SOLAR-TERRESTRIAL PREDICTIONS PROCEEDINGS

VOLUME I

PREDICTION GROUP REPORTS

Edited by

Richard F. Donnelly
Space Environment Laboratory
Boulder, Colorado 80303, U.S.A.

August 1979

The International Solar-Terrestrial Predictions Proceedings and Workshop Program was hosted by the NOAA Space Environment Laboratory. The workshop was held April 23-27, 1979, at the College Inn in Boulder, Colorado.

Science Sponsors of the Program:

AAS: American Astronomical Society
AGU: American Geophysical Union
AMS: American Meteorological Society
COSPAR: Committee on Space Research
IAGA: International Association of Geomagnetism and Aeronomy
IAU: International Astronomical Union
IUWDS: International URSIGRAM and World Days Service
SCOSTEP: Scientific Committee on Solar-Terrestrial Physics
URSI: Union Radio Scientifique Internationale; Commissions E and G

Science and Financial Sponsors of the Program:

Air Force Geophysics Laboratory
Air Force Office of Scientific Research
Department of Energy
National Aeronautics and Space Administration
National Science Foundation
NOAA Environmental Research Laboratories

UNITED STATES DEPARTMENT OF COMMERCE
Juanita M. Kreps, Secretary

NATIONAL OCEANIC AND ATMOSPHERIC ADMINISTRATION
Richard A. Frank, Administrator

Environmental Research Laboratories
Wilmot N. Hess, Director

NOTICE

The Environmental Research Laboratories do not approve, recommend, or endorse any proprietary product or proprietary material mentioned in this publication. No reference shall be made to the Environmental Research Laboratories or to this publication furnished by the Environmental Research Laboratories in any advertising or sales promotion which would indicate or imply that the Environmental Research Laboratories approve, recommend, or endorse any proprietary product or proprietary material mentioned herein, or which has as its purpose an intent to cause directly or indirectly the advertised product to be used or purchased because of this Environmental Research Laboratories publication.

For sale by the Superintendent of Documents, U.S. Government Printing Office, Washington, D.C. 20402 -
(Order by SD Stock No. 003-023-00041-9)

PROGRAM COMMITTEE

F. E. Cook, IPS, Sydney, Australia
A. D. Danilov, Moscow, U.S.S.R.
Y. Hakura, Tokyo, Japan
G. R. Heckman, NOAA SEL, Boulder
A. P. Mitra, NPL, New Delhi, India
G. A. Paulikas, Aerospace, Los Angeles
N. V. Pushkov, IZMIRAN, U.S.S.R.
A. B. Severny, Crimean Observ.,U.S.S.R.
M. A. Shea, AFGL, Bedford, Mass.
P. Simon, Meudon, France
W. C. Snoddy, NASA-MSFC, Huntsville
H. Tanaka, Tokyo Observ., Japan
J. M. Wilcox, Stanford University
D. J. Williams, NOAA SEL, Boulder

WORKING GROUPS and LEADERS

Long-Term Solar Activity Predictions: Mr. P. S. McIntosh, NOAA ERL SEL, Boulder, Colorado 80303 USA

Short-Term Solar Activity Predictions: Dr. P. Simon, Observatory, Meudon, France

Solar Wind and Magnetosphere Interactions: Dr. C. T. Russell, Institute of Geophysics and Planetary Physics, University of California, Los Angeles, California 90024, USA

Geomagnetic Storms: Dr. S. I. Akasofu, Geophysical Institute, University of Alaska, College, Alaska 99701, USA

Energetic Particle Disturbances: Dr. G. A. Paulikas, The Aerospace Corporation, P. O. Box 92957, Los Angeles, California 90009, USA

Magnetosphere-Ionosphere Interactions: Dr. Richard R. Vondrak, Radio Physics Lab., SRI International, Menlo Park, California 94025, USA

High-Latitude E- and F-Region Ionospheric Predictions: Dr Robert D. Hunsucker, Geophysical Institute, University of Alaska, College, Alaska 99701, USA

Midlatitude and Equatorial E- and F-Region Ionospheric Predictions: Dr. Charles M. Rush, Institute of Telecommunications Sciences, National Telecommunications and Information Administration, Boulder, Colorado 80303, USA

D-Region Ionospheric Predictions: Dr. Eivind Thrane, Division for Electronics, Norwegian Defense Research Establishment, P. O. Boks 25, Kjeller, Norway

Solar-Weather Predictions: Dr. K. H. Schatten, Department of Astronomy, Boston University, 725 Commonwealth Avenue, Boston, Massachusetts 02215, USA

Communications Predictions: Dr. A. P. Mitra, Radio Science Division, National Physical Laboratory, Hillside Road, New Delhi - 110012, India

Subsection on Ionosphere-Reflected Propagation: Dr. B. M. Reddy, Radio Science Division, National Physical Laboratory, Hillside Road, New Delhi 110012, India

Subsection on Trans-Ionosphere Propagation: Dr. John A. Klobuchar, AFGL-PHP, Hanscom Air Force Base, Bedford, Massachusetts 01731, USA

Geomagnetic Applications: Dr. Wallace H. Campbell, USGS Box 25046, Denver Federal Center MS 946, Denver, Colorado 80225, USA

Space-Craft Environment and Manned Space Flight Applications: Dr. A. L. Vampola, The Aerospace Corporation, P.O. Box 92957, Los Angeles, California 90009, USA

PREFACE

The International Solar-Terrestrial Prediction Proceedings and Workshop Program (ISTP/P-W Program) included the following: (1) an open call for contributed papers on solar-terrestrial predictions; (2) invited review papers about (a) the prediction, warning and monitoring services of groups that regularly issue solar-terrestrial predictions; (b) the current and future needs for predictions by groups that use solar-terrestrial predictions, and (c) current knowledge of selected topics in solar-terrestrial physics and applications; (3) working groups on fourteen areas of interest for solar-terrestrial predictions; (4) a preprint exchange from October, 1978 through March, 1979; (5) a workshop of representatives of the working groups; and (6) the Solar-Terrestrial Predictions Proceedings. These proceedings consist of four volumes:

Volume I. Prediction Group Reports
Volume II. Working Group Reports and Reviews
Volume III. Solar Activity Predictions
Volume IV. Prediction of Terrestrial Effects of Solar Activity

Volume I reviews the current practice in solar-terrestrial predictions. Volume II presents the recommendations and reports developed by the working groups at the workshop. Topical reviews and papers on the current and future needs for predictions are also included. Volume II reports the results of discussions of questions such as: What predictions are needed? Where are current predictions inadequate? What recent results from solar-terrestrial research should be applied to improve solar-terrestrial predictions? The program did not include a conference where the authors presented their papers orally. Working group participants were asked to read the preprints and correspond with the authors and other group members before meeting at the workshop. Participants included forecasters, scientists and prediction users. Volumes III and IV present individual suggestions for particular prediction schemes.

The goals of the program were as follows: (1) to determine and document the current state-of-the-art of solar-terrestrial predictions, the applications of these predictions, and the future needs for solar-terrestrial predictions, (2) to encourage research, development and evaluation of solar-terrestrial predictions, and (3) to provide indepth interaction of prediction users, forecasters and scientists involved in the research and development of prediction techniques. To achieve the first goal, we invited forecast groups and user groups to review their activities. The working groups concentrated on deriving recommendations for future needs pertinent to solar-terrestrial predictions. The early call for contributed papers was made to achieve the second goal, i.e. authors had more than a year to orient their work towards a paper on predictions. The workshop was aimed at the third goal. The criteria used for selecting working-group representatives to attend the workshop included the goal of having at least one forecaster per group. The working groups on solar-activity, magnetospheric physics, ionospheric physics, etc., were aimed at attracting scientists. On the other hand, the working groups on communications, geomagnetic applications, and space-craft and man-in-space applications were intended to attract prediction users as well as applications scientists.

Richard F. Donnelly

August 16, 1979

Richard F. Donnelly
NOAA/ERL/SEL
Boulder, Colorado 80303 USA

BOB DOEKER - 1920-1978

In 1965, Bob Doeker was given the task of defining and developing the organization in Boulder that became the Space Environment Services Center (SESC) and the IUWDS World Warning Agency. His pioneering efforts brought together separate programs in several government agencies and forged them into a single national center providing a full range of space environment services and predictions. His work laid the foundation for the Solar-Terrestrial Predictions Workshop by identifying a broad range of users who found they needed these services and an organization for delivering them. The remaining necessary element for the program he envisaged — an improved ability to measure and predict the variations that affect the user's systems — was addressed by this workshop and these proceedings.

Bob Doeker passed away September 24, 1978. He had received the first announcement of this workshop and was excited. He would have liked to come and participate. His presence would have provided a formidable critic for new forecasting models. He would have questioned whether they improve on the existing methods and whether the predictions that result produce more benefits than the cost to provide them. If the answers were clearly positive, then he would have pushed for their adoption.

Bob Doeker was born in Covington, Kentucky, on July 20, 1920. He originally trained as a civil engineer, then became a meteorologist specializing in tropical disturbances. By his own admission he was the best weather forecaster in the Air Weather Service. He was one of the pioneers in setting up the Air Force space environment program. At an opportune time, he received the call to come to Boulder. His legacy is a dynamic U.S. space environment program that is left for future development.

Gary R. Heckman
SESC

OVERVIEW

One goal of the workshop was to determine current practices in solar-terrestrial predictions. Invitations were sent to groups that routinely make some type of solar-terrestrial prediction asking them to review their current prediction techniques. We suggested the reviews of predictions include the following: the empirical and/or theoretical basis, customers, applications, examples, input data, and accuracy. This volume presents these prediction-group reviews, some describing particular predictions in detail and others briefly reviewing all the types of predictions issued by the group.

Most prediction groups provide predictions for ionosphere-reflected HF radio propagation, which has always been the dominate application of predictions. A few forecast centers provide services for radiation hazard predictions for manned space flights and high-altitude and high-latitude aircraft flights. Several forecast centers serving countries at high latitudes include geomagnetic activity predictions for geomagnetic survey organizations and long-line electric power networks.

Most predictions are based on empirical techniques. Our knowledge of the physical processes involved has guided the form of the empirical relations used. Recently, models based on physical principles have been developed for science research to describe certain parts of solar-terrestrial disturbances. In most cases, these models are not yet regularly used at forecast centers because they have not yet demonstrated a consistent improvement over older, simple empirical techniques. On the other hand, the route toward improved predictions will undoubtedly follow new understanding of the solar-terrestrial environment. Conversely, the major applications area that needs further knowledge of solar activity and its terrestrial effects is the solar-terrestrial predictions service. Other applications, e.g. for space system design, either already have or are receiving sufficient solar-terrestrial data, or their needs can be met by direct measurement programs.

Solar-terrestrial predictions are disreputable in the eyes of some scientists, as if they were crystal-ball fortune telling. We hope to dispel this by presenting reviews of current prediction practice. We also hope that scientists will be inspired to suggest better scientific prediction techniques. The predominate use of the root "predict" in the scientific literature is distorted in the form that theory predicts something, lacking the sense of time, i.e. the sense of foretelling has been abandoned. We challenge scientists to apply their work more for forecasting and to put the future back into their use of "predict".

Economic factors are an important influence in solar-terrestrial monitoring and prediction services. We are currently capable of certain improvements in short-term forecasting, e.g. through satellite monitoring of the backside of the sun, but the potential improvements have not yet justified the expense. Furthermore, predictions compete with other approaches for minimizing the effects of solar activity on particular systems. Some systems can be redesigned to minimize or even eliminate the undesirable effects induced by solar activ-

ity by reducing the sensitivity of the system to these effects. In other cases, the systems can be made to automatically adapt to the new conditions during solar activity. Economic factors influence which approach is used.

Computers are now used extensively in forecast centers to process, communicate and display data. Some computer terminals are designed to help the user apply the predictions and real-time data to interpret their effect on his particular problems (see the review paper by P. Argo). Some predictions are made by computer algorithms, but so far most predictions are made by experienced forecasters (see the discussion of computer forecasting in the review paper by Severny et al.). In the coming decade, minicomputers with graphical television displays will probably be used more extensively by forecast centers to make routine predictions, as a research tool for developing and testing new prediction schemes, and to improve the forecast-customer interface.

The more intense a solar-terrestrial disturbance, the more important it is to forecast centers; the importance is nonlinearly proportional to intensity. The number of solar-terrestrial disturbances greater than a particular intensity is generally inversely proportional to that intensity. Combining the distribution of events and the importance weighting factor per event still leads to the group of very major events being the most important. The reviews in this volume tend to discuss major disturbances. In contrast, most science research studies in recent years are dominated by small events because of their large number and ease of observation.

The need for long-term solar activity predictions is great, but the accuracy of current predictions is rather low, especially for times longer than ten years. The work in this area is empirical. We lack a scientific understanding of the physical causes of long-term solar activity. Consequently, the time scales considered by forecast centers tend to be less than one solar cycle. During solar minimum and during the start of a new cycle, there is an increase of activity on predicting the new cycle. At the other end of the time scale, forecast centers predominantly warn of events in progress, or predict particle radiation and geomagnetic storms hours to one or two days in advance. Solar-flare-activity is forecast for the next several days. Some forecast centers consider one month in advance for recurrent solar activity related to solar rotation.

The enclosed review papers do not discuss certain approaches apparently because they are not used, e.g. planetary periods are apparently not used. The great hope of the past decade has been the search for a reliable universal flare precursor. None has been found, although certain "precursors" are sometimes helpful in special cases. Also note that many solar flare forecasts depend on ground-based data with fine spatial resolution that are used to study the detailed evolution of active regions. Satellite data have had great success in real-time monitoring, event detection, and warning applications, but have not yet had a major direct impact on predictions. Recent satellite experiments have illustrated how we can observe coronal holes, which should be helpful in predicting the solar wind structure at Earth. However, the time delay between new research results and routine applications is large enough in this area that such satellite measurements are not yet routinely part of the operational forecast services. The possibilities for improved predictions

through improved observations from space and through improved understanding of solar-terrestrial physics are exciting. I hope they will challenge the reader to contribute to making such improvements a reality.

Richard F Donnelly

Richard F. Donnelly July 1, 1979
ISTP/P-W Program Chairman

ACKNOWLEDGEMENTS

The editor wishes to thank the many persons and organizations who helped conduct or support the International Solar-Terrestrial Proceedings and Workshop Program. Without their support, this program would not have been possible. I am grateful for the science sponsors and financial sponsors listed on the title page. I appreciate the help of the Program Committee and the extensive work of the Working Group Leaders listed on the page after the title page. Numerous persons helped with mailing preprints, including the following: Dave Bouwer, Ed Green, Bob Hetzel, Kim Mattison, Dan Watters, Jim Williams, the entire staff of SESC, and my family, Scot, Lora and Betty Ann. I'm grateful to the many typists who participated, including the following: Gloria Baros, Millie Bolme, Kristi Brubaker, and Kim Mattison. I wish to thank NOAA ERL Publications Office and Rush Services for editorial aid. I appreciate the College Inn staff for their help during the workshop. I am thankful for Jim William's help with the bus tour during the workshop and Kim Mattison's help with the banquet. I appreciate Georgina Pickering and Andy Smith for helping to obtain part-time help and solving travel problems during the workshop.

SOLAR-TERRESTRIAL PREDICTIONS PROCEEDINGS

VOLUME I PREDICTION GROUP REPORTS

TABLE OF CONTENTS

N80-18463

THE FORECASTING CENTER OF MEUDON, FRANCE

Paul Simon
Observatoire de Meudon
92190 Meudon

1. HISTORICAL BACKGROUND

The first daily broadcast of solar and geophysical data, now so called URSIGRAM, began at the Eiffel Tower Station, at Paris, on December 1st, 1928 "in order to study the geomagnetic storms and their related phenomena". Formally the Regional Warning Center was established at Bagneux during the AGY (1957) and was moved to the Observatory of Meudon in 1965.

Real solar forecasting began in the summer of 1965, at the request of the SPARMO Secretary, Mr. J. P. Legrand, for coordinated balloon flights carried out in Finland, Norway and Sweden by several European groups interested in the study of auroral X-ray emission and arrival of solar protons. The second campaign was carried out during the winter 1965-1966 for coordinating simultaneous balloon flights in the same countries and in Antarctica. In 1966, during the Proton Flare Project coordinated by Meudon, they succeeded in forecasting three solar proton events: this performance surprised the solar astronomers contributing to the project.

The staff is made up of two solar astronomers and three technicians operating the Center six days a week and nine hours a day. They currently issue a daily solar and geophysical forecast, around 1500 local time, according to the GEOALERT format of the IUWDS. In addition, for temporary campaigns and on request, they issue special forecasts related to the geomagnetic activity and to a few selected categories of solar events.

The scientific environment is a solar observatory in which, since its establishment in 1876, several astronomers were interested in studying solar terrestrial relationship and, since 1956, after the building of the radioastronomical station of Nancay, in uniting both the optical and radio data for studying solar activity.

2. SEVERAL MAIN FEATURES OF SOLAR ACTIVITY AND THEIR FORECAST

Many categories of solar data show "solar activity": spectroheliograms, radio and X-ray data, white light coronal observations, particles data, photospheric images, photospheric magnetic field, etc...However, roughly speaking, all these categories of data contribute to the identification of only two basic phenomena:

a. The active centers built up by a magnetic field which is the origin of different phenomena observed in all parts of the solar atmosphere.

b. The Flares observed in the chromosphere but sometimes accompanied by X-ray and radio bursts which are signatures of phenomena occurring in the corona.

Of course, in a more complete description, we would have to add the recently identified coronal holes, the streamers and the coronal transients which play a key role in solar terrestrial relationship.

Consequently, in order to follow, day after day, the evolution of the solar activity, we need to have series of data related to all the layers of the solar atmosphere: a single series of data would supply us with a very incomplete view of solar activity.

Among the flares, only a few are energetic events. As an example, from 1974 to the middle of 1977, out of 4685 flares, only 50 flares, i.e. close to one per cent, were, according to the microwave data, true energetic events: they occurred in a few selected active centers and only during a short interval of their life.

Consequently, if we issue a daily forecast for all the spotted groups, which are just 50 per cent of the active centers on the solar disk, and if our forecast is "no energetic event" for all these active centers whatever they look like, we will have 95 per cent of right forecast but, of course, we would not succeed in forecasting a single energetic event. Due to the current distribution of the energetic events among the active centers, the useful forecast concerns only a small number of active centers and, sometimes, during a short part of their disk crossing.

There is some evidence for a relationship between the time scale of a phenomena and the accuracy of the relevant forecast: with one forecast a day, one can expect to predict accurately the evolution of an active center (time scale of a few weeks) but not the time of a flare (time scale of a few minutes). At present we just succeed in identifying the magnetic configuration in which "flares like to occur" and we actually forecast (or identify) more the flare buildup than the flare itself: for large flares, it can be done several days in advance. If we succeed in identifying the "flare trigger," we would have the possibility of issuing an accurate forecast but we would have to do it at a very short notice (probably a few minutes or a few seconds in advance). Presently, our knowledge of solar phenomena is so limited that to issue more than one forecast a day does not really improve the accuracy of the prediction.

3. DATA AVAILABLE

Our forecasts are established according to a small set of local data and a large quantity of data circulating in the IUWDS network.

3.1 Local Data

The solar monitoring program carried out at both Meudon and Nançay supply us with a set of "home made" data: sunspot drawing, (disk size 30 cm.), spectroheliograms in Hα, K_{1V}, K_3 (disk size 85 mm.) and, during wonderful

intervals, photospheric magnetograms. On average, the weather permits us to get optical data two days out of three: for preparing the forecast we use the negative plates themselves, sometimes not yet dried. In addition, we have a classical flare patrol which can be used, weather permitting, to identify the flares reported by radio-astronomers or by any other flare effects: SID, SFA, etc... The Calcium plages help us to identify Active Centers, Hα K_{1v} spectroheliograms give the possibility of having the precise sites of sunspots in plages and of the filaments and of the bright Hα features with respect to the spots. Of course, magnetograms when available give additional pieces of information about new emerging flux (which does not have an inversion line surrounded by a filament) and about the gradients of magnetic field intensity. We receive daily reports of radio solar observations carried out with the three radioheliographs of Nançay working respectively at 9800 Mhz, 408 Mhz and 169 Mhz and the radiometers working at 408, and 169 Mhz (the 9800 Mhz radiometer has not worked for several years but a new one is planned): they give us pieces of information about the corona above active centers.

We receive daily reports from an ionospheric station working at Poitiers from a geomagnetic station working at Chambon la Forêt and from the various geophysical instruments operated at Kerguelen Island. In addition, we get daily sunspot reports from Catania which has very beautiful weather during all the year.

3.2 Ursigram Reports

We receive daily messages from Boulder, Moscow, Tokyo (including the Sydney report), Darmstadt, Praha, and Varsaw. Several categories of data are included in these interchange messages following a special request from our side: the URARL messages from Toyokawa which give flux and spectrum of microwave solar sources; the USSPI and USSPY messages (first studied with the collaboration of the Observatory of Roma and now used in several Russian observatories) in which are described the sunspot magnetic polarities. Of course, the best source of event reports is Boulder and their plain language SDF report is an important source of information about the evolution of active centers and flare occurrence.

All these data are used in the preparation of the forecasts. We have in mind the evolution of the active centers, the place and time of flares, the coronal holes when they are reported, the specific consequences of the solar activity and of the solar events: solar particle arrival, sudden ionospheric disturbance, magnetic storm and related ionospheric perturbation. In preparing the forecast, we have in mind models of active centers and of flares and criteria that help in the selection of categories in the relevant models.

4. SCIENTIFIC BACKGROUND

4.1 Active Centers

The simplest active centers are the bipolar ones. The leading part of

the plage plays the key role, with the leading spots appearing first and remaining longest, and the following spots appearing later and having a shorter life than the leading ones. Its inversion line is roughly parallel to a solar meridian and their two sets of spots of opposite polarities have a slow, diverging motion until they have reached their maximum size. According to space observation, they are surrounded by EUV and X-ray loops but their contribution, if any, to the microwave emission is very weak. During their evolution, a filament is forming above the inversion line and will surround the remaining calcium plage. Very few, if any, subflares are reported in these simple bipolar active centers and they occur at the time of the birth.

As a matter of fact, the X-ray images show that most of the active centers and of even weak plages separated by distance up to 30 degrees can be connected by magnetic loops. This magnetic connection can play a role in the evolution of active centers close together (at less than 15 degrees) and bring some anomaly in the ideal scheme described above as a simple bipolar active center: most of the flares occur in "anomalous" active centers.

When two active centers appear close to each other (distance less than 15 degrees) with a lag of several days, and if the younger one is at the west side of the older one, the new sun spot group will evolve in a βf magnetic type and the two closest sets of spots of both active centers will have a slow approaching motion. If, in addition, the two active centers are not at the same latitude, differential rotation can add its proper motion to the motion described above. Sometimes, the two last sets of spots to remain are the leading spot of the eastern center and the following one of the western center: they build a reversed polarity group. Sometimes, the last spot to remain is the following spot of the western group which is a reversed polarity spot for the cycle.

The same kind of influence can be noted in superimposed groups having a more or less large time lag: the detail of their evolution is not fully understood, but this relationship can help to forecast evolution inside a complex group. Another anomaly is the "parasitic polarity", which could be a "satellite spot": a small area of one polarity inside the unipolar part of a plage. Finally, among the "anomalous" spot groups, we must note the so-called "B" configuration. In the "A" configuration, we have in the same penumbra two sets of spots of opposite polarity with nearly equal areas; in the "B" configuration, we have just one large round spot surrounded on one side by an "eyebrow filament" and, sometimes, by a chaplet of tiny spots of opposite polarity situated very near the large spot.

An important item in the forecast is the understanding of the course of evolution of these active centers (A.C.s): are they growing or decaying? During the growing phase, the sunspots, even the large ones, are not seen through the chromosphere. Roughly speaking, during the decay an A. C. becomes simpler and the distance between the opposite polarity spots does not increase. The process of simplification concerns the pattern of the neutral line and could be accompanied by flaring activity.

The microwave brightness of complex active centers (near 3 cm) is linked to the intensity and to the gradient of the magnetic field; their coronal

contribution in terms of 10 cm flux and X-ray emission could be very high.

Another important item of the forecast is the latitudinal extent of the spot group and its mean latitude. Below 10^0, the A. C.s evolve according to their proper motion; above 10^0, differential rotation plays a role and we must take it into account in the forecast of the spot motion. Of course, the same effect can be noted in spot groups at different latitudes but at nearly the same longitude.

In the study of anomalous A. C.s for the forecast, all the data must be used in a "cross-checking" process. A strong gradient of the magnetic field is not always easy to identify according to just a crude real time magnetogram: the microwave and X-ray emission can confirm this identification. In the first step of the forecast, all of these data are not used as criteria, but as pieces of information contributing to success in a jig-saw puzzle.

4.2 Flares

Flares occur on both sides of an inversion line of the longitudinal component of the magnetic field and the chromospheric brightenings are the foot points of coronal loops or arches associated with flares. However, we do not observe flares along all inversion lines and they must be linked to a specific evolution of the magnetic field. As a matter of fact, we could have several categories of flares and of magnetic field evolution driving flares.

Let us start with one model which could be mostly relevant to small flares. Series of magnetograms with a high spatial resolution show the temporal evolution of the fine structure of the magnetic field. In a unipolar field, most of the time we can identify definite peaks of field intensity separated by valleys; the spots, if any, are at the field peaks. The intensity of these peaks is evolving continuously, and after one or a few days, we can notice the disappearance of a few peaks and the growth of new ones inside previous valleys. This evolution seems to be linked to the evolution of the velocity field of the photosphere as it can be presently observed, i.e. with just one component of the field. If two of these "evolving features" of opposite polarities are on both sides of an inversion line and evolve in opposite ways (one growing while the other one is decreasing), a flare is currently triggered during this evolution. This model could explain that satellite spots, kinks along inversion lines, complex centers with e ,edded polarities are flare producers: all these spatial distributions of the fields increase the number of "evolving features" of opposite polarities on both sides of an inversion line.

We do not know if this model is relevant to all the large flares: sometimes it does apply and we can notice either the inverse evolution and flare occurrence or a parallel evolution of the spot area and no flare is reported. It justifies our interest as forecasters in the way in which spots evolve according to the relationship described above.

However, it seems true that several other categories of field evolution can contribute to the "destabilization" of the coronal magnetic field in an active center: emerging of magnetic flux, birth of a new active center near

the first one, proper motion of the sunspots with a field shearing.

We use the evolution of the active centers as described above, in order to forecast the "flare build up" which can be linked to the evolution of several active centers, and we check its actuality by using several categories of data: Hα brightness, microwave spectrum, X-ray emission, but we cannot announce either the hour or the day of the flare: we can have two large flares the same day or wait several days for the second one. In addition, according to the observed or "inferred" gradient of the magnetic field, we can forecast a proton event: of course, the proton flux will not always reach the Earth environment, but both the hard X-ray burst and the strong microwave burst will give the possibility of identifying the acceleration process.

Of course, we cannot pretend to have only two categories of flares, and many flares may not correspond to either of the above descriptions. However, these two models help to prepare the forecast and to understand the difficulty we have in getting a high score in the large flare forecast: the delay between the first forecast and the flare occurrence could reach several days and sometimes we are afraid to "stay" on our forecast; we remove it and the flare occurs at a time when we do not continue to expect it.

Summarizing this forecasting technique, the first step is a forecast of the evolution of all A. C.s taking into account their relationship to the past and actual A. C.s and the "solar cycle" and "latitude" effects. In this work, all the categories of data are used to confirm the evaluation in terms of a coherent A. C. model. The second step concerns the flare forecast itself in which several categories of data supply us with criteria to select the categories of expected flares.

4.3 Geomagnetic Activity

We currently identify two categories of geomagnetic activity.

a. Recurrent activity. Typical recurrent storms have their maximum intensity near the equinox and their minimum at solstice. Most of the time, we have two separate streams of recurrent activity in opposite phase: one around March and the other one around September, and they can be followed from one year to the next one. Several among these storms have a sudden commencement. They are apparently linked to the presence of large coronal holes at low latitude and are well observed during the last three years of a sunspot cycle. However, typical recurrence of weak amplitude can be noted at any time. Our knowledge of the coronal holes is just at a beginning, but it seems that their contribution is questionable during the few years preceding sunspot maximum (their polarity is opposite to the one of the relevant polar hole) and during the two or three years following sunspot maximum: during this interval there are no polar holes at all or they have a very small size.

b. Sporadic storms. Most of them have a sudden commencement and follow a large flare. However, several of the storms which are not in a recurrent stream have no parent flare: sometimes they can be associated with a

disparition brusque.

Looking at the flares, we would notice that most of the large flares or those accompanied by a large microwave burst are followed by a sudden commencement occurring in a delay related to both their order in the flaring activity (the first flare shock wave travels more slowly than the following flare shocks) and the integrated flux of the microwave burst (the larger the integrated flux, the faster the shock wave). Most of them are accompanied by a metric type II burst and the directivity effect is weak: flares from 60^0 East to 60^0 West can be followed by an SSC.

However, the intensity of the geomagnetic storm is not easy to forecast: sometimes the sudden commencement is followed by no definitive increase of the geomagnetic activity, even for large flares near the center of the disk.

5. THE FORECASTING TECHNIQUE

5.1 Data Used for Checking the Model

a. Calcium plage

a.1. A bright and compact plage of small area means a birth or a large temporal evolution.

a.2. Between two bright plages, the brighter one corresponds to the more complex group or to the more evolving group.

a.3. A large scattered plage shows the remnant magnetic field of an old group.

a.4. Many filaments are seen on calcium spectroheliograms as filaments or as corridors.

b. Hα image

b.1. Flares occur in bright Hα features; however, all the Hα features will not have flares.

b.2. In a simple group, the bright features begin between the two polarities, and later on, on both sides of the filament, if present.

b.3. Any bright persisting point which is at some distance from the "normal" bright features described above shows a "parasitic" polarity.

b.4. A very bright feature indicates a point of fast evolution inside the group: increase of one polarity, new birth, young group, parasitic and "huge" polarity.

b.5. The filaments show the inversion line, but they exist only

following the evolution of the group (never at the beginning).

b.6. A spot can be seen in Hα mostly when the group has passed its maximum sunspot area.

b.7. An isolated spot surrounded by a filament is a B configuration (mostly in the decreasing phase of the solar cycle).

c. Radio wave emission

The X-ray and the microwave emission supply us with nearly the same kind of information.

c.1. Strong microwave emission (three centimeters) can correspond either to a large spot (strong field) or to a complex configuration (magnetic field gradient).

c.2. High flux at three centimeters (> 25 f.u.) and a strong ratio (> 1) between the 3 cm and the 8,5 cm flux of a group indicate a strong gradient of the magnetic field.

c.3. Metric wave emission follows flaring activity: strong temporary emission for a large flare, weak or middle-quasi permanent emission for many subflares. However, a group could be a subflare producer without any metric storm (coronal structure and directivity effect).

d. Radio bursts

d.1. A large microwave burst (cm.) corresponds to a strong hard X-ray burst and to strong emission of soft X-rays (SID, etc...).

d.2. A large microwave burst of long duration is accompanied by a large type IV burst (which may not be reported due to a directivity effect). This microwave burst can be used to forecast the time of arrival of the relevant geomagnetic storm.

d.3. The largest microwave bursts correspond to proton accelerations; however, amongst the microwave bursts, many events are not followed by proton arrival at the earth. (propagation effect)

d.4. Any radio burst indicates a particle acceleration, mostly electrons (type III), or a shock wave (type II).

e. X-Rays

e.1. The hard X-rays show strong gradients of magnetic field.

e.2. The X-ray bursts show particle acceleration and flares occurring in strong gradients (sometimes subflares).

5.2 Current Forecast

QUIET Simple bipolar group born far (> 10^0) from another group or from a scattered plage. The inversion line is nearly parallel to a meridian. No radio emission.
Forecast: A few subflares can be expected during the first days.

ERUPTIVE Some weak anomaly in comparison with a quiet group: bright Hα points, born inside an old plage, etc.... They could have weak microwave or metric wave emission.
Forecast: Many subflares, sometimes with weak microwave bursts. Could evolve after several days into an active or proton center.

ACTIVE Large sunspots in white light. B or A configuration (strong magnetic gradient d/D << 1). Bright Hα and Calcium features between spots. Definite microwave emission (≃ 25 f.u.). Ratio 3 cm to 8,5 cm weak (≃ 1.00). Some hard X-ray flux.
Forecast: Flare with large microwave and X-ray emission. However, the evolution can be slow and the flare could be reported only on the second or third day after the forecast.

PROTON An A configuration with all the features of an Active center but:

The inversion line is more strongly drawn. The gradient is stronger but the spot areas are not necessarily larger. The microwave emission is stronger (> 25 fu). The Ratio 3 to 8,5 cm flux is high (> 1.00). The Center is between 30^0 East and the West limb.
Forecast: A Proton Event in the next few days.

MAGNETIC STORM

1. Following a flare with large microwave burst (> 200 f.u.) and some duration (> 15 min.) occurring between 60^0 East and 60^0 West.
Forecast: the delay evaluated according to the microwave importance.

2. Recurrence: Two streams by solar rotation, one having its maximum at the first equinox, the other one at the second equinox.
Forecast: taking into account the seasonal effect.

TEN CM FLUX We try to evaluate the contribution of each center and to use the solar activity forecast in order to predict the evolution of the flux for the next three days.

6. FORECAST AND USERS

We compared our series of forecasts, issued from July 1968 to December 1969, to the actual events reported later on. Our four classes of daily spot group activity are those currently used in the IUWDS: the solar activity is not distributed equally among these four classes since, during this interval, we had 171 Quiet groups, 32 Eruptive groups and 3 Active groups per one Proton group. Consequently, the Quiet Activity is easier to forecast than the Eruptive one, the Eruptive Activity than the Active one, and the

"Active" Activity than the Proton Activity: the study confirmed this expectation with respectively 90 per cent of success in the Quiet Forecast, 50 per cent in the Eruptive one, 18 per cent in the Active one and 30 per cent in the Proton forecast. Starting from the actual activity reported, 92 per cent of the Quiet groups were correctly forecast, and respectively 37, 30 and 64 per cent of the Eruptive, Active and Proton groups. These figures can be linked to the duration of each class of activity during the disk crossing of the sunspot groups: a group is currently eruptive during intervals of two or three consecutive days. This interval is long in comparison to the duration of Active and Proton groups, but very short in comparison to the Quiet groups which can cross the entire disk with only a few subflares reported. In conclusion, we would like to emphasize that even these poor performances are very useful for users: if they follow the forecast, they increase definitely their chance of observing a specific category of event, especially the unusual events like the large X-ray flares or the Proton flares. We did not have a more recent opportunity of evaluating the current accuracy of our forecasts.

We can classify our customers in three categories:

1. Those using a forecast in order to begin or to continue a program of operation: Coordinated International Scientific Programs such as the Proton Flare Project, the Incoherent Scatter WG, the SPARMO Balloon Flights, Solar Satellites and technical programs such as oil or water researches. In order to succeed in these enterprises, we need to have a close and fast contact with our customers: we can add to our forecast special advice, taking into account both the actual trend of solar activity and the constraints under which our customer is put.

2. Those using a forecast as a warning: scientists firing rockets into an aurora, engineers controlling an electric power distribution, operators of radio transmitters, etc.... The current problem is to issue a forecast easy to understand.

3. Those using our forecast in order to issue their own forecast: forecasters of ionospheric propagation, of orbits of low apogee satellites, etc.... The main problem is to understand the accuracy they expect from our forecast.

Acknowledgements

The Forecasting Center of Meudon could not operate without the technical assistance of the Centre National d'Etudes et Telecommunications, the scientific expertise of our colleagues of the Solar Department, the technical assistance of observers operating at Meudon and Nançay, the data supply of our IUWDS colleagues in charge of Regional Warning Centers, the unexpected requests of our customers and the diffuse scientific support of the International Solar Community.

REFERENCES

Avignon, Y., M. J. Martres, and M. Pick (1964): Identification de classes d'eruptions chromospheriques associees aux emissions de rayons cosmiques et a l'activite radioelectrique. Ann. Astro., 27:23.

Caroubalos, C. (1964): Contribution a l'etude de l'activite solaire en relation avec ses effets geophysiques. Ann. Astro., 27:333.

Kundu, M. R. (1959): Structures et proprietes des sources d'activite solaire sur ondes centimetriques. Ann.Astro., 22:1.

Martres, M. J. (1968): Origine des regions solaires actives "anormales", n° 35 IAU Symposium, 25.

Martres, M. J., R. Michard, and I. Soru-Iscovici (1966): Etude morphologique de la structure magnetique des regions actives en relation avec les phenomenes chromospheriques et les eruptions solaires. Ann. Astro., 29:245.

Martres, M. J., R. Michard, I. Soru-Iscovici, and T. Tsap (1968): Structure evolutive magnetique des regions actives solaires. Solar Phys., 5:187.

Martres, M. J., I. Soru-Escaut, and J. Rayrole (1971): An attempt to associate observed photospheric motions with the magnetic field structure and flare occurrence in an active region. IAU Symp. n° 43, 435.

Martres, M. J., I. Soru-Escaut, and J. Rayrole (1973): Relationship between some photospheric motions and the evolution of active centers. Solar Phys., 32:365.

Martres, M. J., J. Rayrole, E. Ribes, M. Semel, and I. Soru-Escaut (1974): On the importance of photospheric velocities in relation to flares. Flare-Related Magnetic Field Dynamics, HAO/NCAR, Boulder, Colo., p. 333.

Martres, M. J., I. Soru-Escaut, and Y. Nakagawa (1977): Hα off-band pre-flare activities. Astron. Astrophys., 59:255.

Pick, M. (1961): Evolution des emissions radioelectriques solaires de type IV et leur relation avec d'autres phenomenes solaires et geophysiques. Ann. Astro., 24:183.

Pick, M., and P. Simon (1973): Solar activity and its forecast. Proc. IEEE, 61:1303.

Ribes, E. (1969): Study of the correlation between flares and the evolution of magnetic field. Astron. Astrophys., 2:316.

Simon, P. (1979): Polar coronal holes and solar cycles. Solar Phys., in press.

Svestka, Z. (1976): Solar Flares. Reidel Publ. Co., Dordrecht, Holland.

Tanaka, H., and T. Kakinuma (1964): The relation between the spectrum of slowly component of solar radio emission and solar proton event. Rep. Ion. Space Res. Japan, 18:32.

D2-32

N80-18464

THE FRENCH SHORT TERM RADIOPROPAGATION PREDICTIONS IN THE DECAMETER BAND

P. Lassudrie-Duchesne, A. M. Bourdila, H. Sizun
C. N. E. T.
Département "Mesures Ionosphériques et Radioélectriques"
Route de Trégastel
22300 Lannion (France)

Ionospheric short term predictions are issued regularly by the "Centre National d'Etudes des Télécommunications" located in Lannion. They are concerned with both weekly and daily predictions of the ionospheric characteristics relevant to radiopropagation. A description of the techniques involved is given as well as examples showing how the prediction messages are prepared.

I. INTRODUCTION

The "Centre National d'Etudes des Télécommunications" (C.N.E.T.) in Lannion prepares and issues short term radiopropagation predictions for the decameter band on a regular basis. The prediction messages are sent by telex to the users. They are mainly the French Army and Post Office as well as a small number of scientific institutes in Europe.

The short term predictions are confined to restricted geographical areas or "zones", namely the "European zone" and the "North European zone". Figure 1 shows the geographical extent of both zones. The predictions are relevant to radio circuits whose terminators are both located inside the same zone. As a matter of fact, they can be used with a reasonable approximation for circuits less than 3000 km of length whose reflection point lies within a given zone.

With the exceptions of special notices and alerts, the short term predictions are of two kinds--weekly and daily predictions.

1.1 Weekly Predictions

They are issued every week and contain a prediction for the next seven days of the radiopropagation conditions. An example of weekly prediction message is given in Figure 2. The first part of the message is a review of the main solar and ionospheric events that occurred during the past week and which are of interest to radiopropagation (S.I.D., P.C.A., auroral absorption, ... etc.).

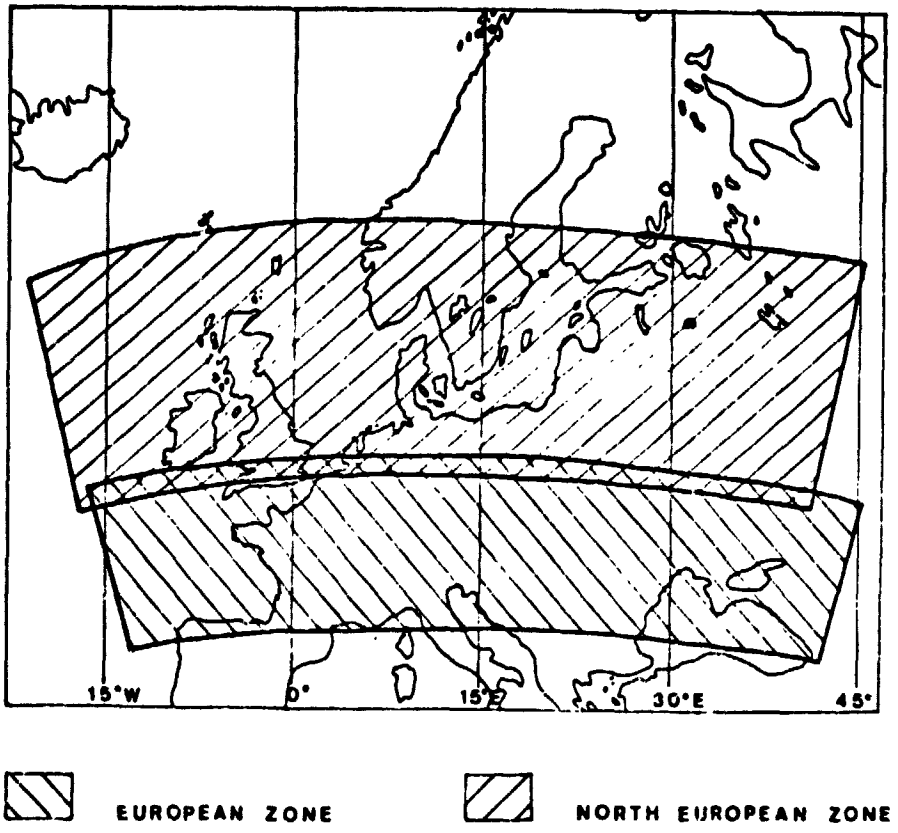

Figure 1. European and North European zones.

The second part of the message of Figure 2 is a prediction of the median radiopropagation conditions (MUF) for the next seven day period. It is concerned with the European and North European zones, as well as with radio circuits starting from France. In this part, reference is made to a "permanent series of bulletins" which the users have at hand and which are normally used for long term predictions. A more detailed description of this permanent series of bulletins will be given in the following section. For the moment we shall simply mention that these bulletins contain monthly median predictions of the MUF and LUF as a function of local time for circuits lying within the zone of interest (Figure 3). The short term prediction message of Figure 2 indicates which of these bulletins is to be selected and the percent corrections to be brought to the curves of this bulletin to match the median MUF expected for the next week. Reference is also made in the message to radio circuits starting from France. The message ends with a brief description of the expected development of the radiopropagation conditions for the future week.

1.2 Daily Predictions

They are issued every day at 15 LT (except weeks end) and contain a more detailed evaluation of the MUF and LUF for the next 24 hours. Figure 4 shows an example of a daily prediction message. The predictions are presented for the European and North European zones separately. The next 24 hours are

Constatation d'anomalies faite au cours d la dernière pé'iode hebdomadaire :

- Propagation médiocre le 9 Septembre 1977 entre 16 H 30 et 18 H 30 et le 10 en début de matinée.
- Faiblesse de l'ionisation durant toute la journée du 11.

PH38 - Prévisions de propagation ionosphérique valable du vendredi 16 12 H 00 TU au vendredi 23 Septembre 1977. Stop.

Primo : Zone Europe - Utiliser les bulletins de la série permanente Septembre IR_5 égale 40. Diminuer de 5 % les valeurs de la MUF 90 %. Stop.

Secondo : Zone Europe du Nord - Utiliser les bulletins de la série permanente Septembre IR_5 égale 40. Augmenter de 10 % les valeurs de la MUF 90 %. Stop.

Tertio : Point à point à partie de la Métropole. Utiliser les bulletins de Septembre. Augmenter de 5 % les valeurs de la MUF 90 %. Stop.

Quarto : Instabilité de l'ionisation en début et en fin de période hebdomadaire.

Disparition des nombreuses réflexions par la couche E sporadique.

Figure 2. Example of weekly prediction message.

divided into 6-hour intervals beginning at 18 LT and ending at 18 LT on the next day. During each of the 6-hour intervals (say 18 to 00 LT in the European zone, for instance), a descriptive cypher is used to evaluate the expected MUF level ("2" placed between 18 and 00 in our instance). The descriptive cyphers refer again to the permanent series bulletin mentioned above. In each 6 hour time interval the descriptive cypher can take the following values (Figure 3): (a) 1 if the MUF is expected to be above the MUF 30% (monthly predicted MUF with a 30% probability of occurrence, (b) 2 if the MUF is expected to be comprised between the MUF 30% and the MUF 90%, and (c) 3 if the MUF is expected to be under the MUF 90%. Roughly speaking, the descriptive cypher is 1 if the expected MUF is higher than normal (i.e. monthly predictions), 2 if it is normal, 3 if it is lower than normal.

In Figure 4 the terms "short distances" ("petites distances") and "median distances" ("moyennes distances") refer to the MUF(0)F2 and the MUF(3000)F2, respectively. A similar presentation is used for the LUF during the day hours (6-12 and 12-18 intervals).

2. AVAILABLE DATA

2.1 Vertical Sounding Data

The vertical ionosonde of LANNION (48.75°N, 3.45°W) is located close to

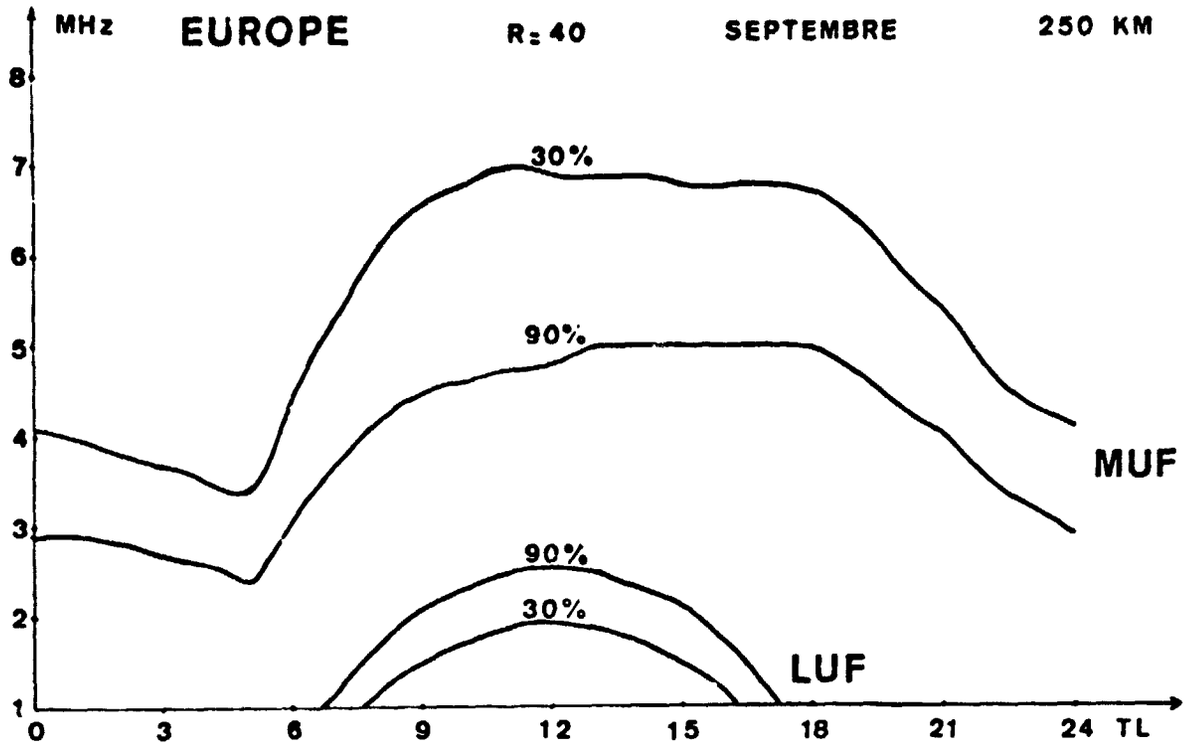

Figure 3a. Example of Permanent Series Bulletin.

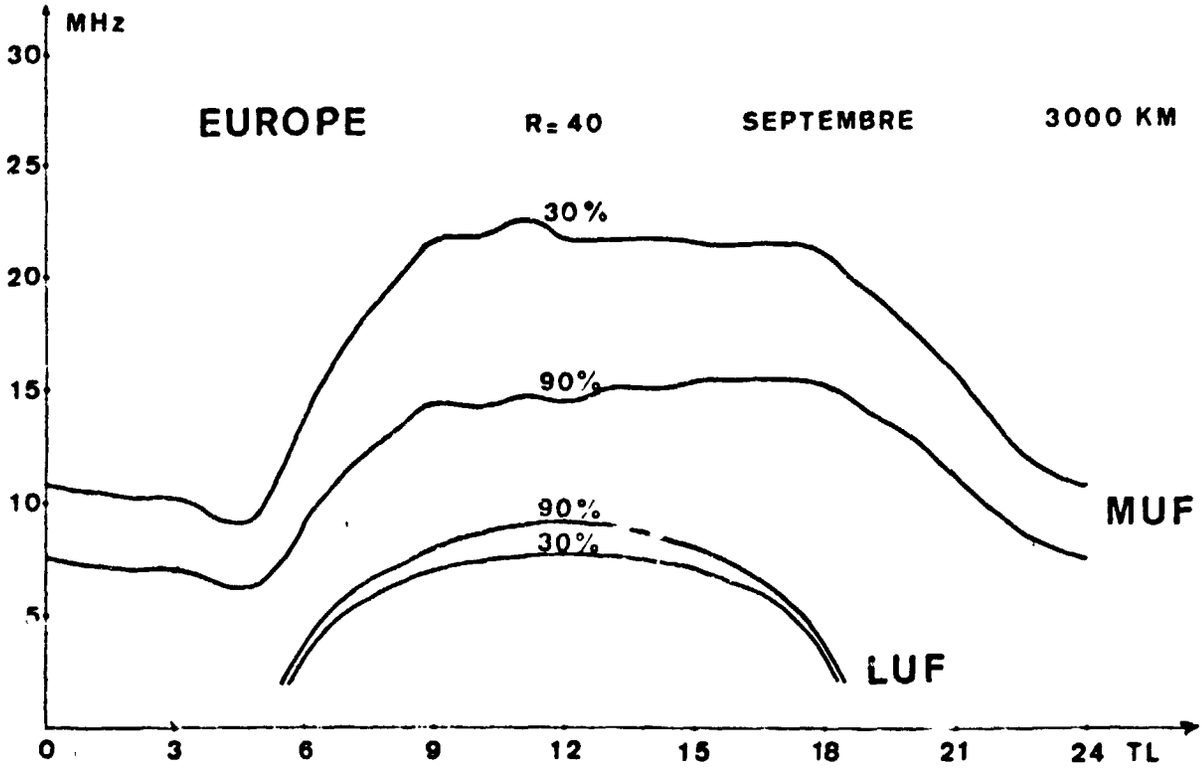

Figure 3b. Example of Permanent Series Bulletin.

PJ263 Prévisions de propagation ionosphérique journalières

Europe moyenne indice 40 Septembre

MUF Petites Distances	18	2	00	3	06	2	12	2	18
MUF Moyennes Distances	18	2	00	3	06	3	12	3	18
LUF	06	1	12	1	18				

Europe du Nord indice 40 Septembre

MUF Petites Distances	18	3	00	3	06	2	12	2	18
MUF Moyennes Distances	18	3	00	3	06	3	12	3	18
LUF	06	1	12	1	18				

Figure 4. Example of Daily Prediction Message.

the prediction center and provides the prediction group with ionospheric measurements. The ionosonde of POITIERS (46.58°N, 0.33°E) (about 320 km away from LANNION) also sends ionospheric data by way of telex or telephone. From Northern Europe, the data of the ionosondes of UPPSALA (60°N, 18°E) or LYCKSELE (65°N, 19°E) are sent daily to LANNION by telex.

2.2 Magnetometer

A magnetometer is located in LANNION and provides the predictors with real time geomagnetic data.

2.3 URSIGRAMS

URSIGRAMS relevant to data measured in observatories from all over the world are received by telex. The data used for short term predictions are concerned with: (a) sunspots, solar flares, solar radio flux, description of solar active centers, (b) geomagnetic indices of activity, and (c) ionospheric critical frequencies, indices of propagation, absorption measurements. Figure 5 gives a synoptic view of the data collected by the prediction center in LANNION.

2.4 Permanent Series Bulletins

The "Permanent series" bulletins mentioned in the previous section are available to the users for long term (monthly) predictions. They also serve as a reference to display short term prediction final results, the latter being presented as a correction to long term predictions. It should be noticed that this is the only interference between short term and long term predictions, the two methods being otherwise independent.

The "Permanent series" bulletins or "Permanent Zonal Predictions" are consistent with the definition of the geographical zones. These are chosen

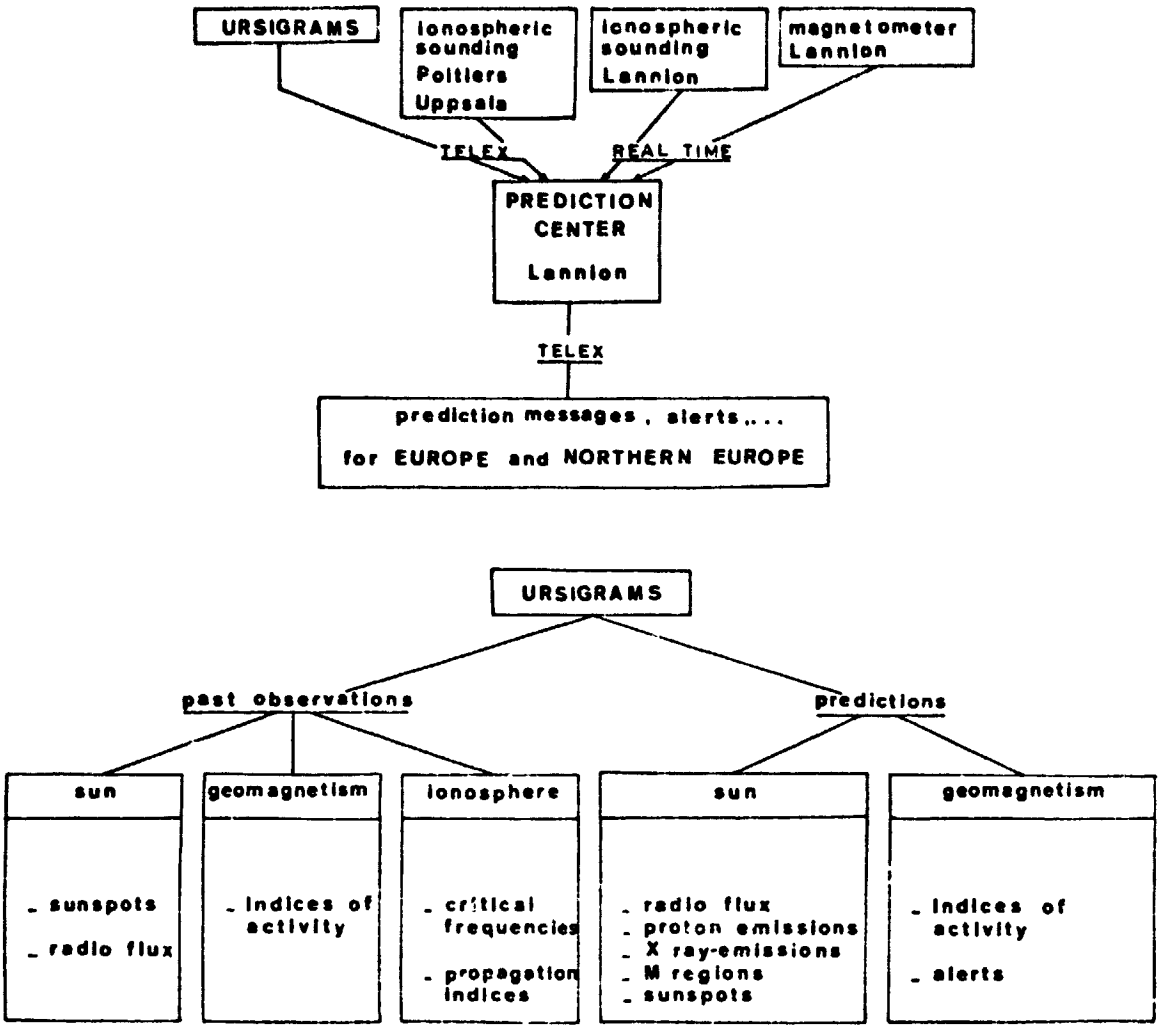

Figure 5. Data collection for the Prediction Center in LANNION.

in such a way that the monthly median foF2 can be regarded as roughly constant (i.e. independent of the geographical coordinates for a given local time) inside a definite zone. In other words, both latitudinal and longitudinal effects are assumed to be negligible within the limits of a zone (the earth's rotation being accounted for by the use of local time). This has made it possible to construct regression curves between the solar index IR_5 and the foF2 for given month and local time where IR_5 is defined by the following relation:

$$IR_5 = \frac{1}{5} \left(R_{m-3} + R_{m-2} + R_{m-1} + R_m + R_{m+1}\right) \qquad (1)$$

with R_m = Wolf number for month m. Any one of these curves is considered to apply for the whole zone.

The results of this analysis is presented to the users in the form of a series of bulletins, each one being relevant to a particular solar index.

The whole series covers the range of solar indices from $IR_5 = 10$ to $IR_5 = 160$ and is applicable to a definite zone. For any given solar index, the corresponding bulletin contains diagrams similar to those of Figure 3 displaying the MUF and LUF as a function of local time. The parameters for each diagram are the month of the year, the distance between the end points of the radio circuit and the attenuation which depends on the particular equipment to which the prediction is applied.

The advantage of such a method for long term predictions is that the user can be given the series of bulletins corresponding to a certain zone once for all. The only information which remains to be regularly sent to him is then the expected solar index for the prediction period (i.e. the bulletin which has been chosen). On the other hand, the drawbacks are that the prediction is available within a restricted area, and that there is a certain loss in accuracy as compared with other methods which calculate the predicted foF2 at the exact point of reflection of the waves.

3. WEEKLY PREDICTIONS

3.1 Foundation of the Method

The method for weekly predictions summarized below has been in use since 1971 and was detailed by Juy (1972). It is based on a linear regression analysis over past data between the 7 day median foF2 at local time h and for week S : $\overline{f}_h(S)$ and the solar index $IR_5(S)$ corresponding to this week (i.e. corresponding to the month which includes week S). Here, the week number S goes from 1 to 52 in the course of a year.

Juy (1972) has shown, by using the data of Freiburg from 1948 to 1968, that there exists a set of linear regression functions L_h^S such that:

$$\overline{f}_h(S) = L_h^S\,(IR_5\,(S)) = a_h^S\;IR_5(S) + b_h^S \qquad (2)$$

In this analysis the most magnetically disturbed weeks were eliminated so that the linear functions L_h^S apply to an approximately quiet ionosphere. Moreover, the L_h^S functions are assumed to be characteristic of the ionosphere not only over Freiburg, but also over the whole European zone.

3.2 Prediction Technique

The prediction technique makes use of the linear regression functions L_h^S as follows: Let S be the number of the last week for which data are available and (S + 1) the week to be predicted. Since $f_h(S)$ is known for every hour h, eq. (1) can be used to determine a value R_h^S of the solar index for week S:

$$R_h^S = (L_h^S)^{-1}\,(\overline{f}_h(S)) = \frac{1}{a_h^S}\,(\overline{f}_h(S) - b_h^S)\ . \qquad (3)$$

The value R_h^S has no physical meaning in that sense that it merely comes from a mathematical relation. It is not in general equal to the actual solar index $IR_5(S)$, which is to be measured for the month including week S.

The main assumption is that the value R_h^S does not change from week S to week S + 1:

$$R_h^{S+1} = R_h^S \tag{4}$$

Now, eq. (2) is again used at step S + 1 to determine $\overline{f}_h(S+1)$ from $IR_5(S+1) = R_h^S = R_h^{S+1}$. The same process can be repeated for every hour h of the day. In practice, Juy (1972) states that the overall level of ionization during the day can be summarized by the values of only three particular hours: h = 10, h = 12 and h = 14 LT. Hence, for simplicity, the level of ionization for the week S + 1 is characterized by the index p(S+1) defined by:

$$p(S+1) = \frac{1}{3}(\overline{f}_{10}(S+1) + \overline{f}_{12}(S+1) + \overline{f}_{14}(S+1)) \ . \tag{5}$$

Let pm be the value of the p index computed from the Permanent Series bulletin values. The percent deviation of p(S+1) from pm is:

$$r(S+1) = 100\ \frac{p(S+1)-pm}{pm} \ . \tag{6}$$

A further assumption is that r(S+1) applies also for the percent deviation of the MUF during the same period.

The correlation between the geomagnetic activity and the ionosphere critical frequency is accounted for according to the following criteria: Let $\Delta Ap = Ap - \overline{Ap}(S+1)$ where $\overline{Ap}(S+1)$ is the predicted average planetary geomagnetic index for week S+1 and Ap the observed index for week S. Then:

If $\Delta Ap \leq -30$, then r(S+1) is reduced by a factor 6%.
If $-30 < \Delta Ap \leq -20$, " " " " " " 3%.
If $|\Delta Ap| < 20$, then r(S+1) is unaltered.
If $20 \leq \Delta Ap < 30$, then r(S+1) is increased by a factor 3%.
If $\Delta Ap \geq 30$, " " " " " " 6%.

A similar technique is used for the North European zone.

3.3 Example of Prediction

The technique will be more clearly explained with the following example which describes how the weekly predictions were made for the week September 16th to September 23rd, 1977 (S+1 = 38). Let us take h = 10 LT as an example. The median foF2 value for the week S = 37 at h = 10 is $\overline{f}_{10}(37) = 5.7$ MHz.

This value plotted on Figure 6a yields $R_{10}^{37} = 21$. By taking $R_{10}^{38} = R_{10}^{37} = 21$ in Figure 6b, we get that $\overline{f}_{10}(38) = 5.6$ MHz. The same process can be repeated for h = 12 and h = 14 LT which gives $\overline{f}_{12}(38) = 5.6$ MHz, and $\overline{f}_{14}(38) = 5.4$ MHz. Hence: $p(38) = (1/3)(\overline{f}_{10}(38) + \overline{f}_{12}(38) + \overline{f}_{14}(38)) = 5.5$ MHz. Let us now compute the value of pm. Figure 3 yields the following values for the MUF 50%: (h = 10, MUF 50% = 6.1 MHz), (h = 12, MUF 50% = 6.4 MHz), and (h = 14, MUF 50% = 6.4 MHz). Hence the value of pm is given by pm = 1/3(6.1 + 6.4 + 6.4) - 1/2 f_H = 5.7 MHz, where f_H = gyrofrequency = 1.2 MHz. This gives $r(38) = 100(p(38) - pm)/pm = -3.5\%$.

The predicted Ap was $\overline{Ap}(38) = 18$ with Ap(37) = 14, hence $\Delta Ap = -4$ and r(38) remains unchanged, i.e. r(38) = -3.5% rounded to -5%. Figure 2 shows the corresponding weekly prediction message.

3.4 Discussion of the Method and Future Prospects

Figure 7 shows a histogram of the prediction errors for the period 1973 - 1977 for h = 10, 12, 14. The total number of values is N = 713. The 90% confidence interval is approximately (-1 MHz, 1 MHz). The main advantage of the method lies in its simplicity. The regression curves, having been established once, for all the weekly predictions, can be done by hand within a few tens of minutes. For criticism it seems that the main causes of errors are the following:

a) The method uses mainly a fixed sample of data (through regression curves) relative to past solar cycles and which are not renewed automatically as time elapses. The only renewed datum is $f_h(S)$, i.e. the last available value of the signal. This only value is, of course, insufficient to take account of the statistical peculiarities of the signal at the time of prediction.

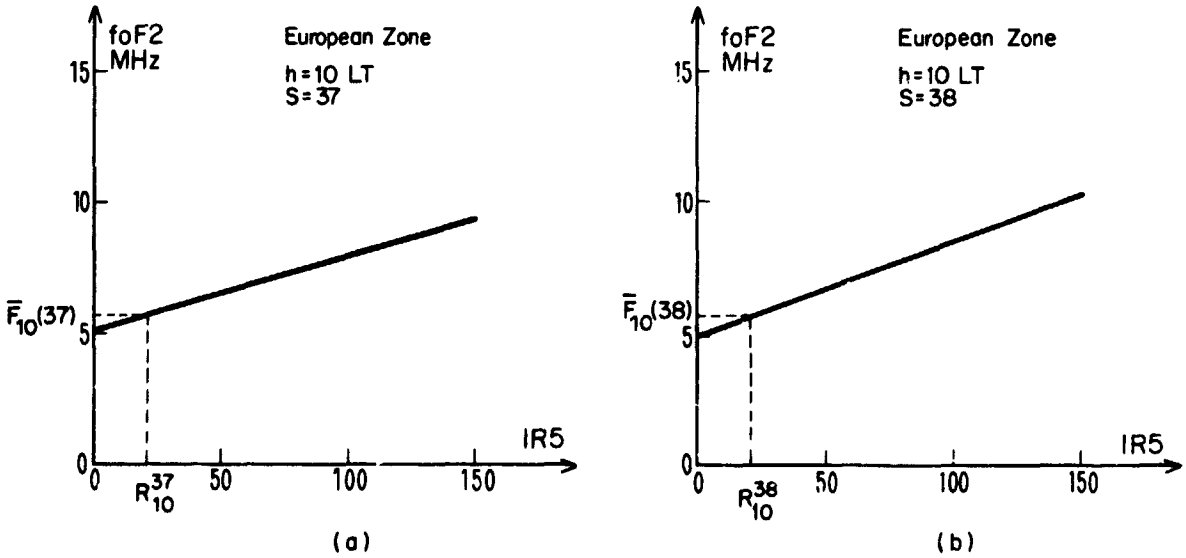

Figure 6. Examples of regression lines for weekly predictions.

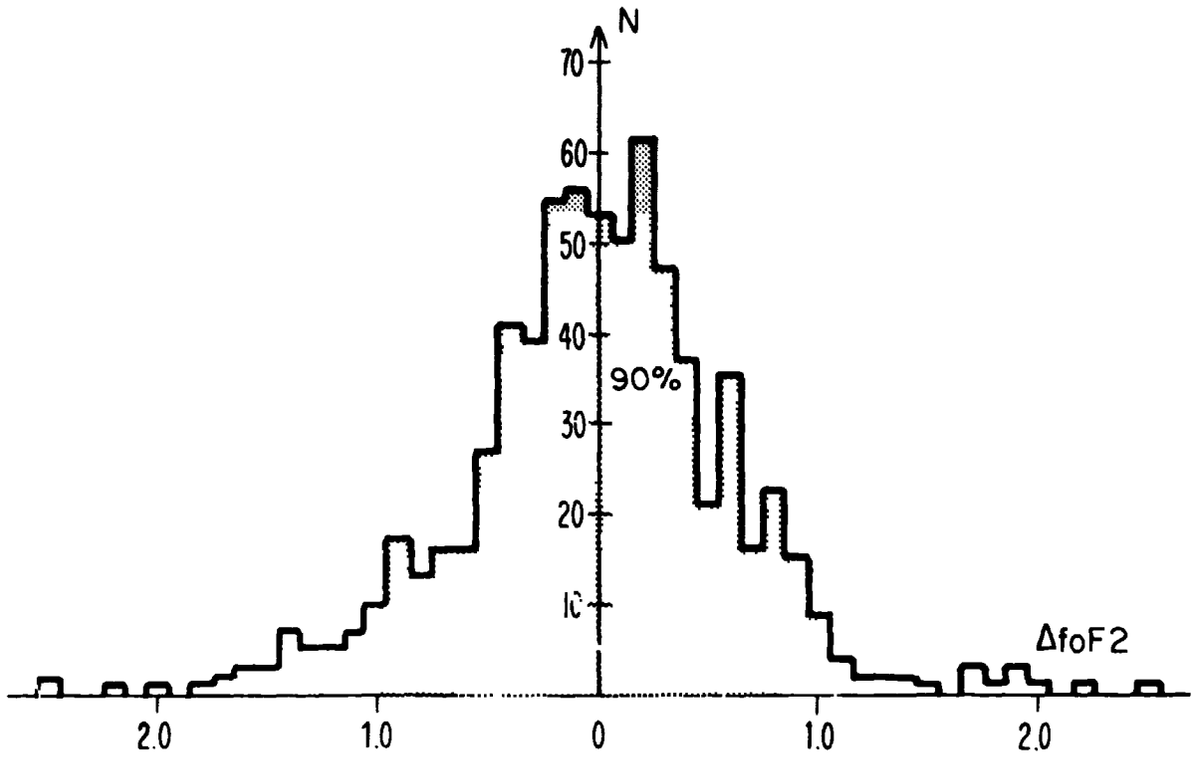

Figure 7. Histogram of the prediction errors for the weekly predictions.

b) Although the regression functions L_h^S, regarded as a serie in S, seem to be able to reproduce adequately the mean annual variation of the signal, it should be noticed that the regression analysis has an averaging effect, which tends to rub out any small scale variation. Hence, errors would rise even if the signal to be predicted had still exactly the same statistical characteristics as that used to produce the regression curves.

These considerations have brought us to the conclusion that ionospheric predictions would be better by means of adaptative methods. So, in the system modelization and identification theory context, ionospheric representation models, particularly fit to prediction settlement, have been recently established. These models have been elaborated by Y. M. Le Roux and will be reported in a contributed paper (2). In fact, the main purpose of this paper will be the weekly predictive case of the foF2 parameter, although it briefly deals with the daily prediction problems. It should be noted that such adaptative predictor models may be established for only one particular parameter (ionospheric, solar or geophysical) or several ones together.

A test of this new weekly method, over past data, has shown an appreciable improvement in the resulting errors with respect to the present method. The predictions algorithms are, moreover, recursive, a fact which can be taken advantage of, whenever desired, to reduce the amount of calculation involved in the prediction to a level sufficiently small to be done manually.

4. DAILY PREDICTIONS

4.1 Prediction Technique

No automatic technique is available. The predictions are heavily dependent on the operator's skill and intuition of the future development of ionospheric events. The following example will give an idea of the way the daily messages are prepared.

4.2 Example of Prediction

Let us take as an example the prediction for September 21st, 1977. The message shown in Figure 4 was prepared on September 20th at 14 L.T. (12 UT). A magnetic sudden storm commencement (S.S.C.) had been reported on September 19th at $11^{H}45$ UT. Figure 8 shows the value of the MUF(0)F2 measured in LANNION plotted on the Permanent series Bulletin curves corresponding to this case. Figure 9 shows the magnetogram of LANNION for this period. A positive phase is observed on September 19th, a few hours after the S.S.C., followed by a decrease in the morning of September 20th.

The predictor has suspected the MUF values to remain at a rather low level during the night and the following day (21st). More precisely, the MUF was expected to remain below the MUF 30%. Hence the descriptive cyphers equal to 2 or 3 in the corresponding message (Figure 4). The operator's intuition has been partially confirmed as shown on Figure 9, where the dotted line represents the values observed in the afternoon of September 20th and the following day.

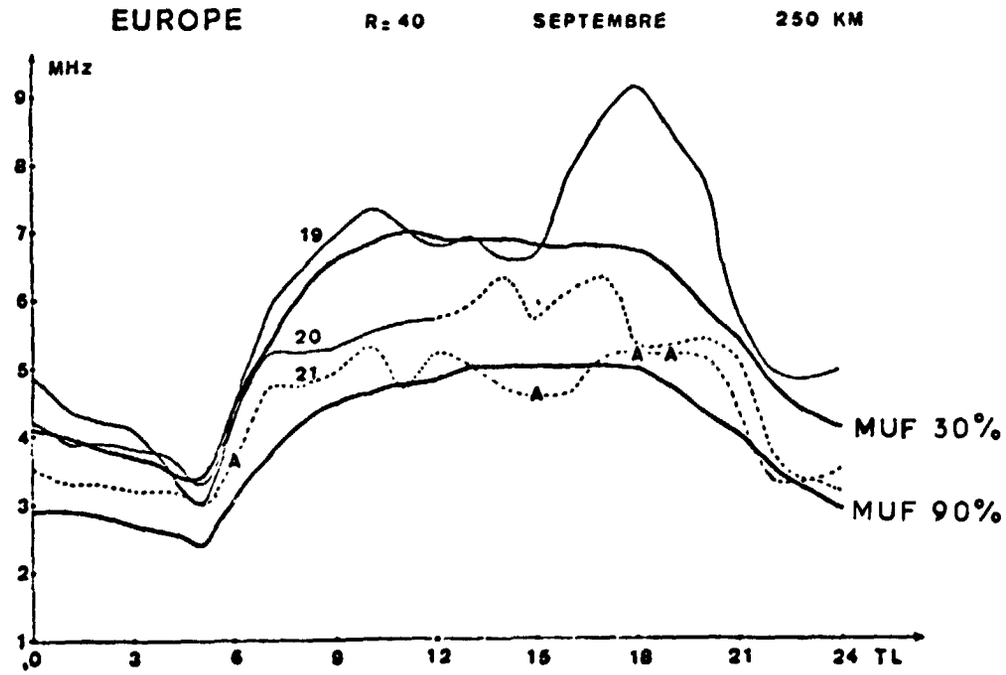

Figure 8. MUF(0)F2 values in LANNION for September 19, 20 and 21, 1977.

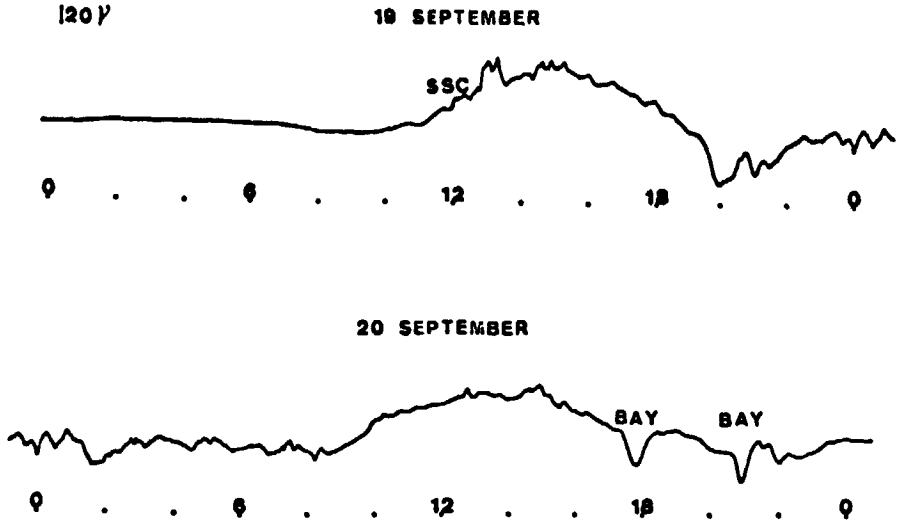

Figure 9, Magnetogram of LANNION (E-W horizontal component) for September 19 and 20, 1977.

4.3 Discussion of the Technique

Telling that the daily ionospheric predictions are an Exact Science would be a questionable assertion. A number of factors are liable to influence the operator's judgment whose individual weight in the final decision can hardly be appreciated. As a matter of fact, two different operators may well produce a somewhat different prediction in the same conditions. Nevertheless, the overall results of the daily predictions are fair (see Figure 10).

The future development in this field tends to make the prediction in a more automatic manner. They are concerned with the modeling of ionospheric disturbances on the one hand and better and more rapid data collection on the other.

REFERENCES

Juy, M. (1972): La prévision ionosphérique hebdomadaire. (Etude sur une base de sept jours de la caractéristique ionosphérique foF2 mesurée en Europe au cours des deux derniers cycles d'activité solaire). Thèse de Doctorat de 3^0 cycle, Université de PARIS VI.

Le Roux, Y. M. (1979): Forecasting methods by means of representation predictive models: Application to the short term ionospheric case. (Private Communication).

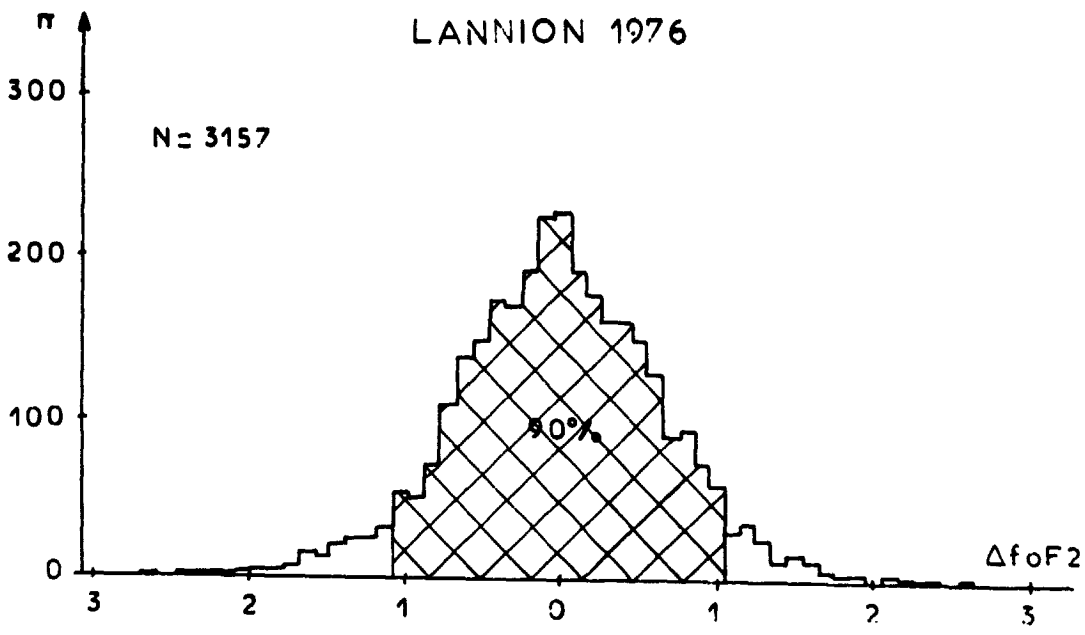

Figure 10. Histogram of the prediction errors for the daily predictions.

PROPAGATION PREDICTIONS FOR THE HF-RANGE BY THE RESEARCH INSTITUTE OF THE DEUTSCHE BUNDESPOST

Th. Damboldt
Forschungsinstitut der Deutschen Bundespost
P.O. Box 5000
D-6100 Darmstadt

This paper describes the long-term and short-term HF propagation prediction service of the Deutsche Bundespost. The long-term prediction method is computer-based and was devised on a philosophy independent from the C.C.I.R. - or any other method. The short-term prediction method is still a manual method which relies mainly on a number of continuous field-strength recordings and on the forecaster's ability to interpret the recordings and to combine this information with all available solar-geophysical data. Examples of the predictions are given and are compared with actually observed HF propagation conditions.

1. INTRODUCTION

Even in our times, where most communications are set up on non-ionospheric circuits, there is a continuing need for reliable radio propagation predictions by a number of users of the HF spectrum. The Research Institute of the Deutsche Bundespost (Post and Telecommunication Administration of the Federal Republic of Germany) provides these users with both long-term and short-term predictions, e.g. for use by its own frequency planning department and coastal radio station. In the following sections a survey of the prediction methods and of the underlying geophysical data will be given.

2. LONG-TERM PREDICTIONS

In this paper the word long-term prediction will be used only for predictions based on published data of the worldwide characteristics of the ionosphere (C.C.I.R., 1974). Long-term predictions are usually computer-based. With the aid of a suitable computer program (e.g. C.C.I.R., 1974) the critical frequencies or the field strength or other propagation data for any month and path can be estimated, provided the only variable, the sunspot number, for the relevant month was reliably predicted.

2.1 The Field-Strength Prediction Method of the Deutsche Bundespost

Current prediction methods (e.g. C.C.I.R., 1974) calculate effective propagation paths (geometrical optics) and compute either transmission loss or field strength taking account of the main geophysical influences on ionospheric radio-wave propagation. In contrast, the method developed here estimates the field strength empirically based on the expressions for deviative and non-deviative absorption (Beckmann, 1965).

A major disadvantage of the other methods of calculating effective propagation paths is that they are incapable of yielding the field strength at frequencies above the "classical MUF" (maximum usable frequency). The classical MUF denotes the highest frequency at which a wave propagates by ionospheric refraction between specified terminals. Experience has shown, however, that reception of the transmitted signal is possible also above the classical MUF. The receiving field strength does not abruptly fall to zero when the frequency of the transmitted signal exceeds the classical MUF, but it decreases gradually. In most cases, therefore, the "operational MUF" is substantially higher than the classical MUF (Beckmann et al., 1965). Several mechanisms are responsible for the propagation of HF radio waves at frequencies above the classical MUF. At present, these are not taken into account by prediction techniques based on theoretical considerations of effective propagation modes. The main mechanisms are:

a) ionospheric scatter propagation by irregularities in the F-layer (e.g. spread-F) and D-layer (ionoscatter),

b) meteor-scatter and auroral scatter,

c) trans-equatorial propagation,

d) scatter on field-aligned irregularities,

e) side-scatter due to ground irregularities,

f) sporadic-E layer refraction,

g) off-great circle propagation, caused e.g. by horizontal gradients in the ionization, and

h) ducting above the maximum of the F-layer.

Apparently several mechanisms are effective at the same time. As a rule, the effectiveness of these modes increases with the length of the radio link and the width of the radiation patterns of the transmitting and receiving antennas.

It has not yet been possible to determine these influences quantitatively by adequate formulae. That is why an empirical factor is applied to the "standard-MUF" values (which are an approximation to the "Classical-MUF" value) taken from the C.C.I.R. Atlas to yield the operational MUF.

The variation of the field strength within the transmission frequency range (i.e. between LUF (lowest usable frequency) and MUF) is computed according to a formula developed by Beckmann, based on the expressions for deviative and non-deviative absorption (Beckmann, 1965). Together with an empirical factor the prediction method now comprises all factors influencing HF radio-wave propagation (Beckmann and Ochs, 1969; Damboldt, 1976).

2.2 Representation of the Predictions

A variety of delineations of the long-term predictions is available to the customers. The oldest and best-known version is the "basic" frequency-versus-time diagram indicating the field strength in the third dimension. Figure 1 shows an example for a certain radio link which is self-explanatory with its legend.

Figure 2 shows an alternative representation where the field strength for the same radio link as in Figure 1 is given in tabular form. In some cases the user of the HF part of the spectrum has available only a limited number of frequencies. In Figure 2 the field strength is given for specified frequencies as a function of time. One advantage of this representation is that transmitter power and antenna gain can be chosen independently for each frequency, whereas in Figure 1 the field strength is normalized to a transmitter power of 1 kW and antenna gains of 0 dB.

Figure 3 shows a printout, where receiver input voltage (upper table) and signal-to-noise ratio (lower table) for the path Tokyo-Germany are given. The receiver input voltage is calculated from the predicted field strength taking into account the antenna gain. Here the signal-to-noise ratio is the ratio of the predicted receiver signal and the noise calculated according to data contained in C.C.I.R. Report 322-1 (C.C.I.R., 1974). The prediction of Figure 3 is shown here to point out the development from field-strength predictions to more user orientated predictions. It is an intermediate stage of the prediction for the coastal radio station of the Deutsche Bundespost at Norddeich and all maritime radio stations of the merchant marine of the Federal Republic of Germany. This prediction, shown in Figure 4, gives for several paths that maritime frequency band which yields the highest receiver input voltage (taking into account the radiation pattern and gain of vertical rod antennas usually used on board ships). Also given is the signal-to-noise ratio in an accompanying symbol A, B, C or *, denoting a signal-to-noise ratio of more than 20 dB, 11-20 dB, 0-10 dB and less than 0 dB, respectively.

The latest version of the predictions is aimed at users with mobile or portable radio stations. Figure 5 shows a sample of these predictions which are accompanied by the text below up to section 2.3:

Explanatory notes on the monthly HF radio propagation predictions for central Europe issued by the Research Institute of the Post and Telecommunication Administration of the Federal Republic of Germany. Each page of the prediction refers to a certain time of the day of a certain month. The time (UT=Universal Time) and the month as well as the sunspot number R upon which the prediction is based are given in the upper right corner. The Tables indicate for different distances between transmitter and receiver that

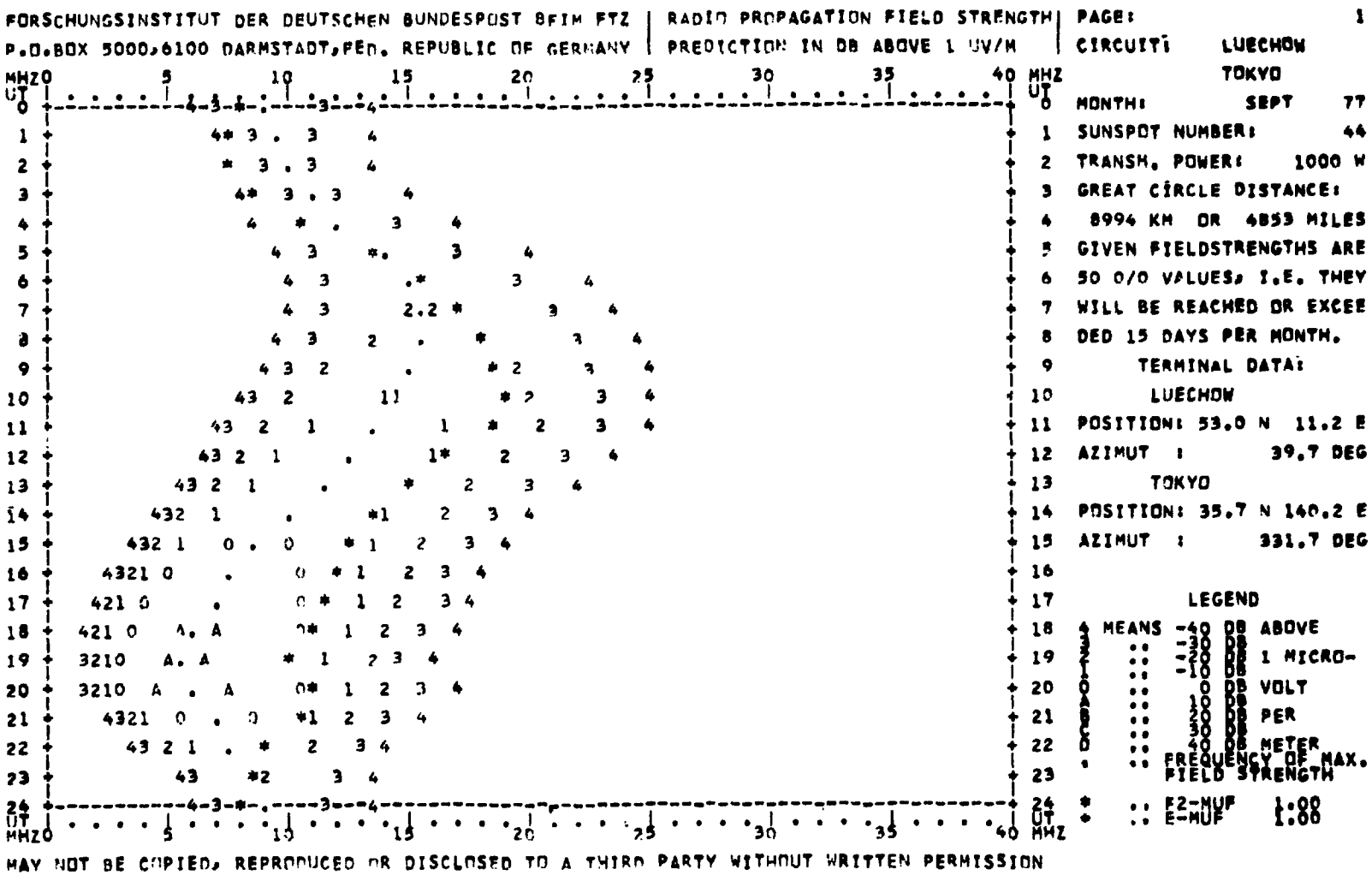

Figure 1. Radio propagation field-strength prediction, diagram form.

FORSCHUNGSINSTITUT DER DEUTSCHEN BUNDESPOST BEIM FTZ P.O.BOX 5000, 6100 DARMSTADT, FED. REPUBLIC OF GERMANY
RADIO PROPAGATION PREDICTION, FIELD STRENGTH IN DB ABOVE 1 MICROVOLT PER METER PAGE: 2
CIRCUIT: LUECHOW - TOKYO MONTH: SEPT 77 SUNSPOT NUMBER: 44.
GREAT CIRCLE DISTANCE: 8994. KM OR 4853. MILES

TERMINAL DATA	TRANSMITTING STATION	RECEIVING STATION
STATION NAME:	LUECHOW	TOKYO
GEOGR. LATITUDE:	53.0 N	35.7 N
GEOGR. LONGITUDE:	11.2 E	140.2 E
AZIMUT:	39.7 DEG	331.7 DEG

FREQUENCY (MHZ)	26.000	22.000	18.000	15.000	12.000	10.000	8.000	6.000	5.000	4.000	3.000
TX POWER (W)	1000	1000	1000	1000	1000	1000	1000	1000	1000	1000	1000
TX ANT.GAIN (DB)	2.0	2.0	2.0	2.0	2.0	2.0	2.0	2.0	2.0	2.0	2.0

UT	1	2	3	4	5	6	7	8	9	10	11	12	13	14	15	16	17	18	19	20	21	22	23	24
CL.MUF MHZ	7.6	7.5	8.3	10.5	13.3	15.6	17.1	17.9	18.5	18.9	18.4	16.5	15.0	13.7	12.6	12.0	11.6	10.9	10.2	11.0	10.3	9.1	8.3	7.9
FREQUENCY																								
26.000 MHZ	-	-	-	-	-	-	-	-	-	-	-	-	-	-	-	-	-	-	-	-	-	-	-	-
22.000 MHZ	-	-	-	-	-	-37	-31	-28	-26	-25	-24	-30	-39	-	-	-	-	-	-	-	-	-	-	-
18.000 MHZ	-	-	-	-	-30	-24	-20	-18	-15	-12	-11	-14	-19	-25	-32	-37	-	-	-	-	-	-	-	-
15.000 MHZ	-	-	-39	-30	-23	-20	-18	-16	-12	-8	-5	-6	-9	-11	-15	-17	-20	-25	-30	-24	-35	-	-	-
12.000 MHZ	-31	-31	-28	-25	-25	-25	-24	-22	-17	-10	-6	-4	-3	-2	-3	-3	-3	-6	-9	-5	-14	-23	-28	-30
10.000 MHZ	-26	-27	-28	-30	-34	-37	-37	-35	-27	-18	-11	-7	-4	0	2	4	5	3	1	4	-4	-12	-20	-23
8.000 MHZ	-29	-32	-38	-	-	-	-	-	-	-35	-25	-17	-11	-2	3	8	10	10	9	11	3	-6	-18	-24
6.000 MHZ	-	-	-	-	-	-	-	-	-	-	-	-	-31	-14	-4	6	10	12	12	13	3	-9	-29	-39
5.000 MHZ	-	-	-	-	-	-	-	-	-	-	-	-	-	-27	-12	1	7	11	12	13	0	-16	-	-
4.000 MHZ	-	-	-	-	-	-	-	-	-	-	-	-	-	-	-28	-8	1	7	9	9	-9	-30	-	-
3.000 MHZ	-	-	-	-	-	-	-	-	-	-	-	-	-	-	-	-27	-12	-2	1	1	-26	-	-	-

Figure 2. Radio propagation field-strength prediction, tabular form.

SEPT. 77 BENUTZER: 1 TOKIO

EMPFAENGEREINGANGSSPANNUNG IN DB AN 50 OHM

GMT	1	2	3	4	5	6	7	8	9	10	11	12	13	14	15	16	17	18	19	20	21	22	23	24
22.4 MHZ	-44	-41	-42	-46	-40	-35	-25	-19	-20	-24	-27	-29	-30	-30	-30	-30	-30	-46	-42	-31	-29	-31	-37	-44
16.8 MHZ	-43	-40	-37	-36	-28	-24	-17	-15	-14	-11	-9	-11	-15	-20	-26	-31	-34	-41	-33	-29	-33	-32	-37	-43
12.6 MHZ	-31	-31	-28	-23	-21	-20	-19	-17	-12	-6	-2	-1	-2	-1	-3	-3	-4	-8	-11	-6	-14	-23	-29	-31
8.4 MHZ	-22	-24	-27	-33	-41	-47	-49	-46	-38	-23	-15	-9	-4	3	7	12	14	14	13	15	8	-1	-12	-17
6.3 MHZ	-35	-40	-48	-61	-61	-61	-61	-61	-61	-55	-41	-29	-20	-5	4	14	18	21	21	22	12	1	-18	-27
4.2 MHZ	-61	-61	-61	-61	-61	-61	-61	-61	-61	-61	-61	-61	-61	-36	-19	4	13	19	21	22	5	-15	-53	-61

STOERABSTAND IN DB

GMT	1	2	3	4	5	6	7	8	9	10	11	12	13	14	15	16	17	18	19	20	21	22	23	24
22.4 MHZ	-99	-99	-99	-99	-99	-99	-99	-99	-99	-99	-99	-99	-99	-99	-99	-99	-99	-99	-99	-99	-99	-99	-99	-99
16.8 MHZ	-99	-99	-99	-99	-99	-99	-99	0	0	3	5	2	-3	-99	-99	-99	-99	-99	-99	-99	-99	-99	-99	-99
12.6 MHZ	-99	-99	-99	-99	-99	-99	-99	-99	0	6	9	10	8	8	5	5	3	-1	-3	2	-5	-99	-99	-99
8.4 MHZ	-99	-99	-99	-99	-99	-99	-99	-99	-99	-99	-4	1	6	11	14	17	16	15	13	14	7	-2	-12	-99
6.3 MHZ	-99	-99	-99	-99	-99	-99	-99	-99	-99	-99	-99	-99	-99	3	11	18	19	19	18	17	6	-6	-99	-99
4.2 MHZ	-99	-99	-99	-99	-99	-99	-99	-99	-99	-99	-99	-99	-99	-99	-99	6	12	14	14	13	-6	-27	-99	-99

Figure 3. Prediction of receiver input voltage and signal-to-noise ratio.

FUNKPROGNOSE FUER VERBINDUNGEN MIT NORDDEICH RADIO SEPT. 77
HERAUSGEGEBEN VOM FORSCHUNGSINSTITUT DER DBP BEIM FERNMELDETECHNISCHEN ZENTRALAMT DARMSTADT R = 44

GMT	1	2	3	4	5	6	7	8	9	10	11	12	13	14	15	16	17	18	19	20	21	22	23	24
GROENLAND	6A	6A	4A	4A	4A	6A	6A	8A	8A	12B	12B	12B	12B	12B	12B	12B	12B	12A	12A	8A	8A	6A	6A	6A
GROSSE SEEN	6B	6B	6B	6B	4B	6A	6A	6B	8C	8C	*	12C	12C	*	*	*	*	12C	12C	12C	12C	8C	8B	8B
NEW YORK	6B	6B	6B	4B	4A	6B	6B	6B	8C	8C	12C	12C	12C	16C	16C	16C	16C	12C	12B	12B	12B	8B	8B	6B
KARIBIK	6B	6B	6B	6B	4B	6B	6A	8B	8C	*	12C	*	*	*	*	*	*	*	16C	12C	12C	8C	8C	6C
RIO DE JAN.	6B	6B	6B	6B	6A	6A	8C	12C	16C	*	*	*	*	*	*	*	*	22C	16B	12A	12A	8B	8B	6B
SANTIAGO	8B	6B	6B	6B	6B	6B	8A	12C	*	*	*	*	*	*	*	*	*	*	*	16C	12C	12C	8C	8C
SANFRANCISCO	8C	6C	6C	6B	6B	6B	6B	6C	8C	*	*	*	*	*	*	*	*	*	*	*	*	*	*	*
VANCOUVER	8C	6C	6B	6B	6B	6A	6B	8C	8C	8C	8C	*	*	*	*	*	*	*	12C	12C	12C	12C	*	*
HAWAII	*	*	*	*	8C	6B	8B	8B	12C	12C	12C	*	*	*	*	*	16C	22C	*	*	*	*	*	*
SIDNEY	*	*	*	*	*	8C	12B	12C	*	*	*	*	12C	12C	8B	8B	6B	6B	6C	8C	8C	*	*	*
PERTH	*	*	*	*	*	*	*	*	12C	*	*	*	*	12C	8B	8B	6B	8B	6B	6B	6C	6C	8C	*
TOKIO	*	*	*	*	*	*	*	16C	16C	12C	12C	12C	12C	8B	8B	6B	6B	6B	6B	6B	8C	*	*	*
COLOMBO	8C	*	*	*	*	*	*	*	*	*	*	16C	16C	12B	12B	8A	8A	8A	6A	6A	6B	6B	6B	8C
ADEN	6A	6A	8A	8B	12B	12B	16B	16C	16C	16C	16C	16C	16C	16B	16B	12A	12A	8A	8A	6A	8A	6A	6A	6A
40S 80E	8C	8C	*	*	*	*	*	*	*	*	*	*	*	*	12C	8B	6B	6C	6C	6C	6B	6C	6C	6C
KAPSTADT	6B	6B	6B	6B	8A	16C	*	*	*	*	*	*	*	22C	22C	22C	12B	12B	8B	8B	8B	8B	6B	6B
MONROVIA	6A	6A	6A	6A	6A	6A	12B	16B	16B	16C	16C	16C	16C	16C	16C	16C	16C	12A	12A	12A	8A	8A	6A	6A

R = SONNENFLECKENRELATIVZAHL
DIE TABELLE GIBT DAS JEWEILS GUENSTIGSTE FREQUENZBAND AN, DER BUCHSTABE HINTER DER FREQUENZ KENNZEICHNET DEN ZU ERWARTENDEN STOERABSTAND, BEZOGEN AUF 300 W SENDELEISTUNG UND 300 HZ BANDBREITE.

ERLAEUTERUNG	A	B	C	*
STOERABSTAND IN DB	GR. 20	11 - 20	0 - 10	KL. 0

Figure 4. Radio propagation prediction, used by all German vessels carrying a maritime radio station.

RADIO PROPAGATION PREDICTION FOR CENTRAL EUROPE MARCH 1979 5 Z
ISSUED BY FTZ DARMSTADT R = 125

TELEPHONY

	SKY WAVE			GROUND WAVE		
	FAIR	GOOD	VERY GOOD	FAIR	GOOD	VERY GOOD
10 KM	1.5- 3.9	1.5- 3.9	1.5- 3.9	1.5-24.0	1.5-16.0	1.5- 5.0
30 KM	1.5- 3.9	1.5- 3.9	1.5- 3.9	1.5- 5.5	1.5- 2.5	-
60 KM	1.5- 4.0	1.5- 4.0	1.5- 4.0	1.5- 1.8	-	-
100 KM	1.5- 4.0	1.5- 4.0	1.5- 4.0	-	-	-
200 KM	1.5- 4.2	1.5- 4.2	1.5- 4.2	-	-	-
300 KM	1.5- 4.3	1.5- 4.3	1.5- 4.3	-	-	-
400 KM	1.5- 4.5	1.5- 4.5	1.7- 4.5	-	-	-
500 KM	1.5- 4.7	1.5- 4.7	2.1- 4.7	-	-	-
600 KM	1.5- 5.0	1.8- 5.0	2.9- 5.0	-	-	-
700 KM	1.5- 5.3	2.3- 5.3	3.3- 5.3	-	-	-
800 KM	1.8- 5.6	2.9- 5.6	-	-	-	-
900 KM	2.0- 5.9	3.5- 5.9	4.8- 5.9	-	-	-
1000 KM	2.5- 6.2	4.1- 6.2	4.8- 6.2	-	-	-

TELEPRINTER

	SKY WAVE			GROUND WAVE		
	FAIR	GOOD	VERY GOOD	FAIR	GOOD	VERY GOOD
10 KM	1.5- 3.9	1.5- 3.9	1.5- 3.9	1.5-30.0	1.5-18.0	1.5- 8.0
30 KM	1.5- 3.9	1.5- 3.9	1.5- 3.9	1.5-13.0	1.5- 4.2	1.5- 1.8
60 KM	1.5- 4.0	1.5- 4.0	1.5- 4.0	1.5- 2.6	-	-
100 KM	1.5- 4.0	1.5- 4.0	1.5- 4.0	-	-	-
200 KM	1.5- 4.2	1.5- 4.2	1.5- 4.2	-	-	-
300 KM	1.5- 4.3	1.5- 4.3	1.5- 4.3	-	-	-
400 KM	1.5- 4.5	1.5- 4.5	1.5- 4.5	-	-	-
500 KM	1.5- 4.7	1.5- 4.7	1.8- 4.7	-	-	-
600 KM	1.5- 5.0	1.5- 5.0	2.1- 5.0	-	-	-
700 KM	1.5- 5.3	1.8- 5.3	3.0- 5.3	-	-	-
800 KM	1.5- 5.6	2.1- 5.6	3.8- 5.6	-	-	-
900 KM	1.8- 5.9	2.6- 5.9	4.3- 5.9	-	-	-
1000 KM	1.9- 6.2	3.2- 6.2	4.5- 6.2	-	-	-

MORSE

	SKY WAVE			GROUND WAVE		
	FAIR	GOOD	VERY GOOD	FAIR	GOOD	VERY GOOD
10 KM	1.5- 3.9	1.5- 3.9	1.5- 3.9	1.5-30.0	1.5-26.0	1.5-16.8
30 KM	1.5- 3.9	1.5- 3.9	1.5- 3.9	1.5-18.0	1.5- 7.0	1.5- 2.8
60 KM	1.5- 4.0	1.5- 4.0	1.5- 4.0	1.5- 4.8	1.5- 2.1	-
100 KM	1.5- 4.0	1.5- 4.0	1.5- 4.0	1.5- 1.7	-	-
200 KM	1.5- 4.2	1.5- 4.2	1.5- 4.2	-	-	-
300 KM	1.5- 4.3	1.5- 4.3	1.5- 4.3	-	-	-
400 KM	1.5- 4.5	1.5- 4.5	1.5- 4.5	-	-	-
500 KM	1.5- 4.7	1.5- 4.7	1.5- 4.7	-	-	-
600 KM	1.5- 5.0	1.5- 5.0	1.7- 5.0	-	-	-
700 KM	1.5- 5.3	1.5- 5.3	2.0- 5.3	-	-	-
800 KM	1.5- 5.6	1.7- 5.6	2.6- 5.6	-	-	-
900 KM	1.5- 5.9	1.9- 5.9	3.0- 5.9	-	-	-
1000 KM	1.6- 6.2	2.3- 6.2	3.8- 6.2	-	-	-

Figure 5. Prediction for mobile and portable radio stations

frequency band which has the signal-to-noise ratio required for various modes of operation (telephony, radioteletype, telegraphy). The following technical parameters are considered in the calculation of the predictions:

Signal-to-noise ratio: As grades for the signal-to-noise ratio (i.e. the ratio of the wanted signal to the atmospheric or man-made noise level at the receiver site) the terms fair, good, and very good were chosen. They are defined as follows:

	fair	good	very good
minimum S/N ratio	10 dB	20 dB	30 dB

The man-made noise level was calculated for rural areas. In the vicinity of large cities or factories this noise increases and, consequently, the signal-to-noise ratio deteriorates.

Transmitter power: The prediction is calculated for a transmitter power of 100 W. For 10 W the frequency range with the next less favourable signal-to-noise ratio applies to all distances (e.g. good instead of very good); for 1000 W the frequency range with the next better signal-to-noise ratio is valid (e.g. very good instead of good).

Antenna: The ground wave bridges only short distances. The prediction calculation assumes a vertical rod antenna (length 8 m). The sky wave is suited for short and long distances. Here the calculations are based on a half-wave dipole (height 12 m above ground).

Bandwidth: The prediction is calculated for a receiver bandwidth of 3 kHz (telephony), 1.1 kHz (radioteletype) and 0.2 kHz (radiotelegraphy).

Electric ground conductivity: The electric conductivity of the ground is the determining factor for the propagation of the ground wave. The higher the conductivity, the longer the range of the ground wave (longest over salt water, shortest over rocky terrain). The prediction calculation assumes poorly conductive ground with a conductivity of 0.003 mho/m and a permittivity of 4.0.

Location: The prediction is calculated for a path-midpoint approximately at 50 degrees north and 10 degrees east. Ground-wave propagation requires a nearly free line-of-sight between transmitter and receiver. This does not apply to the sky wave. Here, for instance, the distant station can also be reached from a valley.

Reliability of prediction: The degree of reliability of the prediction depends on all factors outlined above. Some of them, for instance the noise level and the ground conductivity, are not easily assessible. In the case of the sky wave, the same applies to the unknown actual state of the ionosphere. There is, however, sufficient experience from observations which allows a reliability of about 90% to be expected; i.e. on about 3 days of a month the upper limits of the frequency ranges (i.e. the classical MUF) given for the sky wave will be somewhat lower.

Altogether, it can be said that with a careful choice of the technical

parameters (antenna, transmitter power, bandwidth, location) the non-influencable quantities (noise level, ground conductivity, ionosphere) have been so taken into account in the calculation, that the predicted frequency bands are useful in at least 90% of all cases.

2.3 Comparison of the predictions with measured data

The basis of the activities carried out by the Prediction Group at the Research Institute of the Deutsche Bundespost is the continuous measurement of the signal strength of 26 distant HF transmitters.

For these measurements only radio stations transmitting 24 hours a day are suitable. A number of meteorological broadcast transmitters meets this requirement. Information on these transmitters was taken either from ITU's International Frequency List (power, frequency, site) or from the "Nautischer Funkdienst" (contents of transmissions). Unfortunately, reliable details about transmitter powers and antennas are not always available because most stations are operated by the military. At the present time the field strength of the following stations is recorded: Norfolk (USA), Tokyo (J), Canberra (AUS), Bracknell (GB), and Moscow (SU).

These stations transmit simultaneously on several frequencies. The frequencies on which the field strengths are recorded were so chosen that the HF band (from 3 to 23 MHz) is well represented. The AGC voltages which are a measure for the field strength are recorded on chart recorders, and the charts are evaluated daily.

A fully automatic analyzer or a direct digitization of the AGC-voltage is not advisable because of unforseeable interference. The correct trace on the chart characterized by certain features is marked by an experienced operator. This is possible because all transmitters use frequency shift keying (shift ± 400 Hz). Since the recordings are made with receivers having an IF bandwidth of only 100 Hz, the trace on the chart shows characteristic changes from mark to space. The transmissions received at different frequencies from the same station contain the same information. Therefore, the changes from mark to space must be recognizable on all chart recordings of that path. If a trace does not show these characteristics, there is either interference, technical trouble, or the frequency is above the MUF or below the LUF.

The strip charts are cut off every workday in the morning and hourly values of the measured receiver input voltage are read from the revised charts. The conversion from receiver input voltage into field strength is somewhat complicated because the receiving antennas are rhombic antennas of high directivity and the direction of the incident wave varies unpredictably (Damboldt, 1977). The conversion is made by computer which stores all necessary data to estimate the field strength normalized to 1 kW transmitter power and an isotropic transmitting antenna. These values are then tabulated and depicted in different suitable ways.

One way of representing these data is the "Monthly Report", which

presents data of the preceding month and is published within about ten days of the following month. The Tables contained in the Monthly Report can be used to compare measured and predicted field strength. Figure 6 shows an example for four frequencies recorded on the path Canberra (Australia) - Germany for September 1977. Table 1 shows the corresponding numerical values. The median value for the differences amounts to + 4 dB, - 4 dB, - 1 dB and + 4 dB for the frequencies 19.6, 13.9, 11.0 and 5.1 MHz, respectively. For all four frequencies the median value turns out to be 0 dB. The corresponding rms values for the difference between prediction and measurement are 6.3 dB, 9.6 dB, 6.7 dB and 6.3 dB. For all four frequencies (a total of 62 values) the rms value is 7.9 dB. This value is an estimate for the reliability of the prediction. It is fairly good compared with another prediction method (for comparison see: Pérès, 1978).

3. SHORT-TERM PREDICTIONS

Besides the long-term predictions, the Research Institute of the Deutsche Bundespost also makes short-term predictions for the HF-range. These predictions are issued each workday and are distributed as two separate messages at different times of the day. In the following sections the solar-terrestrial data underlying the short-term predictions as well as a sample of them will be described. Finally a comparison of the predicted radio propagation conditions with observed propagation conditions will be given.

3.1 Solar-terrestrial data available for short-term predictions

The main source of information on the state of the ionospheric transmission channel are the continuous field-strength measurements mentioned in section 2.3. These measurements are available in real time and even a glimpse at the chart recordings reveals details of changes in propagation conditions. Before noon the evaluated measurements of all 26 frequencies for the past 24 hours are available as hourly median values of both field strength and receiver input voltage.

Also available at that time are the readings of a local magnetometer, the readings of the Geomagnetic Observatory at Wingst (near Hamburg), hourly values of the vertical incidence critical frequencies for the past 24 hours from the ionosonde at Lindau and--weather permitting--a chart of sunspots from the observatory on the Wendelstein mountain near Salzburg. Moreover, a variety of data measured in different parts of the world is received through the Ursigram Service. The disadvantage of these data is that they are at least several hours old. Further, very useful information is supplied by the solar daily forecast (SDF) received regularly from Boulder.

With all this information at hand, two experienced forecasters predict the propagation conditions expected for the next 24 hours. The present form of the short-term predictions gives most of the predicted values in relation to the monthly predictions. So, the monthly predicted value is regarded as "normal" and, therefore, it may happen that the short-term predictions

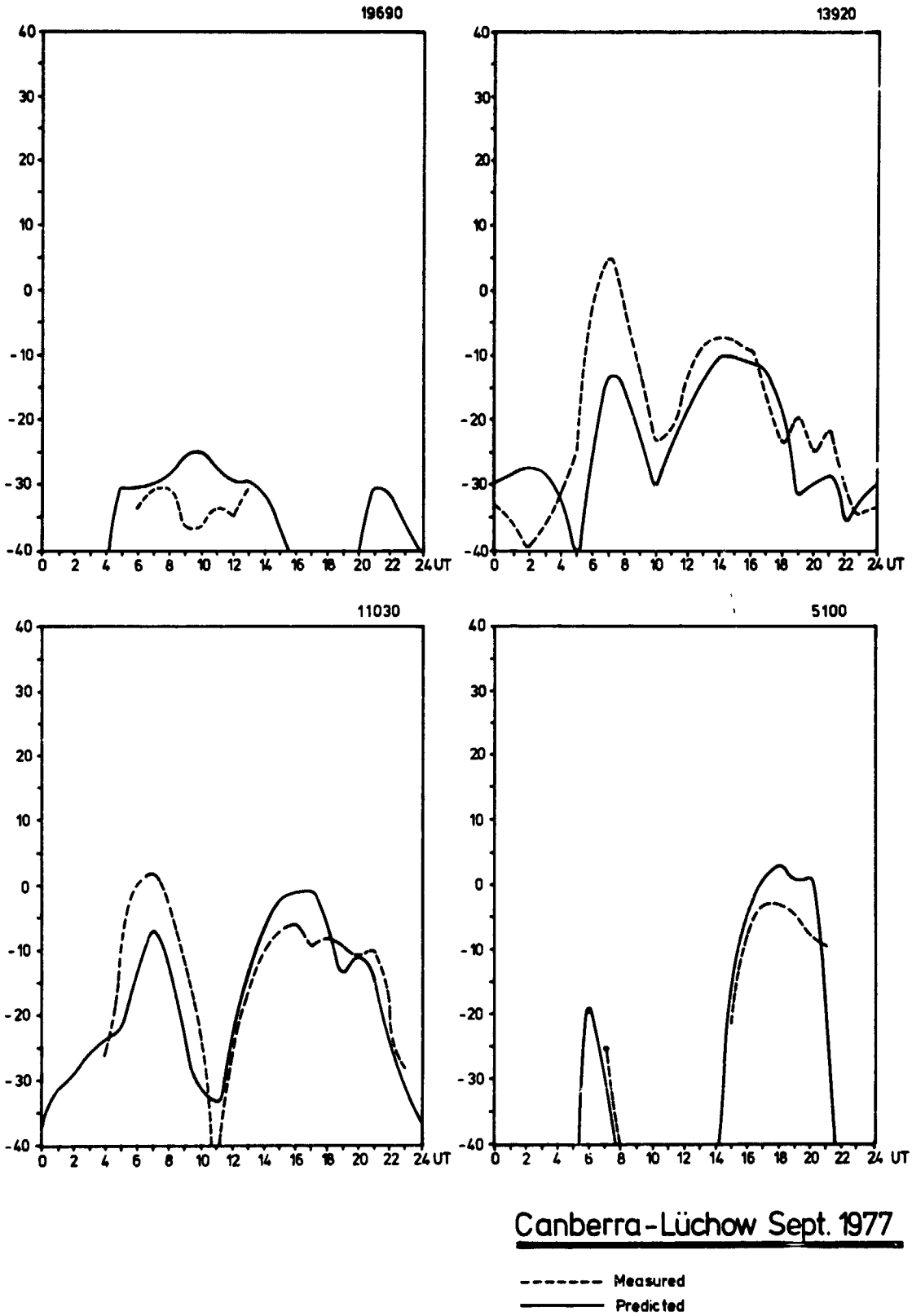

Figure 6. Comparison of measured and predicted field strength.

Table I

Predicted and measured monthly median field strength for the path Canberra - Lüchow, September 1977

	UT	01	02	03	04	05	06	07	08	09	10	11	12	13	14	15	16	17	18	19	20	21	22	23	24
19.7 MHz	Pred.	-44	-46	-52	-47	-30	-30	-29	-28	-25	-25	-27	-29	-29	-31	-37	-41	-45	-58	-	-42	-30	-31	-35	-40
	Meas.	-	-	-	-	-	-33	-30	-30	-36	-36	-33	-34	-30	-	-	-	-	-	-	-	-	-	-	-
	P-M	-	-	-	-	-	3	1	2	11	11	6	5	1	-	-	-	-	-	-	-	-	-	-	-
							median value + 4 dB													RMS 6.3 dB					
13.9	Pred.	-28	-27	-28	-31	-46	-25	-13	-14	-23	-30	-23	-18	-13	-10	-10	-11	-12	-18	-31	-29	-28	-35	-31	-29
	Meas.	-36	-39	-36	-31	-26	- 1	5	- 3	-13	-23	-21	-13	- 8	- 7	- 8	- 9	-16	-23	-19	-24	-21	-30	-34	-33
	P-M	8	12	8	0	-20	-24	-18	-11	-10	- 7	- 2	- 5	- 5	- 3	- 2	- 2	4	5	-12	- 5	- 7	- 5	- 3	- 4
							median value -4													RMS 9.6 dB					
11.0 MHz	Pred.	-31	-29	-26	-24	-22	-13	- 7	-11	-22	-31	-33	-22	-13	- 7	- 2	- 1	- 1	- 5	-13	-11	-14	-22	-29	-36
	Meas.	-	-	-	-26	-12	0	2	- 3	-13	-21	-43	-24	-17	-10	- 7	- 6	- 9	- 8	- 9	-11	-10	-18	-28	-
	P-M	-	-	-	2	-10	-13	- 9	- 8	- 9	-10	10	2	4	3	5	5	8	3	- 4	0	- 4	- 4	- 1	-
							median value -1 dB													RMS 6.7 dB					
5.1 MHz	Pred.	-	-	-	-	-48	-19	-27	-49	-	-	-	-	-	-46	-15	- 5	1	3	1	1	-19	-44	-	-
	Meas.	-	-	-	-	-	-	-25	-40	-	-	-	-	-	-44	-21	- 8	- 3	- 3	- 4	- 8	- 9	-	-	-
	P-M	-	-	-	-	-	-	- 2	- 9	-	-	-	-	-	- 2	6	3	4	6	5	9	-10	-	-	-
							median value +4 dB													RMS 6.3 dB					
All Values:							median value 0 dB													RMS 7.9 dB					

indicate some values as above normal each day if the monthly prediction was too pessimistic. The addressees of the short-term predictions each month receive the explanations given in the next section.

3.2 Explanations of short-term predictions

Explanations regarding the Preliminary Report and the Daily Report of the Research Group Ionosphere (FI 34) in the Research Institute of the Post and Telecommunication Administration of the Federal Republic of Germany.

March 1979: Please keep until next month. Each workday two telex messages are issued on HF radio propagation conditions. The Preliminary Report is made at about 0730 hrs local time and contains in plain language a review of the conditions for the period after the last Daily Report. The basis for the Preliminary Report is provided by all values being available at this early time of the day. The Preliminary Report is intended to give a first picture of the propagation conditions ard a forecast until noon. The Daily Report is issued at about noon and comprises a detailed review for the past 24 hours and a prediction for the next 24 hours (on Fridays for the next 3 days). All times are given in UT.

Situation: Short text describing the general propagation conditions.

Solar activity: The degree of solar activity is characterized by one expression. The following terms are used: very low, low, moderate, high, very high. Generally, the critical frequencies of the F_2-layer increase with increasing solar activity. Consequently, the propagation conditions improve. However, there is a greater probability of disturbances.

10 cm Ottawa: The value given is a measure for the solar radiation at a wavelength of 10 cm. If one deducts 50 from this value, one obtains an estimate for the sunspot number R which is taken as a basis for the monthly propagation predictions.

Critical frequencies in central Europe: Data on the critical frequencies of the F_2-layer are given in percent for four 6-hour periods. The predicted monthly median value, as given in the table below, is taken as 100 percent. The percentages apply not only to the vertical incidence critical frequencies, but also approximately to the critical frequencies at oblique incidence for any distance.

Propagation conditions day/night: The day is defined here as the time between 06 and 18 UT and the night between 18 and 06 UT. The data are given for 5 different paths. The grades used are defined as follows, where mp stands for monthly prediction:

very good: much better than mp, i.e. difference more than + 20 dB.

good: slightly better than mp, i.e. difference between + 10 and + 20 dB.

normal: corresponds to the mp.

fair: slightly worse than mp, i.e. difference between 10 and - 20 dB.

very poor: considerably worse than mp, i.e. difference more than - 30 dB.

Special events: Under this heading special events are mentioned, which are of importance for radio-wave propagation, e.g. moderate or strong short wave fadeouts (SWF). An SWF is an increase in absorption at low frequencies. It is therefore necessary to use as high a frequency as possible during an SWF. In the predection part the probability of occurrence of an SWF is given in percent.

Table of critical frequencies for the current month with an assumed sunspot-number of R = 122

00	01	02	03	04	05	06	07	08	09	10	11	UT
4.8	4.8	4.6	4.2	3.8	4.0	5.0	6.5	7.9	8.9	9.7	10.2	MHz
12	13	14	15	16	17	18	19	20	21	22	23	UT
10.4	10.4	10.2	10.1	9.9	9.4	8.6	7.6	6.6	5.8	5.3	5.0	MHz

Forschungsinstitut der DBP Darmstadt

3.3 Sample of the Daily Report

Figure 7 shows a sample of the Daily Report which is issued in German. It is, however, easily understandable if one consults the explanations given in the previous section.

3.4 Comparison of short-term predictions with observed propagation conditions

A daily quality figure is calculated for each circuit from the 24 hourly values of the received field strength of the transmitters recorded. For each hour the field strength of the frequency with the highest field strength is taken. This is done on the assumption that the optimum frequency would be used for communication. Now the quality figure Q is computed from $Q = 6 + 0.2\ (F_1 + F_2 + \ldots + F_{24})/24$, where the F_i denote the hourly values of the field strength in dB related to 1 μV/m. It follows that a 24-hour average field strength of 0 dB (μV/m) corresponds to a quality figure of 6.0 and that an increase of the quality figure by 0.1 corresponds to a field-strength increase of 0.5 dB. This yields handy values and the quality figures of the paths monitored usually vary between 2.0 (equal to an average field strength of - 20 dB (μV/m) under poor conditions on the long-distance path Australia - Germany and 14.0 (equal to an average field strength of + 40 dB (μV/m) under good conditions on the short-distance path England - Germany. These quality figures were also forecast in the past and a detailed description of the procedure was published (Damboldt, 1979).

One disadvantage of the quality figure is apparent, viz the mean of the logarithmic field-strength values tends to disregard extreme values and this

```
419209 ion d


kurzwellenfunkverbindungen

tagesbericht nr. 37  vom 21.02.79 11.45 mez

rueckblick
----------
zeitraum          : 20/0600-21/0600 ut
situation         : allgemein normale bedingungen
sonnenaktivitaet: maessig
10 cm ottawa      : 238
grenzfrequenzen in mitteleuropa:
        06 - 12     12 - 18     18 - 24     00 - 06  ut
        130-150     125-145     150-170     140-170 prozent
ausbreitungsbedingungen tag/nacht:
mitteleuropa      : normal/normal
nordeuropa        : normal/normal
nordamerika       : normal-maessig/normal, max. +4 mhz
ostasien          : normal, max. +4 mhz/normal, max. + mhz
australien        : 06-12 ut + 20-06 ut um normal, 12-20 ut maessig
besonderes        : magnetstoerung seit 21/0300 ut

vorhersage
----------
zeitraum          : 21/0600-22/0600 ut
situation         : maessige bedingungen
sonnenaktivitaet: maessig bis hoch
10 cm ottawa      : 236
grenzfrequenzen in mitteleuropa:
        06 - 12     12 - 18     18 - 24     00 - 06  ut
       um 100       100-110     90-110      90-110 prozent
ausbreitungsbedingungen tag/nacht:
mitteleuropa      : maessig/maessig
nordeuropa        : maessig/maessig
nordamerika       : maessig/maessig
ostasien          : maessig/maessig
australier        : 06-10 ut normal, danach maessig
wahrscheinlichkeit fuer swf: 50 prozent
besonderes        : andauern der magnetstoerung, in deren folge
                    niedrige grenzfrequenzen

forschungsinstitut der dbp darmstadt fi 34-1  gez. suessmann

419209 ion d  11.55 mez  hoh
```

Figure 7. Sample of daily report.

mean value has no physical meaning. Strictly speaking, the quality figure is connected directly with the field strength only if all 24 hourly values are identical. It is also questionable whether the users of the predictions are satisfied with one value representing 24 hours of a day, if traffic may have been possible during a limited time only (e.g. on long-distance paths).

A comparison of predicted and measured quality figures for the month of September 1977 is shown in Table II. Predicted and measured values agree for 86.7% of the predictions within ± 5 dB. In Table II the wrong predictions are marked with the number 1, correct predictions with a period, ".". As shown in section 3.3, the Daily Report no longer contains predicted quality figures for the reasons mentioned above. The quality figures, however, are still calculated from the measurements and are published in the Monthly Report and in Solar Geophysical Data.

4. CONCLUSIONS

This paper describes the long-term predictions of the Deutsche Bundespost which are computed up to several months ahead using as a data base the C.C.I.R. Atlas of ionospheric characteristics. These predictions are useful for frequency planning purposes. Also described are the short-term predictions and the solar-geophysical data underlying them. These predictions are useful for the operator to change the frequencies in use according to changing propagation conditions.

There is good agreement between predicted and observed field strengths and propagation conditions. However, a problem--not yet solved--is that different users of the predictions have different technical training and different demands for either more detailed or more easily understandable predictions. A closer contact between the forecaster and user is to be aimed at in order to maximize the applicability and the benefit of the predictions.

REFERENCES

Beckmann, B. (1965): Bemerkungen zur Abhängigkeit der Empfangsfeldstärke von den Grenzen des Übertragungsfrequenzbereiches, NTZ 19, S. 649-653.

Beckmann, B., R. Eyfrig, A. Ochs, W. Plage and H. Rauch (1965): Radio propagation predictions by the FTZ Darmstadt. Submitted to C.C.I.R. ... 6/1, 20 Dec. 1965.

Beckmann, B. and A. Ochs (1969): Vorhersage für die ionosphärische Kurzwellen-Ausbreitung. In: Jahrbuch des elektrischen Fernmeldewesens, Bad Windsheim, Germany, F. R.

C.C.I.R. (1974): Report 340-2, Atlas of ionospheric characteristics.

C.C.I.R. (1974): Report 322-1, World distribution and characteristics of atmospheric radio noise.

Table II

Predicted and measured quality figures for the month of September 1977

	Norfolk			Tokyo			Canberra			Moscow			Bracknell		
	Pred	Meas		Pred	Meas		Pred	Meas		Pred	Meas		Pred	Meas	
Thu 1	5.8	7.1	1	5.0	7.3	2	4.3	5.8	1	11.4	11.9	.	11.6	12.4	.
Fri 2	6.5	7.2	.	6.6	6.7	.	5.4	6.0	.	11.8	12.0	.	12.2	12.6	.
Sat 3	6.3	6.4	.	6.3	6.2	.	5.2	6.2	.	11.6	11.5	.	12.0	12.0	.
Sun 4	6.0	6.4	.	6.0	7.1	1	5.0	6.4	1	11.4	11.9	.	11.8	12.4	.
Mon 5	6.4	6.8	.	6.7	6.7	.	6.0	5.2	.	11.7	12.4	.	12.2	11.9	.
Tue 6	6.8	7.1	.	6.8	7.4	.	5.3	5.9	.	12.2	12.1	.	12.0	12.5	.
Wed 7	7.0	7.2	.	7.2	6.7	.	5.6	4.9	.	12.2	11.9	.	12.3	11.8	.
Thu 8	7.0	6.6	.	6.6	6.6	.	5.0	5.2	.	11.8	12.0	.	11.8	11.9	.
Fri 9	6.5	5.0	1	6.5	6.3	.	5.0	5.3	.	12.0	11.7	.	12.0	11.4	.
Sat 10	5.5	4.7	.	5.5	4.9	.	4.0	4.4	.	11.5	11.5	.	11.5	11.5	.
Sun 11	4.5	4.0	.	4.5	4.8	.	3.0	3.7	.	11.0	11.8	.	11.0	11.7	.
Mon 12	4.4	4.6	.	5.2	6.5	1	4.6	4.6	.	11.8	12.3	.	11.8	11.7	.
Tue 13	4.2	4.3	.	5.5	4.1	1	4.2	4.8	.	11.8	11.8	.	11.6	11.2	.
Wed 14	3.8	5.3	1	3.4	4.1	.	4.0	3.2	.	11.4	11.0	.	11.0	11.4	.
Thu 15	5.5	5.7	.	5.2	5.5	.	4.0	4.6	.	11.4	11.5	.	11.6	11.2	.
Fri 16	5.8	6.9	1	5.6	4.9	.	4.5	3.8	.	11.5	12.4	.	11.4	11.7	.
Sat 17	6.0	5.0	.	5.6	4.2	1	4.5	4.9	.	11.5	11.8	.	11.4	11.4	.
Sun 18	6.2	6.2	.	5.6	5.8	.	4.5	5.2	.	11.5	11.7	.	11.4	11.6	.
Mon 19	5.5	5.3	.	5.2	4.0	1	4.6	4.8	.	11.6	11.4	.	11.4	11.6	.
Tue 20	4.6	3.8	.	3.6	2.3	1	4.3	4.7	.	11.0	10.3	.	11.2	11.3	.
Wed 21	3.8	3.8	.	2.5	2.4	.	4.5	3.3	1	10.5	10.3	.	11.4	10.7	.
Thu 22	4.0	3.1	.	2.4	2.2	.	3.3	3.0	.	10.6	11.0	.	11.0	11.1	.
Fri 23	3.5	2.8	.	2.5	2.6	.	3.2	2.9	.	11.0	10.2	.	11.3	10.6	.
Sat 24	4.0	3.2	.	3.0	1.3	1	3.5	3.2	.	11.0	10.7	.	11.3	9.4	1
Sun 25	4.5	3.3	1	3.5	3.5	.	3.8	2.5	1	11.0	11.0	.	11.3	11.2	.
Mon 26	3.5	4.1	.	3.8	2.8	.	3.2	3.8	.	11.0	11.4	.	11.2	11.3	.
Tue 27	4.0	3.3	.	3.0	3.7	.	3.6	3.5	.	11.2	10.4	.	11.2	10.5	.
Wed 28	4.0	4.2	.	4.2	4.1	.	3.8	4.9	1	10.8	11.8	.	11.0	11.8	.
Thu 29	4.5	5.3	.	4.8	3.9	.	5.0	4.3	.	11.8	11.7	.	11.8	11.3	.
Fri 30	5.5	5.5	.	4.3	4.8	.	4.5	5.5	.	11.8	12.3	.	11.6	12.0	.

C.C.I.R. (1974): Report 252-2, C.C.I.R. interim method for estimating sky-wave field strength and transmission loss at frequencies between the approximate limits of 2 and 30 MHz.

Damboldt, Th. (1976): A comparison between the Deutsche Bundespost ionospheric HF radio propagation predictions and measured field strengths. AGARD Conference Proceedings No. 173.

Damboldt, Th. (1977): Lüchow receiving-site measurements: conversion from r.m.s. receiver input voltage to sky-wave field strength, C.C.I.R., IWP 6/1, Doc. 54.

Damboldt, Th. (1978): HF short-term field strength predictions and their agreement with observations. AGARD Conference Proceedings No. 238.

Monthly Report: Published by the Research Institute, FTZ Darmstadt, P.O. Box 5000, D-6100 Darmstadt.

Pérès, M. (1978): Results of comparisons between measured HF field-strength data and values estimated by the method of Report 252-2, C.C.I.R., IWP 6/1 Doc. 76.

N80-18466

A METHOD OF PREDICTING GEOMAGNETIC ACTIVITY BASED ON A CORONAL MODEL OF RELATIONS BETWEEN SOLAR AND GEOMAGNETIC ACTIVITIES

Jaroslav Halenka
Geophysical Institute, Czechosl. Acad. Sci.
Boční II., 1401
141 31 Praha, Czechoslovakia

For the predicting of both disturbed and quiet periods the method uses solar situations along the CM with the key role of filaments, giving indirect evidence of types of directly unobservable coronal structures above them. The time lag, not to be interpreted in terms of propagation speed, between the CM activity and the commencement of the geomagnetic response is about 1 - 2 days. Solar phenomena serve as indicators within approximately 10° of the CM and up to the zone of high-latitude filaments.

INTRODUCTION

The method of predicting geomagnetic activity, being used by the Heliogeophysical Group of the Geophysical Institute of the Czechoslovak Academy of Sciences, was developed during a long-term research into the effect of solar activity on geomagnetic activity, which was begun in 1952. After partial results had been obtained, the new method of predictions based on them was elaborated by Bednářová (1964).

The method tries to connect directly observable phenomena in the Sun's photosphere and chromosphere with the variations of the geomagnetic field observed at the Earth's surface and measured as geomagnetic activity. Predictions can usually be made 1-2 days in advance with great reliability, depending on the solar situation and availability of solar data, or 7-8 days in advance with lower reliability from east limb observations.

This method has been used to issue test forecasts after each observation since 1959. The more than 1000 test forecasts with a reliability of about 90%, issued so far, have mainly been used in verifying and refining our solar-terrestrial relationship results, as we are unable, for technical reasons, to maintain a regular warning service.

The use of the predictions is obvious in all areas of geophysical and related research, as well as in human activities, sensitive directly or indirectly to the condition of the geo-

magnetic field. The predictions need not be restricted to the Earth and its environment, but, without fundamental limitations, they can also be issued even for the half-space above the visible solar hemisphere (Halenka, 1967a).

BASIS FOR THE PREDICTION TECHNIQUE

A good understanding of the true character of the relation between solar and geomagnetic activities is obviously the necessary condition for producing a workable method of predicting geomagnetic activity. The investigation of the connection between the solar and the geomagnetic activities, carried out using material from several solar activity cycles, in the direction from solar to geomagnetic activity and vice versa, as well as the study of the associations between the individual displays of solar activity and of their relation to the corona, yielded the following principal result: a geomagnetic disturbance will occur only if a coronal formation is pointed at the Earth (Bednářová and Halenka, 1969).

There are three possibilities, basically determined by the local magnetic fields in the neighbourhood of the solar central meridian (CM). If the corona is split above the centre of the solar disk, no coronal formation is pointed at the Earth and geomagnetic calm is to be expected. If there is a coronal stream, or a coronal formation of the minimum type above the centre of the disk, a geomagnetic disturbance will follow in both cases. A sudden commencement (SC) disturbance may be expected especially if a coronal stream is generated directly over the centre of the disk, i.e. if the already existing stream is not displaced towards the centre by solar rotation.

The character of coronal formations above the centre of the disk, which cannot be observed from the Earth, must be derived from the groupings and variability of other displays of solar activity in the lower levels of the solar atmosphere. The coronal stream is generated above regions of enhanced instability of local magnetic fields, the instability being indicated by the generation and decay of spots, by changes in area and by the brightness of plages, by the changes of the chromospheric structure in the neighbourhood of the active region, by the occurrence of flares, by changes and, in the most expressive cases, also by temporary or permanent vanishing of filaments. On the contrary, if there is a relatively stable local magnetic field, without indications of an instability mentioned above, the corona is split. A temporary coronal formation of the minimum type may be formed above the centre of the disk, provided that there are no strong local magnetic fields, especially bipolar ones, along the CM.

The coronal model, just outlined, is based mainly on the established significance of filaments and their relations to the coronal structures above them. Filaments, according to

their geomagnetic effects, have been divided into three types, signified by characteristic behaviour, shape, and position with respect to spots, and these were later shown to correspond to various phases of development of the active centre. Bound filaments occur in active centres of little variability, keeping to their basic shape for longer periods and, when observed at the limb, displaying the structure of closed magnetic lines of force. Bound filaments of the first group occur in strong magnetic fields, limited to zones of occurrence of spots in lower and middle heliographic latitudes. The second group occurs in weaker magnetic fields, often already lacking spots, even in high latitudes. Unstable filaments develop from bound filaments of both groups during sudden changes of local magnetic fields, which results in changes of shape and position of the filaments at higher levels of the solar atmosphere and, in extreme cases, in their permanent or temporary disappearance and a change in the fine chromospheric structure, which temporarily loses its magnetic-line-of-force structure, characteristic for the neighbourhood of the spots. Free filaments develop from bound filaments, which have survived the period of sudden changes and, after the disintegration of spots and the weakening of the local magnetic field in the appropriate active centre, they shift to higher latitudes, where they remain as bush-like structures for a period of several solar rotations and gradually dissolve.

Proceeding to the limb, it can be shown from total solar eclipse observations that prominences of the bound type can be observed in the base of the split corona, whereas prominences of the unstable type occur in the base of the coronal stream. The transition of prominences of the first type into the second, over an interval of a few minutes or tens of minutes, is quite usual, and also the corona should respond accordingly: a rapid reconstruction of the originally split corona into a coronal stream may take place. Frequent coronal transients, often characterized by major local injections of mass and energy into the outer corona from the lower solar atmosphere, and some by apparent rearrangements of material in the corona, which are associated mainly with eruptive prominences, have been observed by MacQueen et al. (1976). If the transition in the corona takes place above the centre of the disc, it may explain the occurrence of geomagnetic calm immediately followed by an SC geomagnetic storm.

Above prominences bound in weak magnetic fields, helmet-like or wide radial streams occur, depending on the orientation of the long axis of the prominence, directed radially away from the Sun. Free prominences do not disturb the normal structure of the corona, i.e. a minimum-type corona, characterized by a mighty equatorial streamer. The central meridian passages (CMP) of helmet-like streamers, owing to their position and shape, are rarely followed by geomagnetic disturbances. The CMP of a streamer of a minimum-type corona results in a M-region geomagnetic disturbance, which may be recurrent if the solar situation is stable enough for more rotations, but is in-

terrupted immediately after the CMP of a strong magnetic field, inactive on its own. When no free prominences are present during the CMP of a minimum corona equatorial streamer, the geomagnetic activity becomes only slightly unsettled, but no pronounced geomagnetic calm occurs.

Details on many various investigations, the results of which have served in elaborating the basis for the method of predicting geomagnetic activity, are conveniently summarized in a recent paper by Bednářová and Halenka (1974), where all relevant papers are referenced; references on earlier results are given in a summarizing paper by Bednářová et al. (1963), as well.

PREDICTION TECHNIQUE

In elaborating a prediction of geomagnetic activity one tries to estimate the possibility of a coronal formation being pointed at the Earth. This can be done with greater or lesser reliability, depending on the availability of data and complexity of the particular situation, by analysing individual indicators with their changes and grouping in the central part of the solar disk and along the CM.

Indicators of geomagnetic disturbance

Central. The most reliable and expressive is the sudden disappearance of a filament (SDF). Always followed by a geomagnetic storm or disturbance, usually with an SC. The CMP of a variable filament, especially oriented in the direction of the solar meridian. The duration of the disturbance, which follows, may be short. The CMP of a filament oriented mainly in the direction of a solar parallel may not be reliable; apparently, owing to the slightest deflection by nearby magnetic fields, the related streamer may not point at the Earth. The CMP of a sunspot group with considerable activity of surges. The resulting storm or disturbance need not be an SC one. The generation or decay of sunspots--an SC disturbance or storm is probable.

Non-central, but on the CM; no other local magnetic field in between the indicator and the centre of the disk; decreased reliability. The best indicator in this group is the free filament in a very weak magnetic field far outside of sunspots, the CMP of which is followed by a disturbance or storm, usually long-lasting and non-SC. The duration of the disturbed period corresponds to the duration of the CMP. The disturbance vanishes as soon as a sunspot or bright plage appears in the neighbourhood of the CM during the CMP of a free filament. The SDF and other unstable filaments in weaker magnetic fields (plages without spots) also belong to this group, as well as free filaments of meridional direction with the low-latitude end not too distant from the centre of the disk. Sometimes, especially when solar activity is distributed asymmetrically with respect

to the solar equator (an active region in one solar hemisphere only), other strong changes mentioned above may be effective, apparently as the result of a widening or deflection of the coronal stream, or of the temporary formation of a minimum-type corona. However, as there is no firm evidence of the actual extent and direction of the resulting coronal stream, the prognostic significance of these changes is rather limited. All abrupt processes may cause SC storms or disturbances, as is the case with central indicators.

Indicators of geomagnetic calm

Central. The situation is relatively simple here. The CMP of every sunspot or bright plage, provided ultimately no signs of changes like flares and surges or unstable filaments occur, indicates a period of geomagnetic calm. This is most frequent with early bipolar types of sunspot groups according to the Zürich classification, as well as the oldest stable ones (B, C, H, and J; also type A, if not generated at the CM). Even the higher developed types D, E, F, and G may be used, if sufficiently stable, which is less probable.

Non-central, but on the CM, no other indicator of disturbance at lower latitudes. The same applies as to the central indicators. A stable local magnetic field safely interrupts a disturbance originating from a high-latitude free filament. The effect may be less pronounced with increasing heliographic latitude, as the otherwise undisturbed central part of the solar surface manifests itself by slightly unsettled geomagnetic activity. When there is a pair of indicators, symmetrically located with respect to the solar equator, the probability of sudden changes, mentioned above under non-central indicators of disturbance, synchronous in both, decreases considerably and the resulting geomagnetic calm can be expected more reliably.

Aspects of position, time and intensity

The efficiency of all indicators decreases very rapidly with increasing distance from the CM. Some dependence on the size of indicators may also exist, larger ones being not so sensitive to the decrease. The sudden changes are taken into consideration within about 10^8 of the CM, whereas for the long-lasting indicators the CMP of their centre of gravity is decisive. Sometimes, even more distant large changes, such as big flares, may influence the behaviour of indicators along the CM, apparently due to the magnetic connection of neighbouring active regions which should, therefore, also be kept under observation.

As regards the time interval between the decisive indicator and the commencement of a magnetic disturbance or quiet period, a good typical value is 1.5 d. In well-defined cases, such as the SDF or the CMP of variable and free meridional filaments, values of between 28 and 53 h have been observed. There is a tendency to longer time intervals with decreasing filam-

ent activity. In the best defined cases, when the coronal stream is being newly formed over the centre of the disk, the observed length of the interval is between 28 and 38 h, which is used in the case of unstable filaments. In the remaining cases, when the coronal formation has been displaced over the CM by solar rotation, and, as a result of a longer lifetime, is not sharply defined, the time interval observed is 1 to 2 days.

It is evident, that the value of the time interval may be influenced by several disturbing factors such as the width, deflection from the Sun-Earth direction along solar parallels, or by the asymmetrical position of the coronal formation with respect to the indicator. The duration of the disturbed period, associated with high-latitude free filaments, corresponds to that of the CMP of the indicator.

The presence of unstable filaments in the base of the coronal stream and their occurrence prior to geomagnetic storms indicates that the material escaping from the filaments contributes, after ionization in the coronal region, to the enrichening of the geomagnetically active stream of the solar plasma. This might form the basis for predicting the intensity of magnetic disturbances. Unfortunately, it is not known which part of the prominence material is really ejected and does not return back to the solar surface, as is often observed. Moreover, it is not clear, whether the enrichening is the quality of the coronal stream needed later for generating a magnetic storm during the encounter with the geomagnetic field. At the time, we do not see any objective possibility of predicting the intensity of the expected disturbance on the basis of the indicators mentioned in this paper. The predictions of the maximum Kp index value expected during a disturbance, covered by test forecasts, are, therefore, only rough subjective estimates, based on experience, intended more or less for replacing verbal descriptions of geomagnetic activity. The suitable levels are Kp below or equal to 1 (geomagnetic calm), Kp about 2 (unsettled activity), Kp equal to 3 or 4 (disturbance), Kp equal to or above 5 (storm).

Conditions for issuing predictions

In predicting, the most serious factor limiting the reliability of the forecasts is the availability of the appropriate data. According to the principles explained above, the forecasts should only be issued, when the situation in the corona is derived on the basis of the observation of indicators and decisive changes along the CM. This requires a continuous detailed observation of the Sun, which cannot be ensured at one station.

Therefore, our test forecasts have mainly been issued as the second kind of reliability forecasts, i.e. the decisive changes were not observed directly but only the possibility of such changes was estimated from the character of the solar

situation along the CM.

Even less accurate are forecasts of the third kind, based on observations of the solar situation between the eastern limb and the CM. These forecasts may be of greater importance only in periods of lower solar activity, when the initial data for predicting are mainly long-living free filaments. In any case, their accuracy should be improved later, when the indicators arrive at the CM.

Another possibility often used for tentative long-term forecasts is the observation of the occurrence of prominences at the eastern limb in about the latitude of the centre of the solar disk. Taking into account their types, one can anticipate the possible behaviour of the geomagnetic field 7 or 8 days in advance. Moreover, eastern limb observations provide additional valuable information about the future occurrence of filaments on the disk, since a prominence need not be observed as a filament against the disk due to decreased contrast and Doppler shifts.

In general, although the final judgement should always be made on the basis of the latest possible observations in the vicinity of the CM and, therefore, no period longer than 1 or 2 days can be covered by a reliable forecast, the knowledge of the development between the eastern limb and the CM of all indicators coming into consideration greatly facilitates the task.

EXAMPLES OF USING THE METHOD TO MAKE A PREDICTION

Some contrasting solar-geomagnetic situations will be discussed here in order to illustrate the method of predicting and the role of several indicators.

In Fig. 1 we have an example of sudden changes in the vicinity of the disk centre. One of the most severe geomagnetic storms followed (Kp maximum = 9o), basically of an impulsive character typical of sporadic storms, starting on Feb. 11, 1958 with an SC at 01.25 UT. Suspicious circumstances: sharp geomagnetic activity increase (Kp = 5o) as early as on the 6th, and also in the following three-hour intervals on Feb. 10.

Solar situation: Determining factor - clearly a mighty meridional filament, stretching across the centre of the disk and across the equator, connected with a large active region (E 55) displaying flare activity. Considerable changes of the filament in the centre region during CMP at about 06 UT on Feb. 9. According to the Meudon Observatory report even an SDF was observed in the interval from 09.40 to 12.55 UT on Feb. 9. Last flare before CMP on Feb. 8, at 17.40 UT, 10^{o}E, 20^{o}S, i = 2, first flare after CMP on Feb. 9, 13.37 UT, 5^{o}W, 18^{o}S, i = 2, another flare on Feb. 9, at 21.08 UT, 14^{o}W, 13^{o}S, i = 2, and many other flares of lower importances around CMP.

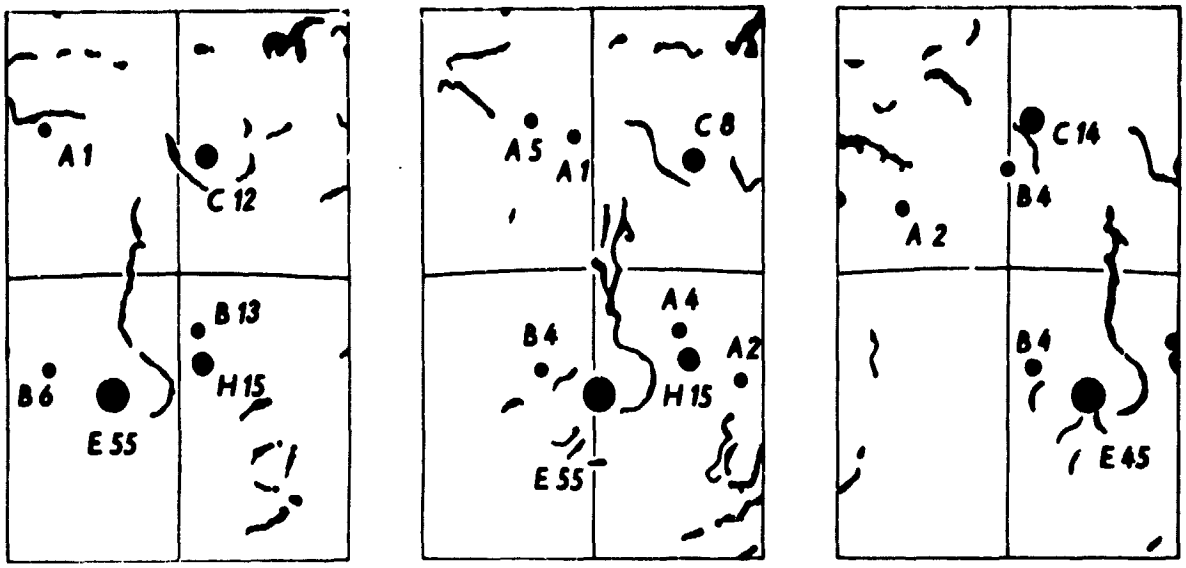

1958 Feb. 8 Feb. 9 Feb. 10

Fig. 1. Unstable filament in the centre of the solar disk prior to the geomagnetic storm of Feb. 11, 1958. Central sections of Freiburg solar daily maps (only spots and filaments are shown). Range 60° in heliographic longitude at the equator and 100° in heliographic latitude along the CM. The equator and the CM are marked. N at the top, E to the left.

Discussion: From observations on a day-to-day basis, on comparing the pictures from Feb. 8 and Feb. 9, we see a clear unstable filament at the centre of the disk. This makes it nearly certain that at least a disturbance would occur in the next 1 or 2 days, measured from the CMP of the filament. Further, an SC of the disturbance cannot be ruled out owing to the presence of a near sunspot group E 55 where sudden changes of magnetic field, indicated by flares, are probable. Now, in actually observing flares, we can take the moment of the one nearest to the CMP as the decisive change which may cause the strong instability of the filament. We can then apply the 28 to 38 h interval measured from the flare at 13.37 UT and expect an SC storm (considering the small distance of the filament to the CM, its meridional direction, dimensions, and probable strong change associated with the near flare a higher level of geomagnetic activity may be assumed), commencing sometime between Feb. 10, 18 UT and Feb. 11, 04 UT. If the latter value is delayed by some ten hours, it will not be surprising as longer time delays also occur. If, however, the SDF is actually observed, which is the highest priority indicator in this situation, it is nearly certain that a geomagnetic storm will take place with a very probable SC, which should occur sometime between

Feb. 10, 17 UT and Feb. 11, 03 UT (taking the moment when the SDF is over as the origin for measuring the delay time).

In an ex-post analysis one is tempted to associate the sharp activity increase on Feb. 10, preceeding the main SC-increase, with the CMP of the filament in its unstable tate before the SDF.

On the contrary, in Fig. 2 we have an example of no sudden changes at the centre of the solar disk, with no filaments, even bound ones, so there is no danger of an unnoticed transition to unstable filaments. Instead, a small stable bipolar B 6 sunspot group is present in a common plage with the following D 19 group, which is flare-inactive before and during the CMP of the B 6 group. Moreover, the area around the centre of the disk is screened on both sides by plages from the possible influence of higher latitude events. Under such circumstances a period of geomagnetic calm should appear 1 or 2 days later. Using our typical value of the time interval (1.5 d) and taking the CMP of the leading edge of the plage, in which B 6 is situated (April 20, around 12 UT), as the origin, we arrive at the almost exact beginning of the actual geomagnetic calm. This occurred on April 21 in the last three-hour interval as a sharp decrease in the surrounding, slightly disturbed activity and consisted of five consecutive values of Kp equal to or below 0+ (see also Fig. 8).

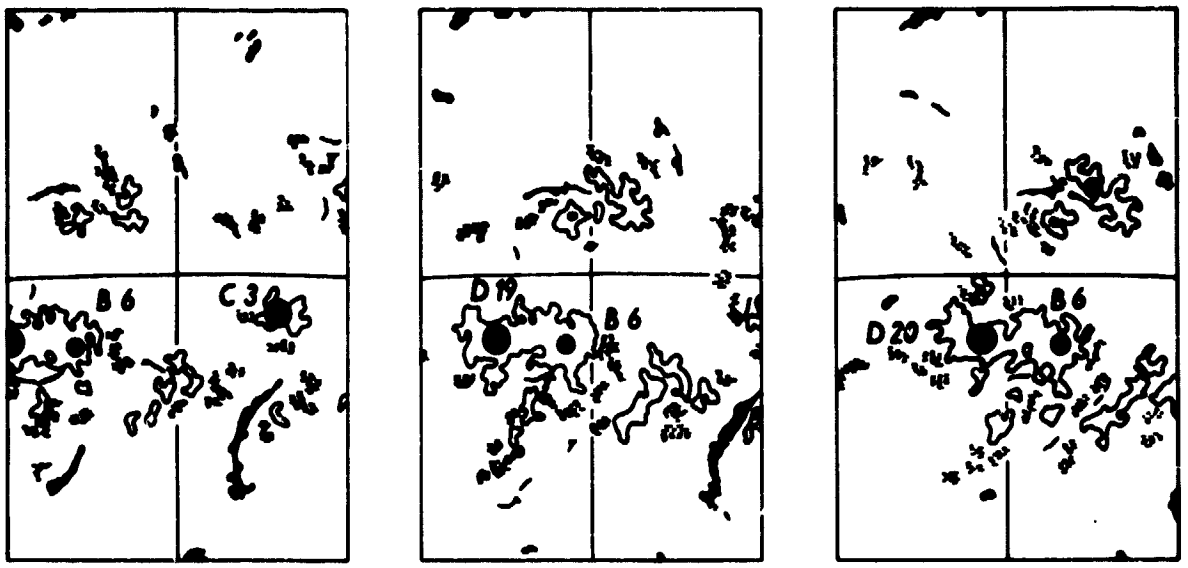

Fig. 2. Stable active region with no filaments at the centre of the disk prior to the geomagnetic calm of April 22, 1972. For explanation see Fig. 1.

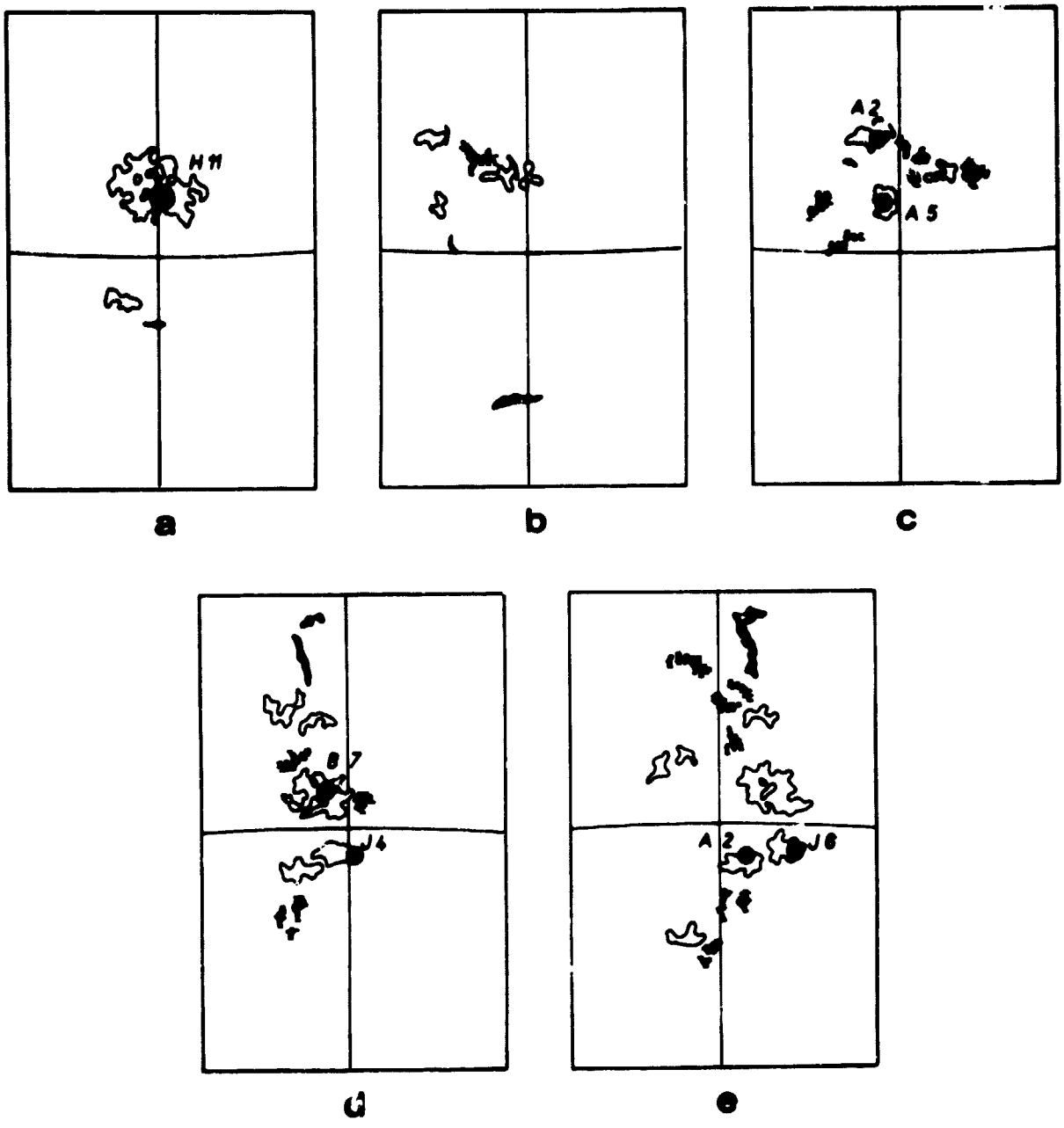

Fig. 3. a) Occurrence of the H 11 group in the centre of the solar disk on Oct. 4, 1971, which preceded the SC of Oct. 5, 1971. b) and c) show the situations on 7 and 8 October during the development of newly observed groups A 2 and A 5 close to the CM, the latter being directly in the centre. The SC followed on Oct. 8, 1971. d) and e) show the changes in the centre of the disk and in its neighbourhood on 17 and 18 March 1971, prior to the SC of March 19, 1971. For explanation see Fig. 1.

Other characteristic situations prior to SC-disturbances or small SC-storms are given in Fig. 3 - 7 taken from a paper by Bednářová and Halenka (1972), showing that even smaller geomagnetic events obey the same laws as the severe ones. The different types of situations are characterized by the presence of unstable groups of sunspots (Fig. 3), or only by unstable plages without spots (Fig. 4), yet again by unstable filaments (Fig. 5), by conditions for a temporary minimum-type corona after the vanishing of disturbing local magnetic fields (Fig. 6), and by the presence of non-central unstable active regions (Fig. 7).

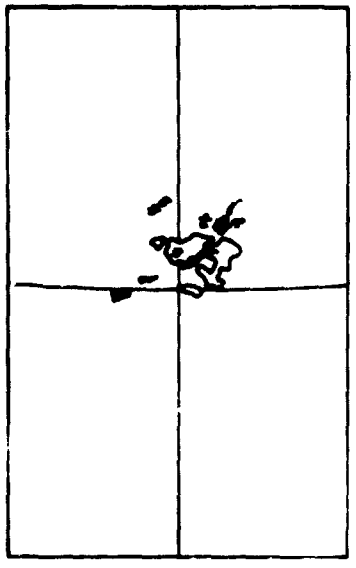

Fig. 4. Plages with a filament, without sunspots, in the centre of the solar disk on Aug. 29, 1971, which preceded the SC of Aug. 30, 1971. For explanation see Fig. 1.

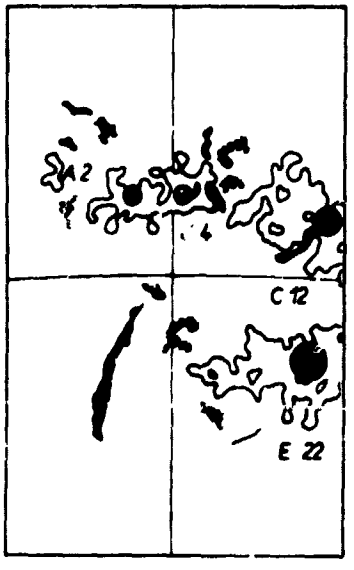

Fig. 5. Unstable filament of Jan. 25, 1971 just prior to the CMP. This situation was followed by the SC of Jan. 27, 1971. For explanation see Fig. 1.

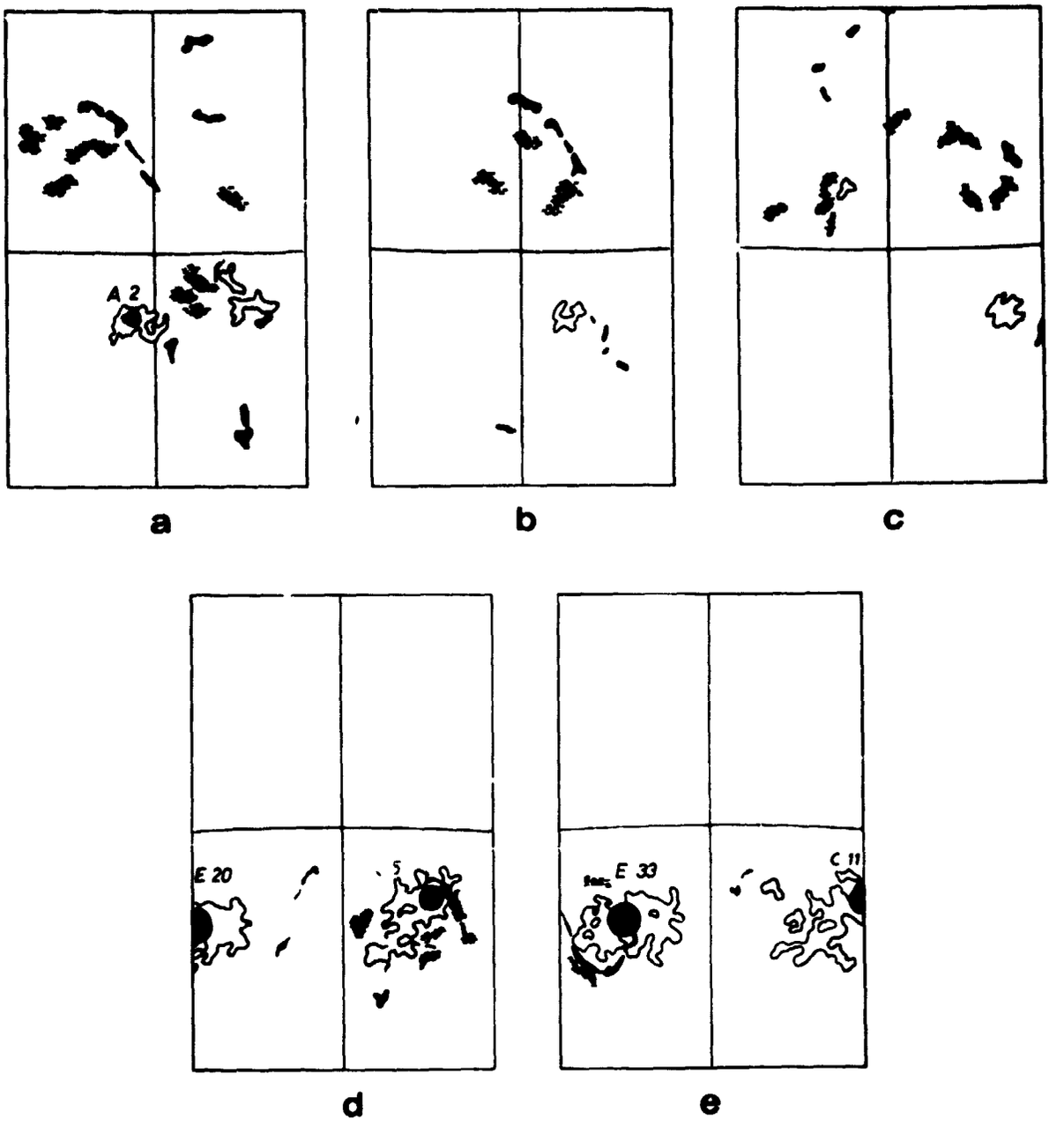

Fig. 6. a, b, c) Situation related to the SC of July 8, 1971. Vanishing of the sunspot group A 2 and other changes on the CM on July 6, 7, and 8, 1971 created conditions for a sudden and temporary forming of a minimum-type corona. d) and e) show the unstable filament between the active regions on Feb. 21 and 22, 1971, when conditions existed for forming a minimum--type corona above the CM. Followed by two SC's on Feb. 23, 1971. For explanation see Fig. 1.

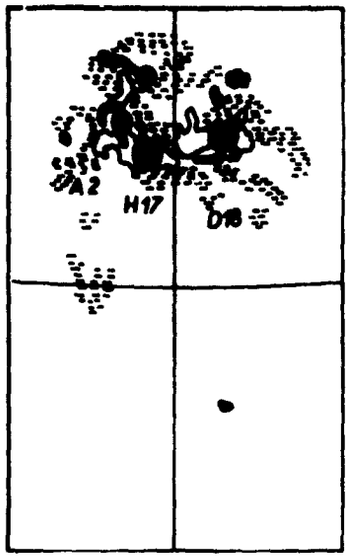

Fig. 7. Situation on Aug. 28, 1971, suitable for the action of an inclined coronal stream, preceding the SC of Aug. 29, 1971. For explanation see Fig. 1.

Many more examples, where the solar situation is analysed in individual cases using daily maps with respect to subsequent geomagnetic activity, may be found in papers by Bednářová (1969, 1972) and Halenka (1967b, 1969). A detailed analysis of solar patrol H-alpha films together with solar daily maps resulted in a detailed co-ordination of geomagnetic activity with central solar situations (Halenka 1975); the main result is reproduced as Fig. 8 here. The types of solar situations associated with geomagnetic activity are given in other papers by Bednářová (1963, 1973).

The forecasts of some remarkable geomagnetic storms are discussed in section 12 of (Bednářová and Halenka 1974).

SUMMARY OF EVALUATIONS OF PREDICTIONS

There are some problems in evaluating predictions, depending on different kinds of reliability of forecasts, their formulations and criteria used. As mentioned, the reliability is determined by the availability of suitable data, length of period to be covered, and complexity of the particular solar situation. From the point of view of checking the accuracy of forecasts the most convenient way of indicating the Kp maximum values expected has no firm objective basis. Sometimes, especially when issuing a forecast without continuous solar observations, an active region may be followed by a storm instead of the expected calm and vice versa, and, sometimes, the expected storm or calm may be displaced to neighbouring days, due to tolerances in the time interval, etc.

Simple evaluations of the test forecasts have shown that agreement between reality and forecasts tends to occur in

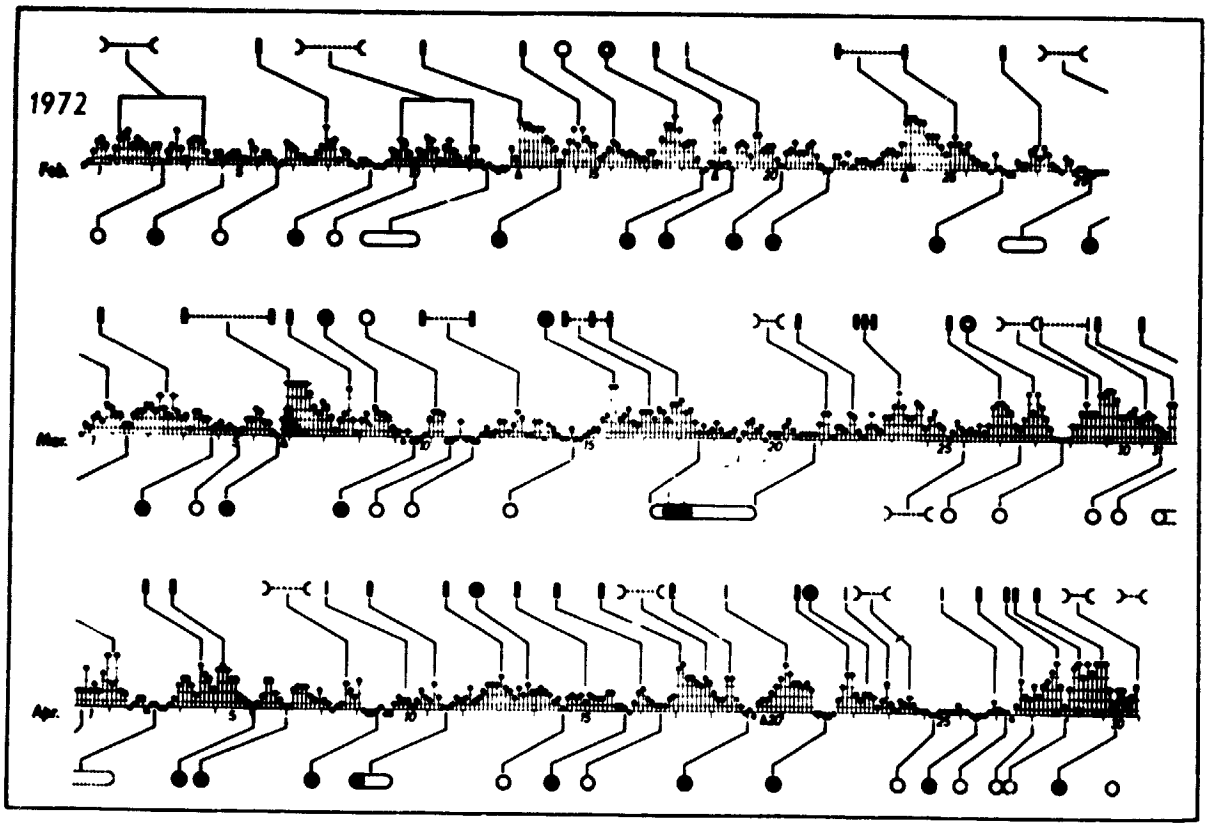

Fig. 8. Co-ordination of geomagnetic activity phenomena (periods of geomagnetic calm, other decreases, revivals and increases of activity), represented by the time pattern of the three-hour Kp-indices, with the solar situations in the immediate vicinity of the solar disk centre, divided into five fundamental types. The times of the individual indicators of the type of solar situation are represented by the following symbols: black circle - group of sunspots (regardless of characteristic but in absence of a variable filament), white circle - plages (in the absence of sunspots and variable filaments), pair of semi-circles - undisturbed area around the disk centre, thin vertical line - undisturbed filament (outside sunspots and plages, unvariable), bold vertical line - variable filament (any changes, arbitrary neighbourhood). The duration of the CMP indicated as required, and combined symbols were used for plages and sunspots in two cases when the sunspot vanished, or appeared close to the CM.

about 90% of the cases. As an example, Table 1 from (Bednářová and Halenka 1968) is reproduced here to show the result of the evaluation from the period between April 1964 and November 1967, covering 94 days with an expected disturbance and 42 days with expected calm intervals.

Table 1. Distribution of the departures of the Kp index from forecast values.

Forecast disturbance	(Actual Kp max.) - (Forecast Kp max.) -3	-2	-1	0	+1	+2	+3	Total
Number of cases	4	4	25	39	16	6	0	94
Per cent	4	4	27	42	17	6	0	100
Forecast calm	**(Actual Kp min.) - (Forecast Kp min.) -3**	**-2**	**-1**	**0**	**+1**	**+2**	**+3**	**Total**
Number of cases	-	-	-	37	3	1	0	41
Per cent	-	-	-	90	7	3	0	100

The published test forecasts for the years 1959-1963, 1964, 1968 and 1969 and their comparison with reality may be found in (Bednářová 1964, 1965, 1970). The ones issued during the retrospective world interval 20 March - 5 May 1976 are evaluated in (Bednářová et al. 1977).

It should be stressed, however, that a straightforward evaluation of the fulfilment of predictions according to any criteria is not enough, regardless of the good or poor accuracy found. One should be able to determine the reasons for discrepancies between predictions and reality which, in our case, can generally be done on the basis of additional analysis using more complete data and which shows the inherent soundness of the predicting method used.

CONCLUDING REMARKS

Experience gained so far has shown that, inspite of the mostly adverse conditions for issuing the test forecast, the method of predicting geomagnetic activity works relatively well. Further improvement and especially its practical use depends on more suitable solar observations and this again on world-wide co-operation. We have had to be content with necessarily seriously limited data, obtained with our spectroheliscope and prominence-coronagraph. Even if all sunshine periods were used at one well-located station, which is not our case, it would not be sufficient for a regular predicting service.

As explained earlier, in connection with the possible extension of the predicting method to the half-space above the visible solar hemisphere, the requirements as to "space" predictions do not differ essentially from the requirements for an optimum terrestrial predicting service (Halenka 1967a). A network of several stations, well distributed around the world,

monitoring the solar image at the centre and wings of the H-alpha line with a time resolution usual for chromospheric patrol films and transmitting the image in near real time to a predicting centre for recording by videorecorder and evaluation by repeated accelerated projection, may be considered as sufficient for the regular issuance of forecasts of the first kind of reliability.

A very efficient supplement would be the observation of the distant white corona, similar to that performed during the SKYLAB mission. In addition to the fundamental importance for further research into the relations between coronal structure and low-level phenomena, otherwise restricted to rare total solar eclipses, such observations would be readily usable for long-term predictions of geomagnetic activity, owing to the stability of some coronal formations.

Even more valuable to the regular predicting service would be the use of a space probe with a coronagraph in Earth orbit, 90^{o} away from the Sun-Earth line, monitoring the white-light coronal structure above the CM.

REFERENCES

Bednářová-Nováková, B. (1963): The active solar region and its relation to geomagnetic activity in the period around the minimum of 1954. Geofysikální sborník, 11:383.

Bednářová-Nováková, B. (1964): A new method of forecasting geomagnetic activity and its practical try-out. Geofysikální sborník, 12:277.

Bednářová-Nováková, B. (1965): An attempt at refining the method of forecasting geomagnetic activity on material from 1964. Geofysikální sborník, 13:419.

Bednářová-Nováková, B. (1969): Sudden commencements of geomagnetic storms at the turn of two solar cycles. Geofysikální sborník, 17:203.

Bednářová-Nováková, B. (1970): Forecast of geomagnetic activity in 1968 and 1969. Geofysikální sborník, 18:379.

Bednářová-Nováková, B. (1972): Comments on the special intervals of January 24 and September 1, 1971. In: Data on solar-geophysical activity associated with the major ground level cosmic ray events of 24 January and 1 September 1971, Boulder, WDC A Report UAG-24, Part I, 277-278.

Bednářová-Nováková, B. (1973): A contribution to the problem of prominences-filaments as indicators of geomagnetic storms. Geofysikální sborník, 21:369.

Bednářová-Nováková, B., V. Bucha, J. Halenka, and M. Konečný (1963): On the problems of the origin of geomagnetic storms. Geofysikální sborník, 11:407.

Bednářová-Nováková, B., and J. Halenka (1968): New method of forecasting geomagnetic activity using features of the solar corona. Nature, 220:250.

Bednářová-Nováková, B., and J. Halenka (1969): A universal interpretation of the generation of geomagnetic storms using features of the solar corona. Planet. Space Sci., 17:1039.

Bednářová-Nováková, B., and J. Halenka (1972): The properties and causes of geomagnetic disturbances with sudden commencements. Geofysikální sborník, 20:391.

Bednářová-Nováková, B., and J. Halenka (1974): Results of investigating the relations between solar and geomagnetic activity obtained at the Geophysical Institute, CSAS. Geofysikální sborník, 22:277.

Bednářová-Nováková, B., J. Halenka, M. Pavluchová, and J. Pýcha (1977): Forecasts of geomagnetic activity. In: Collected data reports for STIP interval II 20 March - 5 May 1976, Boulder, WDC A Report UAG-61, 272-274.

Halenka, J. (1967a): Prognoses of geomagnetic activity and cosmic research. Studia geoph. et geod., 11:101.

Halenka, J. (1967b): On correlating "cosmic" flares with geomagnetic storms. Geofysikální sborník, 15:367.

Halenka, J. (1969): Geomagnetic activity and the solar situation in the neighbourhood of proton effects. Geofysikální sborník, 17:181.

Halenka, J. (1975): A detailed co-ordination of geomagnetic activity with central solar situations during February, March and April 1972. Geofysikální sborník, 23:169.

MacQueen, R. M., J. T. Gosling, E. Hildner, R. H. Munro, A. I. Poland, and C. L. Ross (1976): Initial results from the High Altitude Observatory white light coronagraph on Skylab - a progress report. Phil. Trans. R. Soc. Lond. A, 281:405.

KAZIA - A COMPUTER SYSTEM FOR SOLAR-TERRESTRIAL DATA PROCESSING AND OBJECTIVE PREDICTION

K. Stasiewicz, M. Maksymienko
Polish Academy of Sciences, Space Research Centre, Ordona 21, 01-237 Warsaw, Poland

M. Jakimiec
Astronomical Institute, University of Wroclaw
Kopernika 11, 51-622 Wroclaw, Poland

The present paper describes briefly a computer system for solar-terrestrial data processing, which is currently developed at the Space Research Centre. The data base consists mainly of information contained in Ursigrams exchanged between the IUWDS Regional Warning Centres. The system structure and its functions are presented in this paper. Solar flare forecasting is described, as one of the prediction techniques incorporated in the system.

1. INTRODUCTION

For short-term ionospheric prediction, a vast amount of solar and geophysical data in near real-time is required. The data, describing solar activity, interplanetary medium, the magnetosphere and ionosphere, are monitored by various observatories and satellites. These data are exchanged between IUWDS Regional Warning Centres, usually on a daily basis. The IUWDS - which reads International Ursigram and World Days Service - is an URSI Service established in 1962 for rapid solar-terrestrial data interchange. The exchanged data cover a wide range of solar optical, magnetic and radio parameters, satellite measurements of solar wind, X-ray emission and many ground based ionospheric and geophysical data. These data are coded in 5-digit numbers, according to the IUWDS booklet on Synoptic Codes for Solar-Geophysical Data, and exchanged through teletype service between observatories and Warning Centres in different countries. Anyone who wants to use these data for quick interpretation of other measurements or for short-term forecasting of ionospheric parameters has to decode the data using the IUWDS booklet. The laboriousness of manual decoding of information contained in Ursigrams prompted us into the development of an automatic technique for processing these data.

A group of programs named KAZIA performs the following functions:

(1) decoding of information contained in URSIGRAMS; (2) creation of a data base for further application, i.e. predictions; (3) production of summarized reports on solar, geomagnetic and ionospheric activity; and (4) objective forecasting of solar, geomagnetic and ionospheric activity. The data base for the system is now being expanded by including local measurements of the geomagnetic field, ionospheric absorption, field strength of LW, SW broadcasting stations and solar radio flux on 2800 MHz.

2. SYSTEM DESCRIPTION

KAZIA is written in FORTRAN IV, implemented and tested on a CDC 6000 computer. Figure 1 shows a general flow chart of the system. After entering Ursigrams from the teletype into the computer, Ursigrams are processed by a special program which converts all key words to corresponding numbers, and the whole code content is written numerically on a disk file D2. The sort-modify module checks the date of information and updates it in a permanent disk file D3. The decoding module containing 12 subroutines is capable to decode information from 42 codes described in the IUWDS booklet. The system can generate up to 26 summarized reports on solar, geomagnetic and ionospheric activity. Figures 2 and 3 show examples of such reports. The data necessary for the display reside on a file F2 in a fixed format. This function is similar to that of the SELDADS system, developed in the Space Environment Laboratory in Boulder (Williams, 1976). The latter was of great importance for us in constructing the KAZIA system.

File 2 was designed to serve both display purposes and as a data base for forecasting programs. File 3 in Figure 1 contains values of the locally measured geomagnetic field, riometer data and field strength of LW and SW broadcasting stations. They will be used to complement the global data, near real-time monitoring of solar-geomagnetic activity and radio wave propagation conditions. These data are also incorporated in the prediction procedures. This part of KAZIA is not yet operating. We plan to implement all available prediction methods on three different levels: (1) solar activity, (2) geomagnetic and ionospheric effects, and (3) radio circuits performance. In the next section a technique for solar flares prediction is presented as an example of forecasting programs, which are under development.

3. AN OBJECTIVE TECHNIQUE FOR SOLAR FLARE PREDICTION

An algorithm for predicting the number of flares from a particular active region is incorporated in KAZIA, using an analysis done by Jakimiec and Wasiucionek (1979). The prediction itself is made on the basis for several widely used parameters of active regions observed one day earlier. It does not forecast the exact position, time of occurrence and size of a flare but the probable number and class of the flares which might occur during the considered day. Second-order regression equations were derived from a statistical analysis of solar data for the period 1971-1975. The following

The flow chart of KAZIA

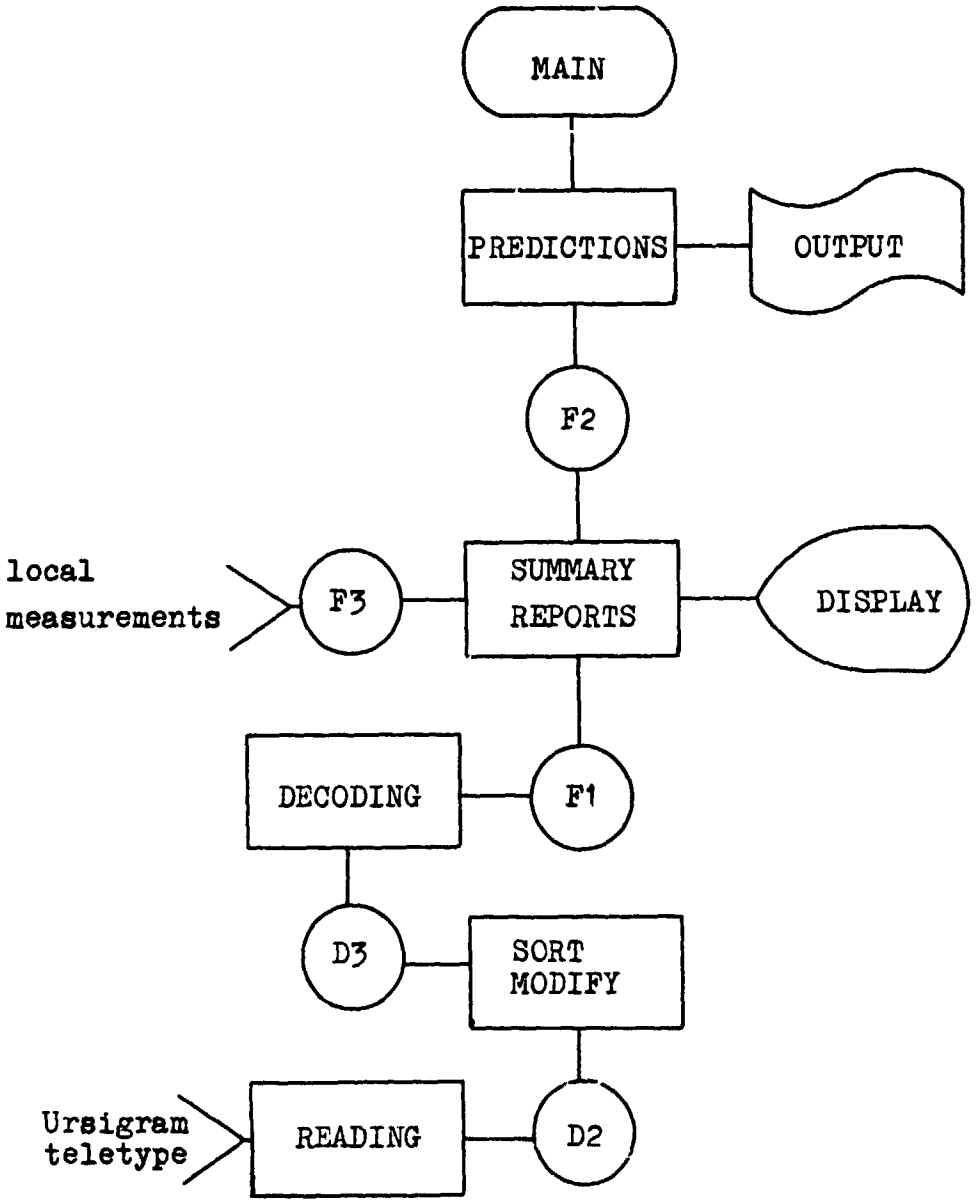

Figure 1. The flow chart of KAZIA.

25/ 2 IONOS EVENTS

STATION	----- TIME ------			OBS	EVENT	DESCRIPTION		
DIXON	1.18	6.18	8.00	RIO	AUR.A	ABSORP	3 DB	
DIXON	3.15	4.58	5.00	RIO	PCA-P	ABSORP	1 DB	
KODAIK	6.02	6.36	8.00	RIO	PCA-P	ABSORP	2 DB	
PANSKA	11.53	12.02	12.16	---	SPA	SID 1+ Q1		
DIXON	19.15	20.30	23.00	RIO	AUR.A	ABSORP	1 DB	
KERGUL	17.2	18.0		VIS	AURORA	TYP-8	COLOR-3	Q-4
	18.0	19.0		VIS	AURORA	TYP-9	COLOR-7	Q-4
	19.0	20.0		VIS	AURORA	TYP-0	COLOR-3	Q-4
	20.0	21.0		VIS	AURORA	TYP-0	COLOR-3	Q-4

Figure 2. Display showing ionospheric events observed at different stations.

14/ 2 SOLAR FLARES

	---------TIME-------			LOCATION	IMP	INT	AREA
	2.45	2.49	3.02	(22:-16)	0	BRIGHT	40
	5.25	5.28	5.35	(20: 90)	0	BRIGHT	40
)	6.00	*****	6.06	(3: 60)	0	NORMAL	80
	6.17	6.19	6.24	(19: 46)	0	NORMAL	40
	6.56	6.58	7.04	(20: 76)	0	NORMAL	60
)	8.05	*****	8.20	(18: 75)	1	NORMAL	80
	8.22	*****	8.27	(3: 59)	1	NORMAL	120

Figure 3. Display containing times of solar flares with their location, importance and area.

parameters have been chosen as the most relevant:

X1 - the magnetic classification of sunspot group,
X2 - the area of sunspot group,
X3 - the calcium plage intensity,
X4 - parameter defined as MFI: (field strength) x (neutral line run) / (distance between the spots),
X5 - the observed number of subflares (sn + sb),
X6 - the observed number of flares of importance 1 (1n + 1b), and
X7 - the observed number of flares of importance 2 and higher (2n + 2b + 3f + 3n + 3b).

The predicted number of subflares (Ns), flares of importance 1 (N1), and flares of importance 2 and higher (N2) are expressed by the second order regression formulae. For groups classified as D (modified Zurich class) the predicted numbers of flares are as follows:

$$Ns = 1.758 + 0.976 \cdot x5 \cdot x7 - 0.467 \cdot x5 \cdot x6 + 0.154 \cdot x3 \cdot x5 + 1.019 \cdot x2 \cdot \cdot x6 - 0.097 \cdot x4^2 + 1.458 \cdot x4 \quad (1)$$

$$N1 = 0.027 + 0.098 \cdot x4 \cdot x5 + 0.021 \cdot x3 \cdot x4 \quad (2)$$

$$N2 = -0.0015 - 0.014 \cdot x4 \cdot x6 + 0.014 \cdot x4 \quad (3)$$

For details see Jakimiec et al. (1979). The above formulae are suitable only for periods of high solar activity. Groups A, B, C have not been considered in this analysis because the probability of a class 2 flare is negligible.

It is known that geophysical effects are correlated rather to X-ray yield than to Hα importance. The transition to the X-ray classification class (C, M, X) is done after Jakimiec (1976) using expressions similar to Bayes formula

$$PC = P(sf) \cdot P(C/sf) + P(1) \cdot P(C/1) + P(2) \cdot P(C/2) + P(3) \cdot P(C/3). \quad (4)$$

The same form of equation applies to PM and PX, where PC, PM, PX are the probability of a class C, M, X flare, respectively, P(sf), P(1), etc., are the probability of a subflare, flare of importance 1, etc. P(C/1) is the conditional probability that a flare of importance 1 is a class C flare. Conditional probabilities are given in Table 1 after Jakimiec (1976). Calculations, according to formulae (1 - 4) are performed for all sunspot groups and summed up to give the total values Ns, N1, N2.

Tabie 1. The probability that the X-ray flare is a particular class (C, M, or X) given tnat an Hα flare of a particular importance has occurred.

	X-ray yield		
Hα importance	C	M	X
sf	0.993	0.007	0.000
1	0.914	0.082	0.004
2	0.156	0.674	0.170
3	0.062	0.438	0.500

4. SYSTEM EVALUATION

The usefulness of the system, in its decoding and report generation functions, is beyond discussion. Preliminary tests on real Ursigrams have shown, however, that improvements of coding forms is necessary to facilitate computer processing. The staff of ARWC Warsaw have sent to the IUWDS a proposal concerning code booklet revision. It is aimed to set more precise and consistent rules for coding in order to avoid ambiguities of present description.

Prediction accuracy depends on the algorithms used in the calculations. We do not have sufficient information to evaluate the whole system. It is designed to be flexible, to permit easy implementation on a minicomputer, ready incorporation of future advances in prediction techniques, and data base expansion.

REFERENCES

Jakimiec, M. (1976): unpublished manuscript, University of Wroclaw.

Jakimiec, M., and J. Wasiucionek (1979): Short-term flare predictions and their stationarity during the 11-years cycle, Solar-Terrestrial Predictions Proceedings, Vol. III.

Williams, D. J. (1976): SELDADS: An Operational Real-Time Solar-Terrestrial Environment Monitoring System, NOAA Technical Report ERL 357 - SEL 37.

D6-32

N80-18468

ESTIMATION OF SOLAR FLARE INFLUENCE ON RADIO CIRCUIT TRANSMISSION LOSS

Z. Klos, K. Stasiewicz
Space Research Centre, Polish Academy
of Sciences
Ordona 21, Warsaw, Poland

A provisional method for determining the hours and frequencies at which solar flares cause major radiopath absorption increase is presented. This technique is incorporated in a computer program for monthly radio propagation prediction, developed in the Space Research Centre in Poland.

1. INTRODUCTION

By increasing the electron production rate in the D and E regions of the ionosphere, solar flare radiation perturbs the propagation of radio waves in the HF band. This effect is manifested in the increase of ionospheric absorption of HF waves, which in relation to specific radio circuits, results in higher transmission loss or complete fadeout (SWF). Although the duration of a solar flare is relatively short during high solar activity periods, the perturbations in the HF-transmission may be significant. Naturally, the radio circuit perturbation effect is closely related to the solar flare intensity, as well as the solar zenith angle along the radio path, during the flare occurrence. For this reason a method of determining the frequencies and times at which a solar flare of a given class can cause significant perturbations (absorption increase) for a specific radio circuit would be very useful. This paper presents a provisional technique incorporated in the monthly radio propagation prediction computer system developed at the Space Research Centre of the Polish Academy of Sciences.

2. BASIS FOR PREDICTION

The absorption of HF waves propagated at oblique incidence via the ionosphere may be estimated if the height distributions of the ionization and electron collision frequency in the D and E region are known. In practice, such calculations are too complex for routine predictions and the knowledge of the electron density distribution profiles for all times and places is poor. This current normal absorption predictions use semi-empirical

formulae based on measurements for different geophysical conditions (Schultz & Gallet, 1970; Barghausen et al., 1969, and recently George & Bradley, 1974). To determine the absorption during a solar flare, model calculations are necessary because of the lack of a vertical-incidence absorption map for flare conditions based on measured data.

In the case of vertical incidence propagation at a frequency f_v, in the frame of magnetoionic theory, the absorption of the ordinary wave is given approximately by the expression for quasi - longitudinal propagation (Ratcliffe, 1962),

$$L\ (f_v) = 2.33 \times 10^{-9} \int \frac{N_e\ \nu e}{\mu} \frac{dh}{(f_v + f_l)^2} \quad (db) \qquad (1)$$

where f_l is the Larmor frequency in MHz, Ne is the electron concentration in electrons/cm^3, νe is the electron collision frequency in s^{-1}, μ is the refractive index. The lower part of the D-region and the height of reflection at frequency f_v, constitute the integration limits.

During a solar flare the main increase in ionization, as well as absorption, occurs in the D and E region. Thus, for the frequencies reflected from the F region, the enhancement of nondeviative absorption (for $f_v >$ plasma frequencies; $\mu \sim 1$) is crucial. In this case, expression (1) takes the form:

$$L\ (f_v) = \frac{2.33 \cdot 10^{-9}}{(f_v + f_l)^2} \int N_e\ \nu_e\ dh = \frac{A(Fl,\ X)}{(f_v + f_l)^2} \qquad (2)$$

Here, the upper limit of the integration is the top of the E region, and A is the function of the flare class (Fl) and solar zenith angle (X).

Model calculations of A(Fl, X) were made using the neutral atmosphere model CIRA-1972, effective electron recombination coefficients during a solar flare (Mitra, 1974), and the flare spectrum of X-ray solar radiation in the range 1-20 Å. The shape of the electron concentration profile $N_e(h)$ in the lower ionosphere during flare conditions depends on the intensity and spectral shape of flare radiation, as different parts of the spectrum contribute at different altitudes.

As the X-rays can be considered as the main source of disturbances in the lower ionosphere, the classification of flares according to the radiation intensity in the range 1-8 Å is introduced. According to this criterion three classes of flares are taken into account: C, M and X. This classification obviously leaves out the spectral shape of the flare. However, the integration on the altitude range in A(Fl) in equation (2) moderates the dependence of HF radio wave absorption on the N_e profile shape, and consequently on the spectral shape of the X-ray flare. On the other hand, the model calculations use X-ray intensities measured by satellite detectors. In this case in the deduction of radiation intensity from the telemetric data, the selection of a standard wavelength-averaged transfer function G is used. It is selected for a given detector to minimize the error resulting from the

variation in radiation spectral shape (Donnelly et al., 1977). Thus the intensity classification can be used as an indicator of HF radio wave absorption increase. The spectra of flares which occurred on August 7, 1972 at 14.36 UT and on August 11, 1972 at 12.16 UT were taken as typical for the X and M class, respectively. Calculations were performed for the maximum phase of the flare and different solar zenith angles (Dymek, 1976). The result of this calculation is presented in Figure 1.

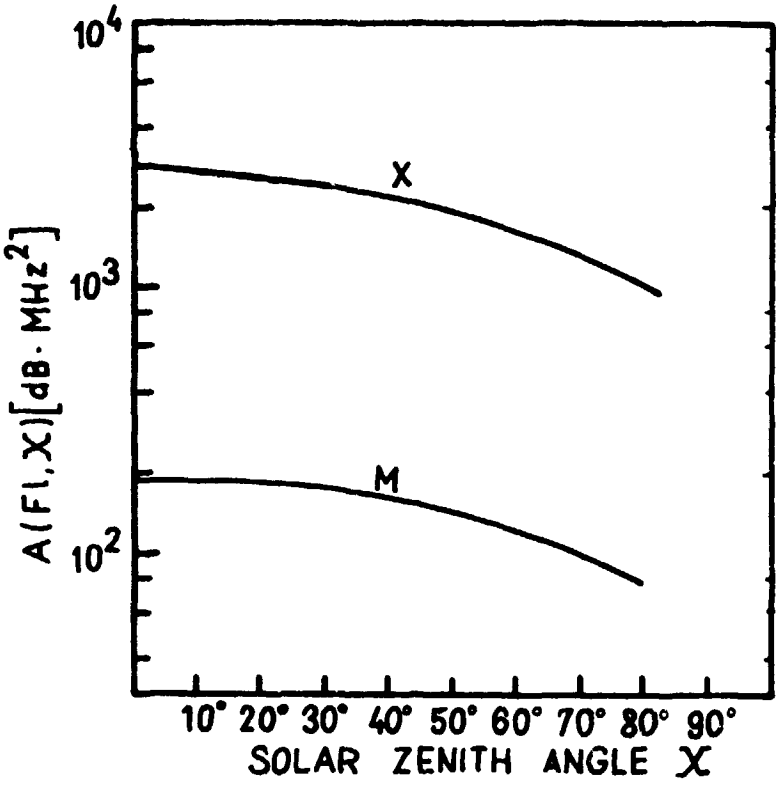

Figure 1. The dependence of $A = 2.33\ 10^{-9} \int N_e \nu_e\ dh$ on solar zenith angle and flare class.

The absorption $L_{ob}(f_{ob})$ of the ordinary wave reflected obliquely from the ionosphere at frequency f_{ob} can be related, quite accurately, to the absorption - $L_v(f_v)$ of the ordinary wave at vertical incidence at frequency f_v (George and Bradley, 1974) as follows:

$$L_{ob}(f_{ob}) = L_v(f_v) \frac{(f_v + f_l)^2}{(f_{ob} + f_l)^2} \sec I_{100}\ , \qquad (3)$$

where I_{100} is the angle of the radio wave incidence at the height of 100 km and $f_v = f_{ob} \cdot \sec I_{100}$.

Using expression (2) the absorption for oblique incidence in flare conditions can be written as:

$$L_{ob}^{Fl}(f_{ob}) = \frac{A(Fl, X)}{(f_{ob} + f_l)^2} \sec I_{100} \qquad (4)$$

The increase of the absorption at oblique incidence is determined by:

$$\Delta L = L^{Fl}(f_{ob}, Fl, X) - L^{N}(f_{ob}, X, R) \qquad (5)$$

where L^N is the absorption in normal conditions given by George and Bradley (1974). The increase in the oblique-path aborption is then the sum of the absorption increase on separate hops.

3. EVALUATION PROCEDURE

The developed computer procedure, which includes the numerical representative of Figure 1 as well as calculations in normal absorption conditions (following George and Bradley, 1974) estimates the possible increase in flare absorption on the oblique radio path in the following way: (1) The geographic coordinates of all the points at which the radio ray hops cross the height of 100 km as well as the incidence angle I_{100} are determined; (2) For a given hour UT of a specific month, the solar zenith angle is determined for each of the above points; (3) From formulae (4) and (5) the increase in the absorption due to flares of different classes at each point is estimated; (4) Next, the summation for all the separate hops determines the total absorption increase ΔL_{tot} along the oblique path; (5) The calculations for a given radio frequency are repeated for all hours of the day, and the hours at which $\Delta L_{tot} > L_o$ are determined, where L_o is an assumed value which depends on the technical parameters of the radio circuit, and (6) The calculations are then repeated for all frequencies in the HF band. The results obtained for a given radio circuit appear in a table which indicates at which hours and on which frequencies the specific type of flare can cause a major ($> L_o$) absorption increase. Of course, if a flare class M has already caused a major absorption increase, a more intense flare class X will cause an even

Table 1
Times and frequencies when an X-ray flare of class C, M or X could produce a major absorption increase.

UT	04	06	08	10	12	14	MHz
1							
2							
3							
4							
5							
6							
7							
8	X	X					
9	M	X					
10	M	M	X	X			
11		M	X	X			
12		M	M				

larger increase. Thus, if in the daily forecast the information about the expected solar flares and their classes is contained, we know on which frequencies and at which hours for a given radio circuit the troubles may appear.

4. CONCLUSIONS

We have presented a provisional method for determining for a specific radio circuit, the hours and frequencies at which solar flares can increase transmission loss more than the assumed value L_o. We have found this method useful in practice. This information in a form similar to Table 1 is included in the monthly prediction of radio circuit transmission parameters issued by the Space Research Centre of the Polish Academy of Sciences. A separate daily forecast of solar flare occurrence is sent to users and thus they can know the hours and frequencies at which they may have troubles.

This method has, however, some disadvantages. First, the model calculation for flare conditions takes into account only nondeviative absorption, which is compared to the deviative and nondeviative absorption for normal conditions. This yields some errors. It is also necessary to analyze many N_e-profiles for different flare classes and for different solar activity periods, to make it possible to determine a typical absorption increase. The elimination of these disadvantages in the presented algorithm is under development.

REFERENCES

Barghausen, A. F., J. W. Finney, L. L. Proctor, L. D. Schultz (1969): Predicting long-term operational parameters of high-frequency sky-wave telecommunication system, ESSA Tech. Rept. ERL 110-ITS 78.

Donnelly, R. F., R. N. Grubb, F. C. Cowley (1977): Solar X-ray measurements from SMS-1, SMS-2 and GOES-1 information for data users, NOAA Technical Memorandum ERL SEL-48.

Dymek, M. (1976): The dependence of ionospheric absorption coefficient on solar flare class and zenith angle. Artificial Satellites, Vol. 11, No. 2.

George, P. L., P. A. Bradley (1974): A new method of predicting the ionospheric absorption of high frequency waves at oblique incidence. Telecommunication Journal, Vol. 41, No. 5.

Mitra, A. P. (1974): Ionospheric effects of solar flares. D. Reidel Publishing Company.

Ratcliffe, J. A. (1962): The magneto-ionic theory and its applications to the ionosphere. Cambridge University Press.

Schultz, L. D., R. M. Gallet (1970): A survey and analysis of normal ionospheric absorption measurements obtained from radio pulse reflections. ESSA Professional Paper 4.

SOVIET SHORT-TERM FORECASTS OF ACTIVE REGION EVOLUTION AND FLARE ACTIVITY

A. B. Severny, N. N. Stepanyan, N. V. Steshenko
Crimean Astrophysical Observatory
p/o Nauchny, Crimea, 334413, USSR

1. CRITERIA FOR FORECASTS

The birth, development and decay of any active region is determined by the evolution of the magnetic field of that region. That is the reason why the most essential criteria for a short-term forecast can be obtained from study of the structure and strength of the magnetic fields of the sun's active regions. The intensity forecast can be made using a gradient of the magnetic field between sunspots of opposite polarity.

It was found that proton flares occur in the regions with the field gradient $\nabla H > 0.1$ gs km^{-1} (Severny, 1958, 1960). After these flares, the gradient decreased to 0.01 - 0.02 gs km^{-1} in the same parts of the active region. This result was obtained for many flares. The mean gradients of the longitudinal magnetic field before and after a flare were obtained by Gopasyuk et al. (1963), as shown in Table 1.

Table 1. Mean gradients of longitudinal magnetic field before and after flares.

Flare class	Flare type	Number of flares	Field gradient G/km	
			Before a flare	After a flare
1	Proton (cosmic rays)	13	0.78	0.27
2	Proton (PCA)	11	0.45	0.27
3	Importance 3 without PCA	12	0.18	0.13
4	Importance 2 and 2+	15	0.054	0.038

The regular records of the transverse fields in active regions performed with the Crimean magnetograph showed a highly inhomogeneous transverse

field $H_\perp$ and a much more inhomogeneous $H_\perp$ structure than than of H . An examination of the position of flares relative to the $H_\perp$ fields (Severny, 1964, 1965; Howard and Severny, 1963) showed the tendency of flares to appear in regions of peculiar behavior of the transversal field such as strong rotation of the $H_\perp$ vector, or the "inclusion" of transverse fields in regions occupied only by $H_\parallel$ or in unipolar regions. Flares also occur in regions where the direction of $H_\perp$ appears to cross. The probability of flare appearance in the points of $H_\perp$ showing peculiar behavior is $\sim$ 83 percent.

The characteristics of the neutral line ($H_\parallel = 0$, $H_\perp = 0$) determined by the magnetic structure of the active region can be the criteria for a forecast. Morton and Severny (1968) showed that bright flare knots appear mostly ($\sim$ 70 percent) near ($\sim$ 10") the neutral line of the longitudinal magnetic field (fig. 1). The same result was obtained by T. T. Tsap together with French scientists (M.-J. Martres et al., 1968).

In figure 2, it is shown that the flare fibrils (low right-hand corner) occur parallel to the neutral line of the longitudinal magnetic field (top left-hand corner) (Zvereva and Severny, 1970). There is a bifurcation of transversal fields in the same regions (lower left-hand corner, fig. 2).

Near the $H_\parallel = 0$ neutral line, as well as in the places of adjoining regions oppositely directed $H_\perp$ and bifurcation of transversal field, mustaches appear more frequently (Severny, 1965; Koval, 1965). Koval found that plage brightening and flares appear in the same places as mustaches. Surges are also more frequent in the period before the flares (Ogir, 1967).

The probability that a flare will occur increases in active regions having their neutral line parallel to the equator. Koval (1974) has analyzed the dependence of flare occurrence on neutral line configuration. She has found out that the occurrence of the neutral line, or even a small part of it, pointed parallel to the equator, will give birth to a flare of importance $\geq$ 1 with a probability of 80 percent (figure 3).

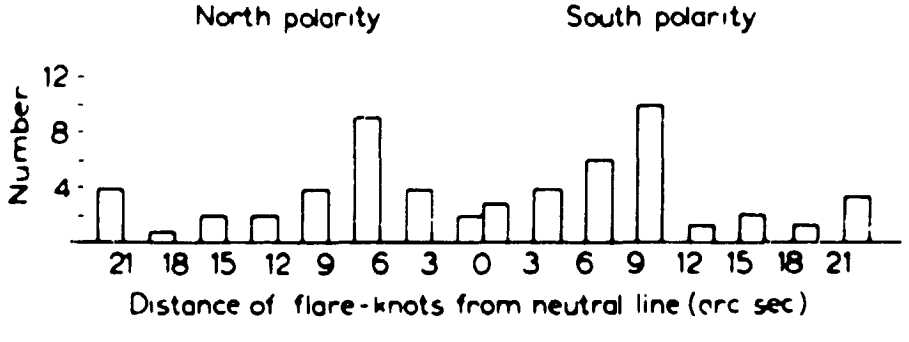

Figure 1. The distribution of 60 separate flare knots according to distance from neutral line.

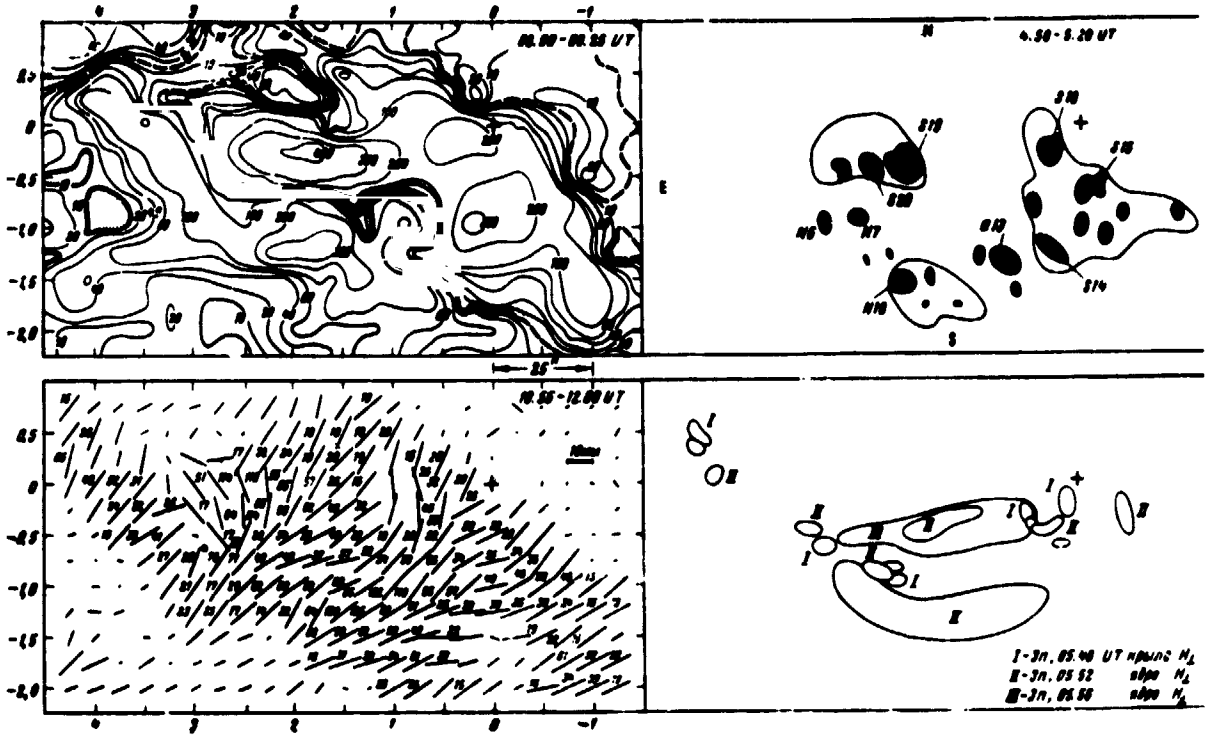

Figure 2. Transverse and longitudinal magnetic fields, spots, and flares in the active region, September 2, 1966.

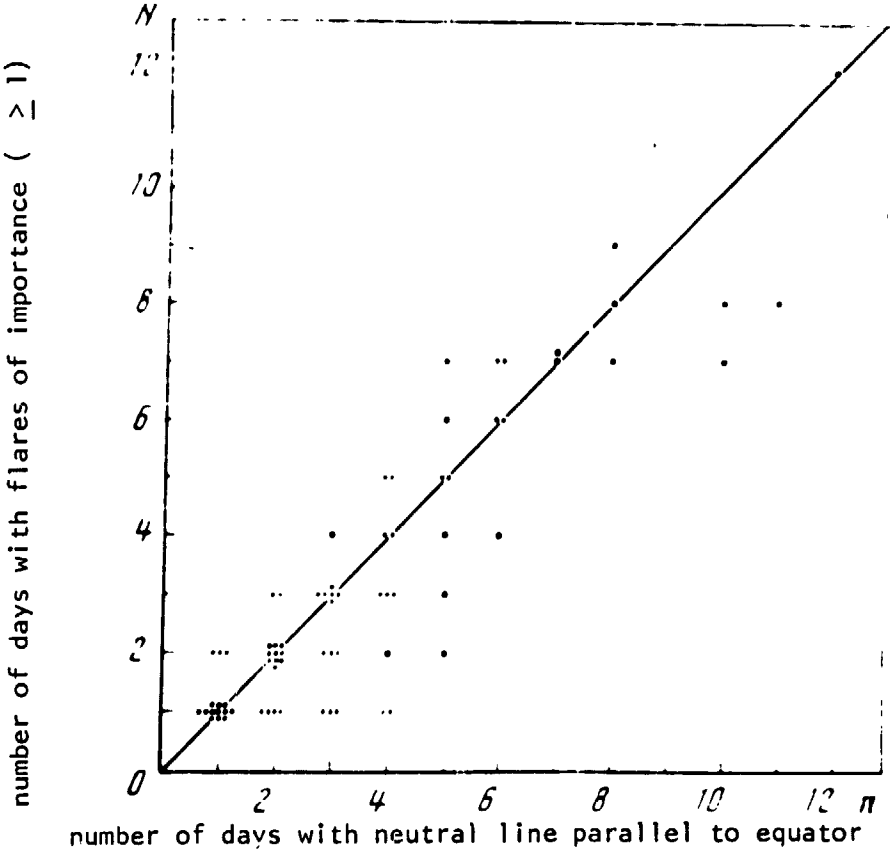

Figure 3. Correlation of neutral line and flares.

It is known that the emergence of new magnetic fields into (or near) an existing area of strong fields is followed by flares. The evidence of field emergence may be indicated, for example, arch filament system, bursts, appearance of new pores, spots, group-satellites, and plage brightenings; but these events are not always connected with flares. They occur frequently during the quiet evolution of active regions. A number of Soviet authors have considered the relation between these events and flares. The aim of such studies is to find quantitative parameters for flare forecasting.

The relations between the number of flares and the age of the group, on the one hand (fig. 4), and plage brightness and the number of nuclei of sunspot umbre, on the other hand (fig. 5), have been obtained by Slonim (1957) for the period 1937 - 1948. The maximum flare occurrence coincides with the seventeenth or eighteenth day of existence of the active region. Similar results were obtained earlier by D'Asambuga (1939) with observations over two years. Slonim derives the empirical equations for calculation of the number of flares Y from the number of umbre nuclei in the group, u, as $Y = 0.035u^2$ and from area of the group, A, as $Y = 0.026A$. The last formula is obtained for the areas measured in the Greenwich system.

For a later period the analysis of observational data was undertaken by Brailovskaya et al. (1972). The dependence of the flare activity on the plage characteristics was confirmed. In addition the solar charts at 9 cm were compared to the solar image in the CaII K - line. It was assumed that there is an interaction between the plages if they are surrounded by the same isoline in the 9 cm chart. The interactions of N-N, S-S type (both plages are in the same hemisphere) and N-S type (the plages are in different hemispheres, with the isoline crossing the equator) were considered (fig. 6).

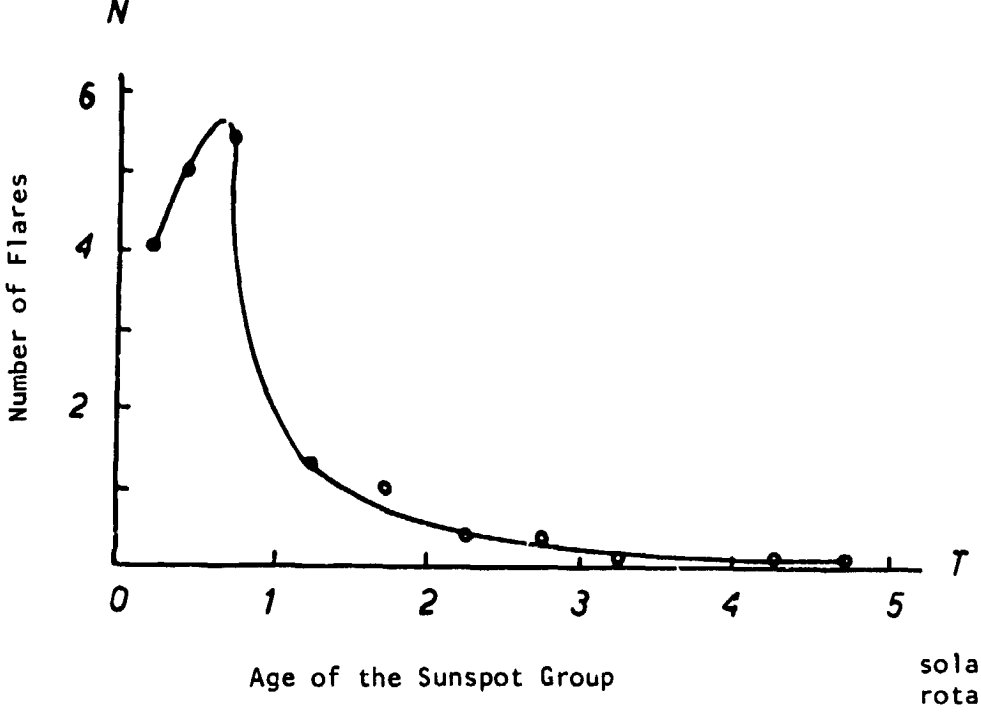

Figure 4. Dependence of the number of flares on age of group.

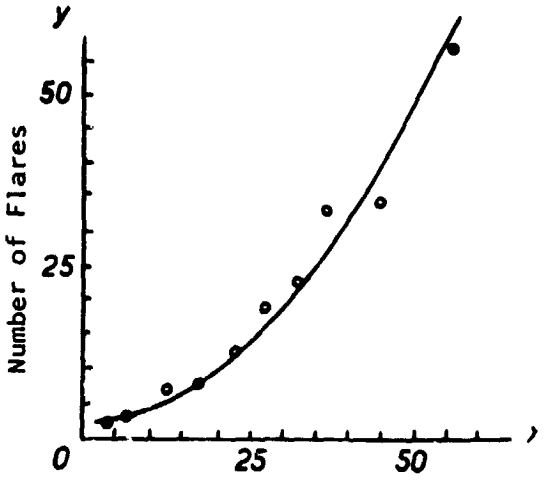

Figure 5. Dependence of number of flares on number of spot nuclei.

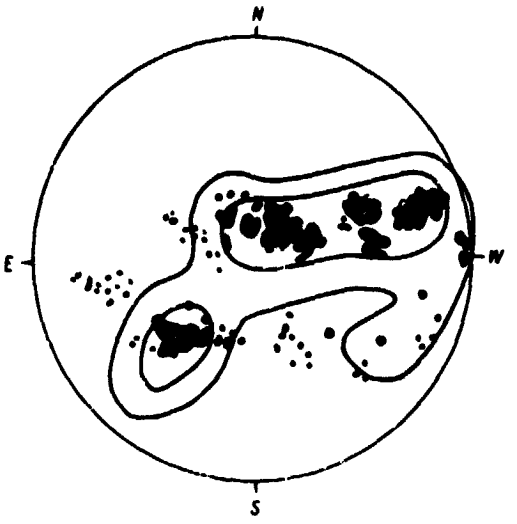

Figure 6. Example of interacting plages.

if there is a N-S interaction, it is always followed by flare activity brighter than a certain value. In the absence of a N-S interaction, the flare activity was lower than the certain value in 10 of 12 cases.

The ratio of the plage brightness in the Hα and K line of CaII can be a criterion of the flare activity as well (Stepanyan, 1974). It was found that in 80 percent of the cases, the intensity ratio of Hα to K permits the determination (with the probability $\geq$ 85 percent) of the level of flare activity of the plage during its pass across the solar disc.

The study of magnetic field strength at two levels inside the sunspots before and after the flares was carried out by Koval and Stepanyan (1972), using the CaI λ 6103 line (top level) and FeI λ 6302 line (low level). It was determined for 70 flares that Δ H ($=H_{6103}-H_{6302}$) in the nearest sunspots increases before the flare and decreases and becomes negative after the flare. Sunspots of the same group but as far from the flare as the sunspots of other groups on the disc do not exhibit this effect (fig. 7).

Kuleshova (1972) has found some characteristics of sunspot groups which are important for the prediction of proton flares. The first characteristic is the diurnal rotation Δφ (in degrees) of the line connecting two stable sunspots in the group (fig. 8). The second is Δ (∇ H), i.e. the diurnal change of the horizontal gradient of the magnetic field of the same stable sunspot pair, where $\nabla H \approx (H_n - H_s)/l_{ns}$ (fig. 9). The mean diurnal changes $|\Delta\phi|$ and $|\Delta(\nabla H)|$ for the active regions with proton flares exceed by two or three times the values for the non-proton flare regions. the $|\Delta\phi|$ and $|\Delta(\nabla H)|$ values increase greatly the day before a flare. The same values remain nearly constant the day before a non-proton flare.

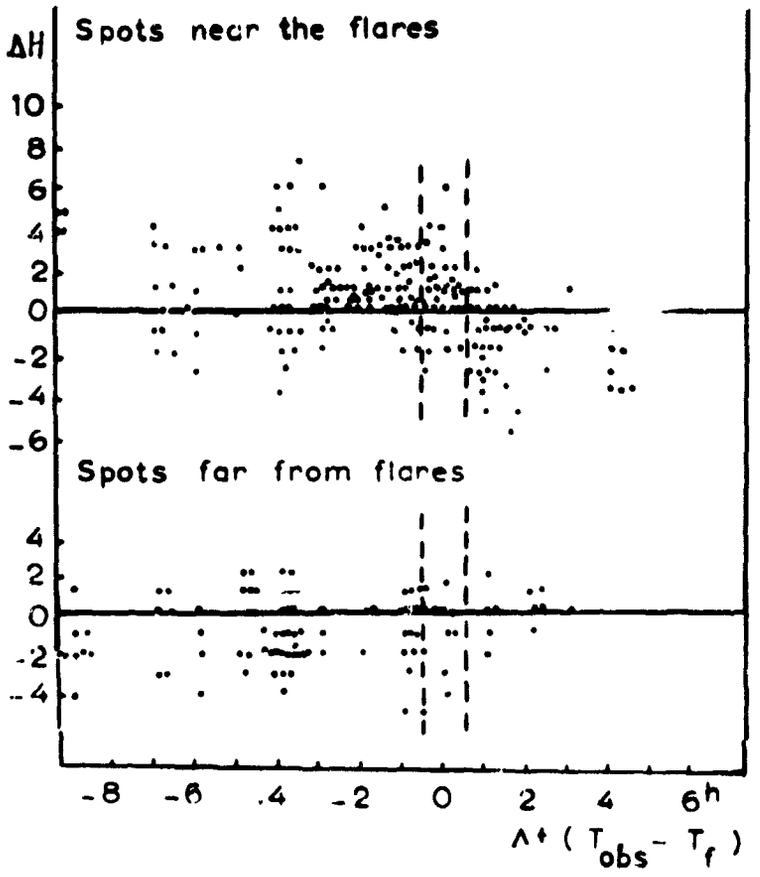

Figure 7. Change of magnetic field difference at two photospheric levels associated with flares.

Group-satellites, which appear 15 to 20 degrees from the main group, can be a criterion for flare prediction. Kusinsky (1972) showed that in 65 percent of the cases the moment of group-satellite appearance precedes the flare. There is good correlation (coefficient of 0.8-0.9) between the positional angle of a satellite and a mean positional angle of flares relative to the center of the main group. Ogir and Shaposhnikova (1965) showed that strong flares follow the appearance of new sunspots or the growing of sunspots near the flare. Bumba and Obridko (1969); Vladimirsky, Levitsky and Severny (1971); Vladimirsky and Levitsky (1974); and Ogir (1978) contributed to the study of the distribution of flare activity relative to the sector structure boundaries of the interplanetary magnetic field, extrapolated to the sun. Flares, especially proton flares, concentrate near sector boundaries; moreover, the most powerful events appear near the boundaries (-,+) in the northern and southern hemispheres.

Summarizing, the authors discussed above have formulated the following criteria for the prediction of flare appearance:

1. the longitudinal magnetic field gradient;

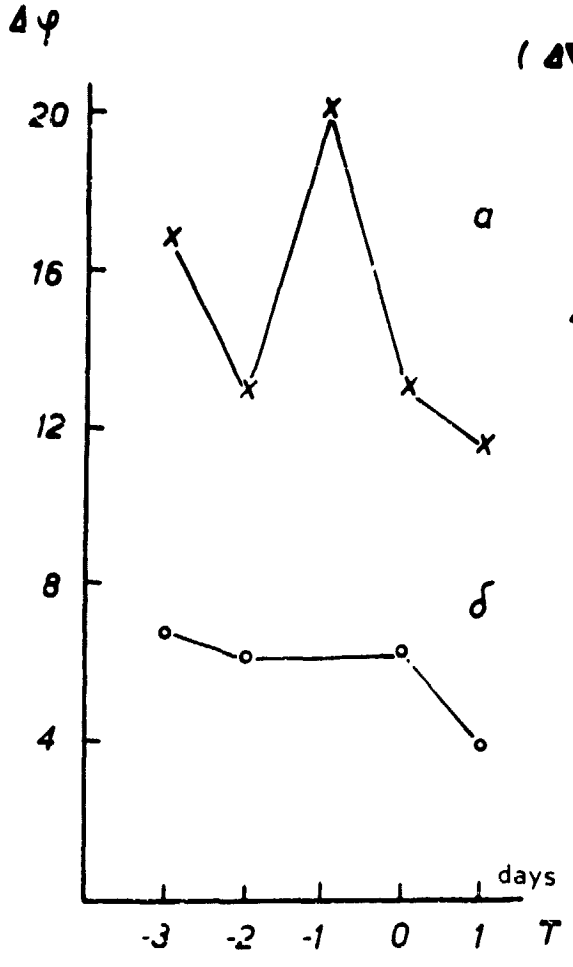

Figure 8. The change in diurnal rotation $\Delta\phi$ of the group's axis before proton flares.

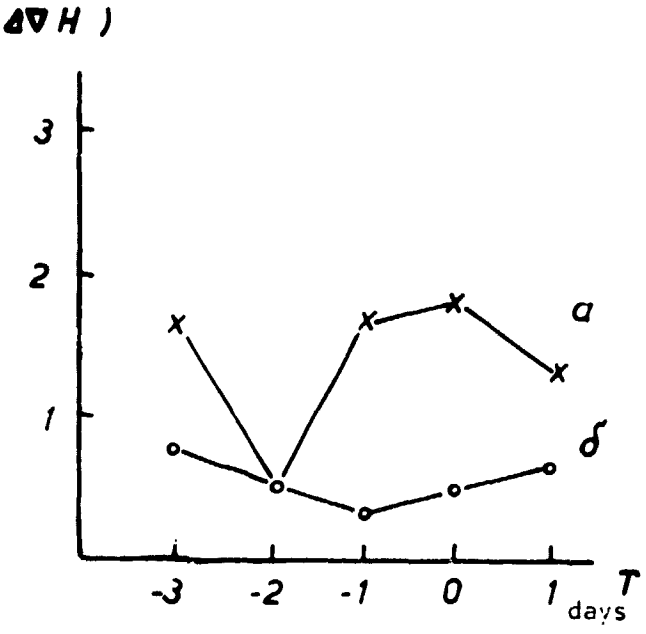

Figure 9. The $\Delta\nabla H$ change before the proton flares.

0 is the day of proton flare appearance

In Figures 8 and 9, the a curve is for active regions with proton flares, and the δ curve is without proton flares.

2. the places of anomalous transverse magnetic fields;

3. neutral line, parallel to the solar equator;

4. the existence of mustaches and surges;

5. the plage brightness in Hα;

6. The relative brightness of Hα and K CaII plages;

7. the interaction of plages on 9 cm wavelength;

8. the change in difference of magnetic field strength in two levels of sunspot depth;

9. the sunspot group rotation;

10. the appearance of satellite groups; and

11. ıe birth of new sunspots in the group.

2. FORECAST METHODS

In the USSR, flare forecasts have been carried out in the Crimean astrophysical observatory during the cosmonaut flights. Such forecasts are based on the measurements of magnetic fields and their gradients in active regions. In addition, data of chromosphere activity (the observations in Hα and K CaII) and radio emission at cm and m wavelengths were used. These data were also obtained in other observatories of the USSR and were sent to the Crimea in real time. Recently two new forecast centers were established in the USSR--in the Institute of Applied Geophysics in Moscow, and at the Astronomical Observatory of the Kiev University.

The forecasts were given three days beforehand in a three-class scale. Forecast I corresponds to the absence of flares or to flares of importance < 1. Forecast II corresponds to flares of importance 2. And forecast III corresponds to flares of importance ≥ 3. If forecast III is given, the forecaster indicates at the same time the probability (in percentage) of proton appearance. The description of this method and the estimation of its probability are given by Severny (1965); Severny and Steshenko (1972a,b); Steshenko (1973); and Gopasyuk et al. (1964).

The comparison of flare patrol data with forecasts issued in Crimea for the period 1965-1971, which includes the solar activity maximum, shows that 78 percent of all forecasts were correct, 14 percent were overestimated, and 8 percent were underestimated.

Comparison of our forecasts with those of other forecast centers is difficult because of the difference in forecast criteria and objects. Thus in Boulder, following Simon and McIntosh (1976), the correct forecasts for M, X and proton events occurred in 69, 78, and 83 percent of the cases, respectively. In Meudon in 1968 and 1969 there were 82.5 percent correct forecasts; 8.4 percent overestimated forecasts, and 9.1 percent underestimated ones.

In connection with the beginning of daily forecast in the USSR, mathematical prediction methods utilizing computers have been developing. The characteristic peculiarity of these methods is the necessity of utilizing the abundant statistical data to formulate the forecast rules. In practice, all investigators have had to use some catalogs of solar data, although it diminished the number of initial parameters. The most essential forecast parameters, e.g. magnetic field gradients, Hα fine structure, X-ray emission of separate regions, and plage brightness, are not yet published with the necessary accuracy and time resolution in catalogs of solar data. Nevertheless, the problems of computer-prediction methods are important to consider. For their decision, one uses some kind of mathematical method, such as linear-statistical methods, logical methods, and different modifications of

pattern recognition methods. Most of these methods give a 70-80 percent probability of correct forecasts. They permit the comparison of predictions based on various parameters, to evaluate the usefulness of each parameter--this is a valuable contribution to the practical application of forecast. But because of the uncertainty or poor quality of the initial data, the most informative parameters in any of the above-mentioned methods cannot be essential in the physical process of a flare.

Two forecast problems were solved by different methods by Slutskaya and Stepanyan (1974, 1976), Burov (1976), Dolgoarchinnyh and Kuklin (1975) on the basis of the same solar observation data from 1967 through 1969. The first problem involved using the plage characteristics in the day of its birth on the solar disc to predict whether it would decay on the disc or pass to the invisible hemisphere and have spots and flares. The second problem concerned using the observations of a plage born on the solar disc during its pass across the disc up to its setting behind the west limb to predict whether it would pass from the east limb or not. The first problem, 4 basic parameters were considered, 15 in the second one. Slutskaya and Stepanyan (1974, 1976) established the construction of the extreme algorithm. The coefficients characterizing the meaning of forecast parameters and typicality of the basic objects are found in the process of computer training. The algorithm of Burov (1976) constructed the discriminative hiper-planes. The solution was in part a logical function of the conjunctions of i-parameters. Dolgoarchinnyh and Kuklin (1975) constructed the logical rule of a "tree" of sequential dissections to subsequences which consist of objects of only one class.

The results of the above-discussed problems were compared by Burov, Kuklin, Slutskaya, and Stepanyan (1976). In conclusion it was assumed that all methods discussed are effective enough, but the best one is the extremal algorithm method. Along with high forecast probability, it permits the choice of the optimal number and kind of parameters.

The forecast of the further evolution of an active region from the moment of a spot appearance in it is discussed by Berlyand, Burov, and Stepanyan (1978) and Stepanyan and Jakimiec (1978). From the same observational data (sunspot groups appeared on the disc from 1967 through 1969), the following problems were solved: the forecast flare activity, the existence duration, and the maximum Zürich class, using the methods of multiple regression and pattern recognition (algorithm "TOPOL").

A number of works on long- and short-term flare forecast were performed in the Astronomical Observatory in Kiev University. Izotov, Izotova, Romanchuk (1976a,b) addressed the long-term forecast. On the basis of the statistical treatment of the sunspot group data and solar flares during 1959-1961 two methods of forecasting the monthly flare number were proposed. The first method was based on the dependence of the number of solar flares on Wolf's number; the second method was based on the dependence of the number of flares in a spot group on the stage of its evolution.

Two forecast methods proposed by Romanchuk, Izotov, Izotova, and Krivodubsky (1977) for a 1-to-7-day period are based on research about the statistical relationship of flares with Zürich class and the maximum size of

the group. The forecast is accurate for 90 percent of the flares in the period from July, 1974, to November, 1975.

Studies by Efimenko, Efimenko and Telnyuk-Adamchuk (1977, 1976); Izotov, Izotova and Romanchuk (1976); Efimenko (1976); and Vaschenko, Efimenko, and Efimenko (1976) were dedicated to the short-term forecast based on sunspot group characteristics. On the basis of these studies, diurnal flare forecasting has been carried out in the Astronomical Observatory of Kiev University. From July, 1974, through December, 1977, 613 forecasts were issued one day in advance of 154 sunspot groups. The occurrence of "no flares", subflares (S) or flares of importance 1, and flares of importance $\geq$ 2 was forecast, as shown in Table 2. Flares were forecast correctly in 71.6 percent, overestimated in 20.6 percent, and underestimated in 7.8 percent of the cases.

Table 2. Forecast justification for every event classification.

Forecast	observations			
	no flares	S; 1	$\geq$ 2	Total
no flares	285	26	1	312
S; 1	117	149	21	287
$\geq$ 2	1	8	5	14
Total	403	183	27	613

During the same period the probability of correct forecasts of the number of subflares and flares of importance 1 given 1-7 days in advance is 82 percent. It is assumed that the forecast is true if the forecast error is not higher than the standard error of the method (the absolute error is 1.5 flares per day and the root mean square error is 2 flares per day).

The forecast and detection of proton flares are of great interest from the point of view of their geoeffectiveness. The studies of IZMIRAN investigators Akinyan, Fomichev, and Chertock (1976) are dedicated to the creation of a method of solar cosmic ray intensity investigation from radio burst characteristics. Earlier, radio burst data were analyzed in connection with flare diagnosis by Straka (1970), Croom (1971a,b), Böhme (1972), Castelli et al. (1973), and Sakurai (1974). But the main advantages of the radio emission were not utilized and a number of important properties of solar cosmic ray propagation were not considered. The method proposed by Akinyan et al. (1976) included the following new points: Successive considerations of the dependence of the proton flux parameters and the character of their relations with radio bursts in the cm- and m-wavelength ranges on the flare heliographic longitude were made. Information in solar

radio data at meter wavelengths about the injection of energetic protons into the interplanetary space was considered. A unified method was used to estimate the proton flux parameters in different energy ranges (E > 10, 30 and 60 Mev). Provision was made for the estimation of the time parameters (the time of beginning and the maximum phase of the proton event in relation to the maximum of microwave flux, the value of decreasing of particle stream), making possible the calculation of particle flux-time profiles. The characteristics of microwave radio emission on 3 and 9 GHz were used to obtain information on the quantity of protons.

· The intensity of the m-component was used to estimate the conditions of protons emerging into interplanetary space and the frequency spectrum of the microwave burst was used to determine the energy spectrum of protons.

Proton events from 1965 to 1969 were analyzed to determine quantitatively the functions of intensity and longitudinal attenuation and the basic time functions of the proton flux near Earth. Then a control study was conducted using independent observations of the events from 1970 to 1976, which confirmed the main features of the relation between proton flux parameters and radio bursts.

Kobrin et al. (1978) have been studying the fluctuations of the solar radiation spectral index in the sm-range. They determined that some days before the proton flare, the amplitude of fluctuations with a period of $\sim$ 30 min increases rapidly (fig. 10). One can make use of this fact for proton flare prediction. At the present time there are some theoretical treatments of the flare forecast. Sirovatsky (1977a,b,c) and Somov and Sirovatsky (1977) have carried out the current sheet theory for a flare mechanism. They make calculations which must permit the determination of the characteristic features of the flare from the observations of pre-flare motions and magnetic fields in the active region.

Another method of forecasting the probability of an event is considered by Mogilevsky (1978a,b). The evolution of the active region is considered as a stochastic process, satisfying the qualification of Markov chains in that the following states are defined only by the preceding states. This method allows the calculation of the probability of the possible following states of the active region from the state being observed. To indicate the probability of the given state one must have a parameter that reflects objectively the energy of the active region. The Fourier spectrum of quasi-periodical oscillations of the magnetic field or radio emission can be used as this parameter. See for example figure 10.

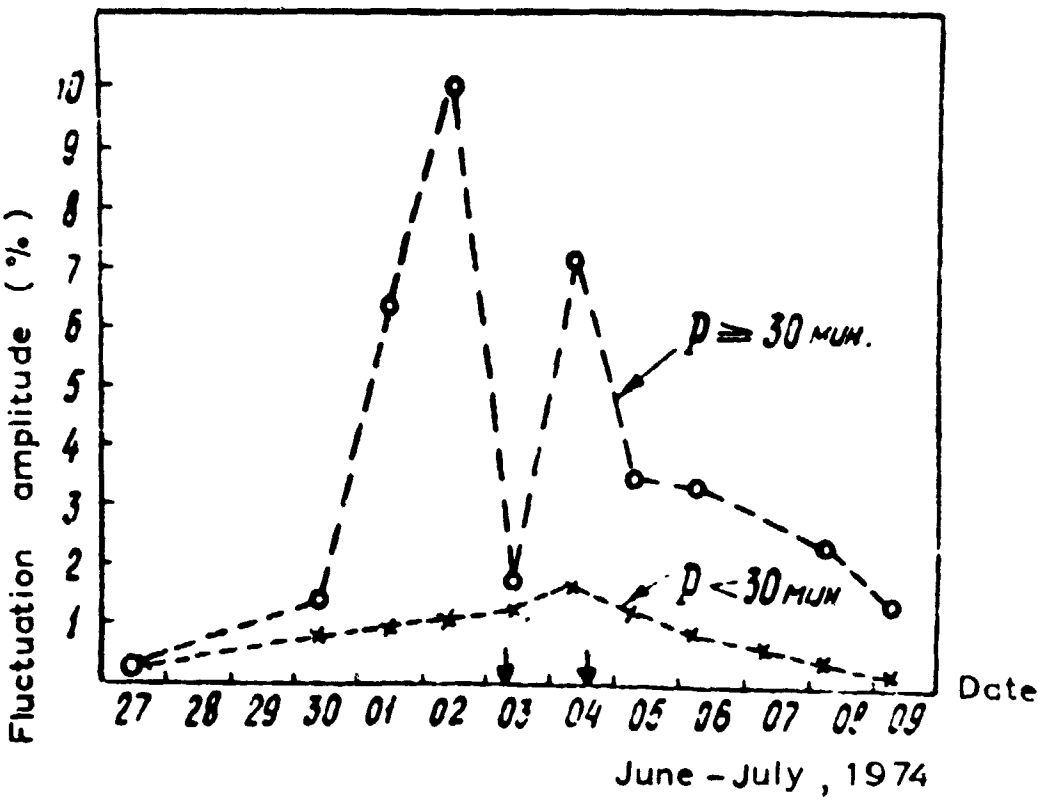

Figure 10. The change of spectral index fluctuation amplitude before proton flares. The moments of flares are noted as arrows along the abscissa.

REFERENCES

Akinyan, S. T., V. V. Fomichev, and I. M. Chertock (1976): The estimation of solar cosmic rays intensity by the characteristics of the radio bursts. In: The Birth and Evolution of Solar Active Regions, Moscow, "Nauka", 190.

Berlyand, B. O. (1978): Characteristics of active region producing high energy proton flares. In: Publ. of IX Consultation on Solar Physics, Wroclaw, Poland.

Berlyand, B. O., and V. A. Burov (1977): The choice of parameters characterizing the solar flares with injections of high energy protons. Trudy IPG, 35:28.

Berlyand, B. O., V. A. Burov, and N. N. Stepanyan (1978): Flare activity of the developing active regions and its prediction. In: Publ. of IX Consultation on Solar Physics, Wroclaw, Poland.

Bernshtejn, P. B. (1978): On long-term prediction of the proton-flare productivity of active regions. In: Publ. of IX Consultation on Solar Physics, Warsaw, Poland.

Bezruchenkova, T. M., N. K. Pereyaslova, and S. G. Frolov (1978): Diagnostics of solar flares and predictions of solar cosmic ray characteristics deduced from data on electromagnetic radiation. In: Publ. of IX Consultation on Solar Physics, Wroclaw, Poland.

Böhme, A. (1972): Spectral behavior and proton effects of the type IV broadband continua. Sol. Physics, 25:478.

Brailovskaya, I. Yu., A. N. Koval, M. B. Ogir, and N. N. Stepanyan (1972): Some parameters of flocculi characteristic for flare activity. Solnechnye Dannye, 6:88.

Bumba, V., and V. N. Obridko (1969): "Bartels" active longitudes, sector boundaries and flare activity. Solar Physics, 6:104.

Burov, V. A. (1976): Forecast of some evolution characteristics of active regions. In: Birth and Evolution of Solar Active Regions, Moscow, "Nauka", 142.

Burov, V. A., G. V. Kuklin, T. L. Slutskaya, and N. N. Stepanyan (1976): The comparison of various methods of forecasting of flocculi appearance at the limb. In: Birth and Evolution of Solar Active Regions, Moscow, "Nauka", 150.

Castelli, J. P., J. Aarons, D. A. Guidice, and R. M. Stzaka (1973): The solar radio patrol network of USAF and its application. Proc. IEEE, 61:1307.

Croom, D. L. (1971a): Solar microwave bursts as indicators of the occurrence of solar proton emission. Solar Physics, 19:152.

Croom, D. L. (1971b): Forecasting the intensity of solar proton events from the time characteristics of solar microwave bursts. Solar Physics, 19:171.

D'Azambuga, L. (1939): La cooperation internationale pour l'observation continue du Soleil et ses premiers resultats. L'Astronomie, 97:1.

Dolgoarshinnich, B. G., and G. V. Kuklin (1975): Forecast of active region evolution by constructing logical recognizing graphs. Res. Geom. Aeron. Sol. Phys., 37:24.

Efimenko, V. I., V. M. Efimenko, and V. V. Telnyuk-Adamchuk (1976): Short-term forecast of flare activity of sunspot groups. In: The Birth and Evolution of Solar Active Regions, Moscow, "Nauka", 182.

Efimenko, V. I., V. M. Efimenko, and V. V. Telnyuk-Adamchuk (1977): On the short-term forecast of the chromospheric flares on the basis of sunspot group characteristics. Vestnik Kievskogo Universiteta, Astronomia, 19:19.

Efimenko, V. M. (1976): On prehistory interval for flare forecast. Solnechnye Dannye, 11:63.

Frolov, S. G. (1977): The solar proton flare diagnosis on the following electromagnetic emission. Trudy IPG, 35:37.

Gopasyuk, S. I., M. B. Ogir, A. B. Severny, and E. F. Shaposhnikova (1963): The structure of magnetic fields and its variations in flare regions. Izv. Krim. Astrofiz. Obs., 29:15.

Gopasyuk, S. I., M. B. Ogir, A. B. Severny, E. F. Shaposhnikova, and N. V. Steshenko (1964): On the forecasting of solar flares. In: Proc. XII International Astronautical Congress, Varna 1962, Wien and New York, 63.

Howard, R., and A. Severny (1963): Solar magnetic fields and the great flare of July 16, 1959. Astrophys. Journ., 137:1242.

Izotov, Yu.I., I.Yu. Izotova, and P. R. Romanchuk (1976a): Flare activity in the process of the group evolution. In: The Birth and Evolution of Solar Active Regions, Moscow, "Nauka", 162.

Izotov, Yu.I., I.Yu. Izotova, and P. R. Romanchuk (1976b): The long-term forecast of the chromosphere flares several months in advance. Solnechnye Dannye, 6:67.

Kasinsky, V. V. (1972): On the large scale interrelation between the chromospheric flare generating sunspots and the satellite groups. Solar-Terrestrial Physics, USSR, 3:296.

Kobrin, M. M., A. I. Korshunov, S. I. Arbuzov, V. V. Pakhomov, V. M. Fridman, and Yu.V. Tikhonov (1978): Manifestation of pulsation instability in solar radio emission preceding proton flares. Sol. Physics, 56:359.

Koval, A. N. (1965): The position of moustaches in a spot group relative to the magnetic field. Izv. Krim. Astrofiz. Obs., 34:278.

Koval, A. N. (1974): A dependence between flare activity of the sunspot groups and the orientation of the line dividing the magnetic field polarities. Izv. Krim. Astrofiz. Obs., 51:13.

Koval, A. N., and N. N. Stepanyan (1972): Variation of the sunspot magnetic fields at two levels and the development of the active regions. Solnechno-zemnaya Fizika, 3:210.

Kuleshova, V. L. (1972): Some features of development of active regions with proton flares. Geomag. Aeronom., 12:328.

Levitsky, L. S. (1979): The flare distribution relative to the sectoral boundaries of the interplanetary field, extrapolated to the sun. Izvestiya Krim. Astrofiz. Obs., 62.

Martres, M.-J., R. Michard, U. Soru-Iscovici, and T. T. Tsap (1968): Étude de la localisation des éruptions dans la structure magnétique évolutive des régions actives solaires. Solar Physics, 5:187.

Mogilevsky, E. I. (1978a): A basis for a stochastic method of quantitative flare prediction. In: Publ. of IX Consultation on Solar Physics, Wroclaw, Poland.

Mogilevsky, E. I. (1978b): Solar magnetic fields and a short-term quantitative forecast of the solar activity. Sbornik "Fizika Solnca", Moscow, "Nauka".

Moreton, G. E., and A. B. Severny (1968): Magnetic fields and flares in the Region CMP, 20 September 1963. Solar Physics, 3:282.

Ogir, M. B. (1967): On some peculiarities of the origin and motion of flares accompanied by type IV bursts. Izv. Krim. Astrofiz. Obs., 37:94.

Ogir, M. B. (1978): The relationship between solar flares and the sector boundaries of the interplanetary magnetic field for maximum and decrease phases of zoth solar activity cycle. Solnechnye Dannye, 9.

Pereyaslova, N. K., L. A. Kolesnikova, M. N. Nazarova, and I. E. Petrenko (1978): Some features of the development of active regions connected with proton events. In: Publ. of IX Consultation on Solar Physics, Wroclaw, Poland.

Romanchuk, P. R., Yu.I. Izotov, I.Yu. Izotova, and V. N. Krivodubsky (1977): The forecast of the chromospheric flares from 1 to 7 days ahead. Vestnik Kievskogo Universiteta, Astronomia, 19:29.

Sakurai, K. (1974): Energetic particles from the sun. Astrophys. and Space Sci., 28:375.

Severny, A. B. (1958): The appearance of flares in neutral points of the Solar magnetic field and the pinch-effect. Izv. Krim. Astrofiz. Obs., 20:22.

Severny, A. B. (1960): An investigation of magnetic fields connected with solar flares. Izv. Krim. Astrofiz. Obs., 22:12.

Severny, A. B. (1964): Observations of transversal and longitudinal magnetic fields connected with solar flares. Izv. Krim. Astrofiz. Obs., 31:159.

Severny, A. B. (1965): On the changes of magnetic fields connected with flares. IAU Symp. 22, 358.

Severny, A. B., and N. V. Steshenko (1972a): Method for forecasting of solar flares. Solar Terrestrial Physics 1970: Part 1:173.

Severny, A. B., and N. V. Steshenko (1972b): Development of the methods of solar flare forecasting. In: XV Plenary COSPAR, Madrid, May 1972, 158.

Simon, P., and P. S. McIntosh (1972): Survey of current solar forecast centers. In: Solar Activity Observations and Predictions. (Progress in Astronautics and Aeronautics, V. 30). McIntosh, P. S., Dryer, M., (Eds.), 343.

Slonim, Yu.M. (1957): Active regions of the sun and chromospheric flares, Trudy Tashkentskoy Astronom. Obs., Series 2, 6:61.

Slutskaya, T. L., and N. N. Stepanyan (1974): Forecast of active region development by the method of potential functions. Izv. Krim. Astrofiz. Obs., 52:131.

Slutskaya, T. L., and N. N. Stepanyan (1976): Estimation of original parameters significance for forecasts of flocculr appearance from behind the limb. Solnechnye Dannye, 1:70.

Somov, B. V., and S. S. Sirovatsky (1977): Quasi-steady magnetic field dissipation in current sheets as the source of heating for solar active region. Sol. Physics, 55:393.

Stepanov, V. E., and A. B. Severny (1962): A photoelectric method for measurements of the magnitude and direction of the solar magnetic field. Izv. Krim. Astrofiz. Obs., 28:166.

Stepanyan, N. N. (1974): Quantitative measurements of the H and K brightness of the plages as a criterion for forecasting of active region development. Izv. Krim. Astrofiz. Obs., 51:8.

Stepanyan, N. N., and M. Jakimiec (1978): Predictions of the development and flare activity of active regions based on the method of multiple regression. In: Publ. of IX Consultation on Solar Physics, Wroclaw, Poland.

Steshenko, N. V. (1973): The study of solar flare appearance. Vestnik A. N. SSSR, 3:42.

Straka, R. M. (1970): Microwave spectral observations of coronal condensations, Report AFC RL-70-0002, Air Force Cambridge Research Labs., Bedford, Mass.

Syrovatsky, S. I. (1977a): On the possibilities to observe preflare current sheets on the sun. Pisma v Astr. Jurnal (USSR), 3:133.

Syrovatsky, S. I. (1977b): The problems of solar activity and cosmic system "Prognoz," Moskva, "Nauka," 5.

Vaschenko, N. D., V. I. Efimenko, and V. M. Efimenko (1976): The formation of conception algorithms and the forecast of chromospheric flares. The Astronomical Observatory of Kiev University, Preprint 12.

Vladimirsky, B. M., and L. S. Levitsky (1974): A solar flare activity distribution around the sector-structure boundaries extrapolated to the sun. Izvestia Krim. Astrofiz. Obs., 51:74.

Vladimirsky, B. M., L. S. Levitsky, and A. B. Severny (1971): In: The Generation of Cosmic Rays on the Sun, Moscow, 314.

Zvereva, A. M., and A. B. Severny (1970): Magnetic fields and proton flares 6 July and 2 September 1966. Izv. Krim. Astrofiz. Obs., 41-42:97.

FORECASTING OF SOLAR ENERGETIC RADIATION AT THE FORECAST CENTER OF THE INSTITUTE OF APPLIED GEOPHYSICS

S. I. Avdyushin, N. K. Pereyaslova, F. L. Dlikman, and Yu.M. Kulagin
Institute of Applied Geophysics
Goscomhydromet, Moscow, USSR

Charged particle fluxes generated in solar flares are the main source of radiation hazard. However, a variety of conditions for injection and absorption of charged particle fluxes exists in a flare region, and even in large flares flux injection does not necessarily take place. The process of particle propagation accompanied by acceleration in interplanetary space is also of importance. Consequently, solar activity disturbances are not unambiguously related to the radiation environment near Earth. The physical mechanism of solar flares is not clearly understood and it is impossible to develop a unique and reliable technique for forecasting the radiation environment.

Investigation of the relationships between the characteristics of solar cosmic ray events and parameters of heliogeophysical phenomena accompanying a flare has made it possible to find out some regularities which are used as the basis for forecasting techniques. For solving forecast problems, a method of simultaneous investigation of a complex of heliogeophysical phenomena accompanying a solar flare is used. Required data on solar activity, the interplanetary medium, and penetrating radiation fluxes in interplanetary space and in the magnetosphere are provided by space, stratospheric and ground-based means, which form the regular observational network of the Forecast Service of the Institute of Applied Geophysics (IAG). Collection, processing and transmission of initial data for analysis are performed with the help of a ground-based automatic system developed on the basis of the "MINSK-32" computer.

The following forecasts are regularly issued by the IAG Service: (1) forecasts of proton flux evolution in solar cosmic-ray (SCR) flares (extrapolation methods), (2) estimations of the integrated SCR flux from a flare based on the accompanying electromagnetic radiation, and (3) qualitative forecasts of flare activity and the magnetosphere and radiation environment for a two day period (issued daily) and for a 27 day period (issued weekly). Observational data from national and foreign sources used to determine the state of solar activity and the interplanetary space include flare data in visible, X-ray and radio bands, and data on sunspot groups and integrated characteristics of solar activity. For penetrating radiation fluxes, the primary data come from measurements on the AES "Meteor" system and supplementary data from stratospheric soundings, riometer data (USA), and neutron monitor data. For the magnetosphere environment, operational information are obtained from magnetic observatories and diagnostics from the AES "Meteor" system.

A method of forecasting SCR flux evolution and integrated flux for the whole event has been developed and is currently used by the IAG Service. This method utilizes a model of isotropic diffusion and SCR flux data from initial records in polar zones on a "Meteor" satellite (Bezruchenkova et al., 1976). To forecast proton fluxes, a linear relation is used,

$$\ln(I \times T^{3/(2-\beta)}) = -a/T + b, \qquad (1)$$

which was obtained from a diffusion equation, where I is the proton flux density determined according to the special program of the operational control of SCR and galactic cosmic ray (GCR) fluxes which was developed for the "MINSK-32" computer (program "Flux averaging in the polar zone"). $T = t_{meas} - t_o$, where t_{meas} is the time of measurement of flux density in the polar zones. The solar source of particle injection is identified from heliogeophysical data operationally available in the IAG Service. The moment of proton injection - t_o is determined. Injection time can be determined from data on X-ray and radio wave emission, accompanying a proton flare, and optical observations in Hα. The time of a hard X-ray burst is preferable. If such data are not available, the beginning of flare observation in Hα is taken as t_o. In case of recording fluxes from beyond-limb flares, the time of radio burst observation (especially type IV radio burst) is taken as t_o.

The diagnostics of the current state of the radiation environment along spacecraft paths in near Earth orbits involves the use of observations of penetrating radiation fluxes in the AES "Meteor" orbit in high-latitude zones of the Earth's magnetosphere to estimate the general structure of particle fluxes, specifically in the orbits of manned space vehicles (MSV) "Saljut"-"Soyuz". This estimate should be primarily made for protons of solar cosmic radiation with regard to the real distribution of threshold geomagnetic rigidities, which depend on the extent of the magnetosphere disturbance. The observed energy spectrum of SCR particles in the polar caps, characteristics of the spatial distribution of cut-off rigidity and the location of the satellite making the measurements are used as the basis for estimating the radiation environment for another prescribed orbit.

In view of the considerable time variations of the magnetospheric state, the solution of this problem requires a dynamic model of threshold rigidities. Such a model is analytically written as (Dorman et al., 1972)

$$R = \frac{15}{L^{2+\delta}}\left[1 - \left(\frac{L-1}{L_o-1}\right)^3\right]^{1.4} \qquad \text{for } L < L_o, \text{ and} \qquad (2)$$

$$R = 0 \qquad \text{for } L \geq L_o. \qquad (3)$$

In this expression parameters δ and L_o include the general characteristics of magnetospheric state. L_o is the polar cap boundary at the nightside of the magnetosphere and δ is quantitatively related to the magnitude of the D_{st} variation which reflects the ring current intensity. For quiet conditions $L_o = 7$ (or $\approx 68^0$ invariant latitude) and $\delta = 0$. An empirical relation given in Table I has been obtained by comparing the SCR proton observations

with the value of D_{st}-variation. The determination of the D_{st}-variation

Table 1. Ring current intensity parameter δ as an empirical function of $D_s t$.

$D_{st}(\gamma)$ =	8	16	26	40	60	100	160	270	380
δ =	0.03	0.10	0.15	0.20	0.24	0.30	0.38	0.47	0.60

magnitude is based on the regularity found from the AES "Meteor" observations and reflected by regular displacement of the bend of cosmic ray latitudinal variation with the increase of ring current intensity (Avdyushin et al., 1976). This relation can be quantitatively described by

$$\Delta L = (L_H - 1)\cdot 10^{-2}|D_{st}|^{2/3} \qquad (4)$$

where ΔL is the displacement of the bend from a quiet level, and L_H is the quiet level of the bend in undisturbed magnetosphere. It should be noted that the main parameters, such as the energy spectrum of particles and characteristics of the distribution of threshold geomagnetic rigidities are obtained simultaneously from AES "Meteor" measurements. In the Institute of Applied Geophysics, this model was used to calculate an operating catalogue of SCR proton integral spectra for a set of turns of MSV "Saljut"-"Soyuz" with different proton initial spectra in the polar caps and the magnetospheric parameters δ and L_o.

While further developing forecasting techniques consideration is given to both physically substantiated premises for forecasting and possibilities of operational availability of heliogeophysical phenomenon characteristics and parameters. Recent investigations have shown that photospheric magnetic fields are the significant factor determining the propagation of flare-generated protons. This was first established by Snyder and Neugebauer (1966) when analyzing the experimental data obtained on "Mariner-2". In subsequent works (Krimigis et al., 1971; Roelof and Gold, 1976), comparison of SCR profiles at proton energies greater than one MeV in interplanetary space with equatorial high-coronal structure was made. It was found that low-energy solar protons are distributed over unipolar magnetic regions in the corona, and the interfaces of magnetic polarities are a serious obstacle to their longitudinal propagation. We analyzed the observed characteristics of of the solar protons with energies of 5-40 MeV recorded in high-latitude zones of the Earth magnetosphere at altitudes 700-1000 km with the configuration of large-scale magnetic fields on the Sun. The investigation of SCR events along with photospheric magnetic fields for the maximum and declining portions of the 20th solar cycle, as well as during the 21st cycle increase, made it possible to establish a relationship between the peculiarities of 5-90 MeV proton propagation and large-scale magnetic structure. The following regularities have been revealed:

(1) The SCR time profile is determined by the temporal location of a flare coupling longitude, i.e. the solar longitude from which the solar wind flows to the Earth, and neutral lines of the longitudinal solar magnetic field, which limit regions filled by flare particles. An equation was developed that relates the decrease constant T to the time of a coupling-longitude displacement to the unipolar region boundary (Δ t) and unipolar region extent (D). In this case the decrease constant was calculated separately from the intensity maximum J_{max} to $J_{max}/2$ according to the following relationship

$$T_1 = (\log D \Delta t)^{2.7} \tag{5}$$

and from the intensity maximum to the intensity at the unipolar region region boundary according to

$$T_2 = 1.6 (\log D \Delta t)^{2.3}. \tag{6}$$

(2) A sharp front of SCR increase up to the maximum was observed for the events in which SCR arrival was recorded after the coupling longitude had crossed the neutral force line. While describing the temporal distribution of proton fluxes by an exponential function, the constant of an increase rate changed from 1.2 to 2 hours. Times up to the maximum did not depend on the flare heliolongitude.

(3) An increase of SCR angular distribution anisotropy up to 30 per cent was observed in the events in which the coupling longitude, after crossing the neutral force line, returned to the region filled by flare particles.

(4) The analysis of SCR spectral characteristics variations showed an effect of spectrum hardening ahead of neutral force lines.

(5) The beginning of a record or sharp increase of 5-40 MeV proton fluxes near the Earth was observed after the coupling longitude had crossed the neutral force line (when moving eastward) separating the unipolar region where protons were injected.

A relationship between the spectrum index γ_{init} and γ_{max} and the decrease time constant T_1 is obtained for the events in which the coupling longitude and flare were in one unipolar region. The effect of the coronal structure on peculiarities of proton propagation with low energies during the solar cycle increase is established in Krimigis et al., 1971. Assuming that the large-scale coronal structure is relatively regular during the whole cycle, the forecasting technique based on the regularities found in the 20th sunspot cycle has been applied to the events of the 21st cycle.

When analyzing the experimental data, the maps of photospheric magnetic fields published in Solar Geophysical Data (1973-1976) were used; their drawing technique is presented in works by McIntosh (1972). The solar synoptical maps drawn on the basis of the pictures taken in Hα, reveal a

large-scale structure of weak magnetic fields and feature continuity over large extent (McIntosh, 1972).

The heliolongitude of the base of the force line connecting the Earth with the equatorial corona was calculated according to the procedure which was called EQRH by the authors Nolte and Roelof (1973). This procedure allows one to estimate the longitude of coupling or that of the solar wind source by extrapolating instantaneous ideal spirals to the Sun. The possibility of such an approximation of the coupling longitude was theoretically supported in Sakurai (1971) and Matsuda and Sakurai (1972), and it was shown in Nolte and Roelof (1973) that the extrapolation of the trajectory of plasma particle motion according to this procedure actually estimates the high-coronal longitude and latitude of a solar wind source.

The relationship for calculating the Carrington longitude of the base of the Sun-Earth force line takes the form:

$$\phi_o = \phi(t) + \frac{\Omega r'_g}{v(t)}, \tag{7}$$

where Ω - mean angular velocity of the solar rotation,

r'_g - heliocentric radius of the detector,

$\phi(t)$ - Carrington longitude of the central solar meridian at t moment.

The error in determining ϕ_o will be of the form:

$$\delta\phi_o = \phi'_o - \phi_o = \Omega\left[\frac{r'_g}{v(t)} - \frac{\Delta r}{\vec{v}}\right] = \Omega\left(\frac{r'_g}{v}\right)\left[\frac{\vec{v}}{v(t)} - \frac{\Delta r}{r'_g}\right], \tag{8}$$

where $\Delta r = r'_g - r_o$, r_o is the distance from the Sun, where the solar wind is radial, and $\vec{v} = (r'_g - r_o)/(t - t_o)$, where t_o is the moment of the solar wind outflow.

Using the known peculiarities of solar proton propagation and taking into consideration the effect of the configuration of large-scale solar magnetic fields (Mikirova and Pereyaslova, 1977; Mikirova and Pereyaslova, 1977; Mikirova and Pereyaslova, 1978; Mikirova, 1977) on the characteristics of SCR proton fluxes, the technique has been developed to forecast the following proton event parameters:

(a) decrease constants T for the fluxes of protons with energies $E_p > 5$ MeV;

(b) times of the maximum of SCR event intensity with $E_p > 5$ MeV;

(c) integrated flux of protons with E_p > 5-10 MeV and E_p > 40-60 MeV, normalized to the maximum intensity;

(d) event beginning and duration; and

(e) indices of the integral spectrum rigidity at the intensity maximum N_{max} and at the beginning of the event at the half-maximum level $N_{max}/2$.

Confidence intervals for reliability values $\alpha = 0.9$, $\alpha = 0.95$, correlation coefficients and the relative error in a forecasted parameter are given in Table 2 for all quantitative relationships involved in the technique. The flow chart of forecasting the SCR event parameters is illustrated in Figure 1. Examples of the time dependence of proton fluxes in the SCR events on September 17-20, 1977, January 7-10, 1978, and April 7-12, 1978, are given in Figures 2, 3 and 4. The analysis of the SCR temporal distribution is performed with the use of the maps of photospheric magnetic fields.

Table 2. Proton Event Forecast Performance

Parameter	Proton energy MeV	Reliability values $\alpha = 0.90$	Reliability values $\alpha = 0.95$	Correlation coefficient	Relative error per cent
Decrease constant (hour)					
T_1	> 5	6	8	0.95	
T_2	> 5	7	9	0.90	45
Times of the maximum (hour)					
(class I) t_{max}	> 5-10	7	8	0.80	70
(class II) t_{max}	> 5	3	4	0.87	30
Integrated flux $\log \frac{F}{N_{max}3600}$	> 5-10	0.2	0.3	0.89	50
	> 40-60	0.3	0.4	0.78	
Spectrum index					
γ_{init}	> 10-30	1.0	1.1	0.78	90
	> 30-60	0.7	0.8	0.94	
γ_{max}	> 10-30	0.9	1.0	0.79	80
	> 30-60	0.7	0.8	0.94	

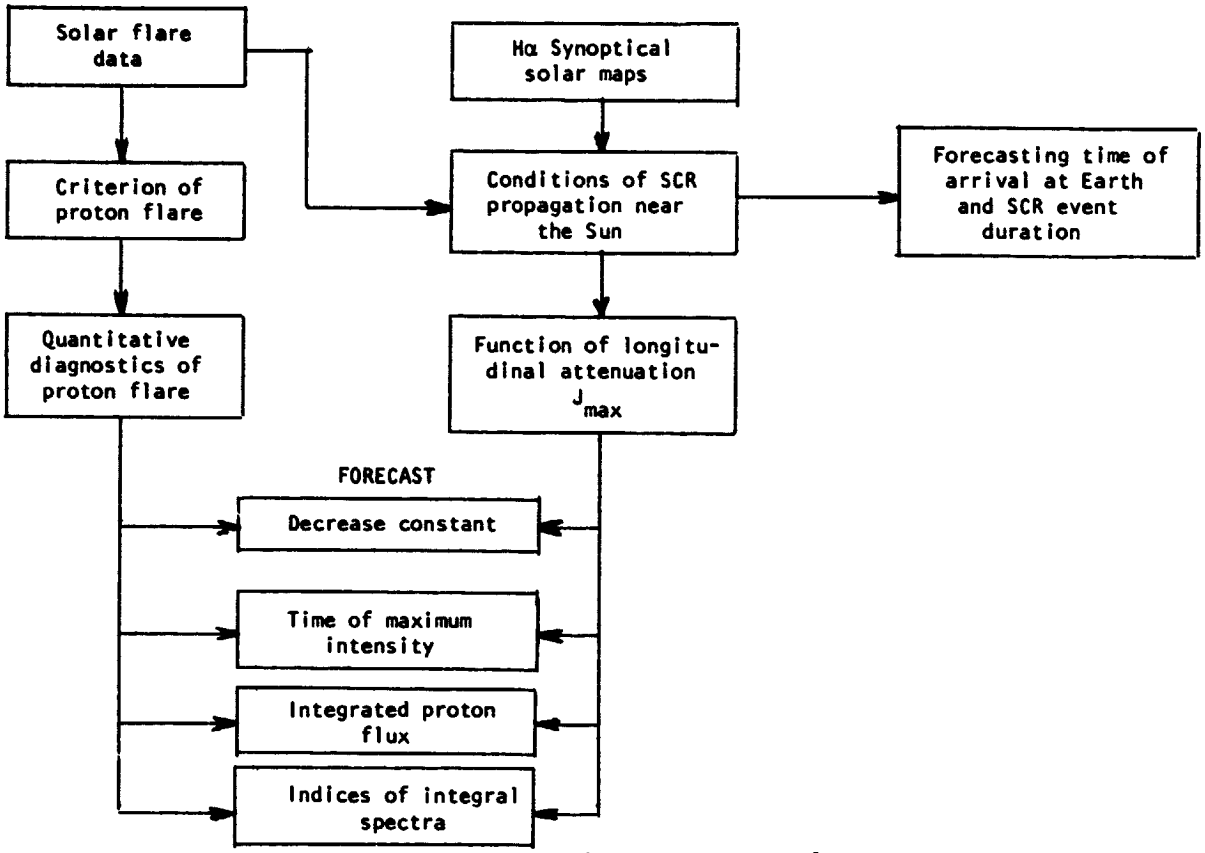

Figure 1. Flow chart of proton event forecasts.

The characteristics of microwave radio bursts and their relation to the proton fluxes in SCR events were investigated as a function of the conditions in the emitting regions and injection source heliolongitude. The following results were obtained (Belovskii et al., 1977; Belovskii et al., 1978; Belovskii and Ochelkov, 1977; Belovskii and Ochelkov, 1977; Belovskii and Ochelkov, 1978; Belovskii and Pereyaslova, 1977) and were used to develop the forecast techniques:

(a) The relation between the maximum proton flux $-J_p$ and peak radio burst flux for ν = 9100 MHz and E_p > 10 MeV was established. The correlation coefficient is 0.64.

(b) The considerable dependence of the maximum proton intensity on the flare heliolongitude (ϕ) was determined. The mean attenuation coefficient for protons with E_p > 30 and 60 MeV is

$$K_p(\phi) = 10^{0.02|60^0-\phi|} \qquad (9)$$

(c) An east-west asymmetry of the microwave burst intensity with the maximum in heliolongitudes of 30^0-60^0E was revealed. The attenuation coefficients of radio emission fluxes $K_{\nu}(\phi)$ were obtained.

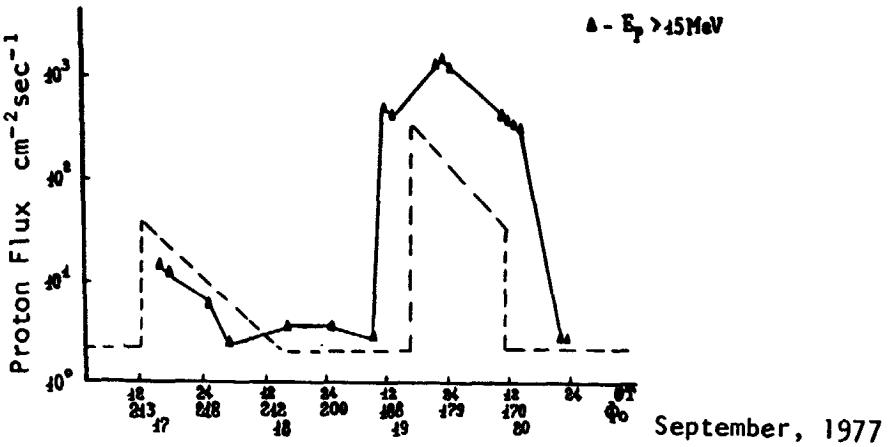

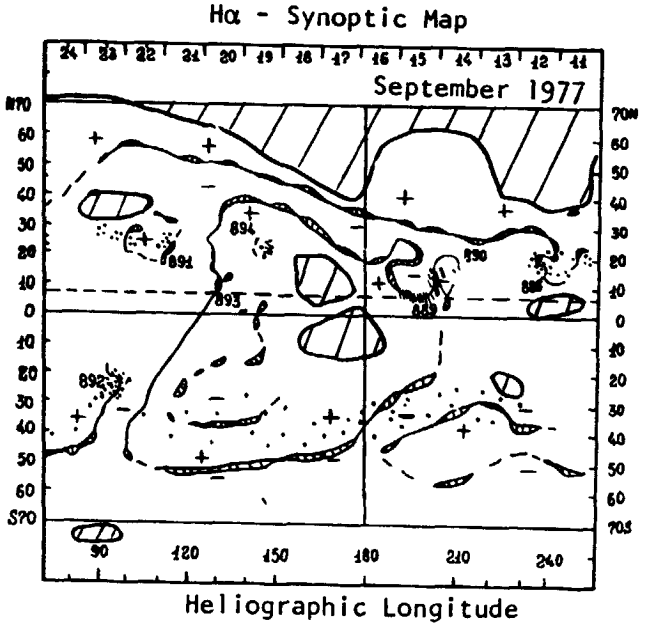

Figure 2. SCR temporal distribution with E_p > 15 MeV in the event of September 17-20, 1977.

(d) The relations between the integral flux for the whole event, the maximum proton flux and the time up to the event maximum was found.

The techniques for forecasting proton event parameters have been developed on the basis of radio observations in the centimeter range.

1. The assessment of the probability of 60 MeV proton record based on the observations on frequencies 8800 and 4995 MHz. The parameters used:

J_λ - radio emission flux in the maximum;

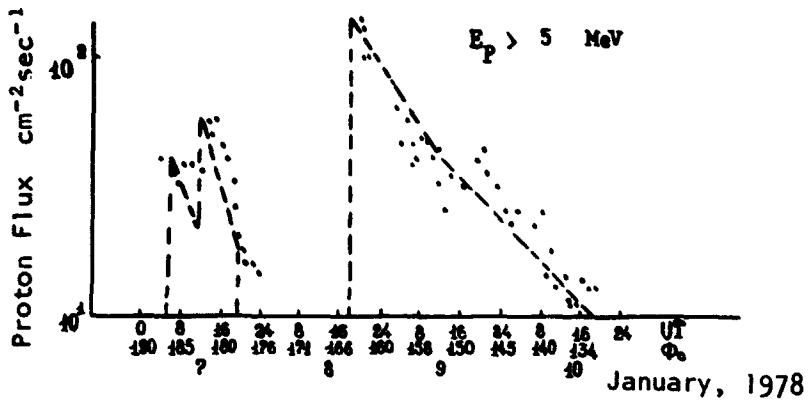

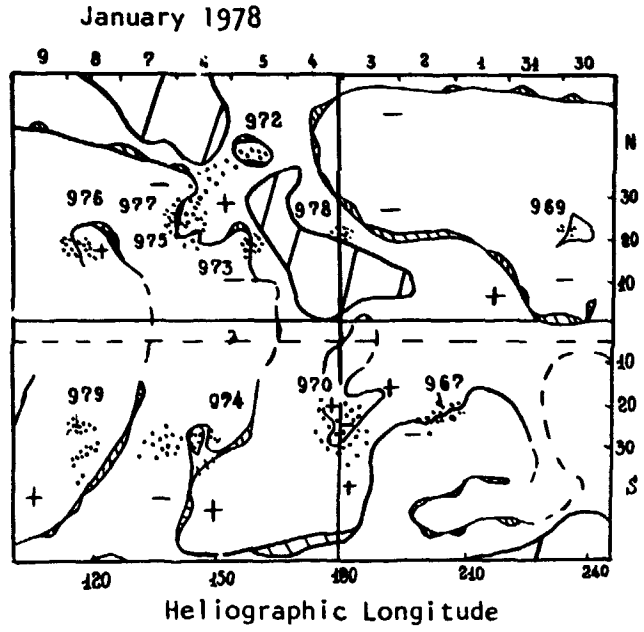

Figure 3. Temporal distribution of proton fluxes with E_p > 5 MeV in the event of January 7-10, 1978.

I - integral flux for the whole event determined as $I = J_{\Lambda}d$, where d is the effective duration.

2. The forecast of the lower limit of the flux of protons with E_p > 10 MeV in the event maximum on the basis of observations on ν = 9100 MHz. Besides data on the flux, the flare coordinates are required.

For the probability of correct forecast being 0.84, 0.89, or 0.92, the value of the lower limit of 10 MeV proton flux is determined with regard to

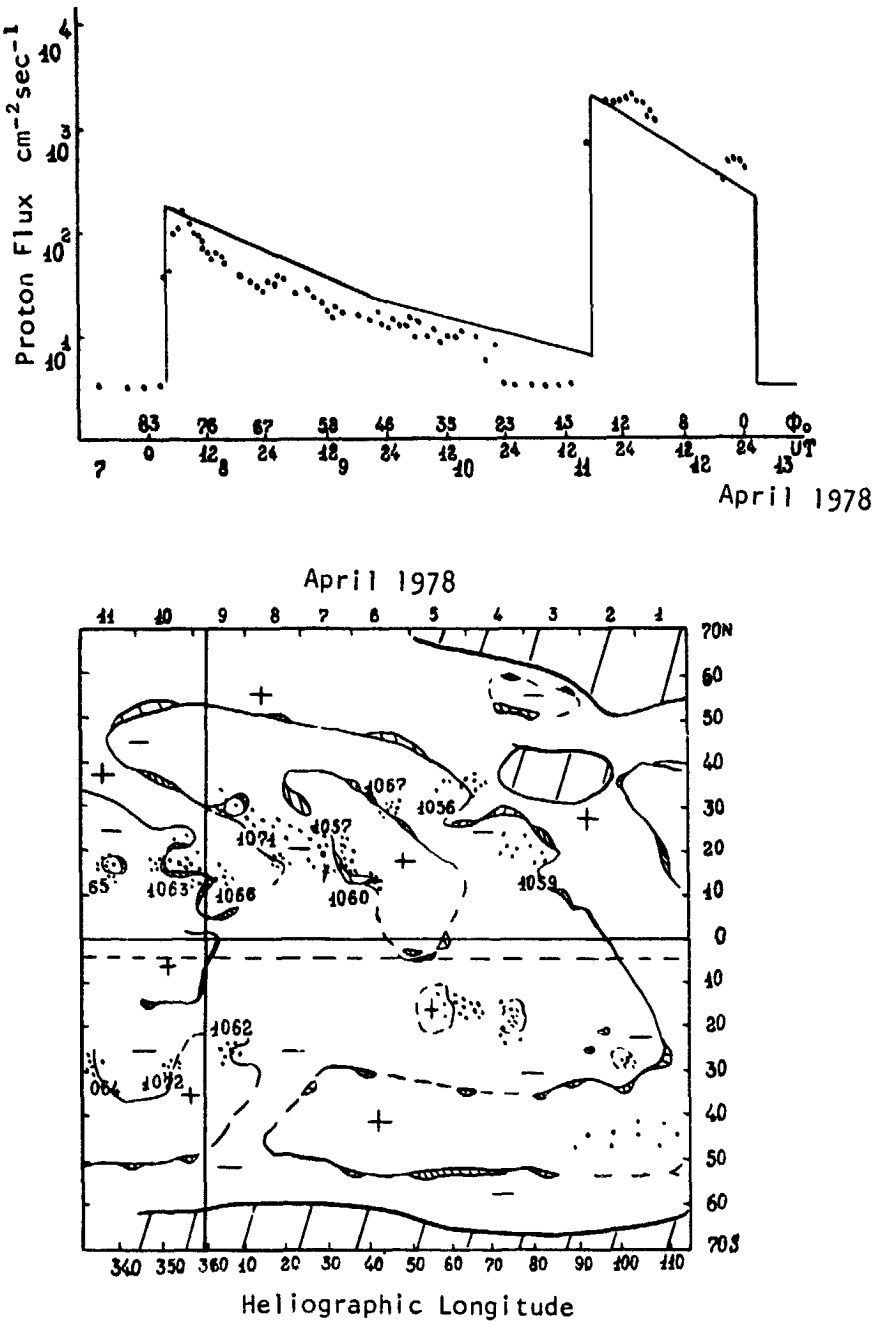

Figure 4. SCR temporal profile with E_p > 5 MeV in the event of April 7-12, 1978.

the attenuation of radio burst intensity by introducing the coefficient $K_{\mathcal{R}}(\phi)$ from the respective relationships:

$$\log J_p^{max} = \begin{cases} 1.279\ \{\log J_\gamma^{max} - 2.26\ K_\gamma(\phi)\} - 1.36 \\ 1.279\ \{\log J_\gamma^{max} - 2.26\ K_\gamma(\phi)\} - 1.45 \\ 1.279\ \{\log J_\gamma^{max} - 2.26\ K_\gamma(\phi)\} - 1.54 \end{cases} \quad (10)$$

The data necessary for forecasting can be obtained from the station Zimenki (USSR) where the patrol is carried out on 9100 MHz with the aid of two identical radio telescopes.

3. Rapid forecast of the integral proton flux for the event. The data on the flux in the event maximum for protons with $E_p > 30$ and 60 MeV and the time up to the maximum are required.

The integral flux of protons I is calculated according to the equation presented by Belovskii and Pereyaslova (1977):

$$I = J_m t_o \alpha\ [\tau^\beta \Theta(1 - \tau) + \Theta(\tau - 1)] \quad (11)$$

where $\tau = t_m/t_o$, J_m is the proton flux at the maximum, t_m - time up to the maximum, Θ is Heaviside's function, and d, β and t_o are numerical constants. The accuracy of forecasting I is not worse than 20-30 per cent. The data required for forecasting are obtained from the "Meteor" satellite.

X-ray emission is a highly informative parameter for predicting the proton flux. Provided that the data on X-ray emission in the range of 0.5-4 Å and 1-8 Å come regularly, it is possible to precalculate the integral fluxes in SCR events before the protons arrive at the Earth's orbit, i.e. before the moment of the accumulation of the maximum dose. By applying regression analysis, the radiation characteristics of exposure dose and spectrum rigidity are forecast step by step. We shall not dwell here in detail upon the method, since this is clearly presented by Bezruchenkova et al., 1977 and Pereyaslova et al., 1978. It should be noted that regular and timely availability of the following information is necessary to enable one to use the proposed method operationally: (a) more complete characteristics of X-ray emission bursts, (b) the maps of photospheric magnetic fields, (c) the solar wind velocity, and (d) flare heliocoordinates.

As stated above, the propagation of solar protons is considerably influenced by the state of the interplanetary space. Therefore questions concerning the diagnostics and forecast of the parameters responsible for the state of the interplanetary space play an important role in forecasting the radiation situation. In a number of papers it was established that SCR characteristics are related to the direction of the radial component of the interplanetary magnetic field (IMF)(Pereyaslova et al., 1976; Darchieva et al., 1973). The conditions in the interplanetary space are mainly governed by the solar wind density and velocity.

The dependence of high-latitude magnetic disturbances on the magnitude and direction of the IMF (Bx, By, Bz) components and quiet solar wind (SW)

velocity forms a physical basis for the forecasting of the SW state. Energy input to the magnetosphere is controlled by the seasonal inclination of the dipole to the SW flux and reorientation of the helio- and geomagnetic equator planes in the Earth orbit. Such geomagnetic disturbances are formed by the superposition of the three current systems: DP_2, DP_3 and DP_4. Each of them depends on $B_z < 0$; $B_z > 0$ and the signs of Bx and By, respectively. In the opinion of Friis-Christensen et al. (1971), the DP_4 currents are to a greater extent governed by ± By and to a lesser extent by ± Bx (IMF components). The maximum of the DP_4 currents is localized at $\phi^0 \sim 80^0$, and the magnitude and direction are determined by the sign and magnitude of ± By (and ± Bx). The delay between the IMF variations and DP_4 disturbances is 25 minutes, and this determines the threshold length of the IMF forecasting by the behavior of the geomagnetic field (GMF). By fluctuations measured in the ecliptic plane are known to produce the additional B_z component of IMF in the solar-magnetospheric system. This "addition" of $\Delta B_z < 0$ is controlled by the dipole inclination to the SW flux. The IMF forecasting techniques based on the well-known Svalgaard-Manssurov effect (Mansurov and Mansurova, 1971; Svalgaard, 1968), should also take into consideration the seasonal dipole variations as a regular effect. The dependence of the high-latitude GMF variations upon the IMF sectoral structure is more pronounced for δZ and less pronounced for δH. This structure manifests itself as the decrease or increase of δZ by 200-300 x 10^{-5} gauss in the N-circumpolar region with IMF directed from or towards the Sun. At the near-polar boundary of the daytime cusp the decrease or increase of H is observed for the same IMF sign reversals. Below $\phi^0 \simeq \pm 75^0$ the effects of the IMF on GMF are insignificant, and this fact determines the selection of stations for observing δZ and δH with the object of the IMF forecasting (stations Tule, Vostok, etc.).

To realize the forecasts of ± By (or Bx) for the period of 1-2 days, it is reasonable to provide the regular income of 3-hour data on δZ and δH from the stations located at $\phi^0 \simeq 77^0$ to 80^0 and near the boundaries of the daytime cusp. The preliminary testing of such stations with the use of δZ and δH data confirmed the feasibility of the ± By (or Bx) forecasts. The income of data from some stations by seasons is insufficiently operational, and the effects of B_z and By on the GMF are superposed. However, having enough information on the morning and evening DP_4 current vortices (since $By \gtrless 0$ with $B_z < 0$) one can attempt to separate B_z and By effects. The technique of the IMF forecasting is based on the extrapolation of the gradients of δZ deviations from the Z trend. The trend takes into account the level of seasonal and recurrence variations of Z (or H) in local warm seasons. The trend averaging takes into consideration the time scales of the Earth's and solar rotations and the maximum duration of IMF sectors $\sim$ 15 days. The rate of changes of δZ deviation gradients from the trend is a measure of the approach of the IMF sign reversal.

For long-range forecasting it is possible to use the method based on the results of the statistical analysis of the information on the solar proton flux characteristics. The peculiarity of the method is in analyzing separately the moments of proton flare occurrence and values of proton fluxes in each flare. This analysis has resulted in the determination of the distribution law for these values, besides the relationships have been found allowing to determine the simultaneous probability of the occurrence of events.

The development and improvement of efforts on direct diagnosis and forecasting are primarily directed towards the application of automated (recorded on machine processable media) global dynamic models of the radiation environment with a limited number of controlling parameters. The estimation and forecast of these parameters is performed on the basis of the operational computer-oriented data bank, which is updated with current observational results, actively using the means of information presentation. Models of the radiation situation for each phase of the solar cycle are assumed to be developed on the basis of the experimental investigations with the purpose of using them when forecasting the radiation characteristics.

REFERENCES

Avdyushin, S. I., Yu. M. Kulagin, E. L. Dlikman, V. A. Kuzmina, G. A. Kirdina, A. B. Malyshev, V. A. Mokhova, and P. M. Svidskii (1976): Variations of threshold geomagnetic rigidities in the period March-May, 1976, and their connection with the ring current. Report UAG-61. Collected data reports for stip interval II 20 March - 5 May 1976, p. 183.

Belovskii, M. N., and Yu. P. Ochelkov (1977): Zavisimost nablyudaemoi pikovoi intensivnosti solnechnykh kosmicheskikh luchei ot geliogeograficheskoi dolgoty. Solnechnye dannye, 1976, 12:73.

Belovskii, M. N., and Yu. P. Ochelkov (1977): O diagramme napravlennosti mikrovolnovykh radiovspleskov Solnza. Doklady AN SSSR, tom 236, N. 6, 51.

Belovskii, M. N., and Yu. P. Ochelkov (1978): O svyazi mehzdu parametrami protonnykh sobytii. Solnechnye dannye, 2:89.

Belovskii, M. N., Yu. P. Ochelkov, and T. S. Podstigach (1977): Metodologicheskie voprosy prognoza protonnyh yavlenii po radiovspleskam Solnza. Tezisy X Vsesoyusnoi konferenzii po radioastronomicheskim issledovaniyam solnechnoi sistemy (1977, Irkutsk), 51.

Belovskii, M. N., Yu. P. Ochelkov, T. S. Podstigach, and M. A. Fasakhova (1978): O prognozirovanii protonnykh yavlenii po radiovspleskam. V sb.: Radioizluchenie Solnza, vyp. 4, izd. LGU, 44.

Belovskii, M. N., and N. K. Pereyaslova (1977): Nekotorye parametry radiovspleskov, svyazannykh so vspyshkami SKI. Trudy IPG, vyp. 35, Gydrometizdat, M., s. 51.

Bezruchenkova, T. M., N. A. Mikryukova, N. K. Pereyaslova, and S. G. Frolov (1977): Diagnostika protonov solnechnykh vspyshek po soprovohzdayushchemu electromagnitnomu izlucheniyu. Geomagnetizm i aeronomiya, N. 5.

Bezruchenkova, T. M., M. N. Nasarova, and N. K. Pereyaslova (1976): Primenenie modeli izotopnoi diffuzii dlya prognozirovaniya razvitiya potokov solnechnykh kosmicheskikh luchei v vysokoshirotnykh zonakh

magnitosfery Zemli. Geomagnetizm i aeronomiya, tom XVI, N. 4, s. 592.

Darchieva, L. A., T. A. Ivanova, E. N. Sosnovets, and L. V. Tverskaya (1973): O strukturnykh i dynamicheskykh osobennostyakh proniknoveniya solnechnykh kosmicheskikh luchei v polyarnye shapki. Izv. AN SSSR, ser. fiz., tom 37, 1313.

Dorman, L. I., V. S. Smirnov, and M. I. Tyasto (1971): Kosmicheskie luchi v magnitnom pole Zemli. "Nauka", M.

Friis-Christensen, E., K. Lassen, J. Wilcox, etc. (1971): Interplanetary magnetic field, Polarity inferred from polar geomagnetic field observations. Nature Physical Science, Vol. 233, 38:48.

Krimigis, S. M., E. C. Roelof, T. P. Armstrong, and J. A. Van Allen (1971): Low energy solar particle observations at widely separated points during 1967. J. Geophys. Res., 76, 5921.

Mansurov, S. M., and L. G. Mansurova (1971): Svyaz mehzdu magnitnymi polyami kosmicheskogo prostranstva i Zemli. Geomagnetizm i aeronomiya, tom II, No. I, s. 115.

Matsuda, T., and T. Sakurai (1972): Dynamics of the azimuthally dependente. Solar wind. Cosmic Electr. dyn., 3:97.

McIntosh, P. S. (1972): Inference of Solar Magnetic Polarities from H-alpha observations, Solar Activity Observations and Predictions, ed. P. S. McIntosh and M. Dryer, MIT Press, pp. 65-92.

Mikirova, N. A. (1977): Osobennosti prostranstvennykh i vremennykh kharakteristik SKI v sobytiyakh 19.IV 1972 i 5.VI 1974. Trudy IPG, 35:24.

Mikirova, N. A., and N. K. Pereyaslova (1977): Vliyanie fotosfernykh magnitnykh polei na osobennosti rasprostraneniya protonov solnechnikh vspishek. Dokladi AN SSSR, 234, N. 4, s. 798.

Mikirova, N. A., and N. K. Pereyaslova (1977): Effect of coronal fields on particularities of distribution of protons from the solar bursts. Abstract. Jaga/JAMAP Joint Assembly 1977.

Mikirova, N. A., and N. K. Pereyaslova (1978): Osobennosti vremennykh i spektralnykh kharakteristik solnechnykh kosmicheskikh luchei, obuslovlennye vluyaniem sektornoi st struktury mehz planetnogo magnitnogo polya. Geomagnetizm i aeronomiya, 4:581.

Nolte, J. T., and E. C. Roelof (1973): Large-scale structure of the interplanetary medium. Solar Phys., 33:483.

Pereyaslova, N. K., S. G. Frolov, and T. M. Bezruchenkova (1978): Diagnosticheskoe prognozirovanie radiazsionnykh kharacteristik solnechnykh vspyshek po parametram electromagnitnogo izlucheniya. Geomagnetizm i aeronomiya, N. 6.

Pereyaslova, N. K., M. N. Nasarova, S. M. Mansurov, and L. G. Mansurova (1976): Nekotorye zakonomernosti svyazi solnechnykh kosmicheskikh luchei v polyarnykh oblastyakh s sektornoi strukturoi mehzplanetnogo magnitnogo polya. Geomagnetizm i aeronomiya, tom XVI, N. 3, 407.

Roelof, E. C., and R. E. Gold (1976): Prediction of solar energetic particle event histories using real-time particle and solar wind measurement. Preprint AFGL-TR-76-0136, Johns Hopkins Univ.

Sakurai, T. (1971): Quasi-radial hyper-velocity approximation of the azimuthally dependent solar wind. Cosmic Electr. dyn., 1:460.

Snyder, C. W., and M. Neugebauer (1966): The relation for Mariner-2 plasma data to solar phenomena. Solar wind, Pergamon Press, 25.

Solar Geophysical Data, 1973-1976.

Svalgaard, L. (1968): Sector structure of the interplanetary magnetic field and daily variation of the geomagnetic field at high latitudes. Inst. Geophys. Paper No. R-6, Danish Meteorol. Inst. Chartlottenlund. p. 11.

FORECASTING IONOSPHERIC AND GEOMAGNETIC CONDITIONS AT THE IAG FORECASTING CENTER

S. I. Kuyushkin, A. D. Danilov, A. B. Malyshev,
G. N. Novikova, and P. M. Svidsky
Institute of Applied Geophysics
Glebovskaya 20b, Moscow 107258, USSR

A description of the Moscow Regional Warning Center activity in the field of geomagnetic and ionospheric forecasting.

1. INTRODUCTION

Since 1975, the Institute of Applied Geophysics (IAG) has been serving as a forecasting center of the national ionospheric and geomagnetic service and as the Eurasian Regional Warning Center of IUWDS. To predict geomagnetic activity and ionospheric conditions, the methods developed earlier in IZMIRAN (Zevakina et al., 1975) are being used, although during the last four years some alterations and additions have been made.

The Forecasting Center issues three principal types of predictions:

1. Short-term predictions of ionospheric and magnetic disturbances;
2. Long-term map-like predictions, giving the MUF (maximum usable frequency) distributions all around the world;
3. Long-term predictions of the radiowave propagation along fixed paths

In this work the main emphasis will be made on the description of the first type of forecasting, because on the one hand this type is the most important for customers, and on the other hand, short-term predictions are the most complicated ones, requiring consideration of the whole set of heliogeophysical events. The methods of long-term forecasting are briefly described at the end of the paper.

Short-term forecasting of ionospheric and magnetic disturbances is principally based on the predictions of different kinds of solar activity. The Forecasting Center collects observational data on the current state of solar activity and the interplanetary medium to produce its own solar forecasts, and also receives solar predictions and geoalerts from the other IUWDS regional centers. In this paper, in speaking about ionospheric and geomagnetic forecasting, we will assume that both solar predictions and current solar data are available. We will not discuss the problems of solar activity forecasting.

Although most ionospheric disturbances are genetically connected to geomagnetic disturbances (storms, substorms, etc.), for our customers the most important are the different kinds of ionospheric disturbances because of their drastic influence on such important aspects of everyday life as broadcasting, radionavigation, and so on. Therefore, the main emphasis of this

paper is the different types of ionospheric predictions produced by the Forecasting Center. Collection and distribution of ionospheric data as well as production of ionospheric forecasts comprise the largest part of its operational activity.

Any forecasting network should be based on current experimental data. In the case of magnetic predictions, the work of the center is based mainly on real-time data on three-hour K-indexes for Moscow (IAG), as well as on diurnal reports on a_K-values and three-hour K-indexes from 10 Soviet stations and 10 stations outside the USSR. Ionospheric forecasting has a large bank of real-time data, collected in the Forecasting Center. The heart of the bank consists of vertical sounding data from the Soviet network of ionospheric stations. A list of the stations sending current information hourly is given in Table 1 (Sukhodolskaya and Shchuka, 1978), and the list of the collected parameters in Table 2. The center receives the vertical sounding data from 14 stations abroad also.

Table 1. List of the vertical sounding stations used in real-time service.

NN	Name	Station number	Type of telegram
1.	Alma-Ata	38401	II
2.	Arkhangelsk	34601	I
3.	Ashkhabad	36401	II
4.	Dixon	38701	I
5.	Irkutsk	40501	III
6.	Kiev	33501	III
7.	Volgograd	34505	I
8.	Leningrad	33603	I
9.	Magadan	45601	III
10.	Moscow	34502	II
11.	Murmansk	33702	III
12.	Novosibirsk	38501	II
13.	Podk. Tunguska	39601	I
14.	Salekhard	37701	III
15.	Sverdlovsk	36602	II
16.	Rostov	34506	I
17.	Tashkent	37401	II
18.	Tomsk	38601	III
19.	Yakutsk	43601	III
20.	Khabarovsk	43501	III
21.	Krenkel	36801	I
22.	Cape Schmidt	28701	III

In addition to the vertical sounding data, the Forecasting Center receives the following real-time ionospheric information: riometer observations in the high-latitude zone (Murmansk, Dixon, Krenkel, Amderma), data on sudden ionospheric disturbances (SID) observed in short wave fade-outs (SWF), and VLF phase anomalies (SPA).

The collection of data is arranged on a regional basis. Together with the Forecasting Center in IAG, four more subcenters operate in Murmansk

Table 2. List of ionospheric parameters sent to the Forecasting Center.

Parameter	Type of telegram I	II	III
foF2--critical frequency of the F2 layer	+	+	+
h'F2--minimum virtual height of the F2 layer	+	+	
M-3000-F2--Maximum usable frequency factor for the F2 layer	+	+	+
f_{min}--minimum registered frequency	+	+	+
foEs--critical frequency of Es	+	+	+
foF1--critical frequency of the F1 layer		+	
h'F--minimum virtual height of the F layer		+	
M-3000-F1--maximum usable frequency factor for the F1 layer		+	
h_pF2--height of the electron concentration maximum		+	
foE--critical frequency of the E layer		+	
h'E--minimum virtual frequency of the E layer		+	
f_bEs--blanketing frequency of the Es layer	+	+	
type of Es	+	+	

(Polar region), Khabarovsk (East region), Novosibirsk (Siberian region), and Tashkent (Central Asian region). The functions of the subcenters are collection and transmission to the center of current data in the region and provision to the local customers of current information and of short-term (less than one day) forecasts.

All the data collected in the Forecasting Center are used both for immediate transfer to the customers and for producing and correcting the short-term predictions described below.

2. VARIATIONS OF THE IONOSPHERIC PARAMETERS

Any detailed consideration of ionospheric aeronomy is beyond the scope of this paper; therefore in this section we mention only the main variations of the ionospheric parameters and the probable sources of their appearance.

Electron concentration [e] in the F2-layer maximum determines the most important parameter of ionospheric forecasting, critical frequency (foF2), and undergoes several well-known regular variations. These are (1) diurnal variations, where [e] decreases from daytime to nighttime following the increase of solar zenith angle χ; (2) variations with solar activity, in which noon values of [e] (under other equal conditions) are higher with higher solar activity index (radiowave flux at 10.7 cm, F_{10}, or Wolf number, W); (3) seasonal variations, due to which noon concentrations in winter are higher than in summer (so-called "winter anomaly" in the F2 layer); and (4) some other less important but known regular changes in electron concentration.

All such changes are being accounted for in long-term forecasts (these forecasts include all regular variations because they are based on the analysis of the huge set of experimental data from the previous years) and in medians in short-term predictions. Short-term predictions themselves are

needed because of the existence of irregular variations of the ionospheric behavior due to different solar and geomagnetic events.

Immediately after a rather strong solar flare the X-ray fluxes with λ = 1-20Å intrude the region of the lower ionosphere, producing a sharp increase of [e] at the D-region heights (60-90 km) in the entire sunlit ionosphere. The increase of electron concentration leads to a strong increase of short-wave absorption as well as to the appearance of some anomalies in the propagation of low frequency and very low frequency radiowaves. The entire set of these events is usually called "sudden ionospheric disturbances" (SID). The duration of SID may vary from several minutes up to an hour or more.

If during the solar flare energetic protons with the energy of tens of mev have been emitted, several hours after the flare they enter the Earth's atmosphere in the polar cap region and produce strong enhancement of the D-region ionization. This event is called "polar cap absorption" (PCA). In its influence on radiowave propagation it is similar to SID, but has much longer duration, very often as long as several days.

The flux of the kev corpuscular radiation (low energy plasma) emitted during the solar flare, as well as that borne in the flare shock waves, arrives in the vicinity of the Earth much later--several tens of hours--after the flare. The low energy plasma and the shock waves influence the Earth's magnetosphere, which causes different events: magnetic storms and substorms, "precipitation" of the particles from the radiation belts, increase of the ring current, and so on. They in their turn produce a whole set of disturbances in the ionosphere. As a result of the intrusion of kev-energy electrons, the electron density at 70-80 km in the auroral zone increases, which produces the event of "auroral absorption" (AA). Simultaneously the heating of the upper atmosphere in the auroral zone takes place because of several factors (Joule heating, absorption of the corpuscular radiation, and so on), which causes a change in the neutral composition of the thermospheric gas. The $[O]/[N_2]$ ratio, which in the F2 region during daytime conditions governs the electron concentration ($[e] \propto [O]/[N_2]$), decreases because of the temperature increase. The effect of the $[O]/[N_2]$ decrease due to dynamic processes, the exact nature of which is still obscure (meridional circulation, gravity waves) is transferred with diminishing amplitude to lower latitudes, leading to a corresponding depletion of [e] in the mid-latitude F2 region. In other words, "negative ionospheric disturbance" takes place. Negative disturbances often follow recurrent magnetic disturbances, and are not connected directly with solar flares, but with the passing through the central meridian of the sun of the geoactive regions. The principal mechanism of the negative ionospheric disturbance in this case is probably the same, but the intensity as well as the duration and the velocity of the penetration to the lower latitudes might differ very much depending on the type of active region and the corresponding geomagnetic disturbance.

Still very poorly understood is the nature of the other type of F2-region events--positive disturbances (enhancements of [e] and correspondingly of foF2). Often positive disturbances appear just prior to or immediately after the so-called "sudden commencement" (SC) of the magnetic storm detected by the ground-based observations. The possible mechanism of this disturbance is associated with the increase of charged particle fluxes from the plasmasphere and with the changes in atmospheric circulation at the F2-region altitudes. Fortunately, since positive ionospheric disturbances do not influence the radiowave propagation in so drastic a way as negative ones, the question of their prediction is not so critical as the prediction of the latter.

A very important event in the ionosphere is the appearance of narrow layers of electron concentration at altitudes of 100-120 km, the so-called sporadic-E layer (Es). Es may influence essentially radiowave propagation, causing an absorption (and sometimes a complete screening) of the short-wave radio signals reflected from the F2 region. The processes of Es formation are still very poorly known (they may be quite different for, say, the mid-latitude narrow layer formed by the wind-shear mechanism than for thick Es in the auroral zone formed probably by corpuscular ionization) and so there is no basis now for Es forecasting.

3. SHORT-TERM FORECASTS

The Forecasting Center issues four types of short-term forecasts of ionospheric and magnetic disturbances:

1. Monthly
2. Five-days
3. Two-days
4. Semidiurnal.

In short-term forecasting a very important device is a synoptic map of helio-geophysical events that is being currently built in the Center. A schematic example of such a map is shown in Figure 1. The following information is presented on the map: active formations on the sun (spots, flares, etc.); proton fluxes with E = 40-500 Mev and X-ray fluxes with λ = 1-8Å; solar radiowave flux at 10.7 cm and 1.2 m, 3-hour magnetic K-index for Moscow; critical frequency deviations δfoF2 for Moscow; and intensity of the cosmic rays according to space monitor data.

For short-term forecasting, maps of the 27-day recurrence of geomagnetic and ionospheric events ("Bartels carpets") are also currently being built in the Center. Such maps are being built for the following parameters: the degree of disturbance of the geomagnetic field for Moscow station; critical frequency deviations δfoF2 and intensity of Es for Moscow, Alma-Ata, Yakutsk, Murmansk, and Krenkel stations; and the probability of the appearance of absorption and diffusivity for Murmansk and Krenkel stations. An example of "carpets" for magnetic disturbances (Moscow) is shown in Figure 2.

While preparing monthly forecasts with the help of corresponding Bartels carpets, the periods of probable geomagnetic disturbances are determined and the probabilities of different kinds of ionospheric events (foF2 disturbances, Es appearance, absorption) are estimated. Carpets, as a rule, show the tendency of the development of the recurrent events--decreasing or increasing--and thus can possibly correct the prediction relative to the previous solar rotation (the previous line in the carpet).

It is worth mentioning that, as is widely known, recurrent forecasting works reliably enough during the years of decreasing solar activity--at the beginning of a new solar cycle the recurrence is often distorted because of the permanent birth of new active regions.

Synoptic mapping allows correction of the above-mentioned recurrent forecast, taking into account the new active formations that have appeared on the sun during the previous rotation.

Monthly forecasts, produced by the Forecasting Center, consist of predictions (for each day of the coming month) of the following parameters: geomagnetic disturbances for Moscow; critical frequency deviations δfoF2 for Moscow, Kiev, Alma-Ata, Irkutsk, Khabarovsk, Krenkel, and Murmansk

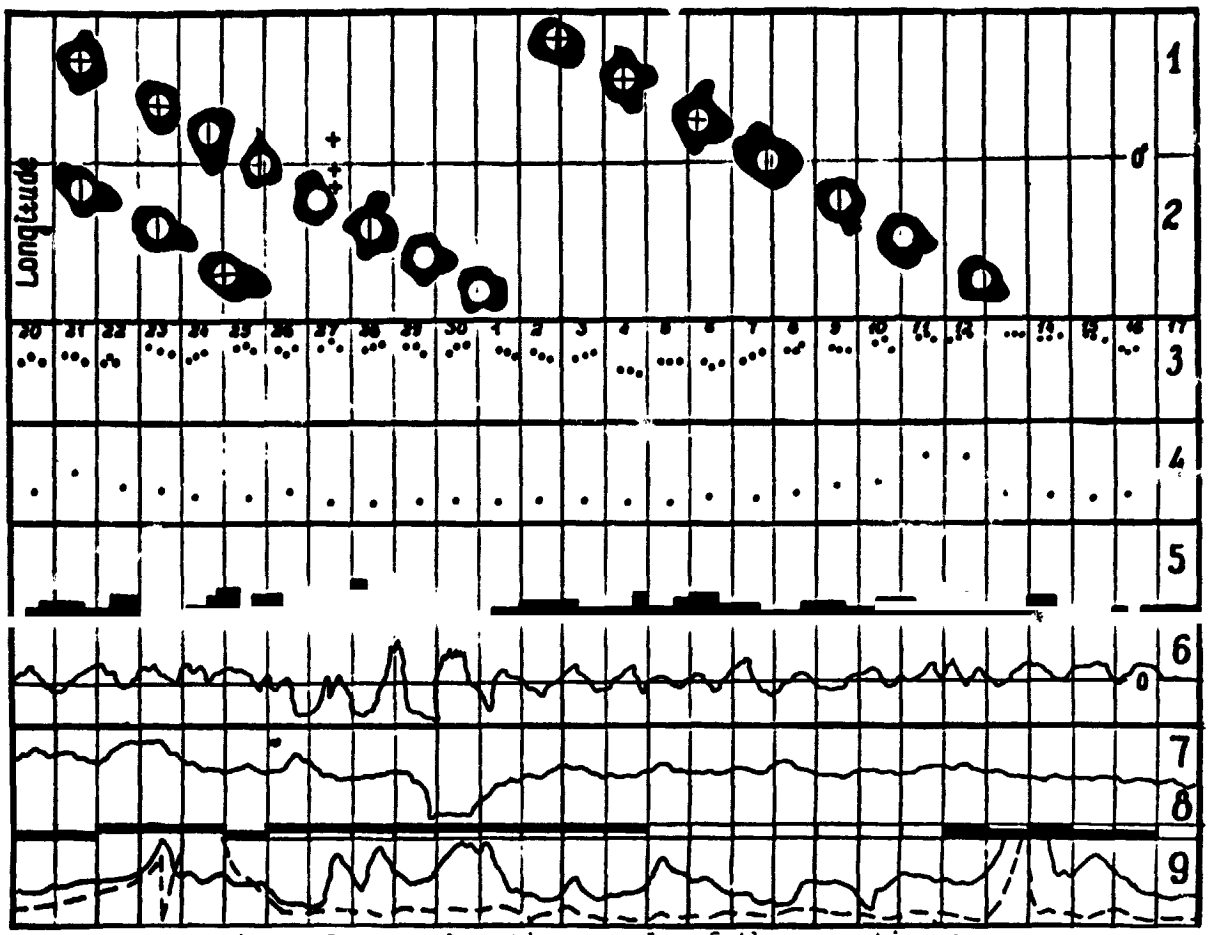

Figure 1. A schematic example of the synoptic map.
1 - Eastern hemisphere of the sun
2 - Western hemisphere of the sun
3 - Solar radiowave flux at 10.7 cm
4 - Solar radiowave flux at 1.2 cm
5 - Geomagnetic K-index for Moscow station
6 - δfoF2
7 - Cosmic rays
8 - Sign of the interplanetary magnetic field
9 - X-ray fluxes with λ = 1-8Å and proton fluxes with E = 40-500 Mev.

stations; intensity and probability of appearance of Es for Murmansk and Krenkel stations; and probability of absorption and diffusivity for Murmansk and Krenkel stations. Monthly predictions are issued on the 25th of each month and are sent to customers by mail and to the regional subcenters by telegraph.

The five-day forecast is a specification of the monthly prediction. The basis of forecasting remains the same as that of the monthly prediction, but emphasis is changed from recurrence (Bartels carpets) to the real events (synoptic maps). Both the events which took place on the sun during the previous days and the forecast of solar activity are taken into account.

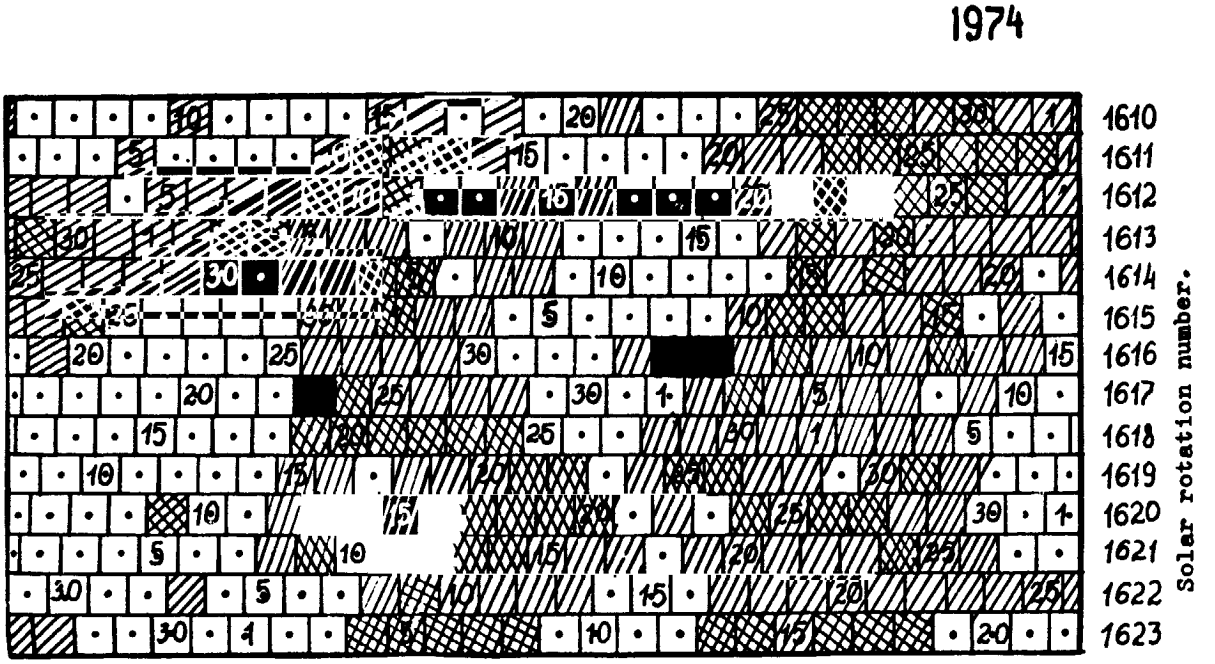

Figure 2. "Bartels carpet," 1974, geomagnetic disturbances, Moscow station.

1 - quiet
2 - weak disturbance
3 - moderate disturbance
4 - strong disturbance

If a geoeffective solar flare is expected, the forecast includes all the corresponding effects mentioned above (magnetic disturbance, PCA, AA, negative ionospheric disturbance). It is assumed that PCA events will begin 1-10 hours after the flare and a geomagnetic storm 25-30 hours after the storm. When flares are relatively weak (not followed by the 4th type radio outbursts), PCA events are not predicted and the time delay for the magnetic storm is taken to be about 50 hours.

Special attempts have been made (Frolov, 1979) to develop an algorithm to decide whether during the flare a geoeffective shock wave has been emitted. Such an algorithm considers the characteristics of the X-ray and the radio-emission of the flare (class and brightness, times of increase and decay of X-ray emission, spectral characteristics of radioemission) to decide if a shock wave has been emitted and what is the expected time of its arrival to the Earth. The average time delay in such a case is about 50 hours and with the above-mentioned method it may be estimated with an accuracy of about 10 hours.

Magnetic storms may also appear 4-5 days after a geoactive region crosses the central meridian of the sun. The duration of the storm depends on the level of solar activity. During solar minimum it generally is 4-5 days, decreasing with an increase of solar activity.

The five-day forecast includes the following parameters for each day: magnetic disturbances; critical frequency deviations $\delta foF2$ for 22 Soviet sta-

tions and 3 stations outside the USSR (Wallops, Juliusru, and Boulder); intensity and probability of Es appearance for Moscow, Murmansk, Alma-Ata, Yakutsk, Krenkel, and Dixon stations; and appearance probability of absorption and diffusivity for Krenkel, Dixon, and Murmansk stations.

In the five-day forecast the mean values of some parameters are included. These values are calculated each five days for the previous five days (running median) taking into account only magnetically quiet days. These mean values serve as a forecast of quiet ionospheric conditions. All the deviations (due to the appearance of some disturbances) given by five-day, two-day, and semi-diurnal predictions, are scaled from these mean values. The five-day forecast includes medians of foF2 and the M-3000-F2 coefficient for 22 Soviet stations and 3 stations outside the USSR (Wallops, Boulder, and Juliusru). The five-day forecast is issued by the Forecasting Center on days 5, 10, 15, 20, 25, and 30 (31) of each month and is sent to customers by telegraph and broadcast.

In the regional subcenters, at the request of customers, the short-term (five-day) forecast of the radiowave propagation conditions for the fixed path is also issued. The forecast is based on two groups of data: mean values of foF2 and M-3000-F2 in the reflection point (if there is no ionospheric station at this place, interpolation is made between the nearest stations) and the five-day forecast of the deviation of both parameters from the median. As a result, the optimal working frequency (OWF) for this particular path for the coming five days in quiet conditions as well as the expected deviations δ(OWF) for each day are obtained directly on the computer.

The next specification of the expected situation in the ionosphere and the geomagnetic field is made in the two-day forecast. This forecast is based on the same current data on solar and geomagnetic activity as the five-day prediction. The two-day forecast gives a non-technical description of the disturbance degree of the ionospheric F2 region for five principal regions of the USSR: Polar cap (Krenkel), Auroral zone (Murmansk), European part (Moscow), East (Yakutsk), and Central Asia (Alma-Ata).

The final specification of the ionospheric prediction is given in the semi-diurnal forecast. In producing this forecast the main emphasis is on the current magnetic and ionospheric data. When predicting the negative ionospheric disturbance the velocity of movement of such a disturbance from the high to the middle latitudes is taken into account. Thus, during the daytime the first minimum on the foF2 curve (maximum of the negative disturbance) appears in Moscow about an hour later than in Leningrad, and in Kiev an hour later than in Moscow. The time delays of δfoF2 minimum relative to the beginning of the magnetic storm for several stations, situated at different latitudes, are shown in Figure 3. It is seen from the figure that the average velocity of the negative disturbance expansion southward along the meridian is about 100 m/sec, which is close to the mean velocity of the meridional circulation at the F2-region altitudes (Kazimirovsky, 1978).

In the southern regions of the Soviet Union the effects of magnetic storms as a rule are not registered in the form of pronounced negative or positive disturbances. The reaction in the low-latitude ionosphere is the appearance of instability of the F2 layer, when the critical frequencies suffer irregular variations with amplitude not higher than 15-20 percent. This fact shows that wave-like disturbances (travelling ionospheric disturbances, for example) generated during the storm in the auroral zone have obviously arrived at these low latitudes.

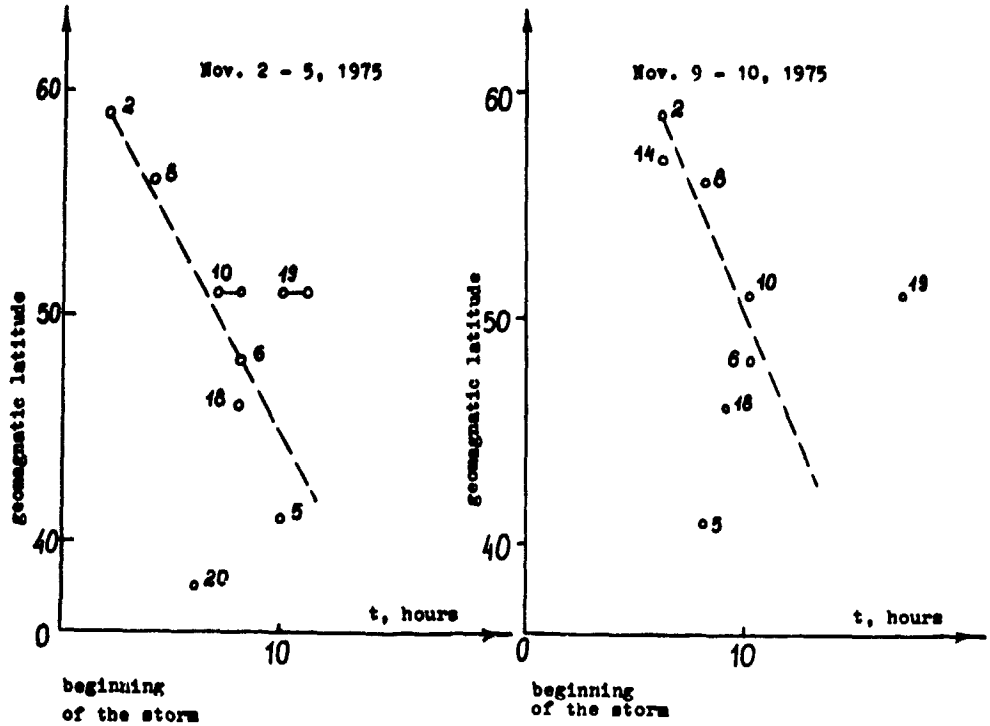

Figure 3. Time delay between the beginning of the magnetic storm and the maximum of negative ionospheric disturbance for different stations (numbers correspond to the station list in Table 1).

When there is no well-pronounced ionospheric disturbance the ionospheric behavior is predicted based on the comparison of the current observational data and the median given by the five-day forecast. The forecaster compares the predicted diurnal curve of foF2 and the experimental points and, based on the behavior of the experimental data, makes corrections to the mean values to produce the forecast for the next 12 hours.

The semidiurnal forecast includes the following parameters: for Polar Cap (Krenkel) and Auroral Zone (Murmansk) stations--δfoF2, intensity and appearance probability of Es, absorption and diffusivity; for European area (Moscow), East (Yakutsk), and Central Asia (Alma-Ata) stations--δfoF2, intensity and appearance probability of Es. The semidiurnal forecast is broadcast twice a day.

The verification of short-term predictions is rather difficult. First of all, whether a forecast proves to be true depends on the method of its estimation. There is no commonly accepted method and creating one seems to be a rather difficult task both because it is very difficult to determine the degree of coincidence between the forecast and the real situation in the ionosphere and also because the deviation of the real situation from the prediction in different directions (for example towards higher or lower values of foF2) have often quite different meanings for different customers.

Table 3 shows the percent of different types of short-term predictions (described above) proved to be true for two months of 1976 (solar minimum) and two months of 1978 (increasing solar activity). The principle of verification

Table 3. Verification of the forecasts of different types (monthly average in percent)

	September 1978	September 1976	July 1978	July 1976
		Magnetic forecasts for Moscow		
Monthly	63	87	68	100
Five-day	87	91	55	100
Diurnal	92	95	87	100
		Ionospheric forecasts for Moscow		
Monthly	82	82	97	100
Five-day	83	82	93	100
Semidiurnal	95	95	93	100

is the one suggested and formerly used by IZMIRAN: the forecast for this particular day and for this particular parameter is considered proved true if the difference between the forecast and the observation does not exceed one step.

As one can see from Table 3, in the years of decreasing and minimum solar activity, the percentage of the forecasts based on recurrence (monthly, five-day) proved true is essentially higher than during the increasing phase of the cycle. This difference confirms the above-mentioned fact that the recurrence "works" well during the second part of each solar cycle and poorly in the beginning of a new one.

For the shorter predictions the difference is smaller and evidently reflects the higher probability of error in the forecast when the number of events to be predicted is higher.

4. LONG-TERM FORECASTS

As mentioned previously, the Forecasting Center issues two types of long-term prediction: map-like forecasts of maximum usable frequencies (MUF) all around the globe and forecasts of radiowave propagation along fixed paths. Both types of prediction are based on the work done by IZMIRAN (Chernyshov and Vasilieva, 1973). In that study, data collected during 15 years (up to 1971) from the world-wide network of ionospheric vertical soundings (129 stations) was analyzed. This analysis allowed a description of the global distribution of the F2-parameters in space and time in the form of a set of spherics functions. Corresponding series coefficients for these functions (Chernyshov and Vasilieva, 1973) provide the basis of long-term predictions.

Monthly forecasts of MUF are issued by the Center 4-6 months in advance and contain maps of the distribution all around the globe of two main parameters, the critical frequency of the F2 layer for vertical incidence of radiowaves, foF2, and the critical frequency of the F2 layer for oblique incidence of radiowaves for the distance to the reflection point equal to 4000 km, MUF-4000-F2.

The maps of these two parameters allow calculation, using the well-known formulas, of values of MUF for any given distance if the radiowaves are reflected from the F2 layer. The maps of foF2 and MUF-4000-F2 are given for even hours of Moscow time. Figures 4 and 5 show examples of the maps.

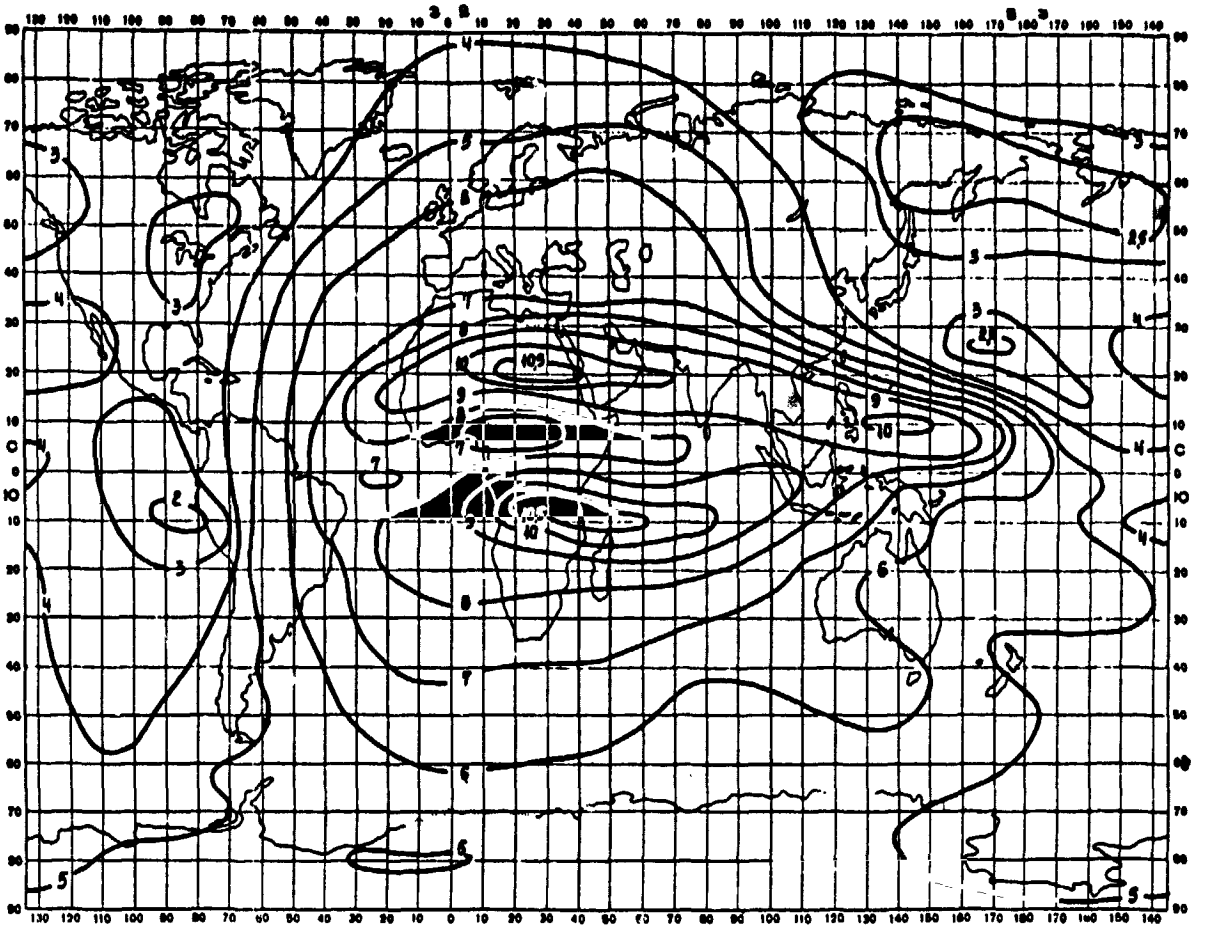

Figure 4. An example of the critical frequency (foF2) distribution (in Mhz) around the globe (long-term forecast; February 1977, 1400 Moscow time).

When radiowaves are propagated a small distance, the reflection from lower layers (F1 and E) may appear to be essential, so in the monthly long-term forecast, figures for MUF determination in cases of F1-reflection (a distance less than 3000 km) and E-reflection (a distance less than 2000 km) are also presented.

The key parameter in long-term forecasting is the smoothed Wolf number of solar spots, W, which is forecast for the center by the Main Astronomical Observatory (Pulkovo) six months in advance.

Long-term predictions of radiowave propagation along fixed paths are made on the request of customers on the basis of the same methods. The predictions contain diurnal variations of MUF and lower usable frequency (LUF) for the particular path and the given month. The variation of LUF is calculated for the fixed transmitter power of 1 kW. An example of prediction of this kind for the path Moscow-Yakutsk (March 1979) is shown in Figure 6.

However, LUF appeared not to be a very convenient parameter for the customers, so now work is being done to substitute LUF by more informative parameters, which characterize the expected weakening of the signal, or its amplitude directly.

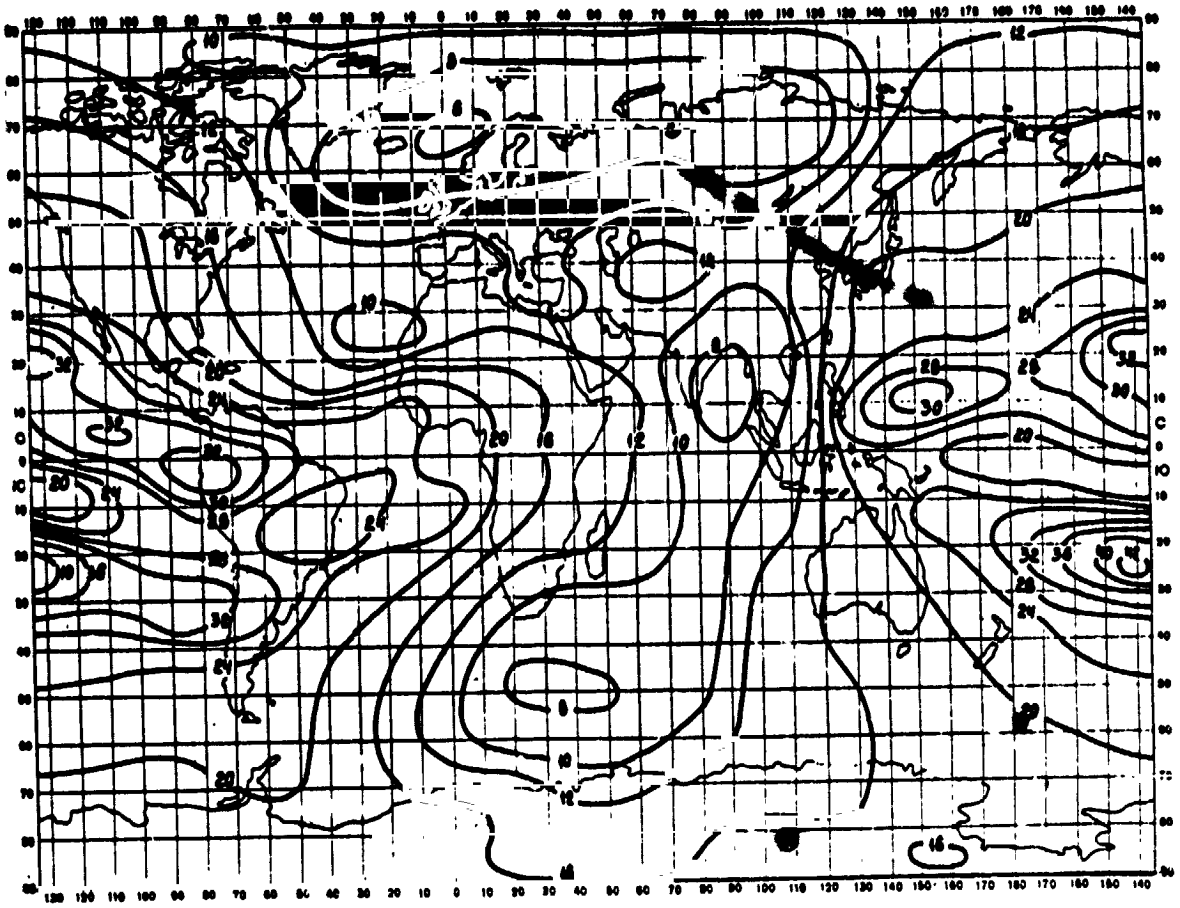

Figure 5. An example of MUF-4000-F2 distribution (in Mhz) around the globe (long-term forecast; February 1977, 0400 Moscow time).

In conclusion, two points should be noted:

- All the work on long-term forecasting in the center is done on computers.
- All the long-term predictions, as was already mentioned, give a mean picture of the forecast behavior of the parameters and thus reflect only regular variations (with latitude, longitude, season, etc.) of the ionospheric layers.

5. CONCLUSION

The above-described activity of the Forecasting Center provides the necessary current information and forecasts for most of the customers. But to increase the amount of distributed information and to improve the reliability of the forecasts, further development of the observational system and the forecasting methods is greatly needed.

Principally, the new method of forecasting should be based not on the previous year's statistics, but on the physical models of the ionosphere (Vlasov, 1979). Presently in the Forecasting Center, appraisal of the

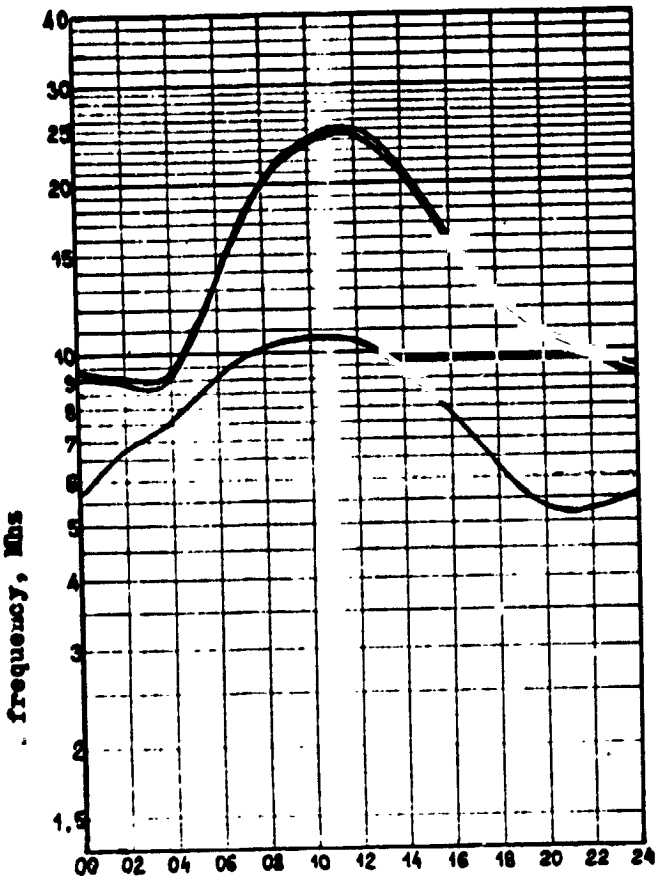

Figure 6. An example of a long-term forecast for the fixed path (Moscow-Yakutsk, March 1979), upper lines--MUF; lower line--LUF.

specially made physical models is being made. The models are being checked from the point of view of the possibility of using them to produce different kinds of forecasts. Evidently such models may be used to predict regular variations of the ionospheric parameters (long-term forecasts) even now. However, as soon as we get more information about the aeronomical parameter variations during ionospheric disturbances, such models may be involved in the forecasting of disturbed conditions (short-term forecasts).

There are very few methods, if any, of D-region state forecasting. At the same time, such forecasts are more and more urgently needed. Presently there is even no real-time information about the lower ionosphere. In vertical-incidence soundings, the only parameter connected with the lower ionosphere is f_{min} (minimum observable frequency), which is not reliable enough because it depends on the characteristics of each particular ionosonde.

The Forecasting Center plans in the immediate future to receive real-time information on the electron concentration profiles in the D region near Leningrad, obtained by the partial reflection method. Having obtained these

data, the Center would be able to provide customers with information on the current state of the lower ionosphere and also to start developing methods for its prediction.

Forecasting of the lower ionosphere (D region) may appear to be something quite different from F2-region forecasting because of the strong influence on the D-region behavior of meteorological factors. According to modern views this behavior is controlled by two groups of parameters: usual geophysical parameters (solar activity, magnetic activity, local time, and so on) and meteorological parameters (stratospheric warmings, circulation at stratospheric and mesospheric levels, thermal regime of the mesosphere, and so on), which makes the problem of D-region forecasting a real burden.

Vertical sounding is still the principal method of getting information about the F2 region. To increase the amount of this information, several additional steps should be made: developing new ionosondes with better potentials; using the network of oblique sounding stations; and launching an ionosonde on-board a satellite. In the latter case, the system of trans-ionospheric sounding may be created, where the signals of the ionosonde are being received by the ground-based network of the ionospheric stations, thus obtaining the real-time distribution over a large range of critical frequencies for different distances.

REFERENCES

Chernyshov, T. V., and T. N. Vasilieva (1973): Forecast of maximum usable frequencies, Nauka Publishing House, Moscow (in Russian).

Frolov, S. G. (1978): Doklady Academii Nauk 243, N. 3.

Kazimirovsky, E. S. (1978): The dynamics of the quiet thermosphere. Review paper presented at STP Symposium, Innsbruk, May 1978.

Sukhodolskaya, A. N., and T. I. Shchuka (1978): Submitted to Bull. INAG.

Vlasov, M. N. (1979): Paper presented at this workshop.

Zevakina, R. A. et al., (1975): Methods of short-term forecasting of magnetic activity and ionospheric conditions. Preprint IZMIRAN N055(02) (in Russian).

D/0-32

N80-18472

LONG TERM SOLAR ACTIVITY AND IONOSPHERIC PREDICTION SERVICES RENDERED BY THE NATIONAL PHYSICAL LABORATORY, NEW DELHI

B. M. Reddy, S. Aggarwal, D. R. Lakshmi,
S. Shastri and A. P. Mitra
Radio Science Division
National Physical Laboratory
New Delhi - 110012, India

The Radio Science Division (RSD) of the National Physical Laboratory is rendering solar and ionospheric prediction services since 1955. RSD is one of the few groups in the world with independent solar prediction activity essentially intended to improve the quality of ionospheric communications. The scope of this paper is to project the data base used in the prediction exercise, to describe the prediction technique and to compare with actual observations. No examples of specific circuit predictions are described, for they are derived routinely from contour outputs with the aid of standard nomograms and conversion tables. Emphasis is laid on the data base and the technique itself so that the present state of art can be appreciated and critically examined. Future plans include more computer-oriented solar predictions and computerisation of all link predictions including required radiated power, field strength and lowest useable frequency calculations.

1. INTRODUCTION

One of the basic objectives of the Radio Science Division (RSD) of the National Physical Laboratory, N. Delhi is to predict the radio environment and advise on communication problems. These include ionospheric and tropospheric radio communications. This paper is purported to summarize our efforts in predicting the ionospheric communication parameters only. Of the various ionospheric regions, the D-region is relevant only in estimating the attenuation, while the E layer is more systematic and easily predictable. This leaves us essentially with the F-region with its two most important communication parameters, the critical frequency and the height factors. Some work has been done at RSD in predicting the sporadic E layer also, but that is not included in this presentation.

The charged particle population in the ionosphere naturally depends upon the neutral atmosphere which presents the ionizable constituents and on the ionizing from the sun (particle effects are also important at high latitudes). While all radiations including the visible and infrared may be responsible

for the neutral atmospheric profiles, the ionizing radiations are essentially the EUV and X-ray radiations which undergo large variations with the solar epoch. The ideal solution of course would be to measure these ionizing radiations and then predict their levels for the future years. These measurements are impossible on a routine basis. One alternative, therefore, is to monitor the sun using those radiations (like the VHF and SHF radio waves) which reach the ground-based sensors unhindered by the intervening terrestrial atmosphere and correlate these measurements with ionosphere producing radiations. However, because of the availability of long series of observations, the sunspot number has been found by us as well as by other groups in the world, to be most suitable for statistical prediction techniques.

The solar activity study, which was started 200 years ago out of scientific curiosity, had assumed great importance by the second quarter of this century because of ionospheric communications. Since recent years, the interest in this study has sky-rocketed because of its potential applications in a wide variety of areas of human interest, such as environmental effects and biological aspects, sun-weather relationships, satellite lifetimes and manned space flights. It was found necessary to start our own solar predictions at RSD because of the special requirements of different user organizations in the country. For example, it is required to predict the activity at different advance intervals like one year, two years or three years to enable long-term planning and frequency clearance from the appropriate governmental authority. Though the ionospheric prediction technique used at RSD is not very different from other techniques, the wealth of data that has gone into the system and the continuous updating as new data pours in, has instilled a certain measure of confidence among the users in the East zone and especially in India where H.F. communications still remain as the backbone of long distance communications. This brings in enormous pressure in conserving the H.F. spectrum and consequently the assignments of frequencies to users is rather involved and time-consuming. This is one reason why short-term forecasting was not very much in demand until recently. We are presently giving short-term forecasting also, but those details are beyond the scope of this presentation.

2. SOLAR ACTIVITY PREDICTIONS

Ever since cyclical variations in solar activity were recognized, there have been many attempts to predict them. When they were found to have close correlation with ionization density in Earth's upper atmosphere, the studies gained impetus from their practical application to radio communications. Sunspots, which are seen as dark patches on the photosphere of the sun, are centers of high magnetic activity that inhibit convection. Many characteristics of the sun such as sunspot number, sunspot coordinates, sunspot area, flare brightness, radio emission level, etc., are observed directly and depict solar activity changes of long- and short-term durations. However, sunspot numbers have the longest series of observed data available in a standard coded form, and this is the single most important reason to continue sunspot numbers for prediction purposes in spite of its subjective nature. Sunspot number prediction methods to-date have been based on analysis of past data as a function of time, the prediction being an extrapolation of the

statistical analysis to some future time. The generally accepted series of observation extends back to over 200 years and when this data is separated into twenty 11-year cycles, the variability of these cycles is found to be so much that each cycle seems to be unique in some way or the other.

2.1 Data Base and its Salient Features

The basic data that supports our long-term solar activity predictions is naturally the Zurich series of sunspot data dating back to 1749. This series has been developed by Rudolf Wolfe in 1848 when he introduced a sunspot number formula and applied it to old records of observed data retrospectively from 1749. There have also been some attempts (Shove, 1955) to obtain maxima and minima for sunspot cycles for periods earlier than 1749 by using other indirect geophysical observations like Aurora.

Considerable efforts have gone into keeping the method of handling observations of sunspot data as nearly uniform as possible and just this feature of the Zurich series makes it particularly useful as a forecasting tool. Other geophysical observations have much shorter histories. Even the ionospheric electron density observations cover something less than four solar cycles. Because these other direct observations cover so few cycles, it is almost impossible to identify and evolve from them any statistical relationships among successive cycles. Instead, it has been noted that during their short histories they exhibit a high correlation with the sunspot number data. It is generally assumed that observed correlations will be equally good over the long-term. In order to study the long-term changes in sunspot activity, the data is smoothed to 12-month running average numbers defined as below:

$$\left[R_{12}\right]_n = \frac{1}{12}\left[\sum_{n-5}^{n+5} R_k + \frac{R_{n-6} + R_{n+6}}{2}\right]$$

for the month n, where R_k is the monthly average sunspot number of the month k. It is this smoothed sunspot number R_{12} with which most of the ionospheric and atmospheric density parameters show a high degree of correlation. The main feature observed in these long series of observations is that besides the 11-years cycle, there is another cycle of period 78-to-80 years in the peaks of the cycle; but cycle no. 19 has been very unusual in all its aspects suggesting that perhaps there is another periodicity of a longer duration. Different methods have been used at different times to sort out the different periodicities in this series. Cole (1973) has used power spectral analysis for detecting the significant periodicities in relative sunspot numbers. The resultant spectra reveal that the mean cycle length of 11.06 years and the 190-year phase modulation are a resultant of two periods of 11.8 and 10.45 years representing a characteristic free running time for the solar cycle and a well-defined periodicity which excites the new solar cycle. Kuklin (1976) has identified several cyclic, secular and super secular variations in solar activity viz. 11, 22, 80-90, 1000 and 1700-1900 year periodicities.

2.2 RSD Prediction Procedure

A number of mathematical and statistical schemes were evolved in this century to arrive at some empirical relationships to predict the sunspot number (Waldmeier, 1946; Stetson, 1947). All of them basically revolve around the game of guessing based on the general pattern of recurrences discernible in the available series of observations.

The sunspot prediction activity was started at RSD during 1955 when the 19th cycle was in progress and the predictions continue ever since. The general principle involved in making a prediction is to predict an average cycle. Instead of mechanically averaging all the previous cycles, the emphasis is laid on the known long-term variations in arriving at the average cycle. Statistical tests are made to identify and evaluate the validity of past cycles and those that belong to an entirely different statistical population are rejected (see for example Slutz et al., 1971). As the cycle progresses, all the observed values from the start of the current cycle are used to update the pattern of growth. Since these constitute standard statistical procedures, the details are not worked out here. However, some empirical relationships were also evolved from the then available eighteen cycles and these relationships were used in the predictions.

Some of the main features observed in the first eighteen cycles which were used as a basis for evolving the empirical relationships are:

a) There is an inverse relationship between the peak value of the cycle and the growth period.

b) Though the cycles with high peaks rise sharply, the decay is slower, thereby maintaining the total duration of the cycle approximately constant.

c) As a corollary to (a) above, the area under the sunspot curve from minimum to maximum will be approximately constant.

d) The initial gradient of a cycle has a definite relationship with the peak of the sunspot cycle.

It may be seen from Figure 1 that a fairly significant straight line relationship exists between the peak value of the sunspot number and the corresponding reciprocal of growth period (plotted as ordinate on the left side as the reciprocal of growth period in months). However, cycle nineteen was an exception and was not bound by this simple relationship. Once it is known that we are in the ascending phase of the cycle, a small right angle triangle is formed in the new cycle with the minimum and the most recently measured value forming the two ends of the diagonal. A triangle is also formed for the previous cycle with the previous cycle with the minimum and the peak of the cycle constituting the two extreme points of the diagonal. With the aid of these two triangles and employing the empirical relationship that the area under the sunspot curve from minimum to maximum is approximately constant, the growth period and the peak of the new cycle can be predicted. Of course, the periodicities other than 11 years are also kept in

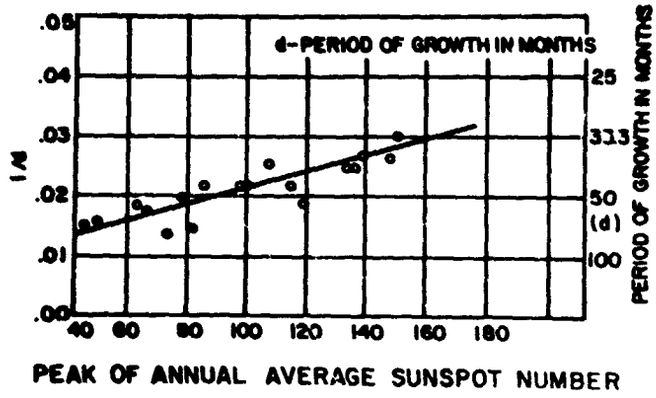

Figure 1. Reciprocal of the growth period (in months) plotted against peak of annual average sunspot numbers for first eighteen cycles. Period of growth, d, (in months) is also shown on the right. A linear relationship can be seen between peak sunspot numbers and (1/d).

mind while making the final estimate of the peak of the cycle. These estimates are updated every month using the most recently observed data.

The characteristic cumulative growth rate from the start of a cycle in successive steps of 6 months is plotted against the peak sunspot number (Figure 2) for the first eighteen cycles and this empirical relationship is used to construct the growing part of the cycle as new observations are added. Once an identifiable peak is reached in the current cycle, the earlier cycles are scanned through to pick up cycles of approximately the same peak value as of the current cycle (within ± 20). These cycles are then superposed on the peaks and an average cycle is evolved which is used to predict the declining phase of the cycle. For example, while predicting the declining phase of the 19th cycle, the average of 2nd and 18th cycles in the series were considered, for these happened to be the two high-peaked cycles in the Zurich series. A comparison is made of the preceding twelve observed values of the current cycle with those predicted from the average cycle. The ratio of the observed values to the values predicted for the declining phase from the average cycle are found to be approximately constant for about 12 months; and this feature is used to predict and update the declining phase continuously. As the trend of the declining phase emerges out more definitely, once again appropriate cycles are chosen from the past cycles to match with the now-emerging trend. This procedure is repeated as often as is found necessary and new adjustments are effected in the average cycle and the prospective minimum. Obviously, near the peak and the grough where the gradients almost disappear, prediction is rather speculative and no reliable method exists to improve this situation.

Comparisons of the RSD predictions and Zurich predictions are presented in Figures 3(a) and 3(b) for cycles 19 and 20 respectively, along with the observed values. It may be noticed that during the unprecedented high

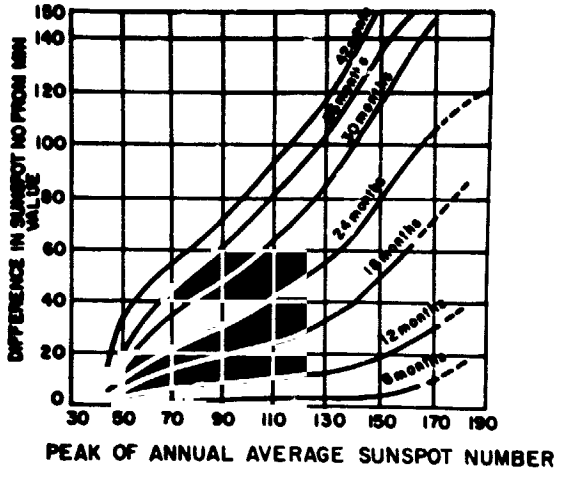

Figure 2. Gradients in sunspot numbers at different stages (6, 12, 18,.....months from the minimum) for growing part of solar cycles are shown against peak sunspot numbers.

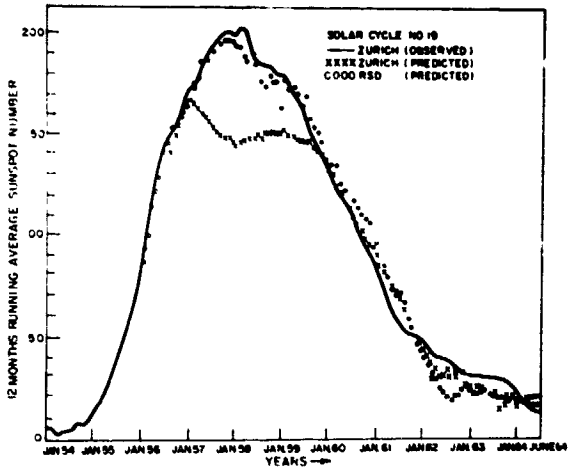

Figure 3a. Running average of Zurich observed sunspot numbers for nineteenth cycle with RSD and Zurich predictions. Near the peak, RSD values fared better.

activity of cycle 19, RSD method fared better. Figure 4 shows the entire predicted twenty-first cycle using just about one year of observations in the cycle.

2.3 Future Plan

All the present methods of long-term solar forecasting essentially center around various forms of statistical analysis of previous cycles. In addition, furtner improvements can be effected by following the growth patterns of the active centers on the solar disk. These centers start

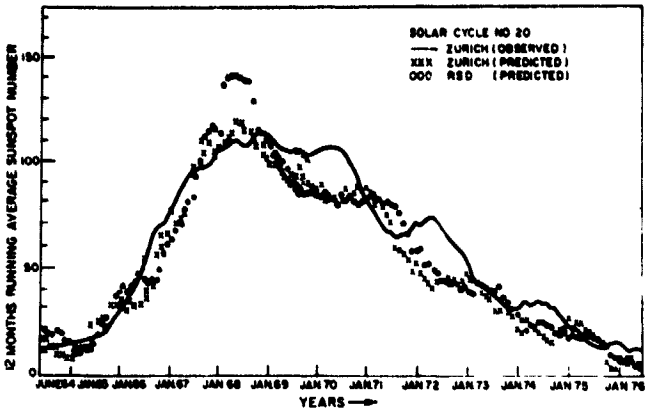

Figure 3b. Running average of Zurich observed sunspot numbers for twentieth cycle with RSD and Zurich predictions.

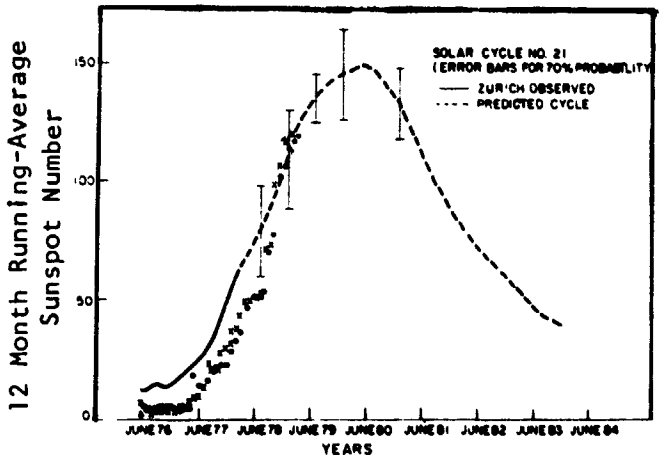

Figure 4. Complete prediction of the twenty-first solar cycle using RSD technique is shown in this diagram. Error bars show 70% probability ranges.

developing around 40-45^0 latitude and drift towards the equator as the cycle progresses. Yet another plan is to use the 22-year periodicity more effectively. For example, one can start with an odd cycle and treat every even cycle as an anti-cycle and predict it as a continuation of the decaying part of the odd cycle. The negative values thus obtained are converted back to positive values, constituting the growing part of the even cycle. The cross-over point from positive to negative values can be readily identified as the minimum. Likewise, odd cycles can be predicted by starting with an even cycle. Standard odd and even cycles are evolved by averaging these cycles separately from the year 1749 A.D. Analyses of results arrived by this technique are too preliminary to be included in this review. There are several other simultaneous attempts being made to improve predictions of different phases of the solar cycle. One such attempt is to evolve an exponential curve to predict the declining part of the cycle. Yet another effort is underway to predict the growth part by using the peak-to-peak range rather than the minimum-to-minimum range.

3. IONOSPHERIC PREDICTIONS

Radio Science Division is responsible for advising the various organizations in India on problems related to radio communications and for providing long-term predictions of propagation parameters for planning of high frequency communication circuits. RSD provides these predictions for the entire latitude range in the eastern region covering a longitudinal extent of 50^0E - 170^0E. The ionospheric parameters viz. foF2 and MUF(4000)F2 are predicted for each of the calendar months. The predicted parameters are presented in the form of contour maps and the values can be read for any latitude for all the 24 hours of the day from the map. Figures 5 and 6 show the contour maps of foF2 and MUF(4000)F2 for September '77. The prediction technique is basically similar to the method developed earlier by CRPL, USA (1948) and used by several predicting agencies with some modifications. So, the method will be described only briefly; however, the data base will be described to show the bulk of observations used in the prediction exercise.

3.1 Data Base

3.1.1 Diurnal Variation for Fixed Solar Activity Ranges

The measured ionospheric data from 27 stations (Table I) obtained over a period of two solar cycles is the basic data that is being used in RSD prediction technique. Data pertaining to 13 more Russian Stations (Table II) has been added to the original data base at a later stage. The incorporation of data from Russian Stations has ensured a good latitudinal coverage in the Eastern zone, especially in the high latitude region.

The data comprises of monthly median values of foF2 and M(3000)F2 for all the stations for each month and hour. Median values are compiled for these 40 stations, using the observations of about two solar cycles. The data is

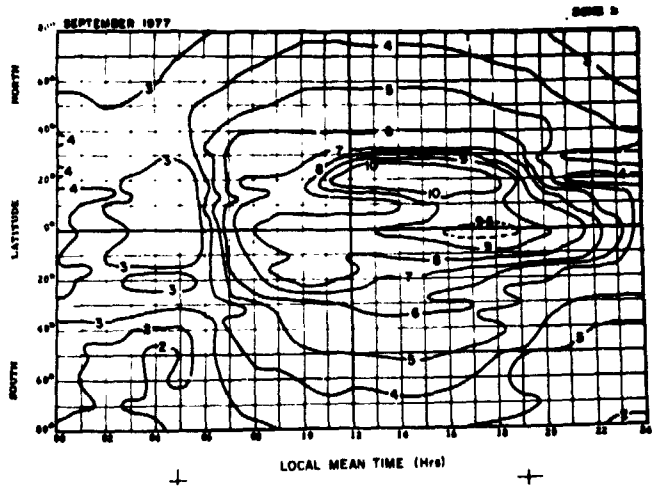

Figure 5. A contour map of foF2 in MHz for east zone (50^0E-170^0E) for September 1977 is shown. The contours are drawn for intervals of 1 MHz.

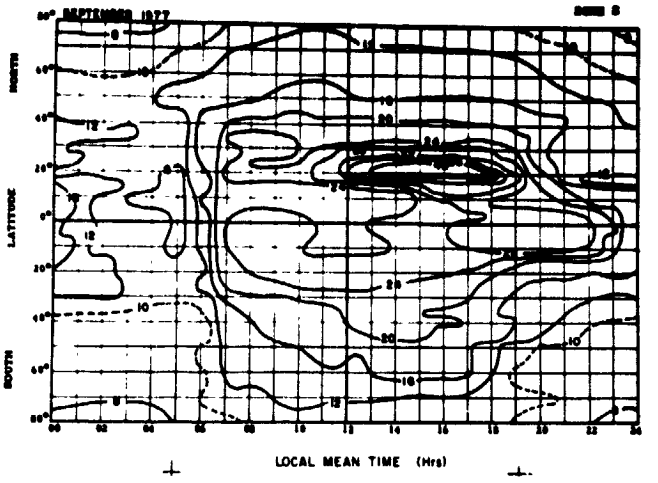

Figure 6. A contour map of MUF(4000)F2 in MHz for the east zone (50°E-170°E) for September 1977 is shown. The contours are drawn for intervals of 4 MHz.

Table 1. Ionospheric observations for two solar cycles.

	Stations	Latitude (°)	Longitude East (°)
1.	Wakkanai	45.4	141.7
2.	Akita	39.7	140.1
3.	Tokyo	37.5	139.5
4.	Yamagawa	31.2	130.6
5.	Delhi	28.6	77.2
6.	Formosa (Tapei)	25.0	121.2
7.	Ahmedabad	23.0	72.6
8.	Haringhata	23.0	88.6
9.	Bombay	19.0	72.8
10.	Baguio	16.4	120.6
11.	Madras	13.1	80.3
12.	Tiruchirapalli	10.8	78.7
13.	Kodaikanal	10.2	77.5
14.	Trivandrum	8.5	77.0
15.	Singapore	1.3	103.8
16.	Townsville	-19.3	148.7
17.	Brisbane	-27.5	152.9
18.	Watheroo (Mundaring)	-30.3 (-31.99)	115.9 (116.3)
19.	Canberra	-35.3	149.0
20.	Hobart	-42.9	147.3
21.	Macq. Isld.	-54.5	159.0
22.	Clyde	70.5	291.4
23.	Vanimo	-2.7	141.3
24.	Cocos. Is.	-12.2	96.8
25.	Port Morseby	-9.4	147.1
26.	Hyderabad	17.4	78.5
27.	Manila	14.6	121.0

Table II. Soviet ionospheric observations.

	Stations	Latitude (°)	Longitude East (°)
1.	Heiss Is.	80.6	58.00
2.	Tikhaya	80.0	52.00
3.	Dixon Is.	73.5	80.4
4.	Tixie Bay	71.6	128.9
5.	Salekhard	66.5	66.7
6.	Yakutsk	62.0	129.6
7.	Syerdlovsk	56.7	61.1
8.	Irkutsk	52.5	104.3
9.	Yuzhno Sakhalinsk	47.0	143.0
10.	Alma Ata	43.2	76.9
11.	Ashkhabad	37.9	58.3
12.	Mirny	-66.5	93.00
13.	Vostok	-78.4	106.87

grouped into three sunspot ranges viz. 0-50, 50-100 and > 100. Using the hourly median values for each station, a diurnal variation curve is obtained for each month and for each of the sunspot range groups. These standard diurnal curves are obtained for both foF2 and M(3000)F2. Figure 7 shows the standard diurnal variation curves for foF2 and M(3000)F2 for Delhi for the month of January. Thus, the observational data base consists of 480 (40 x 12)

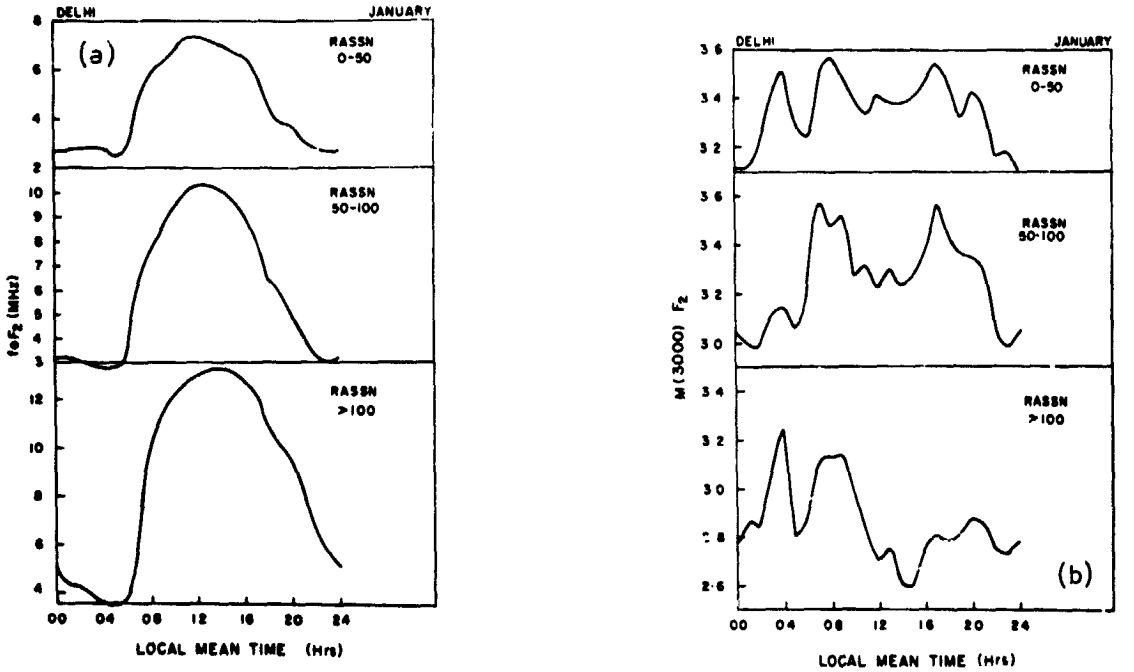

Figure 7. Standard diurnal variation curves for (a) foF2 and (b) M(3000)F2 for Delhi are shown for the month of January. Three curves represent three different ranges of solar activity.

diurnal variation curves for each of the three solar activity ranges for foF2 and an equal number for M(3000)F2. A 24-hour average value is also computed for each of these standard diurnal curves.

3.1.2 Solar Activity Variation Plots of 24-Hour Average Values of foF2 and M(3000)F2

Using the hourly median values, the 24-hour average of the medians is obtained for each month and station and this single value is chosen as the ionospheric index for that particular month for the corresponding running average sunspot number (RASSN). Relationships are obtained between this ionospheric index and the RASSN for each station and month for both foF2 and M(3000)F2. Sample plots are shown in Figure 8 for foF2, and it can be noticed from the figure that a linear relationship is valid for RASSN values less than 150 and saturation effects set in for higher values.

With the help of standard diurnal variation curves for foF2 and M(3000)F2 and plots of 24-hour average foF2, M(3000)F2 against RASSN, the foF2 and MUF(3000)F2 values can be computed for any given sunspot number (RASSN) for any hour of the day and station. MUF(4000)F2 values can be obtained from MUF(3000)F2 by multiplying with appropriate conversion factors recommended by CCIR.

3.1.3 RSD Prediction Technique

The dependence of ionospheric parameters on the Running Average Sun Spot Number (RASSN) is well established and this relationship is the main basis for RSD prediction technique. Radio Science Division starts its prediction activities every month by predicting a RASSN for a month six months hence. After having predicted the Sun Spot Number (refer solar activity prediction section) the corresponding ionospheric parameters are computed using the various sets of diurnal curves and solar activity variation plots described in the data base section. The first step would be to obtain a 24-hours average of foF2 and M(3000)F2 values for each of the stations for the predicted RASSN from the appropriate 24-hour average plots described in 3.1.2 above.

The 24-hour average values so obtained are then plotted against geographic latitude and values are read out at every 5^0 latitude intervals up to 40^0 and at every 10^0 latitude intervals for higher latitudes in both the hemispheres. These 24-hour average values are then converted into diurnal values using one of the three standard diurnal curves that are available for each of the stations depending on the predicted RASSN. The procedure involves use of the standard diurnal curve for appropriate RASSN range. The station used is the one nearest to a latitude grid; for example, the standard diurnal curve of Kodaikanal is used for 10^0N. The hourly values of this curve are then multiplied by the ratio of predicted average at 10^0N to the average of this curve to give diurnal variation at 10^0N.

The diurnal variation curves for foF2 and M(3000)F2 thus obtained at different latitudes are employed to draw the contour maps (Figures 5 and 6) of foF2 and MUF(4000)F2 after converting the M(3000)F2 values into M(4000)F2.

3.1.4 Post-Mortem Analysis and Further Improvement

The RSD (old) method of prediction described earlier indeed has certain limitations such as

i) the diurnal variation in the ionospheric parameter within a specified sunspot range is neglected, and

ii) by choosing the 24-hour average of monthly median as an ionospheric index, the diurnal variation in the index is de-emphasized.

A new RSD prediction method has been developed mainly with the view of reducing these errors. In the new method, plots are obtained between monthly medians and RASSN for every 2-hour intervals resulting in 12 plots for each month, the total number of plots being 5760 (12x12x40) for 40 stations for one parameter for all the months. These large numbers of basic data plots have ensured adequate diurnal coverage and have also simplified the computational procedure considerably. Figure 9 shows prediction of foF2 for September '70 for some low latitude stations obtained by both RSD old and new methods of predictions. They are also compared with the IF2 method (Minnis and Bazzard, 1959) where instead of RASSN, an index IF2 which is

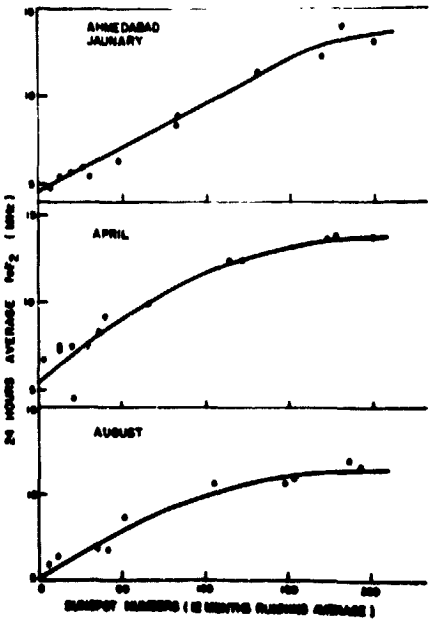

Figure 8. A plot of ionospheric index- 24 hour average of foF2 - against running average sunspot numbers is shown for Ahmedabad for three representative months. The saturation effect can be seen from a value of 150 of RASSN in all the curves.

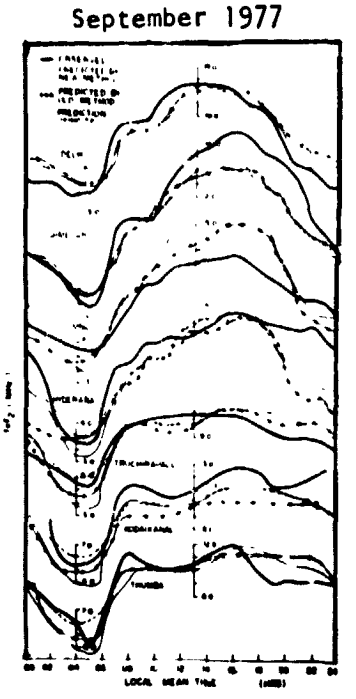

Figure 9. Comparison between observed and predicted values of foF2 for September 1970 are shown. These comparisons are shown for different methods of predictions, for low latitude stations.

derived from sunspot number is used. The bold line in the figure is based on the actual observations. A comparison of different predictions with observed values shows that for latitudes below 20^0, all the prediction methods yield better value for the daytime, while at higher latitudes the nighttime predictions are better.

Figures 10(a,b) also show the comparison of frequency predictions obtained by different methods for two stations, New Delhi (Geographic latitude $28^0 38'N$) and Ahmedabad (Geographic latitude $23^0 01'N$) with the observed values. The predictions are for September 1977 and the methods chosen for comparison are essentially same as the ones used for September 1970 (Figure 9) except for IF2 method; instead, predictions obtained using CCIR - 340 atlas of ionospheric characteristics (1966) are included for comparison.

The comparison of different methods for September 1977 also in general yields results similar to those of September 1970. It can be seen from Figure 10a for New Delhi that both RSD old and new methods show better agreement with the actual observations (bold line in the figure) than CCIR - 340 atlas values. However, for Ahmedabad, which is at a slightly lower latitude than New Delhi, all the prediction methods yield better results during nighttime, especially at post-sunset and pre-sunrise periods. It should also be mentioned here that RSD new method gives more realistic predictions in comparison to other prediction methods.

Saturation effects exhibited by ionospheric parameters at very high sunspot numbers have always been a major limitation in long-term predictions. A systematic analysis of ionospheric parameter variation with RASSN (Figure 8) has conclusively shown that saturation effect is a constant feature at low latitudes irrespective of season for RASSN values above 150. Hence, Radio Science Division had made several studies to overcome this inherent limitation. One such attempt has been to obtain second degree relationships between the ionospheric parameters and RASSN of the kind,

$$foF2 = A + BR + CR^2$$

$$M(3000)F2 = A' + B'R + C'R^2$$

where R represents the RASSN.

Constants A, B, C and A', B', C' are obtained for every two hours for all the stations and the ionospheric parameters foF2 and M(3000)F2 can be computed for any RASSN. RSD currently uses a IBM 1620 computer for all its routine prediction programmes.

Analytical studies are made from time to time to look back and evaluate the accuracy of predictions. However, it is not within the scope of this presentation to give large number of month-by-month comparisons of observed and predicted values. Instead, fairly large statistical samples of these comparisons are presented in Figures 11a and 11b for the northern winter months for low (RASSN ≈ 15) and high (RASSN ≈ 100) solar activity respectively. The curves show the average of all the observed noon values for

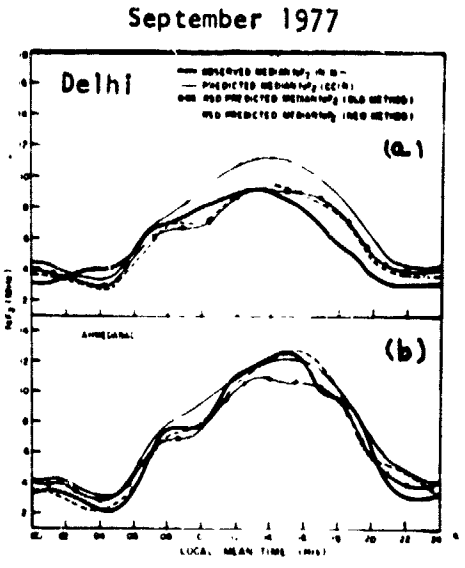

Figure 10. Comparison between observed and predicted values of foF2 for September 1977 are shown for representative stations (a) Delhi and (b) Ahmedabad in India. These comparisons are shown for different methods of prediction.

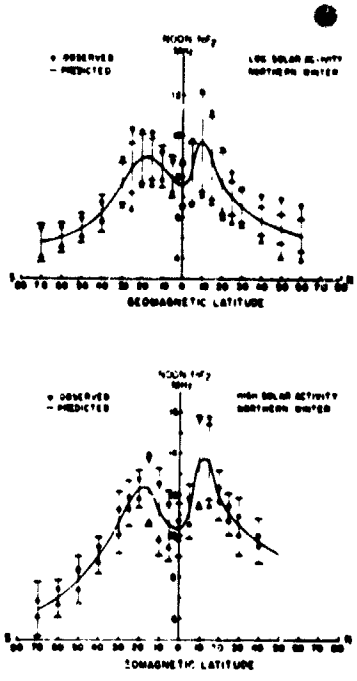

Figure 11. Average of observed noon foF2 values for northern winter are plotted against geomagnetic latitude (line curve) for low and high solar activities separately. The vertical lines bounded by triangles represent the 95% ranges of observed values, whereas those bounded by horizontal bars represent 95% ranges of predicted value.

16 winter months spread over 4 years of low solar activity and 4 years of high solar activity. The vertical lines show the spread in these values, the boundaries set by small horizontal lines indicating the predicted values with 95% probability and the boundaries set by triangles indicating the range of spread in observed values. It may be observed that in general the range in predicted values is not far different from the range in observed values, especially during low solar activity. It may also be noticed that at higher latitudes, the difference is appreciably large because the data base at these latitudes for our longitudinal zone was inadequate earlier. The data is shown against the geomagnetic latitude to emphasize the point that because of large horizontal gradients associated with geomagnetic anomaly and the horizontal movements of the anomaly, the performance of our prediction system even at these latitudes has been satisfactory.

4. CONCLUSIONS

The errors and uncertainties in the finally predicted ionospheric parameters are due to (a) errors in the solar activity predictions, (b) errors in assuming a simplified response of the ionosphere to the sunspot number, (c) errors due to deviations in the ionosphere in response to solar and geophysical events, and (d) errors due to large day-to-day variations apparently unrelated to any specific events. Some attempts have been made at RSD to quantify the uncertainties due to (d) above, and are presented in a companion paper. Other related activities at RSD are as follows:

1. Data services: Ionospheric and solar geophysical data obtained over India are compiled, edited and published.

2. A.R.W.C.: Radio Science Division discharges the responsibilities of an Associate Regional Warning Center (of IUWDS) and disseminates warning messages through the Time and Frequency transmitter of NPL.

3. Short Term Forecasting: Based on the Indian observations and on the data received from Boulder, Sydney, Paris and Moscow, a daily forecast is made and broadcast over the transmitter mentioned above. However, the quality of present service is below threshold.

4. Advisory Services: A large number of communication organizations depend on RSD for advice on frequencies, firing angles, power and antenna requirements for point-to-point H.F. links. Special problems arising due to location of receivers in mountainous terrain and valleys are also attended to. LUF (ALF) and signal strength calculations are also done on special request. Attempts are being made to computerize all these calculations.

5. Special Propagation Studies: Research and analytical studies are continuously made at RSD to solve some of the special low latitude problems arising out of the geomagnetic anomaly and rapid increase and collapse of ionization during sunrise and sunset times. Some of these problems are discussed in another companion paper.

REFERENCES

CCIR Report 340: Atlas of Ionospheric Characteristic, Oslo 1966, published 1967. pp. 404.

Cole, T. W. (1973): Periodicities in solar activity. Solar Physics, 30:103.

Kuklin, G. V. (1976): Cyclical and secular variations of solar activity. Basic Mechanisms of Solar Activity (ed. V. Bumba and J. Kleczek), IAU Symposium No. 71, pp. 147-190.

Minnis, C. M., and G. H. Bazzard (1959): Some indices of solar activity based on ionospheric and radio noise measurements. J. Atmos. Terr. Phys., 14:213.

NBS Circular No. 462 (1948): Ionospheric Radio Propgation, pp. 208.

Shove, D. J. (1955): The sunspot cycle 649 BC to AD 2000. J. Geophys. Res., 60:127.

Slutz, R. J., T. B. Gray, M. L. West, F. G. Stewart and M. Leftin (1971): Solar Activity Predictions. NASA Contract Report No. 1939, NASA CR-1939.

Stetson, H. T. (1947): Sunspots in Action. The Ronald Press Co., USA.

Waldmeier, M. (1946): A prediction of the next maximum of solar activity. Terr. Magn. and Atmosph. Elect., 51:270.

A SIMPLIFIED INDEXING OF F-REGION GEOPHYSICAL NOISE AT LOW LATITUDES

S. Aggarwal, D. R. Lakshmi and B. M. Reddy
National Physical Laboratory
New Delhi - 110012, India

The low latitude F-region, unlike at middle and high latitudes, is protected from direct particle effects as well as indirect particle effects such as ionospheric storms. In fact, during the storms the changes in the F-region critical frequency and the F-region height factors are in such a way as to retain the maximum usable frequency values almost unaltered. However, the day-to-day fluctuations in the F-region parameters, which by themselves are rather large, are compounded by the variability in the equatorial anomaly morphology and may cause considerable deterioration in HF communications, if the median MUF values predicted much in advance are used. The objective of this paper is to describe a simple method of deriving an F-region noise index that can warn the prediction users at low latitudes as to the specific months when they have to be more careful in using the long-term predictions.

1. INTRODUCTION

Long distance H.F. communication supported by the F-region is essentially controlled by the two parameters, foF2 and M(3000)F2. This is so because the Maximum Usable Frequency (MUF) is a function of foF2 as well as M(3000)F2 which includes the information on the height of the reflection level. While prediction of the median values of these parameters for any particular month can be made with some degree of accuracy, it has not been possible to predict their day-to-day changes. These large day-to-day variations, especially manifested in foF2 variations, are apparently unrelated to specific solar or geomagnetic events and may be termed as F-region geophysical noise. Some studies have been made on this topic earlier, especially for mid-latitudes (King and Slater, 1973; Rush et al., 1974). An excellent effort in this direction to quantify the MUF variability is that of Barghausen et al., 1969 (also CCIR doc. 6/1070-E, 1978), but a simpler method of indexing using essentially low latitude data is expected to be more useful because of the special nature of these problems in the low latitude zone.

2. VARIABILITY IN foF2

Several studies were made by the authors to investigate if any kind of

relation exists between the standard solar and geophysical indices and the foF2 fluctuations. The results of one such study using data from Vanimo (geomag. lat. 12.7°S) and Kodaikanal (geomag. lat. 0.6°N) are shown in Figure 1. (Aggarwal et al., 1976). Percentage deviations of foF2, which

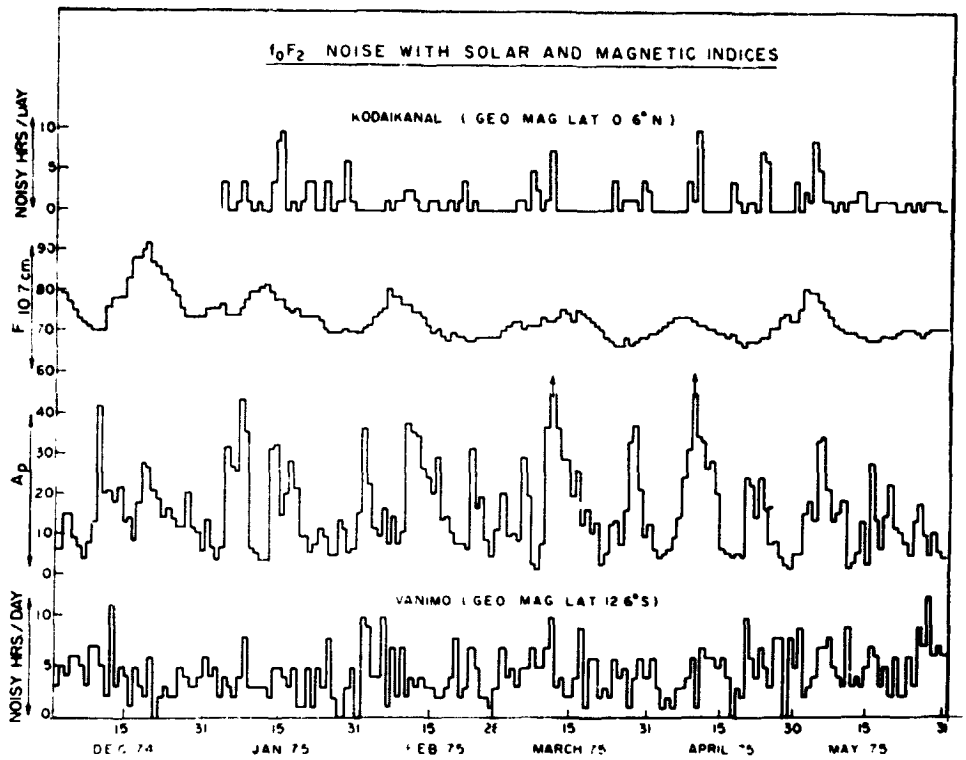

Figure 1. Diagram shows the number of hrs/day when Δ foF2 is beyond the range of coefficient of variation for a low solar activity period for two low latitude stations (A_p and 10.7 cm flux values for the same period are also shown).

are the normalized hourly deviations in foF2 from the monthly median values multiplied by 100, have been calculated for each station. In order to see the dispersion of the percentage deviations around the median, the coefficient of variation for every hour on a monthly basis has been calculated for daytime and nighttime separately, the coefficient of variation being the standard deviation in Δ foF2 itself. To be more explicit, the coefficient of variation 'V' can be defined as the ratio of the standard deviation to its average value in percent (Weatherburn, 1957). For daylight hours, the reference values have been arrived at by averaging the coefficients of variation for the hours 0800 to 1900 local time. Based on these daytime reference values, the number of hours with Δ foF2 values beyond the range of daytime reference values were calculated and it is these number of hours that are shown in Figure 1 as noisy hours per day. It is apparent from Figure 1 that no significant correlation exists between this parameter and the indices A_p and 10.7 cm flux. The correlation coefficients show hardly any improvement when the time lag between the solar and magnetic indices and the foF2

deviations is varied between 0 and 10 days. This study only confirms that the geophysical noise in foF2 is, in fact, a random noise especially at low latitudes, because at middle and high latitudes the large variations in foF2 following magnetic storms may inject some amount of apparent correlation with A_p.

The morphology of the variability in foF2 with local time, season and solar activity for an equatorial station, Kodaikanal, can be visualized from Figures 2 and 3. Figure 2 shows the coefficient of variation 'V', derived as described above for the year 1968 (high solar activity) while Figure 3 is for

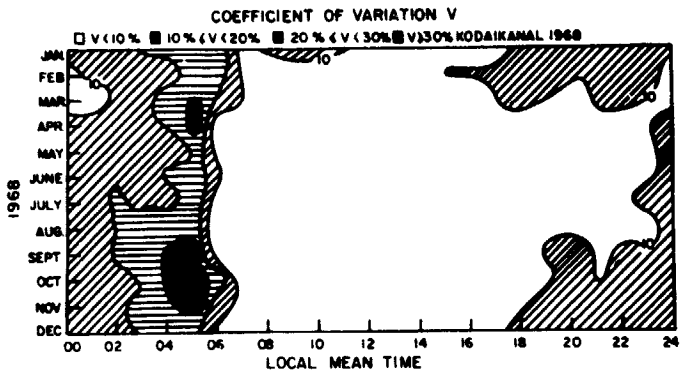

Figure 2. Seasonal and temporal changes in 'V' for a high solar activity year 1968.

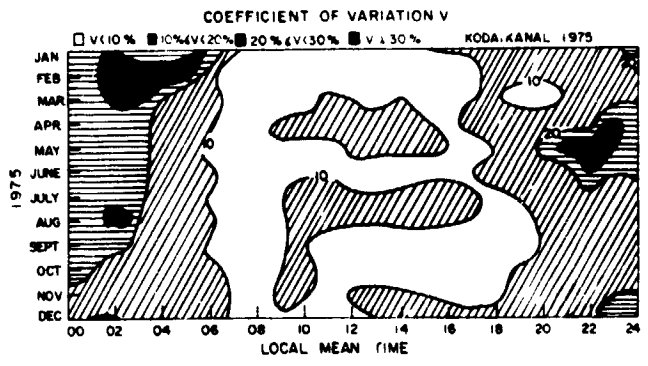

Figure 3. Seasonal and temporal changes in 'V' for a low solar activity year 1975.

the year 1975 representing low solar activity. The variations are much larger, especially for low solar activity period, than the usual prediction accuracy for the median foF2 values.

3. VARIABILITY IN MUF

A comprehensive analysis of a long series of observations (not presented here) at several low latitude stations shows conclusively that the storm-time departures in foF2 are absolutely indistinguishable from usual day-to-day fluctuations. However, rather curiously, the variability in MUF during storms is considerably lesser than the variability on quiet days. This is obviously due to the fact that at low latitudes during magnetic storms, foF2 values undergo marginal enhancements along with increase in the F-layer height. In general, whatever the reasons, whenever the changes in both foF2 and hpF2 are in the same sense, the consequent changes in MUF will only be marginal; for example, an increase in foF2 will tend to increase the MUF while an increase in hpF2 will tend to decrease the MUF. This feature at low latitudes can be used with advantage for indexing the variability, by analysing the morphology of simultaneous variations in foF2 and hpF2.

4. A METHOD OF INDEXING F-REGION NOISE

The simultaneous percentage deviations in foF2 and hpF2 at four different local times in September 1977 for Ahmedabad (Geomag. Latitude: 13.8^0N) are shown in Figure 4. Each point in the diagram represents the value on one day in the month, with the bold points representing the coincidence of more than one point. Figures 5 and 6 show similar plots of percentage deviations in foF2 and hpF2 for Ahmedabad for the months of May-June 1977 (representing summer conditions) and for the months of November-December 1977 (representing winter conditions), respectively. The data points in quadrants 1 and 3 present the situation when both foF2 and hpF2 variations are in the same sense and hence the MUF departures will not be large. So, these two quadrants represent minimum geophysical noise conditions. Quadrant 4 represents increased MUF situation and, consequently, communication using predicted median MUF values will not be a casuality. However, the changes in quadrant 2 (with foF2 decreasing and hpF2 increasing) may reduce the actual MUF much below the predicted median and thus cause communication failure. Obviously, the number of points in quadrant 2 for a particular month and local time may be used to quantify the deterioration. For example, for Figures 4, 5 and 6, a general observation that can be made (from the number of points in quadrant 2) is that the deterioration is considerable in summer and winter compared to equinox.

Attempts are currently underway to use the data from a large number of low latitude ionospheric stations and to compute the number of points in quadrant 2 as also to give different weight factors for these points, so that their actual contribution in bringing down the MUF can be evaluated. A quality index based on this information can be derived and supplied to the prediction users, for the more the number of points in quadrant 2, the

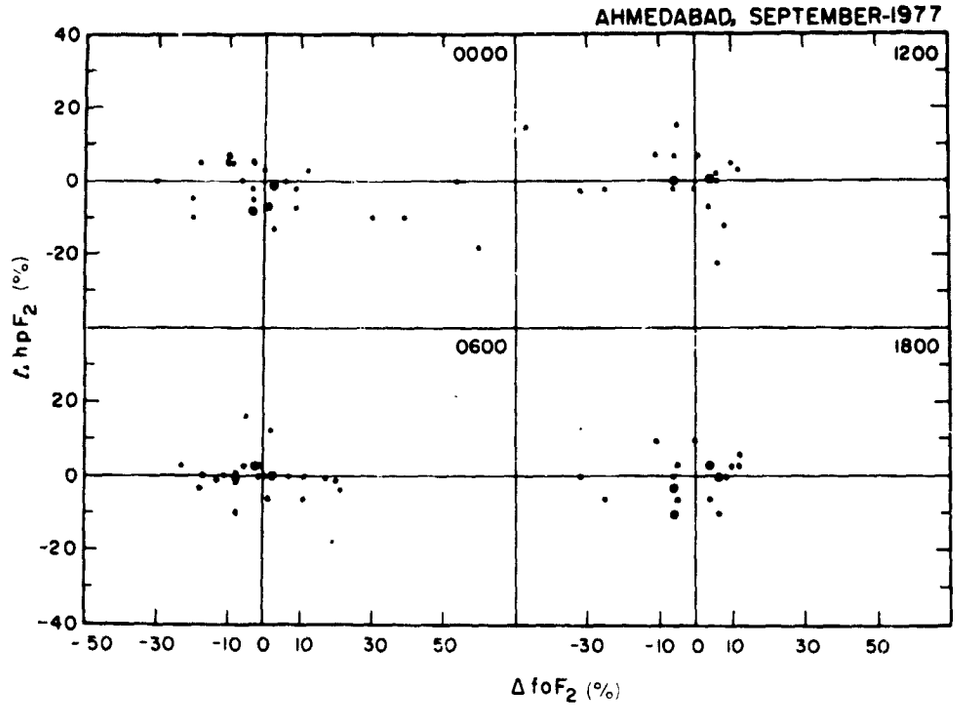

Figure 4. Plots of Δ hpF2 (%) against Δ foF2 (%) for September 1977 at different local times for Ahmedabad.

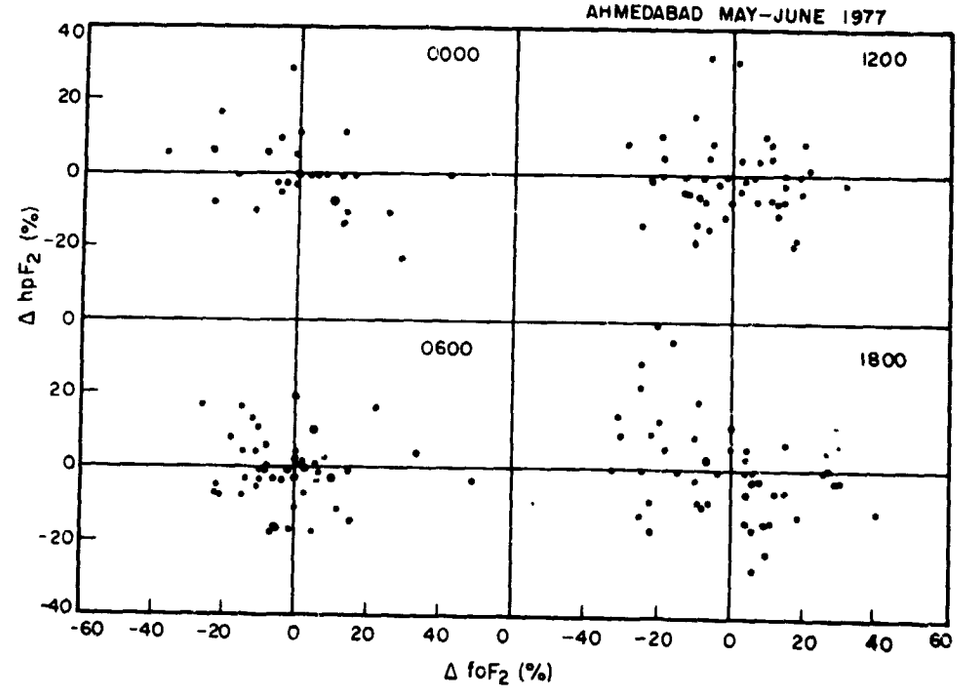

Figure 5. Plots of Δ hpF2 (%) against Δ foF2 (%) for May-June 1977 at different local times for Ahmedabad.

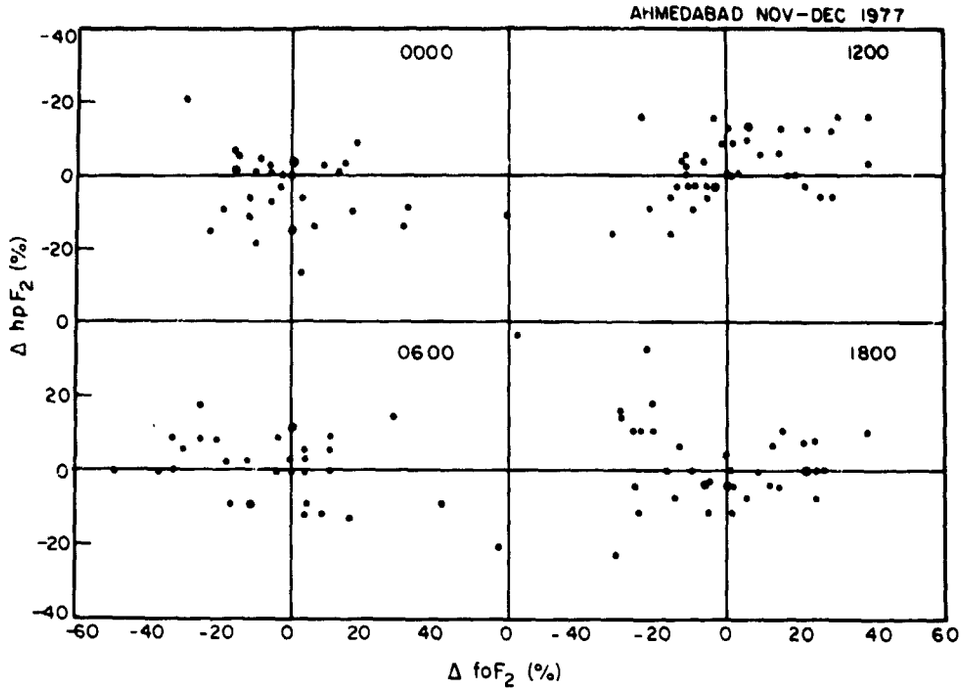

Figure 6. Plots of Δ hpF2 (%) against Δ foF2 (%) for November-December 1977 at different local times for Ahmedabad.

greater will be the chances of deterioration of communication unless short-term predictions are used.

Acknowledgements: The computational assistance rendered by Mrs. S. Shastri and Mr. V. A. Chandrashekharan is gratefully acknowledged.

REFERENCES

Aggarwal, S., D. R. Lakshmi and B. M. Reddy (1976): Some problems of HF communication at low latitudes and possible solutions. I.J.R.S.P., 5:302.

Barghausen, A. F., J. W. Finney, L. L. Proctor and L. D. Schultz (1969): Predicting long-term operational parameters of high-frequency sky-wave telecommunication systems. ESSA Tech. Rpt. ERL 110-ITS 78, U. S. Government Printing Office, Washington, D. C.

King, J. W. and A. J. Slater (1973): Errors in predicted values of foF2 and hpF2 compared with observed day-to-day variability. Telecom. Journal, 40:766.

Rush, C. M., D. Miller and J. Gibbs (1974): The relative daily variability of foF2 and hmF2 and their implications for HF radio propagation. Radio Science, 9:749.

Weatherburn, C. E. (1957): A first course in Mathematical Statistics. Cambridge University Press, Cambridge.

SPIRAL SUNSPOTS AND SOLAR ACTIVITY FORECASTS

Ding You-ji and Zhang Bai-rong
Yunnan Observatory, Academia Sinica,
Kunming, Yunnan Province, China

The definition of a spiral sunspot is given. Three examples illustrate the processes of the occurrence of spiral sunspots and the roles played by them in prominence and flare activities. Finally, we propose a method for solar activity forecasts making use of parameters such as spiral sunspots, prominences and neutral lines.

I. DESCRIPTION AND DEFINITION OF A SPIRAL SUNSPOT

The penumbral filaments of sunspots have a great variety of patterns and forms in the fine structure of sunspots. We roughly divide them into the typical structures such as "spiral", "comb", "net", "radial", etc. These structures show, to a certain degree, that the sunspot groups are at different evolutionary stages.

We define a spiral spot as follows: A sunspot is a spiral spot when either the penumbral filaments of a sunspot, or the outer filaments surrounding a cluster of small sunspots, show a tangential arrangement, either with all the filaments oriented in mutually consistent directions, or if some of the filaments take on other shapes, but they are not directed in the opposite sense. See the regions indicated by arrows in Figures 1 and 2. These spiral filaments generally have the following characteristics: (1) The tangentially arranged filaments are relatively long, and the contrast between the bright and the dark filaments also comparatively large. (2) The penumbral filaments between their roots at the umbra and the outer boundary of the penumbra are usually curved into arcs, and rarely as tangentially arranged straight segments. These characteristics make it rather easy for us to draw an analogy between the spiral spots and hydrodynamical vortices. The physical picture of a spiral spot is simple and clear, namely, the magnetic tube of the sunspot suffers a twist in a certain direction, so that we can directly infer from the morphology that the integral of the magnetic field around the spot,

$$\oint \vec{H} \cdot d\vec{l} = 4\pi I, \qquad (1)$$

is quite large. In other words, we can infer the probable existence, in the active region, of a strong electric current from the penumbral structure. Usually, a spiral structure lasts less than one day, so that when photographed

on the next day, it has disappeared. Perhaps it already changed into a radial or a net-like structure; it is then called a short-lived (or newborn) spiral. Sometimes, it continues to exist for a number of days, its vortex intensity (that is the angle of inclination) weakes gradually until it disappears and changes into a radial structure. We then call it a long-lived spiral. For answering the question whether spirals appear in a sunspot group, we point out the following characteristics: (1) For the active sunspot groups of types C, D, E, F, G and H, the appearance of spirals (especially short-lived spirals) is a rather common phenomenon. (2) It is not a general phenomenon for long-lived (lasting over two days) spirals or recurring spirals to appear. They are only dependent on the peculiarities of a minority of sunspot groups. (3) The time when a spot appears as a spiral pattern is much shorter than its lifetime and usually the spiral stage is at the beginning of its life (Ding You-ji et al., 1976a). We shall describe the formations of spiral sunspots, the relations between them and the activities of flares and prominence, by means of some concrete examples.

2. SPIRAL SPOT IN THE ACTIVE REGION MCMATH 11976

2.1 The Formation of Spiral Spots

We can see from Figure 5 that the spot O_{2N} at the central portion of the large active region McMath 11976 on the second of August in 1972 shows clearly a spiral penumbra. All of its penumbral filaments appear as a clockwise arranged pattern oriented in mutually consistent directions, except that the north-east portion was connected with the umbra O_{1N}. The motions of the spots in this region showed that the distribution and relative position of the four umbrae A_N, B_S, C_S and D_S were stable; however, the large umbra (consisting of O_{1N} and O_{2N}) started an obvious counter-clockwise rotation before 0400UT on August 2. The following features are special: (1) The fibrous penumbral filaments at F in Figures 3 and 4 mostly remained in simple straight-line morphology, but broke up and bent slightly westwards in Figure 5. (2) Comb-shaped penumbrae at G extended toward the south-east in an arc shape on the same day. (3) The tendency of the spirality of the penumbral filaments at H was quite obvious. These morphological consistent changes show clearly the existence of a shearing motion of the magnetic field of the umbra O_{2N} relatively to the solar atmosphere surrounding it. Any other kinds of transfer cannot explain these morphological changes. The association between the directions of the rotational motion of the umbra magnetic field and the arranged pattern of the penumbral filaments mentioned above, however, can be explained with plasma dynamics (Solar Physics Division, Yunnan Observatory, 1974a).

2.2 Relations between Spiral Sunspots and Prominence Activities

According to many photographs of the chromosphere, magnetic fields and flares presented by Zirin and Tanaka (1973), the neutral line ($H_{\parallel} = 0$) penetrated through the penumbra region of the sunspots twice. In the first region it was north-south oriented, situated between two umbral couples, (B_S, A_N) and (C_S, O_{1N}). In the second region it was west-east oriented,

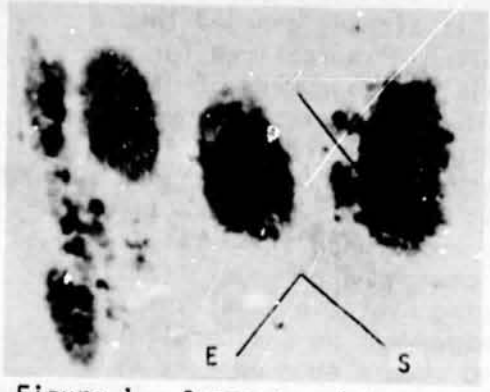

Figure 1. Sunspots of McMath 15266 region at 0300UT on April 28, 1978.

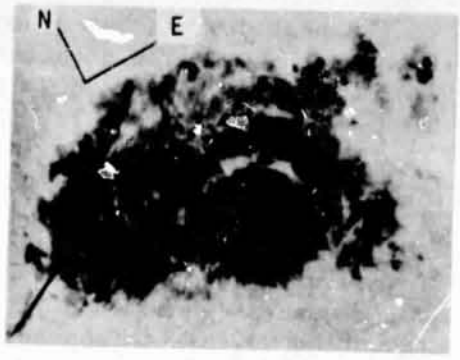

Figure 2. Preceding Spots of McMath Region 11482 on August 21.3, 1971.

Figure 3. Sunspots on July 31.2, 1972

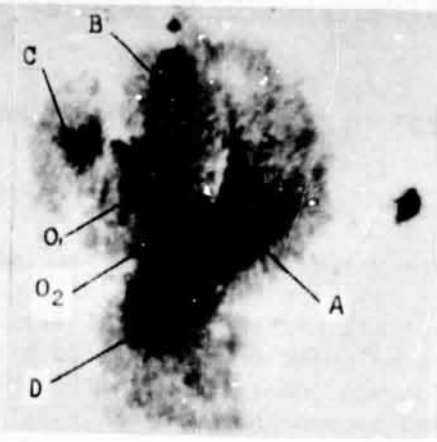

Figure 4. Sunspots on August 1, 1972.

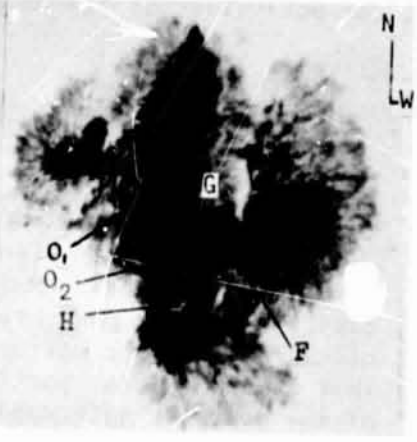

Figure 5. Sunspots on August 2,2, 1972.

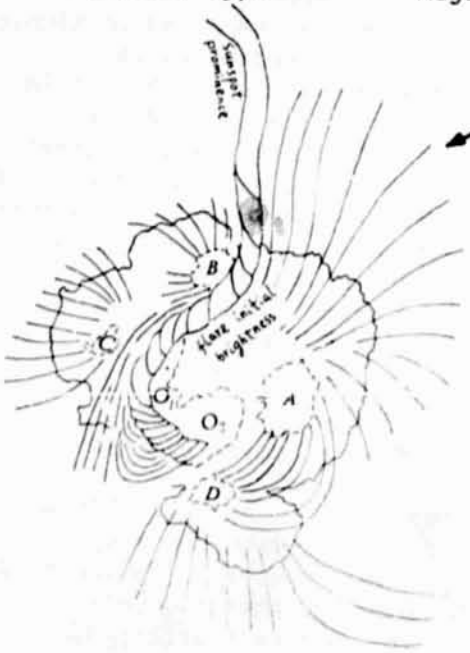

Figure 6. A Twisted Pattern of the Sunspot Prominence at 1837UT and the Initial Bright Filament of the Flare at 1838UT on August 2, 1972.

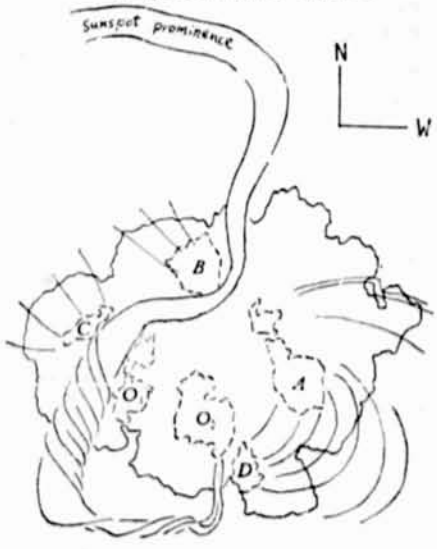

Figure 7. A Twisted Pattern of Sunspot Prominence at 1720UT on August 5, 1972.

situated between the umbrae A_N, O_{2N} and D_S.

The Hα filter photograph of July 31 shows only one twisted sunspot filament, situated over the neutral lines of the two regions, and it had no interruption in morphology. After August 1, the two portions of the filament of the regions suffered different changes. The filament in the second region lost its twisted morphology, replaced by a system of chromospheric threads that connected two umbrae A_N and D_S of opposite polarities. Sometimes they came near to each other and formed a coarse and dark structure; other times they separated from each other, turned into an arc system, and never twisted each other again. The south termination of the filament in the first region evidently pointed towards umbra O_{2N}, (belonging to the following polarity) and ended at the boundary of the umbra O_{2N}, as if it were the source of the filament. But, inside the penumbral region the filament appeared as a tightly twisted prominence magnetic rope with a small width about 3 - 8 arc seconds, and outside the penumbral region it extended northward continuously. See Figures 6 and 7. According to the twisted morphology one can judge that the inner electric current is from north to south, but the current shown by the spiral morphology of the penumbra of O_{2N} is from the top downward. So the prominence magnetic rope may link with the spot magnetic tube; its inner current might be connected, too (Ding You-ji et al., 1976b).

2.3 Relations between Spiral Sunspot and Flare Activity

The morphology and character of the changes of the major flares in this active region were already discussed in detail by the Solar Physical Division of the Yunnan Observatory (1974b). From the former discussion and the paper presented by Zirin et al. (1973), we draw the following conclusions: (1) For all major flares, both the maximum phase of the flare and the prominence magnetic rope associated with O_{2N} were very similar. Perhaps, the flares are the reflexes of the eruptions of the prominence again and again. (2) The region near the second neutral line was anomalously quiet during the eruptions of all major flares. The gradient of the longitudinal field here is about equal to that of the first neutral line, since the maximum values of the magnetic fields of all major spots in this region are approximately equal. The probabilities of magnetic field annihilations and the tearing instability of plasma should also be approximately equal in these two regions, but that did not agree with the observed facts. So we presume that it was very difficult to explain the flare activities in August 1972 with the sheet pinch theory of magnetic neutral layers. The spiral spot, however, may be associated with flare activities through the prominence magnetic rope connected with it. (3) The regions on either side of the first longitudinal field neutral line were pressed by the umbra B_S westwards and by the umbra O_{1N} eastwards. The second neutral line was pressed by O_{2N} southwestwards on one side. From the increase in the longitudinal field gradient, the motions of the spots on either side of the neutral lines, to a certain degree, were similar to each other. But the initial bright points of the flares were largely at the portions pressed by the umbrae B_S and O_{1N}, respectively, and there was no flare activity at the portion pressed by O_{2N}. Therefore, we presume that the sunspots' press on the neutral lines may be an outer factor for the trigger of flares, and cannot provide an energy source of flares and an inner eruptive factor of instability.

3. SPIRAL SPOTS IN THE ACTIVE REGION MCMATH 14943

3.1 The Formation of Spiral Sunspots

We find easily from Figures 8 - 14 that the rotational motion of the preceding spot, which consisted of two umbrae P_{1S} and P_{2S} in this region, became increasingly more rapid during its passage across the solar disk. The relative positions of the major spots in the group, however, were changed rather slowly. The relative position of P_{1S} and P_{2S} rotated about 90^0 on the solar disk during September 15-17, 1977. In response to this, a crack b (Figure 11), due east of umbra P_{2S}, rotated 90^0 during the same period. It indicates that umbrae P_{1S} and P_{2S} rotated together rather than P_{1S} slipping from west to east along a northern arc round the center of P_{2S}. The arranged pattern of its penumbral filaments gradually formed an obvious spiral structure in the same period (Zhang Bai-rong et al., 1978). See Figures 12 - 14.

3.2 Relations between Prominence and Spiral Sunspots

There was a neutral line of the longitudinal field in this active region. It largely penetrated through the central portion of the region in a west-east direction. There was a sunspot prominence over the neutral line, its winding appearance was in accordance with the neutral line very well. The west termination of the prominence connected with spiral spots P_{1S} and P_{2S}. See the portions marked by arrows in Figures 15, 16 and 18. Its east termination extended northwards, pointed to the active region McMath 14942. A twisted structure occurred clearly during the prominence's passage across the central portion of the solar disk on September 15-17th. See the morphologies of the prominence between the spots F_{1N}, F_{2N} and P_{3S} in Figures 16, 17 and 18, and west of the spot P_{2S} in Figures 17 - 18. According to the twisted direction of the prominence we can assert that its inner axial current was from west to east. However, the current shown by the penumbral spiral structures of P_{1S} and P_{2S} was outward toward the chromosphere and the corona. So it should be presumed that the prominence and spots P_{1S} and P_{2S} formed a current circuit and a linking magnetic tube. The areas of other spots approximately equaled to that of P_{1S} and P_{2S} in the region, but there was no obvious prominence activity associated with them.

3.3 Relations between Spiral Sunspots and Flare Activities

Flare eruptions in this active region were recorded 18 times by Yunnan Observatory and Peking Observatory. They were distributed on the whole on either side and near the neutral line or spot prominence. When the spiral morphologies of the spots P_{1S} and P_{2S} were obvious, the flare eruptions tended to occur west of the spot prominences, near the spots P_{1S} and P_{2S}. See Figure 19.

As the spot P_{3S} continuously approached spot F_{1N} their penumbrae connected and formed a δ-structure on September 19. The two spots pressed on both sides of the twisted prominence magnetic rope. This is very similar to the events that occurred over the first neutral line in August 1972 (see section 2.3). After September 19, the plages in this portion were markedly

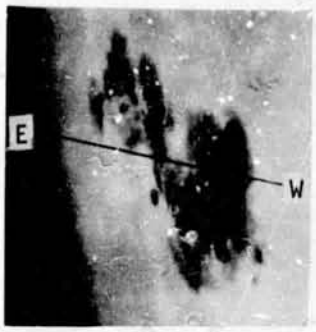

Figure 8. Sunspots at 0150UT on September 10, 1977

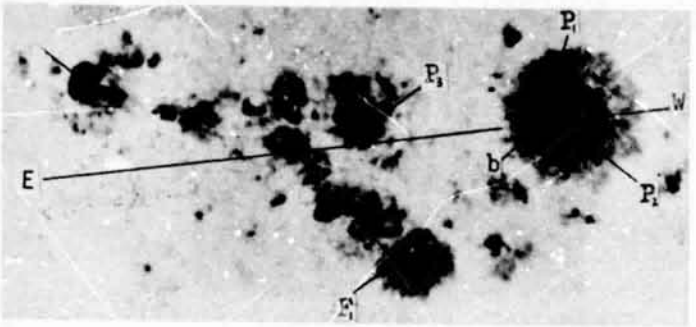

Figure 11. Sunspots at 0930UT on September 15, 1977.

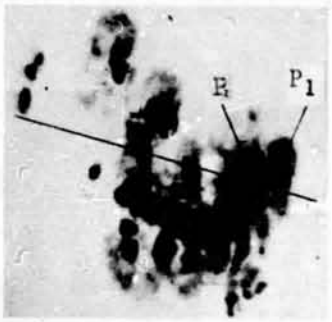

Figure 9. Sunspots at 0122UT on September 11, 1977.

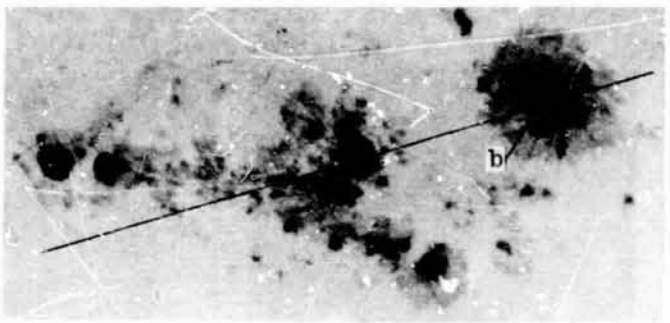

Figure 12. Sunspots at 0230UT on September 16, 1977.

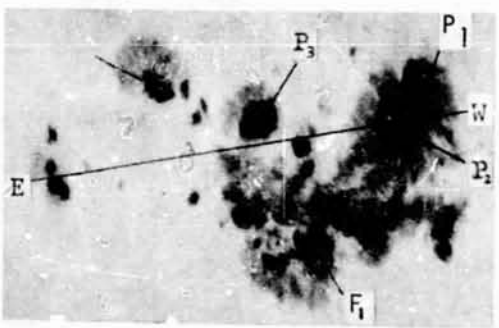

Figure 10. Sunspots at 0330UT on September 12, 1977.

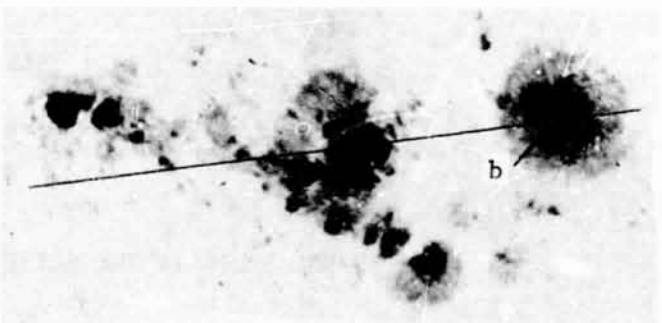

Figure 13. Sunspots at 0820UT on September 16, 1977.

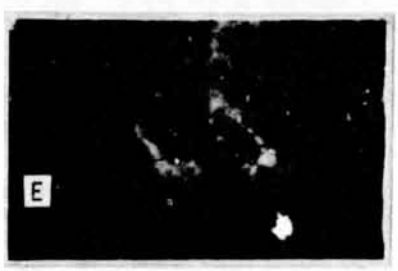

Figure 15. Sunspots filament at 0122UT on September 12, 1977.

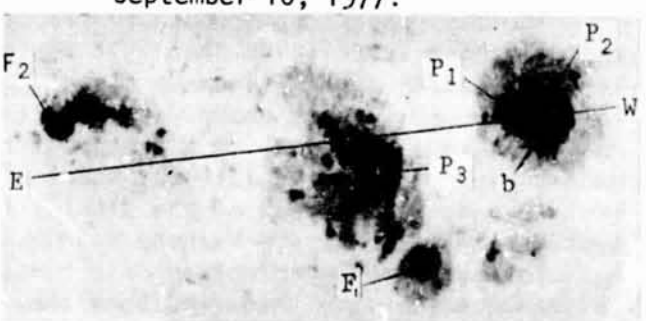

Figure 14. Sunspots at 0315UT on September 17, 1977.

Figure 16. A twisted sunspot filament at 0217UT on September 16, 1977.

Figure 17. A twisted sunspot filament and flare at 0954UT on September 16, 1977.

Figure 18. A twisted sunspot filament and flare at 0112UT on September 17, 1977.

Figure 19. Flare at 0028UT on September 18, 1977 (Peking Obs.).

Figure 20. Flare at 0339UT on September 20, 1977 (Peking Obs.).

bright and major flares erupted. See Figure 20. This also is very similar to the position of the great flare eruptions in August 1972.

4. SPIRAL SPOTS IN THE ACTIVE REGION MCMATH 12094

4.1 The Formation of Spiral Sunspot

The most conspicuous photospheric feature in Figures 21 - 27 of active region McMath 12094 in October 1972 is that the penumbral filaments of the large preceding spot A_N show up clearly as a clockwise spiral pattern. We take the whole sunspot group, of which the characteristic variation and motion were comparatively slow, as a system of reference. There was a stripe of the penumbral bright filament in the shape of a sickle which extended inwards (Point y was at the root of the sickle) in the eastern part of the umbra of spot A_N and an inwards prominent penumbral portion (Point Q) in the west of A_N. To study the inner motion of the spot A_N, we take both of them to be two reference marks. We then find that they revolved counter-clockwise round the center of A_N at the same time with the angular velocity about 15 degrees per day. The evident rotation of the most outside western part (shown as the

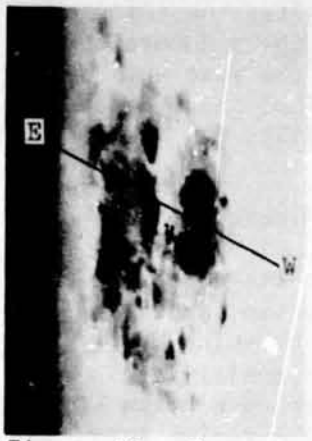

Figure 21. Sunspots on October 24.3, 1972

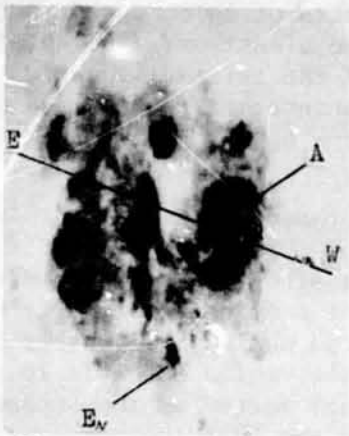

Figure 22. Sunspots on October 25.1, 1972.

Figure 23. Sunspots on October 26.1, 1972.

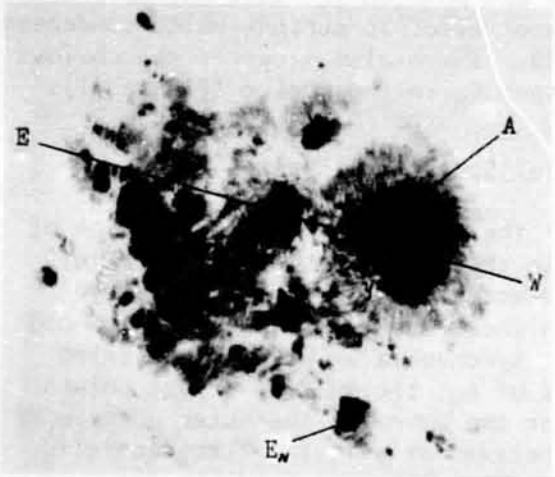

Figure 24. Sunspots on October 27.1, 1972.

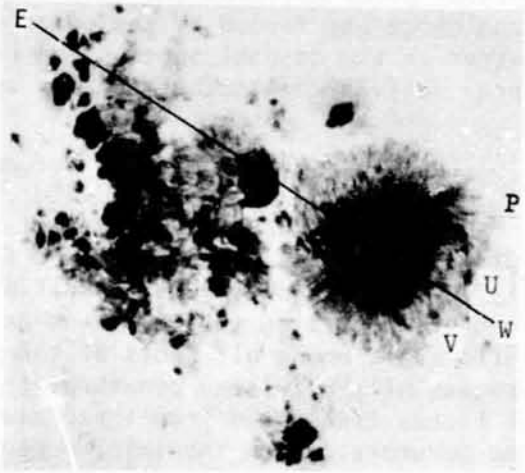

Figure 25. Sunspots on October 28.1, 1972.

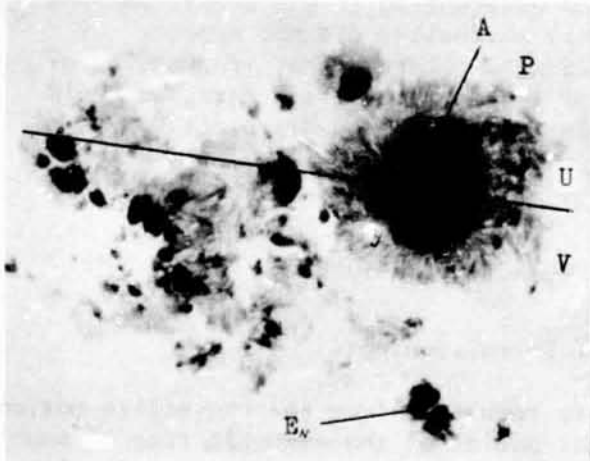

Figure 26. Sunspots on October 29.2, 1972.

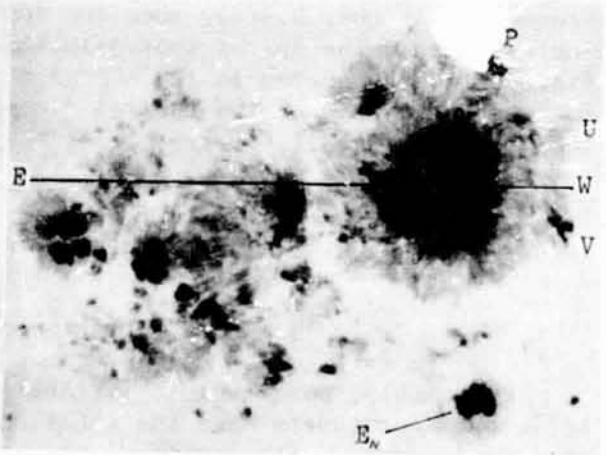

Figure 27. Sunspots on October 30.1, 1972.

points P, U, V) of the penumbra of A_N occurred four days after the spinning of the umbra, but in the same direction. The rotation of the penumbra seemed to be the relaxing motion of the twisted magnetic tube of the spot A_N. We suppose that the spiral structure of the penumbra of A_N might result from the rotational motion of the umbra A_N (Ding You-ji et al., 1977a).

4.2 Relations between Spiral Sunspots and Prominences

In the first three days after the region emerged from the eastern limb of the solar disc, no evident prominence activity was reported. Whole prominence activities occurred during its passage across the solar disc. So the prominence activity in the region was able to reflect sensibly the intensity acted on the coronal matter by the sunspots which were below it. From Figures 28 - 32, we can see that the prominences in the region were associated closely with the large preceding spiral spot A_N. They pointed to this spot unexceptionally and appeared as a divergent arrangement. Ding You-ji et al. (1977b) identified that the attractive center below the largest coronal prominence was the spiral spot A_N, and pointed out that the coronal prominerce was formed by tne powerful sunspot electric current which condensed matter in the coronal space. See Figure 30. There also occurred the obvious spray activity of another smaller spiral spot E_N in the region (Figure 31).

4.3 Relations between Spiral Spots and Flares

Having studied the characteristics of the distribution and evolution of 192 bright points belonging to 68 flares in this region, Ding You-ji et al. (1977b) pointed out: (1) The initial flare activity of the region started over the preceding spot A_N which had the highest energy state of twisted magnetic field among all spots of the group. Synchronizing with the relaxing process of the twisted penumbral filaments of A_N, the initial bright points of flares transposed from three places near the umbra to the outer portion of the penumbra. When the twisted penumbra relaxed at all, the flare activity adjacent to the spot decreased in general. The distances from the flare bright points to the center of A_N changed with time, which was shown in Figure 35. (2) Another spot E_N showed itself in spiral morphology for four days, the frequency of the flare eruption adjacent to it was 5/day, but the frequency was only 0.3/day when the spiral morphology did not appear. It indicated that the spiral spot associated with rather higher frequencies of flare activity. Owing to the shortage of longitudinal field data, we could not study the role of the neutral line in prominence and flare activities of the region in detail.

5. SUMMARY OF THE THREE ACTIVE REGIONS

5.1 The Formation of Spiral Sunspots

Presumably, some dynamic instability resulting from the convective motion below the photosphere made the rotational motion of the magnetic tube of sunspot umbra occur. The penumbral magnetic field lines rooted in the umbral region, the upper portion of them diverged in the shape of a trumpet in the

Figure 28. Flare and coronal prominence at 0315UT on October 27, 1972.

Figure 29. Flare and coronal prominence at 0032UT on October 28, 1972.

Figure 30. Flare and largest coronal prominence at 0257UT on October 29, 1972.

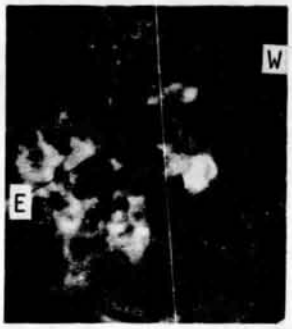

Figure 31. Flare and spray at 2349UT on October 29, 1972.

Figure 32. Flare and coronal prominences at 0731UT on October 30, 1972.

Figure 33. Flare at 0142UT on October 25, 1972.

Figure 34. Flare at 1007UT on October 25, 1972.

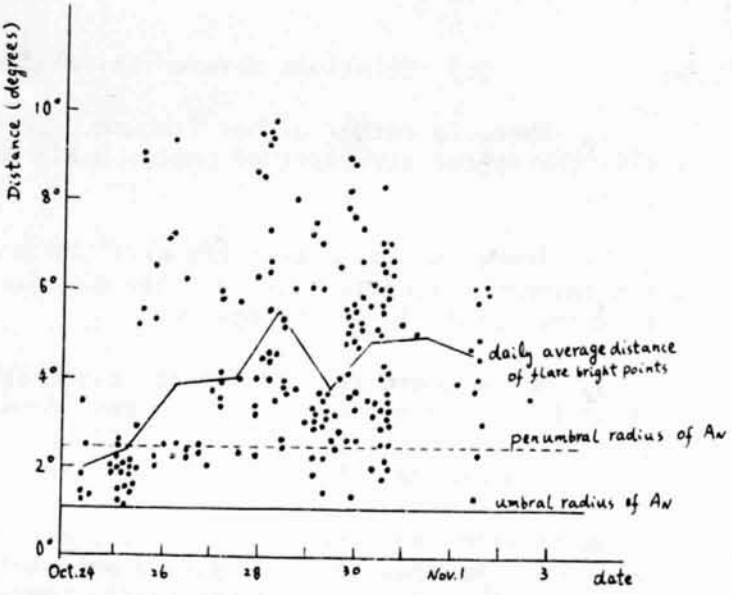

Figure 35. Distances between flare bright points and umbral center of spot A_N. Daily average distances increase with relaxing of twisted penumbral filaments of A_N.

atmosphere of the chromosphere and the upper photosphere. Because the transmission of the disturbance along the magnetic field line takes time, to various extent the phase of the rotational motion of penumbral filaments lagged behind from inside to outside. Therefore, the penumbral helical structure was formed, and the twisted direction of the helical line was opposite to the rotational direction of the spot umbra. The three examples presented in this paper are the observational evidence of this kind of dynamic structure.

5.2 Relations between Spiral Sunspots and Prominences

1. The three examples mentioned above showed unanimously that spiral spots usually associated with the stronger activity of the spot prominences, either of the polarity of them was the preceding (McMath 12094 and 14943) or the following one (McMath 11976). On the photographic data with high quality, the filaments associated with spiral spots usually show up as obvious helical structures, and the twisted direction is mutually consistent with the spiral direction of spots. It means that in both the magnetic tube and current tube they are connected with each other. If the self-inductance coefficient of the prominence is L, then, the twisted free energy stored in it is

$$W = \frac{1}{2} L I^2 \tag{2}$$

2. On the Hα filter photograph, most portions of the prominence magnetic rope keep the general rule of prominence position, that is to say, it extended along the neutral line of the longitudinal field except that a small piece of prominence connected with the sunspot was in the direction of the photospheric magnetic lines.

5.3 Relations between Spiral Sunspots and Flares

1. There is rather higher frequency of the flare eruptions near and inside the spiral structure of photospheric penumbra and chromospheric fibrils.

2. There is also rather higher flare eruptive frequency near and inside the prominence magnetic rope with the obvious twisted structure associated with spiral spots in morphology.

3. Where there is a prominence associated with spiral spots over the neutral line with higher field gradient (δ-magnetic), there will be rather higher probability of erupting major flares; and if not, the major flares were rare, even small flares were very few.

We presume that the points 1 and 2 mentioned above act as sufficient conditions, the point 3 amounts to a necessary condition. There is close physical association between the energy source of flares, the instabilitive factor and the twisted magnetic field (or electric current). The magnitude of the gradient of the magnetic field might show up as the intensity of the outer trigger factor for flares. The major active region McMath 11482 in

August 1971 might be considered as the fourth example (Figure 2). McIntosh (1972) described the motions of the sunspots in the group, and Zirin et al. (1975) described its twisted structure of chromospheric fibrils and flare activities. Babin et al. (1974) reported its spray activities.

6. SPIRAL SUNSPOTS AND ENERGETIC FLARE FORECASTS

6.1 The Possibility of Predicting Energetic Flares with Spiral Sunspots

During the period of 1970-1972, 50 sunspot groups were photographed at Yunnan Observatory. Figure 36 shows the frequency distribution of sunspot groups according to number of days on which spirals are seen. From the figure, we may draw a conclusion that there is close relation between long-life spiral spots and energetic flares (see Ding You-ji et al., 1976a). In addition, the lags of the date between the occurrence of energetic flares and the first sight of spiral spots were researched. The result showed that the spiral spot precedes energetic flares by three to four days. This conclusion is useful for the energetic flare forecast with spiral spots (Figure 37).

6.2 Prediction Technique

1. When the penumbral filaments of a major spot in an active region show up as a spiral pattern on fine structure photographs, it means that the

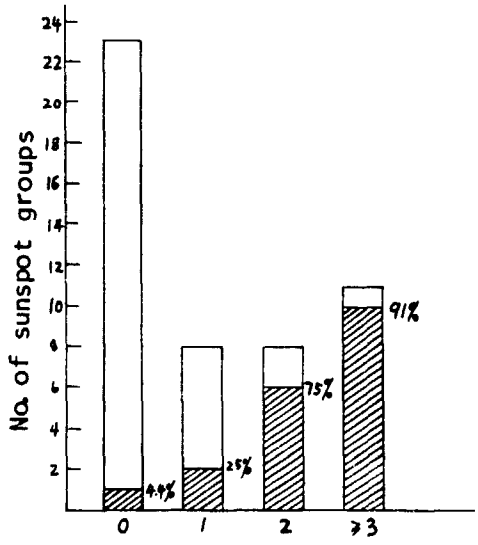

Figure 36. Frequency distribution of sunspot groups according to number of days on which spiral structure was seen. Shaded part with % indicated refers to groups accompanied by larger terrestrial effects.

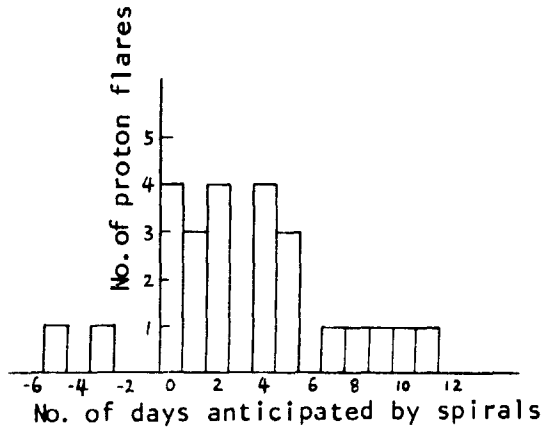

Figure 37. Date difference (date of proton flare minus date of first sight of spiral spot in the same active region) distributions.

flare activity may greatly develop in a few days. Preliminary forecasts should be made, keen joint observations should be taken and close watches should be kept on the development of the active region.

2. In the chromospheric patrol, if a prominence is observed very near or pointing toward the spiral spot, then it shows that the energy, which can be used for flare eruptions, has been transmitted to the upper chromosphere and the coronal space. The flare and prominence activities in the period will then come to a climax.

3. From the shapes of the prominences and flares, and from the types of radio bursts that occur, as well as their corresponding geophysical effects, the future energetic events can be estimated very well.

4. Magnetic field measurements may provide information of the changes of the longitudinal-field gradient on either side of the prominence (neutral line) associated with spiral spots. When the spots with opposite polarities on either side of the prominence approach each other or keep a close distance, it greatly favours the occurrence of a proton flare.

5. When the penumbrae of two spots with opposite polarities have joined together and formed a δ-structure, the prominence associated with the spiral spots over the neutral line is very unstable. Sometimes it turns into a bright plage fibre, narrow and long, and might be extended outside the sunspot group and forms a spot filament, coarse and dark. This kind of situation is almost the foreboding signs of producing proton flares. The necessary alarm must be sent out at once. Many proton flares, though, might occur without so sufficient conditions as mentioned above.

Acknowledgements

We gratefully acknowledge Comrade Ling Zhong-xiu of Yunnan Observatory and Comrade Sheen Lung-xiang of Peking Observatory for their useful help.

REFERENCES

Babin, A. N., L. G. Kartashova, A. N. Koval, M. B. Ogin and N. N. Stepanyan (1974): Izv. Krym. Astrophys. Obs., 52:92.

Ding You-ji, Zhang Bai-rong, Li Wei-bao, Hong Qin-fang and Li Zhi-kai (1976a): Acta Astronomica Sinica, 17:60.

Ding You-ji, Li Wei-bao and Hong Qin-fang (1976b): Acta Astronomica Sinica, 17:110.

Ding You-ji, Li Wei-bao, Hong Qin-fang and Li Zhi-kai (1977a): Acta Astronomica Sinica, 18:40.

Ding You-ji, Li Wei-bao, Wu Ming-chan, Jiang Zhi-zhong, Hong Qin-fang and Liu Zi-zhong (1977b): Acta Astronomica Sinica, 18:143.

McIntosh, P. S. (1972): Sunspots and H-alpha plage in McMath region #11482. World Data Center A. for Solar-Terrestrial Phys. Report UAG-24, Part II, 303-310.

Solar Physics Division, Yunnan Observatory (1974a): Acta Astronomica Sinica, 15:25.

Solar Physics Division, Yunnan Observatory (1974b): Acta Astronomica Sinica, 15:273.

Zhang Bai-rong, Zhong Shu-hua and Wang Hong-zhan (1978): Submitted to Acta Astronomica Sinica.

Zirin, H. and K. Tanaka (1973): Solar Phys., 32:173.

Zirin, H. and B. Lazareff (1975): Solar Phys., 41:425.

SOLAR ACTIVITY PREDICTIONS AT PEKING OBSERVATORY

Solar Activity Prediction Group
Department of Solar Physics
Peking Observatory, Academy of Sciences
Peking, People's Republic of China

Solar activity prediction procedures used at the Peking Observatory are briefly reviewed. Methods for short-term prediction of solar proton events and the results for proton events of importance greater than 1 during the period 1974-1977 are given in detail. The characteristic values of solar cycle 21 are predicted.

Predictions of solar activity have been routinely carried out in the Peking Observatory since 1969. Three kinds of predictions are made. (1), short-term predictions of solar proton events and SID's (72 hours ahead); (2), medium-term predictions (monthly) of solar proton events and SID's; and (3), long-term predictions of solar activity, mainly forecasting of the characteristic values of solar cycle 21. In this paper, we shall describe the principles and methods used for these predictions with emphasis on short-term predictions of proton events (PE).

1. SHORT-TERM PREDICTIONS

For proton events, we are concerned only with the short-term prediction of those with importance greater than 1 according to Smart and Shea's (1971) classification, i.e. E > 10 Mev protons with peak flux value ≥ 10 cm^{-2} sec^{-1}ster^{-1}. Only "danger" (proton event, yes) and "safe" (proton event, no) are forecast. Methods based on the proton-producing-region probability and multiple regression have been developed and used in parallel. The principles and some results are described below.

1.1 Method of Proton-Producing-Region Probability

In establishing the criterion for prediction, we analyzed the features of the solar active regions which produced proton events of greater than importance 1 in the period 1965-1970. We adopted the following four parameters which are available with the present equipment of the Peking Observatory: (i), magnetic field of the sun spot group, (ii), Zurich class of the sun spot group, (iii), Hα flares and (iv), 3 cm radio bursts. Each

parameter is divided into three to four classes according to the "strength" of its activity. In the magnetic parameter, besides the Mt. Wilson classification, factors based on the δ type configuration (Warwick, 1966), "A" configuration (Avignon et al., 1965) and magnetic axis inclination are also taken into account. The flare parameter is taken as a measure of the number and importance of the flares that occurred in the past 24 hours. The parameter of radio bursts is classified according to the number and peak flux of the bursts in the past 24 hours. When an active region has been assigned the above four parameters, classified as i, j, k, l, respectively, the region is given the name of (i j k l) type region. We have determined the types (ijkl) for all active regions that appeared on the surface of the Sun each day in the period 1965-1970. Thus a region that appears on n days is considered as n separate regions. We introduce the idea of "proton producing region", which can be defined as a region that will produce a proton flare within the next 72 hours. The prediction of proton events for the next 72 hours can be performed by the prediction of the occurrence of a proton producing region. By definition, an active region which has a proton event occurring in it during the day or at one and two days before is named a proton producing region. In the 1965-1970 period, we found 43 proton events of importance greater than 1 that could be identified on the visible solar surface, the corresponding proton producing regions were 119 in number. If N_{ijkl} and E_{ijkl} denote the numbers of the (ijkl) active regions and proton producing regions respectively, then the ratio of proton producing regions among various active regions in the years 1965-1970 may be written as $P_{ijkl} = E_{ijkl}/N_{ijkl}$. This can approximately be taken as the probability of occurrence of a proton producing region of the (i j k l) type active region. A table of P_{ijkl} has been compiled. Obviously, when n different active regions appear on the solar surface, the probability of occurrence of a proton producing region for the whole surface will be

$$P = 1 - \prod_{t=1}^{n} (1 - P_{ijkl})_t \qquad (1)$$

We calculated each day's P values for the period 1965-1970 and found that on the day of a proton event and on one and two days before that, one gets P values greater than usual. Especially, on the day of the event, one almost always has a P value greater than the critical value $P_o = 0.05$ (Figure 1). Therefore, in principle, one may establish a criterion of forecasting "danger" or "safe" by estimating the daily P value being $\geq P_o$ or $< P_o$. The actual prediction procedure is as follows:

1. From the solar observations of the day, obtain the classes of the four different parameters for each active region, thus assign the (i j k l) for each region.

2. With the known (ijki), look up P_{ijkl} for each active region from the table of P_{ijkl}.

3. Using equation (1), calculate P, and according to whether P is ≥ 0.05 or < 0.05, forecast the next 72 hours as "danger" or "safe".

For some special occasions, such as when important active regions happened

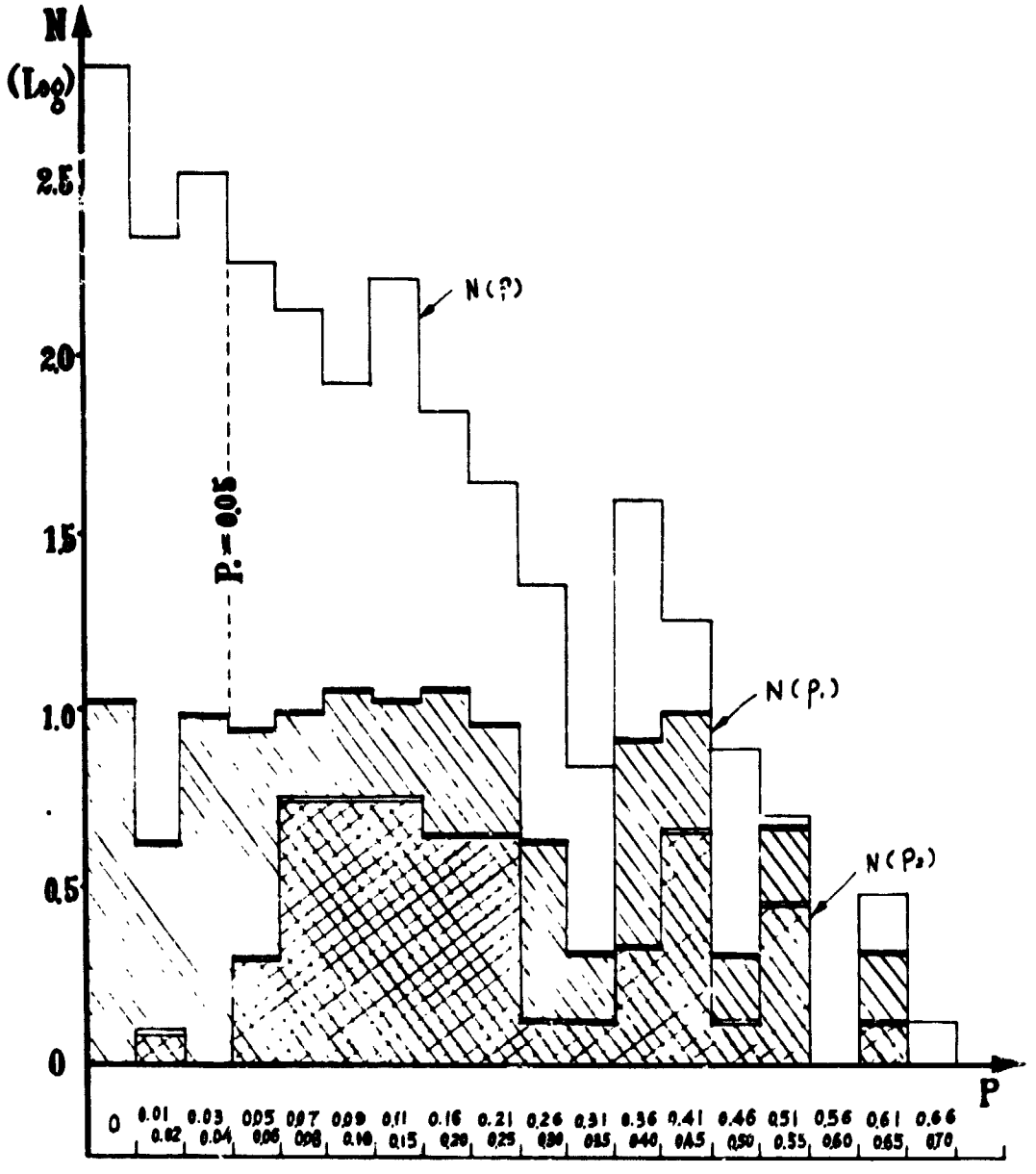

Figure 1. The distribution of the number N of P values (2005 in total) during 1965-1970. P_1 denotes the P value on the day and on one and two days before the proton event, P_2 is the P value on the day of the proton event. N(P), $N(P_1)$ and $N(P_2)$ are respectively the number of days of P, P_1 and P_2 at different intervals.

to be on the limb (so that the magnetic type and configuration were not clear), or that they had just turned behind the west limb (so that the proton stream might still reach the Earth), the experience of the forecaster would be called upon to give a sensible prediction.

1.2 Method of Multiple Regression

Let y denote the occurrence of a proton event (yes or no), i.e. the quantity to be predicted, and let variables x_i be the parameters representing various kinds of solar activity, which are significantly correlated to y. With the help of the "historical" data, one can construct an equation of regression

$$y = b_o + \sum_{i=1}^{m} b_i x_i \qquad (2)$$

where m is the number of variables concerned.

Making use of the standard procedure of multiple regression, one may perform, with a given confidence level, significance tests for any variable in the regression equation, and thus may obtain an equation with as few as possible variables which represent the most significant parameters.

For proton event prediction, we chose as variables a number of parameters including the magnetic type of the sunspot group, the Hα plage, 10 cm flux density....etc. With these historical data, we analyzed the correlation of each of the variables with the proton event, so that relative weights could be assigned to the different classes of each variable. According to the above method, from the relevant data in the period 1966-1972, we obtained the final regression equation with the help of a computer:

$$y = 2.3 + 1.8\, x_1 + 3.2\, x_2 \qquad (3)$$

where x_1 and x_2 are the weighting numbers given respectively to the magnetic type and Zurich class of the principal spot group visible on the solar surface and y, as mentioned above, is the quantity to be predicted.

The procedure for using this method is:

1. From the observed magnetic configuration and Zurich class of the spot group in the principal active region, find the corresponding weighting numbers x_1 and x_2.

2. From equation (3), calculate y.

3. According to whether y is less or not less than a critical number y_o, forecast "safe" or "danger" for the proton event.

Both methods (1.1 and 1.2) have been used for the routine predictions. Some results in the period from January 1974 to October 1977 are shown in table 1. One can see that for proton events of importance greater than 1 (as specified in our case), these two methods yield the same results. During this period all the proton events were duly forecast except the one of importance 1 that occurred on August 22, 1976. In the routine work, when the two methods disagree with each other, which rarely happens, the forecaster would have to decide which to choose.

Table 1. Result of predictions of proton events importance ≥ 1 during the period 1974.1-1977.10. S = Success. F = Failure).

Date of occurrence of proton event	importance	method 1.1	method 1.2
1974 Jul. 3	2	S	S
1976 May 1	2	S	S
Aug. 22	1	F	F
1977 Sep. 17	1	S	S
Sep. 19	2	S	S
Sep. 24	1	S	S
Total number of days when forecast was made:		1056	1076
Total number of days when "danger" was forecast:		40	70
Percent		3.7%	6.5%

Besides the 72 hour forecasts, we also give "immediate" (some ten minutes to several hours ahead) warnings of proton events. For this purpose, we make use of the duration and peak flux density of the centimeter wave bursts. By analyzing the data of 1959-1962 and 1966.9-1969.4, we have found that for proton events of importance greater than 1, the duration Δt and flux density maximum Δs almost always satisfy the following relations:

$$\text{for 3 cm bursts } \Delta t > 15^m, \ \Delta s > 100 \text{ SFU}. \tag{4}$$

$$\text{for 10 cm bursts } \Delta t > 20^m, \ \Delta s > 100 \text{ SFU}. \tag{5}$$

Hence, these relations have been used to decide to issue proton event warnings. With this simple method, we have succeeded on several occasions (e.g. in the events of March 29, 1970, June 14, 1970, and July 3, 1976). When tested by the historical data, we found that this method gives warnings for 92% of the proton events, while the false warning rate amounts to 61%. For further improvement, it becomes necessary to consider the features of the sunspot groups and flares.

It seems to us from experience that the magnetic configuration of the sunspot group plays a dominant role in the prediction of proton events. According to the analysis made on the data of the 20th solar cycle, we have found that it would be useful to classify the magnetic feature of a spot group as "normal" and "abnormal" (Shi Zhong-xian et al., 1975). More

recently, making use of the table of proton events compiled by Svestka and Simon (1973) and the data of proton events in 1970-1972 (Solar Activity Division, Peking Observatory, 1974), we analyzed the proton events of all classes during the period 1965-1972 and the magnetic features of 207 proton active regions in which the events occurred. As a result, we have found that several configurations which appeared "abnormal" had more than usual significant connections with proton events. Applications of this analysis to the work of predictions is yet to be exploited.

For the short term predictions of the SID's, we distinguish four classes of SID events. Thus for the cases of strong, medium, weak and no SID, we assign respectively the numbers 3, 2, 1 and 0. The method adopted for the SID prediction is also based on the principle of multiple regression, similar to that described in section 1.2. The only difference is that the statistics was done separately for the ascending phase and descending phase of the solar cycle. Hence one gets two regression equations:

$$\text{ascending:} \quad y_1 = 11.6 + 8.9x_1 + 5.3x_2 + 4.4x_3 \tag{6}$$

$$\text{descending:} \quad y_2 = 11.4 + 6.9x_2 + 4.7x_3 + 2.9x_4 \tag{7}$$

where x_1, x_2, x_3 and x_4 denote respectively the values given to the types of the magnetic field, plage, 10 cm. flux density and number of centimeter wave bursts of the principal active region. Procedure for the prediction is the same as that described in section 1.2.

2. MEDIUM TERM PREDICTIONS OF SOLAR ACTIVITY

In this program, we are concerned with the monthly predictions of proton events. The following factors have been taken into consideration:

1. Regions of "active longitude". Many authors have already pointed out that active regions which generate proton events have a tendency to concentrate at certain longitudes (Warwick, 1965; Svestka, 1968). We found that the proton active regions in cycle 20 were roughly concentrated near Carrington longitudes 80^0, 130^0, 230^0 and 280^0 (Solar Activity Division, Peking Observatory, 1974). Each region had a width of about 30^0-40^0. Hence when these regions appear on the visible hemisphere of the Sun, the probability of occurrence of proton events will be enhanced.

2. The proton activity of different longitude regions often exhibits different behavior. For example, in the 20th cycle, the region at 80^0 had the greatest rate of proton event production, the majority of events originated in regions having sunspot area greater than 500 (unit: 10^{-6} hemisphere), and the accompanying microwave bursts were comparatively strong; while in the region at 130^0, proton events occurred in sunspot groups with spot areas less than 500, and with only weak microwave bursts.

3. The 80-day cycle of proton activity. A study of proton events in the period 1954-1972 showed that there seems to exist a cycle of 80 days in

proton flare activity(Solar Activity Division, Peking Observatory, 1974). During a certain phase of the cycle, which comprises about 20% of the days in the whole cycle, more than 60% of the proton events of importance 2 and 80% of those of importance 3 were concentrated.

4. Estimation of the evolution and the possibility of recurrence of important active regions. Such estimation is based mainly on the age, shape, rate of evolution and history of recurrence of the region.

In the medium term predictions, we usually plot the Zurich type of spots on the so-called LZT chart, in which date of observation is taken as abscissa and Carrington longitude as ordinate. The "position" of large flares and proton events are then marked on the chart. Taking a sufficiently long period, it is possible by examination of the chart to find the time and space distribution and evolution tendency of the important active regions. This kind of examination, together with the four factors mentioned above, forms the basis of our estimation for the monthly predictions.

The same factors are considered in the medium term predictions of SID's. However, since SID's occur more frequently than the proton events, a larger duration is covered in each prediction.

In addition, studies on the medium term predictions of the total level of solar activities have been conducted. The idea is to consider the active regions with respect to the photosphere, chromosphere and corona as a whole. For this purpose, the magnetic field of the active region, Hα plage and 10 cm radio flux have been taken as parameters signifying these three solar levels. Time sequences of these parameters were treated by the method based on the theory of multi-dimensional stochastic processes. The results have been used as a reference for the medium term predictions.

3. LONG TERM PREDICTIONS OF SOLAR ACTIVITY

In this program we have been concerned mainly with the study of characteristic values of the 21st solar cycle. The long-term behaviour of solar activities have also been investigated (Lin Yuan-chang and Chang Chien-chung, 1977; Chow Yee-hsin, 1977). The study on the prediction of the 21st cycle was carried out in 1974. At that time we predicted that the minimum phase should begin at t_m = 1975.8, which is fairly close to the actual time 1976.25 announced later. Recently we have estimated the time of maximum activity t_M and sunspot number maximum R_M (monthly smoothed value) to be

t_M: 1980.9 ± 0.8 yr

R_M: 115 ± 15

Regression analysis was used for the estimations of t_m and R_M. Thus, let x_1 be the interval between adjacent maxima, x_2 be the length of descending portion and x_3 the length of ascending portion of the last cycle (Figure 2).

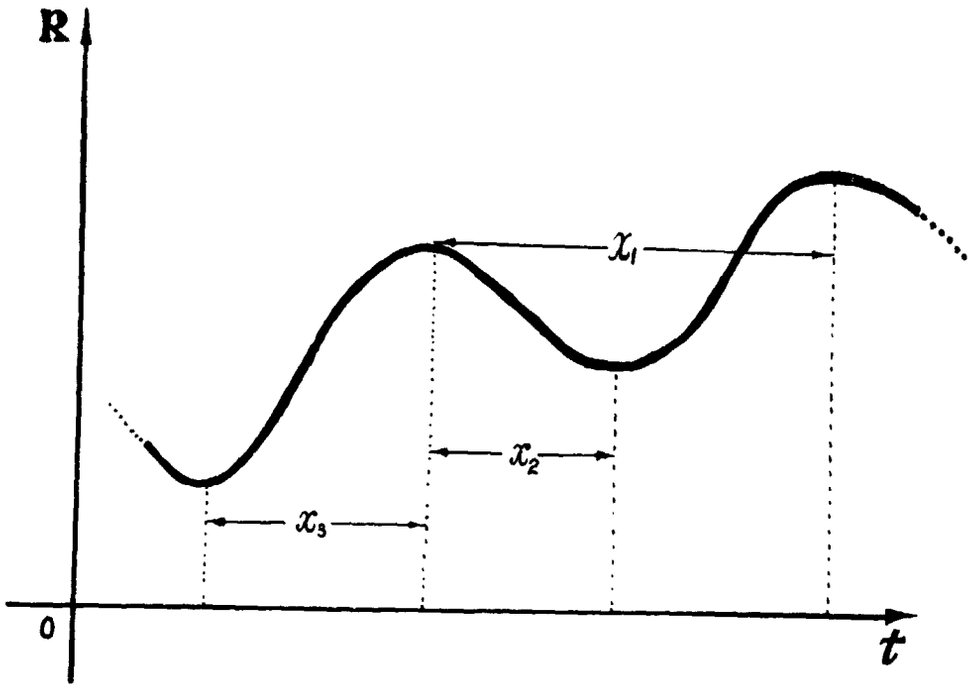

Figure 2. The definitions of x_1, x_2 and x_3.

Making use of the x_1, x_2, x_3, values of 1-19th solar cycles (Waldmeier, 1961), we performed the regression calculations in steps. We obtained, with confidence level of 95%, the regression equation:

$$x_2 = 9.17 - 0.58x_3 \pm 1.15 \text{ (yr)} \tag{8}$$

$$x_1 = 1.73x_2 + 0.55x_3 - 2.89 \pm 0.8 \text{ (yr)} \tag{9}$$

We knew in 1974 that the length of ascending portion of the 20th cycle was $x_3 = 4.1$ years. Substituting this in equation (8), we obtained $x_2 = 6.9 \pm 1.5$ yr and $t_m = 1968.9 + 6.9 \pm 1.5 = 1975.8 \pm 1.5$ yr. Now we also know that $x_2 = 7.2$ yrs in the 20th cycle, so from (9) we have obtained $t_M = 1980.9 \pm 0.8$ yr.

The estimation of R_M has been made in two steps. Firstly, the mean sunspot number R from 1700 through 1974 were smoothed to get an average curve $\bar{R}(t)$. Denoting the deviation of R with respect to $\bar{R}(t)$ by ΔR, we found that in the period of 1700-1974 the distribution of ΔR (214 in total) is nearly a normal distribution. We know that the distribution of peak values G(x) of a random variable which has a normal distribution can be taken as $\Lambda(x)$, thus

$$G(x) \approx \Lambda(x) = e^{-e^{-y}} = e^{-e^{-\frac{x-b}{a}}} \tag{10}$$

In the 1-20th solar cycle, we have 20 peak values of ΔR_n. Substituting in (10), we determine coefficients a and b. With these, we estimate that the peak value R_{21} of the 21st cycle should lie between 30 to 77 with a probability of 0.60. The average value $\overline{R}(t)$ at 1980 may roughly be taken as 50 (Lin Yuan-chang and Chang Chien-chung, 1977), so that we obtain $R_M \approx 80 - 130$.

On the other hand, one can look at the problem from the viewpoint of apparent processes instead of statistical distributions. Thus, the history of solar activity since the 1st cycle, with the exception of 4-6th cycle, has shown that, if during a certain cycle the R_M value decreases with respect to that of the previous cycle, then the R_M value at the next cycle will invariably increase. Even in the case of the 4 - 6th cycles, where the R_M value drops in two successive cycles, the actual amount of drop in the 6th cycle from the 5th is only 0.5. Now, we see that in the period between 19-20th cycle, the R_M values have dropped sharply, reaching 90.7 already. This sharpness of dropping is only surpassed by the historically sharpest drop of 92 during the 4-5th cycle. Holding this in mind, one may expect that possibility of another drop in the 21st cycle would be very small, and since $R_M = 110.6$ in the 20th cycle, the R_M value of the 21st cycle would most probably lie in the greater half of the interval 80-130, so one may predict that for the 21st cycle, $R_M \approx 100-130$.

REFERENCES

Avignon, Y. et al. (1965): in R. Lüst (ed.), Stallar and solar magnetic field, North-Holland, Amsterdam, 373.

Chow Yee-hsin (1977): in Huang Shan Symposium on Astrophysics (in Chinese, to be published).

Lin Yuan-chang, and Chang Chien-chung (1977): Kexue Tongbao, (in Chinese), 22:59.

Shi Zhong-xian, et al. (1975): Acta Astronomia Sinica, 16:12.

Smart, D. F. and Shea, M. A. (1971): Solar Phys., 16:484.

Solar Activity Division, Peking Observatory (1974): Acta Astronomia Sinica, 15:34.

Svestka, Z. (1968): Solar Phys., 4:18.

Svestka, Z. and Simon, P. (1973): Catalog of particle events, 1955-1969, Dordrecht-Holland/Boston, U.S.A.

Waldmeier, M. (1961): Sunspot Activity in the Years 1610-1960. Zurich Schulthess and Co. AG.

Warwick, C. S. (1965): Astrophys. J., 141:500.

Warwick, C. S. (1966): Astrophys. J., 145:215.

LONG-TERM FORECASTING OF SOLAR ACTIVITY

XU ZHEN-TAO, ZHAO AI-DI, MEI YAN-LIN, GUO QUAN-SHI
中国科学院紫金山天文台
PURPLE MOUNTAIN OBSERVATORY, ACADEMIA SINICA
NANKING, CHINA

When the 20th solar cycle was not yet ended, we made a forecast of the basic parameters of the 21st cycle (1). Now that the trend of the ascending phase of the 21st cycle has gradually become clear, we can use the new information to make corrections to the past forecast. Besides this, in consideration of the requirements of meteorological, hydrological, and geophysical units, we shall make an estimate about the level of solar activity in the 22nd cycle.

1. PREDICTION OF R_M AND t_M OF THE 21ST CYCLE

The 20th cycle came to an end in June, 1976, i.e. in the year 1976.5. The corresponding smoothed monthly mean of relative numbers was $\bar{R}_m = 12.2$(2). Therefore, the solar activity at present is in the ascending phase of the 21st cycle. Under this condition, it is convenient to estimate the peak value $\bar{R}_M$ and the epoch of maximum $\bar{t}_M$ of the present cycle by means of the method of Waldmeier (3). According to Waldmeier's formula, we have

$$V = \frac{\bar{R}_M - \bar{R}_m}{12(18.4 - 7.14 \log \bar{R}_M)}, \qquad (1)$$

where V is the rate of rise of the present ascending phase. From the latest issue of S.G.D. (4), we find that the smoothed monthly mean of the relative numbers in November, 1977, is 49.9. From this we may determine the value of V and obtain from equation (1) $\bar{R}_M = 115$, and $\bar{T}_1 = 3.7$ years, where $\bar{T}_1$ is the estimated value of the rise time of the present cycle. Because the epoch of minimum was in the year 1976.5, the epoch of maximum of this cycle must be

$$\bar{T}_M = 1976.5 + 3.7 = 1980.2. \qquad (2)$$

With the yearly mean values of the relative numbers in 1700-1977 some parameters and the rates of rising in the first two years of the

ascending phase of all the cycles may be tabulated in the following:

cycle no.	V_1	V_2	R_m (minimum)	$R_m^{(4)}$ (minimum)	R_m (maximum)	$R_m^{(4)}$ (maximum)	T_1 (years)	T_2 (years)
-4	6	5	5		58		5	7
-3	2	9	0		63		5	6
-2	10	19	11		122		4	6
-1	11	18	5	5.2	111	88.5	5	6
0	6	11	5	5.2	83.4	94.8	6	5
1	0.6	22.2	9.6	7.6	85.9	100.6	6	5
2	26.4	32.0	11.4	7.8	106.1	96.6	3	6
3	12.8	72.7	7.0	8.2	154.4	107.4	3	6
4	13.9	58.8	10.2	9.6	132.0	119.6	3	11
5	2.7	7.7	4.1	8.2	47.5	110.0	6	6
6	1.4	3.6	0	5.3	45.8	94.9	6	7
7	6.7	8.1	1.8	4.0	70.9	74.0	7	3
8	4.7	43.7	8.5	3.6	138.3	75.6	4	6
9	4.3	25.1	10.7	5.2	124.7	94.9	5	8
10	18.4	32.1	4.3	6.3	95.8	107.4	4	7
11	30.3	37.4	7.3	7.7	139.0	124.4	3	8
12	2.6	26.3	3.4	6.4	63.7	105.8	5	6
13	0.8	28.5	6.3	5.3	85.1	95.9	4	8
14	2.3	19.4	2.7	4.9	63.5	87.8	4	8
15	8.5	37.8	1.4	3.4	103.9	79.0	4	6
16	10.9	27.6	5.8	4.0	77.8	82.6	5	5
17	3.0	27.4	5.7	3.9	114.4	89.9	4	7
18	23.6	59.4	9.6	5.6	151.6	111.9	3	7
19	33.6	103.7	4.4	6.4	190.2	133.5	3	7
20	4.9	31.8	10.2	7.5	105.9	140.5	4	8
21	14.9		12.6	9.2				

Where V_1 and V_2 are the rates of rising of the first and second years in the ascending phase respectively. Each of them is the difference between the yearly mean value of relative numbers of the following year and that of the preceding year. R_m and R_M are respectively the minimum and the maximum of the yearly mean values of relative numbers. $R_m^{(4)}$ and $R_M^{(4)}$ are the running mean values in four consecutive cycles. T_1 and T_2 are the lengths of the ascending and descending phases. There can be seen from the above table:

(1) If V_1 is larger than 10, the probability for R_M to be larger than 100 is 0.75. The mean peak value of such cycles is $R_M = 130 \pm 14$, the mean length of the ascending phases is $T_1 = 3.6$ years.

(2) If V_2 is larger than 40, R_M should be larger than 130. The mean length of the ascending phases of these cycles is $T_1 = 3.3$ years. For the 21st cycle there has been obtained $V_1 = 14.9$. According to the

observations of sunspots in the first half of 1978, we guess that the yearly mean of the relative numbers in 1978 will be 70. If this will be true, we shall have $V_2 > 40$. Therefore, we estimate that the peak value of the relative number of the 21st cycle will be $R_M \geq 130$. Considering the above results, we choose

$$R_M = 130 \pm 15, \qquad t_M = 1980.2 \pm 0.3 \tag{3}$$

as the predicted values of the 21st cycle. They are in rather good accordance with the results of Xanthakis and Poulakos (5) and also with those of Hill (6).

2. PREDICTION OF R_M AND R_m OF THE 22ND CYCLE

From the above table, R_M, $R_M^{(4)}$ and R_m, $R_m^{(4)}$ were used to draw Fig. 1 and Fig. 2 respectively. In these figures the curves of $R_M^{(4)}$

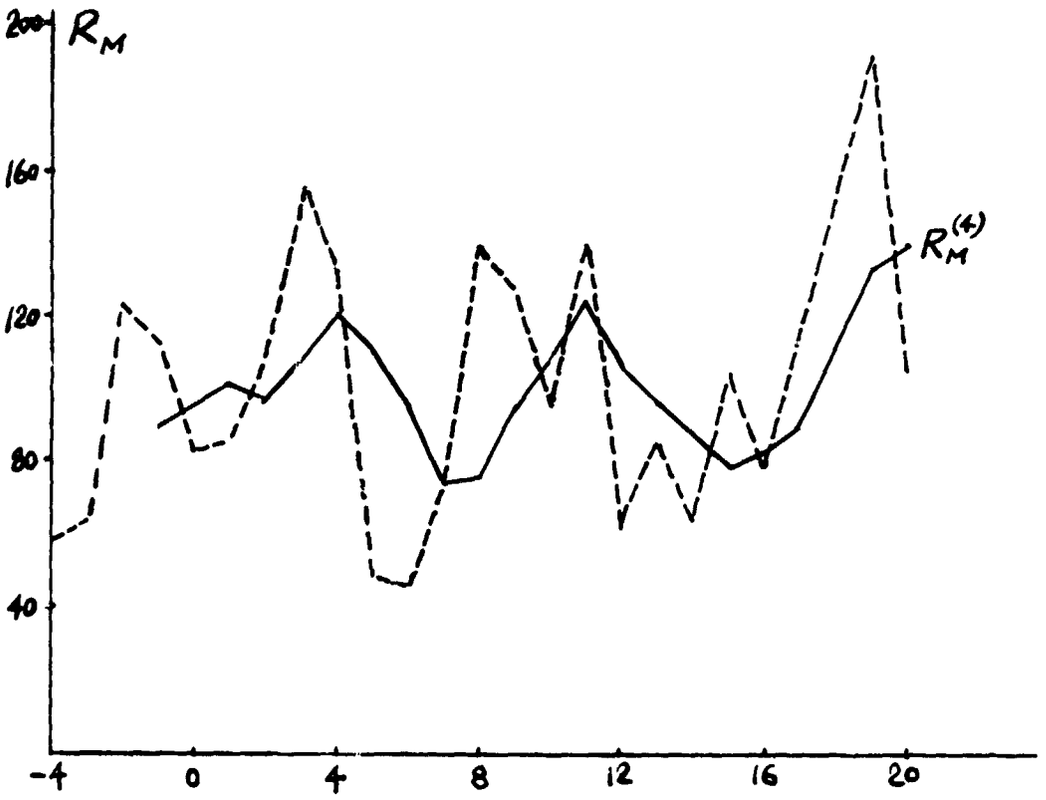

Fig. 1

The long-term forecasting of the yearly maximum sunspot number as a function of sunspot cycle number. Dashed line is the yearly mean sunspot number. Solid line is the running mean from four consecutive cycles.

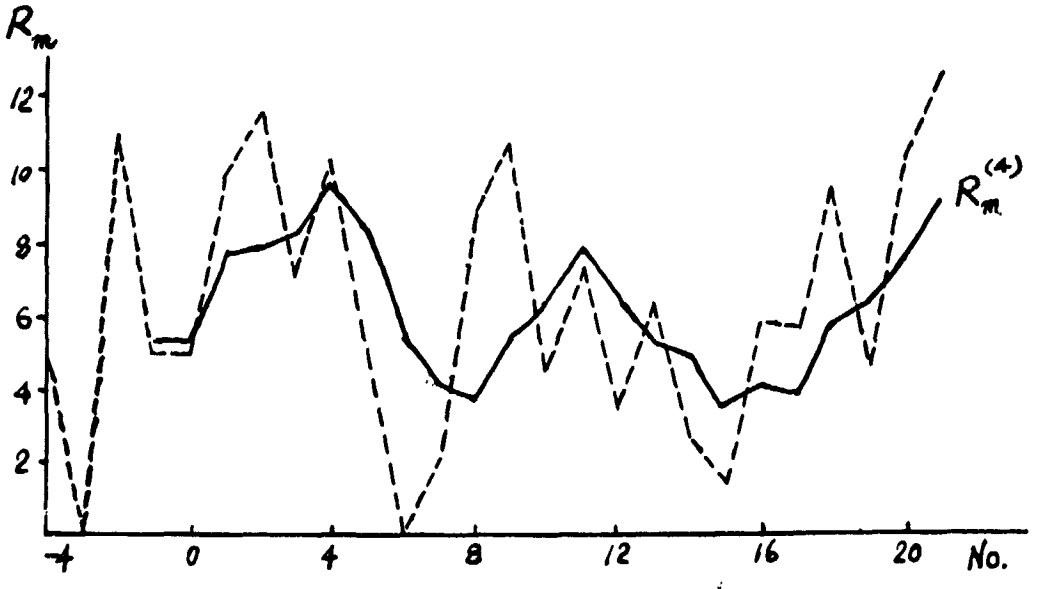

Fig. 2

The long-term forecasting of the yearly minimum sunspot number.

and $R_m^{(4)}$ are the typical representations of the well-known 80-year cycle. It is interesting to note that these two curves are almost completely parallel to each other. Therefore, we have enough reason to confirm that they have the same tendency of variations. It can be seen from Fig. 1 that after the 19th cycle the curve of $R_M^{(4)}$ rises up more and more slowly. It seems to have attained a peak in the 21st cycle. On the other hand, if R_M continued to rise, there should be R_M(No.22) > R_M(No.18) = 151.6. This is very improbable, because the probability of appearance of such a case is only o.12. At the same time, this would make the ascending time of the present 80-year cycle too long, differing much from the past two 80-year cycles. Taking these circumstances into consideration, we think it is comparatively reasonable to take the R_M value of the 21st cycle as the maximum of the present 80-year cycle. The R_m curve should be treated similarly. Therefore, beginning with the 22nd cycle, both R_M and R_m curves will probably enter a descending phase. From the above table, the descending rates of the R_M curves for the past two 80-year cycles are respectively:

$$Q_1 = 15.2, \qquad Q_2 = 11.4. \tag{4}$$

By the same reasoning, the descending rates of the R_m curves are respectively:

$$P_1 = 1.5, \qquad P_2 = 1.1. \tag{5}$$

Taking these as limits, one may get the predicted values of R_M and R_m for the 22nd cycle to be

$$R_M = 90 \text{ to } 106, \qquad R_m = 3.6 \text{ to } 5.2. \tag{6}$$

As for the peak value of the 22nd cycle, (7) and (8) give out very low predicted values. This is worthy of further discussion.

3. PREDICTION OF t_m AND t_M THE 22ND CYCLE

We have the predicted R_M(No.21) = 115 to 145 and take the mean value of the lengths of the descending time of some cycles with peak values lying in this range according with the above table. Then we get T_2 = 7.8 years. By the same reasoning, from the predicted R_M(No.22) = 90 to 106 we may take its mean length of ascending time as T_1 = 3.8 years. It is known that t_M(No.21) = 1980.2 $\pm$ 0.3. Hence t_m(No.22) = 1980.2 + 7.8 $\pm$ 0.3 = 1988.0 $\pm$ 0.3, t_M(No.22) = 1988.0 + 3.8 $\pm$ 0.3 = 1991.8 $\pm$ 0.3.

* * *

In conclusion the results of our forecasting may be tabulated as follows:

	t_m	R_m	t_M	R_M
cycle No. 21			1980.2 $\pm$ 0.3	130 $\pm$ 15
cycle No. 22	1988.0 $\pm$ 0.3	3.6 $\pm$ 5.2	1991.8 $\pm$ 0.3	90 to 106

REFERENCES

1. Xu Zhen-tao, Zhao Ai-di, Xue Yi-sheng and Mei Ya[illegible] Acta Astronomica Sinica, in print.
2. Solar Geophysical Data, No. 405, part 1, (1978).
3. Ю.И.Витинский, Цикличность и Прогнозы Солнечной Активности, (1973).
4. Solar Geophysical Data, No. 406, part 1, (1978).
5. J. Xanthakis & C. Poulakos, Solar Phys., 56, 467, (1978).
6. J. R. Hill, Nature, 266, 151, (1977).
7. T. J. Cohen & P. R. Lintz, Nature, 250, 398 (1978).
8. K. Sakurai, Nature, 269, 401, (1978).

PREDICTION OF LARGE ACTIVE REGIONS AT THE EAST SOLAR LIMB

Guo Quan-Shi
中国科学院紫金山天文台
Solar Activity Prediction Group
Purple Mountain Observatory
Academia Sinica
Nanking, China

1. INTRODUCTION

The execution of space probe plans often requires forecasting of solar activity for a period longer than two weeks. However, while the forecasting for half or one day beforehand is easy, predictions for one or several weeks are extremely difficult. There are two main problems: (1) Because of solar rotation, it is hardly possible to predict active regions which appear about the eastern limb, (2) it is difficult to foresee the sudden birth of solar active regions for several days beforehand. Most of the strong active regions come from behind the east limb by rotation, and only a few of them are born on the solar disk. For instance, throughout the year 1959, there were 103 sunspot groups with magnitudes ≥ 5 (according to the classification used in the Quarterly Bulletin of Solar Activity, the 9th magnitude is the largest and the 1st is the smallest). Among them, 23 groups, or only 22%, were born on the visible disk of the sun. In the years 1970-1972, among the 78 sunspot groups with areas larger than 500, there were 11 groups, or only 14%, that were born on the visible solar surface. Therefore, we shall consider the problem of forecasting the large active regions that appear by rotation around the east limb. From this we attempt to estimate the probability of proton events and propose a method for forecasting quiet periods for the years of high level of activity.

2. FOUNDATION OF FORECAST METHOD

Now the question we would like to study is how to foresee the large active regions that appear at the east limb. At which position on the sun should a sunspot group be born if it is to be seen at the east limb ($E75^0$-90^0) as a ripely developed group of type E or F? The answer to this question is indefinite, because there are many possible ways a sunspot group may develop. But the sunspot groups that are most powerful in producing flares develop according to the curves in Figure 1 (Kuiper, 1953).

If what we see at the east limb is the hatched region in the figure, then spot groups of types E and F should have been born in W 60^0 - > W 90^0 of the western hemisphere of the sun in the preceding rotation. Because it

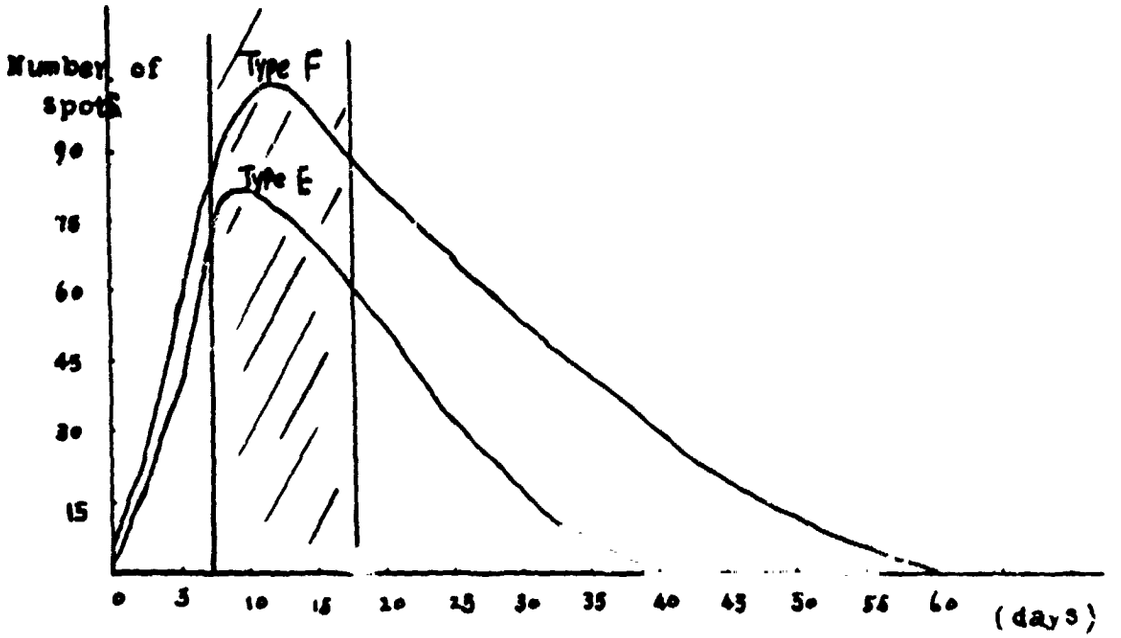

Figure 1. Course of development of spot groups of types F and E.

is easy to observe the birth of spots near the west limb, we may judge the occurrence of large active regions at the east limb after two weeks.

Nevertheless, the further development of a spot after its birth varies greatly. Consider the conditions for it to develop into a type E or F sunspot group. Such development depends upon the degree of intensity of magnetic flux emerging from beneath the photosphere and by the conditions of the background magnetic fields in the vicinity of the emerging magnetic flux. The former can be judged by the small spot groups and the degree of changes of the accompanying chromospheric flocculi. As for the latter, the conceptions proposed by many authors about the birth and development of active regions as well as the conception of complexes are all very useful (Dodson and Hedeman, 1968; Bumba and Howard, 1965; Svestka, 1976; Bumba, 1970; Martres, 1968). With the conceptions of these authors, we think the following is useful to our method of forecasting. The emergence of new magnetic flux is not an isolated process. The structure of the surrounding stronger magnetic fields (including spot groups and background fields) may play a beneficial role for the formation of large spot groups. The emergence of a new magnetic flux in the vicinity of existing spot groups or in residual stronger fields may give rise to a larger probability of the formation of a spot group with proton flares.

3. NECESSARY CONDITIONS OF OBSERVATIONS

With a routine mapping of spots (mapping is more profitable than photography because the latter may miss the small spots in the primary stage of

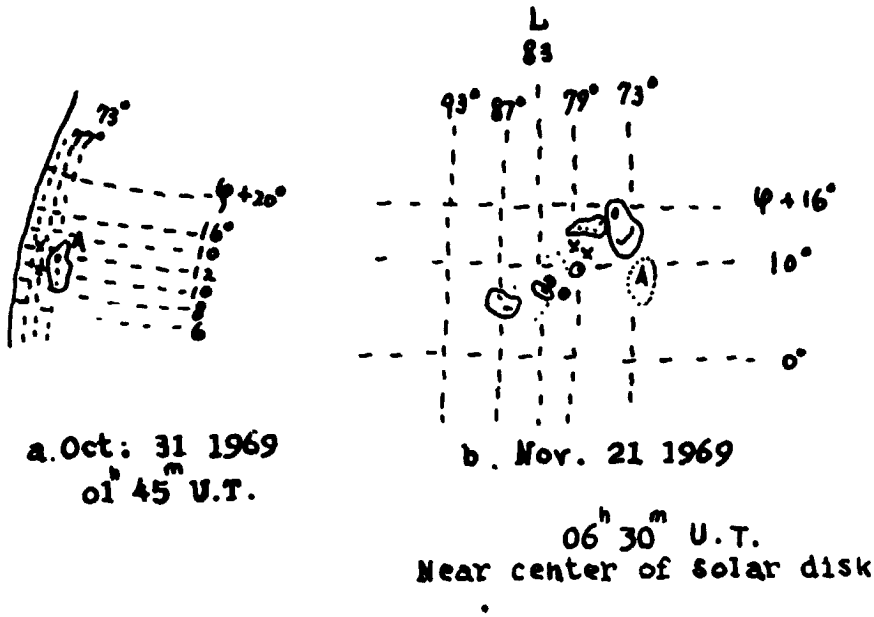

Figure 2. Emergence of new magnetic flux in the vicinity of a spot group gives rise to a proton active region.

the formation of spot groups) and a routine Hα chromospheric patrol, one may observe the outflow of magnetic flux. But if one also possesses magnetic maps and calcium monochromatic images, he can make a better judgement about the appearance of a new magnetic flux. Some authors think that, in two or three days before the birth of spots, the surrounding magnetic fields may be influenced. This perhaps may be measured by a sensitive magnetograph. Having no magnetograph at hand, we wish that this may be perceived from the Hα chromospheric flocculi.

4. CRITERIA FORECASTING

From March to December in 1972, we carried out regular preliminary forecasts of the spot groups that might appear near the east limb. The criteria could be only qualitative. What could most easily be forecast was the fairly strong active regions that produce several proton events. The criterion for forecasting such kind of active regions was that near the west limb there should suddenly appear a very bright flocculus. It must develop very rapidly, the area of the flocculus may increase in 5-6 times on the second day. Simultaneously, if there appear some small spot groups that change quickly, then when the active region of this kind rotates to the east limb, it may give rise to several proton events and short-wave fadeouts in communications.

The criterion for a spot group that produces one or two proton events and short-wave fadeouts is as follows: A bright flocculus appears at the west limb. It increases by two to three times on the second day. At the

same time, there may appear some new small spots.

Besides this, sunspot groups of ordinary degree of activity correspond only to the flocculi of ordinary brightness on the west limb. More attention should be paid to the case mentioned above, when flocculi appear in the vicinity of existing large spot groups. This may give rise to conditions of producing magnetic fields with more complicated structures. We considered the time interval when large spot groups may possibly produce proton events and ionospheric disturbances as being 13 days from the east limb passage to the west limb.

5. FORECASTING RESULTS IN 1972

According to the morphology of flocculi before the formation of sunspot groups as described above, and some other photospheric and chromospheric phenomena and estimating the rate of development of spot groups by the changes of the fields of flocculi, we carried out experimental forecasting of the level of solar activity in the coming month; this was done twice per month. Beginning from March of 1972, we made 18 forecasts in the nine months (on the day of forecasting we took into account the short-term forecasts of the existing spot groups on the solar surface in considering the solar activity in the coming several days). The results of forecasting are partially given in Table 1 as illustrative examples.

We concluded that in the nine months there appeared 41 spot groups of which the maximum areas were larger than 150 in units of millionths of the hemisphere. Among them, 16 spot groups (39%) were forecast comparatively accurately. The estimate of both their positions and levels of activity were generally correct. Fourteen spot groups (34%) were forecast partially accurately. Their positions were foreseen correctly, but estimates of their levels of activity were somewhat higher or lower than reality. Eleven spot groups (27%) were forecast in vain, or nearly in vain. There were another 11 groups which were not foreseen at all, but some of them were born on the solar surface, and properly speaking, one cannot expect to see any evidence of them before one rotation. But it should be pointed out that this was our initial test and our experience was insufficient. Moreover, the data used for forecasting was also not complete or fine enough. Nevertheless, as can be seen from the results obtained, the method we used is effective and applicable for part of the strong active regions. With the accumulation of experience and the improvement of material, it may be possible to make daily forecasts of major groups. As mentioned above, we should be more confident to forecast strong active regions because they have more evident processes of formation. This has some practical significance for forecasting both periods of low activity and periods of strong disturbances in communication. We can examine as examples the three strongest active regions (all of them were active regions with proton flares) in the period of our forecasts (March-December 1972). The predictability of them are as follows:

1. Heliographic location: $L10^0\phi44^0$. Date of central meridian passage CMP was August 4. Three proton events and three strong SWF's. Situation of birth of new active centers: new Hα flocculli

Table 1. Comparison of predicted and observed active regions during March-June 1972.

	Predicted Active Regions				Observed Active Regions			
Date of prediction	heliographic longitude L^0	location latitude ϕ^0	date east limb passage	Comments on degree of activity, group type or area	heliographic latitude L^0	location latitude ϕ^0	type or area	to miss in prediction
1 March 31	(1) 259	-9	April 19	D	251	-7	J	
	(2) 105	-8	April 4	E,F	82	-9	D	
					90	-16	D	
2 April 15	(1) 105	0-10	May 1	all are moderate or small groups	93	17	E 371	D
	(2) 128	-10	April 29		128	-6	C 23	
	(3) 206	15	April 23		in vain			
	(4) 250	-(5-15)	April 26		251	-8	C 22	389
3 April 29	(1) 290-320	10-20	May 13	strong groups	300	13	D 296	E 1111
	(2) 350	-15	May 10		332	-6	F 435 371	
	(3) 105-120	0-10	May 1		93-105	8-17	A,E 371	
	(4) 20	-(15-20)	May 7		10	-8	D 408	
4 May 15	(1) 100-110	5-10	May 27	moderate or small	98	6	C 19	
	(2) 100-110	-(5-15)	May 27		78-91	-(9-16)	C,E 793	
	(3) 35-40	5-15	June 2		46	5	B 9	
	(4) 200	-12	May 21	J	192	-9	B 13	
	(5) 150-170	5-15	May 24	unusual group	165	8	D 501 (1 proton event)	
5 May 31	(1) 290	-(13-23)	June 10	500	302	-13	421	E
	(2) 230	5-15	June 15	300	242	8	53	569
6 June 15	(1) 166	10	June 20	400	165	4	184	
	(2) 84	-8	June 27	600	86	-4	156	
	(3) 95	5-15	June 29	300	106	7	216	

suddenly appeared on solar surface W45^0, after that its area rapidly increased and a spot group appeared.
Predictability: Predicted appearance of strong proton region based on observations of rapid variation of flocculli brightness on July 11-13.

2. Heliographic location: L164$^0\phi$8^0. CMP Date: May 30. One proton event and one strong SWF. Situation of birth of new active centers: sudden appearance of Hα bright point on the solar surface W60^0 during 8^h-19^h U.T. May 8; the next day its area rapidly increased and passed behind the west limb on May 10.
Predictability: predicted appearance of strong proton region based on observation of rapid formation of new region on May 9.

3. Heliographic location: L314$^0\phi$-12^0. CMP Date: October 30. One proton event and one strong SWF. Situation of birth of new active centers: sudden appearance of Hα bright flocculli and small spots, after appearance of two bright points like small flares.

6. IMPROVEMENT OF FORECASTING METHODS

If we introduce the conceptions of the longitudes of activity and complexes of activity into the criteria of forecasting, there may be a better effect for the forecasting of proton active regions.

CRITERION A: The emergence of new magnetic fluxes near the west limb.
- a. birth of new spots on the photospheric background or in the vicinity of spot groups.
- b. emergence of new magnetic fluxes accompanied with the heating of the chromosphere bright points that should be observed in the Hα chromosphere.
- c. comparatively bright flocculli.

CRITERION B: Condition of magnetic fields at the place of emergence of new magnetic fluxes.
- a. within the longitudes of activity (130^0-200^0, 310^0-10^0, 30^0-90^0).
- b. in the vicinity of existing spot groups.
- c. in the regions where before one period of rotation there existed spot groups.

The above criteria have been used to examine the strongest active regions which appeared on the east limb in 1959-1972. The results are listed in Table 2.

Predictions of quiet periods in years of high level of activity may also be deduced from the criteria mentioned above. When the above criteria do not appear near the west limb, one can reliably predict safe quiet periods two weeks in advance during each solar rotation. When only criteria Ac or Bc appeared near the west limb, one can still predict quiet periods. Besides these cases, flares or proton flares may be expected.

Table 2. The analysis of predictability of big spot groups during 1959-1972.

NO	Location L^0	Location ϕ^0	Date of C.M.P.	Max. area (10^Y hemisphere)	Number of prot. event (A) and ≥ 2 SWF (B) or ≥ 2 flare	Aa	Ab	Ac	Ba	Bb	Bc	Est. of predictability
1	57	17	May 14 1959	1850	1(A)15 B			+	+	+		possib.
2	336	17	June 17 1959	1109	1 A,16 B		+		+	+		reliab.
3	330	17	July 14 1959	1847	3 A,11 B	+			+	+		reliab.
4	285	6	Dec. 1 1959	2475	- 15 B			+				imposs.
5	126	14	May 25 1960	1076	- 3 B			+	+	+		possib.
6	351	29	May 8 1960	1750	1 A, 2 B				+			imposs.
7	32	26	Nov. 11 1960	1770	6 A, 7 B	+	+		+		+	reliab.
8	47	-7	July 14 1961	1570	5 A,10 B	?			+			imposs.
9	310	13	Sept 20 1963	1241	4 A,10 B			+	+		+	possib.
10	146	17	Mar. 21 1966	1846	1 A, 9 B	+	+		+	+		reliab.
11	184	22	Aug. 28 1966	1002	2 A, ?	?			+	+		possib.
12	222	28	May 25 1967	2031	2 A, 6 B	+				+		reliab.
13	105	23	June 3 1967	1025	1 A					+		imposs.
14	100	26	July 28 1967	1774	- 6 B	+				+		reliab.
15	87	22	Aug. 25 1967	956	- 4 B				+	+		imposs.
16	173	-16	Oct. 28 1968	1225	1 A, 8 B	?			+	+		possib.
17	344	19	Nov. 11 1968	776	1 A	+			+			reliab.
18	79	10	Nov. 21 1969	1713	1 A,13 B	+			+	+		reliab.
19	130	-8	May 27 1970	532	1 A	+			+	+		reliab.
20	227	16	June 16 1970	1487	1 A						+	imposs.
21	225	17	Jan. 25 1971	1600	1 A						+	imposs.
22	23	8	Feb. 22 1972	1049		+		+			+	possib.
23	164	8	May 30 1972	501	1 A, 1 B		+		+	+	+	possib.
24	10	14	Aug. 1972	1179	3 A, 3 B	+	+		+	+		reliab.
25	314	-12	Oct. 29 1972	2299	1 A, 2 B	+	+		+	+		reliab.

REFERENCES

Bumba, V. (1970): Large-scale magnetic fields and activity patterns on the Sun. In: Solar Terrestrial Physics/1970 (ed. E. R. Dyer), IUCSTP Symposium, Leningrad, D. Reidel Publ. Co., p. 21.

Bumba, V., and R. Howard (1965): Large-scale distribution of solar magnetic fields. Astrophysical Journal., Vol. 141, p. 1502.

Dodson, H. W., and E. R. Hedeman (1968): Some patterns in the development of centers of solar activity, 1962-1966, IAU Symposium (ed. K. O. Kiepenheuer), p. 56.

Kuiper, C. P. (1953): The Sun. University of Chicago Press, p. 344.

Martres, M. J. (1968): Origine des regions actives solaires anormales. In: Structure and Development of Solar Active Regions, I.A.U. Symposium 35, p. 25.

Svestka, Z. (1976): Development of solar active regions. Proceedings of the International Symposium on Solar-Terrestrial Physics, June 7-18, 1976, p. 129, publ. by American Geophysical Union.

D15-92

N80-18477 SHORT-TERM SOLAR ACTIVITY FORECASTING

Chen Xie-Zhen and Zhao Ai-Di
中国科学院紫金山天文台
Solar Activity Prediction Group
Purple Mountain Observatory
Nanking, China

1. INTRODUCTION

Many solar physicists have discussed and reviewed short-term forecasting of solar activity. Extensive observations and statistics have shown that the outburst of flares is closely connected with the magnetic structure of active regions, the morphology of sunspots, spot areas, the morphology and brightness of flocculi, the evolution of active regions, the emission of microwave radiation and X-rays, etc. Because the physical process and mechanism of the occurrence of flares are not yet very clear, the forecasting nowadays is still a probability forecasting based on statistics.

Our project of forecasting is based on the presently available observations at the Purple Mountain Observatory. We try to adopt a comprehensive project of forecasting, as simple and convenient as possible. Its aim is to foresee the level of activity of every active region on the solar surface in the coming 1-3 days and thereby to estimate the possibility of the occurrence of ionospheric disturbances and proton events.

2. SOURCE OF STATISTICAL DATA

This project was formulated in 1972-1973. In order to fit the descending phase of the solar activity cycle, we chose the data of 1959-1963, belonging to the 19th cycle, and those of 1970-1972 in the 20th cycle for separate statistical study. We chose the type, area, magnetic classification and longitude of activity as four parameters. The levels of activity are defined as follows:

0th level of activity: without flares of importance 1 or larger.

1st level of activity: with flares of importance 1B or disturbances of class 1.

2nd level of activity: capable of producing flares of importance 2 or disturbance of class 2.

3rd level of activity: expressing the possibility of occurrence of flares of importance 3 or disturbances of class 3.

Statistical data were chosen from the IAU Quarterly Bulletin of Solar Activity, Solar Data of the Soviet Union, Solar-Geophysical Data of the United States, the coordinated observation in our country and the records of disturbances supplied by radio communication organizations. Active regions on the solar limb are in general not taken into account in our statistics.

Sometimes more reliable forecasts of the quiet periods that are safe from disturbances are necessary. In order to ensure the safety of space flight, we were asked for definite predictions rather than false-alarms. Thus when the level of activity attains or surpasses the 2nd magnitude, we forecast that proton events may occur.

3. FUNDAMENTALS OF TECHNIQUES

First of all we choose K parameters. To fit the conditions of our observations, we have chosen 4 parameters, i.e. (1) type of sunspot group according to the Zurich classification, (2) area of spot group, (3) magnetic classification of spot group, and (4) longitude of activity. Let each parameter have $(i)_k$ factors. For example, the magnetic classification consists of six factors, i.e. δ-structure, abnormal magnetic structure, magnetic axis $\geq 45^0$, γ, $\beta\gamma$ and β. The parameter of spot type has six factors: F, E, G, H, D, C. Spot areas are divided into three classes. For the cycle No. 19 we choose $80^0 \pm 15^0$, $130^0 \pm 15^0$, $330^0 \pm 15^0$ as active longitudes. The total range is equal to 90^0. For the cycle No. 20, we added $230^0 \pm 15^0$ in addition to the three belts of longitude mentioned above. They occupy one-third of the longitude interval on the solar disk. We did not include in the statistical analysis those spot groups which are magnetic type α, or Zurich type B, J, or their area < 200.

To simplify the project, we did not make separate statistics for different levels of activity. Instead, we first calculated the probability $(P_i)_k$ of producing a flare above the importance 1B by every factor of forecasting. To compare the correlation of each parameter with activity, we determined the weighting factor W_k of each parameter from the probability of maximum activity $(P_{max})_k$ corresponding to the forecasting factor of the parameter

$$W_k = \frac{(P_{max})_k}{\sum_{k=1}^{4} (P_{max})_k} \quad . \qquad (1)$$

The weighted probability of activity corresponding to each forecasting factor is $(F_i)_k$

$$(F_i)_k = W_k \frac{(P_i)_k}{(P_{max})_k} \quad . \qquad (2)$$

The probability of appearance of activity in each active region on the visible solar surface is

$$W_p = \sum_{k=1}^{4} (F_i)_k \tag{3}$$

As may be seen by the statistics, the larger the value of W_p, the more frequently strong activity occurs. Therefore, from the magnitude of the value of W_p, we can estimate the possibility of the appearance of activity of various classes.

Besides optical data, we have radio observations at 3 cm and 10 cm. But both are full-disk measurements, and it is impossible to specify the flux of each active region. In order to utilize every kind of material available nowadays, we can also estimate the development of active regions with the rate of increase of radio flux in three days. But this should be considered together with optical observations. Especially when there exist simultaneously many active regions on the solar disk, and they may recurrently rotate off the west limb or turn onto the east limb behind the sun, then the changes of radio flux cannot signify the development of some one active region. It may only characterize the level of activity of the whole solar surface. It is similar in meaning to the total area of spots on the solar disk or the relative number of spots. Hence the rate of change of radio flux is not a quantity that may be used every day. It is taken into account when it can definitely represent the variation of flux of a certain active region.

4. FORECASTING TECHNIQUES

Statistics of the data in 1959-1963 give the following results:

Table 1. Weighted probabilities of activity corresponding to various Zürich types of spot groups.

	Zürich Sunspot Group Type					
	F	E	G	H	D	C
Weighted Probability of Activity F_i:	0.28	0.14	0.05	0.11	0.08	0.05

Table 2. Weighted probabilities of activity corresponding to various areas of spot groups. (The unit of area is 10^{-6} Solar Hemisphere.)

	Area of Sunspot Group		
	> 1000	500-1000	200-500
Weighted Probability of Activity F_i:	0.25	0.13	0.05

Table 3. Weighted probabilities of activity corresponding to various magnetic types of spot groups.

	Magnetic Type					
	δ	abnormal magnetic structure	magnetic axis $\geq 45^0$	γ	$\beta\gamma$	β
Weighted Probability of Activity F_1:	0.38	0.34	0.33	0.29	0.27	0.10

Active longitude: When a sunspot group appears on an active longitude, the weighted probability of activity is 0.09.

Additional parameter: When the rate of increase of radio flux of certain active regions in three days can be definitely evaluated to be $\geq 5.5\%$, the weighted probability of activity is 0.10. According to this project, $(W_p)_{max} = 1.1$. Criteria of forecasting:

$W_p < 0.3$ yields class 0

$0.3 \leq W_p < 0.6$ yields class 1

$0.6 \leq W_p < 0.8$ yields class 2

$W_p \geq 0.8$ yields class 3

In the first two cases, a safe or quiet period may be forecast. In the last two cases, proton events may be forecast.

5. FORECAST EXAMPLES

Example 1: On August 1, 1972 there was observed a large active region with McMath number 11976. Its position on the solar disk was 13^0N, 10^0L. The parametric factor of forecasting is magnetic type δ, spherical area of the whole group was 1197 (10^{-6} area of hemisphere). The Zürich type was E. Rate of increase of radio flux in three days > 5.5%. According to the above project, one can find from the tables that $W_p = 0.38 + 0.25 + 0.14 + 0.10 = 0.87$. Then activity of class 3 could be forecast and there might be a proton event. Actually, there were strong activities on August 2, 4, and 7; proton events happened on the last two days.

Example 2: A large active region appeared on October 24, 1972. McMath number 12094. Position: 11^0S, 314^0L. From the observational data of October 27, magnetic type was δ, area 1746, type E, rise of radio flux in

recent three days < 5.5%. Therefore, we have $W_p = 0.38 + 0.25 + 0.14 + 0.09 = 0.86$. Then an activity level of class 3 could be forecast and there might be a proton event. The outcome was that the proton event took place on October 29.

Example 3: An active region which turned out on September 9, 1974. Position: 8^0N, 268^0L. Judging from the observational data of September 12, it had magnetic type δ, area 935, type H, increase of radio flux in three days > 5.5%. Then according to the project $W_p = 0.38 + 0.13 + 0.11 + 0.10 = 0.72$. One should foresee activity level of class 2, and there might be a proton event. In fact, there occurred a 2N flare on September 13.

6. ESTIMATION OF THE RESULTS OF FORECASTING

The above project was formulated after a statistical analysis of the data in 1959-1963. It differs not very much from the statistics of the data in 1970-1972. The former period is longer and its material more complete; therefore, it was taken as the basis. As a test we applied this project to the material belonging to the period March - July of 1972. When the data were complete, we have for 75 active regions made daily estimates of the levels of activity in the coming 1-3 days. There have been performed altogether 694 forecasts. Among them 532 (77%) were accurate, 98 (14%) were false-alarms, and 64 (9%) were missed. As for proton events, 70-80% of them can be accurately forecast with the project. But the false-alarms were fairly often, occurring on the average 20-30% of the total number of days of forecasts.

7. IMPROVEMENT AND SUPPLEMENT TO THE PROJECT OF FORECASTING

The project described in section 3 was proposed in 1973. With the change of phase of the solar cycle, it has to be revised adequately. It has been found from practice that merely by correcting the standards of areas and active longitudes, this project still holds for quiet years or the ascending phase. For example, near quiet years spots of large area occur quite seldom, and most flares appear in small spot groups with complex magnetic polarities. Accordingly, the areas may be divided into three classes: (1) < 200, (2) 200-500, (3) > 500, but the corresponding F_{1s} value is unchanged.

Active longitudes are incessantly shifting; therefore, they should be adjusted often. After analyzing the data of activity in 1973-1976, we have ascertained four new belts of active longitudes, (1) 30^0-90^0, (2) 140^0-210^0, (3) 260^0-290^0, (4) 320^0-350^0. Examining the material in recent years, we find that several spot groups that appeared earliest of all in the new cycle were all situated in the above-mentioned four belts. The strong active regions that appeared in recent years were all in these longitudes.

In the practical execution of the project, one may also take into account the following aspects:

(1) When several active regions are very closely spaced to each other or when active complexes appear, sufficient estimate should be made about their activity.

(2) Some related parameters cannot be accurately determined for the active regions, which are situated near the limb. In these cases judgements may be made from the circumstances of faculae, Hα plages, limb ejections, etc.

(3) Besides magnetic types one can also consider as reference the gradients of magnetic fields. They can be estimated with the degree of close approaches of spots with opposite polarities.

(4) The growth of spot areas can also be utilized in considering the development of spot groups.

(5) The arrangement of the filaments in the penumbrae of spots, the chromospheric filaments which may shear across magnetically neutral lines, all these may be taken as references in the short-term forecasting.

REFERENCES

Severny, A. B., and N. V. Steshenko (1970): Methods for the forecasting of solar flares. In: Solar Terrestrial Physics 1970, (ed. E. R. Dyer), D. Reidel Publ. Co., p. 173.

Simon, P., M. J. Martres and J. P. Legrand (1969): Flare forecasting. In: Solar Flares and Space Research (ed. C. DeJager and Z. Svestka), North Holland Publ. Co., Amsterdam, p. 405.

Smith, J. B. (1970): Real-time prediction of solar flare locations and region activity levels, AIAA Paper No. 70-1373, from the AIAA Observation and Prediction of Solar Activity Conference held at Huntsville, Alabama, Nov. 16-18, 1970, 799.

Smith, J. B. (1972): Predicting activity levels for specific locations within solar active regions. In: Solar Activity Observations and Predictions (ed. P. S. McIntosh and M. Dryer), MIT Press, p. 429.

Svestka, Z. (1970): Particle event forecasting. In: Intercorrelated Satellite Observations Related to Solar Events (ed. V. Manno and D. E. Page), D. Reidel Publ. Co., p. 90.

D16-32

N80-18478

FORECASTS OF GEOMAGNETIC ACTIVITIES AND HF RADIO PROPAGATION CONDITIONS MADE AT HIRAISO/JAPAN

K. Marubashi, Y. Miyamoto, T. Kidokoro and T. Ishii
Hiraiso Branch, Radio Research Laboratories
3601 Isozaki, Nakaminato, Ibaraki, 311-12 Japan

The Hiraiso Branch of RRL forecasts the geomagnetic activities for a 24-hour period through the IUWDS network. Our prediction techniques are summarized separately for the 27-day recurrent storm and the flare-associated storm. The storm predictions are compared with the actual geomagnetic activities in two ways. The first one is the comparison on a day-to-day basis. In the second comparison, we evaluate the accuracy of the storm predictions during 1965-1976. In addition to the storm prediction, short-term predictions of HF radio propagation conditions are conducted at Hiraiso. The HF propagation predictions are briefly described as an example of the applications of the magnetic storm prediction.

1. INTRODUCTION

The Hiraiso Branch of the Radio Research Laboratories conducts several kinds of solar-terrestrial predictions. They include the predictions of geomagnetic activities and energetic solar flares under the program of the International Ursigram and World Days Service (IUWDS) as the Regional Warning Center/Tokyo, and short-term predictions of HF radio propagation conditions averaged over the long-distance propagation circuits from Japan to various directions. This review concentrates on the forecasts of geomagnetic activities and short wave propagation conditions. More weight is given to the magnetic storm prediction, because the propagation prediction largely relies on the storm prediction.

The daily prediction of geomagnetic activities is issued in the form of either of three key words: MAGALERT for the disturbed period, MAGNIL for the end of disturbed conditions, and MAGQUIET for the quiet period. Our present criterion for the issue of MAGALERT is that the daily sum of Kp indices is expected to exceed 25 or the commencement of such a magnetic storm is expected. The decision of daily prediction is made around 0100 UT and sent through the IUWDS network. In addition, this prediction message is broadcast for the users in the Western Pacific region by Japanese Ursigram Broadcasts, JJD (10,415 kHz) and JJD2 (15,950 kHz) together with other forecasts and all collected Ursigram data. The prediction of magnetic storms provides a basis for the prediction of HF radio propagation conditions. In addition, when an unusually severe magnetic storm is expected, the Hiraiso Forecast Center defines the Special Interval for Ionospheric Observations in which ionograms

are to be obtained every five minutes from five ionosonde stations of RRL. Recently, the magnetic storm predictions are used by satellite tracking, control and telemetry stations, because it has become increasingly evident that the ionospheric radio scintillations associated with magnetic storms can affect satellite communications systems at frequencies from HF and VHF even up to SHF. For this purpose, the storm prediction is communicated directly to some operational stations.

Two types of forecasts of radio propagation conditions are issued from the Hiraiso Forecast Center, which apply to the overall characteristics of HF skywave propagation averaged over the various long-distance propagation circuits around Japan. One is the Weekly Radio Disturbance Forecast (or briefly Weekly Forecast) which predicts the daily propagation quality and the possibility of SWF occurrence for the coming seven days. The propagation quality is defined by deviations both in the time interval during which HF radio signals are received and in the received field strength from monthly average values statistically estimated from long-term observations. The predicted qualities are expressed by the quality figures: 1 = very poor, 2 = poor, 3 = slightly poor, 4 = good, 5 = very good. The expectation of SWF is expressed in three grades from 0 to 2. This Weekly Forecast is sent to the registered users by mail and also sent in RATEF code through the IUWDS network. The other forecast is the Short-Term Radio Disturbance Forecast (or briefly Radio Warning) which predicts the average propagation quality during the next twelve hours. The quality is expressed by the letter code: W = severely disturbed, U = unstable, N = normal. This radio Warning is broadcast on the Japanese standard waves, JJY, in the Morse code every ten minutes.

2. AVAILABLE DATA

The real-time monitoring of the solar-geophysical phenomena is of fundamental importance for any kind of solar-terrestrial predictions. The observations made at Hiraiso and their use for the monitoring and prediction purposes are briefly described below:

(1) Observation of sunspot regions in white light. Sunspot regions are sketched around 0000 UT every morning. The sketches are used to assess the probability of flares from each active region by considering day-to-day variations in the sunspot area, the spot number, and the structural complexity of the spot group.

(2) Measurements of solar radio flux and polarization at 100, 200, and 500 MHz. The flux measurement is made also at 9500 MHz. The spectral features and time variations of solar radio outbursts in these frequencies are useful factors for prediction of subsequent occurrence of magnetic storms.

(3) Riometer observation at 30 MHz. The riometer detects particularly large X-ray flares as the sudden cosmic noise absorption events. The spectral type II solar radio bursts are also detected sometimes by the riometer.

(4) Measurements of short wave field strength. The measurements are made for various long-distance propagation circuits, which include standard waves, commercial communications, overseas broadcasts, etc. The data are used to decide the actual propagation quality. In addition, we can detect SWF phenomena for a considerable part of day by these measurements.

(5) Amplitude and phase recording of pulse signals from Loran C (100 kHz)

stations in Japan. This provides us with a very sensitive detector of SID effects.

(6) Measurements of geomagnetic field variation and earth current. These provide the real-time geomagnetic data which are indispensable for the forecasters to see the progress of magnetic storms. The pattern of geomagnetic variation is an important factor to presume the cause of a magnetic storm and also to infer whether the disturbance will further continue or subside soon.

In addition to these real-time monitorings, near real-time data are provided by some observatories in Japan as listed below:

(1) Reports on solar active regions observed by 3-cm and 8-cm wavelength radio interferometers from Toyokawa Observatory of Nagoya University. They report the east-west position, 3-cm flux, and 3-cm to 8-cm flux ratio for each active region together with their expectation of proton flare in the URALR code of Ursigram.

(2) Geomagnetic K-indices from Kakioka Magnetic Observatory. When a magnetic storm or other special events occur, they supplement description of the events such as the start time, the end time, the maximum range in the horizontal component, etc.

(3) Reports on SPA phenomena detected by VLF recordings from Inubo Radio Observatory, as an indicator of flare activity.

(4) The daytime and nighttime typical values of f_{min} from Wakkanai Radio Observatory of RRL, as an indicator of the ionospheric absorption.

The Ursigram is another important data source, which we rely upon in pursuing the evolutionary changes in the solar-terrestrial environment on a day-to-day basis. Although the Ursigram data provide only simple descriptions of physical phenomena, the full time coverage afforded by the world-wide data exchange is the most important thing. We pay special attention to (1) description of solar active regions by sunspot groups (USSPS) and calcium plages (UPLAK), (2) flare reports (UFLAE), (3) reports on solar radio events (URANJ), (4) reports on solar proton events detected by radio propagation (UABSE) or by satellite measurements (PRESTO messages), and (5) SID event reports (USIDS). Furthermore, the reports from Culgoora in plain language provides us with detailed description of solar active centers and activities of each region obtained from both optical and radio observations. The report on the Culgoora radioheliograph observations is particularly important for the magnetic storm prediction.

In addition to these real-time monitoring and prompt reports cited above, we use later observation reports such as weekly reports and monthly reports from many observatories to identify the cause of each magnetic storm. This identification of the causes of storms is important to understand the recurrence tendency of geomagnetic disturbances correctly. For this purpose, we particularly rely on the coronal hole data from He I 10830 A spectroheliograms of Kitt Peak National Observatory, which is provided by the Preliminary Report and Forecast of Solar Geophysical Data published weekly by ERL/NOAA in Boulder. This is the only data source on coronal holes which is regularly and promptly availabe, and plays an important role in our decision of storm prediction.

3. TECHNIQUES FOR MAGNETIC STORM PREDICTION AND THEIR BASIS

It is well known that there exist two types of magnetic storms, namely, 27-day recurrent storms and flare-associated storms. The prediction techniques for these two types of magnetic storms are quite different because of the difference in the origins of solar wind disturbances which cause magnetic storms. The recurrent-type magnetic storms are caused by high-speed corotating streams which emanate continuously from a certain region on the sun, whereas the flare-produced shock waves trigger the flare-associated storms.

Our techniques for the prediction of recurrent-type magnetic storms are mainly based on recent studies which attempted to identify coronal holes as the origin of the corotating fast streams and their associated geomagnetic disturbances (Krieger et al., 1973; Neupert and Pizzo, 1974; Bell and Noci, 1976; Nolte et al., 1976; Hansen et al., 1976; Sheeley et al., 1976). At present, however, the coronal hole data are used only to identify the causes of recurrent-type magnetic storms and thus confirm the recurrence tendency.

The factors and criteria used in prediction of the recurrent-type storms are listed below:

(1) Recurrence tendency as viewed from 27-day recurrent patterns constructed by K indices from Kakioka. If significant magnetic disturbances were observed in the past two rotations or more, the strong recurrence tendency is assumed for the period concerned. In this case, consideration is given to the rotation-to-rotation trends in the start time and magnitude of magnetic disturbances.

(2) Association between coronal holes and magnetic disturbances in the past rotations. The first priority is given to the association in the last rotation. When the association is evident, the possible recurrence is assumed even if the magnetic disturbance occurred only in the last rotation and not in previous ones.

(3) Evolutionary changes in the coronal hole regions. The return of coronal holes which had caused a magnetic storm in the last rotation is inferred from the distribution of active regions on the present solar disc. If there is a region void of calcium plage or sunspot group at the right place, the return of coronal hole is assumed. Similarity in the magnetic neutral line and active region distributions between the rotations is also taken into consideration.

(4) The return of regions which had produced energetic flares on the previous rotation. This factor is rarely used positively to predict a magnetic storm, but is particularly important with regards to the evolution of coronal holes. There are several examples which show the development of coronal holes in correlation with the occurrence of proton flares. Such examples will be discussed later in some more detail.

(5) Near real-time coronal hole data. The existence of coronal holes is sometimes reported from Culgoora. In such a case, the east-west position of the coronal hole is compared with the coronal hole distribution in the previous rotation to see whether the reported coronal hole is new one or returning one. For the returning coronal hole, the association between the coronal hole and magnetic disturbance in the past rotations is checked. In some cases, large near-equatorial coronal holes are seen which do not cause any significant magnetic disturbance.

The relationships between magnetic storms and solar flares have long been studied, particularly aimed at identifying the characteristics of the

storm-producing flares (see Cook and McCue (1975) for a historical review). Such works provide the basis of the prediction of flare-associated magnetic storms. Among others, our prediction techniques are based on the studies on the solar radio bursts of spectral type II and type IV (DeFeiter et al., 1960; Bell, 1963; Dodson and Hedeman, 1964), the radio energy emitted at meter wavelengths (Sinno and Hakura, 1958; Nishida, 1965; Pinter, 1972), the shock wave propagation from solar corona to the earth's environment (Pinter, 1973; Sakurai and Chao, 1974; Dryer, 1975), and the solar proton events (Hakura and Lincoln, 196.; Castelli et al., 1967, 1977).

When solar flares have occurred, the occurrence of a magnetic storm is predicted considering the following factors:

(1) Hα importance and duration of the flare and the structural complexity of the flare region. The flares of Hα Imp $\geq$ 2 in magnetically complex sunspot groups are considered to be possible to cause magnetic storms.

(2) Position of flare on the solar disc. Flares in the central region of the disc most probably cause magnetic storms, and flares in the western hemisphere tend to cause magnetic storms with higher probability than those in the eastern hemisphere. Flares near the east limb are normally disregarded in magnetic storm prediction.

(3) Occurrence of radio type II and type IV bursts. Greater importance is attached to type IV bursts particularly at meter wavelengths. The highest probability of magnetic storm is expected in case of combined occurrence of type II and type IV bursts.

(4) Intensity and duration at meter wavelengths. The probability of storm occurrence is assessed for each of flare-associated radio events with peak flux around 200 MHz greater than 200 s.f.u. and duration longer than 15 minutes. The highest expectation is given to those events of which the product of peak flux density around 200 MHz (in s.f.u.) and duration (in minutes) is greater than 10^4. The existence of the second part of major radio burst related probably with type IV is taken into consideration when the event is locally observed at Hiraiso.

(5) Frequency coverage of the radio event. The full frequency range coverage from about 100 to 10,000 MHz is an important factor to estimate the flare-released energy. Although we pay more attention to meter wave emission in connection with magnetic storm prediction, the increase in the flux density with frequency in the centimeter range is an important controlling factor of solar proton events.

(6) Occurrence of solar proton events. The occurrence of magnetic storms can be predicted with higher probability of success by knowing that solar protons were emitted from the flare under consideration.

(7) Delay time from flares to magnetic storms. We normally assume two days delay from solar flares to magnetic storms. Shorter delay time is assumed for flares just after fast streams, e.g. in case of successive flares or flares just behind coronal holes.

As is evident, none of the factors cited above is conclusive to predict the occurrence of a magnetic storm for either of recurrent-type or flare-associated storms. The final decision is made subjectively by combining the degreee of expectation judged from each factor.

When a magnetic storm occurs, we must forecast how long the storm would continue. Although it is normally assumed at Hiraiso that the duration of a magnetic storm is about three days on the average, the end times of magnetic storms are actually predicted from some features noticed in the

magnetograms. The techniques are quite different for recurrent-type storms and flare-associated storms. The end of a flare-produced magnetic storm is soon expected when the storm proceeds to its recovery phase as noticed in the H-component variation and short-period fluctuations are small. On the other hand, in some recurrent-type storms, no substantial main phase develops, but bay-type disturbances are repeated in the nighttime for several days. The end times of such events are predicted by considering the following factors: (1) the day-to-day trend in magnitude of bay disturbances, (2) the intensity of short-period fluctuations in H-component, and (3) the definiteness of the regular pattern of diurnal magnetic variation around the morning hours. Thus, it is important for the prediction purpose to know whether the magnetic storm in progress is flare-associated or recurrent-type.

Furthermore, to identify the causes of magnetic storms in the past it is necessary to understand the recurrence tendency correctly. The above-cited factors and criteria for prediction of the storm occurrence provide the ways to discriminate between the recurrent-type storms and the flare-associated storms. Features of magnetic field variation are also taken into consideration. The prompt and tentative identification is later supplemented by examining various data such as those in Solar Geophysical Data (SGD: published monthly by ERL of NOAA, Boulder). It is particularly helpful to examine the variations in the solar wind velocity, density and temperature, and to compare the coronal hole magnetic polarity with the interplanetary magnetic field polarity.

Finally, we must mention the crucial role of the interplanetary magnetic field (IMF) in controlling the development of magnetic storms. Burton et al. (1975) showed that the main phase of a magnetic storm is initiated when the north-south component of IMF becomes negative (southward) and its development is strongly controlled by the product of the north-south IMF and the solar wind speed. This result indicates that the storm prediction based solely on the prediction of high-speed solar wind from coronal holes or flare regions is not sufficient. Fortunately, however, the most intense fluctuations in IMF are generally associated with the region of interaction between the high-speed solar wind and the ambient solar wind, and thus the high-speed solar wind streams are usually accompanied by the southward IMF (Burlaga, 1975).

4. SUMMARY OF MAGNETIC STORM PREDICTIONS DURING BARTEL'S ROTATIONS 1961-1980

The magnetic storm predictions issued by Hiraiso and WWA are compared with the actual geomagnetic activities for the Bartels' rotation periods 1961-1980 in Fig. 1. Geomagnetic activities are exhibited by ΣKp (thick solid line), ΣK from Kakioka (dashed line) and the lowest D_{st} level in every 12-hour interval (thin line with small dots). The magnetic storm intervals and SC's taken from SGD are also shown by horizontal bars and triangles, respectively. In particular, the storm intervals and SC's reported from no less than five observatories are indicated by thick bars and solid triangles. The intervals for which MAGALERT's were issued are shown by black shadings. The shading with a white dot denotes the MAGALERT issued on the day to which the storm prediction is to be applied. The hatching indicates that the MAGALERT having been issued for that day before was cancelled by the issue of MAGNIL. For major magnetic storms and some additional minor disturbances, their possible

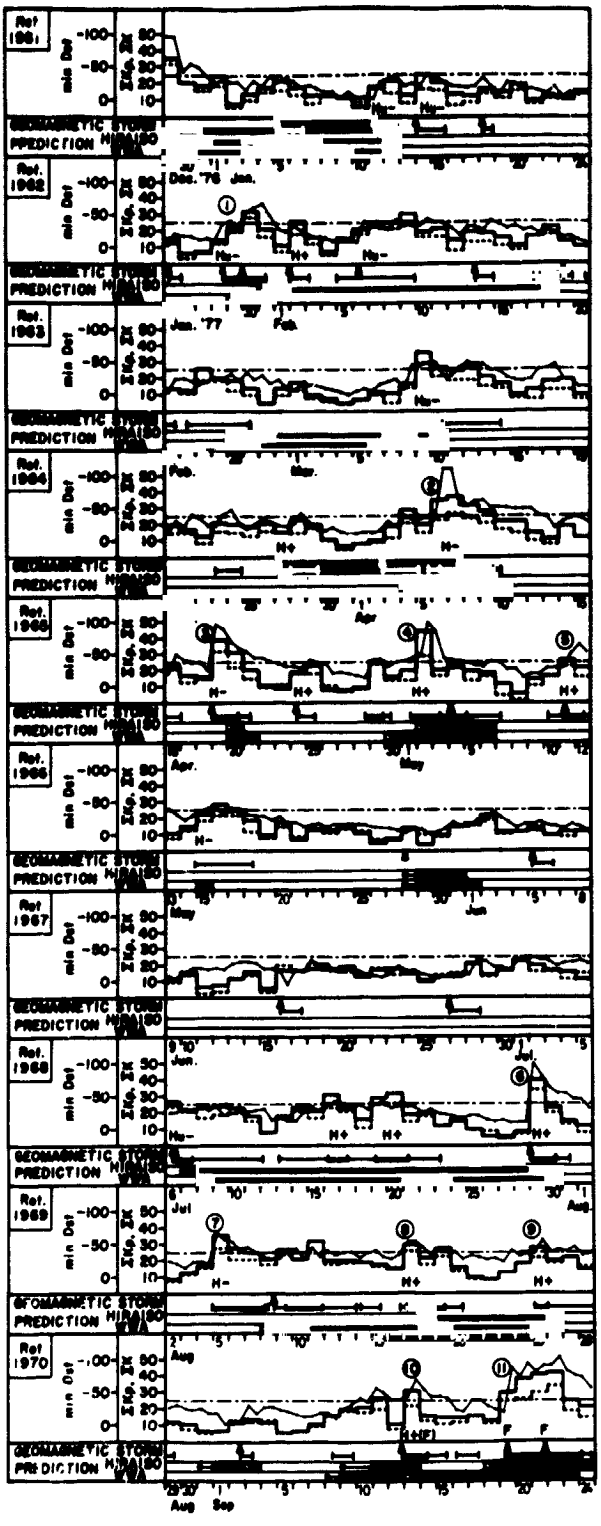

Fig. 1. Comparison of magnetic storm predictions with actual magnetic activities for Bartels' rotations 1961-1980.

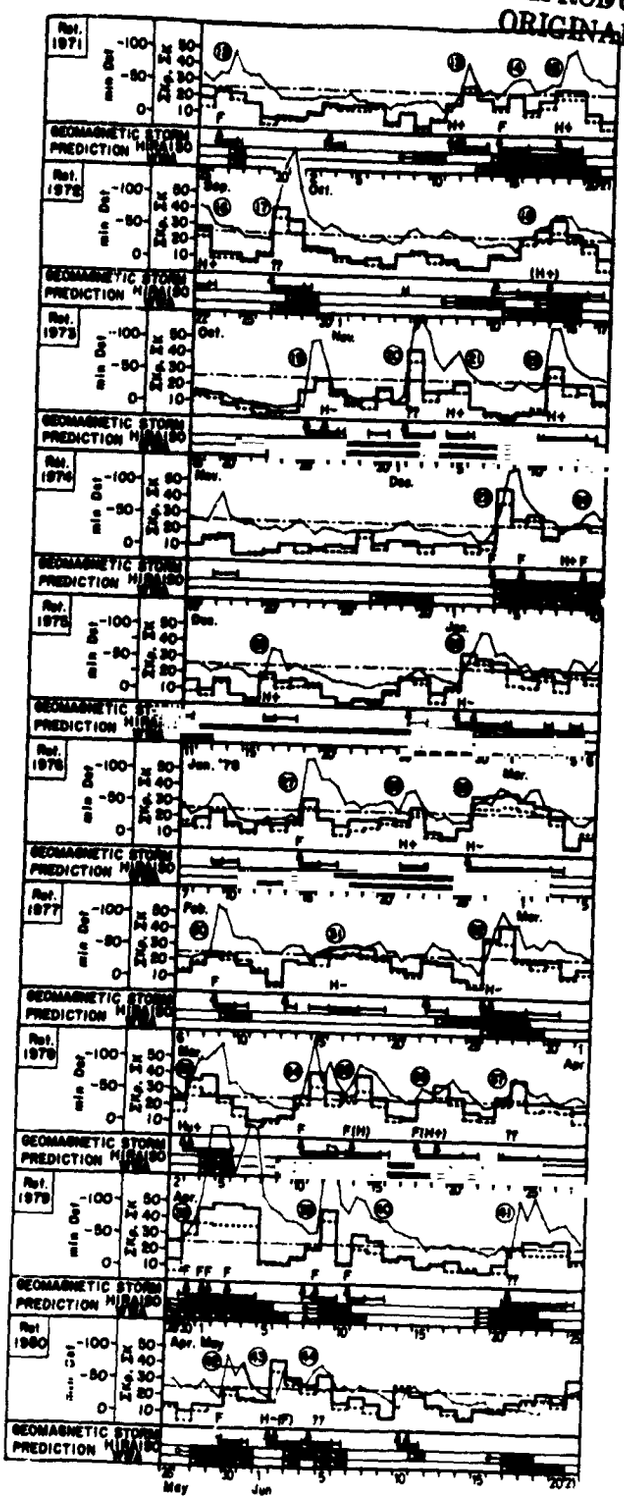

Fig. 1 (Continued)

association with coronal holes or solar flares is indicated by attaching the letter H or F. The association with the unstable or questionable coronal holes is indicated by Hu. The magnetic polarity of the coronal hole is also shown. Here, the major magnetic storm is defined as the storm reported from no less than five magnetic observatories whose D_{st} fell below -50γ (nT). Such major magnetic storms are numbered in Fig. 1.

During the rotation periods 1961-1970, no flare-associated magnetic storm occurred until September, and therefore all storm predictions were made by consideration on the recurrence tendency. It is found that most MAGALERT's were issued after disturbances had started. This is attributed to the fact that the recurrence tendency is not so evident during these periods. The existence of a quiescent period over 40 days from rotation 1966 to rotation 1967 particularly made it difficult to predict magnetic disturbances thereafter. Although weak recurrence tendency is found from rotation 1962 to 1964, the association between these disturbances and coronal holes is not very clear except for the storm No. 2. It is evident that the storm No. 4 is not the return of this recurrent series but is rather to be associated with another coronal hole with positive polarity which disappeared in the next rotation.

There are five intervals for which MAGALERT's had been issued before disturbances were observed. The MAGALERT for January 4-7 was issued on January 3, which was based on the distinct recurrence tendency observed in the previous five or six rotations. This prediction resulted in false alarms, because of breaking-up of the recurrence, though the minor disturbance occurred. The perplexity of the forecasters at Hiraiso and also at WWA is clearly seen by comparing the actual geomagnetic activities and predictions during March 5-10. The MAGALERT's issued beforehand resulted in false alarms in this case, too. The MAGALERT's for May 29-31 and for September 1-3 are other two examples which were issued beforehand and resulted in false alarms. Both of these two predictions were made by the consideration of the apparent association between the coronal holes and magnetic disturbances in the preceding rotations. For the latter case, the magnetic quiescence could have been predicted by closer examination of data, because the UPLAK code of the Ursigram had reported the existence of a calcium plage region at the position of the former coronal hole. The fifth interval of MAGALERT's issued before the occurrence of magnetic disturbance is September 11-13, and this prediction agreed satisfactorily with the actual disturbance.

As is discussed above, there are a number of magnetic storms which are apparently associated with short-lived coronal holes. These storms cause the poor accuracy of our recurrent storm prediction which relies upon the coronal hole data in the previous rotations. However, the above discussion implies the possibility of much improvement by using the near real-time data of coronal holes.

It is clearly seen in Fig. 1 that more MAGALERT messages were issued before the occurrence of magnetic disturbances during the rotation periods 1971-1980 than before. There are two reasons for this change. The first reason is that there occurred storm-producing flares after the major activities of McMath region 14943 during September 7-22, 1977, and therefore MAGALERT's were issued with higher degree of confidence for those events. This is particularly true for the great solar flares such as those at McMath region 15266 in April-May. The second reason is that there were distinct series of recurrent magnetic storms in these periods together with many flare-associated storms.

We can point out three series of recurrent storms for these periods. The first series began with the SC-storm having started at 0027 UT on July 29, 1977 (storm No. 6), and continued to the gradual storm on December 10 (storm No. 22), though we attribute the SC-storms on September 19 and 21 to flares in McMath region 14943. The increase in ΣKp on January 8, 1978 before the storm No. 24 may be regarded as the continuation of this series. The evolution of the coronal hole responsible for this series of recurrent storms seems to have been correlated with the development of active centers in the vicinity, that is, the growth of the coronal hole was seen in September and January. The second series began with the SC-storm at 1853 UT on January 28, 1978, in rotation 1975 and continued to the storm No. 32 in rotation 1977. These storms can be associated with the extension of the southern polar hole with negative polarity. The storm No. 37 in the next rotation seems to be the continuation of this series, though the coronal hole had disappeared in this rotation. This could be an interesting example which exhibits the return of a magnetic storm without a coronal hole. Although the storm No. 41 in the next rotation (1979) appears to be another return of this series, it does not seem true because the magnetic polarity of the solar wind was positive during the period of this storm. The storms, Nos. 8, 10 and 13 (rotations 1969-1971) seem to constitute another series of recurrent storms which are associated with the extension of the northern polar hole.

In addition to the above-discussed storms which are relatively easy to predict, there are number of storms which are associated with sporadic coronal holes in the rotation periods 1971-1980, too.

Table 1 shows further details on the association between storms and coronal holes or solar flares for major magnetic storms. In the table, the storm commencements of uncertain type are indicated by brackets (Nos. 32 and 41, see also Fig. 1). The magnitude of storms is represented by the sum of Kp indices for the 24-hour period which gives the maximum value and the lowest D_{st} level. The coronal holes listed in the table are those within ± 10° longitude from the estimated source location of the solar wind which could cause the magnetic storm and within ± 30° latitude from the sub-earth point on the sun. The estimation of the source location was made with the solar wind speed listed in the table, when the MIT experiments on IMP 7 and 8 are available. Otherwise, the time delay of 2-4 days are assumed between the CMP of coronal holes and the arrival of corotating streams. The longitude ranges of coronal holes are shown as defined within ±30° latitude range of the sub-earth point. The coronal holes are classified into three types: near-equatorial (E), extended from the northern polar region (PN), and extended from south (PS). Unstable or questionable coronal holes are indicated by attaching U. The coronal hole data taken from the Preliminary Report from ERL/NOAA are bracketed. The polarity of coronal holes are determined by comparing coronal hole boundaries with Hα synoptic charts. Coronal holes crossed by neutral lines are indicated by the X polarity. The polarity of the mean solar magnetic field is also listed, which is taken from the Stanford measurements for the date when the solar wind started from the source region near the sun, the constant solar wind speed being assumed. The IMF polarity inferred from magnetograms at Vostok and Thule is shown for three 12-hour intervals, in the first of which each magnetic storm commenced. It is seen that the coronal hole polarity generally coincides with the mean solar magnetic field polarity and the IMF polarity in the second 12-hour interval. The solar flares were taken from the Ursigram data. We listed those flares which seem capable of

Table 1. Association of major magnetic storms with coronal holes or solar flares.

STORM NO.	COMMENCEMENT DATE TIME (UT) TYPE	END DAY HR (UT)	MAGNITUDE Σ Kp	MAGNITUDE Dst	CORONAL HOLE TYPE	CORONAL HOLE LONG.	CORONAL HOLE LAT.	CORONAL HOLE Polarity	MEAN SOLAR MAG. FIELD	SOLAR WIND Polarity	SOLAR WIND SPEED	FLARE DATE TIME (UT)	FLARE POSITION	FLARE IMP.	FLARE AT (HR)	RADIO BURST TYPE II	RADIO BURST TYPE IV	ASSOCIATION CH	ASSOCIATION F
	1977																		
1	Jan.28 1839 SC	31 15	34-	-69	EU	42- 29	18N-37N	-	-	+--	470							△	
2	Apr. 6 12-- ..	9 22	45	-110	E E	212-200 208-185	2N-12N 22S-42S	X -	-	--+	680							○	
3	Apr.19 0106 SC	20 18	40-	-97	E	57- 46	21S-33S	-	-	--X	580							●	
4	May 1 15-- ..	3 12	44	-98	PN	281-270	23N-	+	+	CX+	450							△	
5	May 11 06-- ..	12 14	32	-65	E	164-139	17N-32N	+	+	++X	350							△	
6	Jul.29 0027 SC	30 13	40-	-100	E	182-149	5S-22N	+	+	+X+	450							●	
7	Aug. 4 23-- ..	8 08	36	-62	E	63- 12	20S-40S	-	-	---	700							●	
8	Aug.17 04-- ..	19 14	32-	-54	PN	(262-225)	30N-	+	+	+--	650							△	
9	Aug.25 05-- ..	26 01	31+	-56	E E	179-165 169-153	24S-35S 2N-23N	+ +	+	+++	470							●	
10	Sep.12 2113 SC	14 11	33-	-68	PN	254-243	26N-	+	+	+++	400	Sep. 9 1604	10N 80E	2+	77			△	△
11a	Sep.19 1138 SC	Cont.			E	184-150	8S-25N	+	+	X+X	420	Sep.16 2120	8N 20W	2+	68	Yes	Yes		●
11b	Sep.21 2044 SC	24 04	46-	-103	E	172-162	26S-32S	+	+	-X-	>700	Sep.20 0321	15N 55W	3	41				●
12	Sep.26 0732 ..	27 13	34+	-95	(E	100- 83	31N-40N	-)	U	++-	400	Sep.24(0554)	UNKNOWN		49				△
13	Oct.11 1300 ..	13 16	34-	-81	(E	261-245	27N-45N	+)	-	+++	470							●	
14	Oct.14 1151 SC	16 09	28	-62		NONE			-	X-+	470	Oct.12 0151	8N 3W	1	58	Yes	Yes		●
15	Oct.18 1000 ..	19 20	35-	-108	E	184-172	3N-13N	+	+	+++	480							●	
16	Oct.21 2300 ..	22 23	28+	-79	EU EU E	152-133 140-129 130-120	21S-33S 0N-12N 25N-35N	X - X	+	+++	450							△	
17	Oct.26 2330 SC	29 02	47	-172		NONE			+	CX-	370								
18	Nov.12 01-- ..	16 15	39+	-76		NO DATA			+	+++	420							?	
19a	Nov.25 1227 SC	Cont.							+	++-	350	Nov.22 0930	23N 40W	2	75				○
19b	Nov.26 1704 SC	27 14		-98	PS	15- 0	27S-	-	-	--C	540							●	
20	Dec. 1 2029 SC	3 20	44	-136		NONE			+	-+-	370								
21	Dec. 4 1400 ..	5 23	31-	-85	E	280-253	18N-38N	+	-	++-	430							○	
22	Dec.10 2000 ..	13 15	37	-125	PN	205-148	3S-	+	+	-+U	500	Dec.10 0303	26S 18E	1		Yes	Yes	●	

Table 1 (Continued)

STORM NO.	COMMENCEMENT DATE TIME (UT) TYPE	END DAY HR (UT)	MAGNITUDE ΣKp	MAGNITUDE Dst	CORONAL HOLE TYPE	CORONAL HOLE LONG.	CORONAL HOLE LAT.	CORONAL HOLE Polarity	MEAN SOLAR MAG. FIELD	SOLAR WIND Polarity	SOLAR WIND SPEED	FLARE DATE TIME (UT)	FLARE POSITION	FLARE IMP.	FLARE ΔT (HR)	RADIO BURST TYPE II	RADIO BURST TYPE IV	ASSOCIATION CH	ASSOCIATION F
	1978																		
23a	Jan. 3 2042 SC	Cont.			E	225-193	29S-46S	-	-	-X-	520	Jan. 1 2147	18S 5E	1	47	Yes	Yes		●
23b	Jan. 5 1628 SC	7 03	50-	-129					ND	-X-	650	Jan. 3 1015	15S 7E	1+	54				●
24	Jan. 9 1625 SC	10 22	31	-66	E	189-160	1S-33N	+	+	U+-	540	Jan. 7 0123	23S 60W	1	63	Yes	Yes		●
25	Jan.16 0800 ..	17 01	26	-64	E	107- 90	22S-40S	+	+	+-+	330							△	
26	Jan.28 1853 SC	31 24	35+	-96	(PS	247-230	23S-	-)	-	---	580							○	
27	Feb.14 2147 SC	16 03	35	-118	E	12- 1	10S-23S	-	-	+--	630	Feb.13 0129	15N 15W	2	44	Yes	Yes		●
28	Feb.21 0800 ..	22 23	28-	-73	E E	311-297 296-277	29S-40S 14N-30N	X	+	-++	470							△	
29	Feb.25 1928 SC	3 03	38	-80	PS	220-190	13S-	-	-	+-C	650							△	
30	Mar. 8 1439 SC	10 00	29+	-111	NO DATA					C+-		Mar. 6(1150)	21N 7W	2	51				○
31	Mar.16 0100 ..	18 00	32	-53	E	11-349	13S-30S	-		---								○	
32	Mar.25 2200 (..)	28 22	45+	-110	PS	215-189	18S-	-		X--								○	
33	Apr. 2 2057 ..	6 04	38-	-120	EU	129-116	22S-38S	+		+++								△	
34	Apr.10 1306 SC	12 20	44	-127	NONE					+X+		Apr. 8 0123	19N 3W	1	60		Yes		●
35	Apr.13 1100 ..	15 16	42-	-86	E E	347-342 345-337	10N-19N 20S-28S	- -		---		Apr.11 1334	19N 57W	2+	45		Yes	△	○
36	Apr.17 2345 SC	21 02	39+	-71	E	28S-261	28S-40S	-		-++		Apr.15 0637	15N 8W	0	65	Yes	Yes	○	○
37	Apr.23 1400 ..	25 21	39+	-78	NONE					---									
38a	Apr.30 0951 SC	Cont.			PN	104- 84	11N-	+		X-+		Apr.28 1308	22N 41E	4+	45				●
38b	May 1 0828 SC	Cont.								+--		Apr.29 1854	22N 19E	3+	37				●
38c	May 1 1835 SC	Cont.								--+		Apr.30 1439	20N 11E	3+	28				○
38d	May 2 2318 SC	4 23	55	-218						C-+		May 1 1914	22N 10W	3+	28				○
39	May 8 11-- ..	10 03	46+	-191	EU	34- 23	5S- 8N	-		+C+		May 6(2013) May 7 0320	UNKNOWN 22N 64W	2+	39 32	Yes Yes	Yes Yes		○
40	May 10 2005 SC	11 22	32+	-110	NONE					+--		May 8 1212	22N 76W	2+	56		Yes		●
41	May 20 1600 (..)	24 18	35	-115	(E	224-197	22S-41S	-)		+++									
42	May 29 1831 SC	31 03	26+	-86	NONE					---		May 26 1734	18N 54E	1+	73				△
43	Jun. 1 2143 SC	4 04	47+	-61	PN	87- 70	2SN-	+		-++		May 31 1009	23N 50W	2+	36			○	○
44	Jun. 4 1211 SC	6 02	38	-75	NONE					---									

producing magnetic storms. Therefore, it is not intended to say that all of the listed flares actually caused magnetic storms. For example, the flare on December 10, 1977, cannot be the cause of the storm on December 10 (No. 22). It is supposed, in this case, that the flare-associated stream was just behind the high-speed corotating stream and thus no significant effect could not be detected. The flare-associated type II and type IV events are taken from reports in the Ursigram from Culgoora and Nancay.

In the last column of Table 1, the association between these 44 major magnetic storms and coronal holes or solar flares are shown with the degree of confidence in three grades: triangle = possible, circle = good, and double circle = excellent. These grades are determined by the consideration of the coincidence of magnetic polarity between coronal holes and IMF, the delay time from the coronal hole CMP to the storm commencement, the delay time from flares to magnetic storms, and some characteristic features in the solar wind such as the stream interface and the shock structure. The question mark attached to the storm No. 18 indicates that this storm is probably caused by the coronal hole-associated corotating stream though no coronal hole data are available. The storms of Nos. 11, 27 and 38 are worthy to be specially mentioned, because the times of the flare occurrence nearly coincide with the times of coronal hole CMP for these events. After we concluded that these storms are more likely to be associated with flares as listed in the table, we noticed that the flare position was just on the west side of the coronal hole for the former two cases. It would be reasonable to suppose that the flare-associated shock will arrive at the earth earlier than the corotating stream, because the shock will propagate ahead of the stream.

Finally, it is interesting to note that 40 storms out of 44 major magnetic storms could be explained by coronal holes or solar flares. It can be expected that the causes of the remaining 4 storms may become clearer with more detailed data. The present result provides a strong basis for the storm prediction by observations of coronal holes and solar flares including radio events.

5. SEPTEMBER 1977 EVENTS

During 7-22 September, 1977, McMath plage region 14943 was very active and most solar-geophysical activities were associated with this region, though there was short intermission of activity during 12-15 September. Hiraiso issued MAGALERT's for two intervals, 11-13 and 18-23 during this period as is seen in Fig. 1. In this section, we will show how the magnetic storm predictions were decided and how the predictions agreed with the actual geomagnetic activities during this period. We will discuss the short-term predictions of HF radio propagation conditions made at Hiraiso in association with the activities of McMath region 14943.

Fig. 2 illustrates the solar phenomena closely related with magnetic storm prediction (upper diagram), and the Kp variations for the period concerned (lower diagram, of which dates are two days shifted). The solar phenomena were taken from the Ursigram-interchanged data source, and the following are shown in the figure:

(1) The Hα importance, the starting time, and the longitude of all reported flares which occurred in McMath region 14943 and its vicinity.

(2) The frequency spectrum of peak flux density and the start, maximum,

and end times of selected solar radio bursts with wide frequency range coverage and relatively long duration.

(3) The start, maximum, and end times, and the maximum absorption of PCA events observed by riometers at Russian Arctic stations. Proton events and electron events are indicated by letters P and E, respectively.

The first major solar event occurred at 2227 UT on September 7, when McMath region 14943 was just behind the east limb at about 10°N latitude. We observed a major radio burst event at 100, 200, 500, and 9500 MHz starting at 2228 UT (See Ohbu et al., (1978) for the radio data obtained at Hiraiso during the September 1977 events), and the SWF event of importance 3 at Hiraiso. At 0100 UT on September 8, we did not know the position of the flare which was responsible for above mentioned phenomena yet. Therefore, we postponed our decision on the probability of a flare-produced magnetic storm, and issued MAGQUIET. Later, Culgoora reported the 1B flare at 2227 UT (start time) at the 10°N east limb followed by the 2B flare at 2252 UT. Culgoora also reported a strong type II at 2227 UT and a weak type IV at 2340 UT. The occurrence of a microwave burst event of 1900 s.f.u. was also reported by the PRESTO message from Boulder. The radio heliogram at 3750 MHz sent by facsimile from Toyokawa also informed the flare position. Although MAGALERT 09/10 and MAGALERT 09/11 had been issued by WWA and RWC/Paris, respectively, probably from this solar event, our conclusion was that this flare was too far east to cause a magnetic storm.

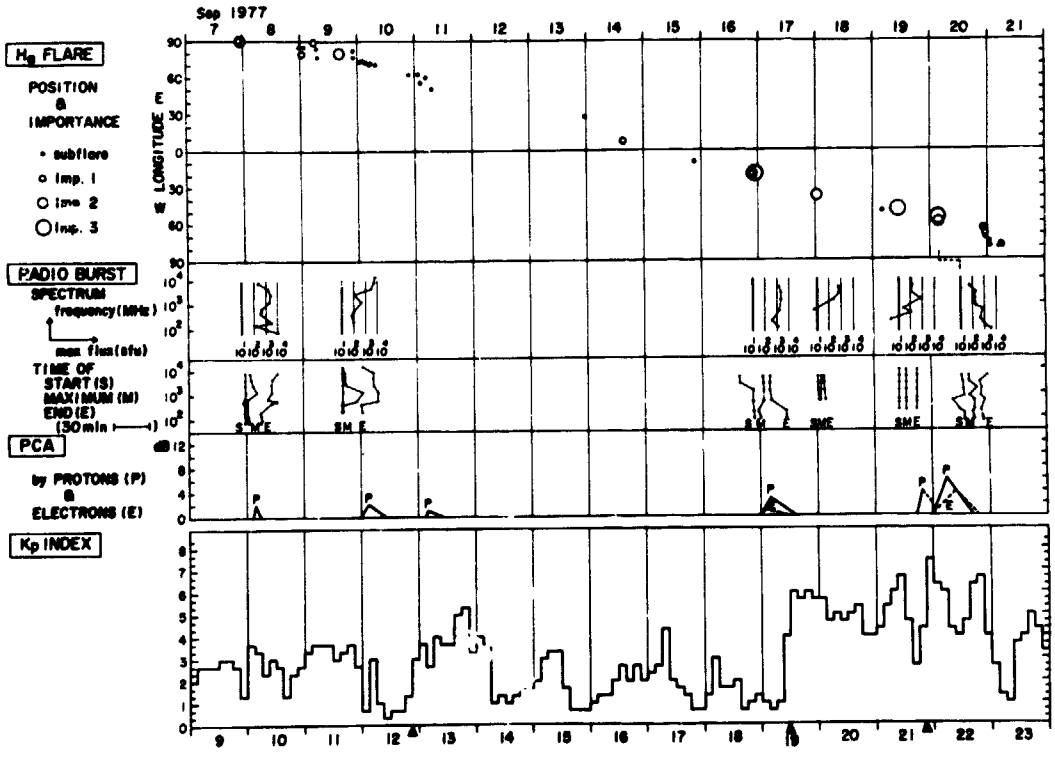

Fig. 2. Solar activities associated with McMath region 14943 during 7-21 September, 1977 (upper), and geomagnetic activities during 9-23 (lower). Note that dates for two diagrams are two days shifted.

The first interval of MAGALERT from Hiraiso (11 to 13) was decided on September 9 from consideration of the recurrence tendency as seen in Bartels' rotation periods 1968 and 1969 in Fig. 1. We issued MAGALERT 11/13 on Sep. 9, intending to express our negative expectation of a magnetic storm by the September 7 solar event, and also our expectation of a recurrent magnetic storm.

The 2B flare at 10°N 80°E at 1604 UT (start time) on September 9 was the second major event which accompanied the major radio event and the PCA event. However, little attention was paid to this flare, because MAGALERT had already been issued for 11 to 13. The values of ΣKp for September 11, 12 and 13 were 27, 11_-, 31_+, and the SC-storm occurred at 2113 UT on September 12. Thus, our prediction, MAGALERT 11/13 appears to have been correct judging from Hiraiso's criterion for MAGALERT issuance. However, we are not quite certain whether the reasoning for the prediction was correct or not. The September 9 solar flare could have caused the SC-storm on September 12, though the flare position seems too far east. On the other hand, this storm could have been caused by the fast stream from the coronal hole which passed the central meridian of the solar disc on September 11, though the delay time between the coronal hole CMP and the magnetic storm for this association seems a little too short if not unthinkably short.

The second interval of MAGALERT from Hiraiso (18 to 2,) can be devided into three epochs according to our decision processes as follows:

(1) The flares on September 16 around 22 hours UT were accompanied by very large bursts of meter waves (Hiraiso's observation available), and Culgoora reported very strong type II and type IV emissions. (The flares were reported as 1N and 3N flares from Culgoora, and as a 2B flare with two maxima from Boulder.) Thus, a magnetic storm was expected to commence on September 18 or later. Therefore we issued MAGQUIET on 17, and MAGALERT 18/20 on Sep. 18. The geomagnetic activity was low on 18, but this prediction was continued as MAGALERT 19/20 on September 19.

(2) The SC-storm commenced at 1138 UT on September 19, we concluded that the disturbed state would continue till September 21. Thus, MAGALERT 20/21 was issued on September 20. The importance 2 solar flare on September 18 was disregarded because the associated radio burst was rather weak at meter wavelengths and its duration was short (Hiraiso's observations available).

(3) On 21 September, we expected one or two magnetic storms to occur on 21 and/or 22 September, judging from the major solar flares on 19 and 20 and the associated radio phenomena. (The latter flare seems more favorable judging from the meter wave intensity; Hiraiso's radio observations being available.) Thus, MAGALERT 21/23 was issued on September 21. This prediction was extended till 24 on September 23, and denied again on September 24. (MAGNIL was issued on 24).

The agreement between the prediction and the actual activity was satisfactory during the second MAGALERT interval. The MAGALERT for 18 was the only false alarm, and no disturbace was missed. It can be said that the solar events in this interval were sufficiently large so that we could predict the occurrence of magnetic storms with high degree of confidence.

Finally, it should be mentioned that these flare-associated storms occurred just in the period when a recurrent magnetic storm could be expected. Two important suggestions can be derived from these events. The flare effects may have arrived at the earth before the corotating stream because the flare position was on the west side of the coronal hole, and that the growth

of the coronal hole may have been associated with the development of this active center.

In Fig. 3, two kinds of short-term predictions of HF propagation conditions made at Hiraiso are compared with the observed HF field strength data from representative propagation circuits for the period September 9-23. The diurnal variation of monthly median values are shown by the smooth curve for each circuit. The dashed curve is drawn for the time interval in which the signal reception rate of this month is lower than 50 %. Values of observed signal strength (in dB; relative value) are indicated by dots, and values affected by interferences are indicated by v-marks. The large (Importance = 3) SWF's detected at Hiraiso are shown by solid triangles. The hatchings in the lower diagram indicate the intervals for which unstable HF propagation conditions were predicted.

In the Weekly Forecast for September 10-16 issued on September 9 (date in Japan Standard Time) the unstable propagation conditions were predicted in accordance with our expectation of a recurrent magnetic storm during September 11-13. The Warning was changed from N (Normal) to U(Unstable) with expectation that the propagation would soon become unstable, when we observed the minor magnetic disturbance of September 11. Although the HF monitoring showed

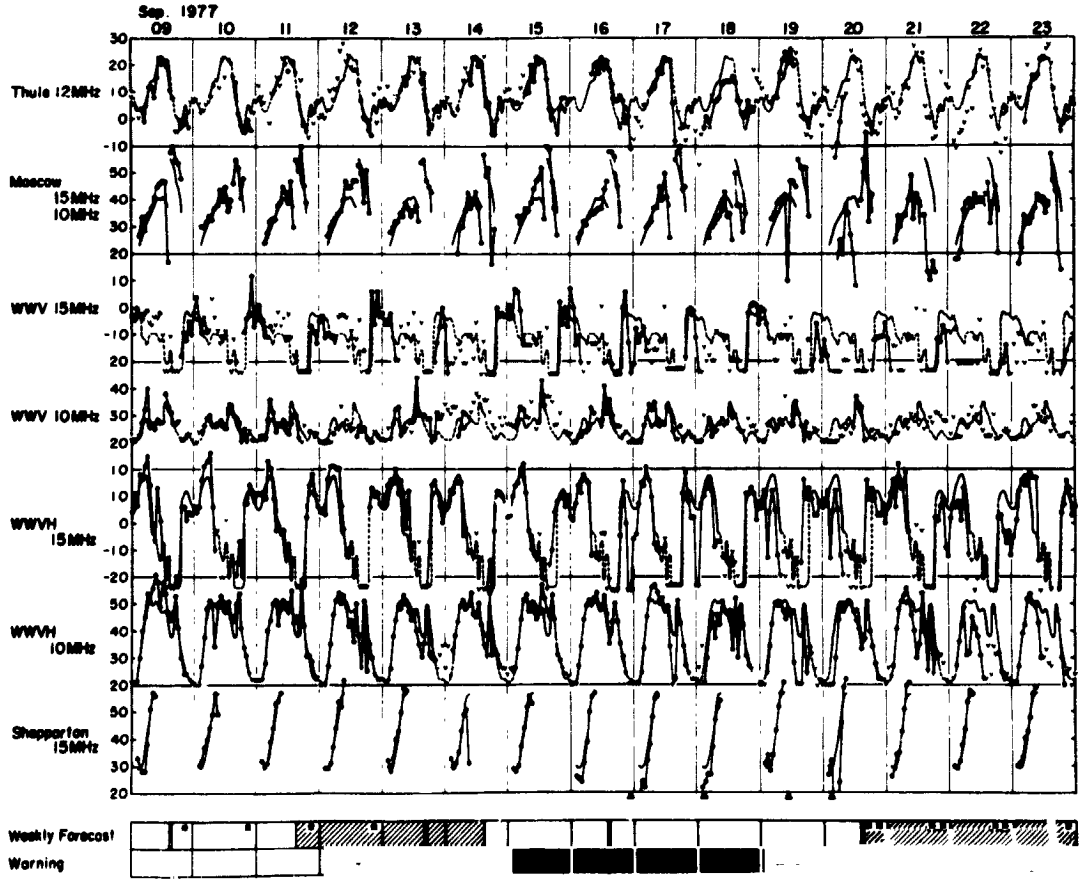

Fig. 3. Comparison between the short-term HF propagation predictions and the HF field strength data during September 9-23.

that this disturbance did not affect the propagation conditions so much, we concluded again that the propagation conditions would become unstable, when the SC-storm on September 12 was observed. Thus, the Weekly Forecast for September 14-20 issued on 13 predicted the disturbance in the HF propagation conditions for September 13. These HF propagation disturbance predictions resluted in false alarms as is evident in Fig. 3.

It can be seen in the figure that the HF signal strength was rather weak during September 19-23 in association with the magnetic storm condition for this period. The Warning was changed from N to U again at 0200 UT on September 19, because we expected a magnetic storm would commence soon. Thus, the Warning seems to have been correct in this case. However, we could not predict the unstable propagation conditions in the Weekly Forecast for 17-23 issued on September 16, because we could not predict the occurrence of the storm-producing flare on September 16.

The difficulty of the short-term HF propagation disturbance predictions is well demonstrated in these two examples, one success and one failure. In the first case, the magnetic storm was not so severe to affect the propagation conditions, whereas in the second case the storm was enough to affect the HF propagation. Thus, the difficulty is that it is needed to predict the magnitude of the magnetic storm, which is strongly controlled by the north-south component of IMF.

6. STATISTICAL EVALUATION OF MAGNETIC STORM PREDICTION

The accuracy of magnetic storm predictions can be statistically evaluated by comparing MAGALERT messages with actual disturbances. Strangely enough, there is no agreed definition of geomagnetically disturbed days among WWA and RWC's according to which MAGALERT should be issued. Therefore, we adopt here our own definition of disturbed days that ΣKp is no less than 25 to compare the disturbance predictions with actual disturbances. In Fig. 4 showing histograms of ΣKp for 1965-1976, the shaded portions present the number of MAGALERT's issued from Hiraiso and WWA vs. ΣKp. The hatched portion indicates the number of MAGALERT's issued for those days on which magnetic storms commenced in late hours and therefore ΣKp is small. These comparison between predictions and ΣKp, particularly those for 1974-1976 suggests that our definition of disturbed days provides a reasonable criterion with which predictions are evaluated.

The accuracy of these storm predictions are statistically evaluated by using the measure of correctness, R, which was originally defined by Sinno (1958):

$$R = x\{D\ (x + y)\}^{-1/2} \qquad (1)$$

where x is the number of disturbed days correctly forecast, D is the total number of disturbed days, and y is the number of quiet days for which storm forecasts were issued (i.e. false alarms). If we define two quantities A and B as

$$A = x / D \qquad (2)$$

$$B = x / (x + y) \qquad (3)$$

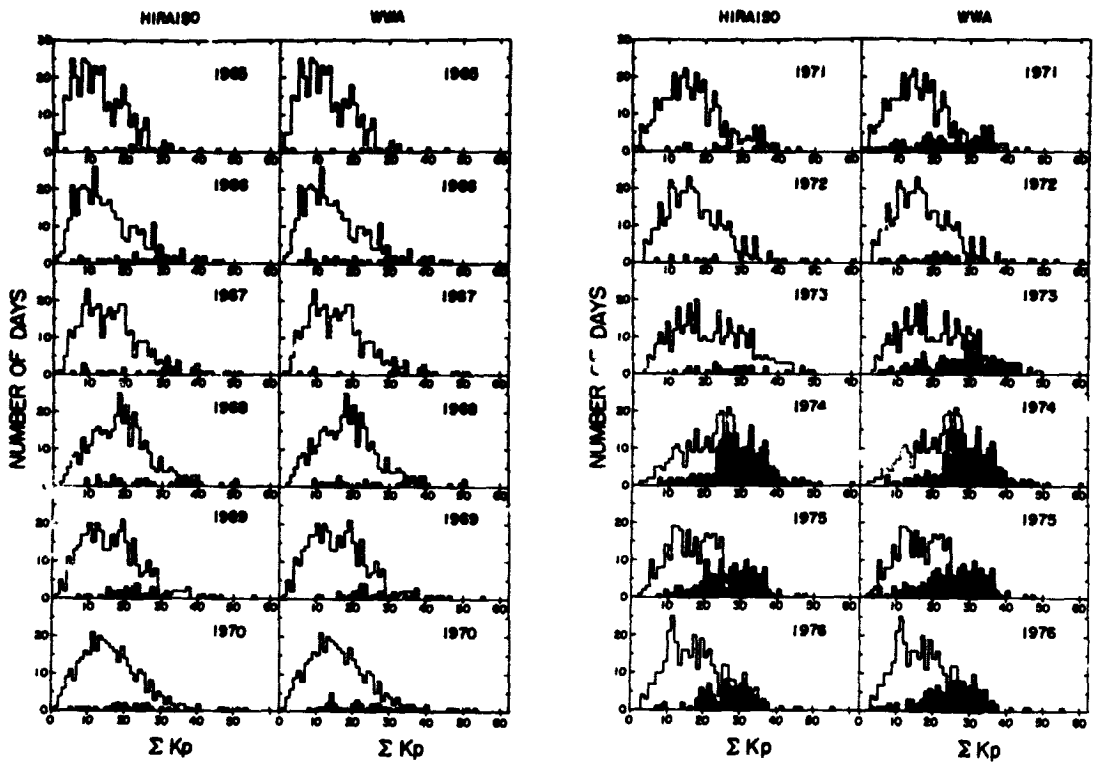

Fig. 4. Number of MAGALERT's issued by Hiraiso and WWA (shading) superposed on histograms of ΣKp for 1965-1976.

then A is the rate of predicted disturbed days to the total disturbed days, and B is the rate of correct disturbance forecasts to the total disturbance forecasts; R being simply the geometric mean of these quantities. We will call A and B the storm prediction rate and the correct alarm rate, respectively, and R the measure of synthetic correctness hereafter. Table 2 shows the values of D, x, and y during the period of 1965-1976 for Hiraiso and WWA. Although the storm predictions are evaluated only in terms of (1)-(3) in this report, evaluation by other methods is possible with this table.

Fig. 5 presents the variations in the storm prediction rate (A), the correct alarm rate (B), and the measure of synthetic correctness (R) calculated for the MAGALERT messages issued by Hiraiso and WWA from 1965 to 1976. It is noticeable that the storm prediction rates are particularly high in 1974-1976 at both Hiraiso and WWA. This is caused by the sudden increase in the number of MAGALERT's in 1974 (see Table 2). As is evident from (2), the more MAGALERT's were issued, the higher storm prediction rate is obtained. The main reason why many MAGALERT's were issued in 1974 and thereafter is that there occurred many recurrent-type magnetic storms in those years, and thus forecasters could easily predict the storm occurrence. The correct alarm rates are also high in 1974-1976 and the correctness measures are at the

Table 2. Numbers of disturbed days (D), correct storm predictions (x), false alarms (y), and total storm predictions (x+y) for MAGALERT's issued from Hiraiso and WWA during 1965-1976.

		HIRAISO			WWA		
Year	D	x	y	x+y	x	y	x+y
1965	21	6	10	16	1	5	6
1966	47	14	17	31	12	19	31
1967	55	16	11	27	12	5	17
1968	73	15	17	32	14	15	29
1969	52	11	24	35	15	18	33
1970	56	11	19	30	19	24	43
1971	55	7	11	18	20	41	61
1972	59	5	10	15	15	26	41
1973	131	16	13	29	69	41	110
1974	167	129	49	178	130	54	184
1975	89	68	59	127	71	70	141
1976	84	61	32	93	61	48	109

highest level of the twelve-year period of this study. The recurrent tendency of geomagnetic disturbances was similarly strong also in 1973 (Ondoh and Nakamura, 1977), and correspondingly WWA issued many MAGALERT's. As a result, the MAGALERT's from WWA in 1973 accomplished rather high storm prediction rate and measure of synthetic correctness. In contrast to this, the number of MAGALERT issuance from Hiraiso does not show any increase until 1974.

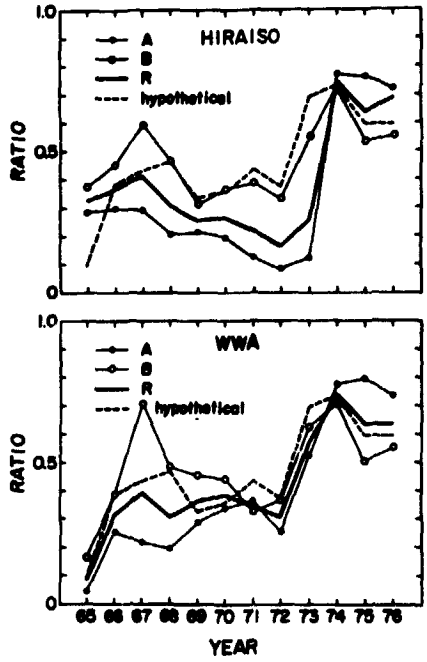

Fig. 5. Year-to-year variations in the storm prediction rate (A), the correct alarm rate (B), and the measure of sythetic correctness (R) for MAGALERT's issued from Hiraiso and WWA during 1965-1976.

In particular during 1970-1973, the number of MAGALERT's were very small in comparison with those from WWA (see Table 2), and thus the storm prediction rates were at the lowest level in those years.

It is also interesting to note in Fig. 5 that the trend of the measure of synthetic correctness (R) is roughly in parallel with the trend of the storm prediction rate (B). This result probably implies the measure of synthetic correctness of storm prediction is more strongly controlled by the storm prediction rate than by the correct alarm rate. The definition by (3) indicates that the highest correct alarm rate is accomplished by minimizing the number of false alarms (y), or in other words, by issuing MAGALERT only when the storm occurrence is expected with high degree of confidence. However this way of MAGALERT issuance will result in the low storm prediction rate and probably in the low correctness measure. It can be concluded from above discussion that the number of MAGALERT's were too small in the earlier times of the twelve-year period of this study, although it depends on the way of application of forecasts which is more important, the storm prediction rate or the correct alarm rate.

Minnis (1977) showed the assessment method of economic values of forecasts by comparing the actual prediction merit with the merit obtained by a simple hypothetical prediction method. Here, we will compare the above statistical evaluation of MAGALERT's with a hypothetical prediction under the assumption that the following day will always be the same as the preceding day. Suppose that there occurred a magnetic storm of the S-day duration, then this hypothetical method yields S-1 correct storm predictions ($x = S-1$), one false alarm for the next day of the storm end ($y = 1$), and one miss of alarm for the starting day of the storm. By counting the numbers of correct storm predictions and false alarms for a given interval, we obtain $D = x + y$ and therefore $A = B = R$. The correctness meaures were calculated for this hypothetical prediction with the actual variations of ΣKp, and the result is shown in Fig. 5 by the dashed line (Note that this one line exhibits the variations of A, B and R). It is really disappointing that the measure of synthetic correctness for the actual prediction is no better than that for the hypothetical prediction. Particularly the results of actual predictions by Hiraiso during 1970-1973 are much worse than those by the hypotnetical method, while the results for WWA are comparable to the hypothetical results. Reversely speaking, the present comparison indicates that the correct and early detection of events is important for the purpose of magnetic storm prediction, and it may be concluded that forecasters at Hiraiso had failed to understand magnetic storms in progress. Fortunately, the trend of improvement can be seen in 1974-1976 at both Hiraiso and WWA. It is also to be noted here again that the hypothetical method considered here can never predict the starting day of magnetic storms nor the isolated storms of one-day duration.

Table 3 shows the results of similar statistical evaluation of MAGALERT messages for the Bartels' rotation periods 1961-1980. The accuracy of the prediction for the first half period is much lower than that for 1976. The statistical accuracy of the hypothetical prediction is also low during this period. These results seem to be similar to those for 1965, and probably caused by the breaking recurrence tendency during the sunspot minimum year as was previously mentioned in Section 4. During the rotation periods 1971-1980, the statistical accuracy of the prediction becomes higher again with increasing flare-associated magnetic storms. The measure of synthetic correctness is much higher than that of the corresponding phase of solar cycle

Table 3. Evaluation of MAGALERT messages from Hiraiso and WWA in terms of the storm prediction rate (A), the correct alarm rate (B), and the measure of synthetic correctness (R).

(a) Rotation periods 1961-1970

Forecaster	D	x	x+y	A	B	R
Hiraiso	44	15	41	0.34	0.37	0.35
WWA	44	18	63	0.41	0.29	0.34
Hypothetical	44	16	44	0.36	0.36	0.36

(b) Rotation periods 1971-1980

Forecaster	D	x	x+y	A	B	R
Hiraiso	69	44	88	0.64	0.50	0.56
WWA	69	49	97	0.71	0.51	0.60
Hypothetical	69	38	69	0.55	0.55	0.55

(c) Rotation periods 1961-1980

Forecaster	D	x	x+y	A	B	R
Hiraiso	113	59	129	0.52	0.46	0.49
WWA	113	67	160	0.59	0.41	0.49
Hypothetical	113	54	113	0.48	0.48	0.48

20 or the solar maximum years. This result probably manifests the improvements of techniques for magnetic storm prediction which have recently been brought about by enhanced data collection and exchange.

REFERENCES

Bell, B. (1963): Solar radio bursts of spectral type II and type IV: their relations to optical phenomena and to geomagnetic activity. Smithonian Contr. Astrophys., 5:239.

Bell, B., and G. Noci (1976): Intensity of the Fe XV emission line corona, the level of geomagnetic activity, and the velocity of the solar wind. J. Geophys. Res., 81:4508.

Burlaga, L. F. (1975): Interplanetary streams and their interaction with the earth. Space Sci. Rev., 17:327.

Burton, R. K., R. L. McPherron, and C. T. Russell (1975): An empirical relationship between interplanetary conditions and D_{st}. J. Geophys. Res., 80:4204.

Castelli, J. P., J. Aarons, and G. A. Michael (1967): Flux density measurements of radio bursts of proton producing and nonproton flares. J. Geophys. Res., 72:5491.

Castelli, J. P., and W. R. Barron (1977): A catalog of solar radio bursts 1966-1976 having spectral characteristics predictive of proton activity. J. Geophys. Res., 82:1273.

Cook, F. E., and C. G. McCue (1975): Solar terrestrial relations and short-term ionospheric forecasting. Rad. Electr. Engineer, 45:11.

DeFeiter, L. D., A. D. Fokker, H. P. Th. Van Lohuizen, and J. Roosen (1960): Solar radio events and geomagnetic storms. Planet. Space Sci., 2:223.

Dodson, H. W., and E. Hedeman (1964): Problems of differentiation of flares with respect to geophysical effects. Planet. Space Sci., 12:393.

Dryer, M. (1975): Interplanetary shock waves: Recent developments. Space Sci. Rev., 17:277

Hakura, Y., and J. V. Lincoln (1963): A suggestion for improving forecasts of geomagnetic storms. J. Geophys. Res., 68:1563.

Hansen, R. T., S. F. Hansen, and C. Sawyer (1976): Long-lived coronal structures and recurrent geomagnetic patterns in 1974. Planet. Space Sci. 24:381.

Krieger, A. S., A. F. Timothy, E. C. Roelof (1973): A coronal hole as the source of a high velocity solar wind stream. Solar Phys., 29:505.

Minnis, C. M. (1977): Ionospheric disturbance forecasts: assessment of their economic value. Telecomm. J., 44:328.

Neupert, W. M., and V. Pizzo (1974): Solar coronal holes as sources of geomagnetic disturbances. J. Geophys. Res., 79:3701.

Nishida, A. (1965): Storm sudden commencements as solar blast waves. Rep. Ionos. Space Res. Japan, 19:201.

Nolte, J. T., A. S. Krieger, A. F. Timothy, R. E. Gold, E. C. Roelof, G. Vaiana, A. J. Lazarus, J. D. Sullivan, and P. S. McIntosh (1976): Coronal holes as sources of solar wind. Solar Phys., 46:303.

Ohbu, K., K. Muranaga, S. Isozaki, A. Mitobe, T. Isobe, and E. Ohuchi (1978): Solar radio emissions of 100, 200, 500 and 9500 MHz observed at Hiraiso. Solar Terr. Environmental Res. Japan, 2:82.

Ondoh, T., and Y. Nakamura (1977): Solar cycle variation of 27-day recurrent tendency of geomagnetic activity during sunspot cycle 20. Solar Terr. Environmental Res. Japan, 1:90.

Pinter, S. (1972): Flare-associated solar wind disturbances and type II and IVm radio bursts. Bull. Astron. Inst. Czech., 23:69

Pinter, S. (1973): Close connection between flare generated coronal and interplanetary shock waves. Nature Phys. Sci., 243:96.

Sakurai, K., and J. K. Chao (1974): Motion of sources for type II and type IV radio bursts and flare-associated interplanetary disturbances. J. Geophys. Res., 79:661.

Sheeley, N. R. , Jr., J. W. Harvey, and W. C. Feldman (1976): coronal holes, solar wind streams, and recurrent geomagnetic disturbances: 1973-1976. Solar Phys., 49:271.

Sinno, K. (1958): Hit rates of radio propagation disturbance warnings and SWI warning. J. Rad. Res. Labs. (Japan), 5:109.

Sinno, K., and Y. Hakura (1958): On the relation of solar eruptions to geomagnetic and ionospheric disturbances, II. On the types of solar radio outbursts. Rep. Ionos. Space Res. Japan, 12:296.

A REVIEW OF SHORT-TERM FLARE FORECASTING ACTIVITIES AT TOYOKAWA

Shinzo Enome
Toyokawa Observatory
Research Institute of Atmospherics
Nagoya University
13 Honohara 3-chome
Toyokawa 442, Japan

Short-term forecasting of solar activity conducted at Toyokawa is briefly reviewed. The forecasts are based on microwave observations of the slowly varying component of solar radiation associated with active regions. Forecasting started in 1966 while participating in the Proton Flare Project on an experimental basis. Since May 1969, daily forecasts have been issued in the URALR Code through the URSIGRAM network.

INTRODUCTION

The main item of prediction at Toyokawa is the occurrence of proton flares. Predictions started in May 1966 to take part in the Proton Flare Project, and were applied, on an international basis, to the selection of a solar active center, which was to be observed in the extensively coordinated studies of solar and geophysical activities, such as Proton Flare Projects (PFP) in 1966, CINOF (1972, 1973). On the occasion of the first PFP in July 1966, the prediction from Toyokawa was entirely successful (Simon, 1969). We will join the coming SMY in 1979 through 1981. Forecasts from Toyokawa are also used, on the regional basis, for fully-prepared observations of active regions and as fundamental data for the warning of shortwave communication condition. Application was made of forecast for the determination of balloon launching timing to observe solar neutrons and gamma rays from flaring regions during the level flight in 1968 in the International Active Sun Year (Takakura and Ito, 1970).

AVAILABLE DATA

Local source of radio emission above an active region is most prominent at microwave frequencies. This radio emission is associated with coronal condensations, with typical density and temperature of 10^8 - 10^9 cm^{-3} and 2×10^6 K, which are permeated by strong magnetic fields of sunspots. At Toyokawa Observatory, we have lambda 3.2-cm (9400 MHz) and 8-cm

(3750 MHz) radio interferometers. Both sets of radio instruments are almost identical in geometrical configuration to give the same spatial resolution of 1.1, 0.4 and 2.2 arc minutes for adding, compound and T modes respectively at 3.2 and 8 cm.

Most useful observational data with these instruments are one-dimensional brightness and polarization distributions at 3.2 and 8 cm with 1.1 arc minutes resolution. The term brightness and polarization, more strictly, correspond to the sum and the difference of right-handed and left-handed circular polarizations.

Active regions usually appear in the middle latitudes of the northern and southern hemispheres of the Sun. When several active regions are visible on the disk, it is in most cases possible to discriminate the contribution of radio emission from each region, so long as the fan beam does not drift across more than two active regions at the same time. If such geometrical alignment of active regions happens, which is not frequent but not entirely rare, we can still discriminate "one-dimensionally overlapped" active regions with pencil beam (T-mode) observations.

After these procedures we have microwave radio flux of each active region, which is called slowly varying component or simply S-component, with information on structure of the region in brightness and polarization at 3.2 and 8 cm. An example of fan beam and pencil beam observations is shown in Figure 1 at both wavelengths.

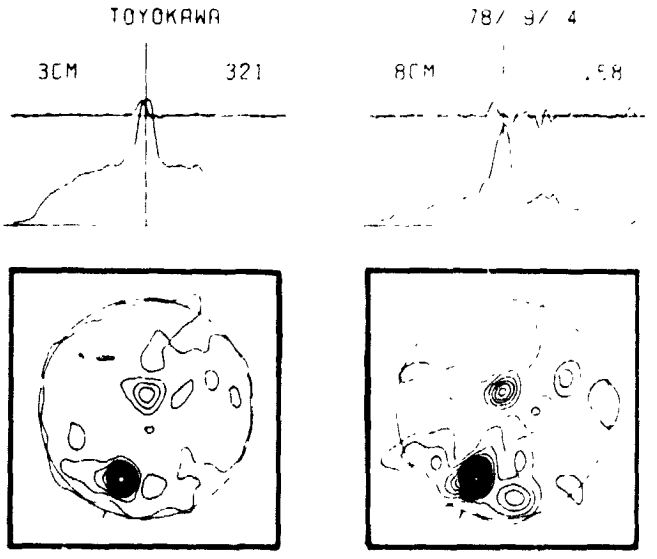

Fig. 1. Fan-beam and pencil-beam observations of the Sun at 3.2 and 8 cm. Contour level and interval are roughly 15000 K at 3.2 cm and 40000 K at 8 cm. North is top and east is left and geographical north and south are indicated by tick marks. Polarization (top) and brightness (middle) are shown for drift curves.

PREDICTION TECHNIQUES

Parameters used in prediction are 3-cm (round number for 3.2), 3-cm to 8-cm flux ratio and spatial polarization distribution at 3 cm of each S-component. For each active region with 3-cm flux greater than 5 s.f.u. (10^{-22} $Wm^{-2}Hz^{-1}$) we report on a message of east-west position, 3-cm flux, 3-cm to 8-cm flux ratio together with observational conditions and observed spatial features. When 3-cm flux is greater than 10 s.f.u. and 3-cm to 8-cm flux ratio is greater than unity, comments are supplemented, which include flux ratio in percent with three digits and proton flare expectation in four grades from 0 to 3. This last expectation number can not be strictly objective, since it depends on the forecaster's personal experience, individual feeling and so on.

These pieces of information are coded according to URALR code of URSIGRAM and sent through its network. An example of URALR message of March 28, 1976 is as follows:

URALR 44301 28096 757XX 20048 X1161.

In plain language, this reads URALR message from Toyokawa that an active region at 57 % east in solar radius has 3-cm flux of 20 s.f.u. with 3-cm to 8-cm flux ratio of 116 %, and is eruptive with spatial polarization feature favourable for proton flares, with proton flare expectation of one, in four grades from 0 to 3.

There was a proton flare on March 28 at 1936 UT, but this prediction was not successful in a strict sense, since March 28, 1976 was Sunday and this message was issued about 0200 UT on March 29 from Toyokawa.

BASIS FOR TECHNIQUE

It was found that the 3-cm S-component is a useful indicator of flare activity by French group (Kundu, 1959; Pick, 1961). In 1964, Tanaka and Kakinuma pointed out that active regions with 3-cm to 7.5-cm (4000 MHz) flux ratio greater than unity are closely related to proton flares. Their work was developed later to investigate spatial structure of S-component in brightness and polarization with respect to proton flare productivity (Tanaka and Enome, 1975).

As for the emission mechanisms of microwave S-component, it is generally accepted that they are free-free emission of thermal electrons and gyro-resonance emission at second and third harmonics of thermal electrons both in a coronal condensation. The former mechanism mainly contributes to unpolarized halo component and the latter to polarized core component.

For intense active regions the brightness temperature of core component is as high as 2×10^6 K at 8 cm and 5×10^5 K at 3.2 cm. Flux of these core component is as much as 20 s.f.u. or more both at 8 cm and 3.2 cm. Our interpretation of these data is that at 8 cm optical depth is thick, where degree of polarization is pretty low, but not thick at 3.2 cm, where degree of polarization is high. This means that electron temperature above an intense active region is as high as 2×10^6 K, where magnetic field is 450

Gauss, if 8-cm radiation is emitted at the third harmonics of electron gyrofrequency. Possible stronger field of 1100 Gauss emerges into corona, inferred from 3-cm radiation.

Tanaka and Enome (1975) have analyzed 259 active regions in the period 1967 through 1971, and have shown that active regions with 3-cm flux greater than 10 s.f.u. and 3-cm to 8-cm flux ratio greater than 80 % have close correlation with the occurrence of proton flares from them. It is also shown that very powerful active regions, which release energetic protons into interplanetary space several times during their disk passage, are associated with an S-component of more than 20 s.f.u. at 3 cm and 8 cm. It is inferred from this that it is neccessary but not sufficient that powerful proton centers are accompanied by electron temperature of 2×10^6 K and by magnetic field of 1100 Gauss permeated into the corona. Tanaka and Enome further have shown that active regions with a definite type of spatial polarization distribution across them are closely related to proton flare production. This polarization distribution at 3 cm is called "P-configuration", which consists of polarized central part with sub-regions on either side of the central part, which are polarized oppositely to the polarization sense of the central part, as seen in Figure 2.

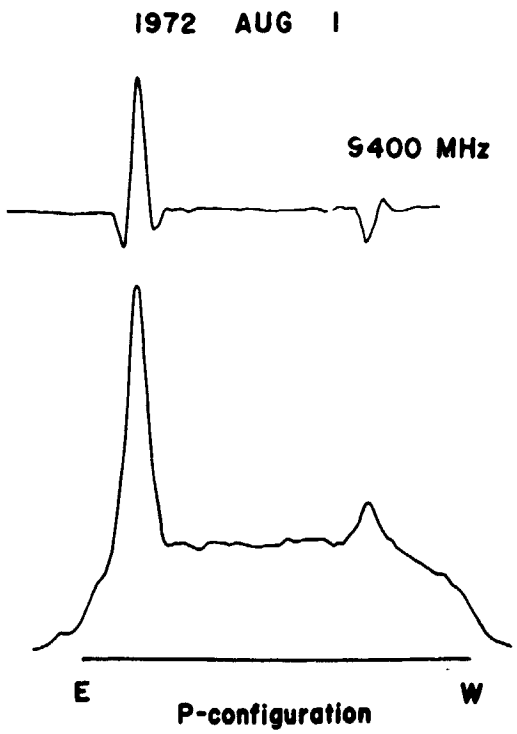

Fig. 2. Strip-scan curves of the Sun in brightness (bottom) and polarization (top) at the wavelength of 3.2 cm on August 1, 1972 (taken from Tanaka and Enome, 1975).

As the gyroresonance theory teaches us (Kakinuma and Swarup, 1962; Zheleznyakov, 1962), right-handed (R) and left-handed (L) polarized waves originate in a hot plasma magnetized negatively and positively respectively. A P-configuration region, therefore, corresponds to field alignment of - + - or + - +, which has close correlation with anomalous magnetic polarization regions at photospheric level such as colliding active regions, shear or rotation of sunspots within single penumbra. From optical and/or magnetograph observations it is well known that those magnetically anomalous regions produce intense flares (e.g. Smith and Howard, 1968).

EVALUATION OF FORECAST

During the periods of July 1974 and of August 1975 through September 1977, fifteen proton event days were recorded by earth-orbiting satellites NOAA 2 and 3 and IMP 7 and 8 (Mangis, 1975; Solar-Geophysical Data) as listed in Table 1.

Table 1
List of Proton Events
in July 1974 and in August 1975 - September 1977

Date	Start	Max	End	Location	McMath	Comment
7/ 3/74	0828	0836	0908	S15E08	13043	Proton Alert (1)*
7/ 4/74	0641	0648	0700	S15W04	13043	Proton Alert (1)
	1353	1354	1500	S16W07	13043	
	2048	2058	2126	S16W12	13043	
7/ 5/74	1509	1514	1522	S15W26	13043	Proton Alert (1)
	2135	2139	2153	S10W26	13043	
7/ 6/74	1842	1905	2028	S15W40	13043	
8/22/75	1027	1028	1029	N26W87	13811	No Alert
	1230	1230	1232	N26W87	13811	
11/21/75	0610	0619	0710	S07W21	13937	No Alert
3/23/76	0840	0843	0909	S05E90	14143	Behind the Limb
3/25/76	1308	1318	1352	S05E69	14143	No Alert
3/28/76	1843	1938	2348	S07E28	14143	Proton Alert (1)
4/30/76	2101	2109	2125	S08W46	14179	No Alert
8/22/76	1158	1212	1230	S02W90	14366	Behind the Limb
9/ 7/77	2225	2258	2420	N10E90	14943	Behind the Limb
9/16/77	2219	2308	2500	N07W21	14943	No Alert
9/19/77	1027	1101	1147	N08W57	14943	No Alert
9/24/77					14943(?)	Behind the Limb

* Proton Flare Expectation Grade in 0 to 3 Range.

Three of these events were certain to be a behind-the-limb event and one is suspected to be it, therefore, it is absolutely not possible to forecast their occurrence with our technique, since it is based on the spectrum of S-component visible on the disk of the Sun. Fifteen events in the above Table were produced by powerful proton centers of McMath 13043, 14143 and 14943, including the above-mentioned four invisible hemisphere events. Among twelve disk event days, five event days were predicted correctly on

24-hour basis. If we take longer predictic interval of, say, three days, prediction is true for seven cases out of t lve. During these periods we have issued 27 messages of proton alert, of which thirteen were positive with expectation grade 1 and one expectation grade 2. The rest of forecasts were negative with expectation grade 0, all of which turned out to be true.

As for the accuracy of the forecast, it may be very difficult to define, since the view point of forecasters may be quite different from that of users. Forecast accuracy of our proton alerts, when they are issued, is evaluated to be 5/27 + 14/?7, which is about 70 % on 24-hour basis. Mean probability of proton event day during these periods is about 15/800, which is about 2 %, while the accuracy of positive proton alerts is 5/13, which is about 38 %. This is about twenty times the mean probability of proton flare day. These values of accuracy may be compared with other forecast center's values (Simon and McIntosh, 1972).

From Table 1 it is readily seen that for very sporadic proton events such as those on August 22, 1975, November 21, 1975 and April 30, 1976, we could not even issue proton alert. It is extremely difficult by the present technique to predict their occurrence, since they are produced in a small active region or they are associated with an active region with very rapid evolution. For reference we list radio status of active regions on the above days in the Table 2.

Table 2
Radio Status of Active Regions on Unpredictable Proton Event Days

8/22/75: No S-component greater than 5 s.f.u.
11/21/75: McMath 13937 at 26 % west with 5 s.f.u. and ratio 60 %, eruptive, low brightness.
4/30/76: McMath 14179 at 80 % west with 13 s.f.u. and ratio 80 %, burst in progress, double structure.

CONCLUDING REMARKS

For proton flares which take place in intense active regions, it is possible to predict their occurrence with certain accuracy, but for certain class of proton flares which occur in a small active region or which are associated with an active region, which evolves very rapidly, or for those which occur behind the limb, it is almost impossible to forecast their occurrence with our present technique.

REFERENCES

Kakinuma, T. and Swarup, G. (1962): A Model for the Sources of the Slowly Varying Component of Microwave Solar Radiations. Astrophys. J., 136: 975.

Kundu, M. R. (1959): Structure et proprietes des sources d'activite solaire sur ondes centimetriques. Ann. Astr., 22:1.

Mangis, S. J. (1975): July 1974 Solar Activity and Related Geophysical Effects. NOAA Technical Memorandum ERL SEL-38, Space Environment Laboratory, Boulder CO, U.S.A.

Pick, M. (1961): Evolution des emissions radioelectriques solaire de type IV et leur relation avec d'autres phenomenes solaire et geophysiques. Ann. Astr., 24:183.

Simon, P. (1969): Introductory. Annales of IQSY, Vol. 3, Proton Flare Project (The July 1966 Event), Ed. A. C. Stickland, The MIT Press, Cambridge MA, U.S.A., p. 3.

Simon, P. and McIntosh, P. S. (1972): Survey of Current Solar Forecast Centers. Solar Activity Observations and Predictions, MIT Press, Cambridge MA, U.S.A., p. 343.

Smith, S. F. and Howard, R. (1968): Magnetic Classification of Active Regions. IAU Symposium No. 35, Structure and Development of Solar Active Regions, Ed. K. O. Kiepenheuer, D. Reidel, Dordrecht-Holland, p. 33.

Takakura, T. and Ito, K. (1970): High Energy Radiations Associated with Solar Flares (in Japanese). Kagaku (Science), 40:340.

Tanaka, H. and Enome, S. (1975): The Microwave Structure of Coronal Condensations and Its Relation to Proton Flares. Solar Phys., 40: 123.

Tanaka, H. and Kakinuma, T. (1964): The Relation between the Spectrum of Slowly Varying Component of Solar Radio Emission and Solar Proton Event. Report Ionosph. Space Res. Japan, 18:32.

Zheleznyakov, V. V. (1962): The Origin of the Slowly Varying Component of Solar Radio Emission. Soviet Astronomy-AJ, 6:3.

D/8-32

N80-18480

RADIO PROPAGATION PREDICTION SERVICES IN JAPAN

Rikio MAEDA
Radio Research Laboratories
4-2-1 Nukui-Kita Koganei, Tokyo 184, JAPAN

Japanese prediction services for HF radio communications are outlined in relation to prediction method, performance and evaluation. The current prediction is based on the CCIR interim method with some modifications matching to a computer system. The principal service is the monthly median prediction issued regularly three months in advance for various communication circuits. A daily prediction for short-distance circuits is being prepared by using real time ionospheric sounding data. It is reportable that an evaluation theory and practice will be introduced in the future prediction service.

1. Introduction

The purpose of this review is to sketch a barest outline of Japanese radio propagation prediction services to professional and amateur users of HF radio communications. It is limited here to the frequency/time and path-loss predictions and excluded from the so-called radio disturbance warnings. The Radio Research Laboratories have been operating the Western Pacific Regional Warning Center of the International Ursigram and World Days Service, the executive facility of which is maintained by the Upper Atmosphere Research Section of the Hiraiso Branch. On the other hand, the regular service on radio propagation prediction is now made by the Ionospheric Radio Prediction Section of the Radio Wave Division which has been conducting the routine ionospheric soundings at Wakkanai (45°N, 142°E), Akita (40°N, 140°E), Kokubunji (35°N, 139°E), Yamagawa (31°N, 131°E) and Okinawa (26°N, 128°E) in Japan for applications to ionospheric radio communications. The Japanese prediction service on ionospheric radio propagation began with issuance of the Radio Propagation Prediction in 1947. This prediction had been based on a manual method before 1971, and at present is similar to a CCIR interim prediction modified for the TOSBAC 5600/160 electronic computer. Objects and forms of the prediction have been considered from a social and economical standpoint for long-term planning and short-term operating of international and domestic communication circuits. There are two monthly predictions published three months in advance, one of which predicts usable frequency-time ranges for various communications among main cities over the world, and the other is a prediction of time ranges appropriate for assigned

operational frequencies on ship-to-shore communications between foreign harbors or fishing banks and Tokyo. These prediction services are regularly offered to hundreds of domestic facilities and a few foreign organizations.

In the following sections, the current prediction is described about its method, performance and evaluation.

2. Method of prediction

In order to plan and maintain an effective communication system, it is desirable to know the upper and lower limits to the range of frequencies within which usable operational frequencies should be chosen. As these frequency limits are generally found for any radio communications via the ionosphere, the radio propagation prediction is intended to provide information about effective usage of assigned frequencies.

HF radio signals for communications are absorbed by and reflected from the ionosphere, therefore the ionospheric propagation is seriously affected by the density distribution of ionization in the D, E and F regions. The quality of communication depends also on the noise field which is notably controlled by man-made noise rather than atmospheric noise at the receiver. It is necessary for radio propagation predictions to take models of ionization and noise in the radio wave medium varying with environment parameters, i.e., the geographic position, time of day, month of year, levels of solar and geomagnetic activity and so on. The modeled ionization and noise can be numerically represented over the world by means of function series with the environment parameters, where the ionospheric characteristics are indicated with monthly median values and the level of solar activity is represented by a predicted twelve months smoothed running average sunspot number. If the normal radio propagation is assumed to be confined within the medium bounded between the ionosphere and the earth's ground, the signal attenuation, direction and mode will be calculated by empirical formulae derived from practical experiences. Accomplishment of the prediction requires further information about circuit parameters such as the transmitter power, the transmitting and receiving antenna characteristics, and the minimun receivable field strength. After the above preparation, the highest and lowest usable frequencies (MUF and LUF) are determined and also the pathloss is calculated for any operational frequency on a communication circuit.

The computer software for the current prediction in Japan is derived from the CCIR Reports 252-2 [Jones and Gallet, 1962] and 340 [Barghausen et al., 1969], with some program conversion to a TOSBAC 5600/160 computer. As an example of the prediction calculation, a computer output is reproduced concerning radio communicative features of the Hawaii-Hiraiso circuit as noted in Table 1 [Ichinose and Yamaoka, 1973]. The monthly median prediction is useful not only for operation plans but also for specification designs of communication circuits. For an actual operation of a communication circuit, a daily prediction service is urgently needed because the day-to-day MUF and LUF are hardly estimated by the monthly prediction.

Table 1. Output of monthly median prediction.

MONTH 3 SSN= 34 135E LOCAL TIME

TR.= HAWAII 20.80N 156.50W RE.= HIRAISO 36.40N 140.60E

BEARINGS T.R 300 H.I 87 DISTANCE 6267KM POWER 1.0KW ANTENNA GAIN TM. 0 RE. 0

3MHZ NOISE=-180DBW TIME= 90 PERCENT REQ.S/N=20DB

GMT	LT	MUF	3.00	5.00	7.00	9.00	12.00	15.00	18.00	22.00	26.00	30.00	FREQ. (MHZ)
2	11	31.8											
			4E	4E	4E	4F	3F	3F	2F	2F	2F	2F	MODE
			5	5	5	17	11	11	4	4	4	4	ANGLE
			21.3	21.3	21.3	22.4	22.2	22.2	21.7	21.7	21.7	21.7	DEL
			584	392	301	200	138	169	161	157	156	155	LOSS
			-443	-240	-148	-65	-20	-8	1	6	9	11	DBU
			-173	-172	-171	-170	-172	-175	-179	-181	-186	-185	NOI.DBW
			-560	-367	-272	-171	-149	-134	-132	-128	-127	-126	SIG.DBW
			-387	-196	-102	-2	22	36	47	52	59	59	S/N DB
			.99	.99	.99	.99	.99	.99	.99	.94	.81	.60	F.DAYS
			.00	.00	.00	.00	.06	.65	.98	.93	.81	.60	S.PROB
			.00	.00	.00	.00	.61	.93	.98	.93	.81	.60	REL
4	13	32.1											
			4E	4E	4E	4F	3F	2F	2F	2F	2F	2F	MODE
			4	4	4	16	10	3	3	3	3	3	ANGLE
			21.3	21.3	21.3	22.6	22.1	21.6	21.6	21.6	21.6	21.6	DEL
			429	305	244	181	166	158	145	154	153	153	LOSS
			-283	-155	-91	-26	-8	2	6	10	12	13	DBU
			-168	-169	-166	-165	-173	-177	-181	-181	-186	-185	NOI.DBW
			-400	-276	-215	-152	-137	-129	-126	-125	-124	-124	SIG.DBW
			-237	-112	-49	13	35	47	55	56	62	61	S/N DB
			.99	.99	.99	.99	.99	.99	.99	.94	.82	.62	F.DAYS
			.00	.00	.00	.01	.68	.99	.98	.94	.84	.64	S.PROB
			.00	.00	.00	.35	.94	.99	.98	.94	.83	.62	REL
6	15	24.3											
			3F	3F	3F	4F	3F	2F	2F	3F	3F	3F	MODE
			7	7	7	12	2	2	2	8	9	8	ANGLE
			15.7	15.7	15.7	22.6	22.0	21.6	21.6	22.0	22.0	22.0	DEL
			190	169	158	152	148	147	148	148	149	150	LOSS
			-44	-17	-4	4	9	12	14	15	16	16	DBU
			-158	-160	-164	-168	-173	-178	-181	-181	-186	-185	NOI.DBW
			-161	-139	-129	-123	-119	-118	-119	-119	-120	-121	SIG.DBW
			-3	21	35	45	54	59	62	61	66	64	S/N DB
			.99	.99	.99	.99	.99	.99	.99	.80	.27	.03	F.DAYS
			.00	.06	.63	.46	.99	.99	.99	.80	.27	.03	S.PROB
			.00	.54	.93	.98	.99	.99	.99	.80	.27	.03	REL
8	17	16.6											
			3M	3F	3F	3F	3F	3F	3F	3F	0	0	MODE
			8	11	11	11	11	11	11	11	0	0	ANGLE
			17.5	22.2	22.2	22.2	22.2	22.2	22.2	22.2	.0	.0	DEL
			127	132	135	137	140	142	143	145	0	0	LOSS
			19	18	18	18	18	18	18	18	0	0	DBU
			-154	-158	-162	-168	-174	-179	-181	-181	0	0	NOI.DBW
			-98	-103	-106	-108	-111	-113	-114	-116	0	0	SIG.DBW
			56	55	56	60	63	65	66	64	0	0	S/N DB
			.99	.99	.99	.99	.99	.81	.24	.00	.00	.00	F.DAYS
			.99	.99	.99	.99	.99	.81	.23	.00	.00	.00	S.PROB
			.99	.99	.99	.99	.99	.81	.23	.00	.00	.00	REL
10	19	13.4											
			3F	2F	2F	2F	2F	2F	2F	0	0	0	MODE
			12	6	4	4	4	4	4	0	0	0	ANGLE
			22.4	21.8	21.8	21.8	21.8	21.6	21.8	0	0	0	DEL
			137	132	135	137	140	142	143	0	0	0	LOSS
			18	18	18	18	18	18	18	0	0	0	DBU
			-153	-157	-163	-169	-174	-179	-181	0	0	0	NOI.DBW
			-98	-103	-106	-108	-111	-113	-114	0	0	0	SIG.DBW
			54	54	56	60	63	65	66	0	0	0	S/N DB
			.99	.99	.99	.99	.78	.20	.00	.00	.00	.00	F.DAYS
			.99	.99	.99	.98	.78	.19	.00	.00	.00	.00	S.PROB
			.99	.99	.99	.98	.78	.19	.00	.00	.00	.00	REL

3. Performance of prediction

Radio propagation prediction services in Japan are remarkably supported by computer systems which have made major contributions to development of prediction calculations and outputs through large data filing and classifying. An important regular service is the monthly radio propagation prediction issued three months in advance with two different output forms.

The first form illustrates diurnal changes in the monthly median MUF and LUF on a frequency-time graph, where the time is denoted by G.M.T. and J.S.T. (Japan Standard Time, 135°E Mean Time). Objective circuits of this prediction are listed in Table 2, where the propagation azimuth is measured in degrees clockwise from north at the communications center and the propagation distance is along the great circle from the center to a terminal in kilometers. For short-distance domestic circuits laid within one hop area over Japan, some predicted MUF and LUF monthly median curves are shown in Fig. 1. These are northern route predictions for special paths with lengths of 500, 1000, 1500 and 2000 km. Fig. 2 illustrates examples of point-to-point predictions for long-distance international circuits between Tokyo and foreign cities.

Table 2. Circuit list for monthly median prediction.

Fig.	Circuit	Center			Terminal			Great Circle (km)
		Lat.	Long.	Azim.	Lat.	Long.	Azim.	
1.1	North from Hakodate	41.8N	140.7E	0	59.8N	140.7E	180	2,000
1.2	East from Hakodate	41.8N	140.7E	90	39.3N	164.3E	285	2,000
1.3	South from Hakodate	41.8N	140.7E	180	23.8N	140.7E	0	2,000
1.4	West from Hakodate	41.8N	140.7E	270	39.3N	117.2E	75	2,000
2.1	North from Tokyo	35.7N	140.8E	0	53.7N	140.8E	180	2,000
2.2	East from Tokyo	35.7N	140.8E	90	33.8N	162.6E	282	2,000
2.3	South from Tokyo	35.7N	140.8E	180	14.8N	140.8E	0	2,000
2.4	West from Tokyo	35.7N	140.8E	270	33.8N	119.0E	77	2,000
3.1	Nouth from Nagasaki	32.4N	130.1E	0	50.4N	130.1E	180	2,000
3.2	East from Nagasaki	32.4N	130.1E	90	30.7N	151.2E	281	2,000
3.3	South from Nagasaki	32.4N	130.1E	180	14.5N	130.1E	0	2,000
3.4	West from Nagasaki	32.4N	130.1E	270	30.7N	105.1E	78	2,000
4	Philippines	35.0N	140.0E	224	14.5N	121.0E	36	2,970
5	Jakarta	35.0N	140.0E	224	6.0S	106.8E	34	5,730
6	Malaya	35.0N	140.0E	236	3.0N	102.0E	43	5,290
7	Southern India	35.0N	140.0E	257	7.0N	80.0E	53	6,840
8	Nouthern India	35.0N	140.0E	281	28.6N	77.2E	66	5,880
9	Beirut	35.0N	140.0E	305	34.0N	36.0E	53	9,000
10.A	Southern Africa (Short Path)	35.0N	140.0E	255	30.0S	25.0E	66	13,990
10.B	Southern Africa (Long Path)	35.0N	140.0E	75	30.0S	25.0E	246	26,020
11	Ghana	35.0N	140.0E	308	5.6N	0.0	39	13,850
12	Iberia	35.0N	140.0E	335	39.0N	9.0W	25	11,190
13	Southern Europe	35.0N	140.0E	323	42.0N	13.0E	40	9,890
14	Central Europe	35.0N	140.0E	335	50.0N	0.0	31	9,770
15	Scandinavia	35.0N	140.0E	333	60.0N	20.0E	47	8,120
16	East Coast U.S.A.	35.0N	140.0E	26	42.0N	76.0W	331	10,700
17	West Indies	35.0N	140.0E	41	23.0N	82.4W	324	12,160
18	Panama	35.0N	140.0E	48	9.0N	80.0W	321	13,520
19	Lima	35.0N	140.0E	64	12.0S	77.0W	310	15,490
20	Alaska	35.0N	140.0E	37	60.0N	145.0W	277	5,880
21	West Coast U.S.A.	35.0N	140.0E	54	37.6N	122.4W	302	8,300
22	Hawaiian Islands	35.0N	140.0E	86	21.3N	158.0W	298	6,170
23.A	Syowa Station Antarctica (Short Path)	35.0N	140.0E	205	69.0S	39.6E	85	14,010
23.B	Syowa Station Antarctica (Long Path)	35.0N	140.0E	25	69.0S	39.6E	265	26,000
24	South East Australia	35.0N	140.0E	175	37.8S	145.0E	355	8,110
25	Moscow	35.0N	140.0E	323	56.0N	37.5E	59	7,550

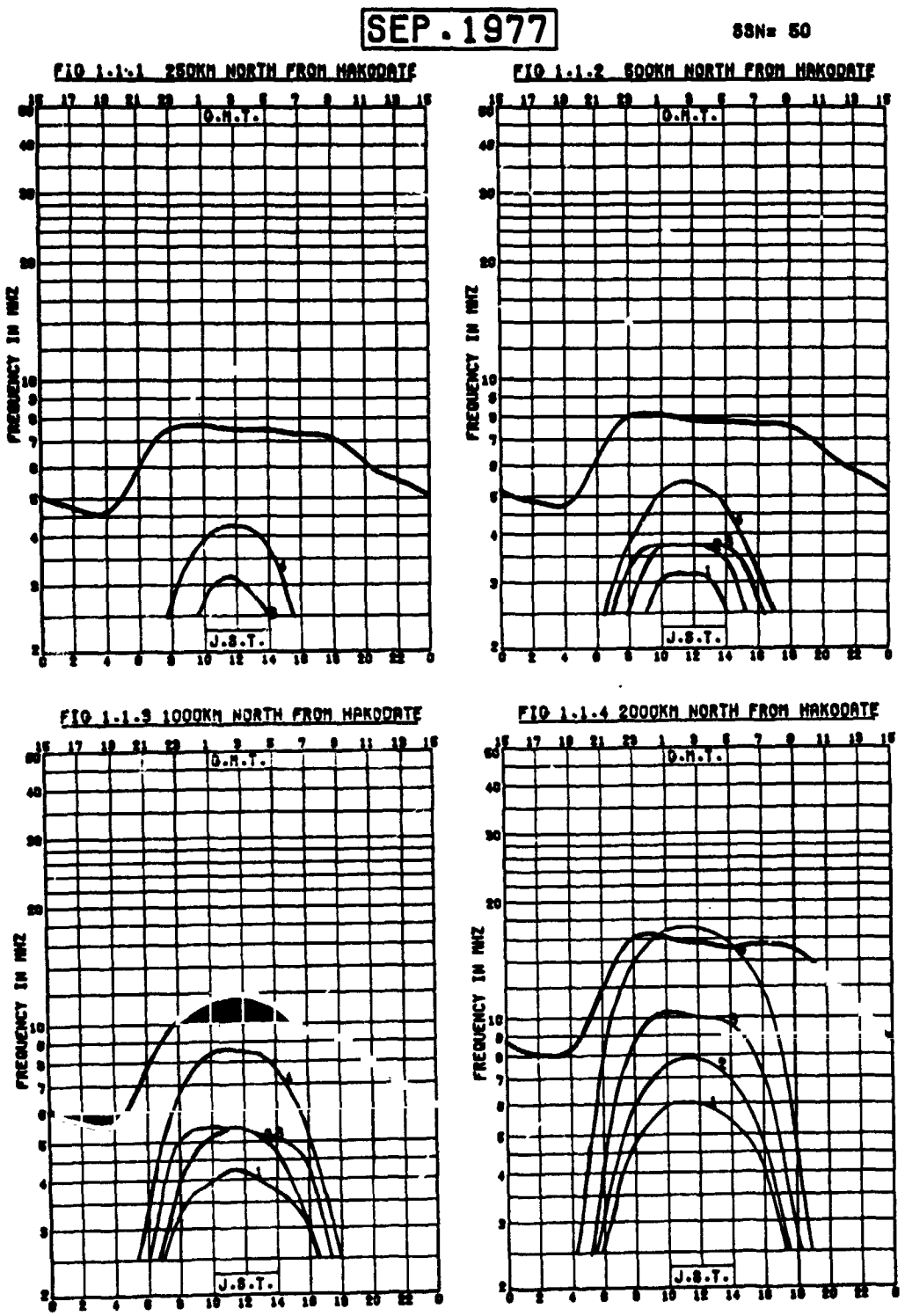

Fig. 1. Frequency-time range prediction for domestic circuits.

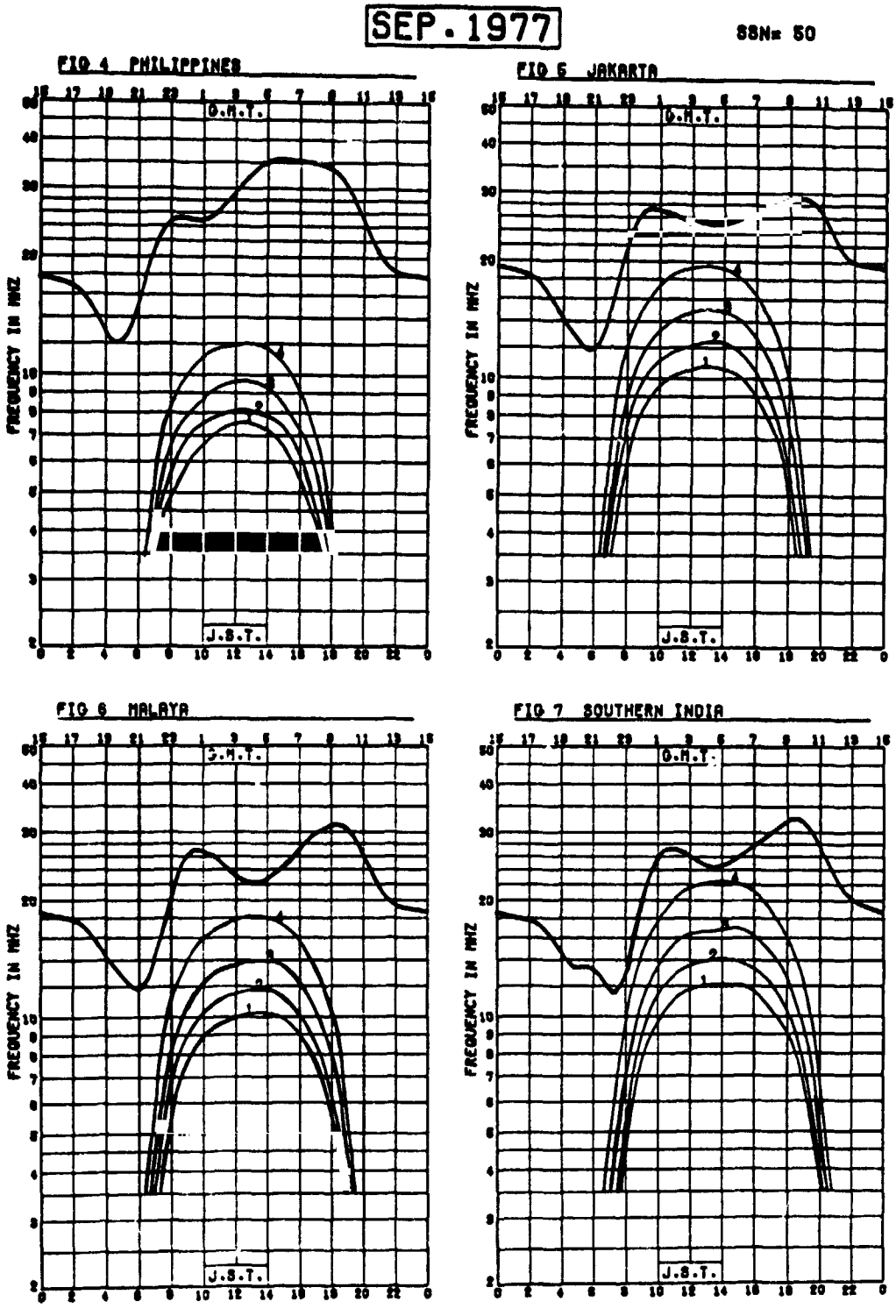

Fig. 2. Frequency-time range prediction for international circuits.

In each of Figs. 1 and 2, a heavy curve means the MUF diurnal change and fine curves numbered 1, 2, 3 and 4 denote respectively the LUF diurnal changes in cases of 10 kW, 1 kW, 100 W and 10 W transmitting powers. The predicted sunspot number (SSN) obtained in twelve months smoothed running average is shown on the right top of each page. It is assumed that the radio wave is propagated along a great circle through the normal ionosphere, the minimum receivable field strength is 3 dB, the transmitting and receiving antenna gains are 0 dB for a radio propagation with a distance less than 2000 km and 10 dB for a radio propagation more than 2000 km long. The other monthly prediction is for ship-to-shore communications. Commercial and fishery ships located on sea areas require customarily point-to-district predictions. Fig. 3 shows a world distribution of communication circuits for commercial ships, where a propagation path with cross marks is a longer route around the great circle. Fig. 4 shows examples of this monthly prediction, where heavy lines parallel to the abscissa denote the time ranges within which the assigned frequencies are operational. Circular marks on the lines indicate critical times, when the operational frequency equals the MUF. At another ending of the lines with no marks, the operational frequency coincides with the LUF. The prediction calculation is carried out under conditions that the transmission type is A1 (telegraph in carrier amplitude modulation), the transmitting power is 1 kW, and the ship and shore antenna gains are respectively 0 dB and 10 dB. In making the fishery communication pre-

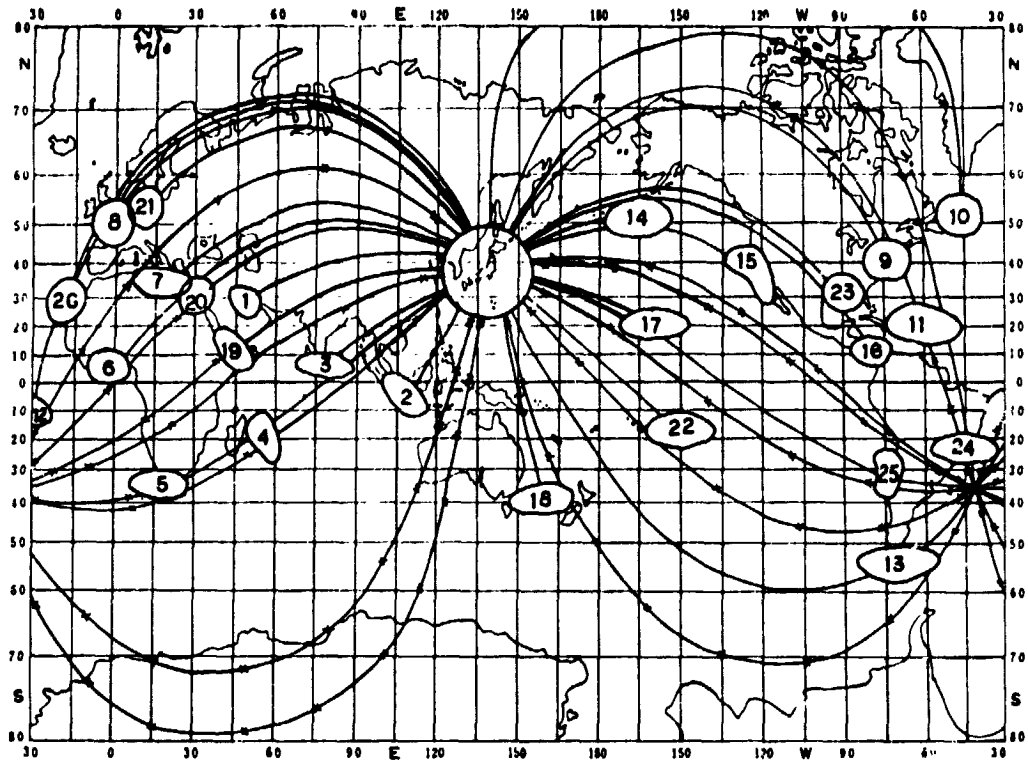

Fig. 3. Circuit map for commercial ship communications.

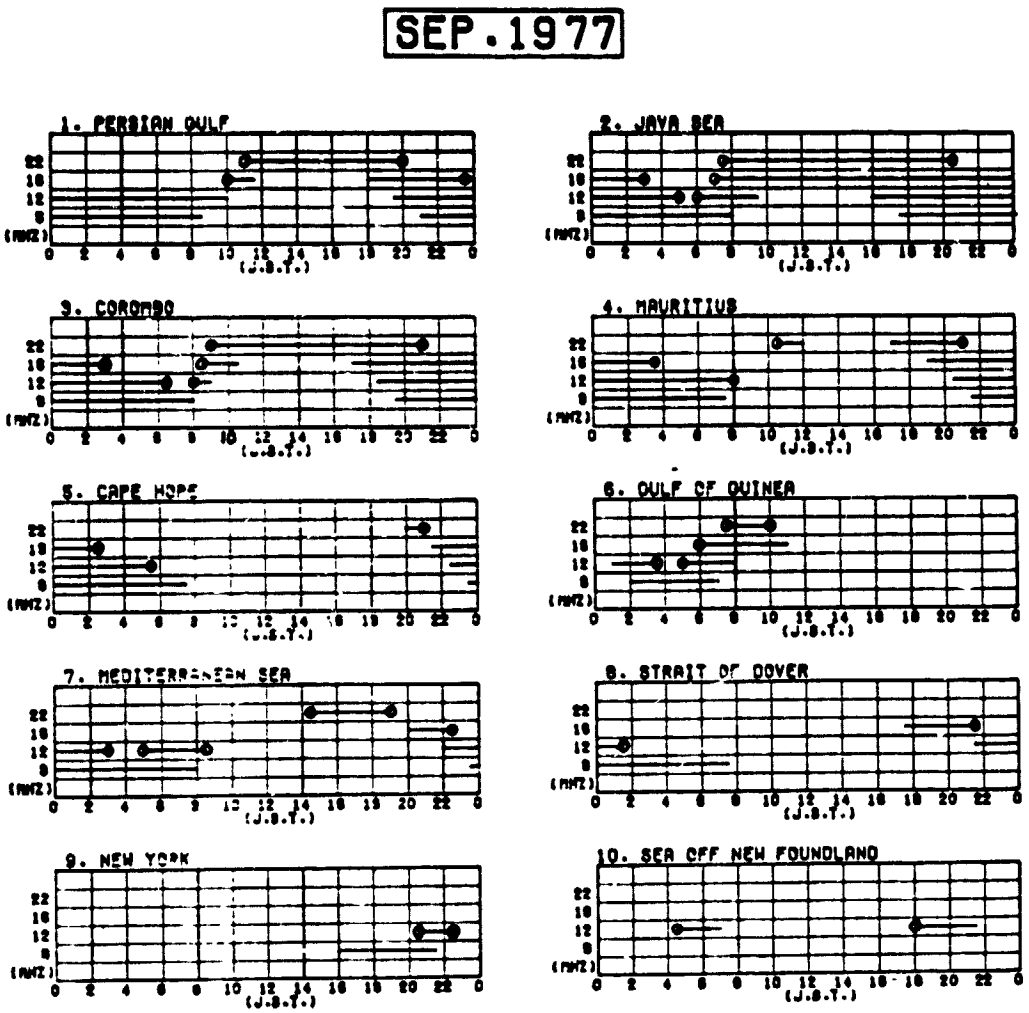

Fig. 4. Time range prediction for commercial ship communications.

diction, it is assumed that the transmission type is A1, the transmitting power is 200 W, and the ship and shore antenna gains are equally 0 dB. The outputs of the above-mentioned predictions can be designated to sheet, graph and 35 mm film/microfiche formats by computer devices.

The monthly median predictions are made on the normal quiet conditions as the ionosphere responds to the daily, yearly and sunspot cycle variations of the ionizing radiation incident on it. When an ionospheric disturbance occurs, the ionospheric characteristics are far from their median values expected in the month, and the MUF and LUF may be depressed or raised and will be different from the predicted medians. It is reasonably required to estimate quantitatively the probable changes in the MUF and LUF. At present, a daily prediction issued one week ahead is being made into reality by using the K-modulation method [Davis, 1970], where any pseudo-objective predicting must be tentatively prepared for the K-index. The daily prediction will be soon applied to only a few hops radio propagation over Japan, by means of the

top-side sounding data telemetered real-time from the Ionosphere Sounding Satellite b (ISS-b).

4. Evaluation of prediction

There are frequently found some differences between predicted and actual circuit conditions, though considerable efforts have been put into the task of improving radio propagation prediction. It is inferred that deviations of the prediction are caused by heterogeneity of source data, defect of model radio media or propagation and incompleteness of empirical formulae. Comparisons of calculation results derived from past data with actual facts will clarify if the models and formulae used in the prediction are valid or not.

For practical survey of the monthly median field strengths, the JJY 5 and 10 MHz waves transmitted from Tokyo (36°N, 140°E) were measured at Wakkanai (45°N, 142°E), and the WWV 15 MHz wave from Washington, D.C. (39°N, 77°W) or Fort Collins (41°N, 105°W) and also the WWVH 15 MHz wave from Maui (21°N, 156°W) were received at Hiraiso (36°N, 141°E). The measured field strengths and predicted MUFs are shown with solid lines in Fig. 5, where broken lines denote usable operational frequencies or calculated corresponding field strengths [Ichinose and Yamaoka, 1971]. The result is fairly satisfactory for short-distance circuits, and the lack of coincidence found be-

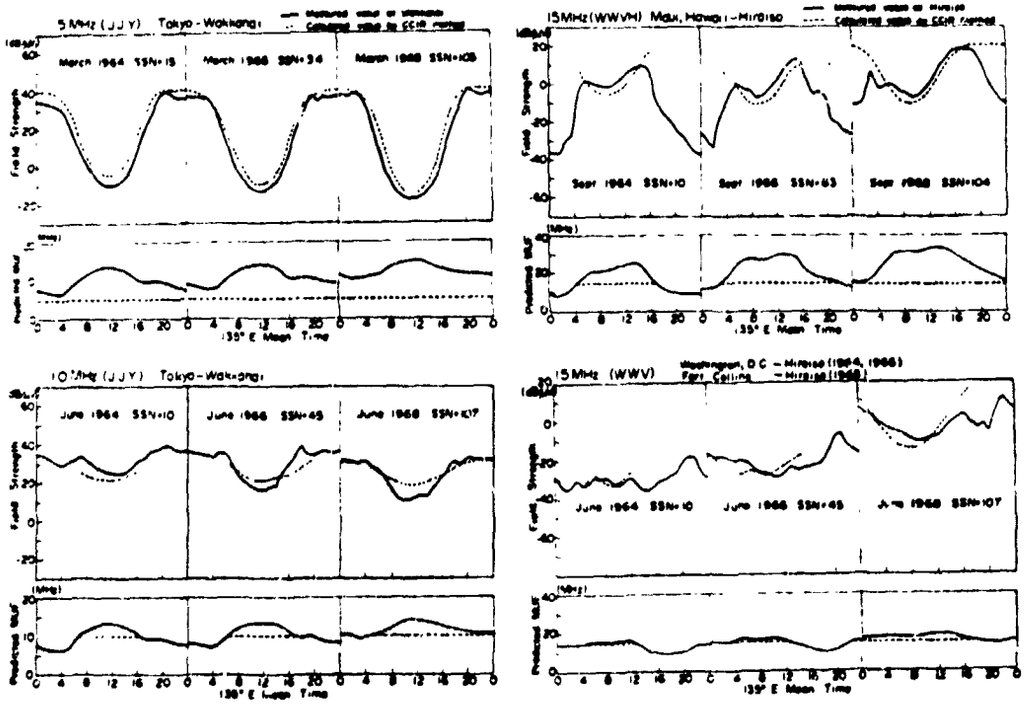

Fig. 5. Observed and calculated field strengths on standard radio wave propagation circuits.

tween observed and calculated fields on long-distance circuits must be caused from incomplete formulation of night ionospheric propagation.

It is necessary for the prediction services to know the degree of their value. Objective methods evaluating differences between predicted and actual propagation conditions were discussed in two papers refered to by the CCIR Report 153 [Sinno, 1958; Minis, 1962]. Both methods are probably said to be based on the statistics of predictions, missing events and false alarms, but are not neccssarily applicable to evaluation of the radio propagation prediction services. Another more general method should be developed that considers prediction probabilities [Maeda, 1971].

5. Conclusion

Radio propagation predictions have been issued in Japan for the last thirty years. During the 1970's, the prediction services have been remarkably improved in various respects by using an efficient computer system. The current prediction was briefly reviewed in the preceding sections, where the following important questions were left to be solved in the near future.

1) Development of solar and geomagnetic activity predictions.
2) Amendment of model ionospheres by using top-side sounding data from the ISS-b.
3) Inquiry of man-made noises.
4) Treatment of ionospheric propagation with irregular modes.
5) Performance of short-term predictions by using real time ionospheric sounding data.

References

Barghausen, A. F., J. W. Finney, L. L. Proctor, and L. D. Schulz (1969): Predicting long-term operational parameters of high-frequency sky-wave telecommunication systems. ESSA Tech. Rep., ERL 110-ITS 78.

CCIR (1966): C.C.I.R. atlas of ionospheric characteristics. CCIR Rep., 340.

CCIR (1970): C.C.I.R. interim method for estimating sky-wave field strength and transmission loss at frequencies between the approximate limits of 2 and 30 MHz. CCIR Rep., 252-2.

Davis, R. M. (1970): Short-term prediction of F2-layer maximum usable frequencies from local magnetic activity. ESSA Tech. Rep., ERL 157-ITS 100.

Ichinose, M., and M. Yamaoka (1971): Methods of calculation of MUF, LUF and HF sky-wave field strength by electronic computer (Japanese). Rev. Radio Res. Labs., 17(93), 480.

Ichinose, M., and M. Yamaoka (1973): Method of calculation by computer of various operational parameters for HF radio circuit designing (Japanese). Rev. Radio Res. Labs., 19(102), 213.

Jones, W. B., and R. M. Gallet (1962): Representation of diurnal and geographic variations of ionospheric data by numerical methods. J. Res. NBS, 66D(4), 419.

Maeda, R. (1971): Weekly forecast of radio propagation conditions (Japanese). Rev. Radio Res. Labs., 17(93), 499.

Minis, C. M. (1962): Ionospheric storm forecasts. Electronic Technology, (May), 172.

Sinno, K. (1958): Hit rates of radio propagation disturbance warnings and SWI warnings. J. Radio Res. Labs., 5(20), 109.

D19-32

N80-18481

RADIO DISTURBANCE WARNING ISSUANCE SYSTEM

Rikio Maeda and Hisao Inuki
Radio Research Laboratories
4-2-1 Nukui-Kita Koganei, Tokyo 184, Japan

Twenty or more years have elapsed since the start of radio disturbance warning services in Japan. In the past decade, many developments in telecommunication techniques have made some radio communications more stable than before, and the efficiency of present radio propagation prediction service has been reconsidered. A radio disturbance warning issuance system was introduced in the Hiraiso Branch of the Radio Research Laboratories in 1972 to reconstruct the current radio disturbance warning service as a social information service. The main theme of this report is a description of the new ideas which were experimentally systematized by means of an electronic computer.

1. INTRODUCTION

During the 1950s HF radiowaves had become a very important means of domestic and international communication among ground facilities and sea-going ships. The bearing and pathloss of radiowave propagation through the ionosphere are always affected and frequently disturbed by variations of ionospheric conditions which depend to a remarkable extent on solar and magnetospheric activities. The Radio Research Laboratories (RRL) have carried out observations of solar and magnetospheric effects on terrestrial and ionospheric environments in order to issue radiowave propagation predictions. At that time, radio forecasting was as useful for the operation plans of practical communications and schedules of scientific observations as weather forecasting for transportation and industries. Communication is an indispensable function in human life as well as in transportation.

A radio propagation prediction service aims at HF radio communication circuits in a normal ionospheric state and issues monthly or weekly medians of usable operation frequencies and probable reception strengths three months or a few weeks in advance. On the other hand, a radio disturbance warning service forecasts indirectly abnormal ionospheric variations, i. e., ionospheric storms, sudden ionospheric disturbances, and polar cap disturbances caused by solar and terrestrial events. Therefore, this service necessarily is maintained on routine monitoring of solar-terrestrial phenomena, e.g., solar flares and geomagnetic storms, which are frequently accompanied by ionospheric and propagational disturbances. Daily and weekly information about these events is coded in the standard ursigrams, and distributed over the Western Pacific region and to warning centers of the International Ursigram and World Days Service (IUWDS).

In the 1960s, radio telecommunication by satellites and submarine cables was comprised, for the most part, of long-distance international communication, except in developing countries. In the 1980s, ship-to-shore communications will also depend on VHF radio waves, but HF radio communication circuits may remain important for broadcasting various information on social news, time-frequencies, navigation, entertainment, and so on. For that reason, the radio disturbance warning service must be improved to adapt, for future radio communication, to circumstances in which the service objects and means will be changeable.

2. RADIO DISTURBANCE WARNING SERVICES

In order to operate current radio communication systems more efficiently, radio propagation predictions concerning abrupt solar-terrestrial events have routinely been offered by the RRL in Japan since the 1950s. The practical services have been conducted by the Upper Atmosphere Research Section of the Hiraiso Branch, as shown in Table 1. The world days service announces information about solar flares and geomagnetic storms daily in GEOALERT (combined data and forecasts including advisory information). Actual abnormal conditions of solar radio emission and ionospheric wave propagation are occasionally reported as URANO (radio noise) and USIDS (sudden ionospheric disturbances). These ursigrams, used for scientific experiments as well as for communication practices, are distributed over the world through Telex networks of the IUWDS and broadcast by the JJD (10.415 and 15.950 MHz) transmitted from Sakura beginning at every 08 UT. The IUWDS has been globally maintained; the world warning center is situated at Boulder and the regional warning centers are located in Tokyo, Sydney, Paris, Darmstadt, and Moscow. The Western Pacific regional Center Tokyo is administered by the RRL. The short-term forecast describes ionospheric radio propagation conditions as normal, unstable, or warning twelve hours in advance. This is broadcast twice every hour from Koganei by

Table 1. Radio disturbance warning services of the RRL.

Type	Title	Description	Forecast Period	Issuance	Distribution
World Days Service	GEOALERT	Solar-Terrestrial Disturbances	A Day	Daily	Telecommunication Facilities (JJD)
Actual Conditions Report	URANO USIDS				WWA & RWC (TLX)
Short Term Forecast	WARNING	HF Propagation Disturbances	Half A Day	Occasionally	Telecommunication Facilities (JJY)
Weekly Forecast	WEEKLY FORECAST ADJ __		A Week	Weekly (Monday, Thursday)	Telecommunication Facilities (Mail) WWA & RWC (TLX)

the JJY (2.5, 5, 8, 10, and 15 MHz) with the Morse code of N, U, or W. The weekly forecast assigns a condition index of radio propagation and an occurrence grade of Delinger phenomenon to each day a week in advance, where the indices 1, 2, 3, 4, and 5 indicate, respectively, very disturbed, disturbed, unstable, normal, and good conditions. Furthermore, the grades * and ** denote fairly expectable and very expectable occurrences, respectively. This message is mailed twice a week to several tens of domestic and international communication facilities.

There are generally two types of forecasting methods. The analytical method is commonly used on astronomical problems which are solved by predicting the future from the present by means of motion and state equations on certain initial conditions. The other method is often applied to aeronomical predictions by means of stochastic relations among environmental phenomena. The radio warnings have been based mainly on the latter method because of easy phenomenological understanding that requires a steady monitoring of the sun for ionospheric radio propagation predictions. Since the data from observatories in only a limited region cannot thoroughly reflect the solar activity, some observations are relayed at least among the three regions of the world, i.e., Asian, American, and European areas, which promise to be able to issue the regional warnings most effectively. For this purpose, the IUWDS developed its function to a remarkable extent during the International Geophysical Years (1957-58) and has operated effectively in Japan for world-wide daily service. Figure 1 shows radio information flows viewed from a side of the Tokyo Warning Center and illustrates an outline of the radio disturbance warning service conducted by the Hiraiso Branch. When an observatory detects outstanding solar-terrestrial events, the preliminary reports are sent as soon as possible to each communication center, which transmits the coded information to respective warning and data centers. The warning center compiles the phenomenological evidence into synoptic forecasts and distributes them to the communication facilities connected with the IUWDS. Although the task has been carried out in Japan by technical forecasters with ten or more years of experi-

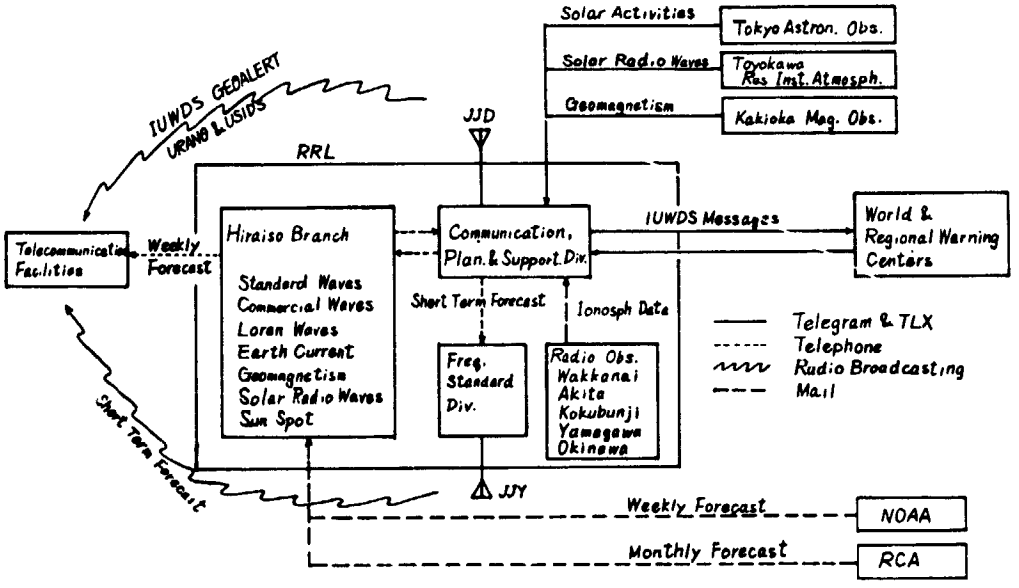

Figure 1. Radio information flows in the RRL.

ence, the issuance of objective radio disturbance warnings is nowadays made smoother by steady observation of phenomena, real-time transmission of data, automatic production of information, and practical evaluation of predictions.

3. AN EXPERIMENTAL SYSTEM

Recent activities of the warning and data centers in Japan were rather backward compared to the remarkable developments in the observation and communication networks. This fact has caused some concern about systematic operation of the present radio disturbance warning service, the efficiency of which is principally based on objective, automatic, steady, and speedy data management. In answer to the demands for more efficient prediction, a radio disturbance warning issuance system (RADWIS) was conceived by the Hiraiso Branch of the RRL in 1972. Radio information, compiled by the Hiraiso Branch for the radio disturbance warning service, is composed of analog data obtained sequentially from its own observatory and digital data accepted randomly from other observatories, as shown in Figure 2. It is desirable for these data processes to be real-time and on-line 24 hours a day. The RADWIS has an electronic computer with a magnetic core memory of 16 kW (16 x 24 kB) which is almost assigned to occupied areas for system programs and overlaid areas for application programs stored in a magnetic drum unit. This system requires a one-way consecutive time slice automatic operation controlled by a non-stop external crystal clock and no manual operation unless unanticipated computer emergencies cause normal process jobs to cease. System breakdowns caused by hardware or software troubles are avoided principally by automatically cutting off the process in the disturbed part and skipping to a consecutive process which admits only a few after-effects into a limited small part. Power out-

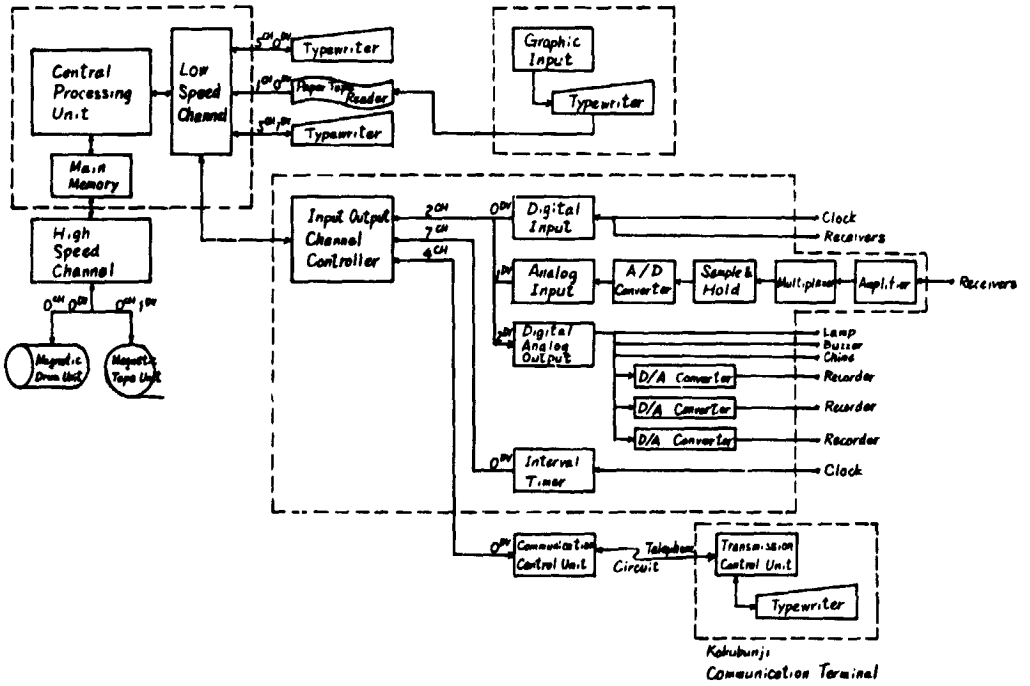

Figure 2. Hardware of the RADWIS.

ages due to artificial or natural events make a transient system breakdown after preparing the system for the future; a system recovery is then automatically carried out by a computer self-restart function when the power becomes normal. If the system breakdown lasts fairly long, operators may achieve an earlier recovery by the use of interrupting manual switches for data compensation--an inevitable task in an on-line and real-time computer system. Figure 2 illustrates hardware of the RADWIS, where data input is through a paper tape reader, a communication terminal typewriter, or analog-digital (A/D) converters, and the output is through the communication terminal typewriter, D/A converters, or monitor typewriters.

The software is shown in Figure 3. In the data acquisition phase, the 24-channel analog data on HF and LF radio signals, solar radio emissions, and geomagnetotellurics are always sampled once a second after data adjustment and calibration to the input apparatus. The data conversion job makes several indices and ursigrams on radio information subject to statistical arrangements. It is most essential for the radio warning to produce forecast information from actual observations. The public telephone circuit between the central processor at Hiraiso and the terminal typewriter at Kokubunji is used mainly for Telex code transmission. Unless commercial power breaks down, the computer is waiting or working for these service jobs scheduled according to the calendar year, month, week, day, hour, and minute designated by non-stop clock signals. The computer constantly monitors the sequentially and randomly accessed data received through observation and communication input, constantly forecasts radio propagation conditions 12 hours in advance, occasionally issues a short-term radio disturbance warning if it is necessary, and also regularly reports to the IUWDS whether solar radio emission and ionospheric radio propagation were severely disturbed or not. The world days service is issued at ten o'clock every day and the weekly forecast is issued at noon every Monday and Thursday by compiling the source data stored in the magnetic drum unit. The results are coded in respective fixed formats, input in the magnetic tape unit, and output to the typewriters at the designated issuance times.

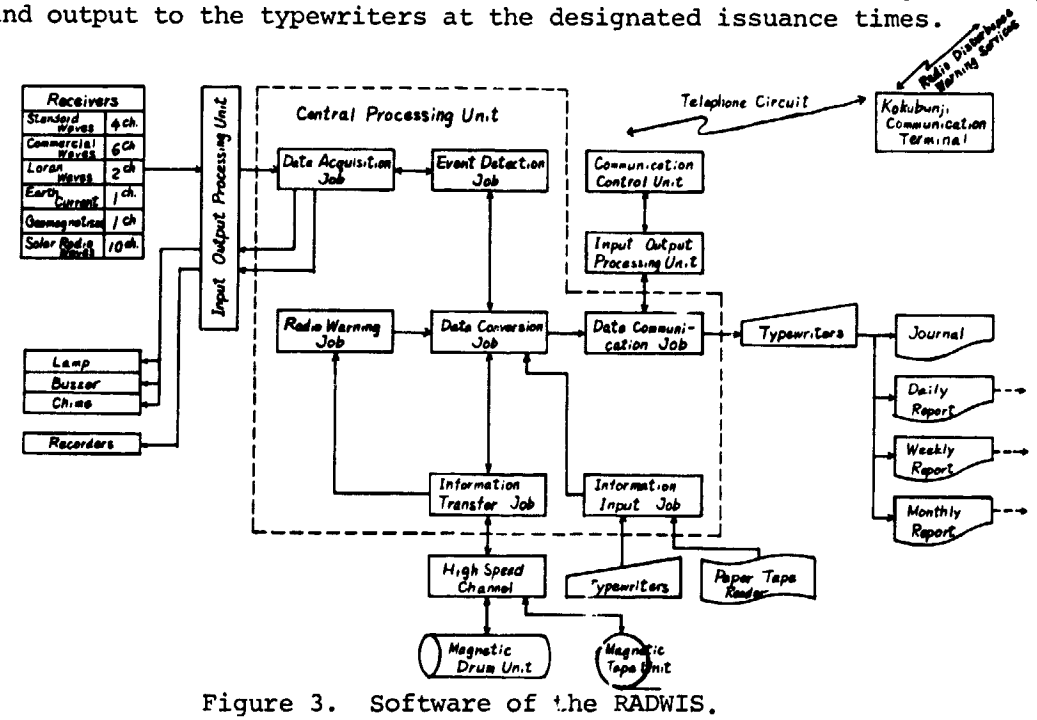

Figure 3. Software of the RADWIS.

Radio disturbance warning services are required to monitor constantly the interplanetary radio waves and plasma generated from the sun or galaxy and modulated through interplanetary space or the magnetosphere. The RADWIS is interested in ionospheric storms, sudden ionospheric disturbances, and polar cap disturbances, which are detected directly through steady monitoring of HF and LF radio propagation circuits. The sunspot configuration and solar radio emission are observed at Hiraiso, but information on the solar magnetic field and solar plasma flow is received from the IUWDS, and these data are effectively used for solar flare forecast. The magnetospheric structures, e.g., the magnetic cusp and tail aspects, are only inferred from ground geomagnetic observations, and information on the radiation belts, interplanetary magnetic fields, and cosmic rays is limited, but real-time utilization of the polar and satellite data is expected in the future. Occurrence of solar flares in an active region is considered over abnormal changes in the sunspot number, area, type, solar radio intensity, temperature, spectrum, and over causal relations between geomagnetic storms and ionospheric storms. The RADWIS forecasts average radio propagation conditions of middle latitudinal circuits, where radio propagation fadeouts and storms are frequently fatal for good HF radio communication. The system was introduced as a trial for automatic routine radio disturbance warnings, but several years of indulgence are still necessary before this will be accomplished. By its nature, this system has aimed at objectification and gradation of the forecasting method, and intends to program, evaluate, and improve the radio disturbance warning service experimentally.

4. CONCLUDING REMARKS

The radiowave propagation forecast has changed its objectives, methods, purposes, and means according to developments in radio communication techniques to which the RRL have consistently devoted themselves throughout recent years. The radio disturbance warning service began early at about the 19th solar minimum in the 1950s, before rockets and satellites opened the new space epoch, and ionospheric physics seemed to dissolve into space research. Thereafter, ionospheric radio communications tended toward space radio communications, losing its technical usefulness for ionospheric experiments and answering to the scientific need for ionospheric studies. A similar reversal in the relation between ends and means is found in earth environmental science. As radiowave propagation depends on ionospheric and magnetospheric conditions, radio environmental information is useful for radio communication circuit predictions, and vice versa. Toward the end of the 20th solar cycle, main frequency bands for long-distance radio communications turned to the VHF from the HF, but HF radiowaves are still important in ship communications and overseas broadcasts. During the 21st solar cycle, the service area of radio disturbance warning will cover the radio communication media between the earth and the sun. To meet the need for space disturbance warnings, the IUWDS network of observation, communication, data, and warning centers must be rearranged. The RADWIS is also intended to be an improved forecasting system for solar-terrestrial phenomena and radio environmental events, a goal which will be attainable with the program revision rendered possible by another large-scale computer.

A REVIEW OF THE OPERATION OF THE IUWDS REGIONAL WARNING CENTRE AT THE IONOSPHERIC PREDICTION SERVICE, SYDNEY

F. E. COOK and P. DAVIES
Ionospheric Prediction Service
Department of Science and the Environment
P.O. Box 702
Darlinghurst NSW 2010, AUSTRALIA

The operation of the Sydney RWC is reviewed. Routine data reports are issued daily, while disturbance warnings (short-term forecasts) are issued as necessary. An outline of the methods used in forecasting solar activity and geomagnetic disturbances is given.

1. INTRODUCTION

The Sydney Regional Warning Centre (RWC) of the International Ursigram and World Days Service (IUWDS), operated by the Ionospheric Prediction Service (IPS) of the Australian Department of Science and the Environment, has responsibility for the Australasia and Antarctica Region. Routine solar activity reports and forecasts are issued daily, and Disturbance Warnings (short-term forecasts) as necessary.

Daily reports consist of the Sydney Geoalert, giving a forecast of expected solar and geomagnetic activity for the next 24 hours, coded data from the solar optical and radio observatories at Culgoora and Fleurs, and a plain language report on solar active regions and activity from Culgoora. Disturbance warnings are issued whenever major solar activity or geomagnetic disturbance is expected to cause the ionospheric radio propagation parameters to deviate noticeably from their predicted quiet-day values.

Data input from the Culgoora and Fleurs observatories and the methods used at Sydney RWC for predicting solar activity and geomagnetic disturbances are described.

2. DATA

2.1 Australian Data

The Ionospheric Prediction Service operates an H-alpha solar patrol at Culgoora, about 600 km northwest of Sydney, where the IPS Observatory is co-located with the CSIRO solar radio and optical observatories operated by the Division of Radiophysics and National Measurement Laboratory. The

observatory is manned daily from sunrise to sunset by a team of three observers (at least one on duty each day) who have access also to data from the CSIRO instruments. Besides visual observations, 35 mm photographs of the sun are taken once per minute. Sunspot data are obtained from a heliograph. Real-time flare data are coded from optical observations, but final flare data are scaled from film records and sent to the World Data Centres.

The CSIRO operates a spectrograph (6-3800 MHz) and the radioheliograph. From the spectrograph real-time display, information on the type of solar radio bursts can be obtained (IUWDS URASP code). The radioheliograph, a unique instrument operating at discrete frequencies of 43.25, 80, and 160 MHz (327.4 MHz to be added), can give information on the position and movement relative to the sun of radio burst sources, for about six hours per day centered on local noon.

Optical and radio data from Culgoora are coded in the IUWDS format and telexed daily to the RWC in Sydney at 0000 UT and after sunset, along with plain language reports describing optical features on the sun and radio bursts observed with the radioheliograph. Major events are reported by telephone or telex as they occur.

One IPS observer is stationed at the Fleurs Radio Astronomy Station of the University of Sydney, about 50 km west of the city. By using the E-W arms of the synthesis telescope, the sun is scanned daily at 0000 UT at frequencies of 692 and 1415 MHz with resolutions of 4 and 2 minutes of arc. These scans are scaled and coded into the URALN code : they are also used to indicate the presence of coronal holes. Also at Fleurs is a radiotelescope operating at frequencies of 1415, 2695 and 4995 MHz (200 and 400 MHz to be added) : the 0000 UT quiet sun flux and data on any radio bursts are coded into the URANJ code. In addition, the station monitors the H-component of the earth's magnetic field, and several radio circuits to detect SID's.

With the exception of the E-W scan, all the data from Fleurs are telemetered to the RWC where they are displayed for the forecasters' use. Fleurs is not usually manned on weekends but E-W scans are carried out automatically and the data reported in the Monday ursigram.

One other local data source is a direct line to the IPS ionospheric research station at Camden, 50 km southwest of Sydney, by means of which one can trigger the ionosonde. A telemetry system transmits the ionogram to the RWC when it may be studied on a long-persistence display or photographed by a polaroid camera. Thus one can know immediately the state of the local ionosphere.

The RWC itself is manned normally from about 2200 UT to 0700 UT on week days and for some hours during the local morning on other days, with provision to extend these hours when the sun is unusually active or to support special programmes.

2.2 Overseas Data

Data are received in Sydney as ursigrams from Tokyo and Moscow during the night and from Boulder in the early morning local time, so that much of

the information is at least 12 hours old (unless it is a PRESTO message). From Boulder comes coded data on calcium plages (McMath-Hulbert Observatory), radio emission (Sagamore Hill and Ottawa, discrete frequencies ranging from 245 to 15600 MHz), sunspots (Boulder) and the AFRED and TENCM forecasts. Flare and radio data from the USAF SOON-RSTN sites are also received. The daily 2200 UT Joint USAF/NOAA Primary Report of Solar and Geophysical Activity is useful as it contains a timely update of the "dark hours" in plain language on solar activity as well as information on X-ray flares and occasionally on coronal holes observed at 10830 A. The Boulder Region Summary provides information on sunspot magnetic classifications. The last two reports are retransmitted to the Culgoora Solar Observatory. From Boulder we receive also the Meudon 1400 UT geoalert and the WWA geoalert issued at 0400 UT.

From both RWC Moscow and RWC Tokyo we receive data on metre wave as well as microwave radio flux and events and both Centres send sunspot and geomagnetic data. The 3-8 cm fluxes and flux ratios from Toyokawa are useful in evaluating large active solar regions, while coronal data from Mt Norikura provide sometimes our earliest indication of the approach of active regions round the east limb. The Tokyo cosmic ray data also allow us to check on the passage of solar plasma clouds ("magnetic bottles") in the absence of definitive spacecraft data.

The data coverage clearly could be improved : in particular, we receive no decimetre or microwave radio spectral information from stations other than Culgoora (although many such report in "Solar Geophysical Data"), and metre wave spectral data only from Culgoora and some USAF-RSTN sites (25-75 MHz).

3. OUTPUT FROM SYDNEY RWC

3.1 Routine Daily Reports

Daily at about 0100 UT the Sydney RWC sends a message (ursigram) to the Centres at Boulder, Delhi and Tokyo from where the data are passed to Meudon (Paris) and Moscow Centres. This message consists of a geoalert, giving a forecast of expected solar and geomagnetic activity for the next 24 hours, followed by coded data from the Australian observations (URANJ, URALN, URASP, UFLAE, USSPS, PTROL, USIDS). Then follows a plain language report from the Culgoora observatory describing the solar active regions and summarizing the solar radio observations. After sunset, a similar message, but without a geoalert part, is sent direct from Culgoora to Boulder and Tokyo and to RWC Sydney. Information on major events is received in near real time from Culgoora and Fleurs and is sent direct to the five Centres mentioned as soon as the data have been assembled.

3.2 Disturbance Warnings

Disturbance Warnings are issued by the Sydney RWC whenever major solar activity or significant geomagnetic disturbance is expected. These Warnings are sent to about 60 users, mainly in Australia and New Zealand and neighbouring countries and to Antarctic stations. The users fall into three main categories,

communicators who are interested in effects on their HF radio circuits, geophysicists, mineral exploration companies and pipeline authorities who are interested mainly in geomagnetic storms, and researchers who need information on expected disturbed or quiet conditions or solar events.

In the Warnings, the probability of flares and storms is given in three grades viz. possible, probable, or expected, and three kinds of warnings are issued, a primary warning to all the users, warning "A" to HF communicators giving more detail about MUF and SID effects, and warning "B" to users concerned with geomagnetic activity. Further details are to be found in the IPS Handbook (Ionospheric Prediction Service, 1977). Special forecasts are issued for certain users (for example, rocket experimenters) as requested.

4. FORECASTING SOLAR AND GEOMAGNETIC ACTIVITY

It is not proposed here to discuss solar-terrestrial relations in detail. The subject was reviewed in relation to short-term forecasting by Cook and McCue (1975), and in CCIR Document 6/177-E (1976) which also listed the services available from the operational forecasting centres around the world. Recent developments have centred on the role of solar sector boundaries, the interplanetary field direction and solar wind parameters, on the relation between coronal holes and solar wind streams and attempts to monitor the passage of coronal holes by ground-based methods, and on the "possible final resolution of the M-region problem". Much effort has also been put into the identification of possible precursors of flares, especially proton flares.

There has been some progress with the "classical" problem of flare distance east or west of central meridian and storm probability, but little new information on the role of metre-wave emission from flares, and the delay time between flares and storms. Meanwhile the solar observers at Culgoora and the disturbance forecasters at RWC Sydney find it useful to begin with a few rules of thumb and these are listed here.

4.1 Flare Forecasting

Forecasting solar activity for the daily geoalert is left to the observers at Culgoora as they have direct access to the sun in H-alpha and white light and to the solar radio data. Points which they bear in mind and which derive from a variety of sources are:

1. Most flares occur near a neutral line : check for complex neutral line embedded in plage. Where the spot magnetic classification is gamma or delta and the region is compact, the likelihood of large flares is greatly increased.

2. Check for large magnetic gradients, complexity of spot group, spot rotation and proper motion of spots. Large spots of opposite magnetic polarity close together indicate steep magnetic gradient.

3. Rapid growth of spot area, 50 to 100% in one day.

4. Presence of active dark filament.

5. Past history of the region with respect to flare production.

6. Region with strong coronal line emission, especially yellow line, at east limb passage (data mostly from Mt Norikura, Japan).

7. Rapid development or decay of a delta configuration.

8. Relation of the 10-cm radio flux value to the 90-day mean : major flares are likely when the current flux is higher.

4.2 Proton Flare Forecasting

1. Most proton flares occur in spot groups with delta configuration.

2. Polar cap absorption events (PCAs) favour the western half of the disc, and particles from western flares travel more quickly, particularly from longitudes 0 to 15 degrees west approximately.

3. Check for umbral coverage and parallel ribbons or Y-shaped flares.

4. Most proton flares are associated with regions where the ratio of the flux densities at 3.2 cm and 7.8 cm is greater than one.

5. Check for U-shaped radio emission spectrum. Proton flares typically give high flux densities at metric and centimetric wavelengths with minima in the decimeter wavelength region (around 1400 MHz). Rise time of microwave burst > 5 minutes and type IV dekametric emission observed. The 10 cm flux maximum tends to occur later than H-alpha maximum.

6. Generally, for proton events, at 19 GHz the peak flux increase should be more than 50% of the preburst value and the flux enhancement more than 10% above it for longer than 5 minutes (but RWC Sydney does not receive any 19 GHz data).

7. PCA events tend to occur in regions on their second or later rotations. Proton events seem to require a mature region. Successive proton events during one disc transit are not uncommon.

8. Large calcium plage (>8 000 millionths) and large spot area (>1 000 millionths) correlate with intense radio bursts and major proton events.

9. Check for moving type IV bursts with the flare.

10. Check size of optical flare, and microwave burst.

11. Check start times of radio events at different frequencies,

indicating movement of plasma out into the corona.

A rough rule is that old regions produce protons, new regions magnetic storms, although storms are produced by mature regions as well. Note also that metre wave flux values can be misleading because metre wave emission cannot escape easily in the sun-earth direction from above the solar limb (the directivity effect).

The sources of most of these "rules" were given in the 1975 review by Cook and McCue and are not referenced again here.

4.2 Magnetic Storm Forecasting

4.2.1 Recurrent Storms

Since the difference between the Mustel' and the Allen-Saemundsson views on the cause of recurrent storms, also mentioned in the 1975 paper, appears to have been resolved (Gulbrandsen 1975) in favour of open magnetic regions or coronal holes, forecasters are now concerned with the detection of these holes and their relation to geomagnetic disturbances, using the data available. The "cone of avoidance" idea in relation to closed magnetic regions and centres of activity now seems firmly established.

Coronal holes have been related to white-light coronal structures (Hansen et al. 1976) and to regions of low 284-A emission (Neupert and Pizzo 1974, Bell and Noci 1976) measured from satellites, and their relation to solar wind streams and disturbances is well documented (Nolte et al. 1976, Sheeley et al. 1976). RWC Sydney however has available only the longer-wavelength coronal line emission data from Mt. Norikura in Japan, from which CMP of weak-emission regions are inferred : and occasional He 10 830 A data from Kitt Peak mentioned in SDF Reports.

More recently Ferguson (1979) has shown that the presence of coronal holes may be inferred, on a regular basis, from the solar east-west scans at decimetre wavelengths, in which the holes appear as stable troughs in the scan data.

The Bartels 27-day chart of magnetic activity continues to be the basic datum for monitoring recurrent storms, supplemented by east limb coronal data and helium line spectrograph data, when available, and now the Fleurs east-west scans. A rough rule is that the presence of a spot group immediately preceding the supposed hole or M-region delays the disturbance a day or two past the usual CMP + 3 days period, and it may begin suddenly. Emergence of a centre of activity within the region will probably disrupt the recurrence altogether. These disturbances are noticeably longer and more severe near the equinoxes. They are also evident throughout the cycle, though most prominent in the years approaching sunspot minimum. A notable feature of the Bartels chart is the regular recurrence of quiet periods : warning of these is important for some users.

4.2.2 Sector Boundary Disturbances and Interplanetary Magnetic Field

The dependence of magnetic disturbance indices on sector boundary crossings,

the interplanetary field direction both parallel and perpendicular to the ecliptic, and solar wind parameters, continues to be investigated by many workers, leading to significance of "away" sectors, south-pointing field, solar wind velocity and number density, and interaction between slow and fast streams in relation to disturbances. In general, the number density first increases, then the field changes direction, and finally the velocity is observed to increase, before the magnetic disturbance occurs at earth.

Many of the published results relate to minor disturbances : for this reason, but mainly because RWC Sydney does not receive solar wind (spacecraft) data and does not have access to very high latitude magnetic observations from which we might infer boundary crossings from the Svalgaard-Mansurov effect, not much attention has been paid to this aspect of disturbance forecasting.

Švestka et al. (1976) list 44 proton events associated with sector boundary transits during the years 1957-1969. Some 17 of these were accompanied by magnetic storms (including two recurrent storms) for which forecasts would have been useful, the rest by minor activity or quiet periods, but advance warning from spacecraft observations would have been required, for forecasting. In about seven cases, the particle event began before the magnetic disturbance.

4.2.3 Flare-induced Storms

While there has been progress in the association of recurrent storms with coronal holes, the rules for forecasting flare-induced storms remain much as they were outlined in the 1975 review already mentioned. For example, it is generally accepted that a major flare near central meridian or west of it, located in a suitable active region and with large radio bursts, especially a spectral II-IV event, is likely to cause a magnetic storm. The same event near east limb (noting that metre wave emission may not be observed from so far east) generally will not. But for users who want a "yes or no" forecast, at what longitude do we change our prediction? And if there is a storm predicted, what will be the delay time from flare to storm commencement? These are the two basic questions for which we still have no simple answers, as is clear from observed differences between forecasts issued by different Centres, based on the same data for the same event.

The paper of Yoshida and Akasofu (1965) gave useful information on the magnitude as well as time-delay distribution according to flare location east or west of central meridian and presence or absence of fast or slow particle events. Pintér (1975) has continued his comparison of travel times of shock waves from type II bursts. Results presented by Sakurai and Chao (1974) are disputed by Lanzerotti (1974) on the grounds of disagreement between different sources of data.

From these and many other sources there emerges another set of "rules of thumb", giving the following criteria for predicting storms following flares:

1. Large flare, generally importance 2 or greater, from about 45 degrees east of CM to far west (especially if cosmic ray data indicate that the earth is inside a "magnetic bottle" connecting

the earth to the emitting region on the sun). Note however that the great storm of February 1956, for example, was caused by a 1B flare : it was near west limb but was accompanied by a very large metre wave event.

2. Spot group usually complex (see also criteria for proton events).

3. Large radio burst with type IV longer than 15 minutes and spread over cm and metre wavelengths and preceded by type II. In the absence of spectral data, which we receive only from Culgoora observatory, the II-IV event may be inferred from "major burst with second part". Note possible directivity effect of metre wave emission from far east or far west events.

4. The type IV should be a moving type IV, not stationary continuum. Again this information is available only from Culgoora, for forecasting purposes. Sometimes a moving IV will be observed, headed east or west into space and not towards the earth : this will not cause a storm (example, the "Westward Ho" event, the first one ever recorded at Culgoora).

5. A rough rule - metre wave emission equates with magnetic storm, microwave with proton events. The largest events across the spectrum produce the major storms.

6. The first flare in a previously quiet region may not produce a storm, but successive events may do so, with the delay time gradually decreasing with each storm but this is not a reliable criterion.

7. SC storms superimposed on recurrent disturbances tend to result in very high Kp values.

8. CMP of metric radio-noisy region is associated with minor disturbance about two days later.

9. Disappearance of a large filament near central meridian is believed to be the cause of some disturbances.

10. Events, even large ones, in small calcium plage areas have a longer delay time than similar events in large regions (up to about 5 000 millionths area).

5. FUTURE DEVELOPMENTS, AND PROBLEMS

In Australia, the IPS observatory at Culgoora is being equipped with a time-lapse video recorder so that H-alpha events which might have occurred during absence of the observer at one of the other sites (or at the telex, for sending data) can be played back and the data supplied to RWC Sydney and the IUWDS network. Telemetry of spectrograph and heliograph observations to

the IPS building is also to be installed. The Fleurs single-frequency radio observations will continue but the east-west scans (for coronal holes as well as active regions) depend on University of Sydney observational requirements : at present, we enjoy regular use of the antennas but this may not always be so.

The USAF SOON-RSTN observatory at Learmonth, North-West Cape area of Western Australia should be in operation by the summer of 1979 and the Ionospheric Prediction Service will station two physicists there. Data from Learmonth will be available to IPS and will be included in our ursigrams, and will be especially useful for proton flare warnings.

Some data problems remain. We receive solar spectral data only from Culgoora (and for some events from Sagamore Hill in the U.S.A.), but several stations at other longitudes supply spectral data to Solar Geophysical Data. It would be very useful to have data from these stations also, in the IUWDS data exchange. A code is being devised for reporting the Culgoora radio-heliograph observations which at present are reported in plain language or in the additional groups in URANJ code. Sydney also receives very little data from Western Europe, under existing arrangements, and the transmission to Centres beyond Delhi, Tokyo and Boulder could be improved : the cost of telex messages is the main difficulty. Another problem is that of PCA data : we have only radio communication with Antarctic bases, with no recourse to land lines or other methods when PCAs and storms interrupt the data flow.

6. IONOSPHERIC DISTURBANCES

Ionospheric disturbances are not considered in this brief review. As mentioned earlier, some indication of expected MUF and absorption changes is given to users, in the Warnings. One problem which should be studied further is that of severe ionospheric disturbance with only moderate magnetic disturbance (example, 1978 October 30), and severe magnetic storm with only slight ionospheric effect, at least at middle latitudes (example, 1978 April 11).

The ionospheric predictions of IPS are described elsewhere in these Proceedings.

REFERENCES

Bell, B. and G. Noci (1976) : Intensity of the Fe XV emission line corona, the level of geomagnetic activity, and the velocity of the solar wind. Journal of Geophysical Research, 81 : 4508.

CCIR Study Group 6 (1976) : Short-term prediction of operational parameters for ionospheric radiocommunications. CCIR Doc. 6/177-E, p. 64.

Cook, F. E. and C. G. McCue (1975) : Solar-terrestrial relations and short-term ionospheric forecasting. The Radio and Electronic Engineer, 45 : 11.

Ferguson, B. G. (1979) : Coronal holes inferred from the "Fleurs" east-west solar scans. Paper submitted to ISTP Proceedings, Boulder, 1979.

Gulbrandsen, A. (1975) : The solar M-region problem - an old problem now facing its solution? Planetary and Space Science, 23 : 143.

Hansen, R. T., S. F. Hansen and C. Sawyer (1976) : Long-lived coronal structures and recurrent geomagnetic patterns in 1974. Planetary and Space Science, 24 : 381.

IPS (Ionospheric Prediction Service), Department of Science (1977) : Handbook IPS H-6 for use with ionospheric prediction services.

Lanzerotti, L. J. (1974) : Comment on (Sakurai and Chao 1974) : Journal of Geophysical Research, 79 : 4823.

Neupert, W. M. and V. Pizzo (1974) : Solar coronal holes as sources of geomagnetic disturbances. Journal of Geophysical Research, 79 : 3701.

Nolte, J. T., A. S. Krieger, A. F. Timothy, R. E. Gold, E. C. Roelof, C. Vaiana, A. J. Lazarus, J. D. Sullivan and P. S. McIntosh (1976) : Coronal holes as sources of solar wind. Solar Physics, 46 : 303.

Pintér, S. (1975) : Deceleration of flare-generated interplanetary shock waves. Bulletin of the Astronomical Institutes of Czechoslovakia, 26 : 169.

Sakurai, K. and J. K. Chao (1974) : Motion of the sources for type II and type IV radio bursts and flare-associated interplanetary disturbances. Journal of Geophysical Research, 79 : 661.

Sheeley, N. R., J. W. Harvey and W. C. Feldman (1976) : Coronal holes, solar wind streams, and recurrent geomagnetic disturbances : 1973-1976. Solar Physics, 49 : 271.

Švestka, Z., L. Fritzová-Švestková, J. T. Nolte, H. W. Dodson-Prince and E. R. Hedeman (1976) : Low-energy particle events associated with sector boundaries. Solar Physics, 50 : 491.

Yoshida, S. and S.-I. Akasofu (1965) : A study of the propagation of solar particles in interplanetary space. The centre-limb effect of the magnitude of cosmic-ray storms and of geomagnetic storms. Planetary and Space Science, 13 : 435.

A DISTURBANCE FORECASTER'S VIEW OF THE SEPTEMBER 1977 EVENTS

F. E. COOK
Ionospheric Prediction Service
Department of Science and the Environment
P.O. Box 702
Darlinghurst NSW 2010, AUSTRALIA

The solar-geophysical events of 1977 September 7-26 presented a variety of disturbance forecasting problems, viz. disc transit of a centre of activity with high microwave flux but relatively low metre-wave flux, flares in this region near east limb, central meridian, and west limb with major radio events, and the presence of two coronal holes. The Sydney daily GEOSYD message and IPS Disturbance Warnings issued during this period are related to the solar-geophysical data available, at the time, about these events.

1. INTRODUCTION

The Ionospheric Prediction Service (IPS) of the Department of Science and the Environment operates the Australasia and Antarctica Regional Warning Centre (RWC) of the International Ursigram and World Days Service (IUWDS). The RWC issues a GEOSYD message about 0100 UT each day. The SOLALERT part of this message, relating to expected solar activity, is prepared usually at the Culgoora Solar Observatory where the observers have access to the optical and radio sun, while the MAGALERT part, relating to expected geomagnetic disturbance, is prepared at the RWC in Sydney, based upon the solar-terrestrial relationships outlined by Cook and McCue (1975) and on more recent developments described in the literature, using data from Australian observatories and from the IUWDS ursigrams (IUWDS 1973). Disturbance Warnings (IPS 1977) are also issued as necessary to HF communicators and other users, mainly in Australia and New Zealand.

The solar-geophysical events of 1977 September 7-26 associated with McMath Region 14943 (Boulder 889), are already well-documented : in particular, the monitoring of these events by means of the ursigram data received at the Japanese RWC is discussed by Nozaki et al. (1978). While much information has now been published, the GEOSYD messages and other forecasts were issued on the basis of information available from day to day, and it may therefore be useful to set out on a day-to-day basis the reasons why particular MAGALERT messages and other Warnings were issued, from an operational Warning Centre, during the period. From this it may be possible to consider what changes, if any, should be made in the selection of data to be exchanged by ursigram, and whether we are correctly applying the data we receive already.

2. THE DATA AVAILABLE

At Sydney, the daily GEOSYD is issued at about 0100 UT which is 1100 hours Standard Time (1200 in Summer), and the data and information usually available at that time are:

(1) The Culgoora visual patrol in H-alpha and white light and radio spectrograph data (8-3800 MHz) for the previous day and up to 0000 UT : the spectrograph data (CSIRO Solar Radio Observatory) are read from a facsimile machine which does not necessarily reveal all the details which are scaled later from the film record.

(2) Location of sources and of some events, at 43, 80, and 160 MHz, from the CSIRO radioheliograph.

(3) Fleurs (IPS) microwave data for the same period (but not usually on weekends and holidays), the E-W scans (University of Sydney), and sudden ionospheric disturbances.

(4) Chart record of the horizontal component of the earth's magnetic field recorded at Fleurs and telemetered to Sydney.

(5) Ursigrams received during the night from Tokyo (data to 0600 UT), Moscow (1400 UT) and Boulder (2000 UT).

(6) The Paris GEOALERT (1400 UT), and usually the Boulder report of solar and geophysical activity issued at 2200 UT.

(7) The World Warning Agency (WWA, Boulder) GEOALERT issued at 0300 UT the previous day.

3. DIARY, SEPTEMBER 8-28, 1977

The Sydney GEOALERT messages are identified by the code word GEOSYD. In these messages, MAGQUIET indicates that no significant geomagnetic disturbance is expected on the day of issue or on the dates listed : at some Centres, because of local time differences, the GEOALERT is issued some time on the previous day. MAGNIL means that a MAGALERT which has been in force should be ended. In some cases the Sydney Centre used MAGQUIET when the correct advice should have been MAGNIL since a world-wide MAGALERT had been in force the previous day; these are recorded here as MAGQUIET (MAGNIL). Similarly, SOLALERT, SOLQUIET and SOLNIL refer to solar activity (IUWDS 1973). All times mentioned are in U.T., the GEOSYD message being issued at 0100 each day.

SEP 08 DATA SEP 07 : 2B flare (Culgoora) north 10 degrees, east limb, SEP 07/2252, maximum at 2308, preceded by 1B 2227/2233/2250 : short type II and V bursts (no type IV) followed by dekametre continuum and bursts on the heliograph frequencies (43, 80, 160 MHz). Fleurs, complex microwave burst (720, 1415, 2695, 4995 MHz) and major S-SWF.

NOTES : Data published later reduced the 2B to 1N, with no mention of the 1B at 2227, and they list also a type IV burst 2230-2245 at metre wavelengths, but these details were not known at the time. The short duration (15 minutes) of the type IV would have made it a borderline case according to Bell (1963), but east limb location makes occurrence of a geomagnetic storm unlikely in any case. The probability of more than a slight disturbance from this location, even if one did occur, is also small : see e.g. Yoshida and Akasofu (1965).
GEOSYD : SOLALERT MAGQUIET.
WARNING : issued SEP 08/0100 "... a solar flare from a region beyond the east limb of the sun, start time 07/2227Z, caused a major short wave fadeout lasting over 30 minutes ... present available data on this event do not indicate that it will cause a magnetic storm."

SEP 09 DATA SEP 08 : The flare SEP 07 was 1B according to Voroshilov Observatory. Hiraiso reported major metre-wave burst, starting first at 500 MHz, then 200, 9100, then 100 MHz. No reports of any PCA.
NOTES : WWA MAGALERT SEP 09/10 in force, Tokyo RWC advised MAGQUIET SEP 08 (Tokyo includes this information in daily ursigram).
GEOSYD : SOLALERT MAGQUIET (MAGNIL).

SEP 10 DATA SEP 09 : IUWDS ADALERT message lists 2B flare north 10 degrees east 80 degrees 09/1604, in McMath Region 14943 (Boulder 889) the site of the SEP 07 flare, and mentions parallel ribbons and umbral coverage which are characteristic of proton flares (Křivský 1963). Sagamore Hill report large complex microwave burst but metre-wave burst not large. Again the 210 and 415 MHz bursts occur before the higher frequencies.
NOTES : Region 14943 is large, complex, and bright in H-alpha. Metre-wave flux is still low but this is possibly the well-known directivity effect. However the flare is still too far east of central meridian (see SEP 08 Disucssion). Also the burst start times at different frequencies are not consistent with disturbance travelling outwards through the corona. WWA MAGALERT SEP 09/11 in force.
GEOSYD : SOLALERT MAGQUIET (MAGNIL).

SEP 11 DATA SEP 10 : Microwave flux increasing, from Region 14943 according to the E-W scans, but not metre-wave. No activity SEP 10.
NOTES : As for SEP 10. Slight recurrent-type geomagnetic activity up to K = 4 : Tokyo RWC recommended MAGALERT SEP 10 probably for this reason. WWA MAGALERT 10/12.
GEOSYD : SOLALERT MAGQUIET (MAGNIL).

SEP 12 DATA SEP 11 : Region 14943 is now magnetically beta/gamma/delta, type E spot group about 50 degrees east of C.M. Microwave flux increasing but metre-wave steady. No significant activity SEP 11.
NOTES : No change. The slight geomagnetic activity continued. WWA MAGALERT 11/13.
GEOSYD : SOLALERT MAGQUIET (MAGNIL).

SEP 13 DATA SEP 12 : No activity reported SEP 12 which was also geomagnetically quiet. Microwave flux still increasing (Ottawa 2800 MHz 106 flux units SEP 12), metre-wave flux still low (Sagamore Hill 245 MHz 9 flux units).
NOTES : WWA MAGALERT continued SEP 12. Fleurs magnetic record indicates possible start of recurrent-type activity.
GEOSYD : SOLALERT MAGALERT 13.

SEP 14 DATA SEP 13 : No activity reported SEP 13 in Region 14943 which is still a large E-type spot group. Recurrent-type geomagnetic disturbance occurred SEP 13. (Later published data show a coronal hole CMP SEP 11 probably associated with this disturbance, but this was not known at the time).
NOTES : WWA MAGALERT in force SEP 13/15. Tokyo advised SOLNIL MAGQUIET SEP 13.
GEOSYD : SOLQUIET (SOLNIL) MAGALERT MINOR 14.
WARNING : issued SEP 14/0200 "... recurrent-type activity 13 September. ... The region (near central meridian) has begun to decline, there is still some chance of flare activity causing minor daylight fadeouts."

SEP 15 DATA SEP 14 : Boulder 14/2200 report mentions a coronal hole visible at 10830A about 20-30 degrees east of Region 14943, that is, about two days east of CMP. Metre-wave flux still low, microwave flux no longer increasing.
NOTES : The coronal hole may cause geomagnetic disturbance about 3 days past CMP, that is, about SEP 19. Unless there are some more major events, CMP of Region 14943 should not produce any significant disturbance SEP 17/18 as it is a "Q" (Radio quiet) region according to the classification of Denisse et al. (1951). Tokyo RWC SEP 14 advised SOLALERT MAGNIL, WWA SOLALERT 14/15 MAGALERT 14/16.
GEOSYD : SOLQUIET MAGNIL.

SEP 16 DATA SEP 15 : Only minor activity reported. Region 14943 retains delta configuration according to Boulder 15/2200 report, with microwave flux steady.
NOTES : No change from previous day. WWA SOLALERT 15/17 MAGALERT 15/16. Tokyo RWC advised SOLALERT MAGQUIET.
GEOSYD : SOLQUIET (SOLNIL) MAGQUIET (MAGNIL).

SEP 17 DATA SEP 16 : Culgoora reports 1N flare north 08 degrees west 19 degrees, in Region 14943, SEP 16/2120 to 2230 with 2N flare starting 2230 still in progress at report time, Y-shaped with umbral coverage, also very large metre-wave bursts and spectral type III and II-IV event, also still in progress. The type IV source was reported as moving to the west from a position (in projection) on the NW limb, at report time. These events occurred too late for mention in the Boulder 16/2200 report.
NOTES : Disturbance Warning and MAGALERT should be issued, with some reservation as Region 14943 is not a metre-wave noise source. The Y-shaped flare with umbral coverage is also characteristic of a proton flare (see SEP 10 data). If a magnetic storm does result from this event, the time delay from a region with calcium plage area of about 5000 millionths of the solar hemisphere as reported by McMath-

Hulbert Observatory, should be at least 24 hours and possibly longer (Cook 1970). The coronal hole disturbance is also due to start about SEP 19. The SOLNIL advice issued SEP 16 has been proved incorrect.
GEOSYD : SOLALERT MAGALERT 18/..
WARNING : issued 17/0200 "confirm severe fadeout SEP 16/2220Z due to major flare in the region now one day past central meridian ... available data on this event indicate severe magnetic storm possible starting late 17 to early 18 September through 19/20 ..."

SEP 18 DATA SEP 17 : Hiraiso 100, 200, 500 MHz data received for the 16/2230 event indicate disturbance travelled outwards through the corona, but the 9500 MHz time is in apparent disagreement (later published data list the bursts at 100, 500, 9500 MHz all starting at 2226). Boulder 17/2200 reports energetic particle event started 17/0300 but subsiding by 1800. Culgoora heliograph observations to 17/0515 describe the type IV source moving from north-west limb to near equator at west limb (later published data show the radial distance from disc centre decreasing, i.e. source moving nearer to sun-earth line).
NOTES : These data support increased probability of geomagnetic storm from the 16/2230 event, but give no indication of the delay time.
WWA SOLALERT 17/18 MAGALERT 17/20 PROTON ARRIVAL ALERT.
GEOSYD : SOLALERT MAGALERT 19/..

SEP 19 DATA SEP 18 : Culgoora 2N flare north 08 degrees west 37 degrees (Region 14943), in progress 18/0050 with umbral coverage, spectral type III and weak type IV events. Hiraiso data list minor bursts 9500, 500, 200, 100 MHz with start times progressively later with decreasing frequency. Other minor events reported in the ursigrams and in Boulder 18/2200. Solar microwave flux decreased today.
NOTES : This event may contribute to disturbance already expected. The coronal hole disturbance is also expected to start today. WWA SOLALERT 18/23 MAGALERT 18/19, Tokyo RWC SOLALERT 18/.. MAGALERT 18/20.
GEOSYD : SOLALERT MAGALERT 19/..
WARNING : issued 19/2330 "moderate magnetic storm began SEP 19/1143Z much later than expected and should continue through SEP 20/21 possibly severe at times. Since previous warning daylight fadeout was observed 18/0022Z and another major solar event occurred 19/1031Z in the same region now four days past central meridian. Further daylight fadeouts probable next three days."

SEP 20 DATA SEP 19 : Geomagnetic storm began about 1140 SEP 19. Boulder 19/2200 reports magnetic SC 1305 (later published data list SC 1143 at some observatories). The storm has recurrent-type appearance on the Fleurs magnetogram, that is, substorms but not a well-developed main phase.
Boulder 19/2200 also reports 3B flare north 09 degrees west 59 degrees (Region 14943) at 19/1045, followed by proton event at 1145 still in progress. Region 14952 (south 23 east 40) now has a D-type spot group with beta/gamma magnetic configuration and is growing. Sagamore Hill data show large complex burst 8800 and 1415 MHz but small at other frequencies including the metre waves.
NOTES : The storm has the appearance of recurrent-type (coronal hole) disturbance with possible SC storm superimposed. If the SC 19/1305 is

due to the flare 16/2230, this represents a long delay of about 63 hours. If the 19/1045 flare also causes a storm, this is likely to be also superimposed on the coronal hole disturbance to produce a severe disturbance with about the same delay, late on SEP 21. MAGALERT and SOLALERTS continue.
GEOSYD : SOLALERT MAGALERT 20/21.

SEP 21 DATA SEP 20 : Culgoora 3N flare, north 15 degrees west 55 degrees (Region 14943) in progress at 20/0321, ended after 0748. Strong type II 0315, wide-band type IV 0257-0520. Complex microwave burst recorded at Fleurs. Hiraiso major metre-wave event. Boulder 2200 report describes this flare as 1N. Other minor events reported.
NOTES : This flare may also contribute to the disturbance. If an identifiable increase in disturbance occurs late today as a result of the 19/1045 event, this will increase the probability of another increase about 15 hours on SEP 22. WWA SOLALERT and MAGALERT continue SEP 20.
GEOSYD : SOLALERT MAGALERT 21.

SEP 22 DATA SEP 21 : Magnetic SC 21/2045 with storm apparently superimposed on the continuing recurrent-type disturbance. No significant solar events.
NOTES : This SC may now be plausibly attributed to the 19/1045 event with a delay of 60 hours (see Discussion SEP 20), and strengthens the probability of another increase late SEP 22.
WWA SOLALERT and MAGALERT continue.
GEOSYD : SOLALERT MAGALERT 22/23.
WARNING : issued 22/0415 "Magnetic storm ... is expected to continue through SEP 23 ... Region producing major activity is now rotating off the sun's visible disc but possibility of major flare activity still exists through SEP 23."

SEP 23 DATA SEP 22 : No significant solar events reported. Fleurs magnetogram shows disturbance ending late SEP 22 with only slight increase in amplitude during the middle of the UT day.
NOTES : No evidence of increased disturbance 60 hours after the 20/0321 flare : Fredericksburg data available only to 1200 hours SEP 22. (On the Bartels Kp charts, the planetary magnetic index does increase on SEP 22 from 4 at 09-12 hours to 6+ at 15-18 hours, but the Kakioka and Fredericksburg indices received next day did not indicate any new storm at this time. Later data from high-latitude stations however do show a marked increase in K index starting with the 12-15 hours interval.) WWA SOLALERT MAGALERT MAJOR SEP 22.
GEOSYD : SOLALERT MAGALERT 23.

SEP 24 DATA SEP 23 : No significant solar events reported. Disturbance has subsided and the magnetometer trace was quiet up to 1300 hours SEP 23 when the magnetometer ceased recording because of a power failure at Fleurs.
NOTES : The Bartels Kp chart for the previous rotation shows a quiet period (at end of 26 August) followed by renewed slight disturbance. This quiet period appears to have recurred early SEP 23. WWA SOLALERT 23 MAGALERT 23.

GEOSYD : SOLQUIET MAGALERT 24.

SEP 25 DATA SEP 24 : Culgoora observed a north-west limb surge about SEP 24/0556 accompanied by strong type III and II bursts. Hiraiso reports short major burst 200 MHz at this time, minor at 500 MHz, no event at 100 MHz. Boulder 24/2200 reports minor PCA event 0600 still in progress. The Fleurs magnetometer began recording again at about 0600, showing no disturbance.
NOTES : Further significant geomagnetic disturbance unlikely. The PCA is apparently associated with the north-west limb event (later published data amended the Culgoora type II to type IV). WWA GEOALERT SOLNIL MAGNIL.
GEOSYD : MAGQUIET SOLQUIET.

SEP 26 DATA SEP 25 : Minor activity in Region 14963 near north-east limb. Boulder 25/2200 reports PCA ended 25/0300.
NOTES : No change from SEP 25. WWA SOLQUIET MAGQUIET.
GEOSYD : SOLALERT 26/28 MAGQUIET.

SEP 27 DATA SEP 26 : Minor flares in north-east (Region 14963) and south-west (Region 14952) with SWF and type III bursts and minor microwave and metre-wave activity. Fleurs magnetometer shows a possible SC at 26/1418Z but no significant disturbance.
NOTES : The possible SC is delayed 56 hours from the behind-the-limb event SEP 24/0556, consistent with delay times from earlier events in Region 14943. WWA SOLALERT 26/28 MAGQUIET.

SEP 28 DATA SEP 27 : Minor activity continues in the north-east and north-west. Boulder reports mention a proton event observed by satellite, beginning SEP 26/0920, now ended. The geomagnetic field was more disturbed during the early part of the day.
NOTES : The recrudescence of geomagnetic activity is possibly related also to the SEP 24/0556 event. WWA SOLALERT 27/28 MAGALERT 27.
GEOSYD : SOLQUIET MAGNIL.

4. DISCUSSION

In these notes we have considered the events during the disc transit of one centre of activity, uncluttered by significant activity from other regions, but complicated by the presence of one or two coronal holes - see Table 1. Forecasting problems brought out, and which still await resolution, include:

(1) Dependence upon meridian distance : the events at east limb and east 80 degrees apparently caused no geomagnetic disturbance, although some Warning Centres expected them to do so. Disturbance can be attributed to all but one of the west hemisphere events including, possibly, one from behind the west limb.

(2) Delay between solar event and geomagnetic storm. All Warning Centres expected a storm to start much earlier after the SEP 16 event. A remarkable feature of the delay times is the consistent value of about

60 hours for each event, reminiscent of homologous flares (Ellison et al. 1960) and homologous flare-associated radio events (Fokker 1967), but homology of flare or radio events is not apparent here. On the other hand, the reported McMath calcium plage area of Region 14943 remained stable during its disc transit.

(3) The recurrent-type disturbance starting about 1140 SEP 19 is consistent with the reported CMP of a coronal hole SEP 16 : a coronal hole CMP SEP 11 was not reported at the time. Earlier separate studies of a coronal hole CMP NOV 24 1970 (Krieger et al. 1973 and Kundu and Liu 1976) identified it as the source of high-speed solar wind streams but no significant geomagnetic disturbance followed its CMP on that occasion.

(4) The occurrence of PCA as a pointer to geomagnetic disturbance. The three flares associated with recognizable geomagnetic SC were all followed by fast PCA events according to the classification of Sinno (1961) while those associated here with recrudescence of activity without SC were not.

(5) No information was received about possible sector boundary crossings, or changes in the direction of the interplanetary magnetic field, during this period.

(6) Positive identification of spectral type events, and interpretation of radioheliograph events is not always possible when the observer is necessarily preoccupied with the optical flare, the solar and radio observatories at Culgoora being located in separate buildings. This results in occasional discrepancies between the events reported at the time (read from facsimile and heliograph display) and the data published later in Sol -Geophysical Data (scaled from spectrograph films and heliograph tapes).

(7) The geomagnetic disturbances beginning SEP 19 had the appearance, on the Fleurs magnetogram, of typical recurrent storms, that is, positive and negative excursions but with no obvious main phase. We are therefore not certain of the reality of the apparent SC storms in this sequence. It has long been known (Allen 1944) that a recurrent storm can begin with a sudden commencement if the supposed M-region is preceded by a centre of activity, in this case by Region 14943.

(8) A centre of activity producing flares with consequent geomagnetic storms would be expected to be a strong metre-wave source as well as emitting bursts with the flares, but Region 14943 was not. The significance of this is not clear.

TABLE 1 : SIGNIFICANT EVENTS 1977 SEP 7-26
AS REPORTED AT THE TIME

Flare					Radio Emission				
Date	UT	Class	Location	PCA type?	micro	metre	PCA event	magnetic activity	Delay (hours)
07	2252	2B	E. limb	-	complex	major II-V[1]	-	-	
09	1604	2B	E.80	Yes	large, complex	small	-	-	
11,13	(Coronal hole CMP 11, not reported)							slight (K=4), recurrent?	
14	(Coronal hole reported two days east of central meridian)								
16	2230	2N	W.19	Yes	complex	large II, moving IV	17/0300	SC 19/1305	63
18	0050	2N	W.37	Yes	minor	weak IV	-	(in recurrent storm)	
19	1045	3B	W.59	?	large	small	19/1145	SC 21/2045	60
20	0321	3N	W.55	-	complex	major II-IV	-	recrudescence 22/1200[2]	57
24	0556	surge	behind W. limb	-	-	major III-II	24/0610	possible SC 26/1418	56
								recrudescence 26/2400	66

(1) Type V later amended to type IV

(2) Shows clearly in high-latitude data (Mawson and Macquarie Island)

REFERENCES

Allen, C. W. (1944) : Relation between magnetic storms and solar activity. Monthly Notices of the Royal Astronomical Society, 104 : 13.

Bell, B. (1963) : Type IV Solar Radio Bursts, Geomagnetic Storms, and Polar Cap Absorption (PCA) Events. Smithsonian Contributions to Astrophysics, 8 : 119.

Cook, F. E. (1970) : On the time delay between solar flares and associated geomagnetic storms. Paper 28 in AGARD Conference Proceedings, No. 49.

Cook, F. E. and C. G. McCu (1975) : Solar-terrestrial relations and short-term ionospheric forecasting. The Radio and Electronic Engineer, 45 : 11.

Denisse, J.-F., J. L. Steinberg, and S. Zisler (1951) : Contrôle de l'activité geomagnétique par les centres d'activité solaires distingués par leurs propriétés radioelectriques. Comptes Rendus, 232 : 2290.

Ellison, M. A., S.M.P. McKenna, and J. H. Reid (1960) : Cape Lyot Heliograph Results 1. Light-curves of 30 solar flares in relation to sudden ionospheric disturbances. Dunsink Observatory Publications 1.1.

Fokker, A. D. (1967) : Homology of solar flare-associated radio events. Solar Physics, 2 : 316.

IPS (Ionospheric Prediction Service), Department of Science (1977) : Handbook IPS H-6 for use with ionospheric prediction services.

IUWDS (International Ursigram and World Days Service) (1973) : Synoptic Codes for Solar and Geophysical Data, Third Revised Edition.

Krieger, A. S., A. F. Timothy, and E. C. Roelof (1973) : A coronal hole and its identification as the source of a high velocity solar wind stream. Solar Physics, 29 : 505.

Křivský, L. (1963) : Y-shaped stage of cosmic ray flares development as phase conditioning ejection. Bulletin of the Astronomical Institutes of Czechoslovakia, 14 : 77.

Kundu, M. R. and S.-Y. Liu (1976) : Observation of a coronal hole at 85 GHz. Solar Physics, 49 : 267.

Nozaki, K., K. Marubashi, Y. Miyamoto, and K. Ohbu (1978) : Overview of Solar-terrestrial physics phenomena associated with McMath Region 14943 based on ursigram data. Solar Terrestrial Environment Research in Japan, 2 : 61.

Sinno, K. (1961) : Preliminary Study of Prediction Aspects of Cosmic Ray Events. Journal of the Radio Research Laboratories (Japan), 8 : 17.

Yoshida, S., and S.-I. Akasofu (1965) : A study of the propagation of solar particles in interplanetary space. Planetary and Space Science, 13 : 435.

D22-46

N80-18484

THE USE OF IONOSPHERIC INDICES TO MAKE REAL- AND NEAR-REAL-TIME FORECASTS OF foF2 AROUND AUSTRALIA

L. F. McNAMARA
Ionospheric Prediction Service
Department of Science and the Environment
P.O. Box 702
Darlinghurst NSW 2010, AUSTRALIA

This paper describes techniques using ionospheric indices which have been developed to make real- and near-real-time forecasts of foF2 at points around Australia. It is divided into two parts, corresponding to two time scales and the corresponding computer programs. Part 1 covers forecasts 1 day ahead using daily ionospheric indices (program DALYPRED), while Part 2 covers forecasts 0-3 hours ahead using hourly ionospheric indices (program HOURPRED). Both programs provide extensive tabulations of errors in the forecast values of foF2, but only heavily compressed results are included here.

The present analysis differs from a previous one (Reference 2) in that it is a more general approach, not relying, for example, on the presence of an ionospheric station at the position where the forecasts are required. It also takes advantage of the ability of the IPS world maps of foF2 to inter-relate values of foF2 at different locations once the appropriate ionospheric index has been specified.

It is found that for forecasts one day ahead the most accurate results are obtained using the past variations of foF2 at several stations to determine a latitudinal-average daily ionospheric index. Forecasts made with lead times of 0-3 hours do not offer significant improvements over these made one day ahead.

Both programs may be used to provide answers to specific questions as they arise from customer requirements.

PART 1 - DALYPRED

1. INTRODUCTION

DALYPRED is a program which makes forecasts of foF2 at a test station one day ahead, calculates the errors in the forecast values and analyses them in various ways. It is not an operational program in that it is not designed to

make forecasts in real time. Rather, it is a developmental program, aimed at investigating the errors inherent in the techniques adopted to make the forecasts and using only "old" ionospheric data recorded over recent years.

Basically, the procedure which has been adopted in making the forecasts is to monitor the ionosphere using five mainland Australian ionospheric stations, project this observed behaviour forward one day at each station and then calculate the expected behaviour at a test station. The five reference stations are Mundaring (Perth), Townsville, Brisbane, Canberra and Hobart. The test station was Norfolk Island although others could just as easily be considered. (In practical applications, this station could also be used as a reference station and the method described here modified appropriately. However at the present stage it is necessary that it be reserved as a test station.)

The principle underlying the present approach is that the behaviour of the ionosphere can be characterised for each day by an ionospheric index "T" in terms of which all calculations may be effected. Several different types of index are investigated, as described in later sections.

DALYPRED requires various forms of pre-calculated input and is in fact the sixth step in the overall problem. The preceding five steps are discussed very briefly below. The logical seventh step is to apply the same techniques to operational situations, provided that the errors involved are acceptably small.

2. PRELIMINARY PROGRAMS

Several of the preliminary programs are used to determine for each station the relationship between a T index and the 24-hour average of the monthly median values of foF2:

$$T = a + b * \frac{1}{24} \sum foF2$$

The T index used initially was the world-wide average monthly index deduced from the calculated indices at 16 particular stations distributed around the world (reference 3).

The above relationship is assumed to hold also for a time scale of one day, so that the average of 24 hourly values of foF2 for a day yields an index which can be used to characterize the behaviour of foF2 throughout that day. This particular index is called IT in the program DALYPRED.

The residuals of T for each month may be used to estimate the size of the error in the forecast values of foF2 caused by the scatter of the points about the fitted line. For Brisbane 1970-74, for example, the average residual in T is 2.2 and the standard deviation is 5.6. The corresponding uncertainties in foF2 can be estimated from the rough figures that a change in 10 in the T index changes foF2 at Brisbane by about 5% or 0.5 MHz.

A second index, TF2, is obtained by averaging the 5 individual values

for each day. The underlying philosophy here is that such an approach might yield an index less affected by the scatter about the regression lines.

A third index, TFX, is obtained from the daily value of 10.7 cm flux using the empirical observed relationship between monthly T indices and monthly average flux values. (Figure 1 of Reference 1.) Note that this index makes no use of foF2 values, and therefore negates any need to monitor the ionosphere. It has been found that, on average, the discrepancy between TF2 and TFX is almost zero, suggesting the TFX may be an adequate index, even without further analysis.

3. PROGRAM DALYPRED

This is the program which makes the forecasts and analyses the errors. Forecasts are made for March, June, September and December for 1970-74 and compared with the observed values of foF2 at the test station.

For a given T index, forecasts of foF2 are obtained by linear interpolation between the values predicted by the standard IPS area MUF program for low (T=0) and high (T=100) solar activity.

Forecasts are made using both the correct daily values, TC, and the projected daily values, TP, of three indices. The three basic indices are as described in section 2:-

IT - the separate indices at the 5 reference stations,
TF2 - the average index for these 5 stations, and
TFX - the index based on the 10.7 cm flux.

TC(1) is calculated for the test station assuming that the index IT for a given day is a function of latitude only. TC(2) and TC(3) are set equal to TF2 and TFX. For later reference, indices derived from IT, TF2 and TFX are referred to as T_1, T_2, and T_3 respectively.

The projected indices TP for day I, say, are calculated using the correct indices TC for days I - 1, I - 2, ... I-NDAY and a least-squares fit subroutine, with all data being given equal weight.

The subject of weights will be referred to again in Section 4. Initially they are set to unity.

This simple projection process was found to be unsatisfactory when ionospheric storms were present, the recovery phase yielding unrealistically high values for several days after each storm. The projected indices are therefore modified in a physically reasonable way.

A storm is defined as a TTOL fractional decrease of TC from the value on the preceding day (presently set at 0.3), and may exist for either one or two days. After a storm, if the projected TP for day I is greater than TC on the day preceding the storm, it is set equal to the average of that value and of TC on the preceding day, I - 1. In this way, TP is forced to recover to

the TC on the day preceding the storm. TP is also forced to recover monotonically.

Forecast values of foF2 are calculated for the test station for each hour for a particular day using the three predicted and three correct T indices, and the T vs. foF2 relationships (actually fxF2) defined by the T = 0 and 100 values of fxF2 described in Section 2. These values are compared with the correct, observed, values and the discrepancies expressed as a percentage of the correct value.

$$\text{IDEL} = (\text{predicted} - \text{observed})/\text{observed} \times 100\%$$

The errors are then analysed in various ways, since no way seems to have any prior advantage. Median and decile values are calculated for the 30 or 31 values at each hour; average values and variances are calculated for the 24 hours of each day, and for the 30 or 31 values at each hour.

The program then works out which is the most successful index, according to the number of times each index gave the smallest (absolute) values of the median, average and variance at each hour.

In order to compare the errors with some absolute standard, rather than just with each other, the error distributions are calculated for the case when the monthly median values are used as the forecast values. Operationally, this would correspond to the use of a correct predicted monthly median. These errors are characterised by interdecile widths and variances and the errors for the most successful index compared against them. Two success counts ($\leqslant 24$) are then made, depending on whether the interdecile width or the variance at each hour is less than or greater than that corresponding to the use of the median value.

4. MODIFICATIONS TO DALYPRED

In Section 2, the T index used for the regression analysis was the worldwide average T index. An alternative approach, which turns out to yield smaller errors, is to use the previously established relationships between a station T index and monthly median values of foF2. This relationship is available for each month for each of the 16 stations used to calculate the worldwide T indices. Unfortunately Townsville is not one of these stations, so DALYPRED needed to be slightly modified.

Further possible modifications to DALYPRED, which have not been implemented, are

1. The lead time could be changed to two or more days.

2. In the projection process, the weighting scheme could be changed in order to give, say, greater weight to more recent data. (Note, however, that the weights had little effect in the forecasts of foF2 a few hours ahead at Brisbane and Canberra - see Reference 2). The length of the reference period, 'NDAY' days,

could also be changed, perhaps going as low as 1.

3. Rather than projecting the T index for each station, and then calculating its value at the test station, perhaps the values should first be calculated for all necessary preceding days at the test station and then these values projected.

4. The criteria for the "best" T index could be changed, for example, by considering only the variances.

5. The success counts for the best T index could be replaced by a reference to an externally defined acceptable error limit.

5. DISCUSSION OF RESULTS

Although DALYPRED provides detailed listings of the errors, we shall limit the discussion here to which is the most successful T index and how often the interdecile widths and variances are less than those obtained using a correct median value as the predicted value.

The program has been used to make forecasts for March, June, September and December of the five years 1970-74. Using world-wide T indices (Section 2) leads to the T_2 index being the most successful for zero lead time:-

$$T_1 : T_2 : T_3 \equiv 6 : 10 : 4$$

For a lead time of 1 day, which means that additional errors are being introduced by the projection process, T_2 and T_3 are equally successful:-

$$T_1 : T_2 : T_3 \equiv 4 : 8 : 8$$

Using station T indices (Section 4), on the other hand, results in T_2 being clearly the most successful index:-

Zero lead time $T_1 : T_2 : T_3 \equiv 0 : 17 : 3$

One day lead $T_1 : T_2 : T_3 \equiv 2 : 12 : 6$

The question of which is the better, the station indices or worldwide indices, can be answered by comparing the success rates for the interdecile widths and variances listed in Table 1. This table shows that the use of the station T indices leads to somewhat higher success rates on average (the highest "score" possible each month is 24), although its overall success rate is still less than 50% (467/960). The use of the station T indices is also indicated by the clearer superiority of one index (T_2).

From the practical point of view, it would be necessary to know which index to choose, T_1, T_2 or T_3. Although the obvious choice is T_2, since it is the best on most (12/20) occasions, other indices are more successful at other times, and no way has been found to predict under what conditions each index will be the best. The best index for each of the months considered is

listed in Table 2. There seems to be no definite dependence, for example, on the presence of ionospheric storms during the month. For real-time forecasts (lead time of zero), T_2 is clearly the best index to use.

	Interdecile widths					Variances				
	M	J	S	D	Total	M	J	S	D	Total
70	11	13	2	13	39	17	17	6	13	53
71	19	5	15	1	40	20	17	20	8	65
72	5	5	11	11	32	12	6	18	15	51
73	7	7	13	10	37	11	10	22	12	55
74	9	7	12	12	40	16	19	11	9	55
Total	51	37	53	47	188	76	69	77	57	279
Equinoxes	104	Solstices	84			Equinoxes	153	Solstices	126	
70	10	12	9	11	42	18	11	14	11	54
71	15	4	15	0	34	17	9	17	8	51
72	8	2	11	11	32	12	6	18	15	51
73	3	4	5	6	18	8	5	16	8	37
74	4	7	12	8	31	9	19	10	3	41
Total	40	29	52	36	157	64	50	75	45	234
Equinoxes	92	Solstices	65			Equinoxes	139	Solstices	95	

Table 1 The success counts (≤ 24) for each month according as the interdecile widths or variances of the forecast errors are less than the corresponding parameters obtained using the post-facto observed median foF2 as the forecast value. The top set of results corresponds to the use of station T indices (Section 4) and the bottom set to the use of world-wide T indices (Section 2). The total success rates (out of 960) for the two are 467 and 391, respectively.

1970	2(Q)	2(Q)	2(Q)	2(Q)
1971	2(Q)	2(Q)	2(D)	2(Q)
1972	2(Q)	3(Q)	3(Q)	3(Q)
1973	2(Q/D)	2(D)	2(Q)	1(Q)
1974	3(D)	3(D)	1(D)	3(D)

Table 2 The T index, T_1, T_2, or T_3, which yields the smallest forecast errors in each of four months for 1970-74. The index T_2 is the most successful index, in the ratios

$$T_1 : T_2 : T_3 \equiv 2 : 12 : 6$$

The letters Q and D denote subjective classifications of each month as being magnetically quiet or disturbed.

6. FUTURE POSSIBILITIES FOR DALYPRED

Since it would be necessary for an operational program to use only one index, presumably T_2, the success rates for forecasts using T_2 may be required. These could be obtained by slight modification of the program, which in its present form calculates the success rates for the best index.

Additional programming could also be added (as was done for HOURPRED) to record the number of times the error in the forecast value was less than some (acceptable) level, say 10%.

7. CONCLUSION-DALYPRED

It has been found that forecasts of foF2 made one day ahead for Norfolk Island are most accurate when made on the basis of the average behaviour of the ionosphere over mainland Australia i.e. using the index T_2 defined in Section 3. Details of the errors for this and the other indices, T_2 and T_3, are available as computer listings.

It has not been found possible to develop an index which is always the best, nor to determine under what conditions T_2 is not the best. However there does seem to be a tendency for T_3 to be better than T_2 when both are small, probably because T_3 varies more smoothly than T_2 and is thus less susceptible to projection errors, especially those caused by rapid changes in T_2 due to ionospheric storms.

PART 2 - HOURPRED

1. INTRODUCTION

The basic approach in HOURPRED is similar to that of the program DALYPRED, the major difference being the time scale which is now hours rather than days. Predictions of foF2 at two test stations (Norfolk Island and Mundaring) are made for lead times of 0 to 3 hours, using the observed hourly values of foF2 at five reference stations (Port Moresby, Townsville, Brisbane, Canberra and Hobart). Data manipulation is done in terms of a T index; it is assumed initially that for a given hour the T index is a function of latitude only; and projections ahead in time are performed using a least-squares fit regression line.

Percentage discrepancies in the predicted values of foF2 are analysed in terms of medians, deciles and variances, and can thus be compared directly with the error distributions obtained using DALYPRED.

It is assumed that the two test stations are at 165° and 120° E longitude, and that the five reference stations are all at 150°E. For an operational program the values of fxF2 at the required location would be obtained by

interpolation in the appropriate world map of fxF2.

2. DETAILS OF PROGRAM HOURPRED

2.1 The projected T indices

For each hour of the given month, hourly values of a T index corresponding to the observed fxF2, T, are calculated, assuming that the relationship defined by the T = 0 and 100 values of monthly median fxF2 is also valid for hourly values of T and fxF2. The projected T indices are then calculated as in DALYPRED, except that no allowance is made for storms since it is expected that the use of hourly data would be one of the most reliable ways of making this allowance.

2.2 T indices at the test stations

As mentioned previously, it was assumed initially that for a given hour the T index is a function of latitude only. The T indices for the test stations were therefore obtained by a simple interpolation in latitude. The interpolation was bypassed and no prediction made if no data were available for Port Moresby or Hobart.

Each interpolated predicted T index for a given local time at the reference stations was then associated with the same local time at the test stations.

This option still exists in the program but the T indices so derived have been overwritten by latitudinal average of all (up to 5) available station T indices, since it was found that the use of the average value significantly decreased the variance of the errors.

2.3 Predicted values of foF2 and errors

The predicted value of foF2 corresponding to each predicted T index is calculated as described in Section 3.

The percentage discrepancies between predicted and observed values of foF2 are then analysed to yield medians, deciles, averages and variances.

In order to facilitate the discussion of errors, the individual errors have been tested to see if they are less than some particular value determined by the parameter TOLER. For the present report, TOLER has been set at 10% and the occurrence rates of errors less than this calculated for each hour and then averaged to yield one value per month for each lead time.

Since it was found in practice that the intercomparison of HOURPRED and DALYPRED variances was too sensitive to just how each program handled missing data, HOURPRED was modified to cycle twice, the first time using some daily T index for all forecasts and the second using the hourly indices. Although any set of daily T indices could be used, the most logical choice is the predicted T_2 index as used by DALYPRED for the same month.

3. DISCUSSION OF RESULTS

Individual errors, median errors, upper and lower deciles, average errors and variances, and success rates for errors less than 10 are all printed out by HOURPPED. However for present purposes it is sufficient to consider average values of the success rate for each month.

Table 3 shows the average success rates for March, June, September and December 1970, for Mundaring (No. 2961) and Norfolk Island (No. 4260), for both predicted daily T_2 indices and for latitudinal averages of the predicted hourly station T indices. The important point to note is that the success rates are about the same for both daily and hourly indices, indicating that the effort of updating forecasts on an hourly basis is not worthwhile. (The December 1970 results are suspect because of small sample sizes, $\lesssim 10$, due to missing data). However the use of the daily index T_2 still requires the collection of hourly values of foF2.

	2961 MARCH 70					4260 MARCH 70			
	0	1	2	3		0	1	2	3
Daily	60	60	60	60	Daily	72	72	72	72
Hourly	61	62	63	57	Hourly	72	69	70	70
	JUNE 70					JUNE 70			
Daily	56	56	56	56	Daily	62	62	62	62
Hourly	60	64	65	57	Hourly	65	64	60	56
	SEPTEMBER 70					SEPTEMBER 70			
Daily	61	61	61	61	Daily	66	66	66	66
Hourly	71	75	75	64	Hourly	69	63	58	58
	DECEMBER 70					DECEMBER 7[illegible]			
Daily	51	51	51	51	Daily	42	42	42	42
Hourly	59	63	63	54	Hourly	61	56	55	51

Table 3 The monthly average success rates for forecast errors of less than 10%. The rates are given for forecasts made using projected values of the daily index T_2 as calculated by DALYPRED and for forecasts made using hourly indices projected 0-3 hours ahead. (Mundaring, No. 2961; Norfolk Island, No. 4260).

REFERENCES

McNamara, L. F. (1976). "The correlation of individual values of foF2 and M(3000)F2 with the solar 10.7 cm flux under magnetically quiet conditions". IPS Series R Reports, IPS-R30.

McNamara, L. F. (1976). "Short-term forecasting of foF2". IPS Series R Reports, IPS-R33.

Turner, J. F. (1968). "The development of the ionospheric index-T". IPS Series R Reports, IPS-R11.

PREDICTION LIMITS FOR foF2

P. J. WILKINSON
Ionospheric Prediction Service
Australian Department of Science and the Environment
P.O. Box 702
Darlinghurst NSW 2010, Australia

Some of the factors limiting the prediction of foF2 are investigated using median and hourly foF2 values recorded at stations in the Australian ionosonde network. Different time and spatial scales together with different levels of solar and geomagnetic activity are considered. The unique feature of this presentation is the display of all data used in the analysis in the form of a series of scatter diagrams which provide an overall view of the accuracy limits for foF2 predictions.

1. INTRODUCTION

Basic to the problem of making ionospheric predictions is the prediction of the F2 region penetration frequency, foF2. The factors limiting the accuracy of foF2 predictions are therefore fundamental to the overall problem of HF prediction.

For a given location, foF2 can have a wide range of values dependent, to a great extent, on the sun's declination (diurnal and seasonal effects) and on solar activity. While the ionospheric F2 region response to these factors is not simple, because of their cyclic nature it is possible to produce empirical models of the ionosphere on the basis of recorded past behaviour. These "models" can then be used for prediction purposes, the only variable requiring prediction being the level of solar activity. Most systems, such as that described, predict average monthly conditions on the basis of a predicted monthly solar index. In this paper the range of average monthly foF2 values is displayed for various stations and the effectiveness of predicting this behaviour is assessed. This 'effectiveness' is demonstrated by comparing recorded median values of foF2 with predicted values, the comparison being made by subtracting the predicted value from the observed values and the results being presented as a scatter plot.

Comparison of predicted median values with recorded hourly foF2 values demonstrates the limitations in using monthly predictions to anticipate daily ionospheric conditions.

Some simple methods to reduce these limitations are investigated. These methods involve the use of previously recorded hourly values to project forward both in time and space in, essentially, a real-time prediction system.

C-3

Because the same data presentation is used throughout it is possible to compare these methods with the use of monthly predictions.

The prediction method used to obtain the monthly prediction is the standard IPS system, but the comparisons presented in this paper are not intended as a test of the IPS predictions. (It is necessary to explain the presence of a systematic offset in the comparisons. The IPS predictions give fxF2, not foF2, as the expected top frequency for the F2 region. Thus, the difference between observed and predicted values will be too low by $\frac{1}{2}f_B$, the geomagnetic split. It was convenient, computationally, not to remove this offset from the data before plotting).

To make useful comparisons of F2 region predictions the known ionospheric index, rather than the predicted index, was used, thereby eliminating errors in predicting the correct level of solar activity.

2. MONTHLY PREDICTIONS

In general, prediction systems based on median maps are only useful for predicting average undisturbed conditions during a month. In making a monthly prediction, three components are allowed for - diurnal, seasonal and solar cycle. Figure 1 gives all the recorded median values for three stations. The format of the diagrams is given in section 6. There is a clearly defined range of values that may be anticipated for each station and it is also possible to identify seasonal and solar cycle components in the time series. However, the diurnal variation makes further interpretation quite difficult.

When only a single UT hour is plotted (figures 2, local midnight, and 3 local midday) the diurnal variation is removed and the relative importance of the solar cycle and seasonal components can be readily assessed. It is apparent that during daytime the solar cycle component is generally more important than the seasonal component.

Most prediction systems can adequately account for these factors. Figure 4 gives the difference between observed and predicted values of the monthly medians for all recorded foF2 data.

Of the three stations, Brisbane is clearly the best behaved. The greatest deviations from predicted values are obtained for the high solar activity in the 1957-59 period. The prediction system in this period gave a false impression of the available frequencies for communicators. If, as has been suggested (Sargent, 1977) cycle 21 is similar in intensity to cycle 19, some thought may have to be given to improving the system for high solar activity.

Seasonal plots (Figure 5) were obtained by folding all data into a one year period. The only significant effect that appears is the diurnal variation in deviations for Vanimo which is more important in Winter than other seasons.

From the small differences shown it can be seen that the monthly predictions are effective to within a megahertz, though for Vanimo there is still a large residual component.

3. PREDICTING HOURLY VALUES

It is the hourly foF2 values which are indicative of the actual HF

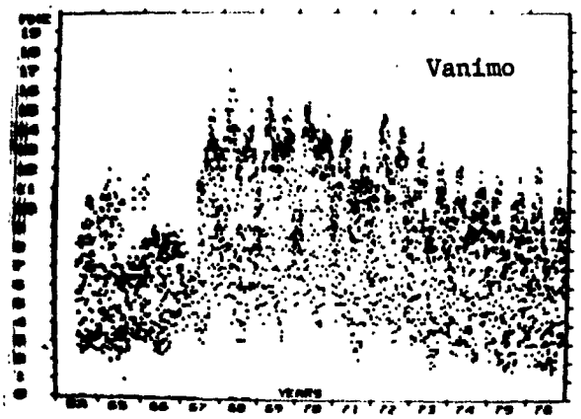

Fig. 1a. Monthly foF2 medians for all 24 hourly medians at Vanimo.

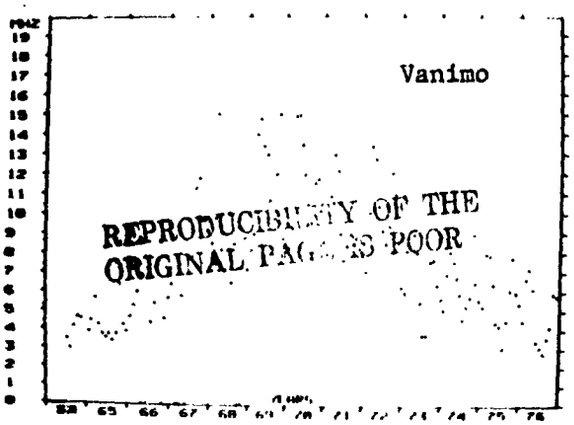

Fig. 2a. Monthly foF2 medians for local midnight at Vanimo.

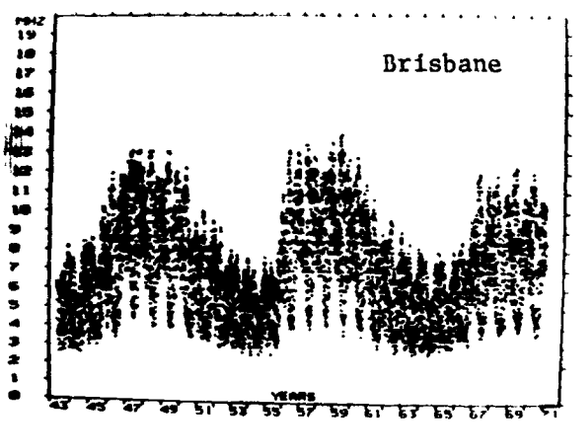

Fig. 1b. Same at Brisbane.

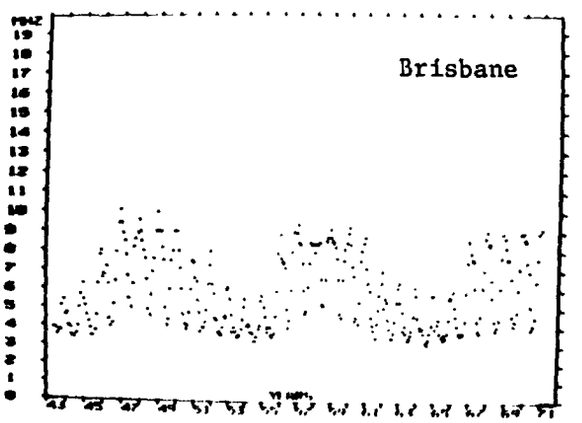

Fig. 2b. Same at Brisbane.

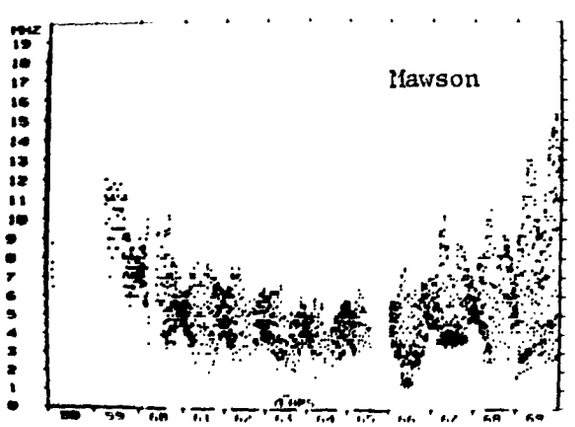

Fig. 1c. Same at Mawson.

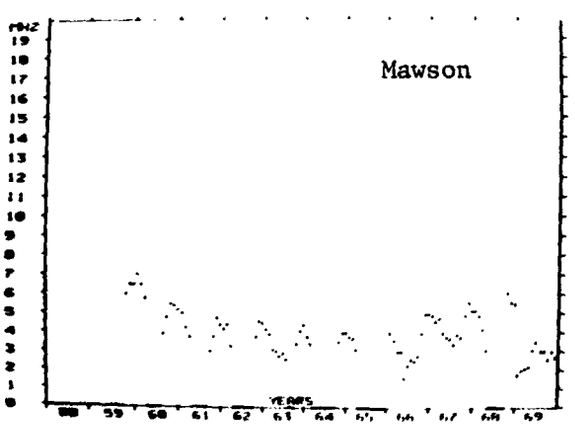

Fig. 2c. Same at Mawson.

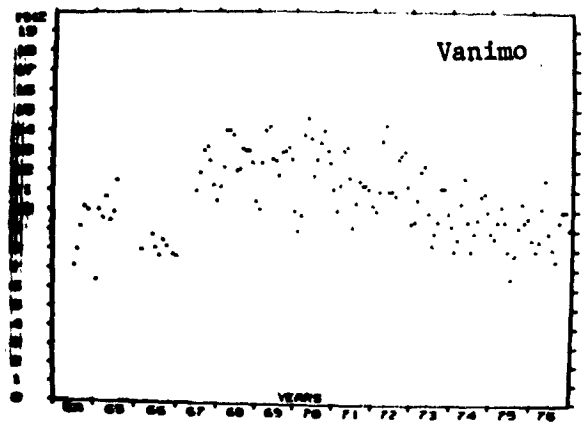

Fig. 3a. Monthly foF2 medians for local noon at Vanimo.

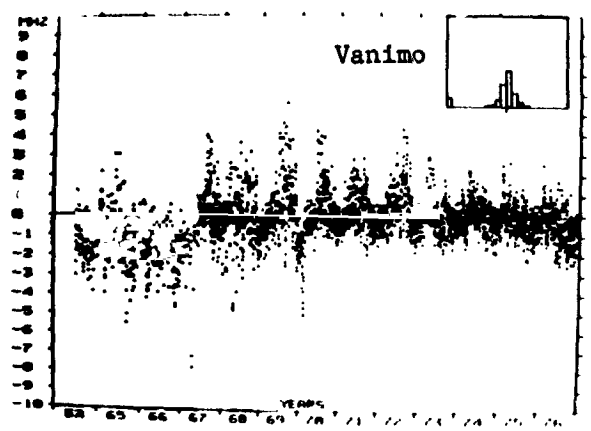

Fig. 4a. Difference between observed and predicted foF2 monthly medians for all recorded data.

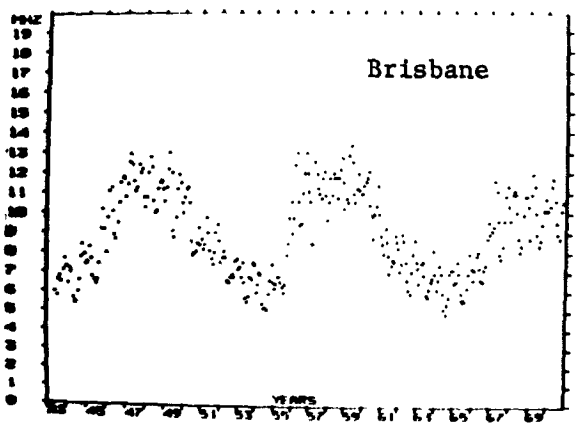

Fig. 3b. Same at Brisbane.

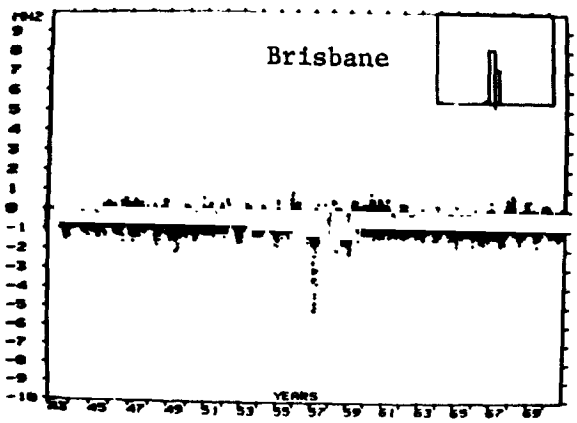

Fig. 4b. Same at Brisbane.

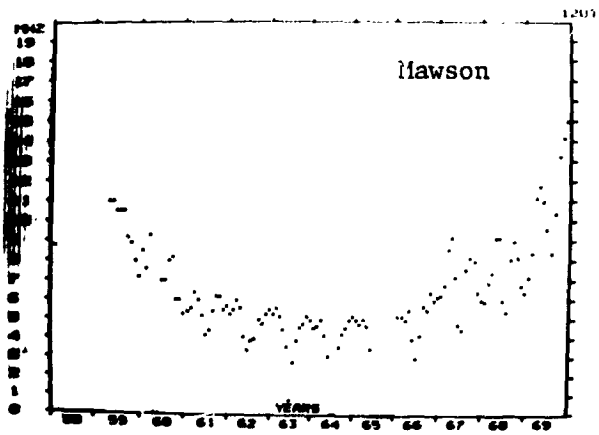

Fig. 3c. Same at Mawson.

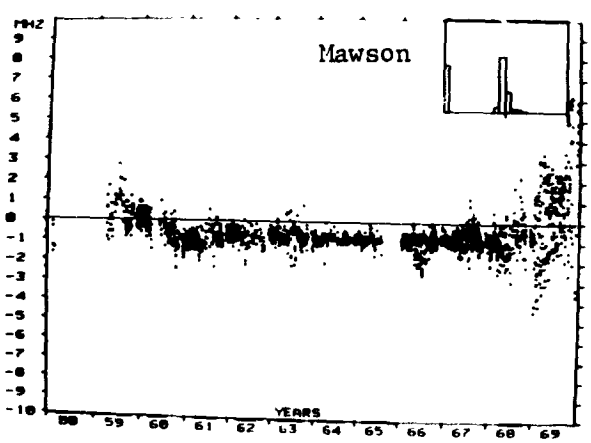

Fig. 4c. Same at Mawson.

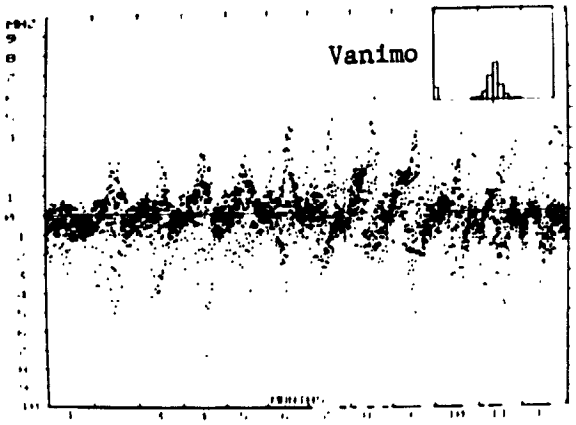

Fig. 5a. Seasonal plot for the same data as in Fig. 4.

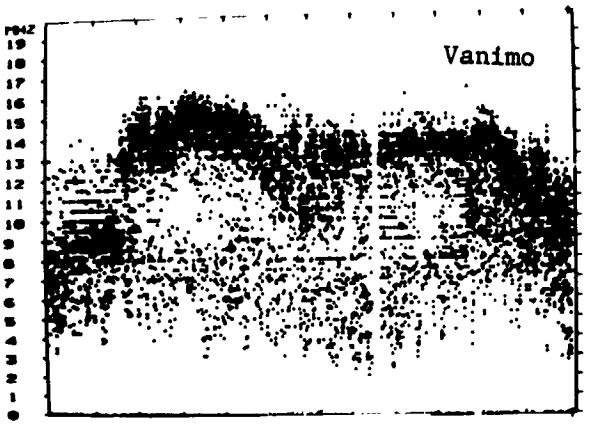

Time During 1970

Fig. 6a. All hourly foF2 values recorded in 1970 at Vanimo.

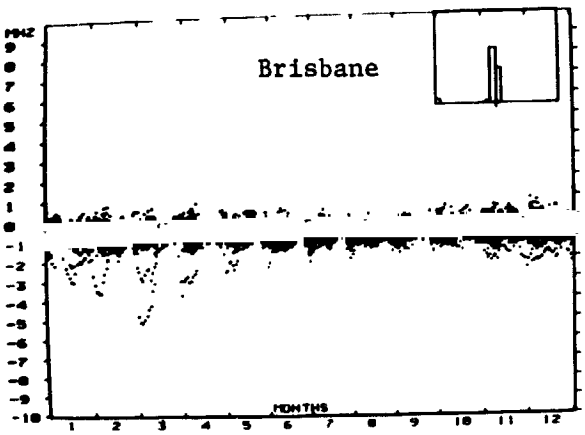

Fig. 5b. Same for Brisbane.

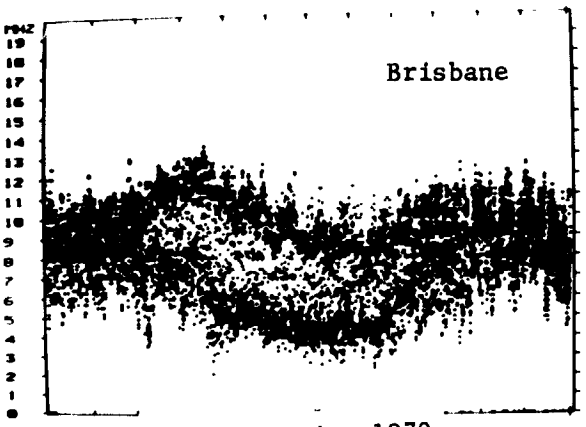

Time During 1970

Fig. 6b. Same at Brisbane.

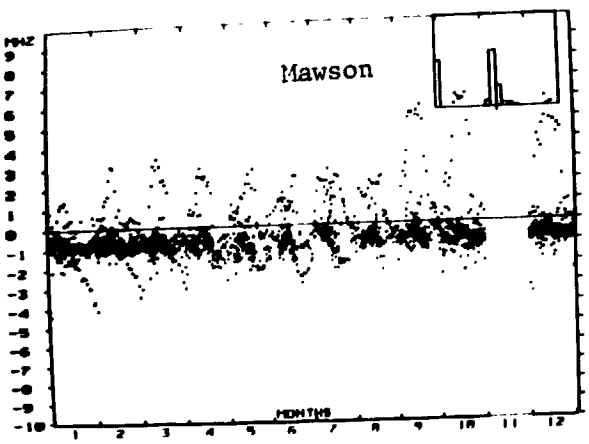

Fig. 5c. Same for Mawson.

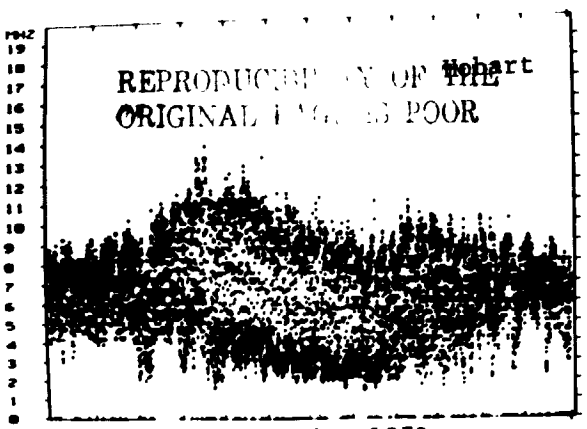

Time During 1970

Fig. 6c. Same at Hobart.

operating environment. As with the median values, the three principal components; diurnal, seasonal and solar cycle, are readily observed in mass plots of all hourly values recorded. Two years of data, 1970 and 1976, for three stations, Vanimo, Brisbane and Hobart are displayed in Figures 6 and 7. It is evident that Vanimo is strikingly different from Brisbane and Hobart, which are representative of all the Australian mid-latitude stations.

While the various components are contained in these plots, they are rather more clear, as before, when the diurnal component is removed (Figures 8 and 9). The day-to-day changes in foF2 are superimposed on a longer period seasonal variation which decreases in amplitude with the change in solar activity from 1970 to 1976. The seasonal component is clearest for 00LT Brisbane and Hobart. Night-time behaviour (Figure 8) at Vanimo is clearly quite different from the mid-latitude stations, showing considerable variability. None of the stations shows very clear seasonal effects for the 12LT data.

The day-to-day component is more evident after the predicted monthly medians are removed. A mass plot for all twenty-four hours for 1970 and 1976 is given in Figures 10 and 11. For Hobart and Brisbane the time series in Figures 10 and 11 show considerable structure much of which can be associated with ionospheric storms. Vanimo, as with the median predictions, shows the greatest spread in deviations by a factor of two.

Figures 12 and 13 show, for the mid-latitude stations, that the 12LT spread is greater than for 00LT while the opposite is true of Vanimo. While there is a diurnal effect, there is no obvious tendency for the deviations from predicted median behaviour to be dependent on the solar cycle level.

Figures 14 and 15 give seasonal plots for 00LT and 12LT for the seven years of data available. Here some structure is apparent, Vanimo showing slightly less spread in summer and Hobart, 12LT, showing increased spread in the equinoxes. Brisbane also shows a marginal summer to equinox increase in spread.

Thus there is a diurnal deviation from the monthly median predictions, a seasonal effect is also present, but is less evident, and there is no obvious evidence for a solar cycle dependency.

These residual deviations indicate the general variability in foF2 that most prediction systems must accept as the 'noise level'. The 'noise' limits can be indicated by statistical limits; normally the upper and lower deciles are predicted. Figures 16 and 17 shows plots of the predicted upper and lower deciles and all data that falls outside these decile limits for 00LT and 12LT. For the mid-latitude stations some of the data falling below the lower limit can be attributed to ionospheric storms. However, for Vanimo over 30% of the data appears both above the upper decile and below the lower decile. This is especially true of the 00LT data. If the deciles were completely reliable, 80% of the observed data would lie between them and for Vanimo this is not the case, suggesting the deciles are not wide enough. For Brisbane, on the other hand, almost 90% of the 00LT and 12LT data lies between the decile limits suggesting that they are too wide.

Evidently, while reasonably adequate for mid-latitudes, the decile limits could be made more reliable.

4. REDUCING THE 'NOISE LEVEL'

To improve the prediction of foF2 further, two basic methods can be

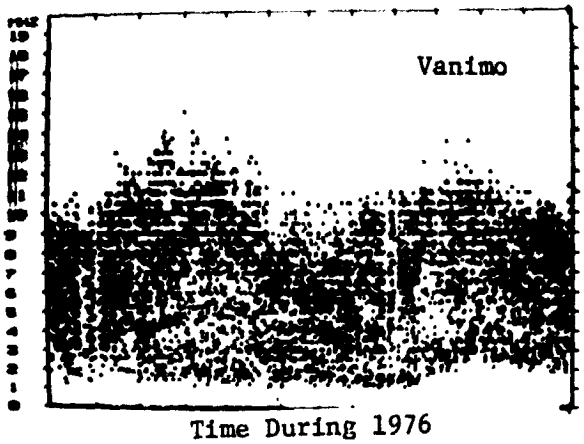

Time During 1976

Fig. 7a. All hourly foF2 values recorded in 1976 at Vanimo.

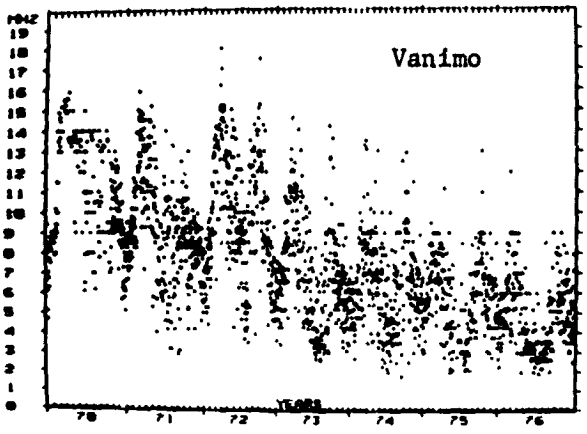

Midnight

Fig. 8a. Midnight foF2 values at Vanimo.

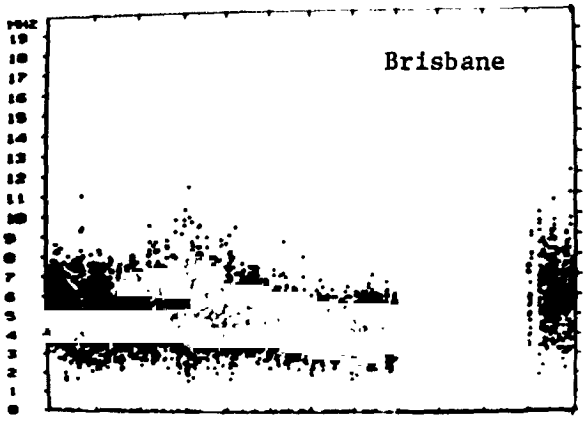

Time During 1976

Fig. 7b. Same at Brisbane.

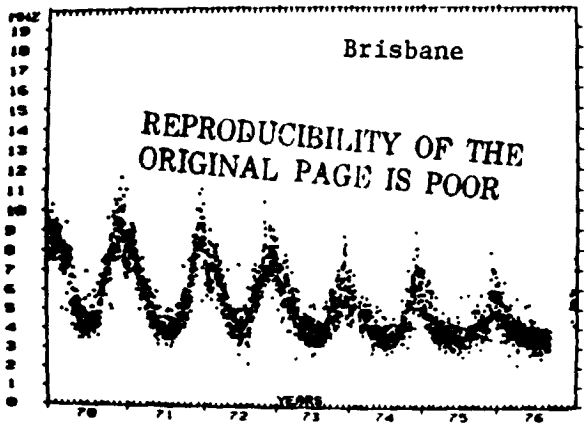

Fig. 8b. Same at Brisbane.

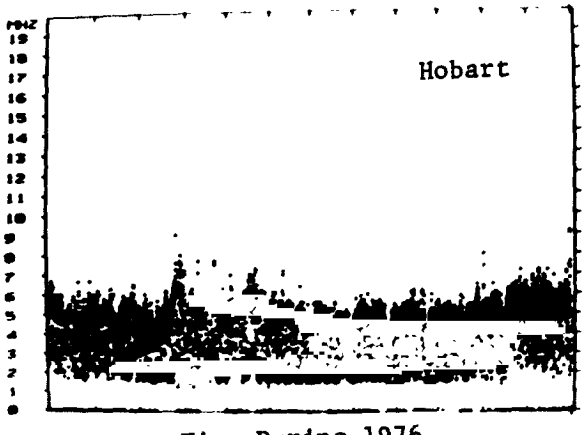

Time During 1976

Fig. 7c. Same at Hobart

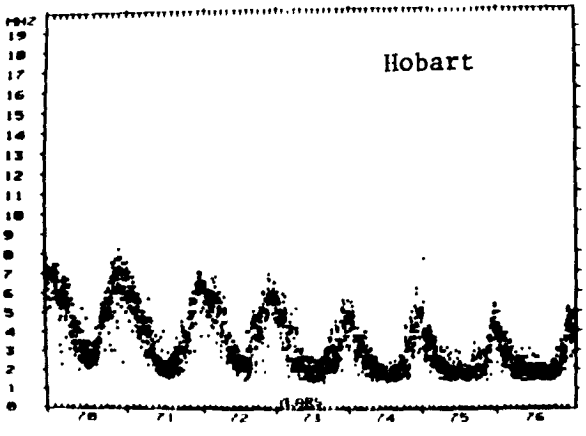

Fig. 8c. Same at Hobart.

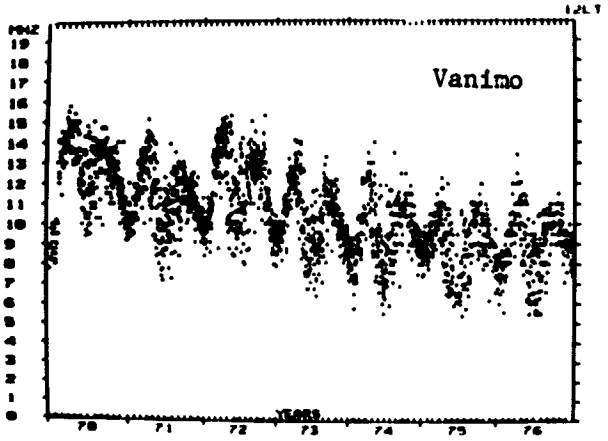

Fig. 9a. Noon hourly foF2 values at Vanimo.

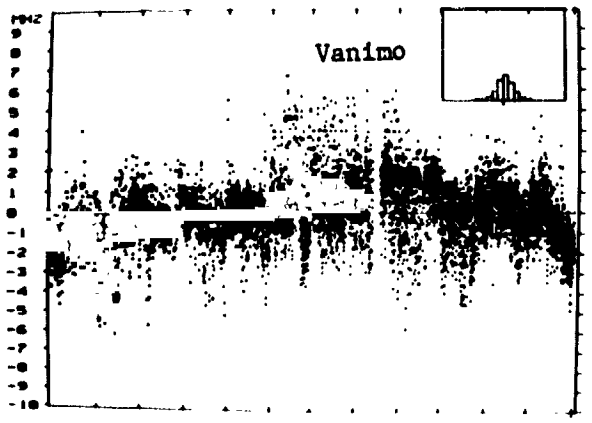

Time During 1970

Fig. 10a. Observed hourly foF2 values minus the predicted monthly foF2 medians.

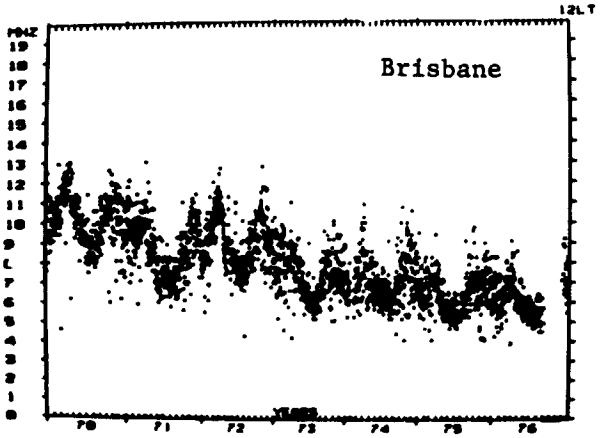

Fig. 9b. Same at Brisbane.

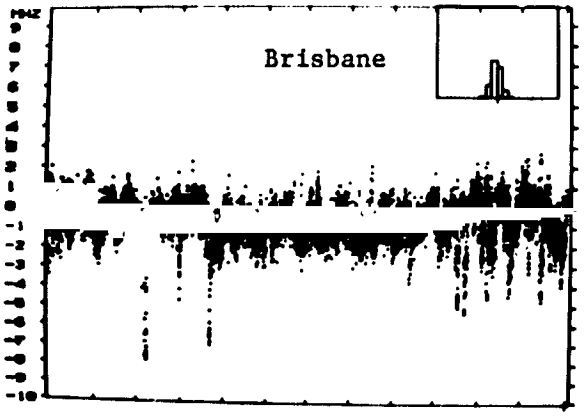

Time During 1970

Fig. 10b. Same at Brisbane.

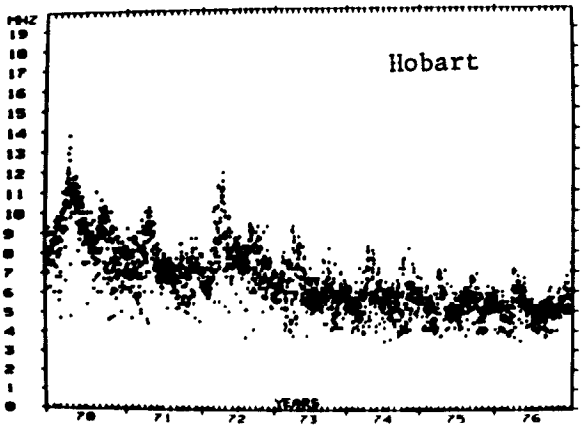

Fig. 9c. Same at Hobart.

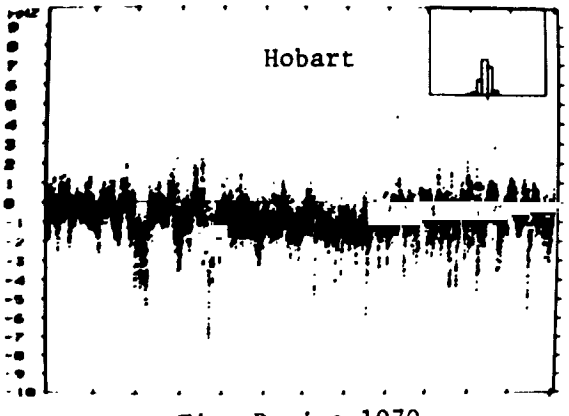

Time During 1970

Fig. 10c. Same at Hobart.

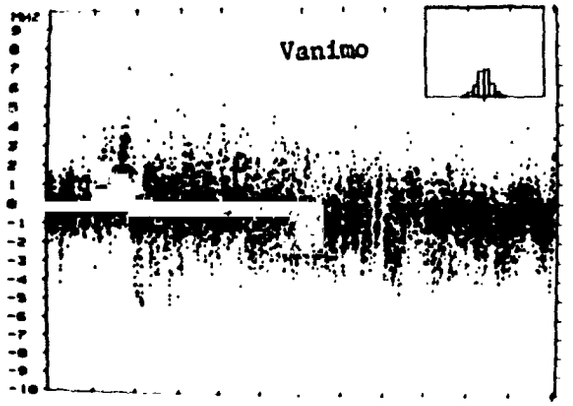

Time During 1976

Fig. 11a. The same as Fig. 10, except for 1976.

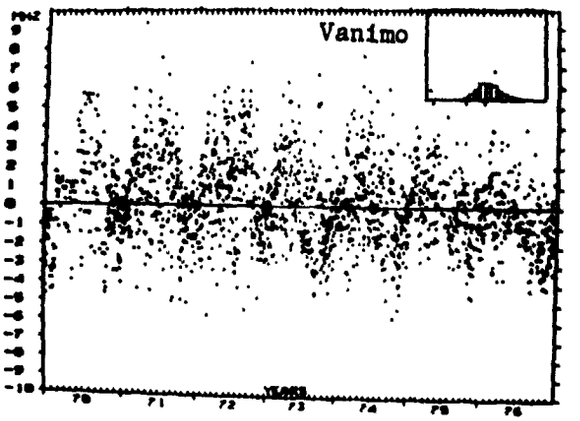

Fig. 12a. Difference between the observed and predicted foF2 values for midnight at Vanimo.

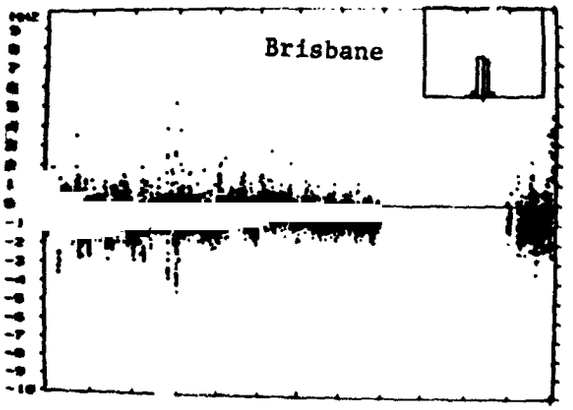

Time During 1976

Fig. 11b. same for Brisbane.

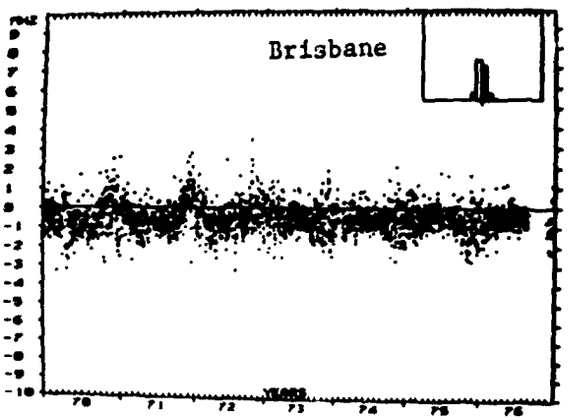

Fig. 12b. Same for Brisbane.

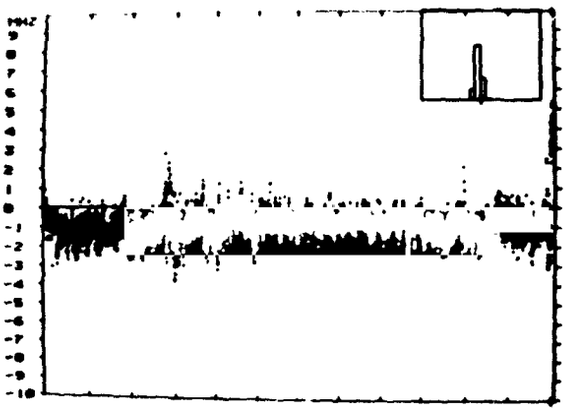

Time During 1976

Fig. 11c. Same for Hobart.

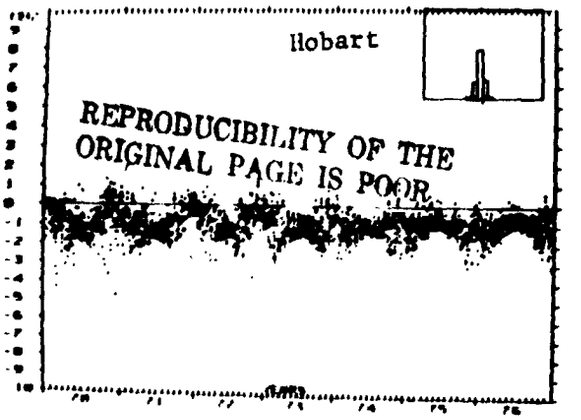

Fig. 12c. Same for Hobart.

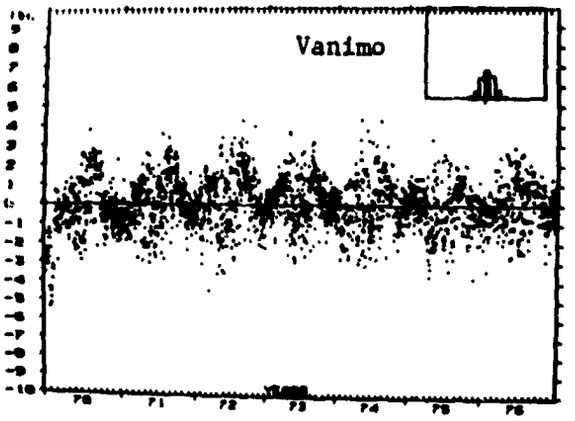

Fig. 13a. Difference between the observed and predicted foF2 values for noon at Vanimo.

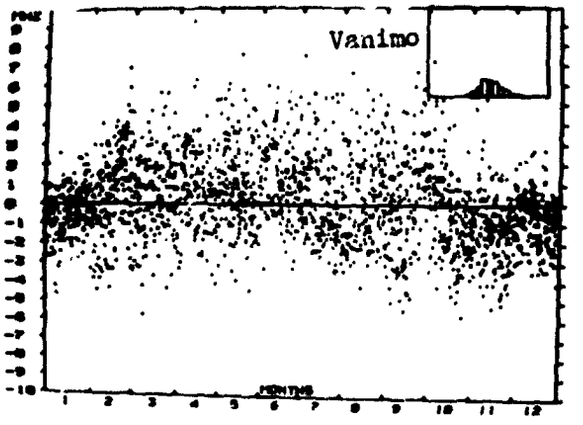

Fig. 14a. Season plot of the data in Figure 12 for midnight at Vanimo.

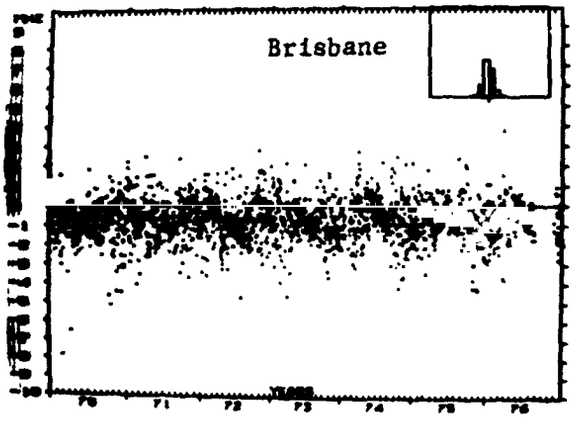

Fig. 13b. Same at Brisbane.

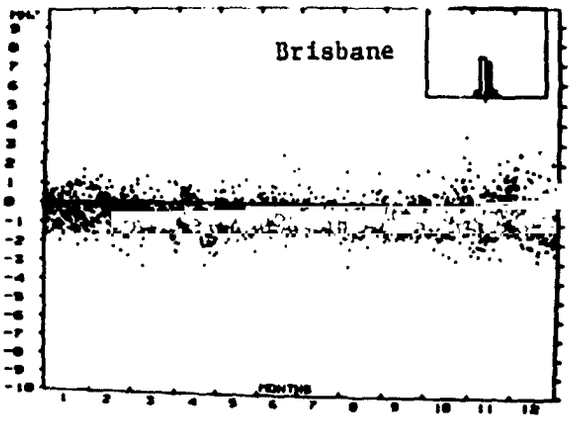

Fig. 14b. Same at Brisbane.

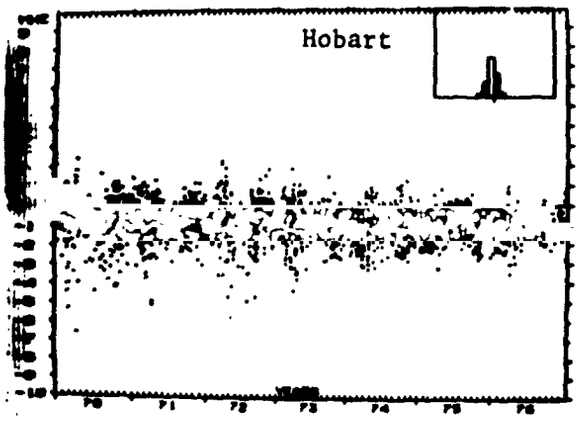

Fig. 13c. Same at Hobart.

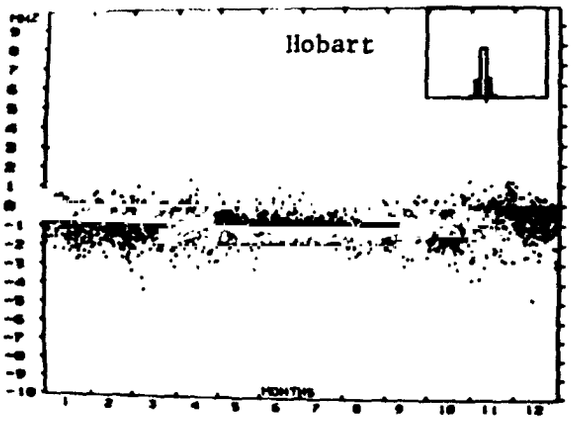

Fig. 14c. Same at Hobart.

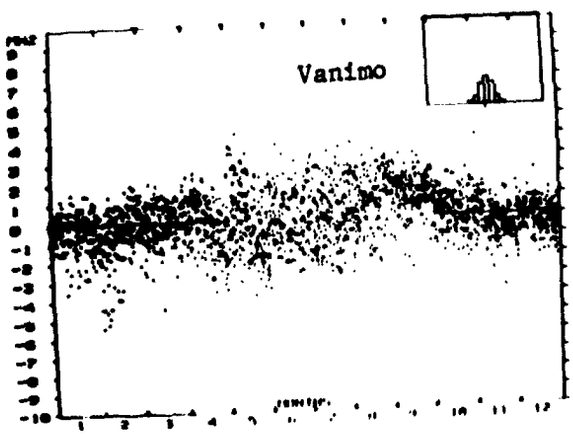

Fig. 15a. Seasonal plot of the data in Fig. 12.

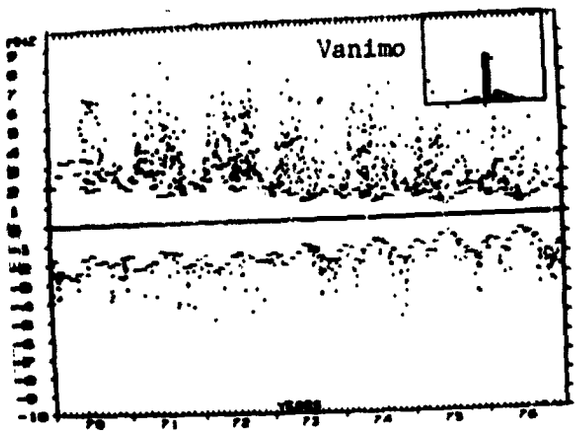

Fig. 16a. Plot of foF2 prediction errors outside the upper and lower deciles for midnight at Vanimo.

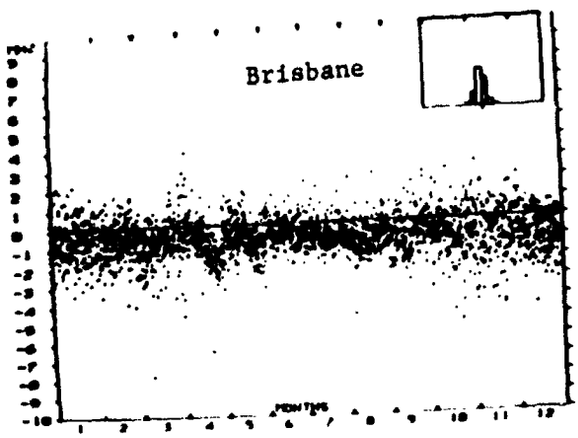

Fig. 15b. Same for Brisbane.

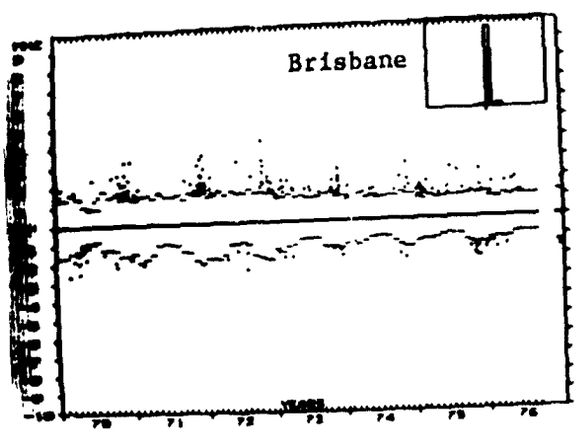

Fig. 16b. Same for Brisbane.

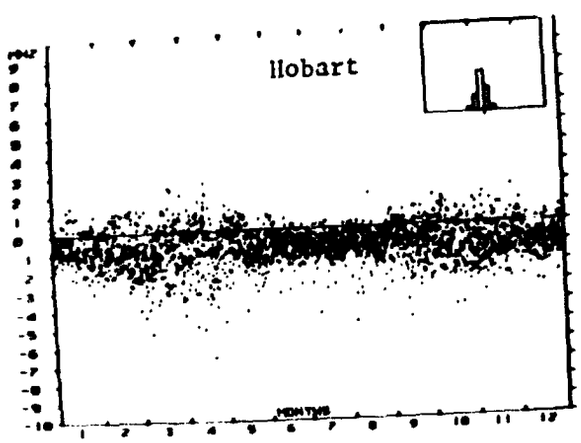

Fig. 15c. Same for Hobart.

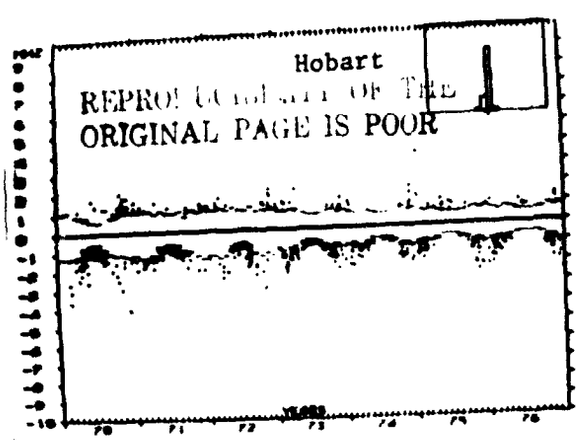

Fig. 16c. Same for Hobart.

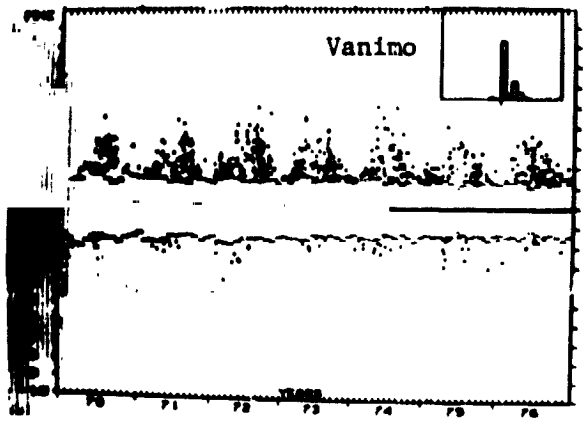

Fig. 17a. Same as Fig. 16 except at noon.

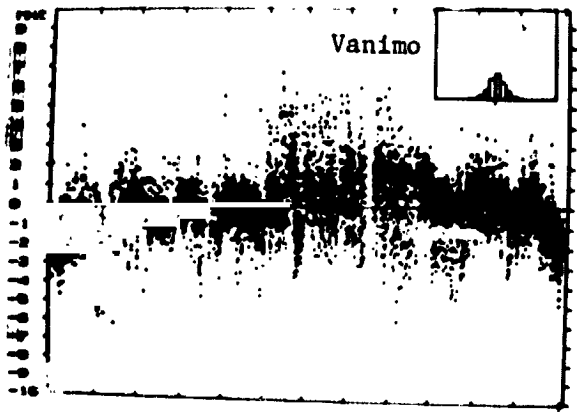

Time During 1970

Fig. 18a. Same as Fig. 10 except data, recorded when the Toclang K index was $\geq$ 3, were excluded.

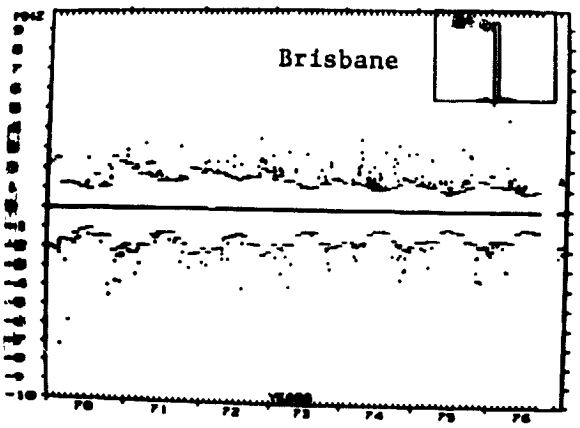

Fig. 17b. Same for Brisbane.

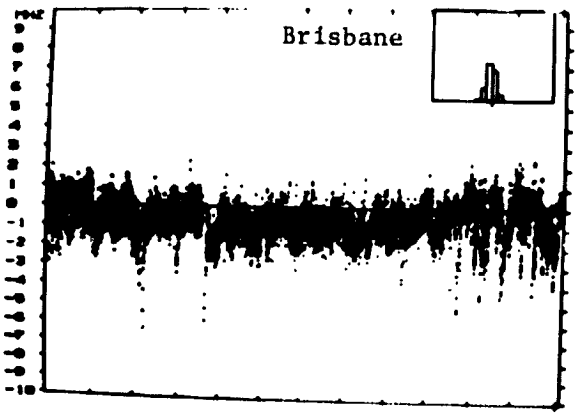

Time During 1970

Fig. 18b. Same for Brisbane.

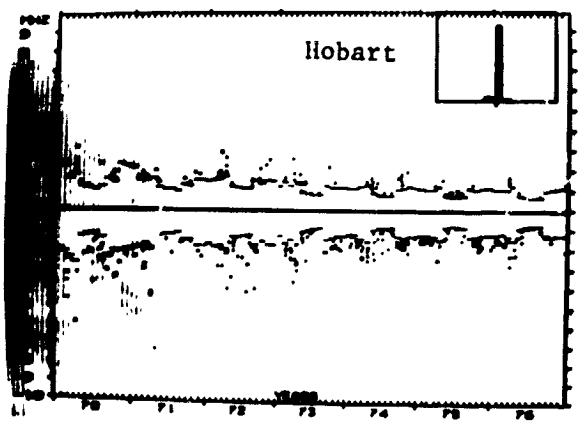

Fig. 17c. Same for Hobart.

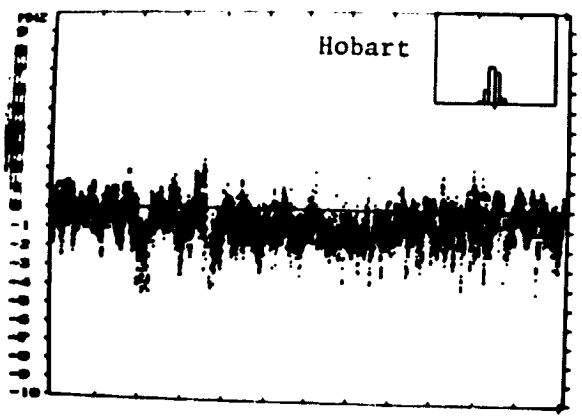

Time During 1970

Fig. 18c. Same for Hobart.

applied.

1. New information may be added to identify periods when observed behaviour will deviate from predicted behaviour. Two solar parameters will be considered here: the 10cm flux, indicative of solar electromagnetic radiation incident on the ionosphere and the K index, indicative of the effects of solar particle fluxes observed at the earth's surface.

2. As mentioned earlier, the time series in Figures 10 and 11 show considerable structure. Knowing past structure, it should be possible, to a certain extent, to anticipate future structure. Furthermore, the Brisbane and Hobart time series are sufficiently similar to make projections from one location to another reasonable. The second method therefore consists of projecting past data to a future time, or current data to a remote location in an attempt to reduce the 'noise level' in the predictions.

4.1 Introducing new information

It is well known that large depressions of foF2 may occur as the high and mid latitude ionospheres respond to changes in the solar wind arriving at the earth. These changes are paramaterized here by the K index for Toolangi. Figure 18 shows deviations recorded when the Toolangi K index was less than 3 during 1970. These can be compared with Figure 10 where all the available data was used. In general, the overall noise is reduced slightly with many extreme values being removed. This is more effective for the mid-latitude stations than Vanimo.

The K index effects are more obvious in Figure 19 where only data for $K \geqslant 3$ are plotted. For Brisbane and Hobart the main effects of ionospheric storms, causing depressed foF2 values, are very clear. For Vanimo the K index information is rather less useful as an indicator, the range of deviations in foF2 being both positive and negative.

Thus being able to anticipate the K index in advance may enable the large excursions of foF2 from predicted values to be anticipated. (This is a convenient method of warning communicators of the likelihood of an ionospheric storm and the extent to which it will affect communications circuits.)

Variations in intensity of the ionizing radiation from the sun may also cause variations in foF2 (McNamara, 1976). This hypothesis is hard to present in the diagramatic fashion used in this paper as no completely reliable method exists to convert a solar flux parameter (the Ottawa 10cm flux, in this case) into a daily ionospheric index that is compatible with the IPS prediction method. Figure 20a shows a plot of daily changes from the monthly mean 10cm flux value (vertical axis) compared with changes in the 12LT foF2 values from the predicted median values for 1970 for midday. While there is a correlation of 0.3 for this data, it is not significant. A similar comparison for 1976 data (Figure 20b) which gave a correlation of 0.02 supports this hypothesis. Thus, while long term changes in 10cm flux can be related to changes in foF2 medians, there is little apparent evidence for day-to-day variations being highly correlated with the changes in foF2. This does not preclude any effect, though it suggests that 10cm flux departures would need to be quite large before associated foF2 departures would be observed. Such large departures are responsible for the presence of any correlation in the 1970 data.

It can be concluded that while some additional information may be

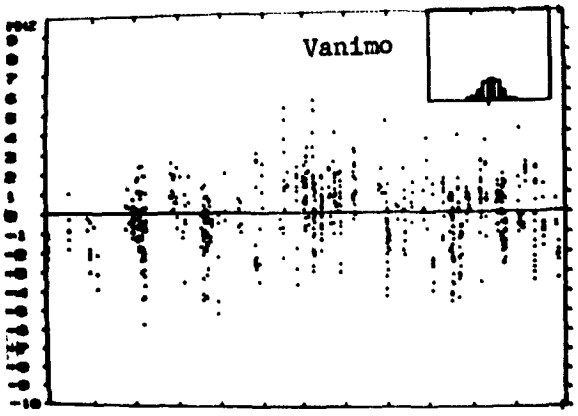

Time During 1970

Fig. 19a. Like Fig. 10 except data, recorded when the Toolang: K index was < 3, were excluded.

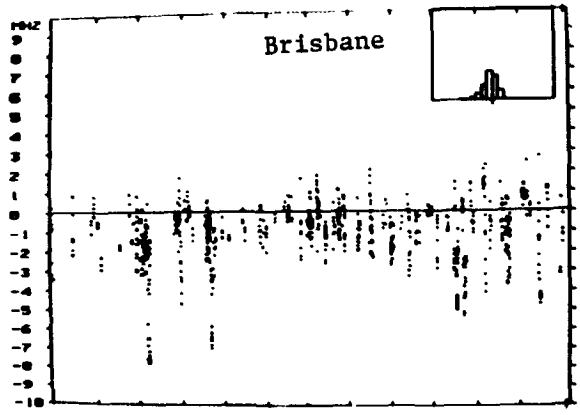

Time During 1970

Fig. 19b. Same for Brisbane.

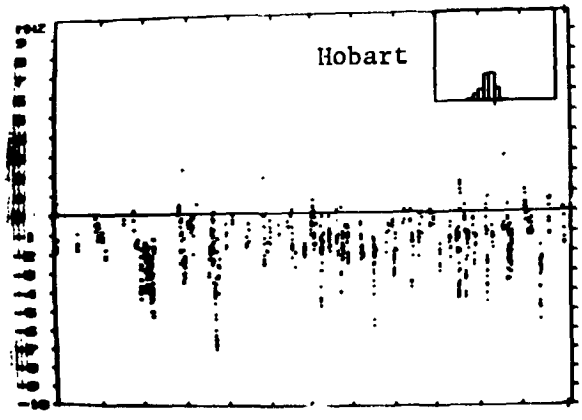

Time During 1970

Fib. 19c. Same for Hobart.

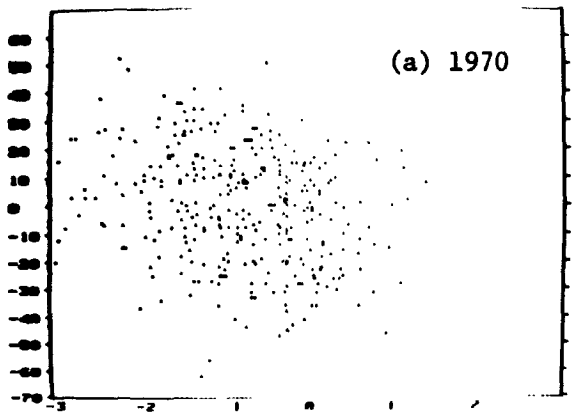

foF2 Deviations, MHz.

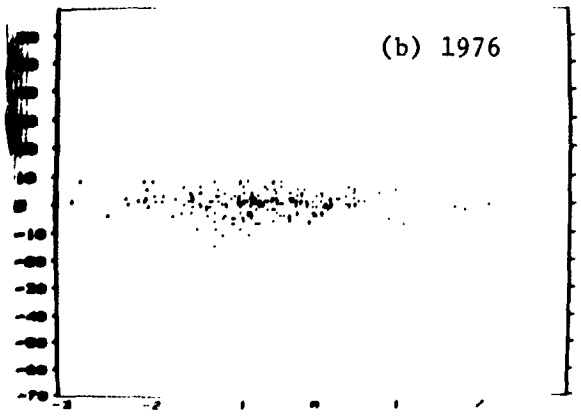

foF2 Deviations, MHz

Fig. 20. Plots of changes in the daily Ottawa 10 cm solar flux with respect to the monthly average (vertical axis, ranging ± 70 solar radio flux units) against deviations in foF2 from the predicted median behavior (horizontal axis, range ± 3 MHz) for (a) 1970 and (b) 1976.

obtained using the K index and 10cm flux observations, in general they will not greatly improve the overall noise level in daily predictions.

4.2 Projecting Data forward in Time and Space

The second approach utilises previously recorded data either at the locations being studied or at some other remote location.

The average condition of the ionosphere at a particular time (and/or place) will vary in the known predictable median fashion. This effect can be removed and predictions made using the deviations from the predicted monthly median foF2, rather than the actual recorded foF2 values.

It is not reasonable to assume that the cause of a deviation from predicted median behaviour at one location (in time and space) will have exactly the same effect at some other location. For instance, the observed ionospheric response to travelling disturbances depends on the electron density gradient which changes during the day and from place to place. This evidently results in travelling disturbances having less effect on foF2 at night compared with daytime. While some scaling factor should be introduced to compensate for this, it is not currently possible to set sensible limits on the proposed effect. In the present work, the ionospheric response is assumed constant.

The simplest case for projection forward in time is considered. The recorded deviation from median behaviour as observed at some particular time is assumed the same as that which will be observed at some future time. Two lead times are illustrated; a one hour lead in Figure 21 and a 24 hour lead in Figure 22. In both Figures, all the data for 1970 is displayed. Figures 23 and 24 give the same data, only now it is folded into 24 hours so that the diurnal variation in spread is more apparent.

It could be argued that projecting percentage departures from median behaviour would be more satisfactory, but as there was no clear diurnal variation in the size of the departures this was not considered necessary.

While a lead of 1 hour (Figures 21 and 23) reduces the spread in values compared with those in Figure 10, its effects are possibly not as great as might have been expected. In fact, for Vanimo the spread is still greater than experienced for the mid-latitude stations when deviations from the predicted medians are considered.

The results for a lead of 24 hours (Figures 22 and 24) are rather disappointing, the spread now being only slightly less than for the monthly predictions. This is partly due to a failure to deal adequately with ionospheric storm data, the time series in Figure 22 being quite spikey (for Brisbane and Hobart) because of this. The effect shows up more clearly in Figure 24 as a halo of extreme deviations for daytime hours superimposed on a relatively structureless background. For Vanimo the day-to-day spread in observed differences is quite large, giving a further indication of the difficulty in predicting the behaviour of foF2 at this location. It also helps explain some of the difficulty experienced in predicting the monthly medians for Vanimo (see Figures 4 and 5).

Different lead times (3, 6 and 12 hours) are illustrated for only one station, Brisbane, in Figure 25. It is apparent that for lead times greater than one hour there is only a slight advantage over the median prediction, the effects of ionospheric storms becoming more evident, while the background

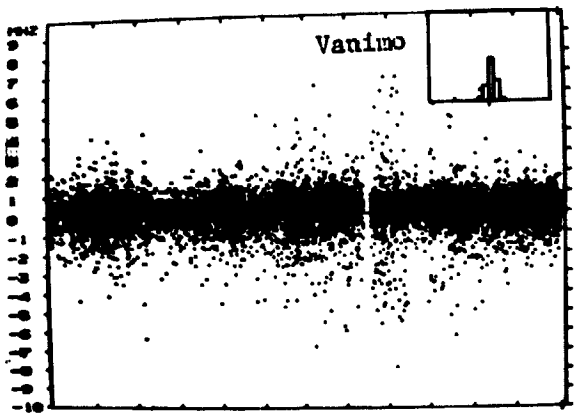

Time During 1970

Fig. 21a. Projection of foF2 of recorded deviations from predicted median behavior with one hour lead time.

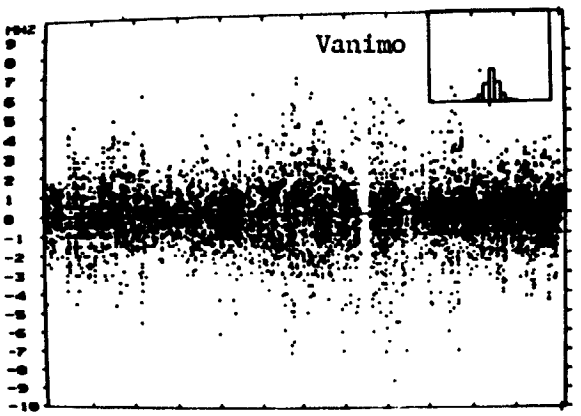

Time During 1970

Fig. 22a. Projection of foF2 with a 24-hour lead time.

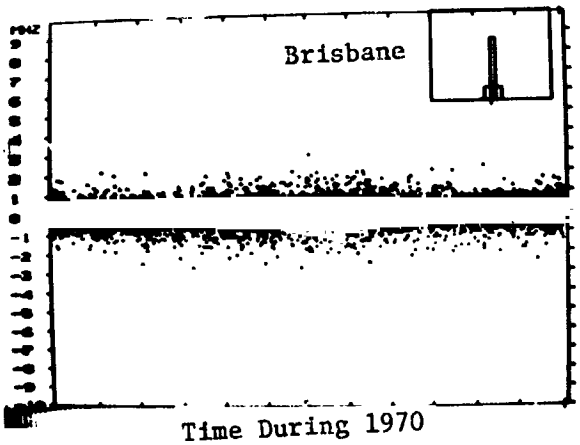

Time During 1970

Fig. 21b. Same for Brisbane.

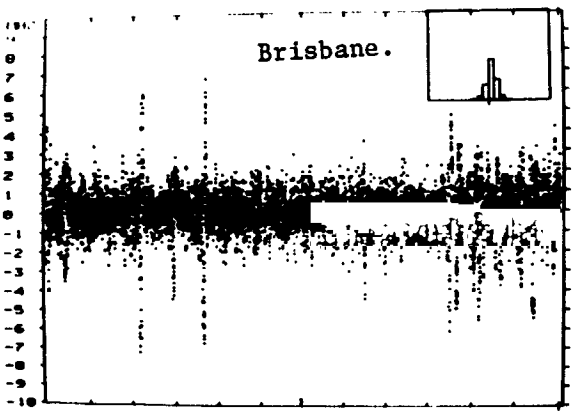

Time During 1970

Fig. 22b. Same for Brisbane.

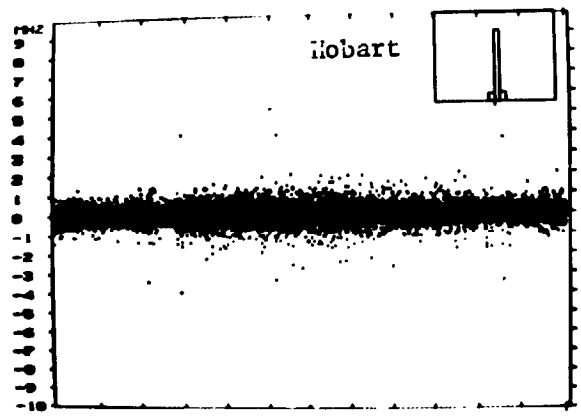

Time During 1970

Fig. 21c. Same for Hobart

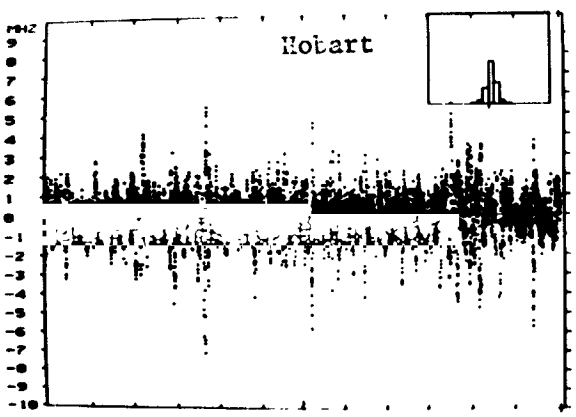

Time During 1970

Fig. 22c. Same for Hobart.

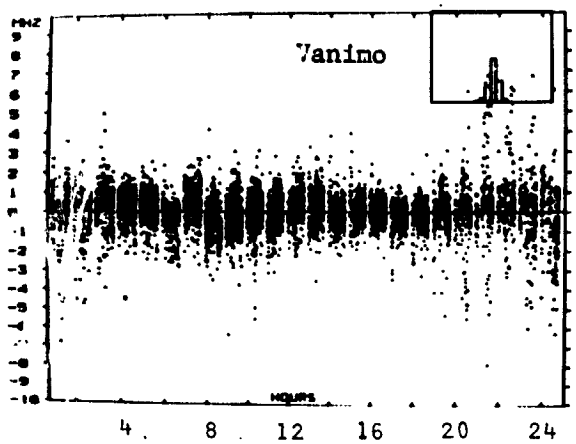

Fig. 23a. Diurnal plot of data in Fig. 21.

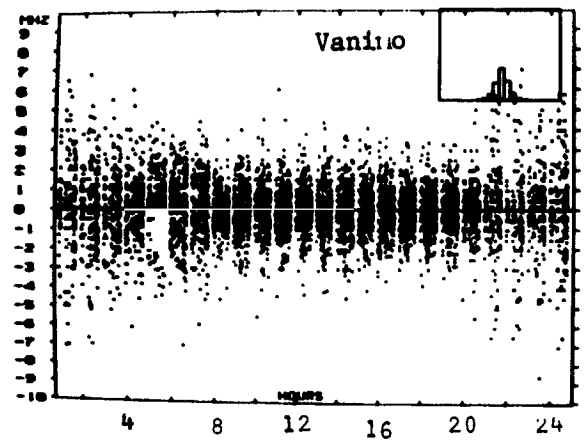

Fig. 24a. Diurnal plot of data in Fig. 22.

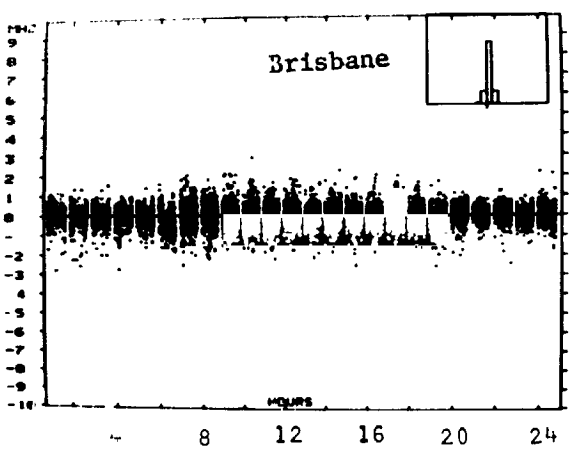

Fig. 23b. Same for Brisbane.

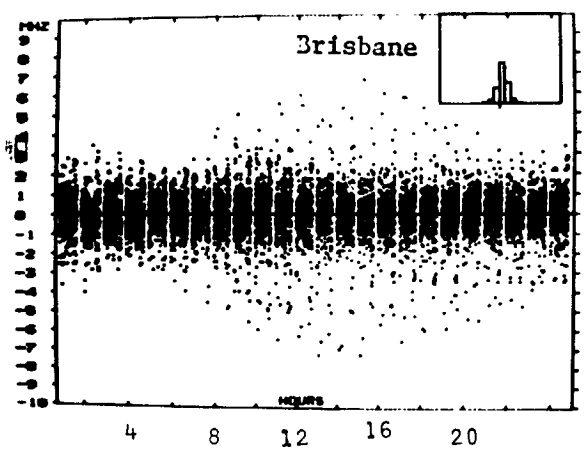

Fig. 24b. Same for Brisbane.

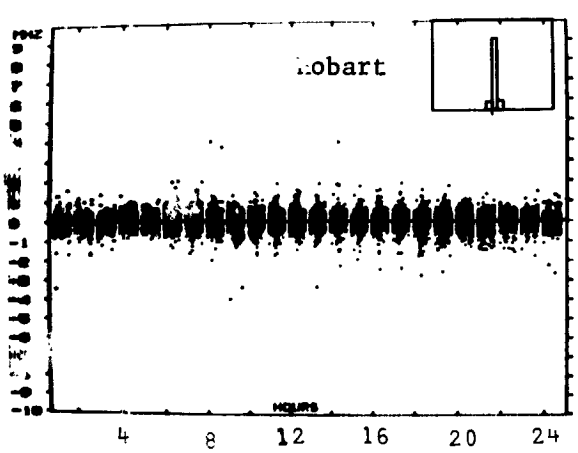

Fig. 23c. Same for Hobart.

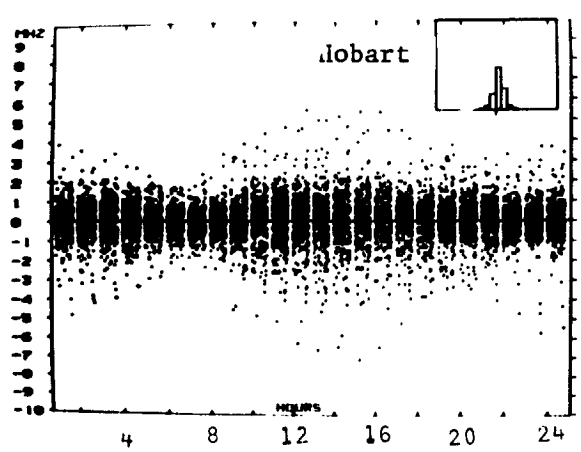

Fig. 24c. Same for Hobart.

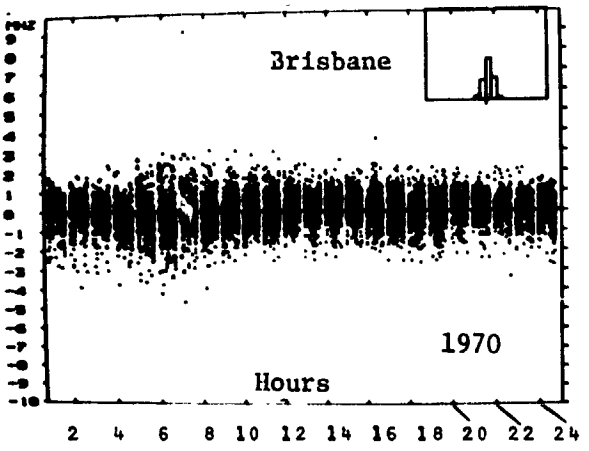

Fig. 25a. Projections with three hours lead.

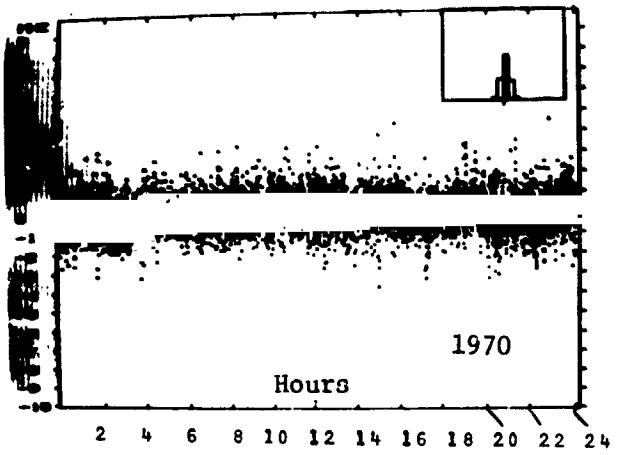

Fig. 26b. Comparing Brisbane and Norfolk Island data with the same local time.

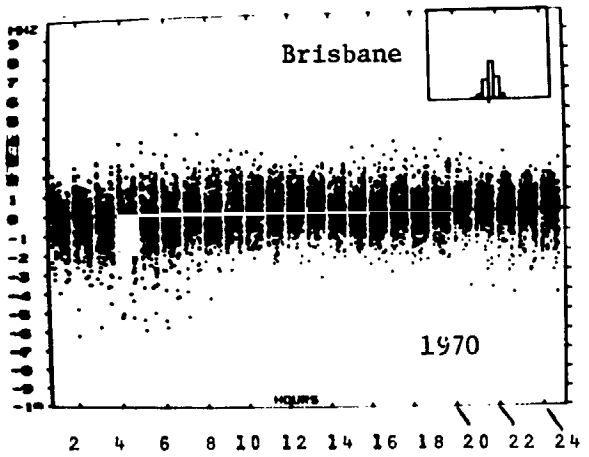

Fig. 25b. Projections with six hours lead.

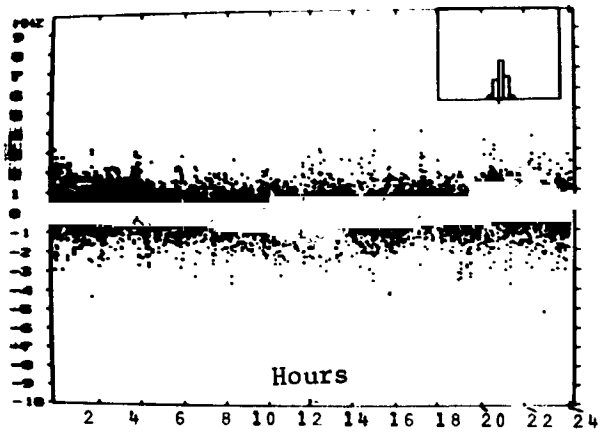

Fig. 26c. Projecting Norfold Island to Brisbane with a 1 hour lead.

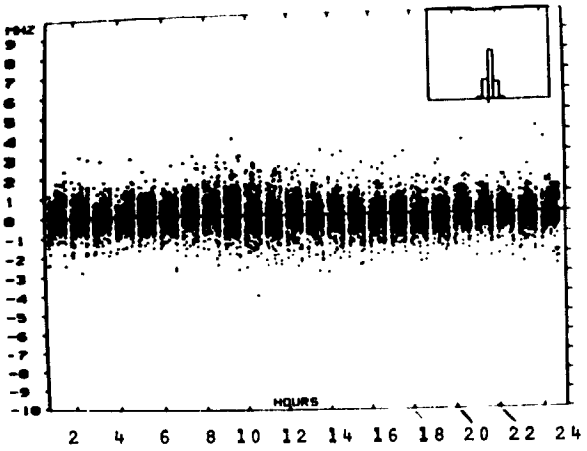

Fig. 26a. Projecting Brisbane data to Norfolk Island with an hour lead.

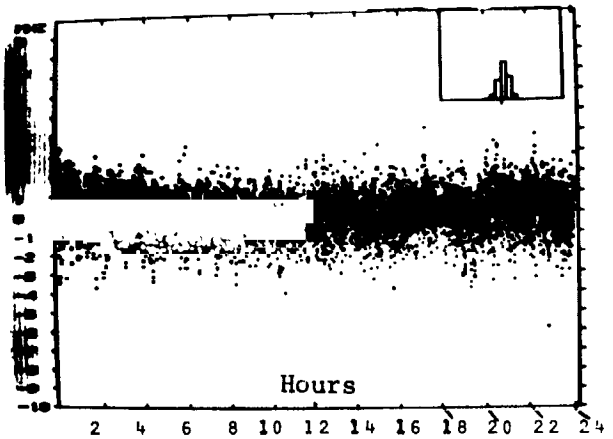

Fig. 26d. The same as Fig. 26c with a 2 hour lead.

spread in deviations also increases.

Using this simple projection model it is evident that while previous data will eliminate gross errors in the predicted index of solar activity, (errors that are not discussed in this paper), it is not until the lead time is reduced to less than 3 hours that this technique can be considered effective. For such short lead times the effects of ionospheric storms and, to some extent, travelling disturbances will be allowed for. However, as many travelling disturbances have periods of the order of one hour or less, probably insufficient information will be available to greatly improve on this even if more careful analysis techniques are used. It could be more necessary to obtain data sampled more frequently than once per hour before significant improvements on this result are obtained.

Most prediction systems requiring improved local predictions also require these predictions to be extended to more remote regions. As with time projections, the simplest approach is to project deviations from the predicted median behaviour at the known location to the required region. This will be adequate for improving on the predicted solar index and allowing for ionospheric storms. The latter will be most effective for regions with the same geomagnetic latitude (McNamara, 1977). As an example of this, the deviations recorded at Norfolk Island are projected to Brisbane. For behaviour that is constant in local time, the deviations at Norfolk Island should lead Brisbane by just over one hour. (Because Norfolk Island data is recorded on 180°MT the lead is two hours for the data used here.) For greater lead times both time and space projections are mixed together. Figure 26 gives a series of different lead times for predicting Brisbane using Norfolk Island and also Norfolk Island using Brisbane. The best results are recorded for data at Norfolk which leads Brisbane data by 1 hour in local time, as anticipated. The spread in deviations is equivalent to a two hour lead time projection for Brisbane data, which might be expected because the projection technique will not allow for travelling disturbances.

Thus, using simple projection methods the 'noise level' in the predictions is reduced, though no substantial improvements are obtained.

5. CONCLUSION

In general, for mid-latitudes, monthly predictions of median foF2 values can be accomplished quite successfully for medium and low solar activity. The spread in recorded hourly values is adequately indicated by the predicted deciles and this spread is not greatly reduced by utilizing past data. Evidently, to significantly reduce the 'noise level', rather more skilful techniques must be applied. One example of skill is the prediction of ionospheric storms, which if successful in both timing and amplitude, will reduce the large depressions observed in foF2.

The low latitude (Vanimo) data was particularly variable and the spread was greater for all categories discussed.

6. THE DIAGRAMS

In addition to the time series plots, for all comparisons a histogram with the same resolution as the vertical axis is plotted in the top right hand corner. It is normalised by the total number of entries thus giving a probability of occurrence of deviations between two scale divisions. The amount of data that was not included because only a descriptive replacement letter was scaled is shown at the side of the histogram. The complete histograms may be obtained from the author if required.

Table 1 gives some information on the stations used in obtaining the diagrams in this paper.

TABLE 1 IONOSPHERIC STATIONS DISPLAYED IN DIAGRAMS

STATION	GEOGRAPHIC COORDINATES		GEOMAGNETIC COORDINATES		GEOMAGNETIC SPLIT (MHz)
Vanimo	2.7S	141.3E	12.6S	211.1E	0.4
Brisbane	27.5S	152.9E	35.4S	228.6E	0.6
Norfolk Is.	29S	168E	34.8S	243.2E	0.5
Hobart	42.9S	147.2E	51.7S	224.3E	0.7
Mawson	67.6S	62.9E	73.1S	102.9E	0.8

Acknowledgements: I wish to thank Mr. D. Carrington, University of New South Wales, for his assistance in copying the data used in this paper from magnetic tape to RK05 disk for use on the IPS PDP11/10 computer.

REFERENCES

McNamara, L. F. (1976): The Correlation of individual values of foF2 and M(3000)F2 with the solar 10.7cm flux under magnetically quiet conditions. Ionospheric Prediction Service Series R 30.

McNamara, L. F. (1977): Ionospheric storm effects on maximum usable frequencies on circuits around Australia. Ionospheric Prediction Service Series R35.

Sargent, H. H. (1978): A Prediction for the next solar cycle. IEEE Vehicular Technology Conference.

D34-46

N80-18486

A WEEKLY IONOSPHERIC INDEX

J. F. Turner and P. J. Wilkinson
Ionospheric Prediction Service
Australian Department of Science and the Environment
Darlinghurst, 2010, N.S.W., Australia

ABSTRACT

For some years the Ionospheric Prediction Service has used a weekly T index as a monitor of the global ionosphere and an aid for predicting the monthly T index. Both the monthly and weekly T indices are discussed and some possibilities for improving the reliability of the weekly T index are considered including extending its applicability to daily variations of the global ionosphere.

1. INTRODUCTION

For the purposes of H.F. prediction the Australian Ionospheric Prediction Service (IPS) uses a monthly ionospheric index produced from the average of the 24 hourly median foF2 values for selected ionospheric stations and the Zurich twelve-month smoothed sunspot numbers. This index, the T index, is the basis of the IPS prediction maps. For prediction purposes, there is usually too great a lag between the calculation of the monthly index and the period for which the next prediction is required. To bridge this gap a weekly index was produced and has been found very useful over the past 10 years. This weekly index is based on the IPS prediction maps and hence on the monthly T index. As groundwork for discussion, the prediction maps and the monthly index are reviewed briefly before the weekly T index is discussed. More details are available in Turner, 1968.

2. THE MONTHLY T INDEX

Using an ionospheric parameter (the average of the 24 hourly median foF2 values for a month) and a solar parameter (the 12-month smoothed Zurich Sunspot number), an ionospheric index is derived by an iterative process.

At each station, given in TABLE 1, a first order relation is found. For the i^{th} station it is of the form,

$$S(t) = m_i F_i(t) + c_i$$

where $S(t)$ is the solar parameter, R_{12}

$F_i(t)$ the ionospheric parameter, all the average of the 24 hourly median foF2 values for a particular mon+h

m_i, c_i regression coefficients.

These relations are used to derive a hemisphere T index by finding the station T index for each data point,

$$tji = m_i F_i + c_i$$

where tji is the station index for the j^{th} iteration.

The hemisphere index, TjH, is then found by averaging the appropriate station T indices,

$$TjH = \frac{1}{N} \sum_{i}^{N} tji.$$

For the first iteration the solar parameter used is R_{12}, but on successive iterations this is replaced by the new solar parameter, the hemisphere T index, TjH. Iterations are continued until a stable T_H is obtained.

Finally, the global T index is obtained by averaging the northern and southern hemisphere T indices. This is now the monthly T index.

Usually three to five iterations are required. Allowance is made for high levels of solar activity, where the first order relation is less reliable, by weighting against this data in the first two iterations.

The averaging in the final step minimises the seasonal dependencies in the index resulting from differences between the two hemispheres and from any imbalance in the number of stations selected from each hemisphere.

The process used is similar to that used for calculating IF2 (Minnis and Bazzard, 1960) with three basic additions. The ionospheric and solar parameters are chosen to reduce the scatter, both being less variable than their IF2 equivalents. Rather than a single cycle, iterations are continued until the new solar activity parameter remains constant. Finally, whereas a global index is calculated in one step for IF2, differences between the two hemispheres are minimised in calculating the T index by averaging indices calculated for each hemisphere.

The index derived by the above method is called the monthly T index and is used in constructing the IPS prediction maps.

TABLE 1. STATIONS USED FOR THE MONTHLY T INDEX

	Station	Geographic Coordinates
1	Adak	N51.9 W176.6
2	Fairbanks (College)	N64.9 W147.8
3	Freiburg	N48.0 E7.8
4	Kiheri (Maui)	N20.8 W156.5
5	Moscow	N55 E37
6	Okinawa	N26.3 E127.8
7	Tokyo	N35.6 E139.7
8	Wallops Is./ Washington	N37 W75
9	Brisbane	S27 E153
10	Canberra	S35 E149
11	Capetown	S34.2 E18.3
12	Christchurch	S43 E172
13	Falkland Is (Pt Stanley)	S51.7 W57.7
14	Hobart	S43 E147
15	Johannesburg	S26.2 E28.0
16	Mundaring/Watheroo	S32 E116

The process used is similar to that used for calculating IF2 (Minnis and Bazzard, 1960) with three basic additions. The ionospheric and solar parameters are chosen to reduce the scatter, both being less variable than their IF2 equivalents. Rather than a single cycle, iterations are continued until the new solar activity parameter remains constant. Finally, whereas a global index is calculated in one step for IF2, differences between the two hemispheres are minimised in calculating the T index by averaging indices calculated for each hemisphere.

The index derived by the above method is called the monthly T index and is used in constructing the IPS prediction maps.

For all available ionosonde station data, the first order least-squares-fit line is found between the monthly T index and the median F region critical frequency for each hour of the day and month of the year. Using the fitted line two values are recorded, the median foF_2 value for T=0 and T=100. (These points are roughly equivalent to sunspot numbers 0 and 100.) These values are then used to construct the IPS F region prediction maps - there being 576 in all (24 hours x 12 months x 2 levels of solar activity) which, together with maps of M(3000)F2, are used to make monthly HF predictions for F region modes.

3. THE WEEKLY INDEX

One of the main reasons for developing the T index and the IF2 index was to allow data recorded in different solar activity cycles to be combined. While the monthly T index is found valuable for resolving such problems, allowing full use to be made of almost all of the recorded ionospheric data, it is not entirely satisfactory for prediction purposes. The time lag resulting from using the 12 month mean Zurich sunspot number together with delays in obtaining station data result in unrealistic lead times for predicting the monthly T index. To reduce this lead time an index was developed based on recorded hourly values at a number of stations.

The data consist of the foF2 values for the four hours (0, 6, 12 and 18 UT) for 26 ionosonde stations (TABLE 2.). This data is made available through the URSIGRAM data exchange system usually within a few days of being recorded.

TABLE 2. STATIONS USED FOR THE WEEKLY T INDEX.

	Station	Geographic Coordinates
1	Ouagadougou	N12 W02
2	Slough	N51 W01
3	Lannion	N48 W03
4	Dakar	N15 W17
5	Wallops Is	N37 W75
6	Boulder	N40 W105
7	Poitiers	N46 E00
8	Lindau	N51 E10
9	Kiruna	N68 E20
10	Djibouti	N12 E43
11	Moscow	N55 E37
12	Alma Ata	N43 E77
13	Irkutsk	N52 E104
14	Kokubouji (Tokyo)	N36 E139
15	Raratonga	S21 W159
16	Mawson	S68 E63
17	Mundaring	S32 E116
18	Vanimo	S03 E141
19	Townsville	S19 E147

TABLE 2. continued.

	Station	Geographic Coordinates
20	Brisbane	S27 E153
21	Canberra	S35 E149
22	Hobart	S43 E147
23	Norfolk Is	S29 E168
24	Christchurch	S43 E172
25	Campbell Is	S52 E169
26	Scott Base	S77 E166

Using this data base and the maps described in the previous section a daily ionospheric index can be derived. For each station monthly predictions for T=0 and T=100 are obtained. These are used to produce two time series for which the fourier components are found. The fourier components of the time series are then used as a convenient interpolation for finding the T=0 and T=100 predictions for any day of the year for each of the UT times of interest. Using these fourier components the recorded data is then converted into a T index by interpolation between the T=0 and T=100 levels of activity, assuming a first order relationship. Figure 1 gives a plot of T indices derived in this way for 1976. As can be seen values range from -100 to +160, the range being marginally less in the equinoxes.

Figure 2 gives an indication of the relationship between magnetic conditions, represented here by the average of the eight daily K indices for Toolangi, solar electromagnetic radiation, represented by the 10.7 cm flux level observed at Ottawa and the daily T index. The T index shown is the average of the station T indices for a day with the length of the bar being twice the standard deviation of the mean for the sample.

During 1976 the geomagnetic disturbances were due to recurrent storms and the solar electromagnetic radiation output was reasonably constant, the daily 10.7 cm flux varying between 60 and 70 flux units during the year. Gross features in these two parameters can be related to the daily T index, increases in the 10.7 cm flux causing increases in the daily T index and increases in the K index occurring at the same time as depressions in the daily T index.

For operational use the daily index is averaged over seven days to produce a weekly index. Experience has shown that the weekly T index, as described, is a useful measure of solar effects on the ionosphere, variations in the index being fairly easily related to known solar variations, as shown by figure 2.

Figure 1. All hourly T indices recorded for all Stations during 1976.

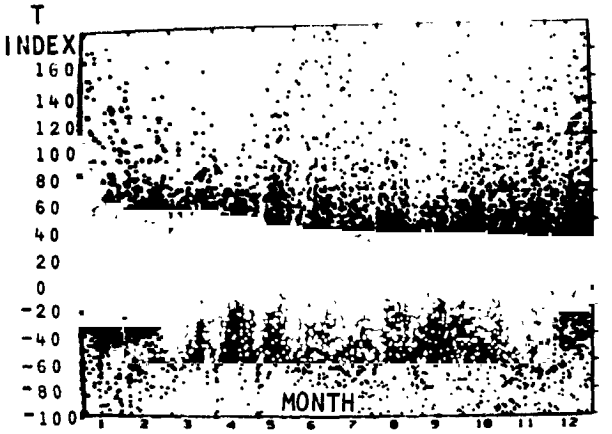

Figure 2. Daily T index, 10 cm flux and Toolangi K for 1976.

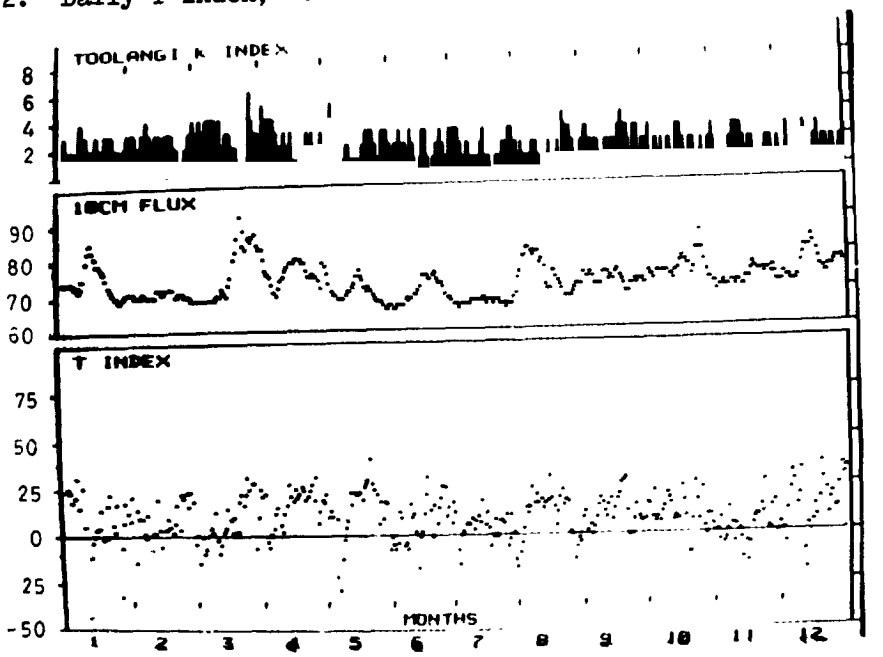

Figure 2(a). Weekly T index for same period.

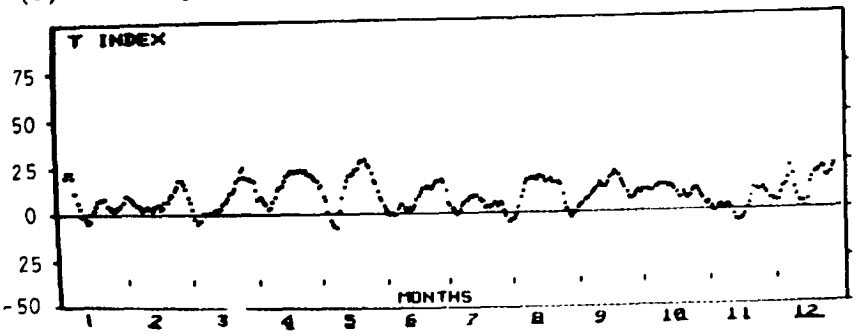

4. IMPROVEMENTS TO THE WEEKLY INDEX

The weekly index, as described in this paper, was initially conceived to improve predictions of the monthly index and also to meet the needs of some of IPS customers who wished to receive prediction updates with as short a lead time as was reasonable. For these purposes the index as described has proven valuable. However, in the course of preparing this paper it has become apparent that various improvements to the index may make it even more useful.

Experimentation has shown that for the 1976 data, provided about half the station data required is available, the daily index is as reliable as the seven day average, with the added advantage of potentially greater resolution. For this reason, all the diagrams presented in the paper have displayed the daily index rather than the weekly index. The results using the weekly index are the same with only a small decrease in the scatter of data points. However, it has not yet been possible to fully investigate the relationship between the two indices (daily and weekly) to decide whether the apparent improved resolution in the daily index is real or related to statistical fluctuations. There is some evidence to suggest that for higher levels of solar activity and with the addition of flare induced storms, as being experienced by the end of 1978, the daily index becomes very variable.

The data base used consists of four data points per day per station, the data being recorded at the same universal time for all stations. Provided the distribution of stations is adequate, this should produce a global average of the ionospheric effects for a particular change in solar output. While the evidence in Figure 2 suggests this is accomplished, it will be necessary to establish that the final result is representative of a global condition.

Using data derived from night-time foF2 values is also questionable as the variation due to solar activity is much less then, giving rise to greater errors. Figure 1 is repeated in figure 3c along with the same plot for only night-time data (figure 3a) and daytime data (figure 3b). The daytime plot shows less scatter suggesting a better index may be obtained either by careful screening of the data averaged, or by using only daytime data.

In calculating the monthly index allowance was made for differences between the two hemispheres. A similar approach is not adopted in calculating the weekly index. In figure 4a, a plot of the difference between the daily northern hemisphere T index and southern hemisphere index is given. To allow some estimate of the significance of this result, the difference between two daily indices constructed by dividing the available station data per day in half by selecting stations randomly is shown in figure 4b. No clear structure appears in figure 4b, though the scatter of points reduces near the equinoxes. In contrast, figure 4a shows a consistent difference between the two hemispheres which is least in the equinoxes. The source of this difference is clearly a seasonal difference between the two sets of data, but it is not clear why it still exists in the data as it should have been eliminated in calculating the station T indices. Further investigation will be required to clear this point up.

Figure 3(a). Daytime hourly station T indices.

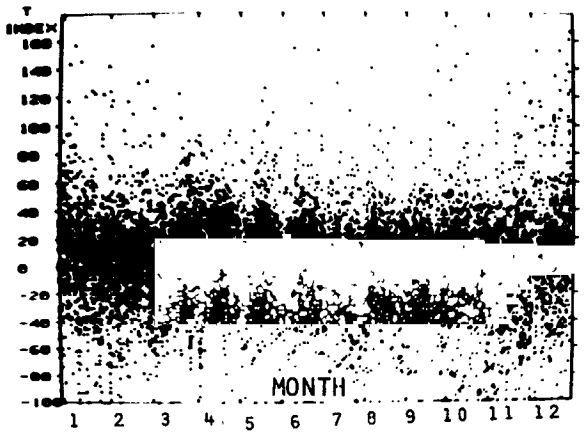

Figure 3(b). Night-time hourly station T indices.

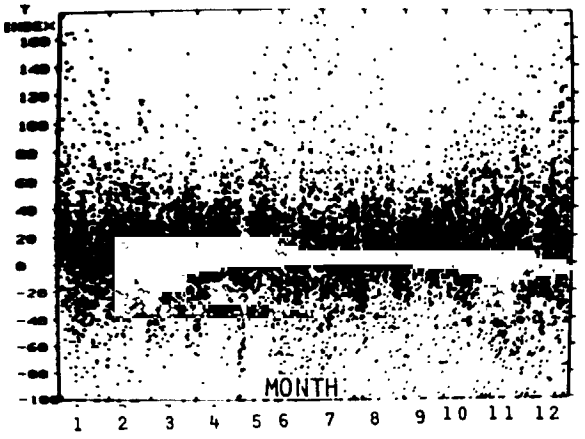

Figure 4(a). Daily T index. Northern Hemisphere-Southern Hemisphere T.

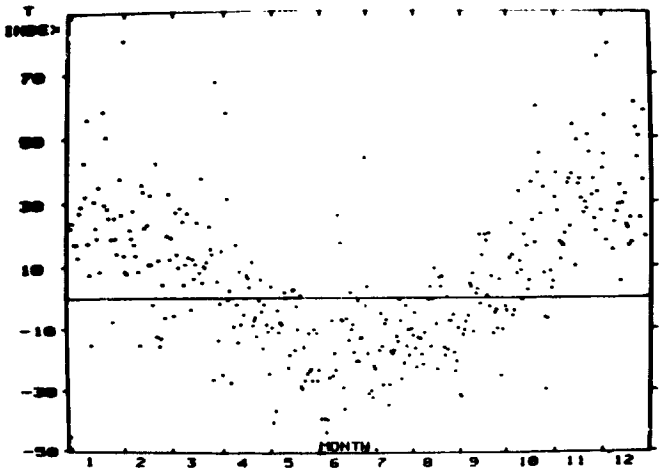

Figure 4(b). Daily T index. Difference between two random samples.

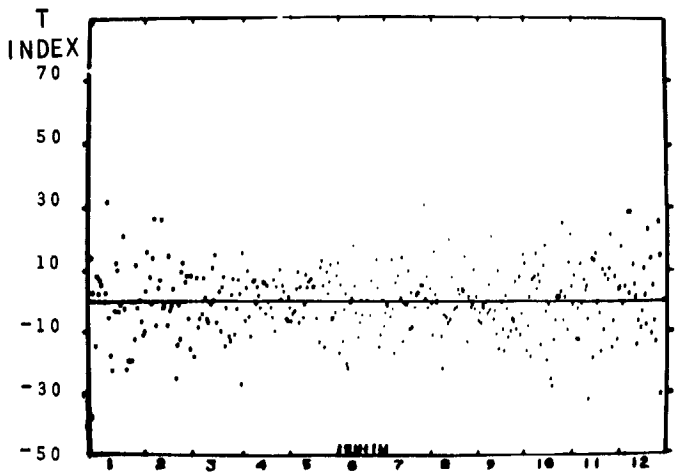

5. CONCLUSION

The weekly T index used by IPS for some years now has proven very useful, operationally, as an indication of conditions in the F2 region of the ionosphere. This information has enabled the lead time for prediction of the monthly T index to be substantially shortened and also enabled IPS to provide some customers with weekly predictions.

Investigation of the weekly T index using the data recorded in 1976 has revealed that a daily index may be just as reliable, though there is a need for more careful analysis of the operation of the index before it can be considered completely reliable.

6. DIAGRAMS

In all diagrams the horizontal axis is the time axis, the scale markers indicating 30 day intervals.

Figure 1. Plot of all recorded T indices derived from the hourly station data for 1976.

Figure 2. Plot of the Toolangi K index the 10.7 cm flux and the daily T index.

(a) The weekly T index.

Figure 3. Plot of all recorded T indices as in figure 1 for

(a) only night-time data
(b) only day-time data
(c) a repeat of figure 1.

Figure 4. (a) The difference between the northern and southern hemisphere daily T indices.
(b) The difference between two daily T indices constructed by selecting stations at random from the daily sample of available station data.

7. REFERENCES

Minnis, C.M. and Bazzard, G.H., (1960). A monthly ionospheric index of solar activity based on F2 layer ionization at eleven stations. Jnl. Atmos. and Terr. Phys., 4, 297.

Turner, J.F., (1968). The Development of the ionospheric T index. Ionospheric Prediction Service Series R12.

D25-92

N80-18487

CORONAL HOLES INFERRED FROM THE "FLEURS" EAST-WEST SOLAR SCANS

BRIAN G. FERGUSON
Ionospheric Prediction Service
Department of Science and the Environment
P.O. Box 702
Darlinghurst NSW 2010, Australia

The presence of coronal holes can be inferred from the "Fleurs" East-West solar scans produced daily on 692 and 1415 MHz. An analysis of these data for the period 1968 to 1973 confirms that coronal holes are stable features displaying significantly reduced electromagnetic emission which can persist for many solar rotations. The coronal hole observations are summarised in a series of tables to provide a consistent set of data for the period 1968 to 1973.

1. INTRODUCTION

Coronal holes are large-scale solar features which have much lower densities and temperatures than the typical background corona. Spectroheliograms at X-ray (Timothy et al. 1975), XUV (Bohlin 1977), EUV (Munro and Withbroe 1972, Neupert and Pizzo 1974) and radio (Dulk and Sheridan 1974, Fürst and Hirth 1975) wavelengths reveal coronal holes as regions exhibiting a localised diminution in electromagnetic emission. Coronal holes appear to possess an open, diverging magnetic field structure and are bounded by apparently divergent coronal loop structures (Vaiana et al. 1973). Thus the characteristic appearance of a coronal hole is one of an open, dark feature with very low levels of emission at coronal wavelengths. Coronal holes have been found to be associated with recurrent, high-speed, solar-wind streams and with geomagnetic activity (Krieger et al. 1973, Neupert and Pizzo 1974, Sheeley and Harvey 1978). Thus the detection of coronal holes is important in Solar-Terrestrial Predictions.

In addition to the two-dimensional spectroheliograms, coronal holes manifest themselves in one-dimensional East-West (E-W) solar scans at metric and centimetric wavelengths (Chiuderi Drago et al. 1977, Covington 1977). The purpose of this paper is to identify and classify coronal holes for the period 1968 to 1973 (inclusive) using the 692 MHz (43 cm) and 1415 MHz (21 cm) solar scans generated daily by the E-W arm of the "Fleurs" Synthesis Telescope.

In Section 2 the production and presentation of the scan data are outlined, whilst in Section 3 the detection of coronal holes and the criterion for recognising them are discussed. A subjective classification is assigned to each hole depending on the degree to which the identification criterion is satisfied.

In Section 4 scan data are presented and analysed for the period January to July, 1973 with the coronal holes being labelled when they appear on the scans. The holes inferred from the radio scans are then associated with the holes evident on the Fe XV (OSO-7) and soft X-ray (Skylab) spectroheliograms. Three tables are presented which summarise the observations of the "radio" holes for 1973 with the central meridian passages (CMPs) for the corresponding "X-ray" holes being included for labelling and comparison purposes.

The analysis is extended to include the period 1968 to 1972 with Section 5 being reserved for tables summarising the coronal hole observations during this time interval.

2. DATA

The solar scan data are made possible by the "Fleurs" Radio Astronomy Station of the University of Sydney, Australia. The E-W arm of the "Fleurs" Synthesis Telescope consists of a row of thirty-two parabolic reflectors 5.8 metres in diameter with an interantenna spacing of 12.2 metres. The signals from the antennas when combined at any moment produce a North-South (N-S) fan beam which is optically equivalent to a slit. As the sun drifts through the beam a one-dimensional brightness distribution is produced. The fan beam inherently integrates all the radio emissions in the N-S direction so all the latitudinal information is lost. Fan beams can be produced on two frequencies 692 and 1415 MHz with resolutions of 4 and 2 minutes of arc respectively.

The sun is scanned daily at around the beginning of the UT day. The scans are traced and reduced for publication in "Solar Geophysical Data". A series of solar scans, obtained on 1415 MHz, is shown in Figure 1. The two short horizontal lines drawn crossing the central vertical line indicate the cold-sky level and the estimated quiet-sun level. The curves are not normalised to account for daily variations in equipment gain or for tilting of the sun's axis of rotation throughout the year.

The scans reveal the presence of discrete emissive sources which give rise to the slowly-varying component (SVC) in solar radio flux measurements. These sources appear on the scans as peaks superimposed on a quiet-sun profile attributed to the undisturbed background-corona and to any conglomeration of broad, faint extensive sources (Covington 1977). The SVC encompasses changes over hours or days in flux measurements and is due to the development and decay of active solar regions. This gives a series of daily scans a dynamic appearance in that the amplitude of the peaks appear to wax and wane from day to day.

Traditionally only the radio source information is of interest with the positions and amplitudes of the peaks being scaled daily. This information is coded and then transmitted to various Regional Warning Centres of the International Ursigram and World Days Service.

This paper adopts the opposite approach in that it is confined to investigating the antithesis of the active regions associated with the peaks.

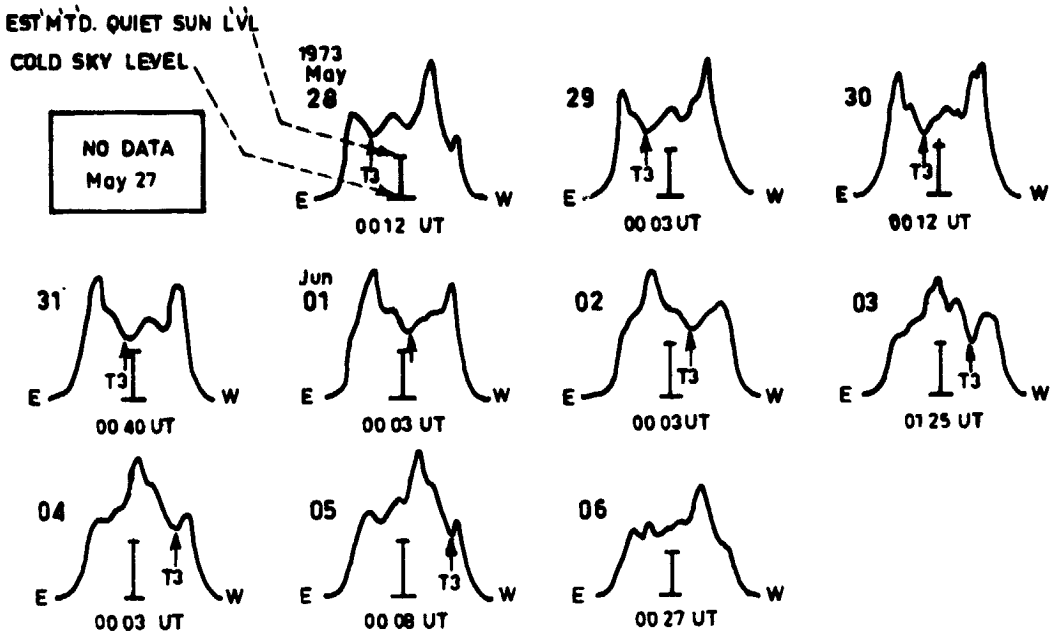

FIG. 1a 1415 MHz E-W SCANS FOR THE PERIOD MAY 27 TO JUNE 06, 1973

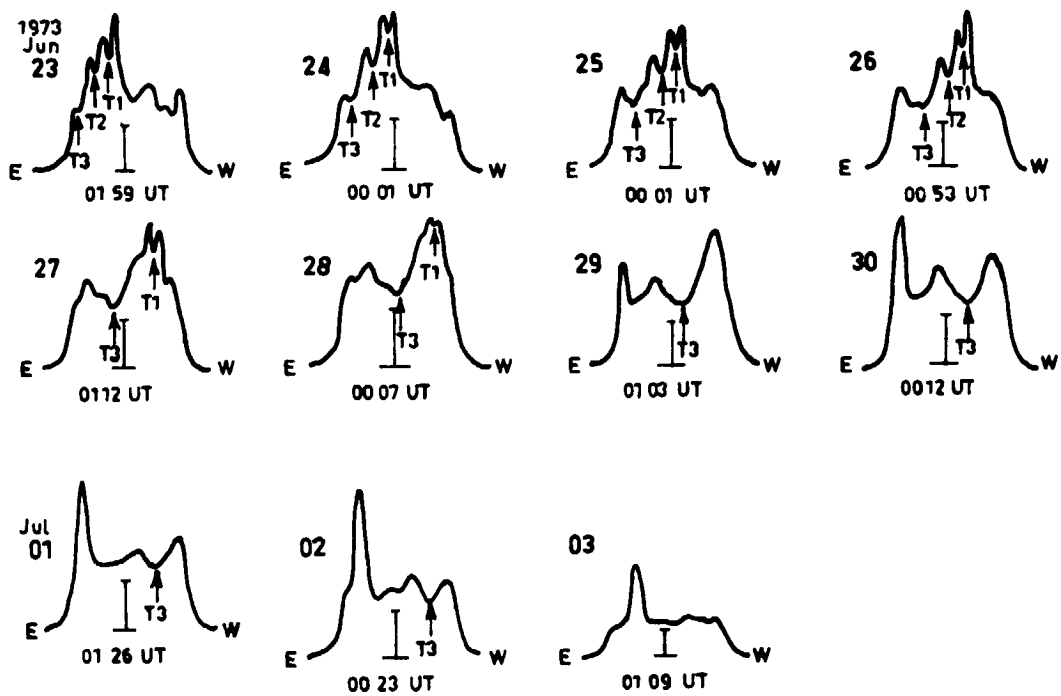

FIG. 1b 1415 MHz E-W SCANS FOR THE PERIOD JUNE 23 TO JULY 03, 1973

Here attention is focused on the trough information to determine whether or not it indicates the presence of coronal holes.

3. DETECTION OF CORONAL HOLES

Not every trough on a scan can be attributed to the presence of a coronal hole and it is necessary therefore to distinguish between quiet regions and coronal holes. The criterion which emerged and was used for inferring the presence of coronal holes is that they manifest themselves as pronounced minima on the scans which endure for days and generally recur on subsequent solar rotations. Other observations at X-ray (Timothy et al.1975) and EUV (Neupert and Pizzo 1974) wavelengths confirm that coronal holes have lifetimes which may span many solar rotations.

The characteristics of a hole profile appear to be preserved over a sequence of daily scans with the trough shifting in position as the sun rotates. Thus the apparent passage of a hole across the solar disc is marked by a deep and stable trough on the scans. On the other hand quiet regions not associated with holes have profiles in which the troughs are prone to change during a solar rotation and can disappear or even be replaced by a peak during a subsequent rotation. In summary coronal holes appear to be steady-state structures whose scan profiles have deep minima which are more or less invariant whereas quiet and active regions have dynamic profiles which can change from day to day.

Consider the series of 1415 MHz scans for June 23 to July 03 1973 which are shown in Figure 1b. For June 23 a number of troughs appear on the scan. Consider the three troughs labelled "T1", "T2", and "T3". By comparing the profiles on subsequent days it may be concluded that the elevated troughs T1 and T2 are associated with quiet regions whilst the lowest trough T3 is associated with a coronal hole. Whereas T1 and T2 are both shallow, T3 is deep. The depth of T3 is preserved on subsequent scans whereas those of T1 and T2 are variable. In fact T2 disappeared on June 27.

In addition, the information obtained for the previous rotation May 27 to June 06 is shown in Figure 1a. Comparing the scan for any one day of one rotation with the scan for the corresponding day of the other rotation suggests the only stable feature common to both rotations was the coronal hole indicated by the small vertical arrow and labelled "T3" in Figures 1a and 1b. The scans indicate the coronal hole underwent CMP late on May 31 and on the subsequent rotation, late on June 27.

The 692 MHz scans for June 23 to July 03 are shown in Figure 2a. The peaks on these scans appear broader than the corresponding ones on 1415 MHz (Figure 2b) for the same period because the resolution is reduced by a factor of 2. A hole is initially detected on the June 27 692 MHz scan and is conspicuous on June 28 and 29. CMP was mid June 28.

In general the 692 MHz observation period of holes is limited to two or three days each side of CMP whilst at 1415 MHz this period is extended to

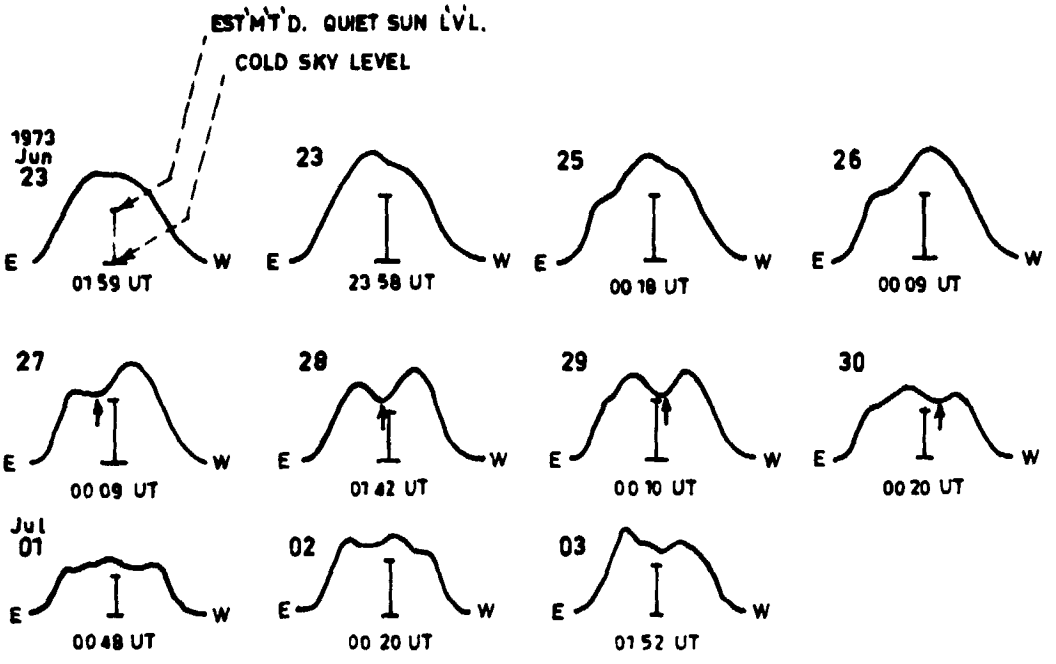

FIG. 2a 692 MHz E-W SCANS FOR THE PERIOD JUNE 23 TO JULY 03, 1973

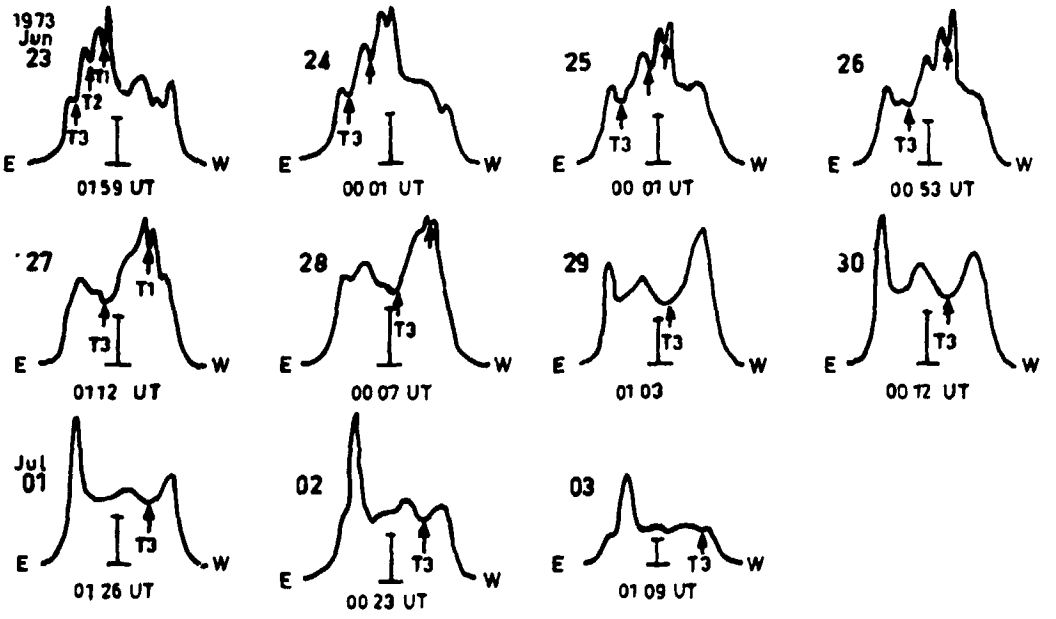

FIG. 2b 1415 MHz E-W SCANS FOR THE PERIOD JUNE 23 TO JULY 03, 1973

four or five days each side of CMP. Also the CMP times for the same hole observed at different frequencies are not necessarily coindicent. For example at 692 MHz, CMP occurred mid June 28 but on 1415 MHz, it occurred late June 27.

Once the presence of a hole is detected from a series of scans, a subjective classification is assigned to the hole. The holes are divided into three groups (labelled "1", "2", "3") depending on the degree to which they satisfy the criterion of being low-emissive, stable features. The group "3" candidates are the most satisfactory in fulfilling the requirements for inferring the existence of a hole. The hole mentioned above was classified as a "3" on 1415 MHz on both rotations, a "1" on 692 MHz for the first rotation and a "3" for the second rotation.

The classification number assigned herein to each coronal hole represents a subjective assessment of the contrast, that is, the depth of the trough in relation to the quiet-Sun background, and the degree to which the contrast is preserved over a series of scans. The class 3 holes have high contrast and the class 1 holes have low contrast. The classification number "2" is reserved for holes which have high contrast around the central meridian but low contrast near the solar limbs. The class 2 and class 3 holes are readily detected on the scan curves but the class 1 holes are more difficult to detect because the contrast is low. Thus with the present technique, difficulties arise in inferring the presence of a coronal hole when the contrast is low. One "low-contrast" situation arises when a radio source is located on the same longitude, but on a different latitude, as a hole because the N-S fan beam sums the contributions from both the source and the hole. Thus the depression associated with the hole is reduced and the contrast degraded. Low-contrast conditions are frequent at Solar Minimum because of a reduction in the number of weak, extensive sources which serve to improve the contrast between the hole and the background reference level.

4. COMPARISON WITH OTHER OBSERVATIONS

Using the criterion mentioned in the previous section to infer the presence of a hole, it is interesting to compare the results with observations made at the same time but at other wavelengths. For instance EUV spectroheliograms at 284Å (Fe XV line) have been published in "Solar Geophysical Data" using the information from the OSO-7 satellite. The maps are presented as a series of contours with the number of counts n_c = 5, 10, 20, 40, ... marked on each isophote. The maps for May 31 and June 27 are shown in Figure 3. These dates correspond to the two CMP dates of the hole inferred from the radio scan data. The EUV analogue of this hole is the area delineated by the isophote n_c = 10. This area has been darkened in the diagram and closely resembles the shape of a coronal hole observed at soft X-ray wavelengths (Timothy et al.1975). The hole is observed at CMP on both EUV maps which is consistent with the radio scan observations.

Similarly observations of holes at X-ray wavelengths (2-32Å and 44-54Å) for the period May 28 to November 21, 1973 were made by the spectro-

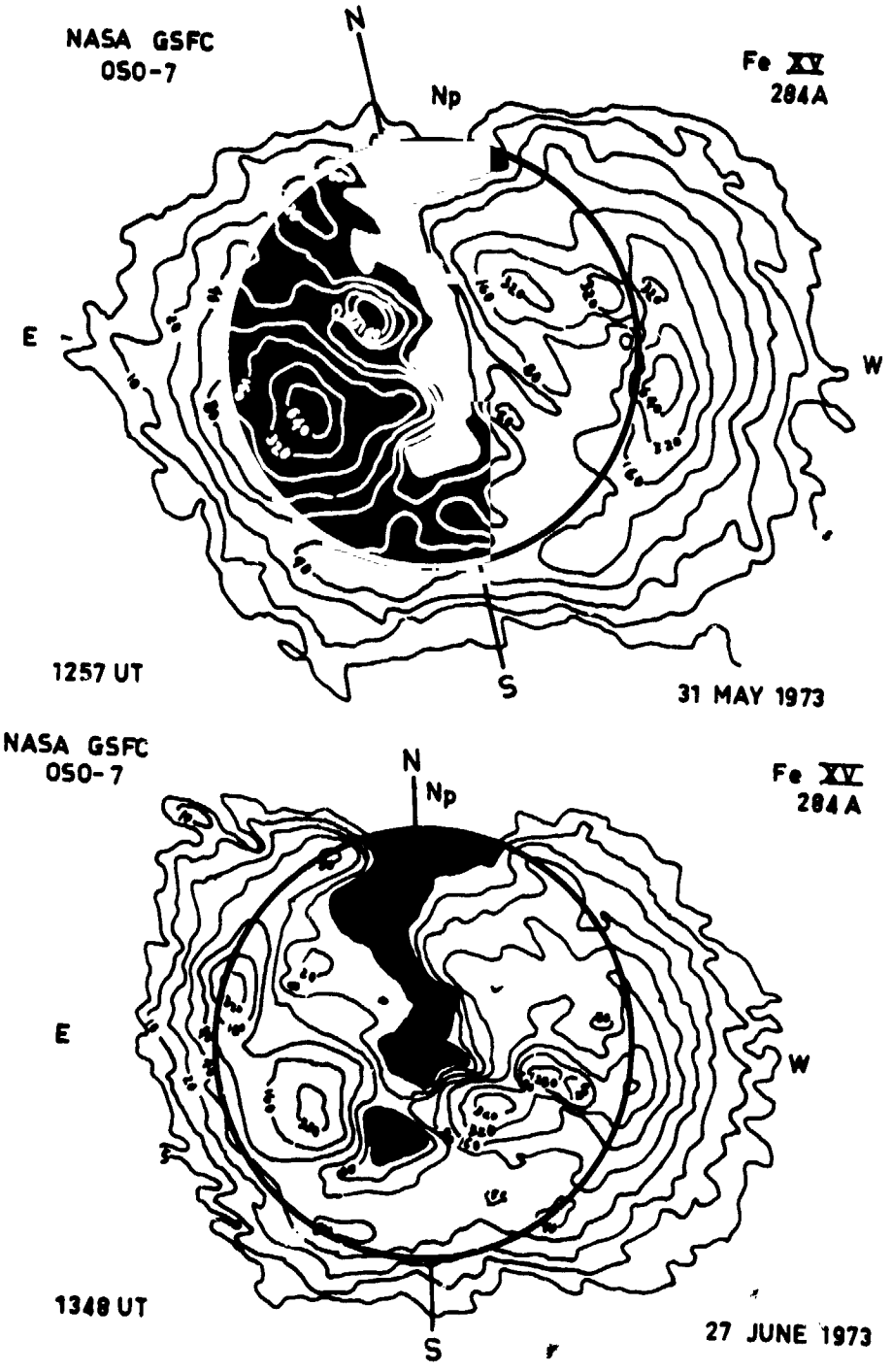

FIG. 3 EUV SPECTROHELIOGRAM SHOWING A CORONAL HOLE AT CENTRAL MERIDIAN ON MAY 31 AND JUNE 27, 1973. THE DARKENED AREA ENCLOSED BY THE ISOPHOTE n_c = 10 REPRESENTS THE HOLE.

graphic telescope on Skylab. An atlas of the coronal hole boundary positions observed during this period has been compiled by Nolte et al. (1976). Six coronal holes were observed during this period four of which can be inferred from the radio scans.

To trace the evolution of coronal holes during the first half of 1973, the 1415 MHz scans for January to July are reproduced in Figures 4 to 10. The CMP dates for these holes are then compared with those obtained using Skylab data when the observation periods overlapped. The notation and numbering of the coronal holes are the same as those used by Nolte et al. (1976) which facilitates comparisons between the two sets of observations. For example the coronal hole T3 observed in Figures 1 and 2 was relabelled "CH1" in subsequent diagrams.

By presenting the radio data for January to July 1973, the history of certain coronal holes can be traced not only for a sequence of days but for a sequence of solar rotations. This set of diagrams shows the evolution of the coronal holes observed by Skylab. In addition the presentation of a long series of scans enables some insight to be gained into the assignment of classification numbers to the "radio" holes.

The Skylab data indicated CH1 underwent CMPs on May 31, June 27, July 25, August 21, September 16, October 14 and November 10 (Nolte et al.1976). The scan data indicated CMPs on February 12, March 12, April 07, May 04, May 31, June 27, July 25 and August 22. The scan data indicated the hole disappeared after August although it was still observed by Skylab. Whereas Timothy et al.(1975) conjectured that CH1 formed only one rotation prior to their first observations in late May, the radio data imply that it existed for five previous rotations.

The passage of CH1 across the disc at the beginning of the Skylab mission is indicated by the labelled arrows in Figures 8 and 9. Data were not available for May 26 and 27 but the existence of CH1 is evident from May 28 to June 05 with CMP occurring on May 31. Similarly Figures 9 and 10 reveal the presence of CH1 on the scans for June 23 to July 03 with CMP late June 27, whilst in Figure 10, the observation period is restricted to July 23 to 30 with CMP on July 25. A summary of these observations is included in Table 1.

The results of the analysis of the scan data for CH3 are shown in Table 2. The information for the other holes inferred for 1973 is presented in Table 3. All these tables show the Skylab number (if applicable), the scan frequency, the classification, the period of observation and the Figure reference number (if observed between January and July) and the CMP dates inferred from the scans and from the Skylab data.

5. SUMMARY OF RESULTS FOR THE PERIOD 1968-1972

The technique of inferring the presence of coronal holes was extended to include the period 1968 to 1972. The results are presented in Tables 4 to 8, each table being reserved for the observations of holes for a

particular year. The tables contain the scan frequency, the classification number and the CMP date for each coronal hole detected.

6. CONCLUSION

Coronal holes can be inferred from solar E-W scan data. The holes manifest themselves as regions of depressed radio emission. The holes appear to be stable structures with lifetimes spanning many solar rotations. The holes inferred from the scans were generally the radio-wave analogues of the holes observed at X-ray and EUV wavelengths.

The inferred coronal hole data were tabulated for the period 1968 to 1973 and should be valuable to users requiring a consistent set of coronal hole observations during this period.

ACKNOWLEDGEMENTS

The author wishes to thank George Daniel for assistance in producing this paper and Eugene Molineux for help in analysing the data.

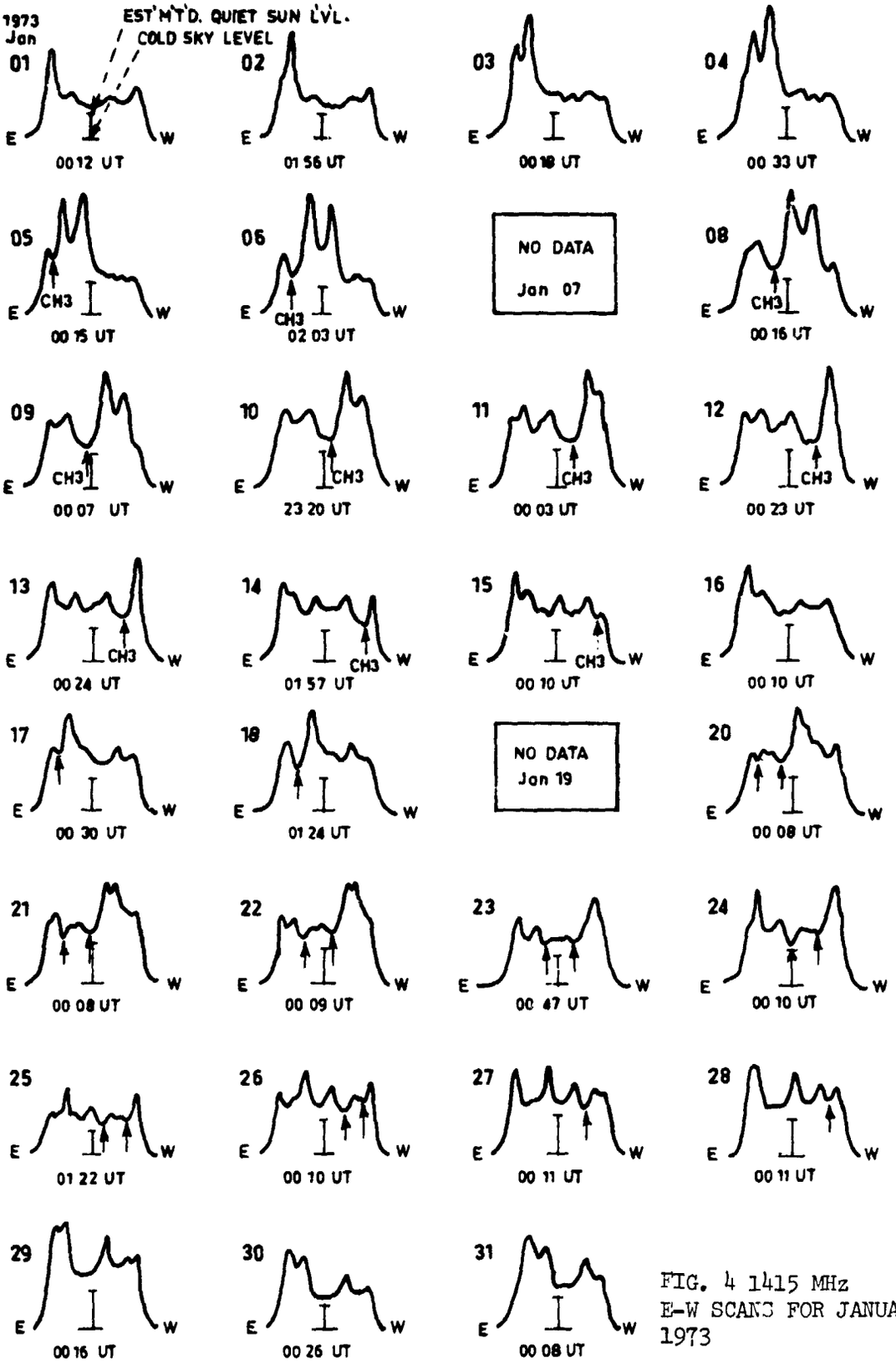

FIG. 4 1415 MHz
E-W SCANS FOR JANUARY
1973

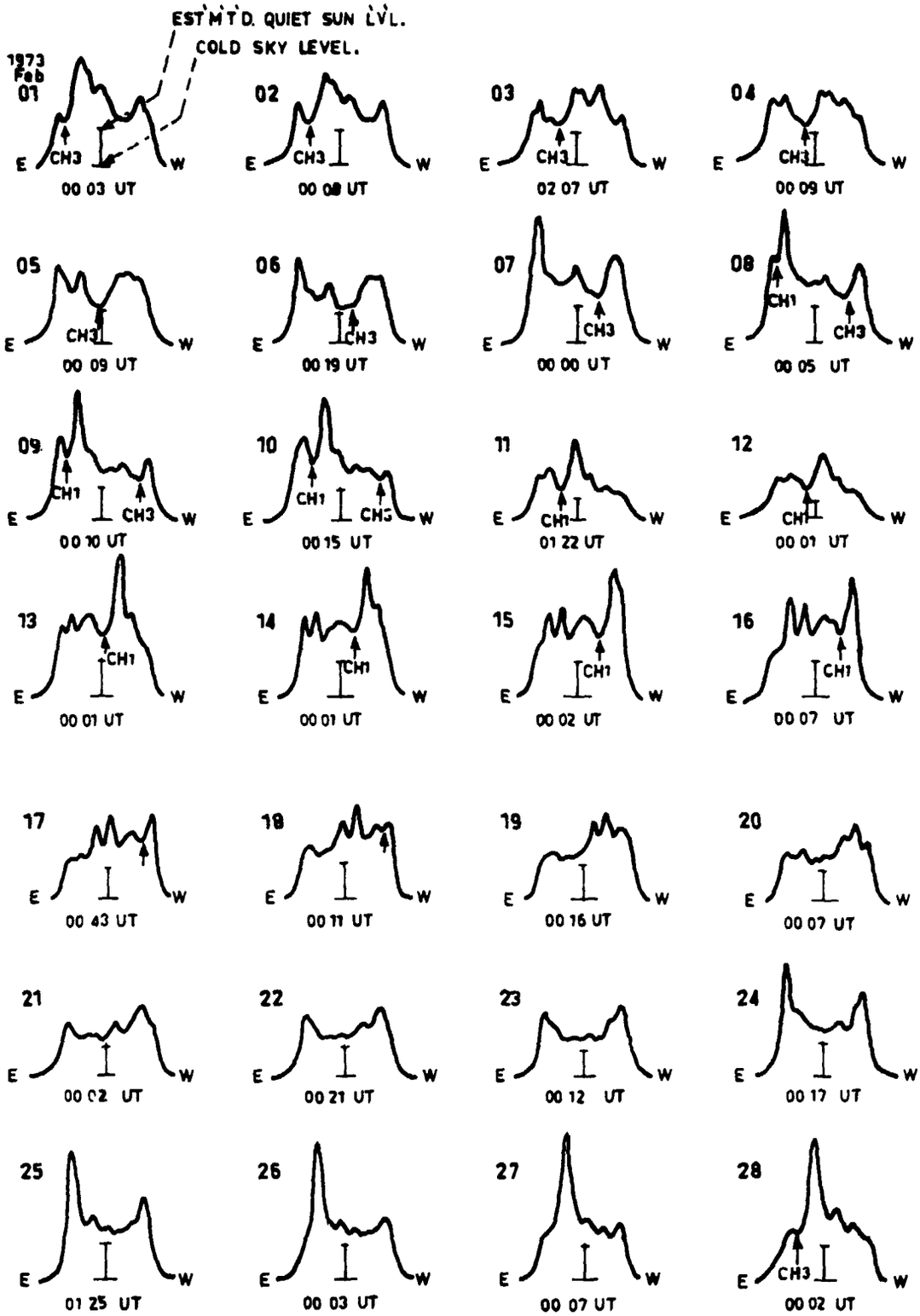

FIG. 5 1415 MHz E-W SCANS FOR FEBRUARY, 1973

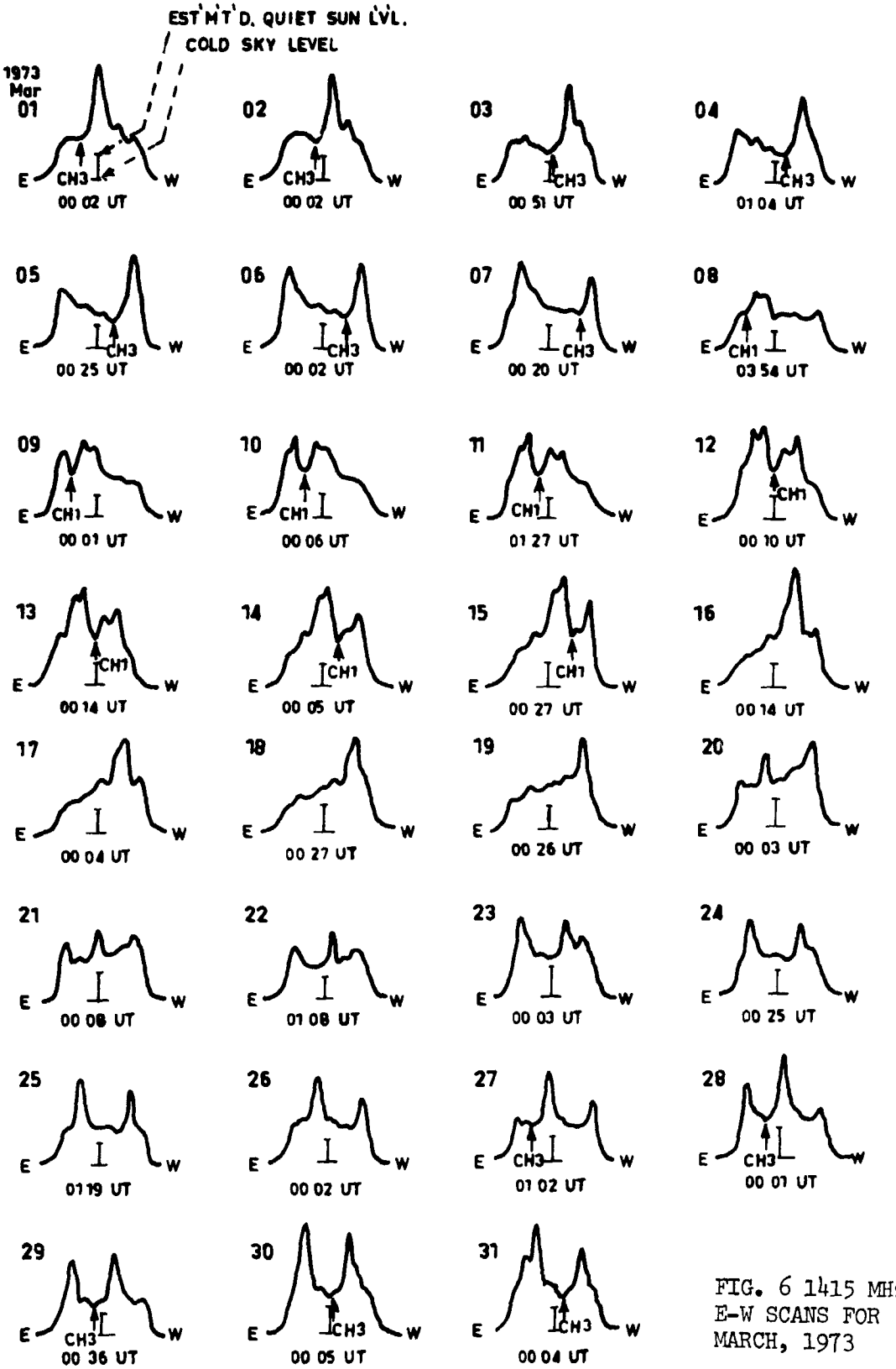

FIG. 6 1415 MHz E-W SCANS FOR MARCH, 1973

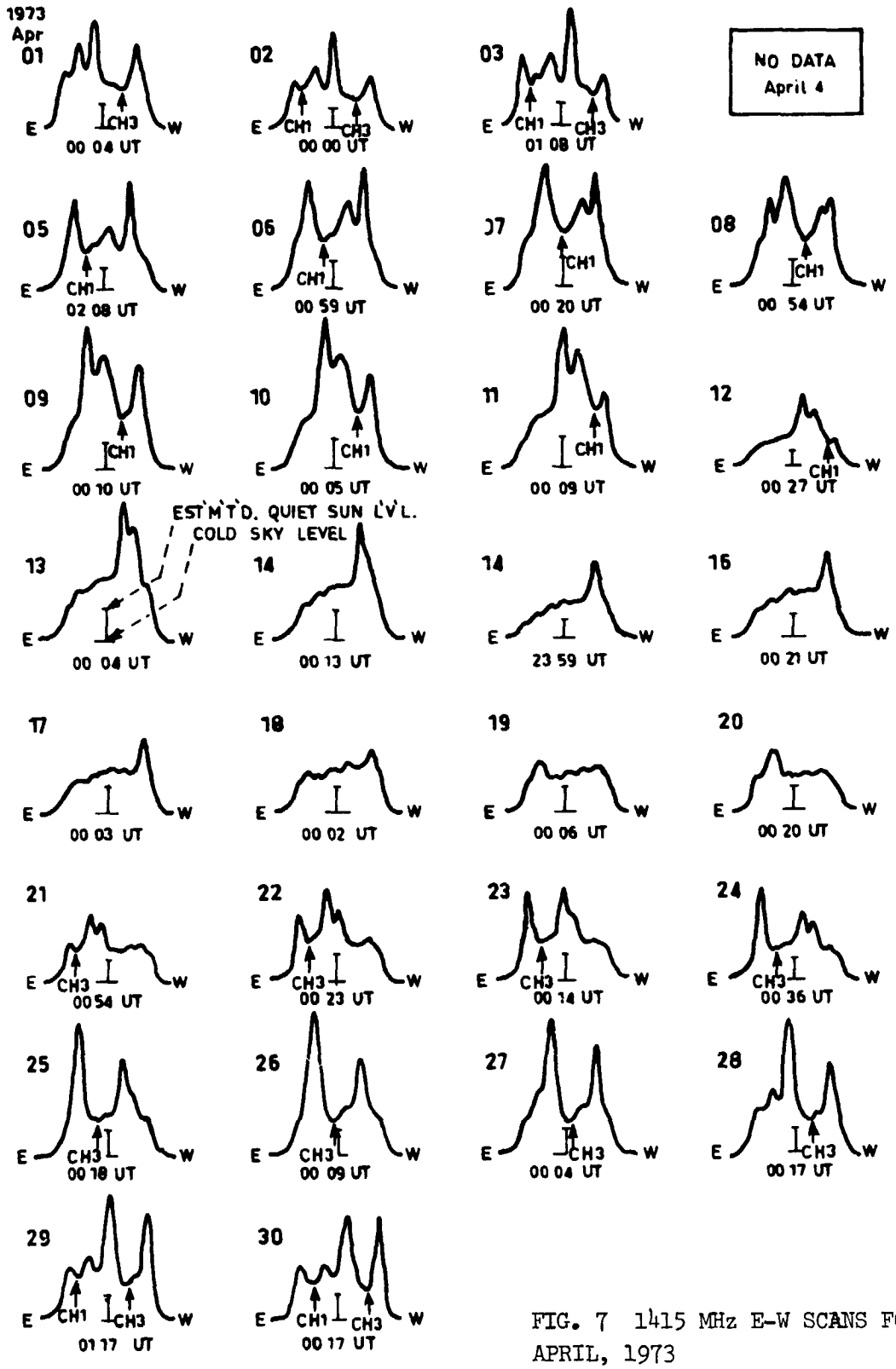

FIG. 7 1415 MHz E-W SCANS FOR APRIL, 1973

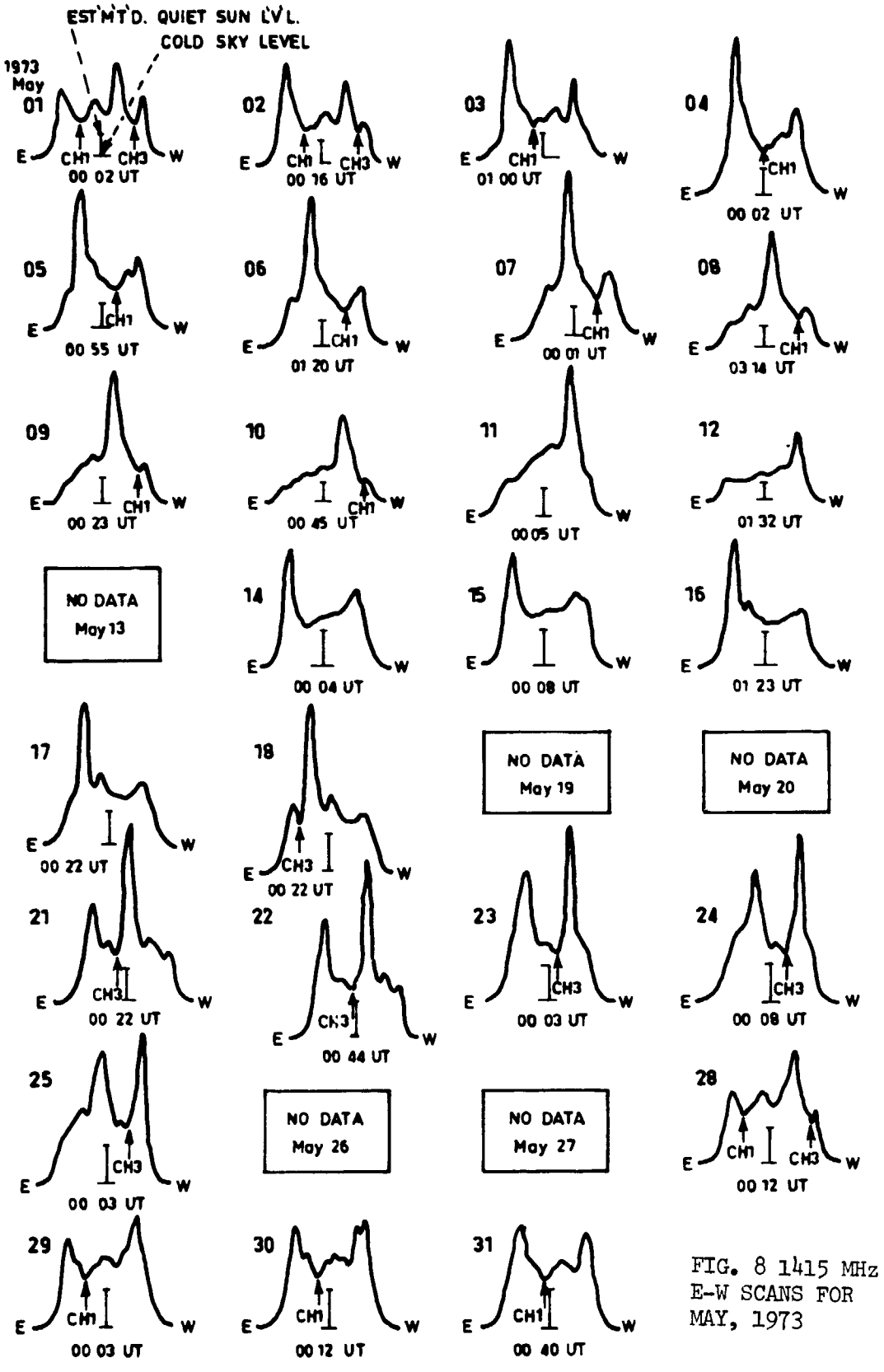

FIG. 8 1415 MHz E-W SCANS FOR MAY, 1973

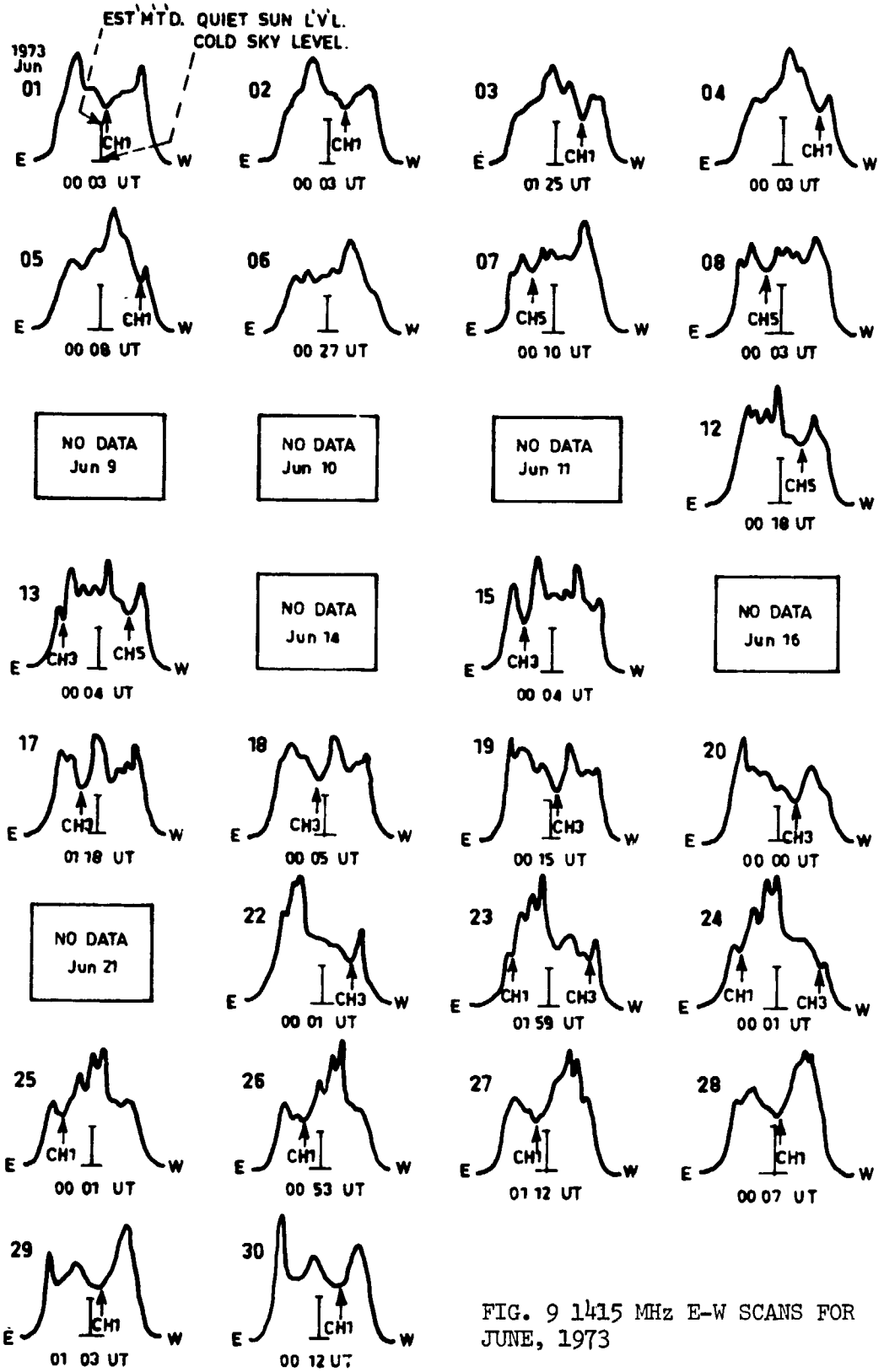

FIG. 9 1415 MHz E-W SCANS FOR JUNE, 1973

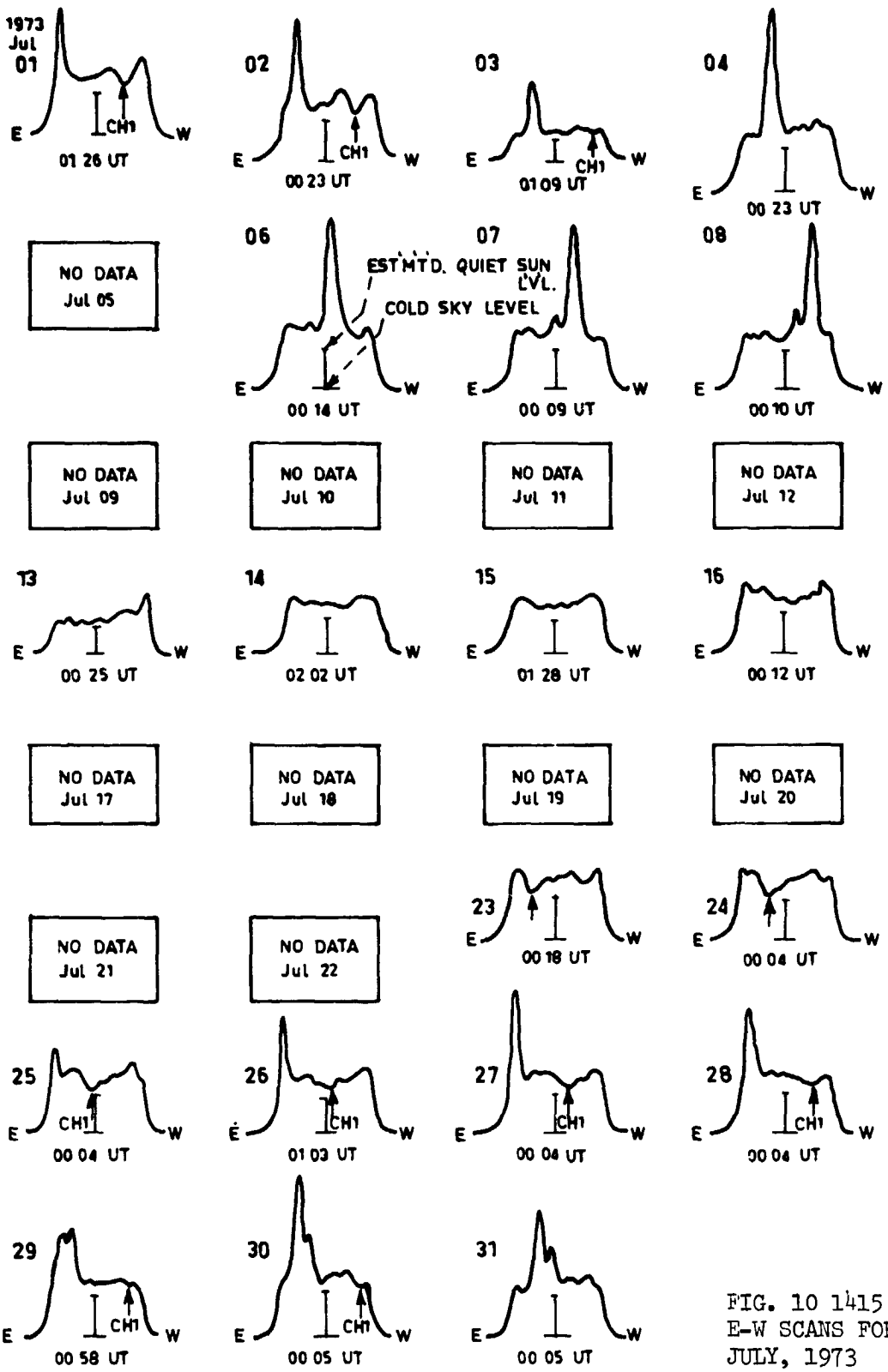

FIG. 10 1415 MHz E-W SCANS FOR JULY, 1973

TABLE 1 SUMMARY OF OBSERVATIONS OF CORONAL HOLE CH1 DURING 1973

Figure	Scan Frequency (MHz)	Class	Period of Observation on Scans (1973)	CMP from Scans (1973)	CMP from Skylab (Nolte et al 1976) (1973)
4	1415	1	Jan 11-Jan 20	mid Jan 15	
5	1415	1	Feb 08-Feb 18	late Feb 12	
6	1415	1	Mar 08-Mar 15	early Mar 12	
7	1415	2	Apr 02-Apr 12	early Apr 07	
7, 8	1415	2	Apr 29-May 10	early May 04	
	692	2	May 02-May 06	early May 04	
8, 9	1415	3	May 28-Jun 05	mid May 31	May 31
	692	1	May 30-Jun 02	May 31	
9, 10	1415	3	Jun 23-Jul 03	late Jun 27	Jun 27
	692	3	Jun 27-Jun 30	early Jun 28	
10	1415	2	Jul 23-Jul 30	early Jul 25	Jul 25
	692	2	Jul 23-Jul 27	early Jul 26	
	692	1	Aug 21-Aug 22	early Aug 22	Aug 21 Sep 16 Oct 14 Nov 10

TABLE 2 SUMMARY OF OBSERVATIONS OF CORONAL HOLE CH3 DURING 1973

Figure	Scan Frequency MHz	Class	Period of Observation on Scans (1973)	CMP from Scans (1973)	CMP from Skylab (Nolte et al 1976) (1973)
4	1415	3	Jan 05-Jan 15	early Jan 09	
	692	2	Jan 08-Jan 12	late Jan 09	
5	1415	3	Feb 01-Feb 10	Feb 05	
	692	3	Feb 04-Feb 07	late Feb 05	
5, 6	1415	2	Feb 28-Mar 07	early Mar 03	
	692	2	Mar 03-Mar 06	mid Mar 03	
6, 7	1415	2	Mar 27-Apr 03	late Mar 29	
	692	3	Mar 29-Apr 02	early Mar 30	
7, 8	1415	3	Apr 21-May 02	early Apr 26	
	692	3	Apr 24-Apr 30	late Apr 26	
8	1415	2	May 18-May 28	early May 22	
	692	2	May 21-May 25	mid May 23	
9	1415	3	Jun 13-Jun 24	mid Jun 18	June 21
	692	1	Jun 17-Jun 20	early Jun 19	
					July 17 Aug 13

TABLE 3 SUMMARY OF OBSERVATIONS OF CORONAL HOLES
(OTHER THAN CH1 (TABLE 1) AND CH3 (TABLE 2) DURING 1973

Coronal Hole	Figure	Scan Frequency	Class	Period of Observation	CMP	CMP from Skylab (Nolte et al 1976
	4	1415	1	Jan 17-Jan 26	mid Jan 21	
	5	1415	1	Feb 12-Feb 20	Feb 16	
	4	1415	1	Jan 20-Jan 28	early Jan 24	
		692	1	Jan 29-Jan 31	Jan 30	
	6	1415	1	Mar 19-Mar 28	early Mar 22	
		692	1	Mar 22-Mar 24	early Mar 23	
CH5	9	1415	1	Jun 07,08,12, 13		June 09
	10	1415	1	Jul 06-Jul 08	Jul 08	
		1415	1	Aug 02-Aug 09	early Aug 05	
CH4		1415	3	Sep 26-Oct 02	late Sep 28	Sep 28
		692	2	Sep 28-Oct 02	early Sep 29	
		1415	2	Oct 22-Oct 29	Oct 25	Oct 25
		692	1	Oct 23-Oct 27	Oct 25	
		1415	2	Nov 18-Nov 26	mid Nov 22	Nov 21
		692	1	Nov 21-Nov 24	late Nov 22	Nov 21
		1415	1	Aug 06-Aug 13	Aug 09	
		692	1	Aug 08-Aug 12	early Aug 10	
		1415	1	Sep 01-Sep 07	late Sep 04	
		1415	1	Sep 19-Sep 27	Sep 22	
CH6						Oct 20 Nov 16
CH2						May 28 Jun 22 Jul 20 Aug 16 Sep 12 Oct 09 Nov 05

TABLE 4 CORONAL HOLE DATA FOR 1968 INFERRED FROM THE "FLEURS" E-W RADIO SCANS

1415 MHz		692 MHz	
CMP e = early m = mid l = late (1968)	Class	CMP (1968)	Class
e Jan 02	2	l Jan 02	3
m Jan 26	1	l Feb 10	2
e Feb 11	3	m Feb 16	1
e Mar 03	2	Feb 23	1
m Mar 14	1	m Mar 22	3
e Mar 22	2	No data Apr 17-May 16	
Apr 08	1	May 16	3
No data Apr 17-May 16		e May 25	1
May 16	2	m Jun 07	3
e May 25	1	l Jun 22	1
e Jun 01	1	e Jul 15	2
e Jun 07	3	e Jul 20	1
e Jun 13	1	e Aug 15	1
e Jun 17	1	e Sep 08	1
m Jun 22	2	m Sep 12	1
m Jul 14	1	e Sep 18	1
e Jul 20	1	e Sep 28	1
m Jul 29	1	e Oct 09	1
e Aug 15	2	e Oct 26	1
m Aug 30	1	e Oct 30	3
m Sep 08	1	m Nov 10	1
m Sep 12	1	m Nov 18	1
e Sep 18	1	l Dec 07	1
l Oct 09	2	e Dec 11	1
e Oct 26	1	e Dec 30	2
e Oct 30	3		
m Nov 10	3		
m Nov 18	2		
e Nov 26	1		
e Dec 08	1		
m Dec 11	1		
m Dec 30	3		

TABLE 5 CORONAL HOLE DATA FOR 1969 INFERRED FROM THE "FLEURS" E-W RADIO SCANS

1415 MHz		692 MHz	
CMP e = early m = mid l = late (1969)	Class	CMP (1969)	Class
m Jan 30	1	m Jan 30	1
l Feb 03	1	l Feb 03	2
Feb 26	2	m Mar 03	1
m Mar 03	1	e Jun 03	1
l Mar 13	1	No data Jun 04-06	
e Mar 28	1	e Aug 08	1
l Apr 09	1	e Sep 11	1
e May 29	2	e Sep 19	1
No data Jun 04-09		e Oct 04	2
m Jun 13	1	m Oct 08	2
e Jul 12	1	m Oct 17	1
m Jul 21	1	l Nov 09	1
e Aug 08	3	m Dec 06	2
e Aug 20	1	m Dec 22	2
e Sep 11	1	No data Dec 25-31	
l Sep 30	2		
e Oct 04	1		
e Oct 08	1		
e Oct 17	1		
l Nov 26	2		
m Dec 06	3		
m Dec 22	2		
No data Dec 25-31			

TABLE 6 CORONAL HOLE DATA FOR 1970 INFERRED FROM THE "FLEURS" E-W RADIO SCANS

1415 MHz		692 MHz	
CMP e = early m = mid l = late (1970)	Class	CMP (1970)	Class
e Jan 04	2	m Jan 11	1
Jan 11	1	l Jan 24	1
m Jan 21	2	m Feb 07	1
l Feb 07	1	e Mar 01	1
e Mar 01	2	e Mar 18	1
e Mar 18	3	e May 12	2
Mar 28	2	e Jun 04	1
e Apr 03	1	m Jun 18	1
m Apr 15	1	m Jun 27	2
m Apr 24	2	e Jul 06	1
m Apr 30	1	e Jul 09	3
e May 08	1	m Jul 26	2
May 12	3	l Aug 06	2
l May 20	1	m Aug 17	2
l May 23	1	l Aug 20	1
m Jun 04	1	e Sep 01	1
e Jun 09	1	e Sep 07	1
Jun 19	3	e Sep 13	1
m Jun 27	2	e Sep 18	1
l Jul 01	1	m Sep 30	3
e Jul 06	2	e Oct 10	2
m Jul 09	3	m Oct 14	2
Jul 26	3	m Oct 27	2
l Jul 31	1	m Nov 11	1
Aug 07	2	m Nov 20	1
l Aug 10	1	m Nov 23	2
m Aug 17	1	l Dec 07	1
e Aug 21	1	m Dec 16	1
m Aug 26	1		
Sep 01	2		
e Sep 07	1		
m Sep 13	1		
m Sep 18	2		
m Sep 30	3		
Oct 10	1		
l Oct 14	2		
m Oct 27	1		
e Nov 02	1		
e Nov 20	1		
m Nov 23	3		
m Dec 07	3		
e Dec 17	2		

TABLE 7 CORONAL HOLE DATA FOR 1971 INFERRED FROM THE "FLEURS" E-W RADIO SCANS

1415 MHz		692 MHz	
CMP e = early m = mid l = late (1971)	Class	CMP (1971)	Class
e Jan 12	1	m Jan 27	3
e Jun 28	1	e Feb 04	2
Feb 01	1	m Feb 22	3
e Feb 04	1	m Mar 21	1
m Feb 12	2	l Mar 25	1
m Feb 22	2	l Apr 29	2
l Mar 02	1	m May 04	1
e Mar 04	1	m May 26	2
m Mar 21	1	m May 31	3
l Mar 25	1	l Jun 26	2
m Mar 30	1	e Jul 01	1
Apr 03	1	e Jul 24	3
m Apr 09	1	l Jul 27	1
e Apr 15	1	m Aug 01	2
e Apr 29	3	l Aug 11	3
e May 04	2	e Aug 19	1
l May 30	3	m Aug 27	2
e Jun 04	2	l Sep 06	1
l Jun 26	3	m Sep 23	3
l Jun 30	3	e Sep 28	2
m Jul 14	2	m Oct 02	2
e Jul 24	3	e Oct 07	1
e Aug 01	1	m Oct 11	3
e Aug 04	1	m Oct 25	3
e Aug 11	1	Nov 03	2
e Aug 19	1	e Nov 08	1
m Aug 27	2	m Nov 22	1
m Aug 31	1	m Nov 29	2
m Sep 23	3	e Dec 05	2
e Sep 28	3	e Dec 19	3
m Oct 02	2	m Dec 26	1
Oct 11	1		
m Oct 20	1		
m Oct 25	3		
e Oct 29	1		
Nov 03	2		
Nov 08	2		
e Nov 22	3		
e Nov 29	1		
m Dec 14	1		
m Dec 18	3		
m Dec 28	1		

TABLE 8 CORONAL HOLE DATA FOR 1972 INFERRED FROM THE "FLEURS" E-W RADIO SCANS

1415 MHz		692 MHz	
CMP e = early m = mid l = lat (1972)	Class	CMP (1972)	Class
m Jan 01	1	m Jan 01	1
m Jan 05	2	l Jan 05	1
l Jan 15	1	Jan 16	2
e Jan 22	1	Feb 11	1
e Jan 25	1	l Feb 23	2
Feb 11	2	m Mar 05	1
m Feb 18	2	e Mar 10	2
m Feb 23	3	m Mar 22	1
l Mar 09	3	m Mar 28	1
e Mar 16	2	e Apr 02	1
m Mar 22	1	m Apr 24	2
m Mar 28	2	m Apr 29	2
e Apr 05	1	m May 26	1
e Apr 24	2	l Jun 01	1
l Apr 28	3	e Jun 19	2
m May 11	1	e Jun 28	1
m May 16	1	m Jul 11	1
m May 26	3	m Jul 21	2
e Jun 02	2	m Jul 25	1
l Jun 19	1	e Aug 17	1
l Jun 24	1	e Sep 13	1
No data Jun 27-30		No data Oct 02-04	
l Jul 04	2	e Oct 17	1
m Jul 06	1	Oct 25	1
Jul 08	1	e Nov 20	1
m Jul 11	1	m Dec 13	2
e Jul 21	2		
m Jul 25	1		
Aug 01	2		
l Aug 10	1		
e Aug 17	1		
e Aug 28	3		
e Sep 06	1		
e Sep 13	2		
No data Oct 02-04			
Oct 04	1		
e Oct 17	1		
Oct 25	3		
m Oct 27	1		
Nov 19	2		
Dec 05	1		
e Dec 13	2		
e Dec 17	2		

REFERENCES

Bohlin, J.D. (1977): Extreme-Ultraviolet Observations of Coronal Holes. I : Locations, Sizes and Evolution of Coronal Holes, June 1973 - January 1974. Solar Physics 51, 377-398.

Chiuderi Drago, F., Avignon Y., and Thomas, R.J. (1977): Structure of Coronal Holes from UV and Radio Observations. Solar Physics 51, 143-158.

Covington, A.E. (1977): Coronal X-Ray Holes and the Quiet Radio Sun at 2800 MHz. Solar Physics 54 393-402.

Dulk, G.A., and Sheridan, K.V. (1974): The Structure of the Middle Corona from Observations at 80 and 160 MHz. Solar Physics 36, 191-202.

Fürst, E., and Hirth, W. (1975): Coronal Hole Observed at 10.7 GHz with a Large Single Dish. Solar Physics 42 157-161.

Krieger, A.S., Timothy, A.F., and Roelef, E.C. (1973): A Coronal Hole and Identification as the Source of a High Velocity Solar Wind Stream. Solar Physics 29, 505-525.

Munro, R.H., and Withbroe, G.L. (1972): Properties of a Coronal Hole Derived from Extreme Ultraviolet Observations. Astrophys. J. 176, 511-520

Neupert, W.M., and Pizzo, V. (1974): Solar Coronal Holes as Sources of Recurrent Geomagnetic Disturbances. Journal of Geophysical Research 79, 3701-3709.

Nolte, J.T., Krieger, A.A., Timothy, A. F., Vaiana, G.S., and Zombeck, M.V. (1976): An Atlas of Coronal Hole Boundary Positions May 28 to November 21, 1973. Solar Physics 46, 291-301.

Sheeley, N.R., and Harvey, J.W. (1978): Coronal Holes, Solar Wind Streams, and Geomagnetic Activity during the New Sunspot Cycle. Solar Physics 59, 159-173.

Timothy, A.F., Krieger, A.S., and Vaiana, G.S. (1975): The Structure and Evolution of Coronal Holes. Solar Physics 42, 135-156.

Vaiana, G.S., Krieger, A.S., and Timothy, A.F. (1973): Identification and Analysis of Stuctures in the Corona from X-Ray Photography. Solar Physics 32, 81.

PROPHET: AN APPLICATION OF PROPAGATION FORECASTING PRINCIPLES

Paul E. Argo
Ilan J. Rothmuller
Naval Ocean Systems Center
San Diego, CA 92152

The performance of a wide variety of Naval electromagnetic systems depends on ionospheric conditions. For example, solar disturbances of the ionosphere can interrupt communications, render surveillance systems useless and cause navigation system inaccuracies. Real-time propagation assessment is a technique to optimize system performance by allowing knowledge of current ionospheric conditions to be used to minimize detrimental effects of an unknown or disturbed propagation environment. An environmental prediction and assessment system (EPAS), comprised of a variety of real-time sources of solar/geophysical data and a center which collects, processes and selectively disseminates these data to regional propagation assessment terminals, can provide real-time knowledge of propagation conditions. The US Naval Ocean Systems Center is developing a terminal called PROPHET (for propagation forecasting), a key element of the EPAS that uses real-time solar/geophysical data to make regional assessments which are tailored to specific system useage. PROPHET uses models to translate data from satellite and ground based sources into performance predictions for specific systems. PROPHET is presently being evaluated at a Naval Communication Station and has proved to be useful to operational personnel.

INTRODUCTION

The performance of electromagnetic communication and navigation systems depends on and is vulnerable to the electromagnetic (EM) wave propagation environment. The Navy's Global Positioning (shf satellite) System, Fleet Satellite Communications, the hf and vlf Fleet Broadcast, vlf and elf strategic communications are all examples of systems which make use of EM waves whose propagation environment is the ionosphere. Changes in the ionosphere, and consequent changes in wave propagation characteristics, may degrade system performance through large signal loss, rapid signal fluctuations, rapid phase changes, changes in angle of arrival, etc. Given foreknowledge of ionospheric changes and the resultant effects on systems, the user is warned of imminent problems and so may be able to take mitigating steps. An Environmental Prediction and Assessment System (EPAS) under development will provide the Navy user with the required foreknowledge.

An effective EPAS contains three functional parts: (1) a number of sensors which obtain raw solar and geophysical data; (2) a data reduction, sorting, and collection function which puts the pertinent data into useable form and forwards it to a forecasting center; (3) a subsystem which digests these data and produces assessments and forecasts of system performance. It gives guidance for frequency selection, antenna selection, transmitter power - all of the factors required to optimize system performance. These outputs are tailored for the specific system and user. Besides providing real time guidance for system users, an effective EPAS will help the Navy satisfy a number of logistic, design, and operational requirements. For example, the Navy needs (1) more efficient frequency management in a world of shrinking available radio spectrum; (2) to minimize the number of transmitters and transmitter power to those actually needed for acceptable communications probabilities (an "overkill" policy is used now); (3) to take into account extreme environmental effects during system design and test, such as accounting for scintillation fading on FLTSATCOM reliability; (4) to develop tactical communication strategies for anti-jam and low-probability-of-intercept operations.

The EPAS under development is designed for those systems whose propagation characteristics are controlled by the ionosphere and magnetosphere. In turn, the characteristics of the ionosphere and the magnetosphere are controlled by the sun's activity. Short term variations in solar activity such as solar flares, x-ray bursts, and high speed solar wind streams cause significant changes in the ionosphere and magnetosphere. Long term cycles of solar activity control the long term average characteristics of the ionosphere. Thus, the first two functions of the EPAS are concerned with the collection and delivery of solar-terrestrial activity data to a propagation assessment and forecasting subsystem.

The third function of EPAS is to provide propagation assessments and forecasts tailored for particular Navy systems and users. NOSC is developing a propagation assessment and forecast terminal (PROPHET) (Richter, et al., 1976; Rothmuller, 1978) to fulfill this function. In the remainder of this paper we will describe the philosophy behind PROPHET and several of the prediction models We will also discuss the future of the PROPHET concept and those areas of solar-terrestrial physics where more information is needed to bring PROPHET to its full potential.

PROPHET DESCRIPTION

"Propagation conditions for the North Pacific are likely to be unsettled for the next 12 hours because of a geomagnetic storm." General advisories of this sort are about all that has been available for the Navy communications officer for the last decade. They are useful in that the communicator is warned to expect erratic system behavior, to expect the usual hf communications frequencies to become unusable, and to understand that when outages do occur it is unlikely they are due to equipment or operator failure. However, the communications officer really wants to know the specific steps to take to minimize the message error rates whenever there is an environmentally caused upset to his system. For example, the hf communicator would like to have predictions of the

lowest useable frequency (LUF), the maximum useable frequency (MUF), and the frequency of optimum transmission (FOT) for each specific circuit. The PROPHET propagation assessment and forecasting terminal is designed to provide him this information.

PROPHET provides this information by taking environmental data from a variety of satellite and ground-based sensors and using these data as inputs to a variety of analytical models that output the specific propagation forecasts required by the communications officer. Figure 1 shows the information flow for the entire EPAS. Data from satellites (SOLRAD HI, SMS/GOES, etc.) and ionospheric assessment centers such as Air Force Global Weather Central and NOAA Space Environmental Services Center pass through a general center (presently NOSC, La Posta), where the data are sorted, converted, and relayed to the individual PROPHET terminals.

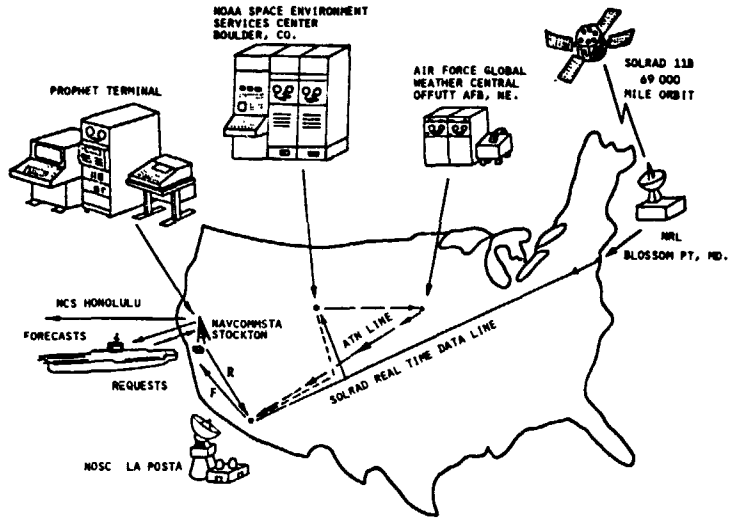

Figure 1. Information flow for the PROPHET environmental prediction terminal

The PROPHET terminal, or minicomputer (presently an AN/UYK-20) contains specific numerical models stored in memory. The models quantify environmental effects on propagation and address specific system vulnerabilities. Initially we at NOSC identify the system characteristics and vulnerabilities, generally through inputs from Naval Communications Officers. Once each problem area is understood then we begin model development. Often the necessary information is available through scientific literature or personal contacts. When it is not available we either do the research ourselves or, when possible, we aid researchers at other institutions in finding support for specific research projects.

Three approaches can be taken to develop models assessing the propagation environment: phenomenological, statistical, and semi-empirical. The phenomenological is based on an understanding of the physical processes relating cause and effect. The statistical approach is based on synoptic studies and assumes that predictions can be made based on historic data. The semi-empirical method

(presently used most often by the NOSC modeling group) combines knowledge of the basic physical causes with observational data to generate simplified models which obviate modeling the complicated processes between the basic driving cause and final effect.

An illustration of a semi-empirical model is the effect of high energy solar proton emission on the Omega vlf navigation system. The physics of the process is that the polar D-region of the ionosphere (50-90 km) is anomalously ionized by high energy (E > 10 MeV) protons. This increased ionization causes greater than normal phase advances on signals crossing the affected region and thus, if unaccounted for, would cause navigational errors. The increased ionization also causes high absorption in the hf (and vhf) band, which has given the name polar cap absorption or PCA to these events.

The Omega correction model developed by NOSC (Argo, 1975) translates the solar proton flux measured at satellite altitudes into phase error corrections (Figure 2). These corrections are in the form now routinely used to account for variations due to time of day, season, etc. The model has as parameters integrated proton flux (E >10 MeV), time of day, and path length through the "polar cap" defined to be greater than 63° geomagnetic latitude. The model will correct the phase back to provide the nominal 2 km accuracy of Omega. The implementation of the model uses an auxiliary look-up table (Argo, 1976) of normalized phase advance, with PROPHET providing a "proton flux factor" that accounts for the event magnitude.

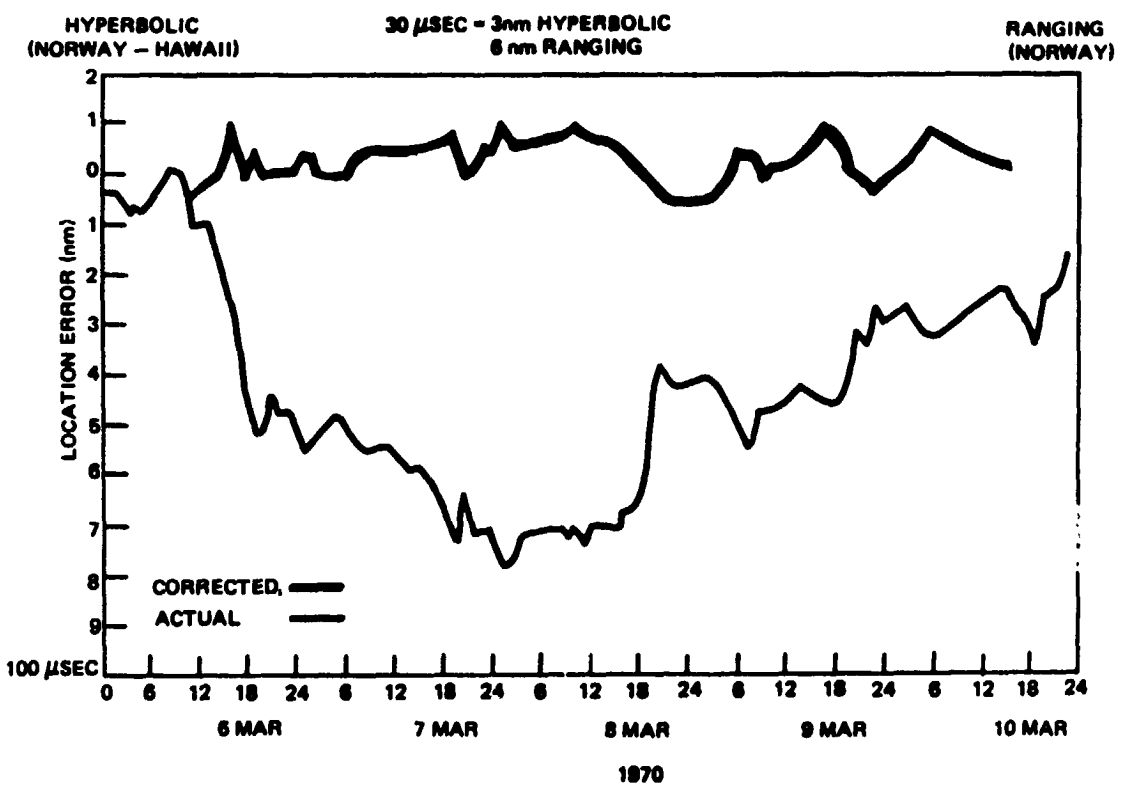

Figure 2. Corrected and uncorrected Omega positioning errors

This semi-empirical approach has yielded other models relating solar proton flux data to systems effects. Argo and Hill (1976) developed a model relating absorption of transpolar hf and polar region vhf/uhf satellite communications to the proton flux. These models use average loss rates (with seasonal variations) to define the D-region electron density, and then calculate the absorption directly.

Another model developed by NOSC is the effect of an x-ray flare on hf communications. This model has two "components." One models the time history of the flare. The flare duration model predicts the duration once the flare has reached its peak. The prediction technique uses the discovery by NOSC that the flare decay can be accurately described with one of a small set of definite decay rates. The rise time and peak amplitude are used to estimate the decay rate (Argo, et al., 1978). The model adjusts itself in case of multiple flares and can update the decay estimate. Figure 3 shows an example of the model using historical SOLRAD 9 data.

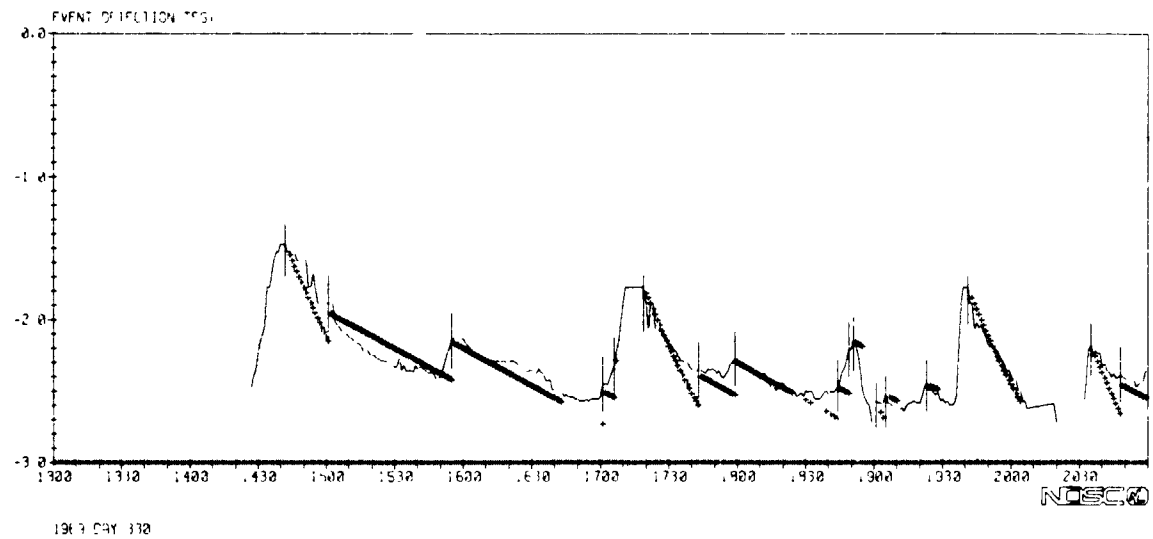

Figure 3. Solar flare 1-8A x-ray flux (solid curve) and flare forecasting results (x's)

Increased x-ray fluxes cause increased absorption of hf signals, with the amount of absorption increasing as the hf frequency decreases. The effect of an x-ray event is therefore to increase the lowest useable frequency (LUF). This relationship between the x-ray flux and the LUF (Rose, et al., 1974) is the second component of the flare model. Once the flare x-ray is modeled then the time to recovery as a function of frequency can be calculated for each communication circuit. The time to recovery will be the point in time that the x-ray enhanced LUF drops below the specified frequency. This output, which now specifically indicates to the communications controller how long his given circuit will be unavailable, is displayed in Figure 4.

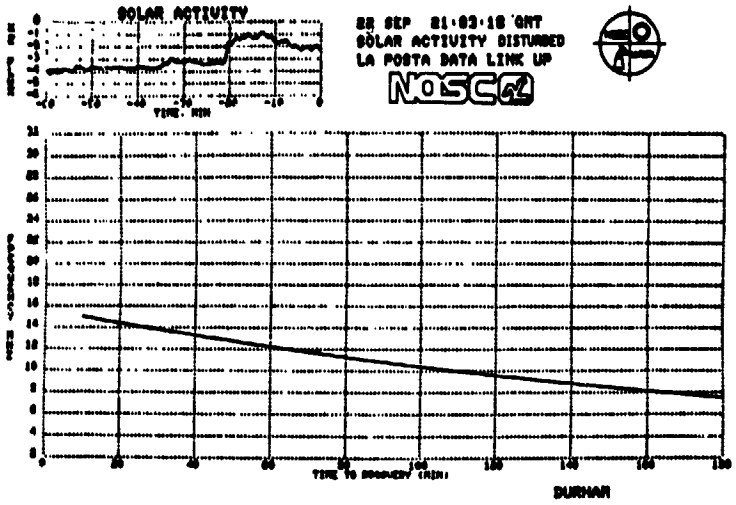

Figure 4. PROPHET display predicting time to recovery from a solar flare for the ship DURHAM

In addition to these propagation predictions during disturbed periods, the Naval Communications Officers expressed interest in having automated the routine predictions of diurnal variations in the MUFs and LUFs. To achieve this models by both the Air Force (1975) and NOSC (Rose, et al., 1978) have been implemented. The Air Force model uses hourly updates to a statistically based model - the updating is done by refitting to data obtained from an hf ionospheric sounder network. The NOSC model is extremely simple, but gives results with nearly the accuracy of the unmodified Air Force model. Therefore it is useful in long term predictions. Figure 5 is an example of the output of the MAP routine, which gives the communications controller the pertinent propagation information such as LUF, MUF, and FOT for his established circuits. The graphics display is used to allow the controller to visualize the area he is responsible for. These dis-

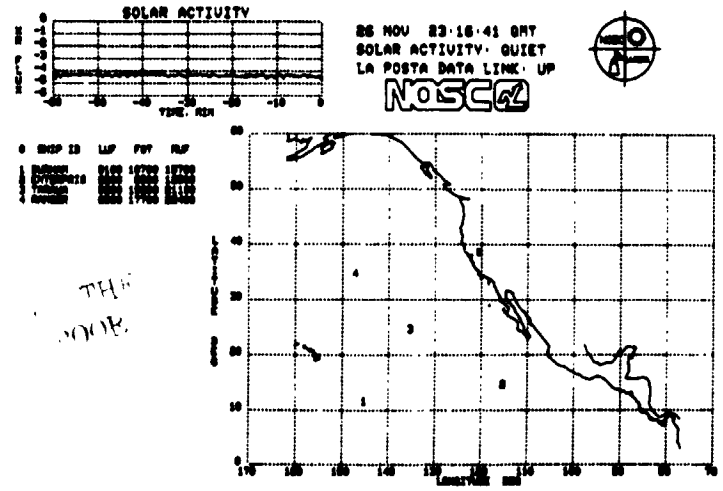

Figure 5. PROPHET display showing controller the LUF, MUF and FOT for the established circuits

plays are also available during disturbed periods (such as x-ray flares), in which case the MUFs and LUFs are those expected at the moment of request.

Another statistical model adapted for Navy use is the scintillation depth of fading model (LaBahn, 1974). This is an adaptation of the model developed by Fremouw and Rino (1973) and modified by Pope (1974).

An important aspect of these models developed at NOSC is that they are tailored to a specific system application and that the output is in easily used terms (e.g. navigation correction in miles, lowest useable frequency, etc.). Table I summarizes the completed forecasting models available to PROPHET.

TABLE 1. DESCRIPTION OF COMPLETED FORECASTING MODELS

Model (source)	Function	Causative source	System	Action
Flare detection	Disturbance warning	1-8Å x-rays	All hf vlf navigation	Warning
Flare duration estimator (NOSC)	Disturbance warning	1-8Å x-rays	All hf vlf navigation	Warning
SID GRID (NOSC)	Disturbance warning-SWF	1-8Å x-rays	All hf	hf comm • Freq shift • Reroute traffic HFDF • Net impact assessment
PCA/vlf (NOSC)	Disturbance warning-PCA	10 MeV particles	vlf navigation (Omega)	Correction factor for transpolar circuits
SPA/vlf (NOSC)	Disturbance warning-SPA	1-8Å x-rays	vlf navigation (Omega)	Correction factor for sunlit circuits
LOF split (NOSC)	Tactical (reduced intercept vulnerability)	Solar diurnal transition 1-8Å x-rays	Covert hf systems	Optimum freq selection against known receivers
Scintillation grid (SRI)	Disturbance warning/ tactical	Unknown (statistical model)	vhf/uhf satellite communica-tions	Advisory - dB fade probability based on location
PCA/hf (NOSC)	Disturbance warning-PCA	10 MeV particles	All hf	Advisory dB • freq shift • reroute traffic HFDF • Net impact assessment
Quiet MUF (ITS/GWC)	MUF during normal times		All hf	hf comm normal operations
QLUF	LUF during normal times		All hf	hf comm normal operations
Raytrace	Receiver accessibility		All hf	hf comm normal operations

NOSC conducted a field test of the PROPHET assessment terminal at the Naval Communications Station, Stockton, CA. The test objectives were to test the utility (and reliability) of real-time tailored propagation assessments in an operational environment. Analysis has shown that: (1) COMMSTA personnel made frequent use of PROPHET - terminal access on an average of once every nine minutes; (2) using PROPHET predictions, QSYs (number of frequency shifts) and outages due to propagation were reduced by 15% with duration of outages reduced by 15%-20%; (3) COMMSTA personnel gave a qualitative general "usefulness" rating of PROPHET of 8 on a scale of 10.

FUTURE PLANS FOR PROPHET AND NEEDS FOR CONTINUED DEVELOPMENT

As use of ionosphere and transionospheric communication channels is increased the impact of and need for solar-terrestrial predictions will increase concommitantly. PROPHET enhances the ability to do individual specific forecasts, and so the Navy will likely move towards increased use of shipboard (and airborne) prediction terminals. These can be used to take tactical advantage of situations such as anomalous intercept opportunities (e.g. Pope, 1976). In addition, the FAA has expressed an interest in a tailored PROPHET-like terminal to ensure adequate communication capabilities for commercial airplanes. Indeed, as the use of the present PROPHET techniques become standard in the communications world then we expect the design of wholly new sophisticated communication systems that will require a new generation of more accurate PROPHET models.

Minicomputers are becoming both smaller and more powerful and so more complicated models (both phenomenological and statistical) can realistically be expected to operate in a real-time environment. These increased capabilities will make tactical propagation advantages available to the user of these forecasting systems. This is important, because presently much effort is being expended in gaining a few dB advantage for communications systems through signal coding and information processing techniques. Intelligent use of a PROPHET system can presently yield advantages significantly higher than that (Rose, 1976; Argo, et al., 1976).

Present modeling capabilities are limited by lack of phenomenological pictures of some solar and ionospheric processes. Future work must be aimed at the removal of these limitations in the following problem areas:

(1) Flare prediction. It is anticipated that by 1980-81 flare activity will be high, and so flare occurrence and flare product prediction models must take high priority.

(2) Scintillation phenomenology. The increased dependence on space borne systems increases the vulnerability to debilitating scintillations caused by irregularities in the intervening medium. Thus, in anticipating outages and to provide circumventing strategies, scintillation morphology and phenomenology must be better known and understood.

(3) Magnetic and ionospheric storms. These disturbances affect a wide variety of military systems such as space track radars, hf communications and surveillance systems, as well as antisubmarine warfare (ASW) and mine warfare systems. An understanding of the energy inputs into the neutral atmosphere and the redistribution of this energy through gravity waves and winds must be attained if the effects of these storms are to be adequately modeled.

(4) Ambient ionosphere. If forecasting is to be developed and used as a tactical operating strategy, better knowledge must be gained of the link between real-time solar geophysical information and ionospheric behavior. Although much work has been done in this area, interactions between the magnetosphere, ionosphere and neutral atmosphere complicate the problem and make the development of an accurate model very difficult. Note that the difference between the ionosphere disturbed by an ionospheric storm and the typically varying ambient ionosphere is strictly a matter of degree, and so problem areas 3 and 4 are closely linked.

CONCLUSION

The effectiveness of Naval Communications is dependent upon establishing and maintaining adequate communication links. Because ionospheric disturbances may be a disrupting factor on these communication links, it is important to have accurate long and short term predictions of solar-terrestrial activity. In order to take remedial action for a specific system we have found it necessary to have real-time forecasts tailored to fit the user's needs. The tailored forecast concept has been implemented through the PROPHET propagation assessment and forecasting terminal. Recent field tests (Levine, 1978) indicate that for the specific systems and disturbances addressed that the PROPHET concept is extremely useful.

PROPHET has only just touched the surface in the application of propagation prediction for communication systems. As computational capabilities increase and costs drop there is much more room for expansion into increasingly sophisticated areas such as propagation channel modeling, where actual statistics of the channel are calculated rather than the more general character such as MUF and LUF. There are also several specific disturbance phenomena (e.g. scintillations and ionospheric storms) that are still inadequately understood in a phenomenological sense, and these must be understood if we are to maximize the usefulness of solar-terrestrial forecasting.

REFERENCES

Air Force Global Weather Central (1973): AFGWC Manual 105-1.

Argo, P. E. (1975): Modeling Omega PCA Phase Advances, NELC Technical Report 1950.

Argo, P. E. (1976): Omega Navigation Disturbance Correction Tables, Polar Cap Absorption Events; East Pacific, 10.2 kHz, NELC Technical Document 480.

Argo, P. E. and J. R. Hill (1976): High Frequency Polar Cap Absorption Model, SOLRAD Application, NELC Technical Note 3249.

Argo, P. E., I. J. Rothmuller and J. R. Hill (1976): Environmental Effects on HF Propagation, NELC Technical Note 3204.

Argo, P. E., I. J. Rothmuller and J. R. Hill (1978): X-Ray Flare and Short-Wave Fade Duration Model, NOSC Technical Report 255.

Fremouw, E. J. and C. L. Rino (1973): Modeling of Transionospheric Radio Propagation, Radio Sci., 8, 213.

LaBahn, R. W. (1974): Development of a Scintillation Prediction Grid, NELC Technical Note 2814.

Levine, P. (1978): SOLRAD PROPHET DT&E Field Test #1 (HF Communications), Megatek Report #R2005-096-F-1.

Pope, J. H. (1974): High Latitude Ionospheric Irregularity Model, Radio Sci., 9, 675.

Richter, J. H., I. J. Rothmuller and R. B. Rose (1976): PROPHET: Real Time Propagation Forecasting Terminal, paper presented at the 7th Technical Exchange Conference, El Paso, TX, 30 Nov - 3 Dec 1976.

Rose, R. B. (1976): Tactical Application of HF Propagation Forecasts, NELC Technical Note 3179.

Rose, R. B., J. R. Hill and M. P. Bleiweiss (1974): Sudden Ionospheric Disturbance Grid, NELC Technical Report 1938.

Rose, R. B., J. N. Martin, P. H. Levine (1978): MINIMUF-3: A Simplified hf MUF Prediction Algorithm, NOSC TR 186, Feb 1978.

Rothmuller, I. J. (1978): Real Time Propagation Assessment, AGARD-CPP-238, Ottawa (24-28 April 1978).

PREDICTIONS OF THE SPACE ENVIRONMENT SERVICES CENTER

G. R. Heckman
Space Environment Services Center
Space Environment Laboratory
National Oceanic and Atmospheric Administration
Boulder, Colorado 80303, USA

A list is presented of all the current types of users of the Space Environment Services Center. All the data collected by the Center are listed and a short description of each primary index or activity summary is given. Finally, each type of regularly produced forecast is described, along with a summary of the methods used to produce each prediction.

1. INTRODUCTION - THE SPACE ENVIRONMENT SERVICES CENTER

The Space Environment Services Center (SESC) in Boulder is operated jointly by the National Oceanic and Atmospheric Administration (NOAA) and the U. S. Air Force Air Weather Service (USAWS) and exists to provide predictions, alerts and real-time data describing solar geophysical disturbances to users throughout the United States. In addition, it is designated as the World Warning Agency (WWA) for the International Ursigram and World Days Service (IUWDS), which is operated under the International Union of Radio Science (URSI). SESC collects data from its own sensors, from cooperating agencies and institutions and from other countries, both through IUWDS and through bilateral exchange agreements. The data collected include images and parametric measurements of the sun, the interplanetary medium and the earth's magnetosphere and ionosphere.

Users of the SESC service can be divided into roughly three equal parts. About one-third find some form of the predictions to be sufficiently accurate to be useful for planning purposes; another third wait until they receive an alert that an event has started before they take action. The final third are users interested in receiving data in some form, which may be indices, activity summaries or high resolution data. A summary of the types of users is given in Table 1.

Table 1. Users and Types of Activity Affecting Their Systems

Customer	Type of Activity Producing Effect
· Civilian satellite communication	· Magnetic storms
· Commercial aviation--mid-latitude communication (VHF)	· Solar radio emissions
· Commercial aviation--polar cap communication (HF)	· PCA, magnetic storms, x-ray bursts
· Commercial aviation navigation (VLF)	· PCA, magnetic storms, x-ray bursts
· Electric power companies	· Magnetic storms
· Long line telephone communication	· Magnetic storms
· High altitude polar flights radiation hazards	· Solar proton events
· Civilian HF communication Coast Guard, GSA, commercial companies, VOA	· X-ray emission, U.V. emission, magnetic storms
· Geophysical exploration	· Magnetic storms
· Satellite orbital variation military and civilian	· U.V. emission, magnetic storms
· DOD SATCOM communication	· Magnetic storms
· DOD HF communication	· X-ray emission, U.V. emission, PCA, magnetic storms
· DOD reconnaissance	· PCA, magnetic storms
· DOD navigation	· X-ray emission, U.V. emission
· ERDA communication (prospective customers)	· X-ray emission, U.V. emission magnetic storms
· International community	· All
· Scientific satellite studies IMS, Solar Maximum mission, Shuttle, solar constant measurements, stratospheric ozone variation, interplanetary missions	· Optical solar flares, magnetic storms, X-ray emission, U.V. emission, solar proton events, solar features
· Scientific rocket studies IMS, magnetosphere, ionosphere, upper atmosphere, sun	· Optical solar flares, solar features, magnetic storms, solar proton emission, X-ray emission
· Scientific ground studies IMS, sun, interplanetary magnetosphere, ionosphere, upper atmosphere, stratosphere, troposphere, seismological/geomagnetic	· Optical solar flare, magnetic storms, solar proton emission, X-ray emission, U.V. emission, solar features

2. DATA SOURCES

All of the observational data in the SESC is listed in Table 2. Though it is presumed that the STP workshop will not limit its coverage to prediction techniques that rely on currently available data, it is possible that some of the discussions may illuminate new and better uses of some of the current data, substitution of more appropriate data sets or elimination of some observations that began with more promise than fulfillment. It should be

Table 2. Data Sources

Type	Wavelength or Energy Range	Time Resolution	Primary Sources
Solar Patrol			
X-rays	1-8 Å, 0.5-4 Å	1 Minute Averages	GOES
Optical	Hydrogen Alpha	Continuous	Several
Radio	202-15,400 MHz	1 Minute	Several
Solar Synoptic			
Hydrogen Alpha Images		Several per day	Boulder
White Light Images		Several per day	Boulder
Ca K Images		Daily	Sac Peak
He 10830 Images		Daily	Kitt Peak
Magnetograms (Full Disk and Regional)		Daily	Kitt Peak, Huntsville
Sunspot Magnetic Fields		Daily	Mt. Wilson, Boulder
Ca K Scaled Reports		Daily	McMath
Sunspot Reports		Several Daily	Several
Solar Mean Field		Daily	Stanford
10.7 Cm Radio Flux	2800 MHz	3 Times Daily	Ottawa (Algonquin)
East-West Radio Drift Scan	2800 MHz	Daily	Ottawa (Algonquin)
Energetic Particle Patrol			
Synchronous Orbit	Protons: 06-500 MeV Alphas: 4.0-329 MeV Electrons: $\geq$ 2 MeV	1 Minute Averages	GOES
Polar Orbit	Protons	30 keV-850 MeV	TIROS-N
Magnetometer Patrol			
Synchronous Orbit	3 Components	1 Minute Averages	GOES
Terrestrial	3 Components	10 Seconds	IMS North American Chain
		10 Seconds	Boulder
		15 Minutes	Air Force Real Time Chain
		15 Minutes	Thule
		15 Minutes	Vostok
Miscellaneous			
Neutron Monitor		15 Minutes	Thule
High Latitude Riometers	30 MHz	15 Minutes	Alaskan Chain, Thule
Auroral Backscatter Radar	50 MHz	15 Minutes	Anchorage
Interplanetary Scintillation	74 MHz	Daily	UCSD
Ionosondes	foF2, M3000, Fmin	One hour or six hours	Several

noted that many of the data sets available to the SESC are provided due to the generosity and cooperative nature of the organizations that make them available.

3. DISTRIBUTION SYSTEMS

In order to give STP Workshop participants an overall view of the SESC operation, a survey of the systems for distributing its produces is given in Table 3.

4. OBSERVED INDICES AND ACTIVITY SUMMARIES

With the exception of research scientists conducting experiments, most users of space environment services do not want a continuous stream of data. They typically refer indices or activity summaries that make it easier for them to relate solar and geophysical variations to problems in their operating systems. Though the topic of the STP Workshop is to study and recommend improved predictions, there are some instances where improved predictions may

Table 3. Distribution Systems

Telephone:
- FTS (Federal Telephone Service)
- WATS (Wide Area Telephone Service)
- Commercial Telephone Service
- Dedicated Telephone Lines (Hot Lines)
- Recorded Information Numbers

Teletype:
- ATN (Astro-Geophysical Teletype Network)
- AUTODIN (U.S. Government Teletype Service)
- Commercial Teletype Services
- Secondary Networks

Computer Links:
- Space Environment Laboratory Data Acquisition and Display System (SELDADS) Public User Access
- Dedicated Data Links

WWV Shortwave Broadcast

Mail

depend on innovative indices that provide a more concise description of the environmental variations. The indices and summaries compiled in the SESC are summarized in Table 4 and described in more detail in this section.

Table 4. Observed Indices and Activity Summaries

- Solar Active Region Summary Report
- Sunspot Number
- Flare (and Other Event) Lists
- Solar Neutral Line Analysis and Synoptic Maps
- Ten-Centimeter Flux
- Solar Proton Events and Proton Flux
- SST Radiation Levels
- Geomagnetic A- and K-indices
- Substorm Log
- Sector Boundaries (at 1 A.U.)

4.1 Solar Active Region Summary Report

Each day, a summary is compiled of all the solar active regions on the visible face of the sun. The summary includes all active regions that contain sunspots plus some additional spotless regions that already have or are believed capable of producing solar flares. The parameters listed for each

region include the following: Boulder Region Number, location (Heliocentric Latitude and Longitude), Carrington longitude, sunspot area, modified Zürich classification, sunspot count, and magnetic classification. All the parameter values assigned each day are a composite summary, made by the Boulder forecaster, from the observatory reports received during the day. The accuracy in the locations reflects the variability in the observatory reports and is typically plus or minus five degrees (heliocentric) unless a special request for higher accuracy has been received in advance.

4.2 Sunspot Number

Using the region summary, a sunspot number is computed each day. The number is unsmoothed and is subject to the considerable variability in the sunspot counts reported by the real time observatories. The numbers are published in the weekly "Preliminary Report and Forecast of Solar-Geophysical Activity".

4.3 Flare (and Other Event) Lists

Each day, a running log is maintained in the SELDADS, of observed solar energetic events including flares (x-ray and optical) and solar radio bursts. The primary flare classification system used is the C,M,X x-ray classes assigned from the SMS/GOES data although optical importance is also included where available. Spectral radio events (Types I-V) are also included in the events list. Non-flare optical events (e.g., erupting filaments, surges) are included although the reporting coverage of these types of activity is less complete.

The primary SESC flare classification system is based on the peak flux Φ in Watts m^{-2} measured on the GOES satellite 1-8 Angstrom ionization chamber. The classes are assigned as follows: Class X for $10^{-4} \leq \Phi$, Class M for $10^{-5} \leq \Phi < 10^{-4}$, and Class C for $10^{-6} \leq \Phi < 10^{-5}$ flux (Watts m^{-2}). An additional digit is added to the C, M, X to indicate the coefficient of the flux. For example, C8 implies 8×10^{-6}, M3 implies 3×10^{-5}, etc.

4.4 Solar Neutral Line and Synoptic Maps

Each day, the SESC forecaster prepares a map of the visible face of the sun using procedures described by McIntosh (1979). The map includes the location of all magnetic neutral lines (the line of separation between the inwardly and outwardly directed magnetic fields) at the solar surface. The neutral line information is compiled from solar magnetograms and inferred using the principles reviewed by McIntosh where lines of magnetic reversal tend to be traced by filaments, by filament channels and plage corridors and where fibrils and arch-filament systems lie perpendicular to the neutral line. Magnetic field polarities are assigned using magnetograph observations and by applying the law of Hale for polarities of sunspots in active regions (leading spots positive in the northern hemisphere in cycle 21, leading spots negative in the southern hemisphere in cycle 21). Active regions are noted by their region number, and following the procedures described in the prediction section, flare probabilities are recorded for each region. The location of

coronal holes, as indicated by x-ray images (when available), or inferred from the Helium 10830 images made at Kitt Peak, are outlined on the map. Most of the information on the daily "neutral line" map (excepting the flare probabilities) is extracted onto a Mercator projection map of the sun that covers 360 degrees of heliographic longitude and latitudes from north 70 to south 70 degrees. This synoptic chart is published in the weekly "Preliminary Report and Forecast of Solar Geomagnetic Activity" and in the NOAA publication Solar Geophysical Data.

4.5 Ten Centimeter Radio Flux

Since 1947, the solar flux at 2700 MHz has been measured daily by the Canadian National Research Council. Because of its relatively long history of careful observation, and because it gives at least a general estimation of solar radiation in EUV wavelengths, the ten centimeter flux has evolved as a well entrenched parameter that is used by a large number of radio communicators and upper atmospheric modelers for a variety of operational applications. The SESC receives the "Ottawa" flux each day and redistributes it to the operational community. In fact, this parameter is probably the most frequently requested and used parameter in the field of solar-geophysical measurements. It has been argued by some of the scientific community that the ten-centimeter flux is too gross a parameter to accurately evaluate the state of the ionosphere and upper atmosphere and that more specific measurements in the EUV would improve the operational models. However, the lack of a consistent and on-going EUV observational program and the expense and disruption of redoing present operational models probably precludes any rapid phase out in the use of the models that operate with ten-centimeter flux as an input.

4.6 Solar Proton Events and Proton Flux

Solar proton flux is collected in real time from the NOAA SMS/GOES satellites at synchronous orbit and the NOAA TIROS-N satellite in polar orbit. The SMS/GOES data are processed in the SELDADS system to provide one-minute (or longer, if desired) (1) averages of proton fluxes above some specified energy levels (4, 10, 16, 40, 80 MeV), (2) spectral and flux parameters R_o and J_o from a least squares fit to an exponential-in-rigidity spectrum and (3) fluxes above arbitrarily selected energies by using the results of the minute-by-minute least squares fit. No processing beyond raw counting rate has yet been done with the TIROS-N data. To simplify communications with the user community, a proton event has been defined as an event where proton fluxes exceed 10 protons cm^{-2} sec^{-1} $ster^{-1}$ for particles with energies greater than 10 MeV. It should be noted that though the SMS/GOES satellites measure alpha particle fluxes over six energy ranges, these data have not yet been integrated into the proton processing and display programs.

4.7 SST Radiation Levels

Using the J_o, R_o parameters calculated for proton events, an estimated radiation dose rate is calculated for a hypothetical aircraft flying at 65,000 feet over the polar cap. The dose is calculated by using the transport equation of Flamm and Lingerfalter (1964) as evaluated by Haurwitz (1971) with J_o and R_o as the independent parameters. The accuracy of the calculation is

reduced by the necessity of fitting the parameters J_o and R_o to spectra for energies measured over the range 1 to 500 MeV (with poor observational resolution toward the upper end) where the primary dose contribution originates. A newer series of particle sensors on future SMS/GOES satellites could improve the higher energy spectral fit but another limitation in the present system is that Haurwitz carried out the numerical integration for relatively modest values of R_o and much higher values have since been measured. As now done, the calculation gives an order-of-magnitude calculation for a quantity that can vary over five orders-of-magnitude.

4.8 Geomagnetic A and K Indices

The A- and K-indices serve as the lowest common denominator for communicating with users whose systems are affected by varying levels of geomagnetic activity. Many scientific users would prefer to have a real time DST or AE for their use and SESC has, in response to some special requests, made real time estimates of DST using the low latitude stations in the IMS North American chain. Continual real time extrapolation of DST and AE, using the same IMS chain, have been discussed but the lack of longitudinal coverage and the uncertain future of the IMS chain has tended to slow the progress toward implementation. The problems with the A- and K-indices are of two kinds. The first is time resolution. The implicit limit in resolution in the present system is three hours for the real time K values (or 90 minutes from some of the Air Force stations). Field perturbations of a few minutes duration but large in magnitude and in rate of change are presumably of greatest concern to several users such as the electric power industry and the K-indices give only an approximate estimate of problems for them. Secondly, the A- and K-indices are global in nature while the effects of magnetic disturbances can be confined to comparatively narrow longitudinal bands so that alerts based on K-indices are not universally applicable.

Like the ten-centimeter flux index, a number of users have large investments in models that use A- and K-indices for measuring geomagnetic activity. Unless, and until, someone redoes all the work that goes into the construction of such models, these users are likely to continue to use A and K values despite the availability of more specific indices. There are some additional problems with the real time A- and K-indices. For many years, users tended to apply a real time K from a mid-latitude station such as Fredericksburg interchangeably with the planetary K_p values which are not available until some months after the fact. In fact, Adams (1975) has shown that the Fredericksburg values vary systematically by up to 25 percent from the planetary values. The Air Force uses a real-time estimation of K and A from a set of about five stations, but the estimated K_p and A_p is frequently made artificially large by the effects of auroral electrojets on their station sample.

4.9 Substorm Log

One type of summary that provides positional information for geomagnetic disturbances is the Substorm Log. The log is compiled from the IMS North American chain and provides a continuous listing of substorm beginning times and longitudinal location. The catalog has attracted interest primarily among

scientific researchers although some operational type users have requested it. Essential shortcomings from the user point of view would probably be the problem of relating the substorm intensity to a threshold at which the user experiences problems and the failure of the equivalent current model, on which the catalog is based, at times of major geomagnetic storms.

4.10 Interplanetary Sector Boundaries

Since the SESC receives no real time solar wind from in situ measurement and because there is a continuing interest among some users in monitoring the current status of sector boundaries in the interplanetary magnetic field, daily inferences of the polarity of the interplanetary magnetic field are made from the Z component of the magnetic field at Thule, Greenland, using the method of Svalgaard (1968) and of Mansurov and Mansurova (1969).

5. ALERT CATEGORIES

Some users of the SESC services find that the predictions as now made are not sufficiently accurate to use as a planning guide, but yet these customers are not interested in monitoring a full data stream at all times. For these users, an alert service is provided that allows them to receive a telephone call or teletype message when a particular kind of disturbance reaches a specific threshold. About one-third of all SESC users fall into this category of service, although a large number of them would prefer to rely on better predictions if such were available. Also, as pointed out in the section on geomagnetic indices, some of the indices are global in nature and the use of a general index at a single threshold typically means that some users are experiencing adverse effects when they receive an alert while others receive what amounts to a false alarm. A complete set of alert thresholds is given in Table 5.

Table 5. SESC Alert Categories

SOLAR FLARES

- X5 (1-8A X-ray Classification)
- X1
- M5
- 3B (Optical Classification)
- 2B
- 1B

MAGNETIC DISTURBANCES

- A $\geq$ 50 (real time A measured at Boulder)
- A $\geq$ 30
- A $\geq$ 20
- K $\geq$ 6 (real time K measured at Boulder)
- K $\geq$ 5 observed in successive three-hour intervals
- K $\geq$ 5

Table 5 (continued).

- $K \geq 4$
- Sudden Commencement

RADIO BURSTS/NOISE STORMS

- 10 CM Radio Burst Greater Than 100 Flux Units
- 245 MHz or Noise Storm
- Type II and/or Type IV Decametric Emission

PROTON EVENTS

Proton Flux (E > 10 MeV) > 10 $cm^{-2}sec^{-1}sterad^{-1}$

6. PREDICTIONS

All the predictions routinely produced by the SESC are included in this section. Each type is discussed separately so that the reader may refer to that section alone. A summary is provided in Table 6.

Table 6. Prediction Products (Lead Time Given in Parentheses)

LONG TERM SOLAR ACTIVITY AND SOLAR RADIATION LEVELS

- Smoothed sunspot number (1 month-10 years)
- Geomagnetic activity and ten-centimeter flux (1 month-10 years)
- General level of solar activity (27 days)

SOLAR ACTIVITY — SHORT TERM

- Solar Flares (1, 2, 3 days)
- Solar proton events (1, 2, 3 days, PFP*)

SOLAR RADIATION LEVELS — SHORT TERM

- Ten-centimeter flux (1, 2, 3 days)

GEOMAGNETIC DISTURBANCE LEVELS

- A, K-indices (1, 2, 3 days)
- Time of sudden commencements (PFP), storm size (PFP)

*PFP: Post Flare Prediction - A prediction of a flare consequence once the flare has occurred.

6.1 Smoothed Sunspot Number

The predictions are made in terms of the smoothed sunspot number, where the smoothing is done according to the standard procedure

$$\bar{R}_n = \frac{1}{24}\left[R_{n-6} + R_{n+6} + \sum_{n-5}^{n+5} 2R_n\right], \qquad (1)$$

where $\bar{R}$ is the smoothed (over 13 months) number, R is the monthly average for month n. SESC cooperates with World Data Center A of the Environmental Data and Information Service (EDIS) of NOAA in issuing predictions of sunspot numbers. EDIS has, for several solar cycles, published predicted smoothed sunspot numbers, along with 95 percent confidence intervals, derived by the method of McNish and Lincoln (1949), for each month remaining in the cycle in progress. Sargent (1978), of the SESC staff, has published a prediction for the maximum sunspot number of cycle 21 along with an expected confidence interval for that cycle. The two predictions for the maximum number are combined, along with the variance for each, to obtain a single value for maximum and a 95 percent confidence interval to go with it.

The many published methods of sunspot prediction can generally be divided into four broad categories as follows:

1. Spectral Analysis: extracting important periodicities in the sunspot record and using these periodicities to extrapolate into the future is a popular method of making the predictions. The dilemma for the user is to choose among the highly variable, but apparently reputable, predictions. For example, the predictions for the present cycle, using spectral methods, have ranged from very small (Cohen and Lintz, 1974) to very large (Hill, 1977). For this reason, spectral methods have not been used in the NOAA predictions.

2. Planetary Influence Models: the published results from this method have also been highly variable and are not included in the NOAA predictions.

3. Comparison of the Rate of Rise of the Current Cycle with Previous Cycles: Figure 1 (from Sargent, ibid) illustrates the time rate of rise of past solar cycles for the first few months following solar minimum. Some ordering of the cycles is apparent and several prediction methods take advantage of this ordering. The most widely used is the method of McNish and Lincoln (ibid). The McNish-Lincoln method accomplishes this statistically by computing an average of all the past cycles and comparing the current cycle to it. If the current cycle lies above or below the mean, that trend is carried forward into the prediction of the future, but it is balanced by a tendency of the predicted curve to move toward the mean. During the rising portion of the cycle, the McNish-Lincoln method is most accurate for the immediate future, with widening confidence intervals as the prediction is taken further and further in advance. This trend reverses later in the declining phase of the cycle when the prediction is for periods when the sunspot is decreasing. As pointed out by other authors (Lundquist and Vaughn, 1978), the principal problems with the McNish-Lincoln method are its

sensitivity to the selection of the time of minimum and the choice of the method of normalizing each cycle to its minimum.

4. The Method of Ohl: Originally suggested by Ohl (1976), the method has been studied by several authors, including Sargent (ibid). Though the various authors have used different indices and techniques of data treatment, they have obtained relatively consistent results. The Ohl method statistically relates the recurrent geomagnetic activity at the end of one solar cycle with the peak sunspot intensity of the next cycle. Sargent's results are shown in Figure 2. The work is interesting because of the possible implications in the association of the nature of the large scale magnetic fields from one cycle to the strength or coverage of the small scale sunspot fields in the next.

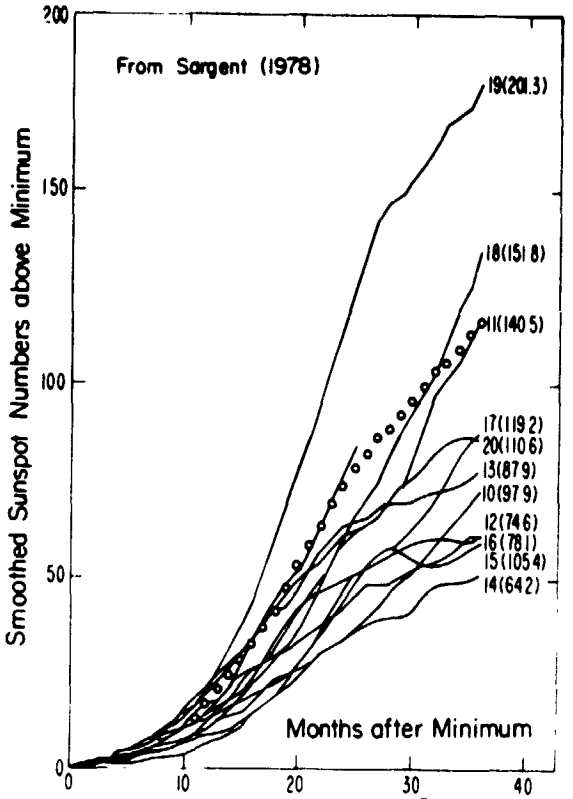

Figure 1. The early phases of the past eleven cycles and progress, to date, in Cycle 21.

6.2 Long Range Geomagnetic Activity and Ten Centimeter Predictions

The predicted quantities are smoothed monthly averages, where the smoothing is the same 13 month averaging that is done on sunspot numbers. The smoothed numbers are not necessarily what are needed by users, but are the limit of what can presently be done. Even so, in the case of the geomagnetic activity, the relationship is tenuous. A plot of smoothed sunspot numbers versus ten centimeter flux is shown in Figure 3 (Slutz et al., 1971). An analytical relationship that has been used in NOAA's recent work is from Slowly (1979) and is given by:

$$F_{10.7} = 49.4 + 0.97 \cdot \overline{R} \qquad (2)$$

$$+ 17.6 \exp(-0.035 \cdot \overline{R}) .$$

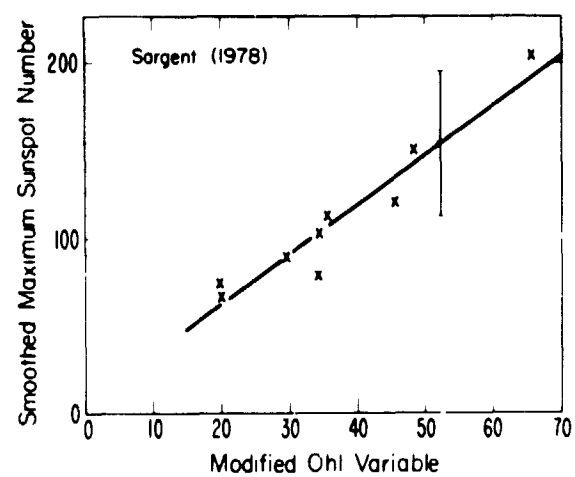

Figure 2. Scatter plot showing the relation of the modified Ohl variable to smoothed sunspot maxima for the past nine sunspot cycles. The predicted value for Cycle 21 is indicated and the 95% confidence limits are shown.

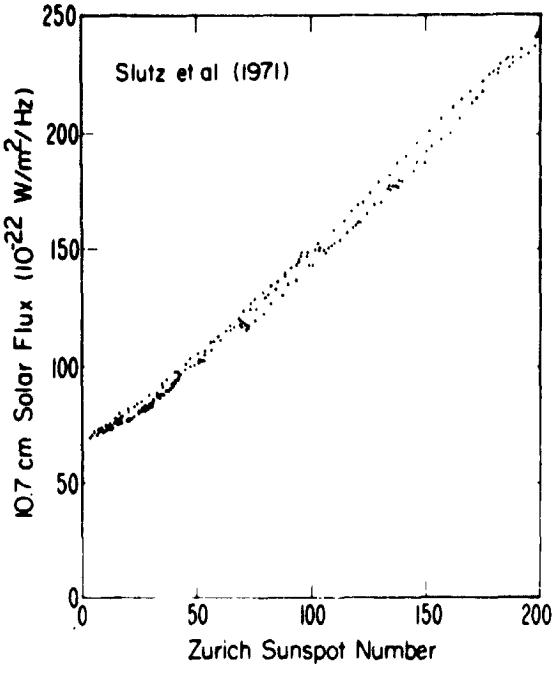

Figure 3. Smoothed Mean 10.7-cm Solar Flux versus Smoothed Mean Zurich Sunspot Number.

6.3 General Level of Solar and Geomagnetic Activity (27 days)

The ability to predict solar flares and associated activity more than a few days in advance is marginal. Therefore, the prediction categories are defined in general terms. For solar activity they are: Very Low — usually only quiet regions on the solar disk and no more than five of these; fewer than ten class C subflares without centimetric radio bursts or SID observed or expected. Low — usually more than five but less than ten quiet regions on the solar disk; only class C subflares without centimetric radio bursts or SID observed or expected. Moderate — eruptive regions on the solar disk; fewer than five class M x-ray events with centimetric radio bursts and SID observed or expected. High — active regions on solar disk; several class M x-ray events with centimetric radio bursts and strong SID; and/or one to two importance 2 chromospheric flares or class X x-ray events observed or expected. Very High — region capable of producing protons on the sun; one or more chromospheric flares of importance 2 or greater with outstanding centimetric radio bursts (500 flux units or greater), class X x-ray bursts, and major SID observed or expected. For the Geomagnetic Field: Quiet - $A_p \leq 7$; Unsettled - $7 < A_p \leq 15$; Active - $15 < A_p \leq 30$; Minor Storm - $30 \leq A_p < 50$; Major Storm - $50 < A_p$.

For predicting the levels of solar activity, primary reliance is placed on the tendency of flare activity to occur in active regions concentrated in bands of active longitudes and on the development and persistence of major active regions for more than one solar rotation in the years around solar maximum. Similarly, the long-range geomagnetic predictions rely heavily on the tendency of coronal holes to persist for several rotations, especially in the years just prior to solar minimum. One area of development that may offer improvement in this area is the construction of maps of the large-scale solar magnetic field and the investigation of whether the large-scale motions, that appear to be related to the formation of active regions and coronal holes, can be reliably predicted.

6.4 Solar Flare Predictions

Solar flares are classed and predicted according to their soft x-ray emission. Predictions are made separately for class C, M and X flares for periods one, two and three days in advance. A prediction is made for each day (0000 UT to 2400 UT) and is stated as the probability of occurrence of at

least one flare of the predicted size during the 24-hour period. It is normally given as a percentage rather than a decimal. The method used to make flare predictions, typically used where physical models of a process are not well defined, is to estimate the likelihood of flare occurrence by attempting to ascertain the presence or absence of certain active region characteristics that have been shown to be associated with flare occurrence. Most of the parameters traditionally used in SESC have been tabulated by Smith (1972) and are shown in Tables 7 and 8. Each forecaster, on the days when he has the duty shift, uses his own method of evaluating these parameters for each active region on the visible side of the sun. He has access to all the data listed in Table 2 while doing this evaluation. He then assigns a subjectively deduced probability of occurrence for each category of flare for each active region. The individual region probabilities are then combined to obtain a whole disk probability for each x-ray category.

Table 7. Primary Forecast Criteria

Magnetic Field Configuration

- Emergence, or growth, of new fields within, or near, existing fields such that the two fields interact.
- Merging of active regions through growth or proper motion.
- Polarities in bipolar region reversed from normal east-west order for hemisphere and solar cycle.
- Number and quality of convolutions in the radial neutral line.
- Magnitude and time-rate-of-change of gradients in radial component;
- Magnitudes of field strength maxima.

Subjective Reference to Past Activity

- H-alpha plage intensity, structure, and size compared with past examples with known associated flare activity.
- Sunspot-group form and area compared with past examples with known associated flare activity.
- Region location with respect to active heliographic longitudes (see Dodson and Hedeman, 1972, and Svestka, 1972).
- Rate and manner of growth or decay.
- Flare activity during past few days, with greater consideration for the past 24 hrs. Evolution of the region during the past 24 hrs. determines whether or not the observed lev ı of flare activity will persist.

Table 8. Secondary Forecast Criteria

Radio Emissions: Rise in background flux at any of several discrete frequencies (preflare heating)

X-ray Background Rise

Optical Coronal Enhancements (green and yellow lines)

Optical Activity at the Solar Limb

- Limb flares
- Surges, sprays
- Coronal rain
- Elevated plage (cap prominence)

In an attempt to determine the consistency with which the forecasters rate the several parameters, a simple survey was made of the forecast staff in the fall of 1978. Each forecaster was asked to rate and weight the parameters listed in Table 9. The results are shown in the columns headed "rank range" and "relative weight". The highest three parameters were equally weighted within the limits of the poll. However, 56 percent of the respondents picked persistence as their highest ranked parameter.

Table 9. Forecasters Rank of Flare Predictors

	Rank Range	Relative Weight (%)
· High or rapidly increasing magnetic field strength and gradient	1-7	11
· Magnetic complexity	2-8	11
· Persistence	1-12	11
· Presence of shearing motion or proper motion indicating shear or twisted fields	1-10	10
· Sunspot classification	1-8	10
· Minor flares that are X-ray rich or high x-ray background	4-10	9
· Emergence of new fields in stable or decaying portion of active region	1-10	7
· Rapid spot growth after initial appearance	4-12	6
· Colliding regions	4-12	6
· Similarity of region to previous flare producers	8-14	6
· Bright plage (or (high) McMath intensity)	3-13	3
· Plage compactness	3-13	3

Coverage of all the papers that relate flare productivity to various active region parameters is beyond the scope of this report. However, those papers that are most reflected by current SESC practice are included. In a pioneering paper, Giovanelli (1939) compiled an equation for the probability of a flare occurrence given by

$$\underline{P} = 2.6 \cdot k \cdot a \cdot f(i) \qquad (3)$$

where a is the spot area and k and f(i) are given in Table 10. The flares included in Giovanelli's study were for all classes and were for the same day as the region parameters. Smith and Howard (1968) extended magnetic field classifications to include active region plages and found that basically bipolar regions with an intrusion of one polarity into another, with islands of opposite polarity or composed of two or more adjacent bipolar regions are about 3 times more likely to produce flares of all sizes. Complex regions with reversed polarities are several times more flare productive. Other applicable papers include Sakurai (1967) and McIntosh (1969) - spot rotation and proper motion preceded some proton flares; Severny (1963) - strong magnetic gradients are associated with major flares; McIntosh (1969) - convergence of strong, opposite polarity spots just before a major flare; Martes et al., (1974) - interaction of growing and decaying portions of an active region as a flare producing condition; Horan and Kreplin (1970) - a

Table 10. Parameter Weights for Giovanelli's Probability Equation

Magnetic Class	k	Change in Area (millionths)	f(i)
α,αf	0	-600	0.9
αp	0.81×10^{-3}	-400	0.9
βf	0.96×10^{-3}	-200	0.9
β	0.96×10^{-3}	0	0.9
βp	0.96×10^{-3}	+200	1.2
βγ	1.20×10^{-3}	+400	1.7
γ	2.05×10^{-3}	+600	2.2

change to variable x-ray emission level accompanied by an overall rise in x-ray emission prior to major flares. Kildahl (1979) has produced the only study that relates active region parameters to the production of class C, M and X flares. The study was done using the McIntosh modified version of the Zürich sunspot classification (McIntosh, 1972-1979) and the results are shown in Figure 4. A knowledge of the history of evolution of an active region is implicit in many of these parameters, though it is not discussed implicitly. However, most forecasters believe that such knowledge is essential for making a good forecast.

What direction should we move in the future? In a promising approach, Neidig et al., (1978) propose a system for estimating energy storage in an active region by using non-potential field models, as done for one active region previously by Tanaka and Nakagawa (1973). Modeling of this kind would appear to be an ideal direction to move to place flare forecasting on a quantitative basis. In this particular, it is not clear that it can be applied to most active regions and it may or may not provide information on the timing of flares. However, we should continue to move the intermediate work in a physically quantifiable direction. For example, a number of large-scale statistical studies were done to relate many different parameters to flare production (Posiadlo, 1973). In an effort to improve this type of study, Hirman and Flowers (1978) have defined a set of parameters that encomposed essentially all of those in use in the SESC. They have attempted to define the parameters so that information on physically meaningful parameters such as magnetic shearing may be gained. Papers evaluating these parameters have been submitted to this workshop.

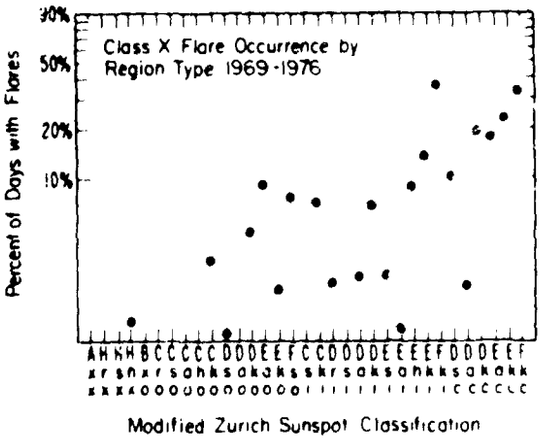

Figure 4. Class X flare occurrence by region type 1969-1976 From Kildahl (1979).

Though it has been over ten years since Smith and Howard (1968) published a system for classifying active region (not just sunspot) magnetic complexity, we still do not have such a system in the real time flare prediction operation. Harvey and Harvey, in a paper in Volume III of these Proceedings, suggest a system to quantify the velocity field complexity. One priority item should be the further development of this system for real time use.

Evaluation of the accuracy of SESC flare forecasts, using the methods discussed in the Verification section, are shown in Figure 5. A summary of the evaluation of the predictions for the years 1969 to 1974 is given by Heckman (1979). The most important results are: (a) The Forecaster has a much greater skill at determining whether an active region will produce a class M or X flare than is his skill at predicting the day of the flare. (b) Predictions made one, two and three days in advance are about equally skillful. (c) The prediction accuracy increases as the frequency of the predicted event decreases.

The current SESC predictions are for 24 hours and most of the flare prediction work has been done on setting the conditions for a flare that persist for several hours or days. There has been some work toward predicting flares on a shorter time scale such as the convergence of sunspots (McIntosh, 1969), filament activity (Martin and Ramsey, 1972) and increasing x-ray levels (Horan and Kreplin, 1970). In fact, many SESC customers - primarily those in operational areas - would be better served by good forecasts in the one-to-three hour range than excellent 24 hour forecasts.

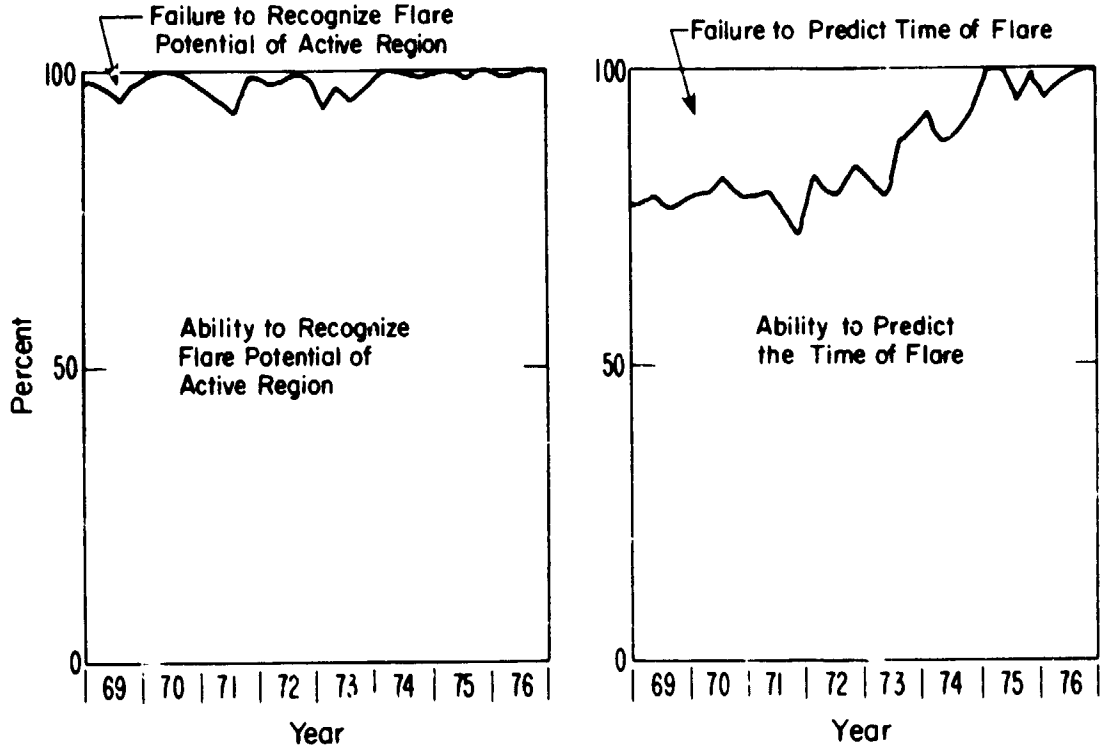

Figure 5. Accuracy of the class M flare forecasts from the SESC for the years 1969-1976.

6.5 Geomagnetic Predictions; A- and K-indices (1, 2, 3 days); Sudden Commencements and Storm Size (Post Flare Prediction)

The predictions are of a mid-latitude A-index (specifically Fredericksburg) as an approximation for Ap, made one, two and three days in advance. Similarly, K values are also predicted for the period 3 to 45 hours in advance. These predictions are done routinely on a daily basis. Another special prediction is made at the time a major flare occurs. It is for the expected time of sudden commencement and the intensity of the magnetic storm that is expected from the flare. Some of the customers who are alerted when a major flare occurs wish to receive this storm prediction at the same time.

The predictions are made by assuming that one of the several possible regimes is dominating the near-earth solar wind environment. The possibilities considered are: (a) A flare produced disturbance is expected to begin or continue. (b) An energetic non-flare solar event is expected. (c) Recurrent (coronal hole produced) activity is expected. (d) Any combination of a, b, or c. (e) None of these.

6.5.1 Flare Produced Disturbance

For the situation where a flare has just occurred, a number of studies have been done to relate the resulting magnetic storm to characteristics of the flare. Most have been statistical in nature. The results can be summarized as a set of guidelines as follows: (a) A major flare with central meridian distance (CMD) less than 45 degrees. (b) A major type IV radio burst at all frequencies from dekametric through centimetric wavelengths. (c) A delay from flare to storm sudden commencement of about one day for the greatest storms to two-three days for lesser storms. (d) A polar cap absorption event (PCA) follows after the flare. These guidelines are based generally on the works of Newton (1943), Dodson and Hedeman (1958), Bell (1965), Sawyer (1965). Further refinement from Akasofu and Yoshida (1967) provides: (a) Scaling of the storm main phase intensity (Dst) is a function of source flare longitude as shown in Figure 6. (b) Delay from flare to storm sudden commencement is not dependent on the longitude of the source flare. (c) Flares moderately east of central meridian produce storms with sudden commencements and Forbush decreases. (d) Flares moderately west of central meridian produce storms with complex forms, typically with less well defined sudden commencements and main phase profiles. Cook (1970) found that the delay from flare to sudden commencement correlates with the area of the calcium plage where the flare occurred (Figure 7).

In order to further quantify the parameters of storm producing flares, Sutorik (1978) examined a set of events classified according to the Comprehensive Flare Index (CFI) devised by Dodson and Hedeman (1971). His summary is: (a) For flares with CFI $\geq$ 14 and CMD $\leq$ 50 degrees, 76 percent were followed by a major magnetic storm in one to four days. Eleven percent were followed by no magnetic activity. (b) For flares with CFI $\geq$ 14 and located anywhere on the visible disk, 67 percent were followed by a major storm in one to four days. Twelve percent were followed by no activity. (c) Flares with CFI of 10 to 13 may be followed by major storms, especially if they occur in a series or following a flare with CFI $\geq$ 14.

The following routine has been developed to provide a simple but quantitative model for storm predictions. For flares near central meridian, storm intensity is related to the total energy in the flare. The time-integrated x-ray flux from the 1-8 Angstrom GOES sensor was taken as a measure of total flare energy. An A_p index for the 24 hours following the sudden commencement was taken as a measure of the storm intensity. For the limited number of isolated events, where a clear one-to-one matching from flare to storm could be made, the relationship was that shown in Figure 8. To predict delay times from flare to sudden commencement, a simple calculational model was devised that allows a perturbation in the form of a Huygenian wave to propagate outward from a point on the solar surface to intercept the earth. The velocity transverse to the radial direction is allowed to vary as a fixed percentage of the radial velocity. The radial velocity remains constant. For a range of initial velocities and flare locations from east limb to west limb, hypothetical delay times can be computed.

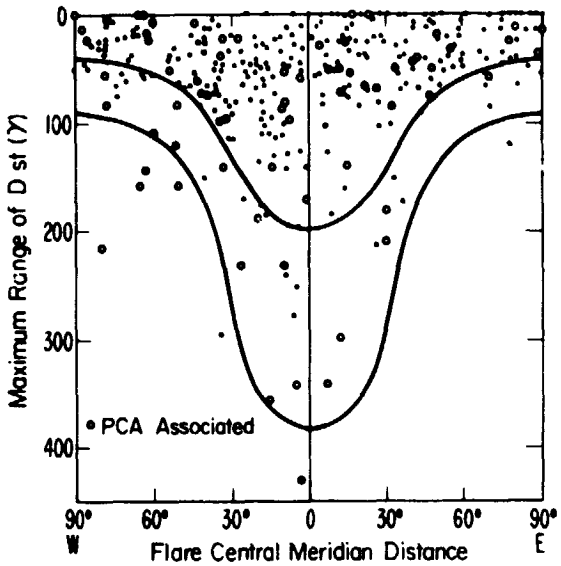

Figure 6. Intensity of geomagnetic storm main phases as a function of the longitude of the source flare. After Akasofu and Yoshida (1967).

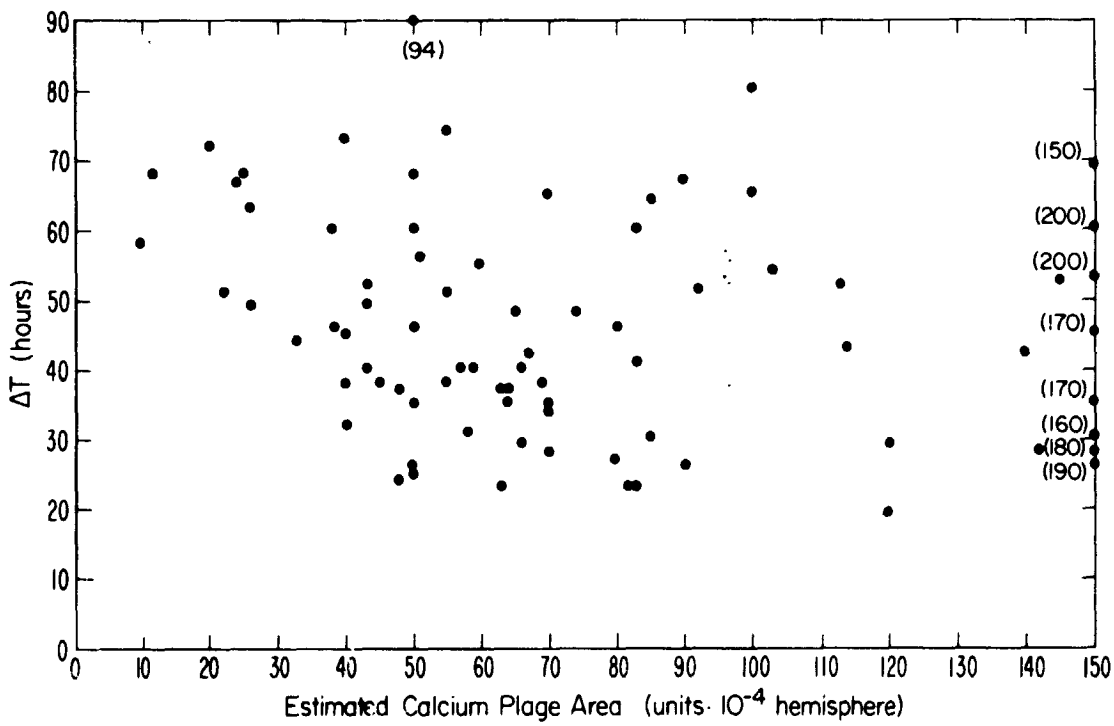

Figure 7. Relation between flare-storm delay time and areas of corresponding calcium plages during IGY-IGC. From Cook (1970).

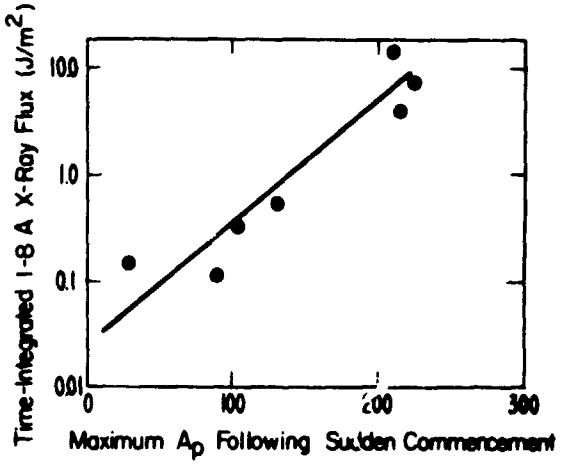

Figure 8. Magnetic storm intensity as a function of the flare x-ray energy.

Two sets of data were run: one for transverse velocity equal to radial velocity, producing a spherical front, and one where transverse velocity was about 0.8 of the radial, yielding an elliptical front. The results are shown in Figure 9.

6.5.2 Recurrent Activity

With some exceptions, Bartels (1932) and Allen (1944) summarized many of the features of recurrent storms that are applicable to forecasting. One of the exceptions is that we now know that M-regions, of which these authors spoke, are now identified as coronal holes. Bartels said: (a) M-regions (read coronal holes) recur at 27-day intervals. (b) They produce disturbances of minor to moderate intensity. (c) They apparently do not correlate with solar features visible in most ground-based observations. (d) There is an average three-day delay from the time each transits central meridian until a disturbance reaches the earth.

Allen said: (a) There are nearly always two or three on the sun at the same time. (b) They often precede (lie to the west of) major spots by about 40 degrees. (c) The disappearance of one often coincides with the appearance of another. (d) The appearance of a major spot where an M-region was previously located means the end of the region's ability to produce a recurrent disturbance. (e) The storms produced may reach moderate intensity. (f) The probability of a recurrent disturbance is about twice as high at the equinoxes as during the middle of June and December. (g) About 12 percent of the disturbances begin with a sudden commencement.

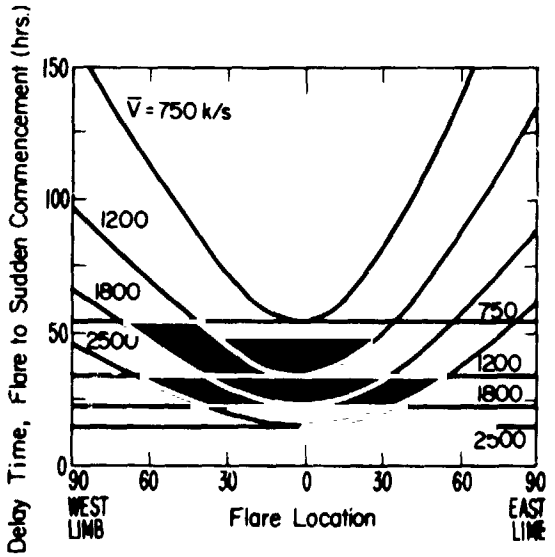

Figure 9. Delay times from flare to sudden commencement for various average shock velocities.

Coronal holes are monitored on a regular basis by using the daily helium photographs from Kitt Peak (Harvey and Sheeley, 1977) transmitted by wire photo imaging to Boulder. As noted by Neupert and Pizzo (1974) and Sheeley et al. (1976), we found that in the declining phase of solar cycle 20, the coronal holes were near the equator, large, long-lasting and regular sources of geomagnetic disturbances. But, in agreement with Sheeley and Harvey (1978), we have found the smaller, shorter lived and less-well-defined holes that are typical of the rising years of cycle 21

to be irregular sources of geomagnetic disturbances. Some holes have produced regular disturbances--mostly those near the equator. We have not been able to apply the relationship between the area of the equatorward holes and the velocity of the solar wind that was found for the 1973 period by Nolte et al. (1977). Ideally, this relationship $V = 80A + 426$, where V is the solar wind velocity and A is the area of the coronal hole, could be combined with the empirical relation between solar wind velocity and geomagnetic disturbance $V = 33A_p\ 0.79 + 250$ given by Gardner (1975) to make predictions of the size of the geomagnetic disturbances produced by particular coronal holes. All these findings for cycle 21 are consistent with the results of Sargent (1979), who finds, by defining an index of recurrence, that for declining portions of the solar cycle, beginning about three years past maximum for even cycles and five years past maximum for odd cycles, the geomagnetic activity is dominated by recurrent, coronal hole type disturbances. This condition persists until about the time of minimum. Both the beginning and end of these periods occur rather abruptly.

6.6 Ten Centimeter Flux

The quantity predicted is the radio flux of the sun as measured at 1700 UT daily by the National Research Council of Canada. The wavelength is nearer to 10.7 centimeters (2800 MHz). As a starting point, the forecaster has the prediction from a regression algorithm run at the Global Weather Center. The algorithm establishes a trend based on the past three solar rotations (weighted toward the most recent rotation) and the trend for the past two or three days of the current rotation. If both trends are in the same direction, the predicted flux moves in that direction. If the two trends are in opposite directions, the prediction follows the direction of the recent trend for the next day, but regressing toward the direction of the long-term average. The forecaster can vary this prediction by using the east-west 10.7 centimeter scan, received daily from the National Research Council, Ottawa. From this scan, which shows the relative east-west location of the radio plages, he can estimate the effects of solar rotation. In the same manner, he can make use of the images in Hydrogen-alpha and calcium.

6.7 Proton Events

The proton event predictions are made for several energy ranges. As described in an earlier section, the primary level of proton event prediction and monitoring is for the flux as a function of time for protons with energies greater than 10 MeV, with some special requests going down to about 1 MeV. Dose predictions done for past manned space applications were for fluxes greater than 30 MeV, while high altitude aircraft doses are generally dependent on the fluxes greater than 100 MeV.

Proton event predictions, while far from satisfactory, are probably the best developed of the prediction routines. The various phases of the process, from acceleration in a flare to propagation to the earth, have been individually identified and then modeled. Some of the phases are models of physical processes while others are heuristic descriptions based primarily on observations made in the satellite era. Those phases that are usually considered in proton event prediction are: (a) Prediction of a proton flare

before it occurs. (b) Estimation of the number of particles, and their energy spectrum, that are accelerated in a flare. (c) Describing the propagation of the particles from the flare location and the effects of the propagation on the flux and energy spectrum. (d) Prediction of the solar source of the magnetic field encompassing the earth. Part (a) is similar to the flare prediction problem with some additional criteria. Primarily, the region must be far enough west on the solar disk to be in a favorable position for the particles to easily reach the earth. Eastward regions have some chance of producing proton events, though it is much lower. Secondly, there is some additional reliance placed on the radio productivity of the active region. Many forecasters prefer to make a yes/no decision on part (b) before doing a quantitative estimate of the accelerated particles. Some of the traditional elements that are associated with proton flares are parallel ribbons, umbral coverage, U-shaped radio burst spectra, long-lived x-ray and radio bursts. It is not clear whether these are distinguishing characteristics of proton flares or whether they are other manifestations of more energetic flares in general.

An example of a prediction model is one done by this author for use in the Apollo and Skylab space programs. The only references are in SESC working documents. The predictions were for the flux and spectral parameter for protons with energies greater than 30 MeV. The predictions were for use with parametric dose equations (Robbins, 1964) that required that the spectrum be described as exponential in rigidity $F\ (E > Eo) = F_o\ e^{-P/Po}$, where F is flux, E is energy and P is rigidity. For phase b: the particle flux accelerated was estimated from the total (time integrated) energy of the flare in the radio spectrum at ten centimeters or from the total energy in the 1 to 8 Angstrom x-ray flux during the early part of the flare. An average spectral parameter was assumed for all events and was taken as P_o = 200 Mv. These quantities were estimated based on average values for flares where the earth, to first approximation, was directly connected to the flare location. Phase c: Burlaga (1967) described an anisotropic diffusion model to describe the propagation of the several hundred MeV protons which produce Ground Level Events. His solutions were especially useful in that the rise time to proton maximum (from flare time) and the scaling of the maximum particle intensity is correlated with the angle between the flare longitude and the connection point of the solar wind intercepting the earth. For the 30 MeV energies, a least squares fit was done from Explorer data published in Solar Geophysical Data (SGD, 1972). The spectral parameter at the peak of the event was found to have a similar dependence. An important feature of this model is the additional use of the equation for the flux (I) as a function of time (t)

$$I(t) = A \exp(S/t)\, t^{-5/2} \qquad (4)$$

After differentiation, a linear relationship can be found between the flux at each point of time and the lapsed time from the flare maximum to that point. The slope of this line, determined from a least squares fit for each proton event while the event is still in progress, is the rise time to proton event maximum. Using this relationship, observations made early in the event can be used to obtain a more accurate prediction of the maximum proton flux yet to come. Experience has shown that this portion of the model works well for some events, but not so well for others. Phase d: in building real-time

prediction models, the modeler must be careful to insure that the model be computationally simple and quick and that it does not rely on parameters that are beyond the prediction capability of the user of the model. Estimation of the solar wind velocity for five to fifty hours in advance is an example of such a parameter. For this model, the forecaster assumes a single value that will be "typical" of the hours from the flare through the peak of the proton event. The typical values are low solar wind velocity, implying a connection point near the west limb of the sun, moderate, with a connection about 45 to 50 degrees west and high, with a connection near central meridian.

The results with this model, used operationally through the declining years of solar cycle 20, was that the peak flux, which can vary by five orders of magnitude, would typically be off by one order of magnitude. The time of rise, from flare to proton flux maximum, which can vary from around three to 100 hours, would be off by about 50 percent. The results of the model, as applied to the August, 1972 events, can be seen in Figure 10. This model is still used in a quick look version in the SESC.

The Smart-Shea Proton Prediction Study: Smart and Shea (1978) have constructed a model that provides a comprehensive treatment, especially of phases c and d. Their model is available in on-line computers at both the SESC and at GWC. In phase b of their model, Smart and Shea provide a variety of radio frequencies that can be used to estimate the size of the proton flux. However, they must rely on the same kind of correlative relationships that were done previously. Part of the SERF (Solar Energy Release in Flares) portion of the Solar Maximum Year is an observational program dedicated to

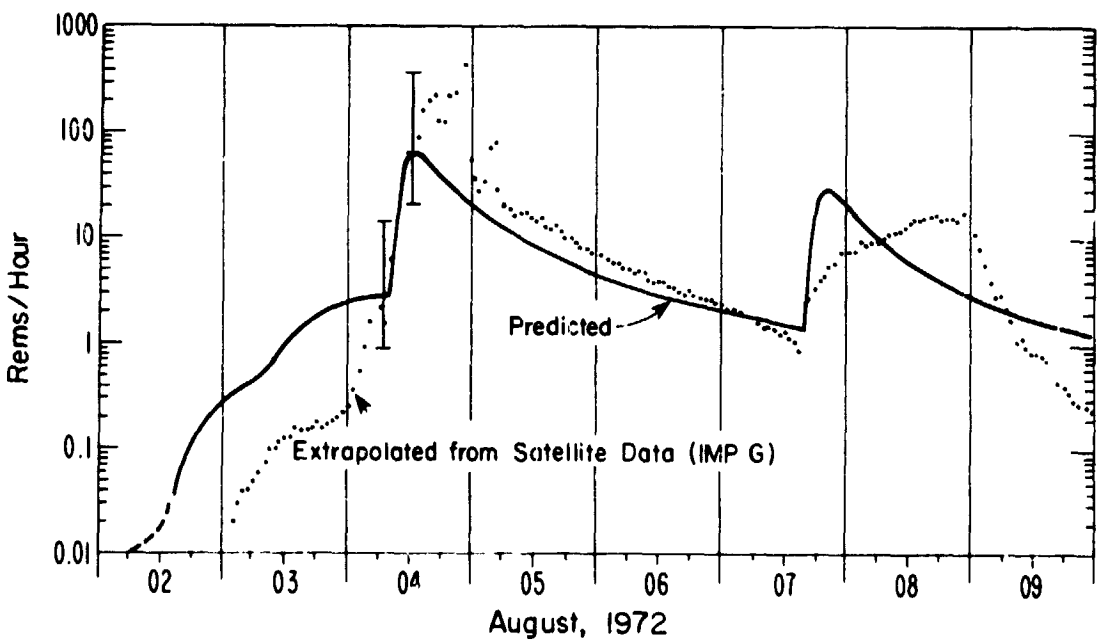

Figure 10. Predicted and extrapolated radiation doses in August, 1972. The predictions were made on the basis of the flare x-ray and radio energies. From McKinnon (1972).

this problem, and if successful, may promise the first real progress in this phase in some time. In their treatment of phase c, Smart and Shea provide for two aspects of the particle propagation. First is the diffusion of the protons from the flare location through the solar corona to the magnetic field line connected to the earth. Second is the travel of the particles along the interplanetary magnetic field lines to the earth. The Smart and Shea approach appears to be a more realistic treatment of the propagation problem and may provide more consistency from event to event. Smart and Shea also assume a more complex spectral form in order to obtain an improved match to the observed particle fluxes from low (one MeV) to high (several hundred MeV) energies. Smart and Shea handle phase d by allowing for continual co-rotation and varying solar wind velocity through the event.

As pointed out in a number of recent papers, the coronal phase of the propagation is more complex than that modeled by assuming uniform coronal diffusion and escape. For example, Gold et al. (1977) discuss an instance where the primary particle release was above the flare site for two days, then apparently shifted to a location about 100 degrees away. This effect probably accounts for much of the order-of-magnitude error in the flux predictions. At present, there is no clear method of predicting the anomolous escape locations in advance.

7. VERIFICATION

Verification of forecasts is a complex and controversial subject, and many of the methods used are misleading or inaccurate. Vertification of forecasts in the SESC are intended to serve four purposes: (1) Ascertain whether the subjective probability forecasts show skill in relation to other forecast methods. (2) Determine sources of error in the forecasts. (3) Determine the utility of the forecasts for operational customers of SESC. (4) Provide a baseline for evaluating the usefulness of future developments in statistical or physical forecast models. The most important restriction on verification systems is that they be "proper" (Murphy and Epstein, 1967) in the sense that the forecaster expresses his true belief in order to obtain the best verification score. A mathematical definition exists so that a scoring system can be shown to be proper or not. An example of an improper scoring system is the one where the evaluation is done by simply counting all the correct forecasts and dividing by the total number issued--the percent of correct forecasts. Specifically, if ten major flares occur per year, a forecaster should issue a "no" forecast every day and he will have a 97 percent score.

For evaluating flare forecasts, SESC uses the Brier P-score (Brier, 1950) as modified by Sanders (1963). This system is mathematically proper. Let the verification score P be defined by

$$P = \frac{1}{M} \sum_{k=1}^{K} \sum_{i=1}^{M} (f_{ik} - o_{ik})^2 \quad , \tag{5}$$

where M is the number of forecasts made, K is the number of states or categories on each forecast occasion, f is the forecast probability with range 0 to 1 in each category k ($\Sigma_k f = 1$), and O is the observation and is 1 if the event in category k occurs and is zero if it does not. If the forecaster is able to interpret current conditions, he will forecast high probabilities when he expects an event and low when no event is expected. If he is correct in his evaluation, the difference ($f_{ik} - O_{ik}$) will be small and the Brier P score will be small. If the forecaster is perfectly competent, he will have predicted $f_{ik} = 1$ for every occasion when an event subsequently occurred and $f_{ik} = 0$ when an event did not follow. Then his Brier P score will be zero. If the forecaster is perfectly incompetent, the difference ($f_i - O_i$) will be ± 1 and his verification score will approach the value 1.0. In summary, the lower the score, the more skillful the forecaster.

Sanders' modification is to divide the forecasts being evaluated into subsets according to the probability f. For each subset s, the score is partitioned into two terms ($f_s - \bar{O}_s$) (where $\bar{O}_s$ is the average for subset 5) and $\bar{O}$ ($1-\bar{O}_s$). Sanders called the first term "sorting" ability. As applied to solar flare forecasts, it is the forecaster's ability to estimate whether a region will produce a class C, M or X flare, but not when it will occur. The second term, which Sanders called "labeling" ability, measures how well the forecaster predicts the day of the flare. Figure 5 illustrates these two terms and shows that the forecaster, using current methods, can estimate the amount of energy stored in a flare, but he cannot predict the time of the flare— that is, he cannot anticipate the "flare trigger".

REFERENCES

Adams, H. A., III (1975): A comparison between Fredericksburg and planetary geomagnetic A values, National Oceanic and Atmospheric Administration Technical Report ERL 350-SEL 36.

Allen, C. W. (1944): Relation between magnetic storms and solar activity, Monthly Notices Roy. Astron. Soc., 104:13.

Akasofu, S.-I., and S. Yoshida (1967): The structure of the plasma flow generated by solar flares, Planet. Space Sci., 15:39.

Bartels, J. (1932): Terrestrial-magnetic activity and its relations to solar phenomena, Journ. Terr. Magn. Atm. Electr., 37:1.

Bell, B. (1965): Major flares and geomagnetic activity, Smithsonian Contr. Astrophys., 5:69.

Brier, G. W. (1950): Verification of forecasts expressed in terms of probability, Mon. Wea. Rev., 78:1.

Burlaga, L. F. (1967): Anisotropic diffusion of solar cosmic rays, J. Geophys. Res., 72:4449.

Cohen, T. J., and P. R. Lintz (1974): Long term periodicities in the sunspot cycle, Nature, 250:398.

Cook, F. E. (1970): On the time delay between solar flares and associated geomagnetic storms. Paper 28 in AGARD Conference Proceedings, No. 49.

Dodson, H. W., and E. R. Hedeman (1958): Geomagnetic disturbances associated with solar flares with major premaximum bursts at radio frequencies 200 MC/S. Journ. Geophys. Res., 63:77.

Dodson, H. W., and E. R. Hedeman (1971): An experimental comprehensive flare index and its derivation for "major" flares, 1955-1969. UAG Report-14, U. S. Department of Commerce, Boulder, Colorado 80303, USA.

Flamn, E. J., and R. E. Lingenfelter (1964): Neutron and proton dosage in the upper atmosphere from solar flare radiation, Science, 144:1556.

Gardner, L. J. (1975): Geomagnetic forecasting based on EUV coronal intensity, NOAA Tech. Rep. ERL 320-SEL 33.

Giovanelli, R. G. (1939): The relations between eruptions and sunspots, Astrophys. Journ., 89:555.

Gold, R. E., E. P. Keath and E. C. Roelof (1977): Coronal structure of the April 10, 1969, solar flare particle event, in 15th International Cosmic Ray Conference, Conference Papers, Vol. 5.

Harvey, J. W., and N. R. Sheeley, Jr. (1977): A comparison of He II 304A and He I 10830A spectroheliograms, Solar Physics, 54:343.

Haurwitz, M. (1971): Procedures of the Space Environment Services Center, U. S. Department of Commerce, Boulder, Colorado 80303, USA (Unpublished).

Heckman, G. R. (1979): Verification of the solar flare forecasts at the Space Environment Services Center for the years 1969-1974. Technical Report (to appear), U. S. Department of Commerce, National Oceanic and Atmospheric Administration.

Hill, J. R. (1977): Long term solar activity forecasting using high-resolution time spectral analysis, Nature, 266:151.

Hirman, J. W., and W. E. Flowers (1978): An objective approach to region analysis for flare forecasting. Proceedings of the Symposium on the Effect of the Ionosphere on Space Systems and Communications, Naval Research Laboratory, Washington, D. C. (in press).

Horan, D. M., and R. W. Kreplin (1970): Predictions of solar flare activity based on solar x-ray energy flux measurements. Paper 28 in AGARD Conference Proceedings, No. 49.

Kildahl, K. (1979): Private communication.

Lundquist, C. A., and W. W. Vaughn (1978): Private communication.

Mansurov, S. M., and L. G. Mansurova (1969): New evidence of a relationship between magnetic fields in space and on earth, Geomagn. Aeron., :622.

Martes, M.-J., J. Rayrole, E. Ribes, M. Semel and I. Soru-Escaut (1974): On the importance of photospheric velocities in relation to flares, in Flare-Related Magnetic Field Dynamics, Manuscripts presented at a conference held in Boulder, Colorado, 23-25 September, 1974.

Martin, S. F., and H. E. Ramsey (1972): Early recognition of major solar flares in H-alpha, in Solar Activity Observations and Predictions, Progress in Astronautics and Aeronautics 30, MIT Press, p.

McIntosh, P. S. (1969): Sunspots associated with the proton flare of 23 May 1967, in UAG Report 5, U. S. Department of Commerce, Boulder, Colorado 80303, USA.

McIntosh, P. S. (1972): Inference of solar magnetic polarities from H-alpha observations, in Solar Activity Observations and Predictions, Progress in Astronautics and Aeronautics 30, MIT Press, p. 65.

McIntosh, P. S. (1972-1979): Sunspot classification, in Solar Geophysical Data Descriptive Text, p. 25.

McIntosh, P. S. (1979): Annotated atlas of Hα synoptic charts for solar cycle 20, 1964-1974, UAG Report 14; U. S. Department of Commerce, Boulder, Colorado 80303, USA.

McNish, A. G., and J. V. Lincoln (1949): Prediction of sunspot numbers, Transactions of the American Geophysical Union, 30:5.

Murphey, A. H., and E. S. Epstein (1967): A note on probability forecasts and "Hedging", J. Appl. Meteor., 6:1002.

Neidig, D. F., H. L. DeMastis, and P. H. Wiborg (1978): Flares, force-free fields, emerging flux and other phenomena in McMath 14943 (September, 1977), AFGL-TR-78-0194.

Neidig, D. F., H. L. DeMastus, and P. H. Wiborg (1978): Flares, force-free fields, emerging flux and other phenomena in McMath 14943 (September, 1977), Air Force Geophysics Laboratory Environmental Research Paper, No. 637.

Neupert, W. M., and V. Pizzo (1974): Solar coronal holes as sources of recurrent geomagnetic disturbances, J. Geophys. Res., 79:3701.

Newton, H. W. (1943): Solar flares and magnetic storms, Monthly Notices Roy. Astron. Soc., 90:820.

Nolte, J. T., A. S. Krieger, A. F. Timothy, R. E. Gold, E. C. Roelof, G. Vaiana, A. J. Lazarus, J. D. Sullivan and P. S. McIntosh (1976): Coronal holes as sources of solar wind, Solar Phys., 46:303.

Ohl, A. I. (1976): A preliminary forecast of some parameters of cycle no. 21 of the solar activity, Solnechnaya Dannyye No. 9, p. 73.

Posialdlo, R. T. (1973): An objective baseline for flare prediction, COSPAR Symposium 15, Academie-Verlag, Berlin, p. 817.

Robbins, D. E. (1964): Apollo shielding analysis, in Second Symposium on Protection Against Radiations in Space, NASA SP-71.

Sakurai, K. (1967): Solar cosmic-ray flares and related sunspot magnetic fields, Rept. Ionospheric and Space Res Japan, 21:113.

Sanders, F. (1963): On subjective probability forecasting, J. Appl. Meteor., 2:191.

Sargent, H. H., III (1978): A prediction for the next solar cycle, 28th IEEE Vehicular Technology Conference, p. 490.

Sargent, H. H., III (1979): A geomagnetic activity recurrence index, Solar-Terrestrial Influences on Weather and Climate, Reidel, Dordrecht, Holland, p. 101.

Severny, A. B. (1963): On the behavior of magnetic fields associated with solar flares, AAS-NASA Symposium on the Physics of Solar Flares, NASA SP-50.

SGD (1972): Solar Geophysical Data, No. 330 (supplement), U. S. Department of Commerce, Boulder, Colorado.

Sheeley, N. R., Jr., J. W. Harvey, and W. C. Feldman (1976): Coronal holes, solar wind streams and recurrent geomagnetic disturbances: 1973-1976, Sol. Phys., 49:271.

Sheeley, N. R., Jr., and J. W. Harvey (1978): Coronal holes, solar wind streams, and geomagnetic activity during the new sunspot cycle, Naval Research Laboratory Skylab/ATM Preprint.

Slowley, E. (1979): Private communication.

Slutz, R. J., T. B. Gray, M. L. West, F. G. Stewart, and M. Lerch (1[illegible] Solar activity prediction, NASA CR-1939.

Smart, D., and M. Shea (1978): Private communication.

Smith, J. B., Jr. (1972): Predicting activity levels for specific locations within solar active regions, in Solar Activity Observations and Predictions, Progress in Astronautics and Aeronautics, Vol. 30, MIT Press, p. 429.

Smith, S. F., and R. Howard (1968): Magnetic classification of active regions, in Structure and Development of Solar Active Regions, IAU Symposium No. 35, Reidel, Dordrecht.

Sutorik, J. (1978): Procedures of the Space Environment Services Center, U. S. Department of Commerce, Boulder, Colorado (Unpublished).

Svalgaard, L. (1968): Sector structure of the interplanetary magnetic field and the daily variation of the geomagnetic field at high latitudes, Geophys. Papers, R-6, Danish Meteorol. Inst., Copenhagen.

Svestka, Z. (1972): Several solar aspects of flare-associated particle events, in Solar Activity Observations and Predictions, Progress in Astronautics and Aeronautics, Vol. 30, MIT Press, p. 41.

Tanaka, K., and Y. Nakagawa (1973): Force-free magnetic fields and flares of August, 1972, Sol. Phys., 33, 187.

GEOPHYSICAL FORECASTING AT AFGWC

Richard L. Thompson
Lt Col USAF

and

James A. Secan
Capt USAF

Air Force Global Weather Central*
Offutt Air Force Base, Nebraska, USA

*mailing address: AFGWC/DOX, Offutt AFB, NE 68113, USA

Advanced systems that either use or are affected by the environment above 50 kilometers require forecast support. The Air Weather Service provides a worldwide network of sensors and a central facility to monitor and forecast the state of the space environment; the sun, interplanetary field, magnetosphere and ionosphere. This paper discusses forecast methods and problem areas requiring additional advances in scientific understanding to support ever increasing operational requirements.

1. INTRODUCTION

The Air Weather Service (AWS), through its operational forecast centers of the Air Force Global Weather Central (AFGWC), provides space environmental support to the entire Department of Defense. Although the types and intensity of support are varied, the overall driving requirement is to minimize system effects caused by impulsive solar/geophysical activity and ionospheric variations. The knowledge of these effects, preferably beforehand, provides the decision maker with information to utilize his resources effectively. AFGWC provides around-the-clock service in forecasting and specifying the aerospace environment by applying varied data to the problem. The Air Force has been active in space environment research and forecasting for over a decade. Many earlier papers (Snyder, 1974; von Flotow, 1978; Thompson, 1978) have described data sources and techniques used to provide real-time and post-analysis support.

In this paper, we will describe in greater detail the method and problems of real-time space environmental forecasting and specification. Although the ionosphere will be the area of greatest concentration, the areas of magnetospheric and energetic particle forecasting will be addressed.

2. HISTORY/REQUIREMENTS

The Air Force has been active in space research for many years. Most of this effort has either been completed or directed by the Air Force Geophysical Laboratory (AFGL). Through the cooperation of AWS and AFGL, a worldwide network of observatories was established to observe solar activity during the maximum years of solar cycle 20. This network helped to support national requirements during the Apollo and Skylab missions and direct support to operational decision-makers concerned with environmental effects on electronic systems. We are again prepared to support both national and defense oriented missions during the maximum years of solar cycle 21.

Two major advances in observational equipment are the deployment of the new solar observing optical network (SOON) and radio solar telescope network (RSTN). These systems are partially in place and we expect to complete deployment during 1980. Both systems employ on-site automation to provide AFGWC with reliable data in minimum time. During solar cycle 20 we were able to provide only limited real-time information that a flare was in progress. With the data from SOON, RSTN, and X-ray data from the Geosynchronous Operational Environmental Satellites (GOES) we can provide a real-time comprehensive analysis of the flare and its effects on the space environment. These data can also be used to predict, with reasonable confidence, high energy solar particle events. The requirement for reliable predictions of high-energy solar events was a primary driving force behind the installation of the SOON/RSTN.

In the late sixties, AWS installed a series of real-time magnetometers to observe and forecast the state of the magnetosphere. This network allows real-time specification of a pseudo A_p. This A_p data coupled with the 10.7 cm solar radio flux remain the main inputs to upper atmosphere neutral density models. However, new requirements concerning the interaction of spacecraft and the magnetosphere dictate a more comprehensive understanding and observational database to provide effective support.

The importance of the ionosphere to AFGWC supported operations increased significantly during the solar minimum years of the mid seventies. AWS has been active in ionospheric prediction and specification since 1967, but not at the present magnitude. Early efforts were generally manual analyses for special cases of limited areas, both in time and space. However, as technology advanced, previously neglected errors caused by the ionosphere reached parity with other error sources. Interest in reducing these ionospheric errors placed new demands on AFGWC for more accurate analyses and forecasts. It soon became apparent that manual methods would not be able to satisfy increased demands. A major break-through occurred with the development and implementation of the Flattery-Ramsay (1975) model which coupled the data handling and processing techniques of meteorology with observa-

tions of the ionosphere. This permitted a hemispheric real-time update of the Institute of Telecommunication Services (ITS) ionospheric coefficients. This model was continuous only in three dimensions (latitude, longitude, and time) which was an operational limitation. This limitation led to preliminary development of the four dimensional ionospheric (4D) model, continuous in latitude, longitude, time, and height, with great potential for using a "build and apply" concept. Using the "build and apply" approach, we build the most comprehensive specification/forecast of the ionosphere, then apply this data base to generate automated products needed to satisfy a variety of customer requirements.

3. CURRENT FORECASTING

3.1 Solar Flare Particle Emissions

The forecasting and observation of high energy solar protons remains one of the highest priority functions within the Space Environmental Support System (SESS). Solar flare-produced protons can cause damage to satellites operating in the near-earth space environment and are an ever present danger to people in space. Rapid gathering and processing of flare data are essential in providing useful forecast services. High speed communication links between world-wide observatories and AFGWC, such as the Automated Weather Network (AWN), supply the rapid transfer of data. Automation at both the observatories and AFGWC aids in rapid data reduction.

The data used in proton prediction and observation come from a myriad of ground-based and satellite-borne sensors. Most of the ground-based data is from SOON and RSTN currently being deployed by AWS. Table 3.1 gives the location, data types available, and status of the various sites in the SOON/RSTN and other sites which provide data to AFGWC. While these ground-based observations are used primarily as inputs to various proton prediction schemes, satellite observations are used for direct proton observations as well.

Most of the satellite observations used at AFGWC come from the National Oceanic and Atmospheric Administration (NOAA) GOES satellites. These data, which include solar x-ray and high-energy proton observations, are collected at the NOAA in Boulder and transmitted to AFGWC in real-time via a dedicated computer-to-computer data line. A small amount of solar x-ray and particle data is still received from the VELA 5 and 5B satellites, but this data source has deteriorated significantly over the last several years and its use is scheduled to be terminated at AFGWC in the near future. Other operational Department of Defense satellites provide nearly continuous proton/electronn data.

Both ground-based and satellite data are transmitted to AFGWC in real-time via several data links, such as the AWN and NOAA-AFGWC lines. Once at AFGWC, these data are processed in real-time and made available for preparation of various prediction and observation products for AFGWC customers.

OBSERVATORY	LATITUDE	LONGITUDE	OPTICAL									
			RAZDOW	SOON	245	410	606	1415	2695	4995	8800	14500
SAGAMORE HILL	43N	71W			X	X	X	X	X	X	X	X
RAMEY AFB	18N	67W		X								
ATHENS	38N	24E						X	X	X		
MANILA	15N	121E	X		X		X	X	X	X	X	X
PALEHUA	21N	158W		X	X	X	X	X	X	X	X	X
HOLLOMAN	33N	106W		X								
LEARMONTH[1]	22S	114E		X	X	X	X	X	X	X	X	X
MIDDLE EAST[2]	-	-		X	X	X	X	X	X	X	X	X

[1]OPERATIONAL IN LATE 1979

[2]OPERATIONAL IN 1980

TABLE 3.1 GROUND-BASED SOLAR OBSERVATORIES

The AFGWC prediction of solar proton events is divided into two areas:

(1) Did a given flare produce protons? (Yes/No forecast, qualitative)

(2) If protons are produced, how will the particle spectrum grow and decay near the earth as a function of time? (particle flux forecast, quantitative)

Both of these forecasts are time critical; the yes/no qualitative forecast must be transmitted within 10 minutes of flare maximum, the particle flux forecast within 30 minutes of maximum. The yes/no forecast is primarily a subjective one, based on flare signatures such as parallel ribbons on the H-alpha flare, the Castelli U-shaped radio burst, the type-II radio burst, and many others. For this forecast, the computer acts as a data collector, with the forecaster providing the actual forecast intelligence. The particle flux forecast is done almost entirely by the computer. After the incoming data has been processed, the Smart-Shea Proton Prediction Study (PPS) program is run to produce the forecast. Further details on the yes/no forecast techniques used and the Smart-Shea PPS program can be found in Smart and Shea (1977 a, b) and Cliver, et al., (1978).

Although AWS SESS has recently made several improvements in ITS proton prediction capability, most notably the SEON data and the Smart-Shea PPS program, there are still many problems and shortcomings. In the area of yes/no prediction the most frustrating problem is the subjective nature of these forecasts. Almost every worker in this field has his own list of proton signatures and while most all lists include roughly the same signatures, the emphasis is often different. This lack of agreement within the scientific community on the importance of various signatures coupled with the often ambiguous collection of signatures from a given event (parallel ribbon flares without a Castelli-U burst, etc.) makes it very difficult to produce a reasonable yes/no forecast within the required timelines. Ambiguity is also a problem with the Smart-Shea PPS Program. Different input parameters often produce very different forecasts. While this problem can be often resolved by forecaster experience and expertise, a far more serious problem is the lack of interplanetary medium observations. Without up-to-date knowledge of the structure of the solar wind between the sun and the earth, only a rough estimate can be made of the propagation of high energy protons from their source to the earth. This can seriously affect the timing and intensity of the proton event at the earth. Finally, flares which occur behind the west limb of the sun, producing at best only weak radio signatures are a problem.

3.2 Magnetospheric Variations

Magnetospheric forecasting at AFGWC is still in its infancy. Real-time observations of geomagnetic indices and magnetospheric protons and electrons are only the beginning of a comprehensive

forecasting and specification scheme. These observations are currently used to give the forecaster a subjective "feel" for the current state of the magnetosphere rather than to drive specification and prediction models.

As in the solar proton area, magnetospheric data are collected by a number of ground-based and satellite sensors. The majority of the ground-based data consists of magnetometer observations. These data come from a network of magnetometers operated in near real-time for AWS and from various magnetometers located around the world which provide geomagnetic indices 12-36 hours after the fact (table 3.2) A wide range of data is collected by the NOAA/AWS High Latitude Monitoring Station (HLMS) and transmitted every 15 minutes to AFGWC. A partial list of these data includes magnetometer observations, riometer observations, and auroral backscatter radar measurements. These ground observations are complemented by observations in two different magnetospheric regimes, the geostationary satellites and the low altitude (840 KM) polar orbiting Defense Meteorological Satellite Program (DMSP) satellites. Table 3.3 lists the data available from the GOES and EP (1976-059A and 1977-007A) satellites. The DMSP satellites provide visual observations of the aurora (Snyder, et al., 1974) and precipitating electron data (pitch angle = 0^{o}) in the energy range 50 eV to 20 KeV from the SSJ/3 sensor. The GOES and EP data are transmitted to AFGWC in real-time via high speed data lines; the DMSP data is collected and processed on a nearly rev-by-rev basis at AFGWC.

Gross magnetospheric variations are monitored using a pseudo ap or Kp index calculated using a subset of the ground-based magnetometers indicated in table 3.2. This index, calculated within 30 minutes of the end of each three hour period, can be used as an input to models that require an integrated measure of global geomagnetic activity. The 24 hour Ap index is forecast daily for the upcoming seven days using a variety of largely subjective techniques. The K_p calculated in real-time normally has a mean difference of roughly one K_p unit from that by the Geophysikalisches Institut at the University of Gottingen, F.R. of Germany (Snyder, 1974).

Auroral substorm activity is monitored using DMSP visual and SSJ/3 data. These data are used to calculate two indices of auroral activity; an effective Q index, Qe (Snyder, 1974); and Ca, a subjective measure of the level of auroral activity on a given DMSP photograph (Pike, 1975). The Qe index is derived from the equatorial boundary of the diffuse aurora on the DMSP photographs or the equatorward point where auroral electrons are detected on the 0.652 KeV channel of the SSJ/3 sensor, mapped down to 100KM. Qe is calculated from these measurements using a variation of the technique discussed by Gassman (1973), Feldstein and Starkov (1967), and Starkov (1969). This measure of the size of the auroral oval is used with Ca to monitor substorm activity.

	GEOGRAPHIC		GEOMAGNETIC	
OBSERVATORY	LATITUDE	LONGITUDE	LATITUDE	LONGITUDE
THULE*	77N	69W	+87	+ 38
KRENKEL	80N	58E	+75	+144
DIKSON	73N	80E	+68	+154
TIXIE	71N	129E	+66	+196
GOOSE BAY*	54N	60W	+65	+ 21
COLLEGE*	65N	148W	+65	+260
MURMANSK	68N	33E	+64	+114
ANCHORAGE	61N	150W	+61	+261
LORING AFB*	48N	68W	+60	+ 8
TUNGUSKA	60N	90E	+56	+161
LENINGRAD	60N	30E	+56	+107
MAGADAN	60N	151E	+54	+217
SVERDLOVSK	56N	61E	+52	+132
FREDRICKSBURG	38N	77W	+51	+353
MOSCOW	55N	37E	+51	+111
WINGST	54N	9E	+51	+ 88
BOULDER*	40N	105W	+50	+316
IRKUTSK	52N	104E	+48	+175
PETROPAVLOVSK	53N	158E	+47	+225
CHAMBON	48N	2E	+46	+ 81
KAKIOKA	36N	140E	+30	+210
MANILA	15N	121E	+ 9	+190
KERGUELEN	49S	70E	-58	+121

*RECEIVED AND PROCESSED IN REAL-TIME

TABLE 3.2 MAGNETOMETER DATA NETWORK

GEOSYNCHRONOUS SATELLITE DATA

A. GOES DATA

PROTON	ELECTRON	ALPHA
0.8 - 4.0 MEV	2.0 MEV	8.2 - 10.0 MEV
4.0 - 8.0 MEV		10.0 - 16.0 MEV
8.0 - 16.0 MEV		16.0 - 60.0 MEV
16.0 - 215.0 MEV		85.0 - 182.0 MEV
36.0 - 215.0 MEV		156.0 - 228.0 MEV
80.0 - 215.0 MEV		326.0 - 412.0 MEV
215.0 - 500.0 MEV		

B. EP DATA

PROTON		ELECTRON	
50 - 500 KEV	0.30 - 0.40 MEV	30 - 300 KEV	0.20 - 2.0 MEV
63 - 500 KEV	0.40 - 0.53 MEV	44 - 300 KEV	0.20 - 2.0 MEV
80 - 500 KEV	0.53 - 0.71 MEV	64 - 300 KEV	0.43 - 2.0 MEV
100 - 500 KEV	0.71 - 0.94 MEV	95 - 300 KEV	0.63 - 2.0 MEV
126 - 500 KEV	0.94 - 1.25 MEV	139 - 300 KEV	0.93 - 2.0 MEV
158 - 500 KEV	1.25 - 1.66 MEV	204 - 300 KEV	1.40 - 2.0 MEV
198 - 500 KEV	1.66 - 2.20 MEV		
252 - 500 KEV	2.20 - 4.73 MEV		
316 - 500 KEV	4.73 - 8.00 MEV		
396 - 500 KEV	8.00 - 13.50 MEV		
	13.50 - 22.80 MEV		
	22.80 - 33.20 MEV		
	33.20 - 48.40 MEV		
	48.40 - 70.60 MEV		
	70.60 - 103.00 MEV		
	103.00 - 150.00 MEV		

TABLE 3.3 GOES AND EP DATA

There are many problems encountered in forecasting magnetospheric activity beyond the simple seven day Ap forecast mentioned earlier. The main difficulty is forecasting the occurrence and duration of substorm activity prior to onset. Most of the methods of short term forecasting of substorm onset (lead times <1 hour) depend on solar wind measurements taken "upwind" of the earth's magnetopause. With the gradual failure of the VELA solar wind sensors, AFGWC has become essentially blind to structures in the solar wind which can cause substorms. This blindness affects our ability to observe newly formed fast stream structures in the solar wind which could be used by the forecast center to warn customers of an upcoming disturbance. Until the problem of forecasting substorms is better understood, and the data to make such forecasts available, magnetospheric forecasting at AFGWC will remain in its infancy.

3.3 Ionospheric Variations

During the time between the maximum of solar cycle 20 and the start of cycle 21, AWS SESS has seen its involvement in ionospheric prediction and specification grow from reporting flare-induced ionosphere variations (SWF's and PCA's) to modeling and forecasting large scale ionosphere behavior. The remainder of this section will deal with techniques used in forecasting and specifying ionospheric fields. Details on the products produced from the ionospheric parameters drawn from these fields, such as radio propagation forecasts, can be found in Thompson (1978) and von Flotow (1978) and will not be covered here. The data used in current ionospheric work was also covered in detail in von Flotow (1978), Thompson (1978), and Snyder (1974), and will be only briefly discussed here. Table 3.4 summarizes the ground-based and satellite (DMSP) ionospheric data available at AFGWC.

A variety of methods and models are used at AFGWC to forecast and specify the ionosphere, but generally they all follow the same lines. An automated model is used to combine observations and climatology to provide a "best guess" specification of the ionosphere. The forecaster then manually, or with the aid of various computer software "tools", makes any modifications required to fill in data sparse areas of a specification. He also makes changes he believes will occur during the forecast period which are not reflected in the computer produced analysis. Currently, two models are used to provide the "best guess" base field; the Flattery-Ramsay Hybrid Model (Flattery and Ramsay, 1975), and the new 4D model (Tascione, et al, 1978). Details of these models can be found in the given references; here we will discuss how these models are used and indicate the advantages and limitations of each.

3.3.1 The Flattery-Ramsay Hybrid Model

This model was developed at AFGWC in the early 1970s (Flattery and Ramsay, 1975) and is still being used operationally by SESS forecasters. It is a two stage model in which input data (foF2 and M3000)

VERTICAL IONOSONDES

OBSERVATORY	LATITUDE	LONGITUDE	OBSERVATORY	LATITUDE	LONGITUDE
MANILA	14N	121E	MAGADAN	59N	151E
DJIBOUTI	12N	43N	OTTAWA	45N	76W
OUAGADOUGOU	12N	1W	ST. JOHNS	47N	52W
TAIPEI	25N	121E	SVWEDLOVSK	56N	61E
DAKAR	15N	17W	KENORA	50N	97W
MAUI	21N	156W	TOMSK	56N	85E
KOKUBUNJI	36N	133E	GOOSE BAY	53N	60W
ASHKHABAD	40N	58E	YAKUTSK	62N	130W
VANDENBERG AFB	35N	121W	COLLEGE	65N	147W
ALMA ATA	43N	77E	CAPE SCHMIDT	69N	179W
PATRICK AFB	29N	80W	KIRUNA	68N	20E
POITIERS	46N	00W	MURMANSK	69N	33E
LANNION	48N	03W	TUNGUSKA	61N	90E
KHABAROBSK	48N	135E	CHURCHILL	58N	94W
BOULDER	40N	105W	NARSSARSUAK	61N	45W
PETROPAVLOVSK	53N	159E	SALEKHARD	67N	67W
WALLOPS IS	37N	75W	DISON	73N	80E
KIEV	51N	31E	KRENDEL	80N	58E
IRKUTSK	52N	104E	GODHAVEN	69N	54W
MOSCOW	55N	32E	RESOLUTE BAY	75N	95W
DOURBES	50N	5E	QANAQ	76N	68W
LINDAU	51N	10E			
SLOUGH	51N	1W			

FARADAY POLARIMETERS

OBSERVATORY	LATITUDE	LONGITUDE	OBSERVATORY	LATITUDE	LONGITUDE
ATHENS	34N	15W	SAGAMORE HILL	39N	71W
GOOSE BAY	48N	62W	BOULDER	37N	105W
OSAN AFB	35N	128E	TAIWAN	23N	122E
PATRICK AFB	27N	80W	PALEHUA	20N	157W
RAMEY AFB	17N	70W	SHEMYA AFB	49N	179W

DMSP SPECIAL SENSORS

SENSOR	DESCRIPTION
SSJ/3	PRECIPITATING ELECTRONS (16 CHANNELS, 6EV-20KEV)
SSIE	IN-SITU PLASMA PROBE (NE, TE, NI, TI, MI)
SSIP	PASSIVE FOF2 MONITOR (NOISE BREAKTHROUGH)

TABLE 3.4 IONOSPHERIC DATA

are first meshed with the ITS-78 ionospheric climatology (Barghausen, et al 1969) to produce updated fields of foF2 and M3000. These fields are passed to an electron density profile (EDP) model, a modified version of the Damon and Hartranft model (Damon and Hartranft, 1970), to produce ionospheric variations in the vertical, Z, coordinate. The type of input data will determine the nature of the output fields: single day observations of foF2 and M3000 provide a specification; five-day means of these same parameters provide the base "best guess" field for a forecast.

As an example of the use of this model, let us suppose the forecaster wishes to produce an EDP forecast over North America on 5^{o} x 5^{o} latitude/longitude grid. The first stage of the model is run on five-day means of whatever foF2/M3000 observations are available. This stage is accomplished in two phases. First, the sunspot number (SSN) used as input to the ITS-78 model is varied to provide the best overall fit of the ITS-78 foF2 to the five day mean foF2 values (Thompson, 1978). Then the foF2/M3000 fields produced using this SSN are meshed, with the mean observed foF2 and M3000 values to produce an updated set of coefficients in ITS-78 format. This coefficient set is then used to produce a grid of foF2 and M3000 for the forecaster to modify as he requires. This modified grid is then passed to the second state, EDP model, to produce the required profile forecast.

The major advantage of this model is that it provides a global ionosphere based on actual observations. It is used to give a single hour forecast of foF2 at a single point, or a global grid of total electron content (TEC), depending on the forecaster's need. The fact that the output of the first stage of the model is a set of coefficients identical in format to those used by ITS-78 is another major positive attribute of this model. Any computer software which uses the ITS-78 ionosphere, such as the HF propagation program for which the ITS-78 climatology was developed (Barghausen, et al., 1969), can use the output of this model. This adds what is essentially a "real-time" capability to such software. There are four major deficiencies with this modeling scheme:

(1) It is mathematically continuous in only three dimensions (latitude, longitude, and time);
(2) It is computationally clumsy and slow;
(3) It cannot handle strong spatial and temporal gradients such as the high latitude trough; and
(4) It can use only foF2 and M3000 as input observations.

The combination of these deficiencies, particularly the last two, led to the development of what has become known as the 4D ionospheric model.

3.3.2 Four Dimensional (4D) Ionospheric Model

The 4D model was developed in the mid-1970s to remedy some of the problems of the Flattery-Ramsay model (Flattery and Davenport, 1977; Tascione, et al., 1978). All four dimensions (latitude, longitude, height,

and time) are incorporated within a single mathematical framework which is computationally far more efficient than the earlier model. The 4D model will accept a variety of observations as input data. It is currently configured to use foF2, M3000 (or Hmax), TEC, and electron density (N_e) or plasma scale height (H_e) at any level in the topside ionosphere. This last feature allows the use of N_e and H_e data at 840 km from the DMSP SSIE plasma probe. Finally, the ability to fit sharp gradients can be controlled through the number of wave numbers used in the latitude/longitude/time spectral analysis of the model.

As with the Flattery-Ramsay model, this model runs in two stages, but both stages are within the same program. All input data are first used to produce density profiles using a modified version of the Damon-Hartranft EDP model. Each profile is reduced to four coefficients by fitting a set of climatological height eigenvectors to the profile (Tascione, et al., 1978). These coefficients are then analyzed and merged into a climatological analysis to provide the final output of the model. The coefficients output by the model can then be used to produce any macroscopic ionospheric parameter desired.

This model would be used as follows to provide the forecast discussed earlier in section 3.3.2. All available data, including DMSP observations, are input to the 4D. After the model provides the "best guess" field grid the forecaster can make modifications to whatever parameter desired, including electron density at any level. The modified grids are then passed back to the 4D which provides an internally consistent analysis based on the forecaster's modifications. The forecaster can then use this analysis to produce the desired EDPs, or run through the modification loop again to produce another set of 4D analysis coefficients. Figure 3.1 shows the process schematically.

The two primary advantages of the 4D model are its ability to use a wide spectrum of input data and the flexibility that a system built around the 4D model gives the ionospheric forecaster. The example given above shows only a fraction of the options available. The forecaster can selectively delete or modify data initially input to the 4D, use different base climatology fields including the field produced by a prior run of the 4D, and can pass a manually produced analysis of any input parameter to the 4D for analysis.

For all its flexibility the current version of the 4D model has some problem areas. The model is data starved, i.e., there is not enough data currently available to take advantage of the profiling and gradient reproducing features of the model. This problem can be dealt with by acquiring more data, such as the new SSIE and SSIP (Rush, et al., 1978) sensors on the DMSP satellite, or by using the forecaster's inputs to "spread" the available data in latitude and longitude. A second problem, which is proving more difficult to address, concerns the height eigenvectors. The current set was derived from a collection of EDP observations from the

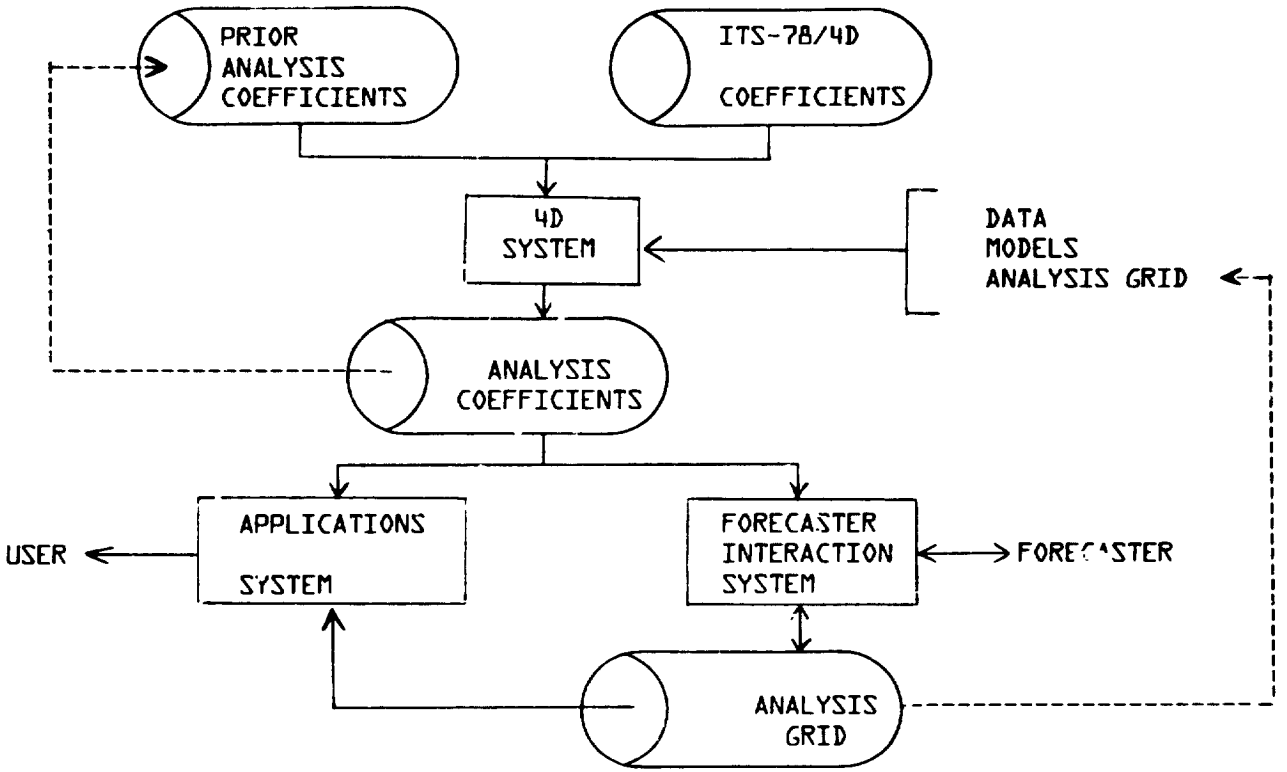

FIGURE 3.1 4D IONOSPHERE SYSTEM

incoherent backscatter facility at Millstone Hill, Mass. (Tascione, et al., 1978). This set has proved to be unable to fit profiles adequately from low and auroral latitudes, and has become marginal at middle latitudes with the upswing in the solar cycle. A number of studies are currently underway at AFGWC to improve the current eigenvector set, but a more representative set of EDP data, including high and low latitudes, will be required to produce a more universal set of eigenvectors.

4. IMPROVEMENT EFFORTS

4.1 Proton Forecasting

Improved modeling of solar particle events has led to improved forecasting capabilities. The models require consistent high quality data in order to perform at their capability. The SOON and RSTN systems are two ways AWS is trying to improve the data. The SOON, with its multi-wavelength features and real-time data processing, enhances the solar optical observing ability, both in quality and timeliness. Continuing research is presently in progress to exploit the improved capabilities of the SOON. Improved capabilities can be translated into better data required to improve our comprehension of the energy balance of a flare. While these data are not a panacea in themselves, they are and will continue to be an important part of the international solar patrol.

A significant portion of modeling efforts in high energy solar particles has been devoted to exploiting the radio portion of the flare spectrum. The current production model in use at AFGWC (Smart and Shea, 1977 a, b) is based on and fed by radio data. The RSTN was designed to monitor solar radio emissions from 25 MHz to 15 GHz. Eight fixed frequencies from 245 MHz to 15 GHz give a profile of each solar radio burst which can be translated into energy release by proton prediction models. On site computer systems will allow immediate evaluation of peak intensities, rise times, and integrated energy on each fixed frequency channel. These data, from worldwide standardized sites will allow more accurate and reliable input to the proton prediction models. The net result of these improvements to the observational system will have a significantly positive effect on the reliability of proton forecasting.

4.2 Magnetospheric Forecasting

Improvement in this area isn't quite as visible as in the proton area. However, the level of understanding is increasing due to data from such systems as DMSP. The specification of the magnetospheric processes which affect the density and composition of the upper atmosphere remain in need of improvement as discussed earlier, and the methods we use to observe the magnetosphere are presently rather crude. We feel considerable improvement can be gained by techniques and models in this area.

Coupling of the magnetosphere and ionosphere is another area which needs considerable definition and study. We are making improvements to the observational phase by observing the plasma environment at 6.6 earth radii using sensors on EP satellites. These data are fed into AFGWC in real-time (5 min averages of 56 channels of electrons and protons). There is usually a sensor in the midnight sector, so changes associated with substorm activity can be observed. Observations shortly after-the-fact (approximately 1-2 hours) from the polar orbiting DMSP satellites provides data about precipitating electrons, electron density and visual aurora. These, coupled with the ground based data could supply a magnetospheric model with enough data to describe some of the upper atmospheric processes. Presently, modelers hold the key to full exploitation of these data sources.

4.3 Ionospheric Modeling

Improvements are planned in three areas:

(1) The 4D model

(2) Use of the 4D model system, and

(3) Input data.

Most of the improvement efforts for the 4D model concern its profiling techniques. As was mentioned earlier, several programs are currently underway to improve the Millstone Hill eigenvectors. We hope to acquire additional data from other latitudes, as well as more current data from Millstone Hill, to extract a more representative eigenvector set. The techniques used to fit these eigenvectors to input profiles, and those used to integrate input TEC into these profiles, are being improved to provide more accurate and efficient profiling techniques.

A number of improvements and additions are planned for the 4D model forecasting and specification system. Current work is centered on improving the interfaces between the forecaster and the modeling system, such as software that enables the forecaster to add features to the forecast fields such as the high latitude trough. Other areas include adding a polar model as a front end to the 4D model, modifying current raytrace software to use the 4D output, and provide better base field climatology including a topside climatolog. We are also investigating the possibility of developing storm-line templates to pass to the 4D model as data grids when geomagnetic disturbances are expected or in progress.

As was mentioned in section 3.3, one problem with the 4D model is that it is data starved. In addition to the two new ionospheric sensors on the DMSP satellites, two other data sources are being explored. Work was recently begun to investigate the possibility of putting an active topside sounder on the DMSP spacecraft. These data would improve not only the specification of the ionosphere, but would also the model by using a set of topside measurements from over the entire globe to develop the

height eigenvectors. If this instrument is successfully developed, it will be first flown sometime in the early 1980's. Another avenue being explored is the possibility of using the dual frequency beacons of the Global Positioning System (GPS) satellites to observe TEC. These data will also be available sometime in the 1980's. The use of these new data, along with that now available from ground-based observatories and the DMSP SSIE and SSIP sensors, should provide enough data to begin using the 4D model to its fullest potential.

5. SUMMARY

The Air Weather Service has responded to Air Force requirements by development of capabilities in space environmental support. We have reviewed this involvement and indicated where our capabilites, efforts, and shortcomings exist. We feel our operational forecast centers of AFGWC utilize state-of-the-art techniques and data, but as demands increase, improved data and forecasting techniques are needed. It is our intent to identify these to the research community and hopefully to channel efforts toward solutions of problems we have identified. We fully realize the complexity of these problems and advocate further research efforts throughout the spectrum of the solar-terrestial sciences.

REFERENCES

Barghausen, A. F., J. W. Finneg, L. L. Proctor, and L. D. Schultz (1969): Predicting Long-Term Operational Parameters of High Frequency Sky-Wave Telecommunications Systems, Institute of Telecommunications Sciences, ESSA TR ERL 110-ITS-78.

Cliver, E. W., J. A. Secan, E. D. Beard, and J. A. Manley (1978): Prediction of Solar Proton Events at the Air Force Global Weather Central's Space Environmental Forecasting Facility, Proceedings the 1978 Symposium on the Effect of the Ionosphere on Space and Terrestrial Systems (in press).

Damon, T. D., and F. R. Hartranft (1970); Ionospheric Electron Density Profile Model, Aerospace Environmental Support Center Technical Memorandum 70-3.

Flattery, T. W. and G. R. Davenport (1977): Four Dimensional Ionosphere Model, Presented at URSI meeting, Stanford University, 22-24 June 1977.

Flattery, T. W. and A. C. Ramsey (1975): Derivation of Total Electron Content for Real-Time Global Applications, Effects of the Ionosphere on Space Systems and Communications, Edited by J. M. Goodman.

Feldstein, Y. I. and G. V. Starkov (1967): Dynamic of Auroral Belt and Polar Geomagnetic Disturbances, Planetary Space Science, 15:209.

Gassman, G. J. (1973): Analog Model 1972 of the Arctic Ionosphere, AFCRL Air Force Surveys In Geophysics No. 259, March 3.

Pike, C. P. (1975): Defense Meteorological Satellite Program Auroral Interpretation Guide, AFCRL Air Force'Surveys in Geophysics No. 306, 4 April 1975.

Rush, C. M., A. L. Snyder, E. Ziemba, V. Patterson, T. Tascione, and D. Nelson (1978): Global Behavior of the HF Radio Noise in the Topside Ionosphere, (submitted) Radio Science.

Smart, D. F. and M. A. Shea (1977a): Proceedings of the 15th International Cosmic Ray Conference, Vol 5, pg 131.

Smart, D. F. and M. A. Shea (1977b): Prediction of the Solar Proton Time-Intensity Profiles for the 30 April 1976 event. Space Research 18:373.

Starkov, G. V. (1969); Analytical Representation of the Equatorward Boundary of the Auroral Oval Zone, Geomag and Aeronomy (English Translation), 9:614.

Snyder, A. L. (1974): Real-Time Magnetospheric and Ionospheric Monitoring, 6th Conference on Aerospace and Aeronautical Meteorology, El Paso, TX.

Snyder, A. L., S-I. Akasofu, and T. N. Davis (1974): Auroral Substorms Observed Above the North Pole Region by a Satellite, J. Geophys Res. 77:3419.

Tascione, T. F., T. W. Flattery, V. G. Patterson, J. A. Secan, and J. W. Taylor, Jr. (1978): Ionospheric Modeling at AFGWC, Proceedings of Solar-Terrestial Predictions, Boulder, CO (in press).

Thompson, R. L. (1978): User Requirements of Aerospace Propagation - Environment Modeling and Forecasting, Proceedings of the AGARD Symposium on Operational Modeling of the Aerospace Propagation Environment, Ottawa, Canada (in press).

von Flotow, C. S. (1978): Ionospheric Forecasting at Air Force Global Weather Central, Proceedings of the Ionospheric Effects Symposium, Arlington, VA, Jan 1978 (in press).

D27.46

N80-18491

IONOSPHERIC MODELING AT AIR FORCE GLOBAL WEATHER CENTRAL

Capt Thomas F. Tascione
Col Thomas W. Flattery
Maj Vernon G. Patterson
Capt James A. Secan
Capt James W. Taylor Jr.
Air Force Global Weather Central
Offutt Air Force Base, Nebraska, 68113, USA

This paper describes the Four-Dimensional Ionospheric Model (4-D) which is under development at Air Force Global Weather Central. The 4-D integrates a wide variety of ionospheric data types into a consistent ionospheric specification. At each observing location, the 4-D reduces an entire electron density profile to four weighting coefficients. These weighting coefficients are interconnected in time and space by spectral analysis techniques. The resultant field of spectral coefficients can be used to reconstruct an electron density profile at any latitude, longitude and time.

1. BACKGROUND

The Air Weather Service (AWS) provides environmental support to Department of Defense (DOD) and other federal agencies in the form of ionospheric specifications and forecasts. The AWS Space Environmental Support System (SESS) generates these products based upon ionospheric models run on computer systems located at Air Force Global Weather Central (AFGWC), Offutt Air Force Base, Nebraska. This paper will describe the new Four-Dimensional Ionospheric Model and the impetus behind its development.

Observations of foF2, the critical frequency of the F2 region, and of M3000, a dimensionless quantity from which the altitude of the electron density peak may be computed, are received at AFGWC in real-time or near real-time from over 40 stations around the world. Observations of total electron content (TEC) are received from eleven stations. The locations of both the TEC and foF2 (M3000) observing stations are indicated in Figure 1. The frequency of observation varies from hourly to six-hourly and the reporting frequency varies from hourly to weekly. The foF2 and M3000 observations form the foundation upon which AFGWC models its ionospheric products.

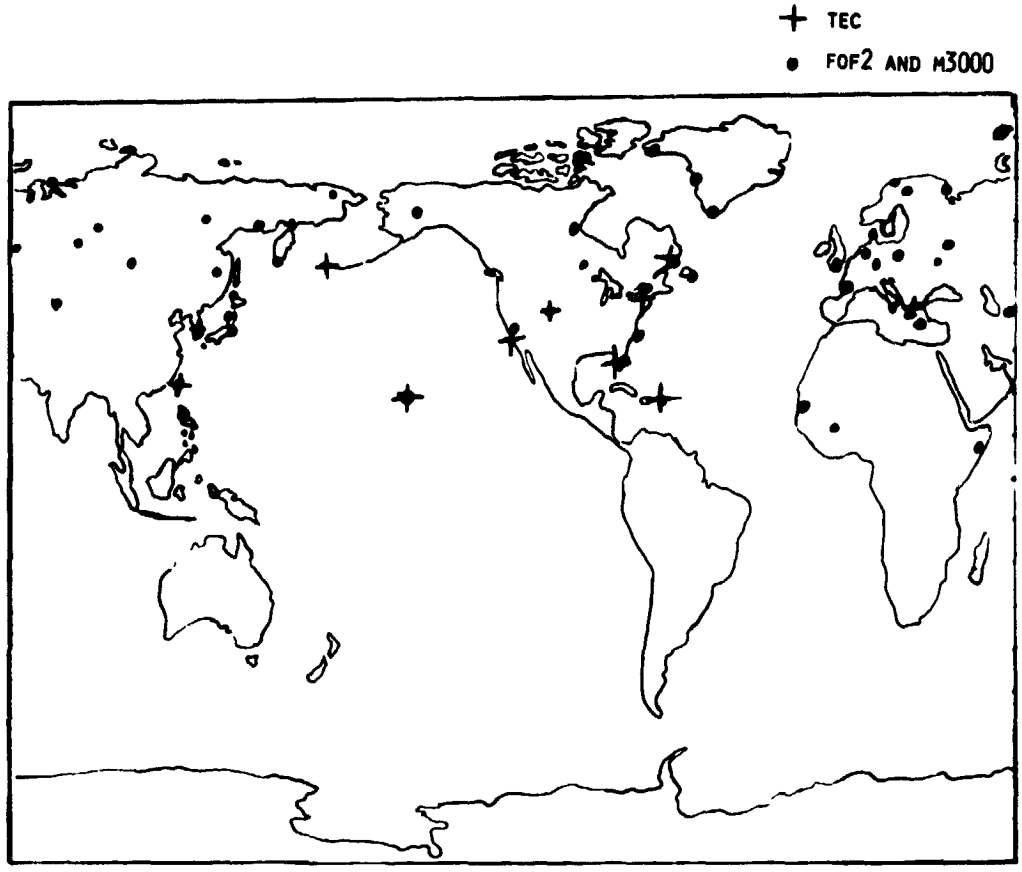

Figure 1. Map of foF2, M3000, and TEC observing locations.

Additionally, electron density observations, at approximately 840km, are provided by the SSIE sensor. This sensor is aboard a sunrise-sunset, sun-synchronous Defense Meteorological Satellite Program (DMSP) satellite. In the future, an SSIE sensor is to be flown on a noon-midnight DMSP satellite.

The SSIE sensor is an ion-electron plasma probe which provides in-situ measurements of electron and ion densities, electron and ion temperatures, and mean ion mass. The plasma scale heights, at 840km, can be deduced from the SSIE data and are useful in determining the shape of the topside ionosphere. More detailed information about the AFGWC data sources can be found in a paper by von Flotow (1978).

Currently, a need exists at AFGWC for a comprehensive ionospheric specification model which can ingest any or all of the above mentioned ionospheric data. The Four-Dimensional Ionospheric Model (4-D) is being developed to satisfy this need. The 4-D produces a consistent ionospheric specification anywhere in the Northern Hemisphere for a 24 hour period. Note: The 4-D is not a forecast model. No attempt is made to solve the multitude of complex equations necessary to describe ionospheric dynamics.

2. PROGRAM FLOW CHART

Figure 2 is a program logic flow chart. It outlines the principle stages of the model. It might be useful to use this figure as a guide as you read the model description section.

3. THE MODEL

An appropriate starting point for any ionospheric model is to build a vertical electron density profile at each observing location. Numerous investigators have considered the problem of modeling electron density profiles. A summary of several profile modeling techniques is given in Table 1. This table is not intended to be all inclusive, rather, it highlights a variety of methods.

Table 1. Electron Density Profile Models

Model (Year)	E Region	F1 Region	F2 Region	Remarks
CCIR (1970)	Parabola		Parabola	
Damon and Hartranft (1970)	Chapman Layer	Chapman Layer	Chapman Layer	
Nisbet: Penn State NRI (1970)	Solution of Equation of Continuity		Solution of Diffusion Equation	Daytime Model
Bent (1972)	Parabola Squared	Parabola Squared	Parabola	Topside: Exponential Decay Functions
Cookingham (1972)	From Nisbet	From Nisbet	Chapman, Parabola, or Sine Squared Function	
Bradley and Dudeney (1973)	Parabola below E layer max	Linear up to level of 1.7 foE	Parabola	
Ching and Chiu (1973)	Phenomenological	Phenomenological	Phenomenological	
Miller and Gibbs (1973)	Parabola	Parabola	$sech^2$ in daytime parabola at night	Topside: Exponential Decay Functions
Rush and Miller (1973)	Parabola	Parabola	$sech^2$ in daytime parabola at night	Topside: sech function
Jasperse (1976)	Solution to electron distribution function			Daytime Bottomside Model

Presently, AFGWC uses a modified version of the Damon and Hartanft (1970) technique to build the profile. In this version, the electron density at any level is the sum of an E layer, F1 layer and F2 layer contribution. Each layer is represented by a Chapman distribution,

$$Ne(h) = Ne\ max\ \ exp(a(1-Z-exp-z)) \qquad (1)$$

where a is a function of the electron loss mechanism. For the E layer, a is equal to 1/2 (recombination predominates); a is equal to 1 for the F1 and F2 layers (attachment predominates). The variable z is given by:

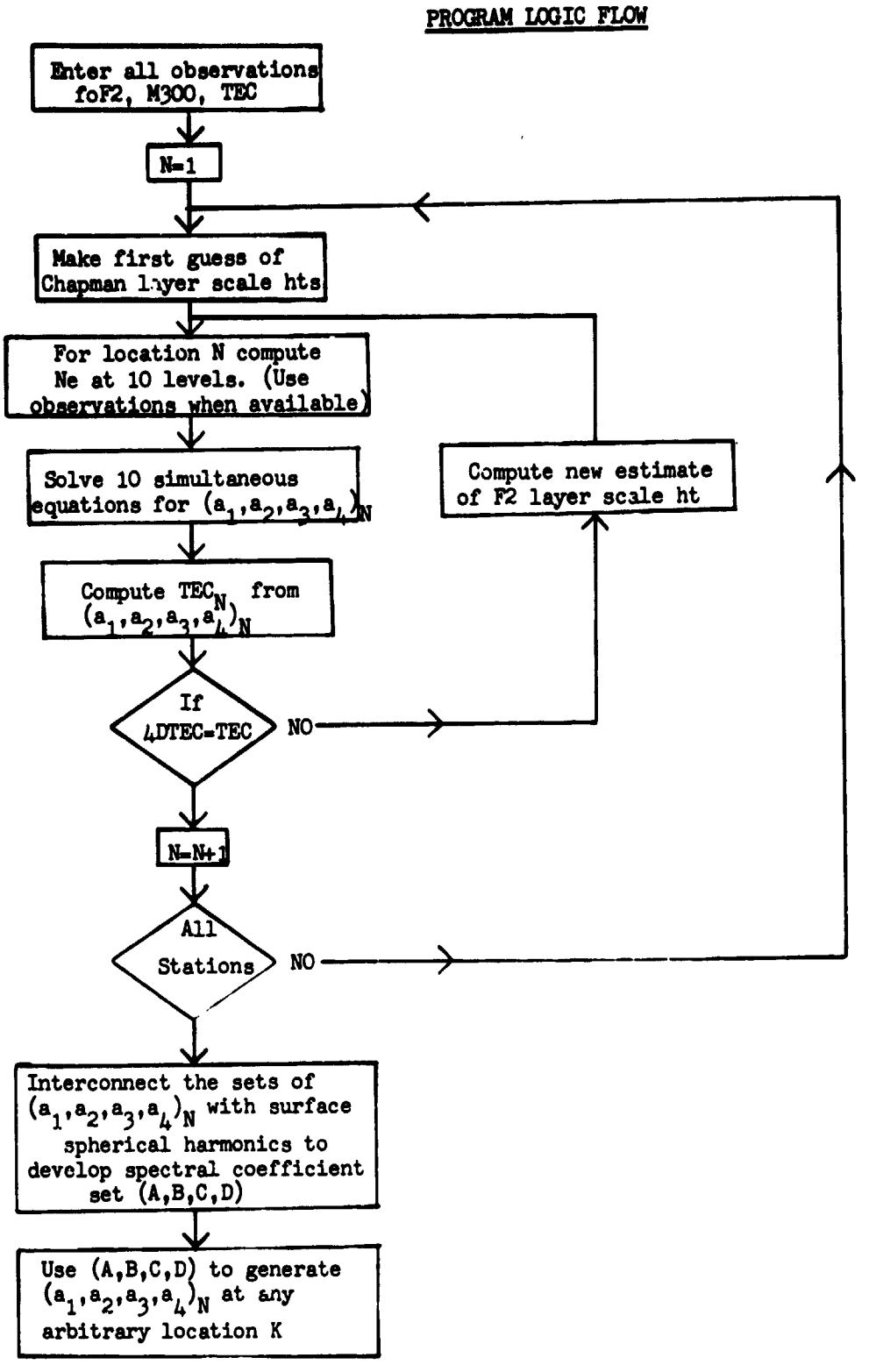

Figure 2. Program logic flow chart.

$$Z = \frac{h - hmax}{h_s} \qquad (2)$$

where h is the height, hmax is the height of Ne max, and h_s is the scale height. The E layer hmax is fixed at 120 km. The F2 layer hmax (HMAX) is computed via a modified version of Shimazaki's equation (1955) from observed M3000. The F1 layer hmax is allowed to vary in a predetermined manner between the E and F2 peaks. Figure 3 illustrates an electron density profile which is the sum of the E layer, F1 layer, and F2 layer Chapman distributions. The next step is to reduce an electron density profile (computed via equation 1) to a set of weighting coefficients.

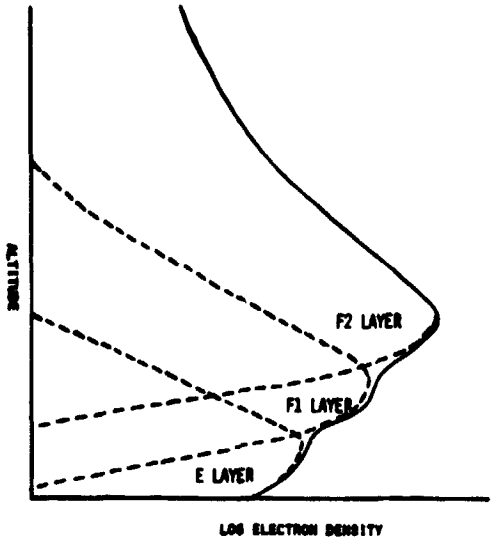

Figure 3. Electron density profile as the sum of the E, F1, and F2 Chapman layer contributions.

In gneral, at any height (h), an electron density profile can be approximated by a partial sum of orthonormal basis functions and an appropriate set of weighting coefficients. That is:

$$Ne(\ell) = \sum_{k=1}^{N} a_k W_k(\ell) \qquad (3)$$

where $W_k(\ell)$ represents an empirically derived set of discrete orthonormal basis functions evaluated at level ℓ and the a_k's are weighting coefficients. These basis funcitons are provided as input variables to the model. Presently 127 levels span the physical distance between 95 and 2000km. The interval spacing between each level is: 5 km for level 1 through 81 (95-500 km); 20 km for levels 82 through 106 (520-1000 km); and 50 km for levels 107 through 127 (1050-2000 km). A detailed discussion of the derivation of a suitable empirical orthonormal basis set is given in a paper by Flattery, et al. (1979). Presently, we only use the first four terms of the partial sum given by equation 3. This choice represents a trade-off between model accuracy and computer run time. The sum can easily be extended as computer resources permit and accuracy demands. Figure 4 is an example of the first three empirical orthonormal functions which were derived from Millstone Hill backscatter radar observations.

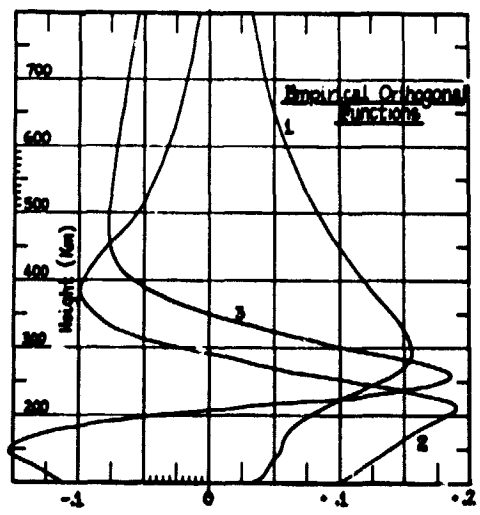

Figure 4. Empirical orthogonal functions.

The next step is to determine the values for the weight coefficients, a_k. Currently we evaluate (using equation 1) the electron density at 10 different heights: 50 km below HMAX; 20 km below HMAX; at HMAX; 20, 50, 100 and 200 km above HMAX; 740 km; 840 km (DMSP height); and 940 km. These points maximize the profile shape definition with a minimun of points. There is nothing unique about the points selected; the number and location of points can be changed as required. Whenever possible, real observations are inserted at HMAX and 840 km. Therefore, from equation 3, we have ten simultaneous equations:

$$\begin{aligned} Ne(50\ \text{below}) &= a_1 W_1(50\ \text{below}) + a_2 W_2(50\ \text{below}) + \ldots + a_4 W_4(50\ \text{below}) \\ &\vdots \\ Ne\ (940) &= a_1 W_1\ (940) + a_2 W_2\ (940) + \ldots + a_4 W_4\ (940) \end{aligned} \qquad (4)$$

From this set of equations we can find a least squares fit solution of a_1, a_2, a_3, a_4. Once the weighting coefficients are known, we can compute the TEC by using:

$$4DTEC = \int_{95}^{2000} Ne(h)\ dh$$

-or-

$$4DTEC = \Delta L_1 \sum_{m=1}^{81} \sum_{k=1}^{4} a_k W_k(m) + \Delta L_2 \sum_{m=82}^{106} \sum_{k=1}^{4} a_k W_k(m) + \Delta L_3 \sum_{m=107}^{127} \sum_{k=1}^{4} a_k W_k(m) \qquad (5)$$

where

ΔL_1 = 5 km
ΔL_2 = 20 km
ΔL_3 = 50 km

The 4DTEC is then compared against any nearby observed TEC. We can minimize any differences by appropriately modifying the F2 layer scale height (h_s) in equation 2. That is, F2 layer h_s controls the topside thickness of the profile; we can add or subtract electrons by adjusting this h_s. Therefore, our complete set of equations includes 4, 5, 1 and 2. Presently, we solve this set of equations by an iterative technique.

In practice it is better to do the entire profile analysis in terms of plasma frequency rather than plasma density. The variance of plasma frequency over the profile is much smaller than the variance of plasma density. This smaller variance allows for more stable computational solutions. However, conversion to plasma frequencies can cause some problems. In terms of plasma density, equation 3 becomes:

$$f(\ell) = \sum_{k=1}^{n} a_k Z_k(\ell) \qquad (6)$$

where $f(\ell)$ is the plasma frequency at level ℓ and $Z_k(\ell)$ is a discrete (empirical) orthonormal basis set which spans the frequency space. Difficulties arise in the 4DTEC equation because it becomes quadratic. That is,

$$4DTEC = \Delta L_1' \sum_{m=1}^{81} \left(\sum_{k=1}^{4} a_k Z_k(m) \right)^2 + \Delta L_2' \sum_{m=82}^{106} \left(\sum_{k=1}^{4} a_k Z_k(m) \right)^2 + \Delta L_3' \sum_{m=107}^{127} \left(\sum_{k=1}^{4} a_k Z_k(m) \right)^2 \quad (7)$$

where

$$\Delta L_1' = 1.24 \times 10^4 \, \Delta L_1$$
$$\Delta L_2' = 1.24 \times 10^4 \, \Delta L_2$$
$$\Delta L_3' = 1.24 \times 10^4 \, \Delta L_3$$

In equation 7, the conversion of plasma frequency to plasma density is given by:

$$Ne(\ell) = 1.24 \times 10^4 \, f^2(\ell) \quad (8)$$

The analogous set of simultaneous equations becomes:

$$\begin{aligned} f(50 \text{ below}) &= a_1 Z_1(50 \text{ below}) + \ldots + a_4 Z_4(50 \text{ below}) \\ &\vdots \qquad\qquad\qquad\qquad \vdots \\ f(940) &= a_1 Z_1(940) + \ldots\ldots + a_4 Z_4(940) \end{aligned} \quad (9)$$

Therefore, in practice, we solve for the weighting coefficients (a_1, a_2, a_3, a_4) by an iterative technique using equations 9, 7, 1, 2, and 8. In effect, this analysis reduces an entire electron density profile to just four weighting coefficients. That is, once a_1 thru a_4 are known, one can reconstruct an entire electron density profile from equations 6 and 8. Remember, the empirical basis functions, $Z_k(\ell)$, are input parameters to the model. This analysis is applied at every observing location.

The next step is to interconnect the weighting coefficients with "best fit" functions which are continuous in time and space. These continuous functions can then be used to compute a weighting coefficient set anywhere on the surface of the Northern Hemisphere (i.e. we can compute a_1 thru a_4 for any given latitude, longitude, and time). In this way, the model expands a discrete set of observations into a continuous specification of the ionosphere.

Presently, we use surface spherical harmonic functions for the spacial connections and simple trigonometric functions are used for time relationship. In the near future, we hope to replace the trigonometric time functions with a more representative set of empirically derived functions.

These new time functions should have a basic shape which characterizes the ionosphere's very strong sunrise gradient and its weaker (but still strong) sunset gradient. A potential benefit of these new functions is that fewer terms would be needed in the temporal partial sum in order to match diurnal ionospheric behavior.

The current equation for plasma frequency is given by:

$$f(\ell) = \sum_{i=0}^{I}\sum_{j=0}^{J}\sum_{m=2j}^{2(j+m-1)}\sum_{k=1}^{4}\left(A_{m,k}^{i,j}\cos j\lambda\cos it + B_{m,k}^{i,j}\sin j\lambda\cos it \right. \tag{10}$$

$$\left. + C_{m,k}^{i,j}\cos j\lambda\sin it + D_{m,k}^{i,j}\sin j\lambda\sin it\right) p_m^j(\sin\phi)z_k(\ell)$$

where ϕ is the latitude, λ is the longitude, and t is the time. The wave numbers, I,J,M are selected on the basis of ionospheric gradients. That is the steeper the gradients, the more terms we need to include in the partial sums. Presently, I, J, and M are set at 17, 12, and 10. The terms $p_m^j(\sin\phi)$ are associated Lengendre polynomials. Equation 10 is the result of substituting the solution for the a_k's (surface spherical harmonics) back into equation 6. Therefore, if one knows all the spectral coefficients (A, B, C, and D), then one can produce an electron density profile anywhere in the ionosphere.

The 4-D is initialized from a data grid of foF2's and M3000's extracted from ITS78 (See Barghausen, et al (1969)). Each grid point will affect certain spectral coefficients and the wave numbers I, J, and M determine the grid spacing necessary to initialize all spectral coefficients. Presently the grid is 10^0 of longitude by 10^0 of latitude. Points separated by more than 15^0 will have minimal influence on one another.

After the 4-D is initialized, all observed data are entered. These observations will change specific spectral coefficients; those spectral coefficients outside the range of influence of a given observation will remain virtually unchanged. Therefore, if observations differ significantly from the initial field, unrealistic gradients can be introduced into the ionospheric specification. Figure 5 has an example of scattered observations which differ appreciably from the initial field. The spectral coefficients for observations 1 and 2 are 50% higher than the initial coefficient field. In figure 5a, the observation points are separated by more than 30 degrees and in figure 5b, the observation points are within 10 degrees of one another. Notice, in figure 5a, that the observation points are too far apart to influence one another. The 4-D solution (solid line) returns to the initial (dotted line) field about 15 to 20 degrees beyond an observation. The dashed line is the desired solution. In figure 5b, the observations are close enough to affect each other; about $15\text{-}20^0$ beyond the observation region the 4-D reverts back to the base field. Therefore, we have a two-fold problem. First, the data points must be close enough together so that they influence one another. Secondly, the data network must be extensive enough so as to avoid unrealistic gradients as the field changes from the observations back to the base field. In fact, to avoid these artificial model gradients completely, we would need an entire Northern Hemisphere 10^0 by 10^0 grid. Realistically, this 10^0 by 10^0 grid need only exist in the areas of interest. Beyond these areas, we could blend back into the base field, generating model gradients in areas which would not affect our solution.

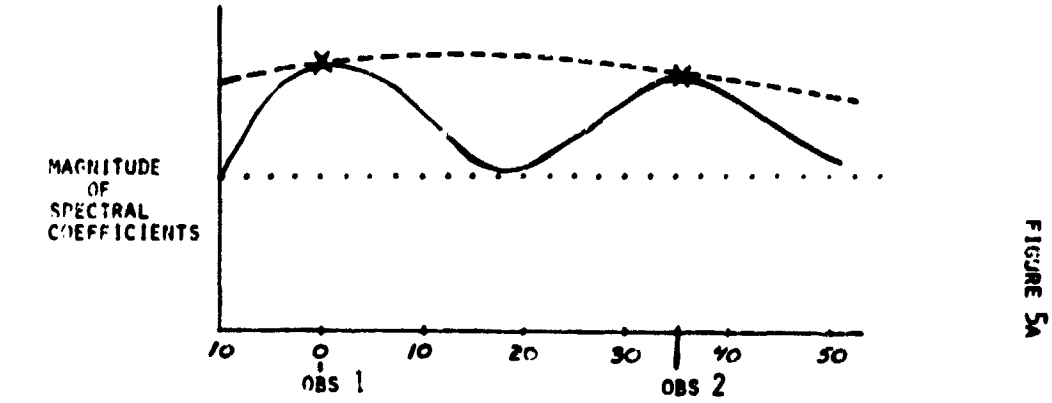

FIGURE 5A

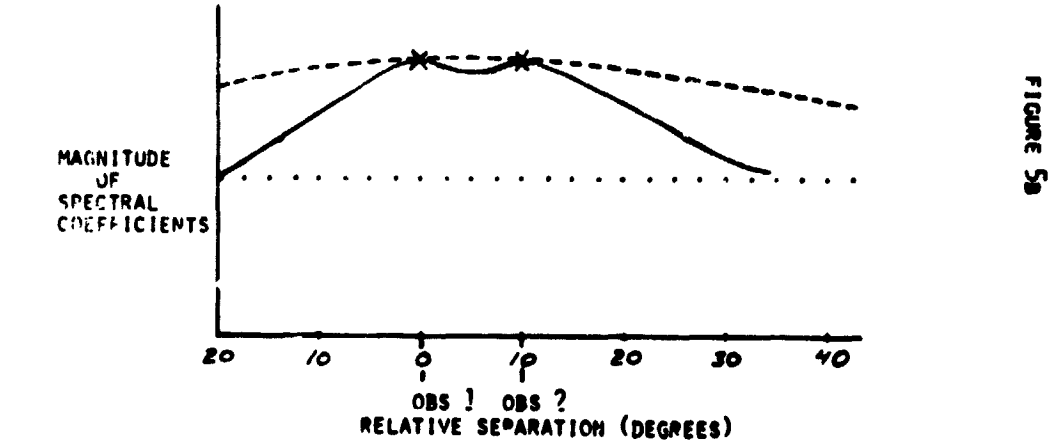

FIGURE 5B

Figure 5. Examples of artifical gradients induced by observations which differ significantly from the base field. Base field (····); 4-D analysis (——); Desired solution (- - -).

Presently, we are developing modeling techniques which can spread out the information from our observation network into a space/time grid of "psuedo observations" (See Flattery, et al. (1979)). These techniques have shown great promise and they will soon become preprocessors for the 4-D model.

4. CONCLUSIONS

The 4-D model is being developed to provide a continuous and comprehensive specification of the ionosphere. No attempt has been made to develop a dynamic forecast model. Instead we have concentrated on providing a representative reproduction of the complete ionosphere from disperse observations.

The model reduces the entire ionosphere into a small collection of coefficients which can be easily transmitted to a customer or stored for future reference. Given a coefficient set, a user can reconstruct an electron density profile anywhere in the Northern Hemisphere for the valid 24 hour specification period.

The 4-D model is currently in limited use at AFGWC as part of an ionospheric specification and forecasting system (See Thompson and Secan, 1978). While there are still some operational limitations to the current version of the model, there is a great deal of potential in the flexibility of the model. Work is currently underway at AFGWC in learning how to exploit this flexibility to meet current and future operational requirements.

REFERENCES

Allen, R.S. and J.D. Tardelli (1973). Interim Technical Report - Model Evaluation Program, Air Force Cambridge Research Laboratories, Hanscom Air Force Base, Massachusetts 01731.

Bradley, P.A. and J.R. Dudeney (1973). A simple model of the vertical distribution of electron concentration in the ionosphere, Journal of Atmospheric and Terrestrial Physics, 35, 2131-2146.

Bryon, F.A. and R.W. Fuller (1969). Mathematics of Classical and Quantum Physics, Addison-Wesley Publishing Company; Reading, Massachusetts.

Barghausen, A.F., F.W. Finney, L.L. Proctor, and L.D. Schultig (1969). Predicting Long-Term Operational Parameters of High-Frequency Sky-Wave Telecommunication Systems, ESSA Tech. Rept. ERL 110-ITS78 (U.S. Govern-Printing Office, Washington D.C. 20402).

Ching, B.K. and Y.T. Chiu (1973). A phenomenological model of global ionospheric electron density in the E-, F1- and F2-regions, Journal of Atmospheric and Terrestrial Physics, 35, 1615-1630.

Cookingham, R.E. (1972). Modeling the Bottomside Ionospheric Electron Density Profile, AFCRL-72-0340, Air Force Cambridge Research Laboratories Hanscom AFB, Massachusetts 01731.

Damon, T.D. and F.R. Hartranft (1970). Ionospheric Electron Density Profile Model, Aerospace Environmental Support Center Technical Memorandum 70-3, Ent Air Force Base, Colorado 80914.

Flattery, T.W. (1971). Spectral Models for Global Analysis and Forecasting, Air Weather Service Technical Report 242, Air Weather Service, Scott AFB, Illinois 62225.

Flattery, T.W., T.F. Tascione, J.A. Secan and J.W. Taylor, Jr. (1979). A Four Dimensional Ionospheric Model (to be published).

Jasperse, J.R. (1976). Boltzmann-Fokker-Planck Model for the Electron Distribution Function in the Earth's Ionosphere, Planetary and Space Science, 24 (1), 33-40.

Llewellyn, S.K. and R.B. Bent (1973). Documentation and Description of the Bent Ionospheric Model - Delay Model Version, SAMSO TR 73-252, Space and Missile Systems Organization, Los Angeles, California 90009.

Miller, D.C. and J. Gibbs (1974). Ionospheric Analysis and Ionospheric Modeling, AFCRL-TR-74-0364, Air Force Cambridge Research Laboratories, Hanscom Air Force Base, Massachusetts 01731.

Nisbet, J.S. (1970). On the Construction and Use of the Penn State MKI Ionospheric Model, Scientific Report No. 355, Ionospheric Research Laboratory, The Pennsylvania State University, University Park, Pennsylvania 16802.

Nisbet, J.S. (1971). On the construction and use of a simple ionospheric model, Radio Science, 6, 437-464.

Nisbet, J.S. (1975). Models of the Ionosphere, Atmospheres of Earth and the Planets, edited by B.M. McCormac, 245-258, D. Reidel, Dordrecht, Holland.

Rush, C.M. and D. Miller (1973). A Three Dimensional Ionospheric Model Using Observed Ionospheric Parameters, AFCRL-TR-73-0567, Air Force Cambridge Research Laboratories, Hanscom Air Force Base, Massachusetts 01731.

Shimazaki, T. (1955). Worldwide Daily Variations in the Height of the Maximum Electron Density of the Ionospheric F2 Layer, J. Radio Res. Labs, Japan, 2, 85-97.

Thompson, R.L. and J.A. Secan (1978). Geophysical Forecasting at AFGWC, (these proceedings).

von Flotow, C.S. (1978). Ionospheric forecasting at Air Force Global Weather Central, Ionospheric Effects Symposium, Arlington, Va, Jan 78. (in press).

MSFC SOLAR ACTIVITY PREDICTIONS FOR SATELLITE ORBITAL LIFETIME ESTIMATION

H. C. Euler, C. A. Lundquist,
and W. W. Vaughan
Space Sciences Laboratory
NASA Marshall Space Flight Center
Marshall Space Flight Center, Alabama 35812, USA

The procedure to predict solar activity indices for use in upper atmosphere density models is given together with an example of the performance. The prediction procedure employs a least-square linear regression model to generate the predicted smoothed $\overline{R}_{13}$ and geomagnetic $\overline{A}_{p(13)}$ values. Linear regression equations are then employed to compute corresponding $\overline{F}_{10.7(13)}$ solar flux values from the predicted $\overline{R}_{13}$ values. The output is issued principally for satellite orbital lifetime estimations.

INTRODUCTION

The purpose of this paper is to present the Marshall Space Flight Center (MSFC) solar activity prediction technique and the basis for the procedure used. The motivation for issuing the predictions monthly is the need for a current and systematic input for use in an upper atmosphere density model employed in satellite orbital lifetime estimates. The mission analysis and planning for launches require estimates of orbital lifetimes up to 10 to 15 years in the future for satellites at various orbital altitudes, inclinations, and eccentricities.

The upper atmosphere density model used (NASA, 1973) is based on the work and models developed by Jacchia (1970, 1971) and his colleagues of the Smithsonian Astrophysical Observatory (SAO). To compute neutral density at the pertinent orbital altitudes and times, the model requires as an input the mean value of the 10.7 cm solar flux ($F_{10.7}$) evaluated over $\pm$ three solar rotations, the mean daily value of solar flux ($F_{10.7}$), and the three-hourly geomagnetic index (A_p) taken 6 to 9 hours prior to the time of desired orbital density calculation. The behavior of the daily solar flux and geomagnetic indices precludes the long-term prediction of the daily values with any degree of accuracy. Therefore, 13-month smoothed, solar-activity-related indices for $F_{10.7}$ and A_p are predicted using a least-square linear regression procedure. The predicted smoothed values of $\overline{F}_{10.7(13)}$ and $\overline{A}_{p(13)}$ are

used as input to the upper atmosphere density model instead of the shorter time period values of $F_{10.7}$ and A_p. This produces the necessary values of the neutral density applicable to the computation of medium and long-term satellite orbital lifetime estimates.

PREDICTION TECHNIQUE

The MSFC solar activity prediction technique uses a modified McNish-Lincoln (1949) method to project the remainder of a current sunspot cycle based on data for the past 20 cycles and the current smoothed Zürich sunspot number $\overline{R}_{13}$. The statistical prediction technique uses a least-square linear regression model to generate the predicted smoothed sunspot number $\overline{R}_{13}$ (Avaritt, 1972). Prior to being used as input data the values for each cycle are reduced so that the cycle minima at the start of the cycles are normalized to zero.

A mean cycle is computed based on all past cycles used in the prediction. This provides a first approximation to the predicted cycle. All 20 cycles used in the prediction model data base use the Zürich established minima as the starting point. However, because of the behavior of the minimum for cycle 20, whereby two identical values of $\overline{R}_{13}$ in March and June 1976 are given, an interpolation procedure using the shape of the descending and ascending curve for cycles 20 and 21, respectively, was employed (Lundquist and Vaughan, 1978). This interpolation gave April 1976 as the index for the starting point of cycle 21. This point and the most recent value of $\overline{R}_{13}$ for cycle 21 are used in the prediction. The variance of the prediction error of the predicted deviations from the mean cycle is minimized by the model. The predicted deviations are then applied to the mean cycle to obtain an updated projection for the remainder of cycle 21.

The least-square linear regression procedure assumes that if the current cycle is running above (or below) the ensemble mean cycle, then in the future the current cycle is likely to follow the course of previous cycles than ran correspondingly above (or below) the mean. The variance is computed for each updated prediction as the average squared error obtained when the corresponding point of each previous cycle is predicted by the same procedure as that applied to predicting the current cycle. The best estimate of the standard deviation for the predicted smoothed sunspot number $\overline{R}_{13}$ is then computed by taking the square root of this variance. The resulting computer output includes predicted nominal $\overline{R}_{13}$ and associated plus- and minus-two standard deviation values arranged in a time sequence.

Since upper atmosphere model inputs are needed for orbital lifetime estimates used in the design of missions beyond the current cycle, the later entries in the output of the least-square linear regression model are slightly modified. The modification involves the selection of June 1987 as the initialization point for cycle 22. The $\overline{R}_{13}$ values of zero, six, and twelve are then used, respectively, for the minus-two standard deviation,

nominal, and plus-two standard deviation values for the minimum of cycle 22, with the balance of cycle 22 being represented by the mean and standard deviation values computed from cycles 1 through 20. The predicted sunspot values for the final 3 years prior to June 1987 are interpolated from the least-square linear regression model prediction for cycle 21 to the estimated start of cycle 22.

To compute the smoothed $\overline{F}_{10.7(13)}$ solar flux values, a relationship

$$\left\{\overline{F}_{10.7(13)} = 49.4 + 0.97\ \overline{R}_{13} + 17.6\ \exp^{-0.035\overline{R}_{13}}\right\}$$

is used. This regression equation is used with each predicted nominal and two-standard-deviation value of $\overline{R}_{13}$. The values are arranged in a time sequence on the computer output. A linear correlation coefficient of 0.98 was obtained for this fit of the data which extend back to 1947.

The data base for the geomagnetic index A_p extends back to 1932. Its behavior is poorly correlated with the solar cycle, even for 13-month smoothed values. Therefore, the 13-month smoothed values of the geomagnetic index $\overline{A}_{p(13)}$ are employed in a prediction model using the least-square linear regression technique. The output is an estimate of the nominal $\overline{A}_{p(13)}$ and associated plus- and minus-two standard deviations arranged in a time sequence.

BASIS FOR TECHNIQUE

Yu. I. Vitinskii (1965) conducted a very extensive survey and analysis of solar activity forecasting methods. While recognizing the considerable importance of the problem and encouraging studies of active processes taking place on the Sun as a contribution toward the solution of the problem, he well stated what is still the current situation. Vitinskii concluded: "...we have shown that the reliability of the results obtained using these methods still leaves much to be desired." However, his analysis showed that the linear regression method gives the best accuracy for $\overline{R}_{13}$ predictions up to a year in advance. For predictions several years in advance the linear regression method becomes increasingly less accurate. The uncertainty of this prediction method is given by the standard deviation estimates as computed by the MSFC least-square linear regression method reliability procedure. Therefore, with the lack of any proven deterministic prediction scheme based on physical laws, the statistical predictions produced by this technique are used as a basis for developing future orbital lifetime estimates needed for mission planning and analysis.

EXAMPLE OF TECHNIQUE

The Marshall Space Flight Center generates a monthly memorandum which contains data on the recently determined solar activity indices and the current predictions for the smoothed values of $\bar{R}_{13}$, $\bar{F}_{10.7(13)}$, and $\bar{A}_{p(13)}$. Part of the output given in the November 1978 memorandum is reproduced in Table 1 as an example of the results of the prediction technique.

SUMMARY OF EVALUATIONS

Obviously, no evaluation is yet possible relative to the prediction accuracy for the magnitude of cycle 21 peak $\bar{R}_{13}$ values. The least-square linear regression model technique is sensitive to the initiation date of the cycle being predicted, the ensemble of cycles used in the historical data base, etc. Figure 1 summarizes the application to date of the linear regression procedure to the prediction of cycle 21. The choice of the date for the start (minimum) of cycle 21 strongly influences the results. The data base and normalization choices have significant effects in the early phase of cycle 21 development, relative to the predicted peak $\bar{R}_{13}$ values, but become less significant as the cycle develops. This figure is helpful in representing the range of rational linear regression projections for the forthcoming maximum of cycle 21. The current MSFC nominal prediction employs the interpolated April minimum and uses a normalized data base of cycles 1 through 20.

There is a need for a systematic representation of solar activity predictions for use in upper atmosphere density models employed in satellite lifetime studies. The MSFC solar activity predictions are intended to serve that function.

TABLE 1. PREDICTED SOLAR ACTIVITY SMOOTHED 13-MONTH MEANS.[a,b]

TIME	SUNSPOT NUMBER $\bar{R}_{13}$			10.7 CM SOLAR FLUX $\bar{F}_{10.7}$			GEOMAGNETIC INDEX $\bar{A}_p$		
	NOMINAL	PLUS TWO SIGMA	MINUS TWO SIGMA	NOMINAL	PLUS TWO SIGMA	MINUS TWO SIGMA	NOMINAL	PLUS TWO SIGMA	MINUS TWO SIGMA
1978.333 MAY	79.41	83.01	75.80	127.52	130.88	124.16	16.25	16.87	15.63
1978.417 JUN	83.51	90.14	76.88	131.35	137.59	125.17	15.99	17.10	14.88
1978.500 JUL	87.03	95.77	78.30	134.66	142.91	126.49	15.79	16.91	14.67
1978.583 AUG	89.92	100.42	79.42	137.38	147.33	127.53	15.89	16.51	15.26
1978.667 SEP	92.88	106.01	79.75	140.18	152.66	127.84	15.70	16.40	14.99
1978.750 OCT	96.22	112.63	79.82	143.34(16)	158.99(0)	127.90(31)	16.25	17.60	14.89
1978.833 NOV	99.61	118.25	80.97	146.56(10)	164.38(0)	128.97(20)	16.93	18.87	14.99
1978.917 DEC	103.48	123.79	83.17	150.25(6)	169.71(0)	131.03(10)	16.98	18.51	15.46
1979.000 JAN	107.21	129.55	84.87	153.81(0)	175.25(0)	132.63(0)	17.15	18.68	15.63
1979.083 FEB	110.27	135.35	85.18	156.73	180.84	132.92	17.37	19.07	15.67
1979.167 MAR	112.68	139.80	85.55	159.04	185.14	133.27	17.59	19.68	15.47
1979.250 APR	115.07	143.03	87.11	161.33	188.25	134.73	17.86	20.22	15.49
1979.333 MAY	117.00	146.46	87.54	163.18	191.57	135.14	17.63	20.08	15.17
1979.417 JUN	118.91	151.30	86.52	165.02	196.25	134.18	17.41	20.50	14.32
1979.500 JUL	121.29	155.35	87.23	167.30	200.17	134.84	17.57	21.00	14.14
1979.583 AUG	123.15	157.31	89.00	169.10	202.06	136.51	17.78	21.71	13.85
1979.667 SEP	124.15	158.25	90.05	170.05	202.97	137.50	17.82	22.58	13.07
1979.750 OCT	124.34	157.85	90.84	170.24	202.59	138.25	17.34	21.66	13.02
1979.833 NOV	124.23	157.54	90.91	170.13	202.29	138.31	16.67	20.80	12.54
1979.917 DEC	123.53	157.61	89.44	169.45	202.35	136.92	16.38	20.78	11.99
1980.000 JAN	122.33	157.01	87.66	168.31	201.77	135.25	16.37	20.10	12.64
1980.083 FEB	121.77	157.36	86.17	167.76	202.11	133.84	16.40	20.21	12.59
1980.167 MAR	121.48	157.86	85.10	167.49	202.60	132.85	16.50	19.83	13.16
1980.250 APR	120.72	157.36	84.09	166.76	202.11	131.89	16.65	19.31	13.99
1980.333 MAY	119.59	156.42	82.76	165.67	201.20	130.65	16.65	19.02	14.28
1980.417 JUN	117.96	154.88	81.04	164.10	199.71	129.04	16.70	19.11	14.30
1980.500 JUL	116.17	154.10	78.25	162.39	198.96	126.44	16.52	18.94	14.10
1980.583 AUG	114.58	154.39	74.77	160.86	199.24	123.21	16.49	19.11	13.86
1980.667 SEP	113.56	154.71	72.41	159.89	199.55	121.04	16.75	20.04	13.47
1980.750 OCT	113.22	155.91	70.52	159.56	200.71	119.30	16.78	20.76	12.79
1980.833 NOV	112.88	157.00	68.76	159.23	201.76	117.68	16.71	21.54	11.88
1980.917 DEC	112.29	155.97	68.62	158.67	200.77	117.55	16.84	22.48	11.20
1981.000 JAN	111.53	153.43	69.63	157.94	198.31	118.48	17.02	22.95	11.09
1981.083 FEB	110.26	151.42	69.09	156.72	196.37	117.99	16.88	22.91	10.84
1981.166 MAR	108.39	150.38	66.40	154.93	195.36	115.53	16.52	22.89	10.15
1981.250 APR	106.14	148.78	63.50	152.79	193.82	112.90	16.24	22.51	9.96

a. Because orbital lifetime programs require a specific date to associate with the input of solar flux ($\bar{F}_{10.7}$) and geomagnetic ($\bar{A}_p$) prediction to compute a corresponding atmospheric density, the data points are identified with the midday of the given month.

b. Values in parentheses beside the solar flux predictions are estimates of the near-term average values for $F_{10.7} - \bar{F}_{10.7}$ projected 3 months into the future. The first value shown in parentheses is based on the actual average value of $F_{10.7}$ for the month given. See Equation A-10 of NASA SP-8021 for use of these data.

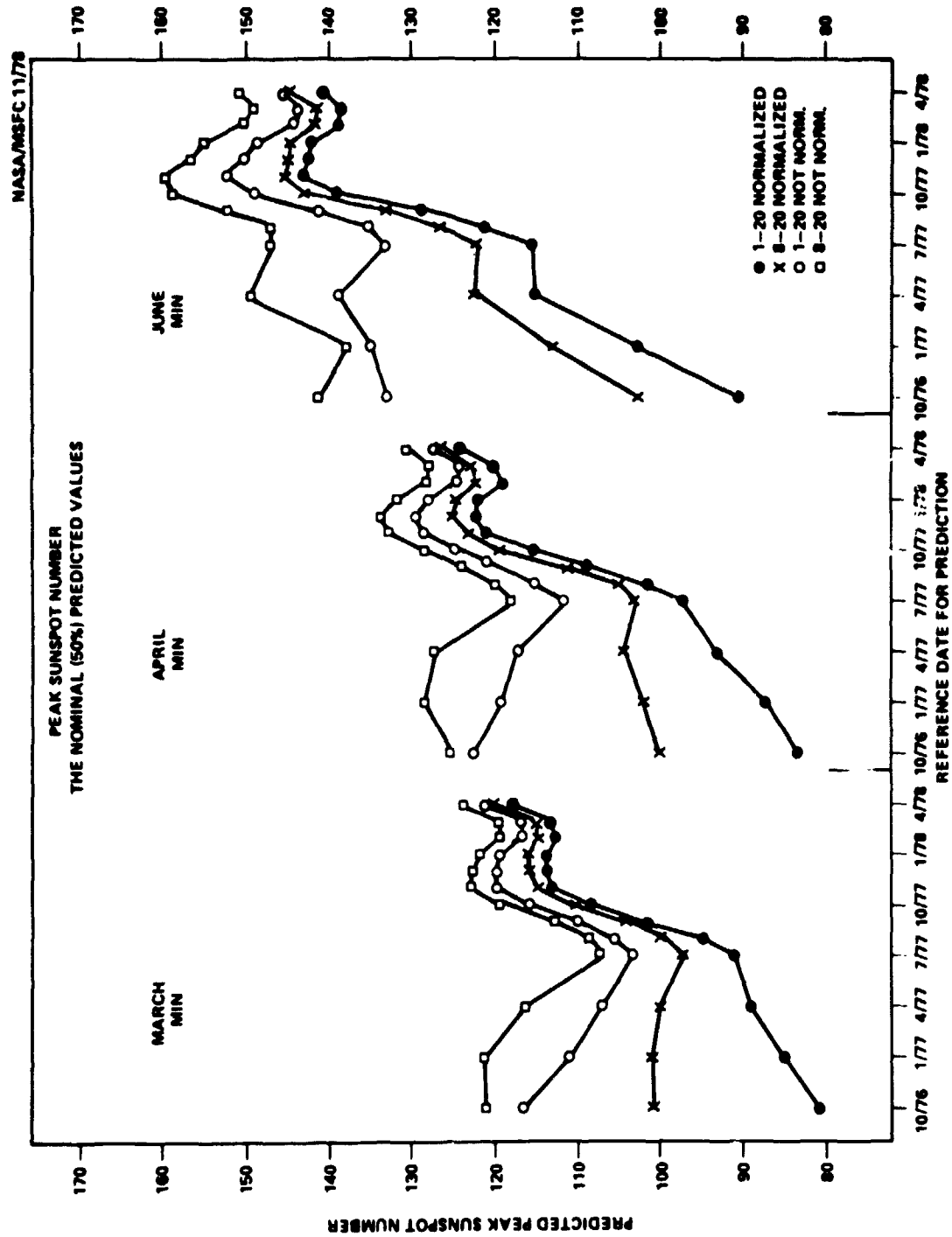

Figure 1. Predicting cycle 21 by linear regression.

REFERENCES

Avaritt, D. (1972): Sunspot prediction program (sunspot deck). Program Document 3F0360, Computer Sciences Corporation, Huntsville, Alabama.

Jacchia, L. G. (1970): New static models of the thermosphere and exosphere with empirical temperature profiles. Special Report No. 313, Smithsonian Astrophysical Observatory, Cambridge, Massachusetts.

Jacchia, L. G. (1971): Revised static models of the thermosphere and exosphere with empirical temperature profiles. Special Report No. 332, Smithsonian Astrophysical Observatory, Cambridge, Massachusetts.

Lundquist, C. A., and W. W. Vaughan (1978): Analysis of regression methods for solar activity forecasting. Symposium/Workshop on Solar-Terrestrial Influences on Weather and Climate, Columbus, Ohio, July 24-28, 1978.

McNish, A. G., and J. V. Lincoln (1949): Prediction of sunspot numbers. Transactions, American Geophysical Union, 30:673.

NASA Space Vehicle Design Criteria (1973): Models of earth's atmosphere (90 to 2500 km). NASA SP-8021, National Aeronautics and Space Administration, Washington, D. C.

Vitinskii, Yu. I. (1965): Solar-activity forecasting. Translated from Russian, Israel Program for Scientific Translations, Jerusalem. NASA TT F-289, Clearinghouse for Federal Scientific and Technical Information, Springfield, Virginia 22151.

Examples of "Problem" Flares or Situations in Past Solar-Terrestrial Observations

H. W. Dodson, E. R. Hedeman, O. C. Mohler
McMath-Hulbert Observatory of
The University of Michigan
895 Lake Angelus Road
Pontiac, Michigan 48055

An effort is made to recall instances of solar activity in past years that probably would have presented difficulties in prediction. Unexpected flares of significance include the so called "spotless" flares in centers of activity with only small or no spots. Isolated major flares in relatively flare-poor centers of activity also can be a surprise. Centers of activity with atypical levels of flare production with respect to their spot associations can introduce confusions in prediction. Flare-rich centers of activity without significant associated geomagnetic disturbance likewise are often misleading to forecasters. At the present time, energetic particle events stemming from flares on the invisible hemisphere present almost insurmountable difficulties for those who carry the responsibility of prediction.

1. Introduction

It has been suggested by Dr. Donnelly and the Program Committee of the Solar-Terrestrial Predictions Workshop that we at the McMath-Hulbert Observatory might be able to recall certain flares or solar-terrestrial situations that would have presented unusual difficulties had efforts been made to forecast their occurrence. In the hope that experiences of the past may be of value to future efforts, we will try to share, informally, some of the non-typical or unexpected solar and/or geophysical circumstances that we remember from past years.

2. Flares, probably unexpected, with significant geophysical effects.

2.1 Major flares in centers of activity with small or no spots

Although the majority of flares occur in centers of

activity with well developed spots, especially those with spots with complex magnetic configurations, it has been known for many years that a small proportion of flares, including a few important flares, develop in regions with small or no spots. It seems probable, that major flares in regions with only small or no spots may present especially difficult prediction circumstances. In 1970 we published a report (Dodson and Hedeman, 1970) of flares of Hα importance ≥2 in such regions in the years 1956-1968. These "spotless" flares included approximately 7% of all flares of Hα importance 2 and 3 in the years in question. At the time that we prepared the above paper we indicated that only a small proportion of the important "spotless" flares were accompanied by significant geophysical effects. The identification of the geophysically important major flares in "spotless" regions thus becomes a prediction problem with double difficulty. Such flares do occur, and over the years have presented interesting geophysical circumstances. Table 1 lists examples of such major "spotless" flares with information relating to their geophysical associations.

TABLE 1

Examples of Major "Spotless"+ Flares
with Significant Geophysical Associations

Flare Date and Time	Position	Hα Imp.	CFI	Geophysical Effects
1957 Nov.29^{d}00^{h}45^{m}	N41 E63	3+	4	Geomagnetic storm Dec. 1. Max 3-hr. K_p = 6.
1959 Jul.14^{d}14^{h}00^{m}	S25 E37	3	8	SID imp.2. There were so many great flares in another center of activity in mid-July 1959 that it is impossible to evaluate other possible geophysical effects of this flare.
1967 Jan.11^{d}01^{h}37^{m}	S27 W45	3	5	Geomagnetic storm Jan.13, max. 3-hr. K_p = 8; Sat. proton emission >90 MEV.
1967 Feb.13^{d}17^{h}47^{m}	N21 W11	3b	≥8	SID imp. 1; geomag. storm Feb. 15, max. 3-hr. K_p = 8, Polar Cap Absorption.

TABLE 1 (con't)

Flare Date and Time	Position	Hα Imp.	CFI	Geophysical Effects
1969 Sep.25^{d}06^{h}58^{m}	N13 W15	3n	5	This large flare had no reported associated SID. Nevertheless, it was apparently the source of >30 MEV protons and Polar Cap Absorption. A moderately severe geomagnetic storm began late on Sep. 27.
1970 Nov. 5^{d}03^{h}07^{m} (This was the only flare of Hα importance 3 in the year 1970)	S13 E35	3b	14	SID imp.3; geomag. storm Nov.7, max. 3-hr.Kp = 7. Sat. proton emission >60 MEV; Polar Cap Absorption
1973 Jul.29^{d}13^{h}12^{m} (This large two-ribbon flare occurred during the Skylab mission but it apparently was not predicted because the astronauts did not obtain observations until four or more hours after the start of the flare. It was the only flare of Hα importance 3 in 1973.)	N14 E45	3b	11	SID imp. 2; Geomag. storm Jul.31. max. 3-hr. K_p = 5, weak proton emission and weak Polar Cap Absorption.

+ The term "spotless" means a region with only very small or no spots

The locations in which these large "spotless" flares develop, generally include a large and relatively bright calcium plage (intensity ~2.5 on McMath scale). More importantly, the flare is generally associated with a large, dark, previously existing filament in Hα observations. Prior to the onset of the flare, the filament often shows motion through the presence of Doppler shifts in the dark gases. The filaments associated with "spotless" flares either traverse a plage or lie between regions described as two plages.

2.2 Other possibly unexpected significant flares.

Sometimes when the general level of solar activity is low, unexpected events occur. Were "major" flares with Polar Cap Absorption expected on 1964 March 16^{d}15^{h}53^{m} and 1965 February

$5^d17^h50^m$? It seems unlikely. Some months later, in late September and early October 1965, Plage 8005 (CMP October 3, N21°) a bright plage with a relatively large γ-type spot was crossing the solar disk and producing a modest number of flares and subflares. On October 3, a new spot and plage formed on the disk south of this active region and near a previously existing plage. The newly formed region was Plage 8012 at S19°. This newly formed region grew rapidly, and on October 4, to our surprise, developed a "major" flare, Comprehensive Flare Index of 8 and Hα importance 2, associated with a proton event and Polar Cap Absorption. This was the first "major" flare since June 13, 1965 and it did not occur in the center of activity that was attracting our primary attention.

Later, in September 1968, when solar activity was at a relatively high level, there was a good example of an important flare event that probably was hard to predict. It was what we refer to as an "isolated major flare" and it had significant geophysical effects. On 1968 September $29^d16^h17^m$, in Plage 9678 (CMP September 25, N16°) there developed a 2b flare. It was the only "major" flare, and the only flare to be associated with a Short Wave Fade in the history of the plage. This unique flare event was the apparent source of very energetic protons, Polar Cap Absorption, and a very small Ground-Level Enhancement of cosmic rays. The plage in which this isolated major flare occurred included several spot groups. The largest had a maximum area of ~800 millionths and was classified as magnetically complex (γ) on September 21, 25, and 26. Relatively isolated major flares do occur throughout the solar cycle and probably present especial difficulties for forecasters.

3. Centers of Activity with atypical levels of flare production.

3.1 Unexpectedly low levels of flare production.

Centers of activity with large spots (maximum area $\geq$1000 millionths of the hemisphere) and complex magnetic structure ($\beta\gamma$, γ, and δ configurations) are well known to be the sites of numerous Hα flares and SID-associated subflares during the transit of the region across the solar disk. Memory does not at once recall an outstanding exception to this pattern, though numerous large, spotted, plages do, indeed, traverse the disk without producing exceptionally great flares. A survey of our records shows that regions with large spots that are not magnetically complex frequently traverse the solar disk without producing more than ten flares of Hα importance $\geq$1, or ten SID's. It is rare, however, for the disk passage of large magnetically complex groups to fail to be associated with at least ten flares of importance one or with at least 10 SID-associated

flares or subflares. If our records are correct, at least two such atypical regions can be pointed out. (A) McMath Plage 9073, CMP, 1967 November 19, N16°, with a spot of maximum area 1085, and mean area 825 millionths of the hemisphere.

The spot was classified as $\beta\gamma$ and δ. According to our reevaluation of flare importance values for 1967 (UAG-19) there were only four flares of importance ≥ 1 in this region. These four flares, however, included one event of importance 3, two flares of importance 2, and one of importance 1. The plage was large and very bright and was in its third rotation. The region returned in December, underwent additional growth and had a β type spot with maximum area 2427 millionths, developed 11 flares of importance ≥ 1, and was associated with 18 SID's. Failure of a large complex region to produce many flares, such as Plage 9073 in November, apparently is not a reliable indication that that region on the sun has lost its potential for increased activity.

(B) McMath plage 11883, CMP 1972 May 20, N09°, with a spot of maximum area 1262, and mean area 1020 millionths of the hemisphere.

The spot was classified as $B\gamma$ and δ. The region developed only five flares with importance ≥ 1 and none of them qualified as "major" flares. Only six flares and subflares in the region were associated with SID's. Meter wave-length radiation was enhanced during the central meridian passage of this plage and spot. Geomagnetic disturbance was not associated with this region or its flares.

Over the years we apparently have not been especially mindful of the potentially active regions that failed to live up to their solar expectations. It might be worthwhile in the future to try to keep track of large, complex spot groups that do not develop a reasonable number of flares or SID's, perhaps 10 flares of Hα importance ≥ 1 and 10 SID's associated with flares or subflares. Suggestions of such regions are given in Table 2. Should plage 14822 with the large spot group with CMP June 29, 1977 be considered in this category? The region developed only six flares with Hα importance as great as one and only one X-ray enhancement as great as M 1. Thirteen flare associated SWF's were reported. All of the flares and SWF's took place during the days when the region was in the east and when the spot group was generally magnetically complex and with maximum area of the order of 1000 millionths of the hemisphere. During transit of the western half of the disk, the spot lost its magnetic complexity, decreased in area, and the production of flares of importance ≥ 1 and SWF's stopped. Perhaps the real challenge in flare prediction is to try to anticipate when the magnetic complexity of a spot group will cease, and when the spot area will diminish.

TABLE 2

Possible Examples of Apparently Significant Centers of Activity with below Average Flare Production

Plage	Date CMP	Lat.	Long.	Spot Area	Spot Mag. Class.	Number + Flare Imp.	Number + SWF
3747	1956 Nov. 9	N27	273°	1007 (max.) 520 (mean)	βp	4	0
5491	1959 Dec.15	N15	106	1413 1034	βp	6	1
5505	1959 Dec.26	N09	314	1282 589	β	5	0
5556	1960 Feb.11	N24	56	1191	β	5	0
8609	1966 Dec.11	S23	250	1218	β	3	3
8629	1967 Jan. 2	S22	320	1803	βp	6	3
9073	1967 Nov.19	N16	35	1085	βγ - δ	4	3
10242	1969 Aug. 5	S13	67	825	βγ	1	0
10344	1069 Oct. 3	S12	14	511	βγ	1	2
10918	1970 Sep. 5	N18	239	1100	βγ	7	10
11111	1971 Jan.10	S04	5	1255 970	βp	4	4
11137	1971 Feb. 3	N13	55	1320 1003	βp, βγ on Δ d	5	0
11565	1971 Oct.22	N10	208	1571 1167	βp βγ on 2 days	4	2
11619	1971 Nov.27	S13	93	734 670	βp βγ on 3 days	5	2
11883	1972 May 20	S14	299	1262 1020	βγ - δ	5	6

+ Data not homogeneous over the years.

3.2 Unexpectedly flare-rich centers of activity.

Efforts to identify in past experience centers of activity that produced more flares of Hα importance ≥1 or more flare-associated SID's than the area and magnetic complexity of the spot would suggest, encounter the effects of changing standards in flare-reporting and the more abundant modern techniques for detection of ionospheric disturbances. Regardless of these inhomogeneities, it seems clear that large Plage 4065, CMP 1957 July 20, N21°, which included spots no larger than 500 millionths of the hemisphere and β magnetic classification, was an above average flare producer. It apparently was the site

of 74 flares called importance one or greater and produced 17 of the relatively rare SID's of those years.

On March 25, 1970, a very large bright plage, McMath 10641, with numerous small spot groups crossed the central meridian. Several of the spot groups were reported as having magnetic complexity on one or two days. During the course of its transit across the disk, the plage was the site of 27 flares of importance ≥ 1, including 6 "major" flares, for two of which the Comprehensive Flare Indices were 11 and 14 respectively. These "great" flares on March 25 and 29 were associated with important SID's, well defined proton enhancements, and the onsets of geomagnetic storms. The region seems to have been well above average in flare production for a center of activity with such unpretentious spots. There are probably many other such above average flare producers in the records. A list of suggestions for regions in this category is given in Table 3.

TABLE 3

Possible Examples of Unexpectedly Flare-Rich Centers of Activity

				Spot		Number +	
Plage	Date CMP	Lat.	Long.	Area	Mag. Class.	Flare Imp.	SWF's
4065	1957 Jul.20	N21	175°	465	βf	74	17
4436	1958 Feb.25	S21	144	450	βρ	15	2
4634	1958 Jul. 7	N28	203	373	β	23	?
5315	1959 Aug.10	N18	342	311	βρ	52	7
5627	1960 Apr.13	N08	319	804	β	31	5
5680	1960 Jun. 4	N28	351	494	β	34	9
5863	1960 Sep.25	S15	297	452	βρ	33	2
7812	1965 May 23	N24	176	440	βρ	6	0
9946	1969 Feb.23	N16	60	897	β	16	31
9966	1969 Mar. 6	N13	275	293	β	15	19
10109	1969 May 26	N13	292	397	βρ	26	23
10477	1969 Dec.19	N12	72	170	βρ	19	7
10568	1970 Feb.10	N16	94	797	βρ	22	37
					(δ on 2 days)		
10584	1970 Feb.22	S15	296	284	βρ	17	8
10607	1970 Mar. 5	N08	158	604	βρ	18	28
10641	1970 Mar.25	N16	247	358	β		
				271	βρ	27	18
					(βγ on 2 days)		

+ Data not homogeneous over the years.

4. Flare-rich centers of activity with associated geomagnetic disturbance at relatively low levels.

4.1 Plage 3400; CMP February 17, 1956; N20°.

There are so many instances of the occurrence of significant geomagnetic storms and well defined proton increases in time association with the transit across the disk of great, flare-rich centers of activity that one tends to forget that there have been conspicuous exceptions to this pattern. We well remember the circumstances in February 1956 when McMath Plage 3400 with its large spots and γ classification crossed the disk with an impressive series of flare events starting on February 10 with a great flare and ejection at the east limb. At least 6 "major" flares took place in the region between February 10 and February 19 (UAG-14). All had severe SWF's and assorted radio frequency emission. At least one event (February $14^{d}05^{h}38^{m}$, E32°) was a "great" flare with Comprehensive Index of 12. Geomagnetic storms were expected but did not materialize beyond the most minor of disturbances. It was not until February 23 when this "disappointing" region was at W80° that another "great" flare (CFI $\geq$13) developed and initiated the severe and well known GLE and Polar Cap Absorption of that date. A significant geomagnetic storm began on February 25. We often have puzzled over the series of circumstances presented by Plage 3400. Were propagation circumstances at the sun, in the interplanetary medium, or both, especially unfavorable for the transport of particles from the sun to earth until the flare at W80° took place?

4.2 Plage 2325; CMP May 16, 1951; N10°

Another great, flare-rich region of earlier decades that crossed the disk without initiating geomagnetic disturbance that was commensurate with its flare production was McMath Plage 2325 with CMP May 16, 1951. This region, like 3400 described above, began its flare activity at the east limb (May 8). It produced many significant flares throughout its entire transit of the solar disk. Included in its record were especially important flares on May 18 and 19.

A geomagnetic storm with maximum 3-hourly K_p of 7 began on May 9, lasted for two or three days but the disturbance appears to have been primarily sequential in nature. During the remainder of the region's transit across the disk, geomagnetic disturbance was most moderate, and what did occur seems sequential rather than flare associated. It was a time when forecasters might indeed have expected greater geomagnetic storms.

4.3 Plage 8223, CMP April 4, 1966; N27°.

The difference between the geomagnetic effects of somewhat comparable centers of activity was well exemplified in early 1966 by the Polar Cap Absorption and geomagnetic storms associated with the great March region of that year (Plage 8207, CMP March 22) and the near absence of such effects with the usually forgotten April region (Plage 8223, CMP April 3). From the purely solar point of view, the two regions were rather similar with large, magnetically complex spots, high levels of radio frequency emission, many flares, and many flare-associated SID's. Our evaluations lead to Active Region Indices of 14 and 12 respectively, the two highest Active Region Indices in 1966. It should be noted, however, that the "major" flares in the April region took place east of the central meridian. In addition, the two regions were located almost exactly 180° apart in solar longitude. Did this special geometrical relationship play any part in the probable difference in propagation patterns relative to the two regions?

4.4 Plage 8704, CMP February 27, 1967; N23° and
Plage 8740, CMP March 27, 1967; N21°.

These two plages are successive rotations of the same center of activity. In both the February and March (1967) transits, the regions were flare-rich and had abundant x-ray emission as exemplified by the numerous flare-associated SID's. Their Active Region Indices were high, 16 and 12 respectively. In spite of these circumstances, geomagnetic disturbance was at a low level or absent during the time of transit of the regions. During each rotation the plage developed eight events that we identified as "major" flares on the basis of ionizing, radio frequency, or optical radiation (UAG-14) but there was only <u>one</u> flare in each transit for which the Comprehensive Flare Index was ≥ 11, indicating a "great" flare (UAG-14). Polar Cap Absorption was not confidently associated with any flare in these two plages (Svestka and Simon Catalogue).

4.5 Plage 8905, CMP July 28, 1967; N27° and
Plage 8942, CMP August 26, 1967; N22°.

These two plages again constitute successive rotations of the same center of activity. Plage 8942 in August (1967) was a return not only of 8905 but also of 8907 (CMP July 29) in latitude N16°. In July, 1967, Plage 8905 with its large spot and complex magnetic field developed large numbers of flares and very large numbers of associated SID's. Its Active Region Index is 18, the highest value we have assigned to any plage in all of solar cycle 20. In its return in August as Plage 8942, the spots continued to be large and magnetically complex, flare and SID production was high, and the Active Region Index was 12. Again, in spite of these circumstances, during the

July and August transits of this center of activity, geomagnetic disturbance was low or absent and Polar Cap Absorption was not recorded. It may be noteworthy that during both the July and August rotations of the region, only four flares in each rotation qualified as "major" flares (UAG-14) and for none of these events was the Comprehensive Flare Index ≥ 11. We would therefore comment that although flares in these regions were numerous, and abundant X-ray producers, none of them was "great."

4.6 Plage 9184, CMP January 31, 1968; N15°.

Plage 9184 (CMP January 31, 1968) with its very large spot and complex magnetic field was another flare-rich region with below average geomagnetic storm association. The maximum area of the spot was 2769 millionths and mean area, 2176. The magnetic classification was $\beta\gamma$ with δ on January 31. Twenty-three flares of importance ≥ 1 and 21 SID's were recorded in the region. In spite of these manifestations of activity, only four of the flares qualified as "major" on the basis of ionizing, radio frequency, or optical phenomena, and none was "great" (i.e. Comprehensive Flare Index ≥ 11). Did this absence of "great" flares account for the fact that geomagnetic disturbance during the transit of this significant center of activity (Active Region Index = 16) was at a relatively low level? Polar Cap Absorption recorded on February 8, 1968 has been ascribed to this region (Plage 9184) when it was two days beyond the west limb. (Svestka-Simon Catalogue).

4.7 Plage 10432, CMP November 22, 1969; N11°.

We also should point out Plage 10432, CMP November 22, 1969 as another center of activity with large spots, complex magnetic fields, many flares and short wave fades, and enhanced radio frequency emission, but with perhaps less than anticipated geomagnetic disturbance. Its Active Region Index was 13. More importantly perhaps, it was, according to our records and reevaluations, the center of activity in cycle 20 with the largest number of flares of importance ≥ 1. There were 55 such flares in this region (Dodson, Hedeman, and Mohler, 1974). Nine of the flares qualified as "major" (UAG-14) and three of them fall into our category of "great" flares. The three "great" flares occurred on November 18, November 24, and November 27 (E40°, W31°, W82°) with Comprehensive Flare Indices of 14, 12 and 13 respectively. Polar Cap Absorption was observed following the flare on November 24 and a "moderate" SC, geomagnetic storm developed on November 26. In general, however, geomagnetic disturbance during the transit of this especially flare-rich region seems not commensurate with the observed level of solar activity. It also seems noteworthy that the "great" flare with CFI of 13 at W82° on November 27 was <u>not</u> accompanied by a recorded increase in proton flux in the neighborhood of the earth in spite of its favorable location

in the far western part of the solar disk. Even the low energy 1-10 MEV flux shows no increase and continues its steady decline following this flare.

5. Comments on geomagnetic disturbance associated with centers of activity with as many as four "great" flares (Comprehensive Flare Index ≥11).

The foregoing significantly flare-rich centers of activity can indeed be considered as having been "disappointing" in their geophysical consequences if one has in mind the severe geomagnetic disturbances associated with such centers of activity as Plage 8818 (CMP May 25, 1967), Plage 9740 (CMP October 28, 1968), and Plage 11976 (CMP August 4, 1972). We have often noted that these three regions were all plages in which as many as four "great" flares (Comprehensive Flare Index ≥11) occurred. We have been led to ask if the occurrence of at least four "great" flares in a center of activity provides sufficient grounds for the confident expectation of severe geomagnetic disturbance. In solar cycle 19 we identified five plages with at least four "great" flares (Dodson, Hedeman, and Mohler, 1974):

Plage 4134, CMP September 10, 1957
Plage 5265, CMP July 14, 1959
Plage 5615, CMP March 31, 1960
Plage 5925, CMP November 12, 1960
Plage 6171, CMP July 14, 1961

All of the above regions were accompanied by geomagnetic storms of marked severity attributed to flares within these regions.

In solar cycle 20, five regions with at least four "great" flares also have been identified:

Plage 8818, CMP May 25, 1967
Plage 9740, CMP October 28, 1968
Plage 9946, CMP February 23, 1969
Plage 10607, CMP March 5, 1970
Plage 11976, CMP August 4, 1972

As mentioned earlier, for three of these regions, 8818, 9740, and 11976, the associated severe geomagnetic disturbance is something that many solar astronomers and geophysicists remember well. For the other two regions, a few comments seem needed.

In 1969, Plage 9946 with CMP February 23 was the site of 16 flares of importance ≥1 including 10 "major" flares for which four had Comprehensive Indices ≥11. The greatest of these flares (February $25^{d}09^{h}00^{m}$, W37°) was a white light flare associated with a ground level cosmic ray enhancement, proton

increase, and Polar Cap Absorption. Geomagnetic storms are indeed reported as starting on February 26 and 27, but these storms were not severe. A glance at plots of Kp and C9 values for the interval in question shows that the geomagnetic disturbance, though clear cut, was not unusually severe. Why was the geomagnetic disturbance not greater?

In 1970, Plage 10607, CMP March 5, also might have been misleading to forecasters of geomagnetic disturbance. This region with 18 flares of importance ≥1 had all of its seven "major" flares, including the four "great" flares, when the plage was east of the central meridian (February 27-March 2, E69°-E35°). Moderate geomagnetic storms occurred March 1-2 and March 5-6, perhaps attributable to the foregoing flares. However, starting on March 6 and March 8, two storms, moderately severe and severe, respectively, take place, long after Plage 10607 has ceased having "major" flares. It is probable that these two later storms were flare associated, but not with flares in Plage 10607. Why was this geomagnetic disturbance so great? Considerable caution seems indicated in efforts to anticipate the magnitude of geomagnetic disturbances. Sometimes it is much greater than expected as was the case with the great "problem" geomagnetic storm of October 5-7, 1960.

6. Final Comments

At times the forecasting of proton enhancements and geophysical phenomena is practically impossible. We remember especially the great events of January 28, 1967 -- ground level enhancements of cosmic rays, Polar Cap Absorption, and great energetic proton enhancements. If association of these events with a flare or flares far on the invisible hemisphere is correct, the forecaster, under present circumstances, had practically no way of anticipating these events. Lesser, but probably similar events seem to have occurred at other times. For example, did anyone anticipate the significant geophysical phenomena that occurred around May 12-16, 1969? One of the most severe geomagnetic storms of 1969 began on May 14, Polar Cap Absorption was reported on May 13. Faced with no suitable observed phenomena to account for the PCA, in the Svestka-Simon "Catalogue of Solar Particle Events," we suggest activity on the invisible hemisphere as the particle source. Perhaps, in years ahead, satellite data will provide information about the invisible hemisphere of the sun that will be of assistance in forecasting certain solar and/or geophysical phenomena.

The foregoing comments so emphasize the problem cases and disorder in solar and geophysical phenomena that they may give the wrong impression. Comments could have been prepared that would have stressed the general accord that exists between the development of large, magnetically complex spots in large bright

plages, and the occurrence of flares, ionospheric disturbances, energetic particle enhancements, and frequently subsequent geomagnetic storms. The prediction of such phenomena appears to be a possible, but difficult, undertaking. The frequency of atypical phenomena or situations suggests that notes of caution in a forecast will often considerably increase its credibility. Those who carry the responsibility of forecasting solar and geophysical circumstances deserve the highest level of support in their difficult task from all who observe the sun or try to keep track of its effects on terrestrial circumstances.

The authors gratefully acknowledge support from the following grants and contracts in the preparation of this report:

NASA - NGL 23-005-275, NOAA 03-4-022-94, and Johns Hopkins Applied Physics Laboratory Contract No. 600868.

References and Data Sources

Dodson, H. W., and Hedeman, E. R. (1970): Major Hα Flares in Centers of Activity with Very Small or No Spots. Solar Physics, Vol. 13, 401.

Dodson, H. W., and Hedeman, E. R. (1971): An Experimental Comprehensive Flare Index and its Derivation for 'Major' Flares, 1955-1969. Report UAG-14, WDC-A, NOAA, Boulder, Colorado.

Dodson, H. W., Hedeman, E. R., and Mohler, O. C. (1974): Comparison of Activity in Solar Cycle 18, 19, and 20. Reviews of Geophysics and Space Physics, Vol. 12, 329.

Dodson, H. W., and Hedeman, E. R. (1975): Experimental Comprehensive Solar Flare Indices for Certain Flares, 1970-1974. Report UAG-52, WDC-A, NOAA, Boulder, Colo.

Quarterly Bulletin of Solar Activity of the International Astronomical Union: Publisher Eidgen, Sternwarte in Zurich.

Solar Geophysical Data: National Geophysical and Solar-Terrestrial Data Center, Coulder, Colorado.

FORECASTS OF GEOMAGNETIC ACTIVITY BY OTTAWA MAGNETIC OBSERVATORY: THEIR RELIABILITY AND APPLICATION

J. Hruska
Earth Physics Branch
Dept. of Energy, Mines and Resources
Ottawa, Ontario, Canada

Ottawa Magnetic Observatory issues a 27-day forecast of geomagnetic activity based on the forecasts from the Environment Services Center in Boulder, Colorado and on data from Canadian geomagnetic observatories. To evaluate the reliability of the forecasts, the predicted activity has been compared with the actual geomagnetic activity at five geomagnetic observatories located in different magnetic zones: Ottawa (57.0°N, 351.5°E,) Meanook (61.8°N 301.0°E) Fort Churchill (68.8°N, 322.5°E), Cambridge Bay (76.7°N, 294.0°E), and Resolute Bay (83.1°N, 287.7°E). The percentage of correct predictions varies with the geomagnetic latitude of the observatory used for comparison. The percentage is on the average highest for lower latitude stations and lowest for the northern stations. The number of incorrect predictions ranges from 4.7% for Ottawa to 8.4% for Churchill.

The 27-day predictions of Geomagnetic Activity are used for geomagnetic surveys and in various research projects. User evaluations of the reliability and usefulness of these forecasts are summarized.

1. Canadian Forecasts of Geomagnetic Activity.

Beginning in 1974 the Ottawa Magnetic Observatory, Earth Physics Branch, issues a "27-day Forecast of Geomagnetic Activity" every three weeks especially designed for use by mining and geophysical survey companies and by various government agencies. The predictions are based on the "27-day Forecast of Solar and Geophysical Activity" issued by the Space Environment Services Center in Boulder, modified to more closely reflect the characteristics of the geomagnetic field at higher latitudes [K. Whitham, E.I. Loomer, E.R. Niblett (1960)]. The records from the Canadian Observatories are used to monitor the 27-day recurrence of geomagnetic activity. The trends of activity estimated in this manner are compared with the 27-day forecast issued by the Space Environmental Services Center. A new forecast which respects the predictions from Boulder as well as the trends of activity expected from the 27-day cycle observed in Canadian data, is then issued.

Since the predictions are destined mainly for practical use in magnetic surveys, they cover every day of the interval for which they are issued and describe the geomagnetic activity in simple, easily understood terms. They also include a review of the magnetic activity during the past month as given by the K-indices from Ottawa and Meanook observatories--see example of the Forecast of Geomagnetic Activity by Ottawa, Review of Geomagnetic Activity and the Boulder Forecast, for July 1978.

FORECAST OF GEOMAGNETIC ACTIVITY FOR PERIOD:
LA PREVISION DE L'ACTIVITE GEOMAGNETIQUE POUR LA DUREE:

June (juin) 28 to (à) July (juillet) 30 1978

The geomagnetic field is expected to be:
Le champ geomagnetique sera probablement:

active (actif)	:	July (juillet) 4-8, 16-19
unsettled (agite)	:	the rest of forecast period (le reste de la period prevue)
quiet (calme)	:	July (juillet) 1-3

Ottawa Magnetic Observatory
L'observatoire magnetique d'Ottawa

THE REVIEW OF GEOMAGNETIC ACTIVITY IN JULY 1978
LA PREVISION DE L'ACTIVITE GEOMAGNETIQUE DE MOIS DE JUILLET

OTTAWA Geomag. Co-ord.: 57.0^0 Lat. N., 351.5^0 Long. E.

active (actif)	:	4-5, 13-16, 18
unsettled (agite)	:	the rest of July (le reste du juillet)
quiet (calme)	:	29-31

MEANOOK Geomag. Co-ord.: 61.8^0 Lat. N., 301.0^0 Long. E.

active (actif)	:	4-5, 7, 13-14
unsettled (agite)	:	the rest of July (le reste du juillet)
quiet	:	1-2, 6, 9, 11-12, 15-16, 19-20, 23-31.

R 260400Z JUN 78
FM SPACE ENVIRONMENT SERVICES CENTER BOULDER COLO

UNCLAS WU 27 DAY FORECAST OF SOLAR AND GEOPHYSICAL ACTIVITY
ISSUED 0201Z 26 JUNE 1978
SOLAR ACTIVITY SHOULD BE MODERATE EARLY IN THE PERIOD, BECOMING LOW AS REGIONS 1170, 1172 AND 1176 DISAPPEAR FROM VIEW. THE ACTIVITY SHOULD REMAIN RELATIVELY LOW UNTIL ABOUT 14 JULY WHEN THESE REGIONS WILL RETURN TO THE VISIBLE DISK. SOLAR ACTIVITY MAY BECOME HIGH AT THAT POINT.
THE GEOMAGNETIC FIELD IS EXPECTED TO BE GENERALLY UNSETTLED THROUGH THE NEXT 27 DAYS WITH OCCASIONAL QUIET PERIODS. SHOULD A MAJOR FLARE OCCUR, A MAJOR MAGNETIC STORM IS A POSSIBILITY.
SOLTERWARN

The geomagnetic activity is defined as quiet, unsettled or active. The latitudinal dependence of the activity is reasonably well eliminated from the predictions with the help of an empirically determined hourly index P which effectively normalizes activity levels in three geomagnetic zones: sub-auroral (50° - 60°); auroral (60° - 70°); and polar cap (above 70° north). The values of P in nanoteslas are listed in the following table. The index has been based on values of K-indices for the subauroral zone and on R-indices, derived from the hourly ranges, for the auroral and polar cap zones.

geomagn. activity / geomagnetic lat. N	50° - 60°	60° - 70°	over 70°
quiet	$P \leq 30$nT	$P \leq 100$nT	$P \leq 80$nT
unsettled	$30 > P \leq 60$	$100 > P \leq 230$	$80 > P \leq 150$
active	$P > 60$	$P > 230$	$P > 150$

2. The Reliability of Geomagnetic Predictions during 1975 to 1977.

The Ottawa predictions for the period 1975 to 1977 have been evaluated by comparing the forecasted activity with the activity actually observed at five magnetic observatories located in different geomagnetic zones: Ottawa -- OTT (subauroral), Fort Churchill -- FCC (auroral), Resolute Bay -- RES (polar cap), and the transitional stations Meanook -- MEA and Cambridge Bay -- CBB [E.I. Loomer (1976)]. The geographic location of these stations is shown in Fig. 1.

Canadian Magnetic Observatory Network

Symbol	Station	Geographic Lat.	Geographic Long E	Geomagnetic Lat.	Geomagnetic Long E.
ALE	Alert	82.50	297.50	85.9	168.2
RES	Resolute Bay	74.42	265.10	83.1	287.7
MBC	Mould Bay	76.2	240.6	79.1	284.7
CBB	Cambridge Bay	69.10	255.0	76.7	294.0
PEB	Pelly Bay	68.53	270.49	78.6	320.45
BLC	Baker Lake	64.33	263.97	73.9	314.8
YKC	Yellowknife	62.50	245.5	69.0	293.1
RII	Rankin Inlet	62.63	268.08	72.9	321.9
EKP	Eskimo Point	61.10	265.93	71.1	321.8
FCC	Fort Churchill	58.80	265.77	67.8	323.0
FSV	Fort Severn	55.98	272.35	66.8	333.0
GWS	Great Whale River	55.27	282.22	66.8	347.2
GIM	Gillam	56.35	265.32	66.2	323.4
TMP	Thompson	55.72	262.12	65.4	319.3
MEA	Meanook	54.60	246.7	61.8	301.0
ISL	Island Lake	53.88	265.32	64.0	324.4
WHS	White Shell	49.75	264.75	59.9	325.3
STS	St. John's	47.60	307.3	58.7	21.4
VIC	Victoria	48.50	236.6	54.3	292.7
OTT	Ottawa	45.40	284.5	57.0	351.5

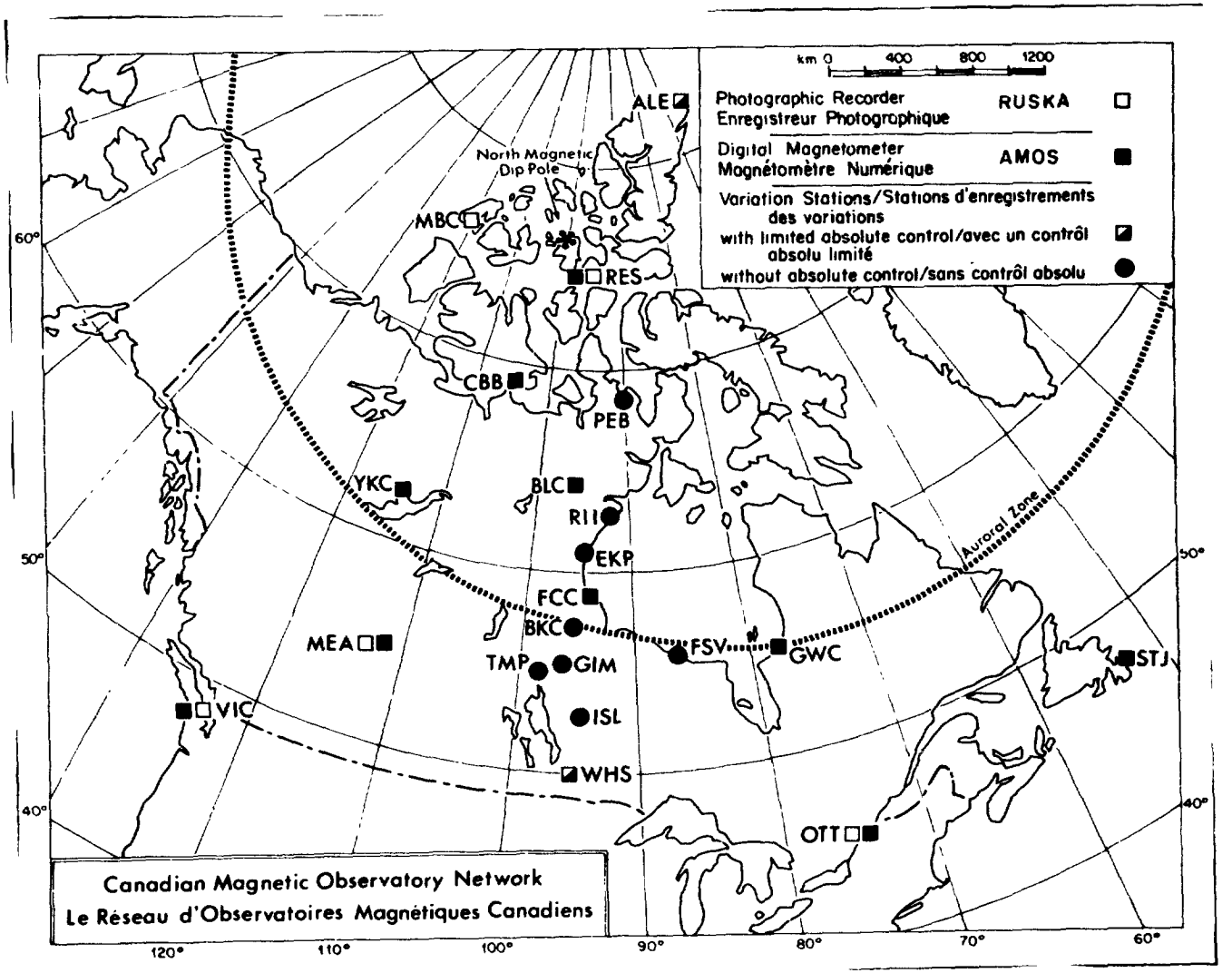
km 0 400 800 1200
Photographic Recorder
Enregistreur Photographique
RUSKA
Digital Magnetometer
Magnétomètre Numérique
AMOS
Variation Stations/Stations d'enregistrements des variations
with limited absolute control/avec un contrôl absolu limité
without absolute control/sans contrôl absolu
North Magnetic Dip Pole
ALE
MBC
RES
CBB
PEB
YKC
BLC
RIK
EKP
FCC
BKC
MEA
TMP
GIM
FSV
GWC
STJ
VIC
ISL
WHS
OTT
Auroral Zone
60°
50°
40°
120°
110°
100°
90°
80°
70°
60°
Canadian Magnetic Observatory Network
Le Réseau d'Observatoires Magnétiques Canadiens

Figure 1.

The period from 1975 to 1977 is centred on the minimum of solar geomagnetic activity and the terms "active", "unsettled" and "quiet" characterize the levels of activity on a chosen day with respect to the average activity during solar minimum. [E.I. Loomer, G. Jansen van Beek (1969)]. The comparison of the predictions with the activity actually observed at individual stations has been made by dividing the predictions into three groups: correct, uncertain and incorrect. For a given reference observatory the prediction is classified as correct (uncertain or incorrect), when the observed and the predicted levels (i.e. quiet, unsettled, active) are the same (differ by one level, or differ by two levels, respectively). The results of this comparison are summarized in Figures 2a, 2b and 3.

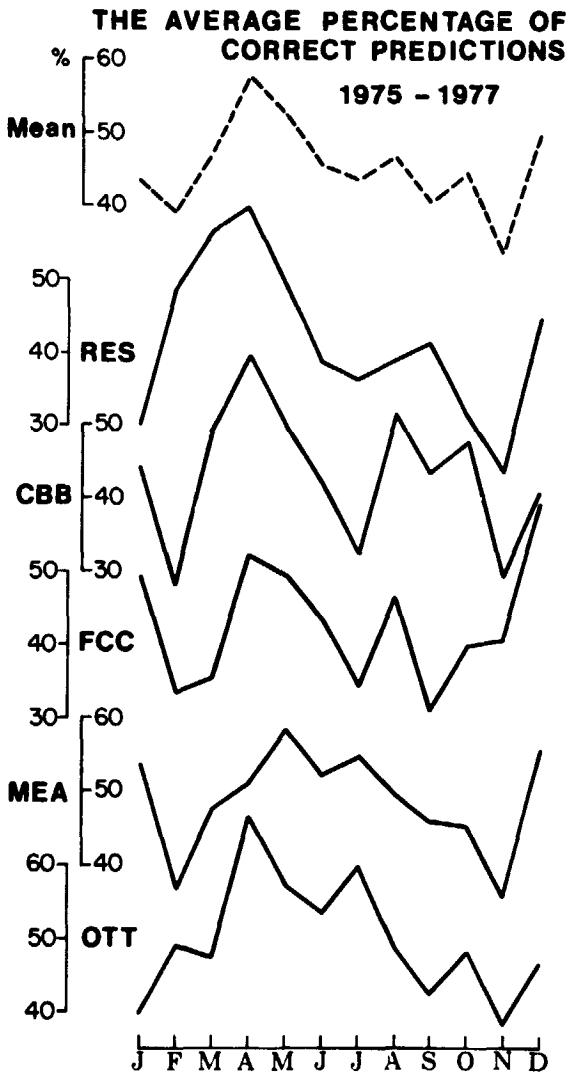

Figures 2a and 2b show the annual variation of the percentage of correct and incorrect predictions for the individual observatories It is interesting to note that the number of correct predictions was greatest in the period March to May and least in November. The dependence of the percentage of correct predictions on geomagnetic latitude is shown in Fig. 3 (curve 2). It is evident that the level of activity is more accurately predictable at lower latitudes. The percentage of uncertain predictions (curve 1) does not vary substantially with latitude. In summary, 7.1% of the predictions were incorrect, 47.4% were uncertain and 45.5 were correct in the three-year period 1975-1977 as evaluated using the 5 reference observatories.

Figure 2a.

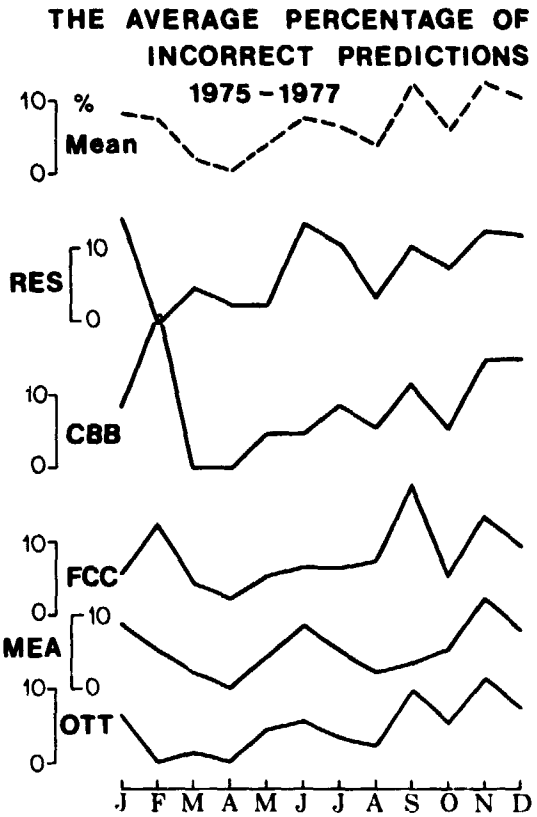

Figure 2b.

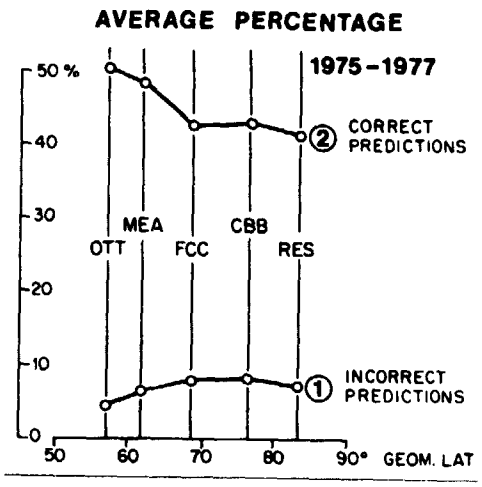

Figure 3.

3. Application of the predictions.

To evaluate the usefulness of the predictions and to find out the needs of our users, a survey was made of 70 users in January, 1978 [Hruska, J. (1978)]. The predictions are being used by the private sector (geophysical surveys and mining companies, etc.), by government agencies (observatories, Geological Survey, etc.), and by universities. Sixty-five percent of our users are in the private sector, 32% in government agencies and 3% in universities. The predictions are used on a continuing basis by 32% of users, regularly in certain periods by 43% of users, and occasionally by 25% of users. The predictions are used over a wide range of geographic latitude as seen in the following table:

Geographic Lat. N.	% of Users
30 - 40 °	7%
41 - 50	25%
51 - 60	27%
61 - 70	18%
71 - 80	15%
over 81	8%

They are used for various types of work as is described in the following table:

	% of Users
Ground survey (general)	28%
Mineral exploration	22%
Observatory work	20%
Airborne survey	19%
Research	8%
Telluric methods	3%
Education	1%
Other (information, calibration, radio communications-citizen bands, etc.)	17%

Users classify the value of predictions for various purposes as follows:

	very useful	useful	not useful	no. of replies
Planning and organizing	25%	70%	5%	53
Reduction of operational expenses	15%	59%	26%	46
Time saving	17%	74%	9%	54

On the basis of their experience only 6% of the users estimated that predictions are correct in less than 50% of cases. Forty-eight percent found the predictions correct in 51 to 65% of the cases and 26% estimated that the probability of correct predictions is 66 to 80%. Seven percent of users estimated that the forecasts are correct in more than 81% of the cases. Twelve percent of the users stated that they did not have enough experience to estimate the reliability of the forecasts.

Acknowledgments: We would like to express our thanks to the Space Environment Services Center in Boulder for their provision of the data which are basic for our forecasts of magnetic activity. The author extends special thanks to P. H. Serson and E. I. Loomer for their interest and helpful comments.

REFERENCES

Hruska, J. (1978): Consulting Services Provided by the Ottawa Magnetic Observatory. Internal Report of Earth Physics Branch, DEMR, Ottawa.

Loomer, E. I. (1976): The Canadian Magnetic Observatory Network. Seminar of Earth Physics Branch, DEMR, Ottawa.

Loomer, E. I., G. Jansen van Beek (1969): The Effect of the Solar Cycle on Magnetic Activity at High Latitudes. Publ. of the Dominion Observatory, Vol. XXXVII, No. 6.

Whitham, K., E. I. Loomer and E. R. Niblett (1960): The Latitudinal Distribution of Magnetic Activity in Canada. J. Geophys. Res., 65, 3961.

D33-92 N80-18495

PPS76 - A COMPUTERIZED "EVENT MODE" SOLAR PROTON FORECASTING TECHNIQUE

D. F. Smart and M. A. Shea
Air Force Geophysics Laboratory
Bedford, Massachusetts, 01731, USA

A procedure has been developed to generate a computerized time-intensity profile of the solar proton intensity expected at the earth after the occurrence of a significant solar flare on the sun. This procedure is a combination of many pieces of independent research and theoretical results. It is not a comprehensive self-consistent analytical method, but is a construction of selected experimental and theoretical results from the entire domain of solar-terrestrial physics.

1. INTRODUCTION

Any proton prediction system intended to be operationally useful must conform to the available data and operational constraints of the environment in which it is to be utilized. The prediction system described in this report is designed to operate with the information likely to be available in real time or near real time to the Air Weather Service Space Environmental Support Branch of AFGWC and the NOAA Space Environmental Services Center. The information available to these organizations is currently limited to the following:

a. H-alpha flare reports (onset time, position, time of maximum, flare importance and end time);

b. Radio observations at discrete frequencies (606, 1415, 2695, 4995, 8800, and 15400 MHZ);

c. Soft X-ray fluxes from satellites such as SMS/GOES or SOLRAD;

d. Very limited solar wind data from spacecraft;

e. Real time solar particle data from satellites such as SMS/GOES; these particle data are needed for verification of events and prediction updates.

The overall objective of the computer program is to be able (at the time of the H-alpha maximum) to make a prediction of the solar proton flux at the earth for the next 300 hours. The program must be able to operate on the data available at any time the forecaster selects. Since some of the desired input data may not always be available, algorithms are included to calculate nominal values for essential data that may be missing.

The program also has an update capability so when additional data are available they can be included for new prediction attempts. In addition if the solar particle data available in real time has features grossly different from those initially predicted, then the update capability can be utilized to include these gross features in calculating the future behavior of the event.

This procedure is intended to be a tool for forecast personnel in making decisions for warnings and alerts. Users are cautioned that the computer merely executes algorithms included in the program. The closer a predicted profile conforms to actual obervations, the more confidently the prediction may be utilized.

2. CONCEPTS INVOLVED

2.1 General Concepts

Solar protons are assumed to be accelerated in solar active regions during solar flare events. The X-ray, radio and optical emissions during the solar flare event are the indicators that proton acceleration is occurring. We interpret the "U-shaped" spectral signature of the radio emission (Castelli, et al., 1967) as the indicator that solar protons are being released from the solar active region. This assumption is based on a comparison of those flares having a "U-shaped" characteristic signature in the radio power spectra (Castelli and Guidice, 1976) with the proton events given in the "Catalog of Solar Particle Events, 1955-1969" (Dodson et al., 1975) along with those of Castelli and Tarnstrom (1978). For operation of this program no minimum radio flux is required. Any "U-shaped spectral signature in the power spectrum of the radio outburst in time coincidence with an observed optical flare is assumed to release solar protons from the accelerating region. The computer program algorithm will compute a predicted maximum proton intensity expected at the earth; this may range anywhere from a very large event to a solar proton flux so small it cannot be discerned in a particle sensor channel above a cosmic ray induced background.

After the solar protons are released from the confines of the accelerating region, they will travel through the solar corona and some will propagate outwards along the interplanetary magnetic field lines.

Those emitted from the inner solar corona at a "favorable" position may intercept the earth. From examining the solar proton data acquired during the past two solar cycles, we can generalize to the following phases of a solar proton event observed at the earth as illustrated in Figure 1.

a. There is a propagation delay from the time of the solar flare until the first particles are observed at the earth.

b. After the initial onset of particles, there is a rise in the solar proton flux until a maximum flux is observed.

c. After the time of the maximum solar proton intensity, there is a general exponential decay of the particle flux to background levels. This decay is usually much slower than the rising phase of the event.

We employ the same generalizations to predict the time-intensity profile to be expected at the earth after the occurrence of a solar proton producing flare on the sun. Specifically, we know there will be some propagation delay time necessary for the particles to travel from the sun to the earth. If we specify the maximum flux and the time of maximum, we can construct an exponential curve from the onset of the event to the maximum of the event. Then by specifying an exponential decay and appropriate decay constant, we can complete the calculation of the time-intensity profile expected for a particular solar flare. The actual profile may be quite different from the idealized curve illustrated in Figure 1, but the generalizations provide an adequate description of the time history of a solar proton event.

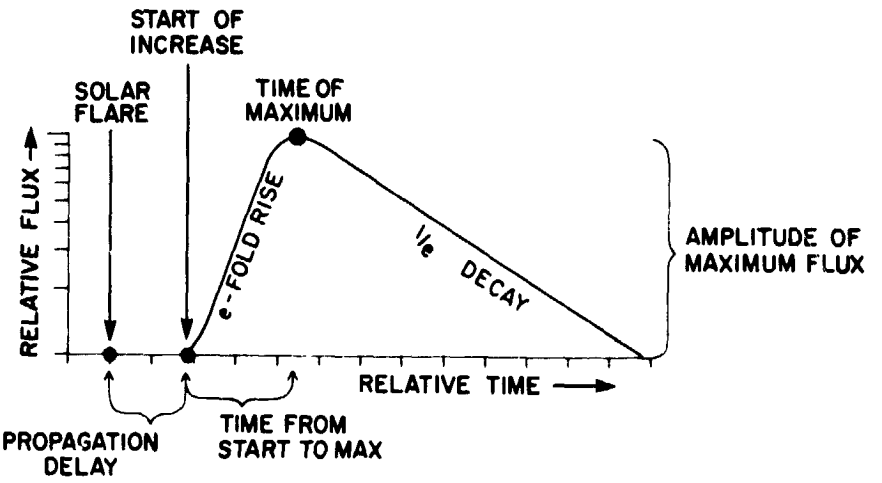

Fig. 1. Illustration of the general characterstics of solar proton events.

2.2 Solar Flare Generalizations

The sudden release of large amounts of energy in localized regions of the sun results in the acceleration of some of the ambient solar plasma to high energies and in characteristic electromagnetic emissions from the site of the energy release. The optical phenomenon viewed when this occurs is called a solar flare, and there are concurrent emissions in the radio and X-ray wavelengths. At times the radio and X-ray emissions are detected without a corresponding optical emission, a phenomena that can occur when the solar flare is located behind the visible portion of the disk, particularly near the eastern or western limb. The exact process by which particles are accelerated is still a matter of scientific debate with a number of mechanisms currently proposed (see Svestka, 1976); however, these mechanisms are not germane to this report.

The optical emissions, usually viewed in the H-alpha absorption line, are well suited for defining the position of the solar flare, although the dynamic range available in the actual emission above the solar background is somewhat limited besides being a somewhat subjective measure. There are statistical trends between the brightness of a flare and particle emission; however, the variance in the data between individual flares is approximately the same size as the total range of the flare brightness scale. In the radio emissions, the amount of energy released at various frequencies may increase by many orders of magnitude. Consequently, radio patrols of the sun are an excellent method of identifying solar activity, although the resolution of the location of the emitting source on the solar disk may be very poor. The soft X-ray emission may have a dynamic range of many orders of magnitude above the quiet solar background; however, as with the radio emission, there is generally no resolution of the position of the emitting source.

For the proton prediction program described in this report, we utilize the optical emission to provide the position of the accelerating region on the sun, and use the radio and/or X-ray emission to determine the size of the particle event to be expected from this sudden release of energy into the solar corona. If the "U-shaped" spectral characteristic signature is present in the radio data, we assume that some of the accelerated particles were able to escape the confining magnetic fields of the active region into the solar corona. If the "U-shaped" spectral characteristic signature is not present, we assume that the energy release was insufficient to allow these particles to escape from the region.

3. PROPAGATION OF SOLAR PARTICLES

We will consider the propagation of solar protons from the flare site to the earth as being separable into two distinct and independent phases. The first phase is diffusion from the flare site through the

solar corona to the "foot" of the Archimedean sprial path formed by the interplanetary magnetic field line between the sun and the earth. The second part is the propagation in the interplanetary medium from the sun to the earth along the interplanetary magnetic field lines. Figure 2 provides an illustration of the propagation concepts.

3.1 Propagation in the Solar Corona

The concepts we have used for the propagation of solar protons in the solar corona are similar to those advanced by Reinhard and Wibberenz (1974). We will make very few assumptions as to the manner of coronal transport except that some stochastic processes dominate and the particles have many interactions between their source at the flare site and their release point along an interplanetary magnetic field line. In this context we take the fundamental elements of solar particle diffusion theory as developed by a number of researchers, some of the original results being those of Axford (1965), Reid (1964), Burlaga (1967) and Krimigis (1965), and assume that almost all of the diffusive effects occur in the solar corona.

The distance the solar particles travel in the solar corona from the presumed source (i.e. the solar flare site) to the foot of the Archimedean spiral path from the sun to the earth is designated by the symbol Θ . For measurement of this distance we will use a heliocentric coordinate system where 0 degrees is the longitude of the plane containing the earth-sun line (positive in the sense of solar rotation), and latitude is measured either "up" or "down" from the solar equator. The solar flare will have coordinates defined as solar latitude, λ_F,

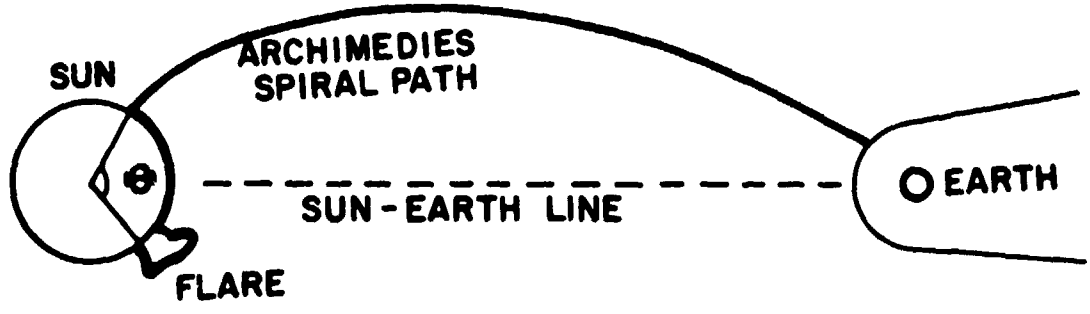

Fig. 2. Illustration of the propagation concept. The coronal propagation distance Θ is illustrated by the heavy arc on the sun. Interplanetary propagation proceeds along the Archimedean spiral path from the sun to the earth.

and heliocentric longitude Φ_F. If we make the assumption that the "foot" of the Archimedean spiral will be at the solar equator, it will have heliocentric longitude of Φ_A. The heliocentric longitudinal distance from the flare site to the "foot" of the Archimedean spiral will be $\Phi_A - \Phi_F$. If we also consider that there may be a heliocentric latitude effect, and assume that the simplified geometry of a right spherical triangle is adequate for simple calculations, then

$$\cos \Theta = \cos (\Phi_A - \Phi_F) \cos \lambda_F. \qquad (1)$$

We assume that coronal propagation is a function of Θ. From diffusion theory we would expect it to be proportional to Θ^2. (See Wibberenz (1974) for a contemporary discussion of diffusion theory.) For large values of Θ the propagation delay time is dominated by the diffusion time, and so we select a normalization contant such that we can obtain some of the very long delay times reported for Eastern hemisphere flares. Typical data sets containing onset times of particle events at the earth are those of Barough et al. (1971), and Lanzerotti (1973).

As a result of diffusion in the solar corona from the flare site to the "foot" of the Archimedean spiral, and the inherent assumption that some stochastic processes are operating, we would expect that there is a solar particle gradient existing in the solar corona such that the proton intensity decreases as a function of distance from the flare site. There is some observational evidence for the existence of such a gradient (Gold et al., 1975; McCracken and Rao, 1970; Roelof et al., 1975; McCracken et al., 1971; Roelof, 1976). The observational evidence suggests that the gradient may vary from case to case; however, for this program we have assumed that this gradient from the presumed particle source (i.e. the flare location) to the release point of solar protons observable at the earth (i.e. the "foot" of the Archimedean spiral of the interplanetary magnetic field line between the earth and the sun) is 3e per radian. Therefore, an observer at one astronomical unit who is connected via the interplanetary magnetic field line to the heliographic longitude of the flaring region would observe the maximum possible particle intensity, I_F. An observer whose interplanetary magnetic field connection is at a distance of Θ from the flaring location would observe an intensity of $I_F \exp(-3\Theta)$.

3.2 Propagation in the Interplanetary Medium

After the particles propagate through the solar corona and are released into the interplanetary medium, they essentially propagate along the interplanetary magnetic field line. During this phase of their propagation we assume that their mean free path length is of the order of 0.1 to 0.3 AU. These assumptions appear to be consistent with some of the more recent studies of solar particle propagation (Roelof and Krimigis, 1973; Roelof, 1975; Palmer et al., 1978). While these assumptions are not

"scatter free" propagation, the number of scattering centers the particle may encounter between the sun and the earth is relatively small; therefore, much of the early work regarding diffusive cosmic ray transport is applicable under these conditions.

For this computer program we have made the simplest possible assumptions regarding transport in the interplanetary medium. These assumptions are as follows:

a. The particles travel essentially along the interplanetary magnetic field lines with a velocity which is a function of the particle energy.

b. Diffusion perpendicular to the interplanetary magnetic field is assumed to be negligible.

c. The minimum distance to travel from the sun to the earth is the distance along the Archimedean spiral path.

The minimum propagation delay will be for particles that essentially travel along the interplanetary magnetic field lines with very little scattering, so for scatter free onsets the propagation time from the sun to the earth will be the distance traveled divided by the particle velocity. After the initial onset it is reasonable to expect that some scattering has taken place and that some aspects of diffusion theory are applicable. Almost all theories involving differential transport show that the time of maximum is proportional to the square of the distance traveled. (See Wibberenz, 1974).

We will further make the assumption that the average particle propagates through the interplanetary medium with a bulk velocity which is half the speed to be expected from the particle energy of an average pitch angle of 60 degrees.

The polar form of the equation of the Archimedean spiral is

$$\rho = a\theta \quad . \tag{2}$$

If we normalize to the earth's orbit then a = 1 AU and $\theta = \Phi_A$ in our heliographic coordinate system. The distance along the Archimedean spiral path from the sun to the earth is the integral along the arc length

$$D = \int_0^{\phi_A} [\rho^2 + (\frac{d\rho}{d\theta}) d\theta]. \tag{3}$$

The results in our system, normalized to 1 AU is

$$D = 1/2 \left\{ \sqrt{\phi_A^2 + 1} + [\ln (\phi_A + \sqrt{\phi_A^2 + 1})]/\Phi_A \right\} \tag{4}$$

The solar longitude of the "foot point" (Φ_A) of the Archimedean

spiral path on the sun can be computed by considering that a plasma element leaves the sun at the earth-sun line and propagates rectilinearly to 1 AU with an average velocity v. When this plasma element reaches 1 AU, the sun will have rotated such that the solar longitude of the starting point on the sun will be to the west of central meridian and equal to Φ_A. If the plasma carries "frozen in" magnetic fields, then the "foot point" of the interplanetary magnetic field lines that extends from the sun to the earth can be given by

$$\Phi_A = \frac{\omega_s r}{V} \tag{5}$$

where ω_s is the solar synodic rotation rate (13.333 degrees/day) and r is 1 AU. If we express the Archimedean spiral equation in the polar form normalized to 1 AU, then

$$\Phi_A = \frac{404}{V_{sw}} \tag{6}$$

where V_{sw} is the measured solar wind velocity in km/sec at the earth (1 AU) and 404 is the nominal solar wind velocity when the solar rotation is equal to one radian during the time it takes the plasma element to travel 1 AU.

The proton velocity is given by

$$\beta = \sqrt{1 - \frac{1}{[(E/mc^2) + 1]^2}} \tag{7}$$

where E is the kinetic energy of the particle in MeV, β is the velocity of the particle compared with the velocity of light, and the rest energy of the proton, mc^2, has the value of 938.323 MeV. (Note: $\beta = V/c$).

The minimum time in (hours) required for a proton to propagate along the Archimedean spiral path from the sun to the earth with a zero pitch angle is $0.1333\ D/\beta$.

4. EVENT PROFILE CONSTRUCTION

4.1 Particle Increase Onset Time

Review articles on solar particle propagation note that there is an apparent anomalous delay of about 15 minutes even for relativistic solar particles to propagate from the sun to the earth. Beginning with this constant the propagation delay time is the sum of the coronal propagation time plus the interplanetary propagation time along the length of the Archimedean spiral from the sun to the earth for the fastest (highest energy) protons detected in a specific solar proton sensor. We assume that for a given channel this is

$$\text{Onset} = 0.25 + 0.1333\ D/\beta + 4\ \Theta^2 \tag{8}$$

where D is the distance along the length of the Archimedean spiral from the sun to the earth and β is the velocity of the most energetic proton measured by the channel. This calculation is carried out for each energy channel to compute the particle onset time.

The distribution of onset times expected for 30 MeV protons for nominal solar wind speeds (taken as 404 km/sec) is shown in Figure 3. The data points shown on the figure are taken from Barouch et al., (1971) and indicate typical variations that may be expected. The minimum in the figure corresponds to a flare at the "foot point" of the Archimedean spiral path between the sun and the earth (57.2 degrees west of central meridian). Variations in the solar wind will result in changes in the computed "foot point" of the Archimedean spiral path.

When dealing with actual data, the onset cannot be recognized until the additional flux is larger than the background of the channel. The onset time that will be apparent from the program output is the time when the particle flux increases above the background.

4.2 Time of Maximum

The time of maximum in each channel is computed by assuming the particles have an average bulk velocity that is about half of the speed of particles of the same energy traveling rectilinearly. Most theoretical models find the time of maximum proportional to the square of the distance along the field line from the sun and so this factor is included.

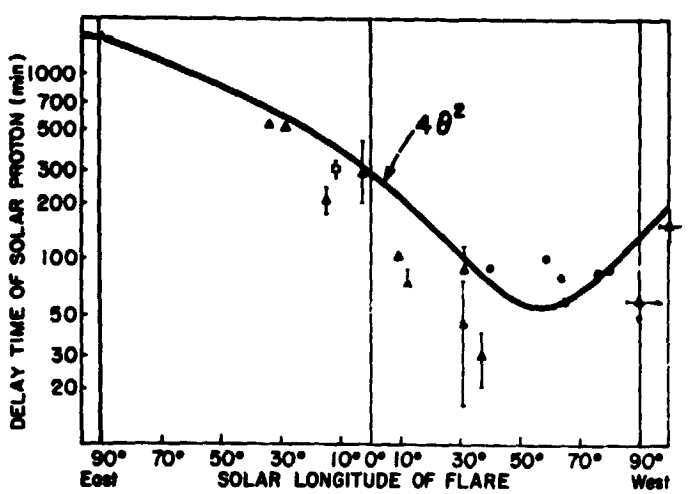

Fig. 3. Distribution of onset time of 30 MeV protons as a function of solar longitude. The data points are the measurements of Barouch et al., (1971)

The maximum number of particles in a specified energy range is assumed to be at the lowest energy of the channel. The time of maximum is computed by

$$T_m \text{ (in hours)} = 2.0\ (0.1333\ D^2/\beta\ ) + 8\Theta^2. \qquad (9)$$

The distribution of the computed time of maximum as a function of solar longitude is illustrated in Figure 4. The data points are from Reinhard and Wibberanz (1974) and show the typical range of variations that can be expected. The minimum in the curve corresponds to a flare at the "foot point" of 57.2 degrees for the Archimedean spiral path between the earth and the sun computed from a nominal solar wind of 404 km/sec. Similar curves for 30 MeV protons and 60 MeV protons cannot be shown here for lack of space, but they are not significantly different from the curve given in Figure 4.

Figure 5 illustrates the computed curve for our nominal solar wind speed (heavy solid line) as compared with the extensive data set of Van Hollebeke et al.(1975) showing the distribution of the time of maximum of 20 to 80 MeV protons with solar longitude.

Variations in the solar wind speed will shift the curve to correspond to the position of the "foot point" of the Archimedean spiral path. As an example a fast solar wind velocity of 808 km/sec results in the foot point of an idealized Archimedean spiral to be at 28.6 degrees west of central

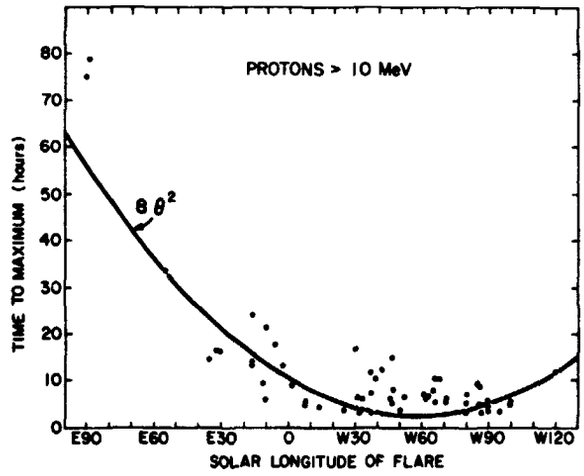

Fig. 4. Distribution of time of solar proton event maximum as a function of solar longitude. The data points are those of Reinhard and Wibberanz (1974).

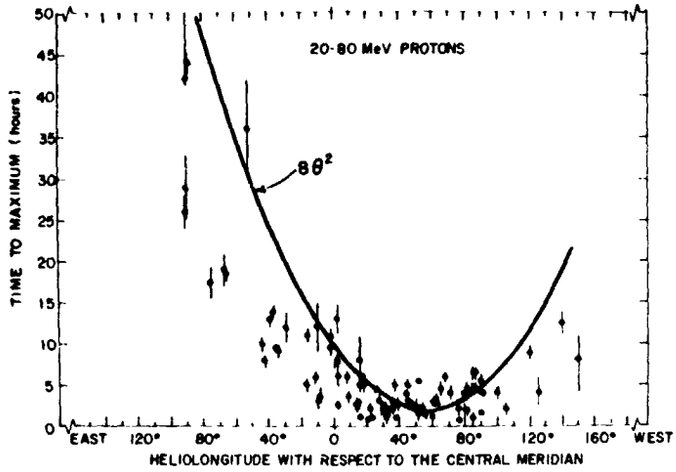

Fig. 5. Distribution of the measured time of maximum of 20 to 80 MeV protons obtained by Van Hollebeke et al. (1975) as compared with our coronal propagation parameter.

meridian while a slow solar wind velocity of 323 km/sec results in a "foot point" at 71.6 degrees west of central meridian. Thus, the variation introduced by changes in the solar wind velocity can result in large displacements from the idealized curve of maximum times. The sun's rotation introduces other effects that modulate the shape of the idealized time of maximum curves shown in these figures. (Co-rotation effects are discussed in more detail in section 4.4.2 of this paper.)

4.3 Maximum Intensity

4.3.1 Maximum Intensity Along the Archimedean Spiral Path From the Flare

The maximum intensity at some energy is predicted by converting an electromagnetic emission parameter (usually radio flux or x-ray flux) to a proton flux. Many different algorithms can be used but we have followed the procedures developed by Castelli and co-workers (private communication) and have used relationships between integrated or semi-integrated radio flux and peak proton flux. We have modified the results obtained by Straka (1970), Newell (1972), Castelli et al. (1973) and Cliver (1976) to develop a set of forecast parameters for the peak flux of protons > 10 MeV or protons > 5.2 MeV from radio burst data, and we have modified the results of Kuck et al. (1971) to develop forecast parameters for peak proton flux > 10 MeV from integrated x-ray data. A summary of some of the algorithms used is given in Table 1.

TABLE I.1 ALGORITHMS FOR CONVERTING SEMI-INTEGRATED RADIO FLUX DATA (F_S) TO PEAK PROTON FLUX (J)

FREQUENCY (MHz)	ALGORITHM
1415	$J(>5.2) = \frac{1}{C}(2.97 \times 10^4 \; F_{SW}^{0.243})^2$
2695	$J(>5.2) = \frac{1}{C}(8.63 \times 10^8 \; F_{SW}^{0.513})^2$
4995	$J(>5.2) = \frac{1}{C}(5.97 \times 10^7 \; F_{SW}^{0.453})^2$
8800	$J(>5.2) = \frac{1}{C}(9.12 \times 10^6 \; F_{SW}^{0.406})^2$

TABLE I.2 ALGORITHMS FOR CONVERTING EVENT INTEGRATED RADIO FLUX DATA (F_I) TO PEAK PROTON FLUX (J)

FREQUENCY (MHz)	ALGORITHM
1415	$J(>5.2) = \frac{1}{C}(1.74 \times 10^6 \; F_{IW}^{0.376})^2$
2695	$J(>5.2) = \frac{1}{C}(1.66 \times 10^6 \; F_{IW}^{0.380})^2$
4995	$J(>5.2) = \frac{1}{C}(4.57 \times 10^5 \; F_{IW}^{0.352})^2$
8800	$J(>10) = 3.4 \times 10^{24} \; F_{IJ}^{1.43}$
2800	$J(>5.2) = \frac{1}{C}(0.0116 \; F_{IS}^{0.555})^2$

TABLE I.3 ALGORITHMS FOR CONVERTING INTEGRATED X-RAY FLUX (F_X) TO PEAK PROTON FLUX (J)

SENSOR WAVELENGTH RANGE (ANGSTROMS)	ALGORITHM
1 – 8	$J(>10) = 2.222 \times 10^3 \; F_{XW}^{\;2}$
0.5 – 4	$J(>10) = 5.555 \times 10^4 \; F_{XW}^{\;2}$

NOTES: 1 SFU = 10^{-22} Wm^{-2} Hz^{-1}

1 JOULE = WATT SEC.

F_{SW} DESIGNATES UNITS FOR SEMI-INTEGRATED RADIO DATA AND MUST BE (Wm^{-2} Hz^{-1}) SEC.

F_{IW} DESIGNATES UNITS FOR EVENT INTEGRATED RADIO DATA AND MUST BE (Wm^{-2} Hz^{-1}) SEC.

F_{IJ} DESIGNATES UNITS FOR EVENT INTEGRATED RADIO DATA AND AND MUST BE Jm^{-2} Hz^{-1}

F_{IS} DESIGNATES UNITS FOR EVENT INTEGRATED RADIO DATA AND MUST BE SFU SEC.

F_{XW} DESIGNATES UNITS FOR X-RAY DATA IN UNITS OF Wm^{-2} SEC.

C IS A CONVERSION FACTOR RIOMETER ABSORPTION SQUARED TO >5.2 MeV PROTON FLUX DATA. $C = (0.115)^2 \pi$

We solve for a differential energy spectrum such that

$$P(>E) = K \int E^{\gamma} \, dE = \frac{K}{|\gamma + 1|} E^{\gamma + 1} \qquad (10)$$

where γ is the slope of the differential energy spectrum and K represents the flux at 1 MeV. For example, if we are using an algorithm for the > 10 MeV peak flux, the above equation is solved by an iterative technique so that

$$\sum_{E = 10 \text{ MeV}}^{E = 1000 \text{ MeV}} KE^{\gamma} = P(>10) \qquad (11)$$

where γ is the variable slope described in section 4.5.

The radio data input to the program is assumed to be in SFU (solar flux units); however, it can accept a large variety of different units (SFU, Joules, watt sec) as long as the units are identified during the input. The software makes an internal conversion to the correct units for use in the algorithms. The X-ray data input can be in either units of watts per square meter-second or ergs per square centimeter-second.

The various algorithms given in the following tables are formated so the term inside the parenthesis is the riometer absorption. The conversion from riometer absorption to proton flux follows the conventional form of $J = CA^2$ where C denotes a conversion constant. (See Section 5 for a further discussion of these conversions.)

4.3.2 Maximum Intensity at the Earth

After the maximum intensity along the Archimedean spiral path from the flare has been computed, the maximum intensity at the earth is derived by attenuating the flux through the coronal gradient over the heliocentric distance in the corona between the flare position and the solar equatorial longitude of the foot point of the Archimedean spiral path from the sun to the earth. (See Section 3.1 for a previous discussion of this concept.)

If the coronal gradient can be specified as a simple exponential function in terms of the heliocentric angle between the flare site and the foot of the interplanetary magnetic field line "connecting" the earth to the sun, then the flux at the earth's Archimedean spiral "foot point", I_e, will be reduced from the flux at the flare site I_f by

$$I_e = I_f \exp - (g \Theta) \qquad (12)$$

where g describes the coronal gradient.

There is another factor that attenuates the earth-sensed solar flare proton flux. We contruct a pseudo time-intensity profile for the proton flux at one AU along the interplanetary magnetic field line "connected" with the flare site. We assume that the decay rate discussed in section 4.4.1 commences immediately after the particle acceleration. This, coupled with the time delays associated with the coronal propagation effects to other heliolongitude positions, (See Section 4.2) implies that the flux along interplanetary magnetic field lines removed from the flare site will have an additional flux decrease by a factor of $\exp -(t_m/t_d)$. For practical applications of proton flux prediction at the earth, t_m is the time of maximum intensity for the specified channel and t_d is the 1/e decay constant in the co-rotating reference frame of the interplanetary magnetic field line "rooted" to the flare site (See Section 4.4.2).

4.4 Event Decay

4.4.1 Decay Constant

The decaying portion of the event is modeled after the principles of collimated convection (Roelof, 1973). After making a number of simplifying assumptions (some of which are that the particle flux can be represented by a simple power law, the anisotropy of the particle flux is small, the interplanetery magnetic field falls off as r^{-2}, and that the particle flux gradient is field aligned and small), the decay constant, as derived by Roelof (private communication) can be represented as

$$\tau \approx 3D/[4V(|\gamma| + 1)] \qquad (13)$$

where τ is the 1/e decay constant, D is the distance along the Archimedean spiral path, V is the solar wind velocity, and γ is the differential spectral exponent.

4.4.2 Effect of Coronal Gradient on Apparent Decay Rate.

By assuming that the source of the particle flux is the active region of the flare, and that there exists a particle gradient in the corona as described earlier, and that after the particles are released from the corona the particle propagation is along the interplanetary magnetic field with negligible diffusion perpendicular to the field lines, then the rotation of the sun affects the apparent decay rated observed at a fixed location in space (such as the earth at 1 AU). An example of this effect is shown in Figure 6. In this case the decay rate on the Archimedean spiral path corotating with the solar particle source position is constant. If the particle flux along the interplanetary magnetic field lines is considered as a corotating structure being convected out of the system, and if the particle source is rotating toward the "foot point" of the Archimedean spiral from the sun to the earth, such as is the case for flares on the eastern hemisphere or near central meridian, the apparent decay rate will be slower than if the particle source is rotating away from the "foot point", such as is the case for extreme western hemisphere flares. Also, the solar wind velocity

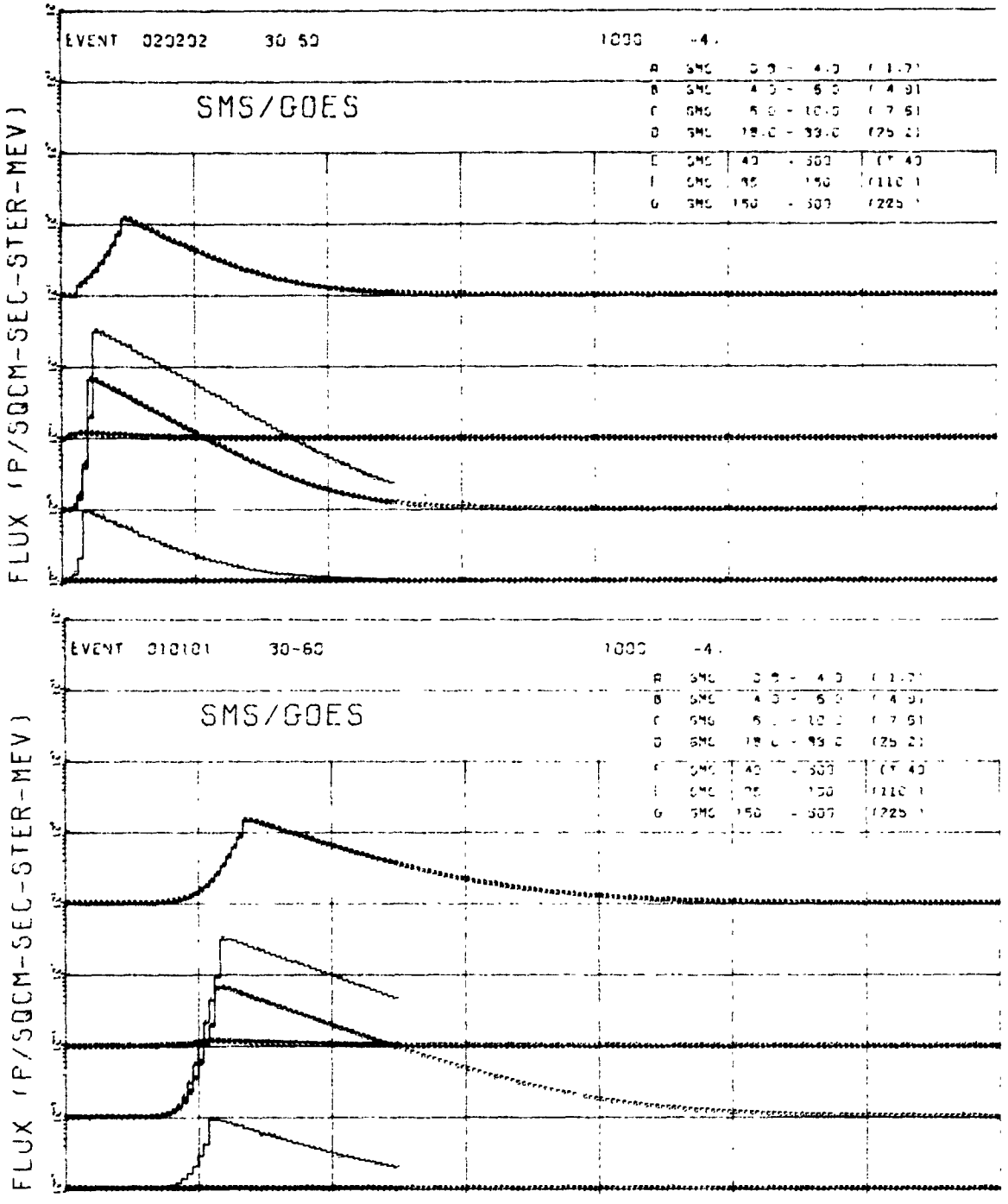

Fig. 6. Predicted solar proton time intensity profiles for the earth from a solar flare at 0000 relative time (positioned at the left axis). The top panel illustrates the profile for a western hemisphere flare at 30^{O}N, 60^{O}W. The bottom panel illustrates the profile for an eastern hemisphere flare at 30^{O}N, 60^{O}E. For both cases a nominal solar wind velocity of 404 km/sec and a differential spectral slope of -4 was used. Each horizontal line is one day and each vertical line is a factor of 10 in flux.

will affect the decay rate so the effects of co-rotation and solar wind velocity changes must be considered in constructing time-intensity profiles.

4.5 Differential Energy Spectra

We assume that at the time of the maximum flux of 1 MeV protons it is possible to construct a differential energy spectrum that is representative of the entire event. Our representative spectra have an average reference value of γ_R between 10 and 200 MeV; however the energy dependent slope becomes slightly shallower at low energies and slightly steeper at higher energies. The slope of the spectrum is modulated as a function of the particle velocity (β = v/c) so that at any energy slope of the differential energy spectrum γ_β is $\gamma_R + \alpha - \beta$ where α is the normalization constant necessary to give the proper average value between 10 and 200 MeV.

For a predicted reference slope we prefer to utilize the techniques developed by Bakshi and Barron (1974, 1975, 1979) to derive the slope of the integral solar proton spectrum (which we convert to a differential energy spectral slope) when appropriate maximum and minimum flux values of the U-shaped signature in the radio power spectrum at radio burst maximum are available.

If a prediction of the spectral slope is not available, and no explicit specification of the spectral slope has been entered as input data, a default value is computed. The default spectral algorithm is based on the work of Van Hollebeke et al. (1975) shown in Figure 7.

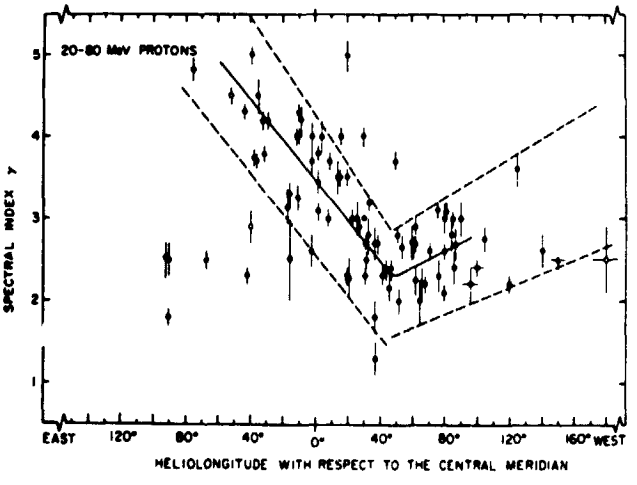

Fig. 7. Variation of the spectal index γ in the 20-80 MeV range as function of the heliolongitude. The dashed contour lines enclose 92% of the "normal" events. The solid line is a least square fit that can be represented by = 2.7[1 + θ /2].

We have modified their function by assuming that the hardest spectra (the minimum in the solid curve of Figure 7) should be along the interplanetary magnetic field lines leading away from the flare site, and that it will vary at other heliolongitudes approximately as the Van Hollebeke et al. (1975) function. The default differential energy spectral slope algorithm used is

$$\gamma_R = -2.5\ (1.0 + \Theta/2) \tag{14}$$

5. PREDICTION OF POLAR CAP ABSORPTION

After the event time intensity profiles have been computed for each energy range of interest, it is possible to convert to specialized outputs such as the prediction of the profile of the riometer absorption in the polar ionosphere. We have used the concepts and relationships developed by Sellers et al. (1977) to derive simple equations that in their opinion were relatively independent of the slope of the solar proton energy spectrum to convert satellite measured proton fluxes to equivalent riometer absorption that compared favorably with the output of more elaborate calculations employing the solar proton energy deposition and ionization rates in the atmosphere with the reaction rates of atmospheric ions and electrons in the ionosphere. These authors selected the integral proton flux greater than 5.2 MeV to be a good predictor of the riometer absorption in the sunlit polar ionosphere and the integral proton flux greater than 2.2 MeV for predicting the expected riometer absorption in the night time polar ionosphere. There equations are:

$$A\ (\text{day}) = \sqrt{0.115\,\pi\,J(>5.2)} \tag{15}$$

$$A\ (\text{night}) = \sqrt{0.02\,\pi\,J(>2.2)} \tag{16}$$

By including the integral flux above 2.2 and 5.2 MeV in the solar proton time intensity profiles it is possible to generate displays of the predicted riometer absorption expected in the polar cap during a solar proton event.

The general application of equation 15 was used in converting the original algorithms between radio flux and riometer absorption in the polar cap developed by Straka and Barron (1969), Straka (1970), Newell (1972) and Cliver (1976) to equivalent integral proton fluxes so a relatively standardized set of algorithms could be employed for conversion of radio data to peak proton flux, (see Table 1 for listing of the various algorithms used in PPS76).

6. MULTIPLE FLARE INJECTION OF PROTONS

PPS76 makes calculation of the predictions of the proton flux for up to 15 different proton energy ranges in addition to calculations of the predicted day and night riometer absorption in the polar cap. The program computes the projected time intensity profiles for the next 300 hours, and if there are subsequent new flares accelerating solar protons, these new solar proton injections are added to the residual flux from the previous flare(s). Variations in the amplitude of the new events, variations in spectra, and changes in the solar wind velocity provide for a fascinating variety of possibilities.

7. OPERATIONAL USE OF PPS76

PPS76 has been in operational use at both of the principal forecast centers in the United States since 1976. This composite prediction procedure appears to be a very useful tool for the prediction of "normal" solar proton events and polar cap absorption events. It is more limited when it is used for high energy (more than a few hundred MeV) or relativistic solar proaton events. Cliver et al. (1978) have discussed the prediction generated by this technique during the September 1977 series of solar proton events and the comparison of these predictions with the actual observations available in near real time at one of the forecast centers.

An example of some of the capabilities of this prediction technique is given in Figure 7. These time intensity profiles (or would be predictions from the input data listed at the top of the figure) may be compared with the actual measurements of the IMP 8 spacecraft shown in Figure 8. The prediction illustration in Figure 8 does not allow for enough high energy protons to produce a gound level solar cosmic ray event when in fact the 30 April 1976 event was a relativistic solar cosmic ray event detected at the surface of the earth. A somewhat similar event occured on 7 May 1978. The forecast information available predicted only a small PCA with a hard energy spectrum. A small PCA of the forecast magnitude (2.5 Db) did occur at the forecast time; however the 7 May 1978 event was the largest relativistic solar proton event since 1960.

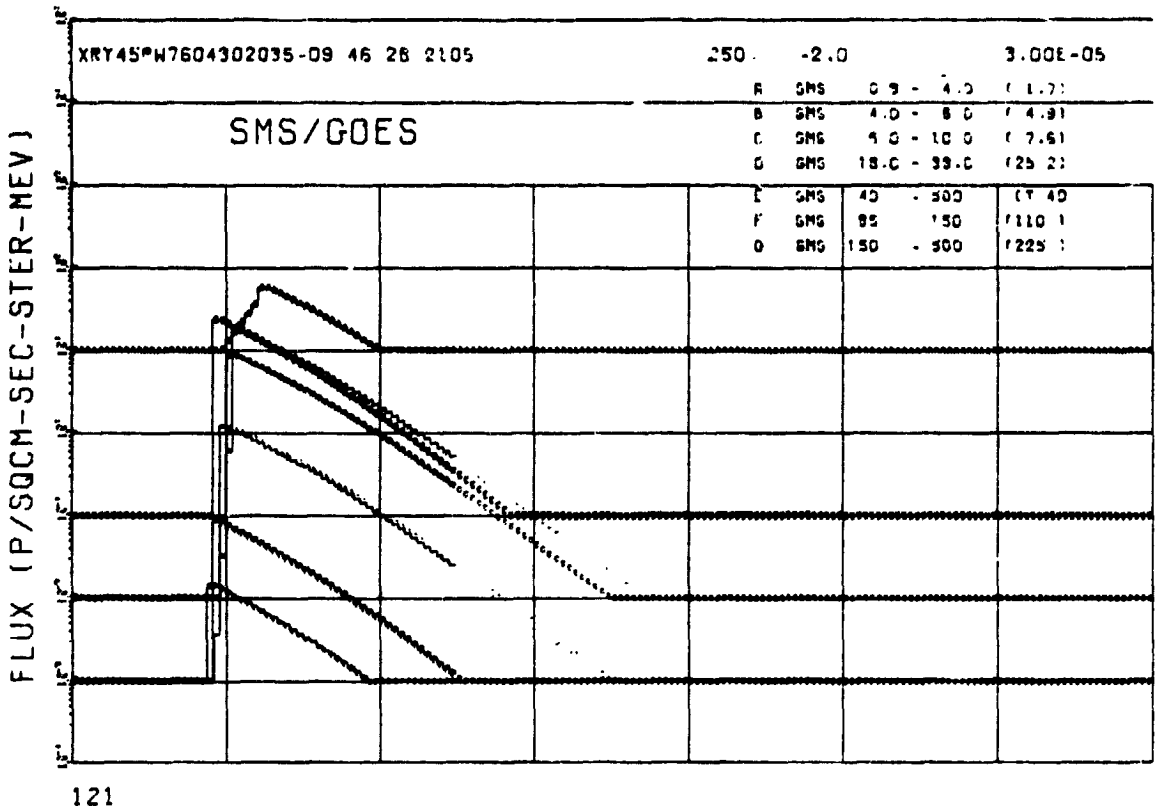

Fig 7. Predicted time intensity profile for the 30 April 1976 solar proton event. The energy channels shown are those monitored by the SMS/GOES satellite.

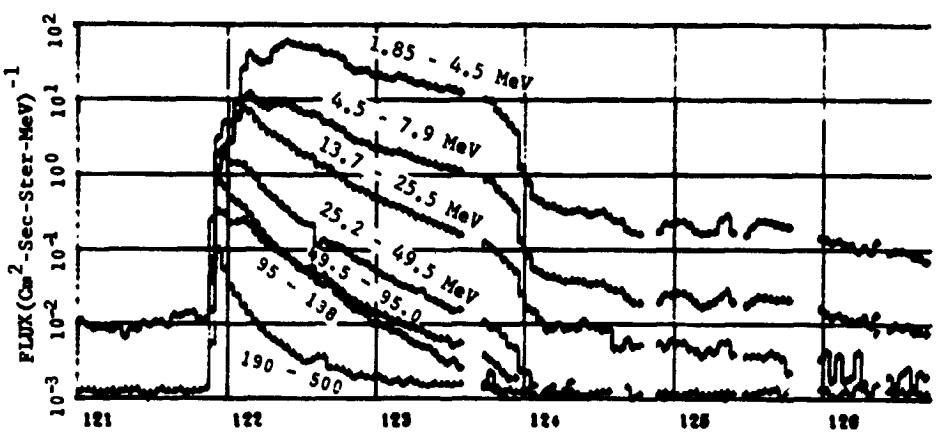

Fig. 8 The 30 April 1976 solar proton event as observed by the Johns Hopkins University Applied Physics Laboratory experiments on IMP 8.

REFERENCES

Axford, W. I., (1965): Anisotropic diffusion of solar cosmic rays. Planet. Space Sci., 13:1301.

Bakshi, P., and W. Barron, (1974): Spectral Correlations Between Solar Flare Radio Bursts and Associated Proton Fluxes I. AFCRL-TR-74-0508. Air Force Cambridge Reesearch Laboratories, Hanscom Air Force Base, Massachusetts.

Bakshi, P., and W. R. Barron, (1975): Spectral Correlation Between Solar Flare Radio Bursts and Associated Proton Fluxes, II. AFCRL-TR-75-0579. Air Force Cambridge Research Laboratories, Hanscom Air Force Base, Massachusetts.

Bakshi, P. and W. R. Barron, (1979): Prediction of Solar Flare Proton Spectral Slope From Radio Burst Data. J. Geophys. Res., 84:131.

Barouch, E., M. Gros, and P. Masse, (1971): The Solar Longitude Dependence of Proton Event Delay. Sol. Phys., 19:483.

Burlaga, L. F., (1967): Anisotropic diffusion of solar cosmic rays, J. Geophys. Res., 72:4449.

Castelli, J. P., J. Aarons, and G. A. Michael (1967): Flux Density Measurements of Radio Bursts of Proton-Producing Flares and Nonproton Flares. J. of Geophys. Res. 72:5491.

Castelli, J. P., W. R. Barron, and J. Aarons (1973): Solar Radio Activity in August 1972. AFCRL-TR-73-0086. Air Force Cambridge Research Laboratories, Hanscom Air Force Base, Massachusetts.

Castell, J. P., and D. A. Guidice (1976): Impact of Current Solar Radio Patrol Observations. Vistas in Astronomy, 19:355.

Castelli, J. P., and G. L. Tarnstrom (1978): A Catalog of Proton Events 1966-1976 Having Non-Classical Solar Radio Spectra. AFGL-TR-78-0121. Air Force Geophysics Laboratory, Hanscom Air Force Base, Massachusetts.

Cliver, E. W., (1976): Parent Flare Emission at 2.8 GHz As A Predictor of the Peak Absorption of Polar-Cap Events. NELC-TR-2015. Navel Electronics Laboratory, San Diego, California.

Cliver, E. W., J. A. Secan, E. D. Beard and J. A. Manley (1978): Prediction of Solar Proton Events at the Air Force Global Weather Central's Space Environment Forecasting Facility. In: Proceedings of the 1978 Symposium on the Effect of the Ionosphere on Space and Terrestrial Systems.

Dodson, H. W., E. R. Hedeman, R. W. Kreplin, M. J. Martres, V. N. Obridko, M. A. Shea, D. F. Smart and H. Tanaka (1975): Catalog of Solar Particle Events 1955-1969. Vol. 49 of the Astrophysics and Space Science Library, Edited by Z. Svestka and P. Simon, D. Reidel Publishing Co., Dordrecht, Holland.

Forman, M. A., (1970): The Equilibrium Anisotropy in the Flux of 10 MeV Solar Flare Particles and Their Convection in the Solar Wind. J. Geophys. Res., 75:3147.

Gold, R. E., E. C. Roelof, J. T. Nolte and A. S. Krieger (1975): Relation of large-scale coronal x-ray structure and cosmic rays: 5. Solar wind and coronal influence on a Forbrush decrease lasting one solar rotation. Proc. 14th International Cosmic Ray Conference (Munich), 3:1095.

Krimigis, S. M., (1965): Interplanetary diffusion model for the time behavior of intensity in a solar cosmic ray event. J. Geophys. Res., 70:2943.

Kuck, G. A., S. R. Davis and G. J. Krause (1971): Prediction of Polar Cap Absorption Events. AFWL-TR-71-1. Air Force Weapons Laboratory, Kirtland AFB, New Mexico

Lanzerotti, L. J., (1973): Coronal Propagation of Low-Energy Solar Protons. J. Geophys. Res., 78:3942.

McCracken, K. G., and U. R. Rao (1970): Solar Cosmic Ray Phenomena. Space Science Reviews, 11:155.

McCracken, K. G., U. R. Rao, R. P. Bukata, and E. P. Keath (1971): The Decay Phase of Solar Flare Events. Sol. Phys., 18:100.

Newell, D. T., (1972): Forecasting Peak Proton Flux and PCA Event Magnitudes Using "Flash-Phase" Integrated Radio-Burst Flux Density. AFCRL-TR-72-0543. Air Force Cambridge Research Laboratories, Hanscom Air Force Base, Massachusetts

Palmer, I. D., R. D. Zwickl, W. R. Webber and F. B. McDonald (1978): Spectrum of Mean Free Paths Near the Earth in the Solar Cosmic Ray Event of April 29, 1973. J. Geophys. Res., 83:2461.

Reid, G. C., (1964): A diffusive model for the initial phase of a solar proton event. J. Geophys. Res., 69:2659.

Reinhard, R., and G. Wibberenz (1974): Propagation of Flare Protons i the Solar Atmosphere. Sol. Phys., 36:473.

Roelof, E. C., (1973): New aspects of interplanetary propagation revealed by 0.3 MeV solar proton events in 1967, in: Solar-Terrestrial Relations 411. University of Calgary, Canada.

Roelof, E. C., (1975): Scatter-free collimated convection and cosmic-ray transport at 1 AU. Proc. 14th International Cosmic Ray Conference (Munich), 5:1716.

Roelof, E. C., (1976): Solar Particle Emission. In: Physics of Solar Planetary Environments, 1:214. Published by the American Geophysical Union, Washington, D.C., USA.

Roelof, E. C., R. E. Gold, S. M. Krimigis, A. S. Krieger, J. T. Nolte, P. S. McIntosh, A. J Lazarus and J. D. Sullivan (1975): Relation of large-scale coronal x-ray structure and cosmic rays: 2. Coronal control of interplanetary injection of 300 keV solar protons. Proc. 14th International Cosmic Ray Conference (Munich), 5:1704.

Roelof, E. C. and S. M. Krimgis, (1973): Analysis and synthesis of coronal and interplanetery energetic particle, plasma and magnetic field observations over three solar rotations. J. Geophys. Res., 78:5375.

Sellers, B., F. A. Hanser, M. A. Stroscio and G. K. Yates (1977): The night and day relationships between Polar Cap Riometer Absorption and Solar Protons. Radio Science, 12:779.

Straka, R. M., (1970): The Use of Solar Radio Bursts as Predictors of Proton Event Magnitude. AFCRL Space Forecasting Research Note 2.

Straka, R. M. and W. R. Barron, (1969): Multifrequency Solar Radio Bursts as Predictors for Proton Events. AGARD Conference Proceedings, No. 49.

Svestka, Z. (1976): Solar Flares, Volume 8, Geophysics and Astrophysics Monographs, D. Reidel Publishing Co., Dordrecht, Holland.

Van Hollebeke, M. A. I., L. S. Ma Sung, and F. B. McDonald, (1975): The Variation of Solar Proton Energy Spectra and Size Distirbution with Heliolongitude. Sol. Phys., 41:189.

Wibberenz, G., (1974): Interplanetary Magnetic Fields and the Propagation of Cosmic Rays. J. Geophys., 40:667.

Summary of Forecasters' Meeting on April 25, 1979, During the International Solar-Terrestrial Predictions Workshop

J. B. Smith

1. INTRODUCTION

The presence at the workshop of many who are involved in Solar-Terrestrial predictions and of others who are the users of the monitoring and prediction services offered a unique opportunity to discuss currently available data and forecast services and to suggest improvements in those products. Therefore, a meeting of solar-environmental forecasters and customers was held on April 25, 1979, (following two days of Working Group meetings) to discuss the early progress of each of the working groups. To introduce some order to the discussion of several subjects by the large group of individuals, the working groups were first discussed by representatives of those working groups — followed by open group discussion. Notes of the discussions and recommendations are presented below. A summary of the discussion of solar activity forecast verification appears after the working group remarks and is followed by a list of the participants in the forecasters' meeting. Although recommendations generally represent a majority view, some comments may be neither a consensus statement nor a majority opinion.

2. WORKING GROUP DISCUSSIONS

2.1 Long-Term Solar Activity Predictions

1. Historically, the sunspot count, particularly as recorded by the Zurich Observatory, has served as a valuable index of solar activity and offers the primary long term data base for analysis and prediction. (A more objective and much used activity index is the solar radio flux at 10.7 cm, observed and reported by Ottawa since 1974.) The continuation of these observations is considered of primary importance to long-term solar activity predictions and to the understanding of the cyclic variations in solar activity.

2. For physical reasons, forecasters and users emphasize that observations and predictions from other non-traditional data, particularly EUV, are very desirable. Improvement in more traditional data bases, such as solar radio flux and geomagnetic indices, is needed.

3. The validity of the short-term, mid-term, and long-term periodicities in the data should be verified. Are the periodicities real and predictable? Statistical analysis should be applied to determine the validity of the data fluctuations.

4. It was suggested that the long-term predictions working group could have benefited by the addition of a representative from the area of dynamic modeling. This was certainly a popular opinion and should be considered for any future meeting.

5. Group discussion indicated that intermediate time-scale forecasting (on the order of a solar rotation to a few months) has not been given deserved attention. Techniques for predicting the evolution of active regions and of active longitudes should be evaluated for current application. A 27 day forecast of daily 10.7 cm flux and Ap values is a recently added service at SESC in Boulder.

2.2 Short-Term Solar Activity Predictions

1. Users and potential users of solar-terrestrial forecast services are not always fully aware of the services and data available and of how to interpret the data provided. Similarly, the forecasters may not always understand the requirements of the users. Increased interaction between the forecasters and their customers is clearly desirable.

2. Forecast centers, although closely related by data and product exchange, do not presently share all available data. Different data sets are available to the different forecasters, although an internationally exchanged subset is available to all. A real-time exchange of more of the important information is strongly suggested. The discussions and submitted workshop papers have also made apparent some difference in the forecast techniques applied by the centers. The various forecasting techniques should be shared among centers and perhaps similarly evaluated.

3. Although many current solar prediction techniques are quite qualitative, or input data are used quite qualitatively, objective solar prediction techniques have received a good deal of attention and are discussed at length in separate sections of these proceedings. It seems necessary to quantize the forecasts where possible. New observational parameters may be necessary for further progress. The opinion was expressed that prediction accuracy has progressed as far as is possible with the data currently available.

4. Forecasts for periods of less than 24 hours are usually made on an as-required basis. Forecasters should determine whether there is a recurring need for forecasts of a few hours, as was implied here.

5. Predictions of an active regions' flare potential should include a prediction of its capability for producing proton events.

6. RECOMMENDATION. There is a strong recommendation (with general agreements) for forecaster exchange between centers.

2.3 Geomagnetic Disturbances

There were no members of these study groups present in the forecasters meeting. Discussion of the forecasting techniques and application was therefore limited.

2.4 Magnetosphere - Ionosphere Interaction

Only questions were posed: Why does a geomagnetic disturbance produce, or not produce, ionospheric effects? What are the cause and effect relationships, the coupling mechanisms, and the geomagnetic distribution?

2.5 Ionospheric Predictions

1. Improved measurements of more directly involved wavelengths, e.g. EUV, may be beneficial in ionospheric monitoring and prediction.

2. There is a need to know what ionospheric instrumentation is currently operational.

3. An expressed opinion that ionospheric predictions are not always based on "real physics" was perhaps not fully subscribed to.

2.6 Solar - Weather Predictions

1. Further identification should be made for solar parameters that should be evaluated for possible correlation with long-term (drought, climate, planetary wave studies) and short-term (pressure changes, electrical storms, etc.) weather phenomena. Greater interaction with solar-activity prediction groups is desirable.

2. The coupling of the troposphere to solar activity is certainly not understood. Some things to be looked at are the energy input, the solar constant, coronal holes, sector boundaries, chemistry, triggering, geomagnetic storms, etc.

3. At this point, it appears that the need for data and research is greater than for solar predictions. We are clearly not now in a position to use solar forecasting to predict the Earth's weather.

2.7 Propagation Predictions

Those who use the propagation forecast were well represented and the discussion and comments centered on communication between the forecaster and the user. Those who use the predictions are not always familiar with the standard terminology and may not understand the implications of the forecast. A partial solution is certainly user education and some forecaster education about tailoring their product for the customer. Dissemination of the short-term predictions is still often too slow.

2.8 Geomagnetic Applications

1. This area is of interest to many commercial users. The predictions are important and are used because that can be translated into financial savings. The emphasis should be strongly toward the geomagnetic effect, not the cause of the activity. Very specific daily forecasts are of value, and forecasts that can be simply interpreted are desirable.

2. Not only the predictions of an active geomagnetic field are of value, the prediction of quiet conditions is also very important.

3. Division of geomagnetic predictions according to geographic zones would be beneficial.

4. Problem Areas: Again the too slow dissemination of short-term forecasts was mentioned.

3. FORECAST VERIFICATION

Many of the principles and problems of forecast verification schemes mentioned in the meeting are discussed in NOAA-ERL-Technical Memorandum (in press) by Gary R. Heckman, entitled "Verification of Solar Flare Forecasts at the Space Environmental Services Center for the Years 1969-1974". This paper has an excellent discussion of several scoring methods and considers them in light of a "proper" scoring method . A "proper" verification scoring method is one where the best forecast for scoring purposes represents the forecaster's true belief about what will happen. This paper also considers how to weigh probability forecasts according to the "cost" to a particular user of making one of two types of error. One type of error is predicting an event which does occur. A method by which this can be done is explained fully in Heckman's paper.

Some comments made in the general discussion of forecast verification are summarized below:

1. There is a need for more utilization of statistical analysis to develop and verify forecasting techniques.

2. Verification may indicate which variables are the good predictors as well as indicate the quality of the forecast. Verification is valuable as feedback to the user and the forecaster.

3. A summary of all currently used verification techniques and their advantages is needed.

4. It is imperative that all published forecast accuracy statements include: (a) a clear statement of exactly what is being forecast, (b) the climatology during the forecast period, and (c) a clear statement of exactly how the verification was performed.